Spatiotemporal Dynamics in Regulating Ecosystem Services of Urban Green-blue Infrastructure

Fraser Alan Edward Charles Baker

2020

Spatiotemporal Dynamics in Regulating Ecosystem Services of Urban Green-blue Infrastructure

Fraser Alan Edward Charles Baker

A thesis submitted in partial fulfilment of the requirements of Manchester Metropolitan University for the degree of *Doctor of Philosophy*

2020

A society grows great when old men plant trees whose shade they know they shall never sit in

Greek Proverb

Acknowledgements

This project was funded through an Ecology and Environment Research Centre PhD studentship at Manchester Metropolitan University. The European Space Agency (Category – 1 Proposal ID. 38972) provided the PLEIADES and SPOT 7 satellite imagery. The Ordnance Survey (3-month research licence; commencing 2nd July 2018) supplied the Addressbase plus data. Thanks to Bryan Cosgrove and City of Trees for use of the Greater Manchester *i-Tree* survey data. Also, I would like to thank the independent reviewers for their important corrections and inputs to the published papers of this thesis (Baker et al. 2021).

Firstly, I would like to express my sincere gratitude to Dr Gina Cavan. Gina has been an exceptional Director of Studies, helping me overcome practical obstacles and offering much needed personal support and encouragement over the past three years. She has provided invaluable pragmatic advice and reason during all stages of this thesis, and has helped me to develop my scientific communication skills considerably. Our collaboration on numerous projects during this thesis has been a pleasure and I am confident we will continue collaborative work in the future. I would also like to extend the deepest of gratitude to the rest of the supervisory team: Graham Smith MSc. and Stuart Marsden, Professor in Ecology. Their advice, good humour, patience and ability to help me view this project from alternative perspectives has proved an immeasurable benefit.

I would also like to thank Dr Elias Symeonakis and Dr Christian Devenish for their technical support during this project, and also thanks to fellow PhD candidates and staff in the Ecology Environment Research Centre (too many to list here unfortunately) who have provided an excellent and supportive research environment. Finally, the deepest of thanks to my parents and family for their understanding and support.

Abstract

Synoptic citywide maps of green-blue infrastructure (GBI) and associated regulating ecosystem services (RES) can indicate priority locations for GBI investment to build urban resilience to future climate stressors. However, current approaches are typically static in view, and may fail to consider change in services over different temporal cycles. Planned GBI investment may not offer optimal RES solutions when considering seasonal fluctuations in climate and ecological conditions, or environmental change due to future urban development. In response, this thesis aimed to develop a range of spatiotemporal analysis methods to improve the usefulness of current RES map information. The city of Manchester, UK, is the study area, as the environmental impacts of considerable urban development, since the turn of the century, is currently poorly understood by local planning stakeholders.

Overall, findings indicate that seasonal variation in RES is a limited concern for the city. Incorporation of seasonally adjusted indicators for temperature regulation and stormwater storage RES, against typical assumptions of static year-round RES functions, result in less than 5% discrepancy in identified RES deprived areas. In contrast, environmental change is more evident over an inter-year period (2000 – 2017). The city lost approximately 11% of existing GBI, although net GBI increases were recorded in a minority of areas. GBI declines were recorded for most land uses, with losses of between 5.7% and 28.3% a concern for residential land uses where residents live and consume RES. In response, scenario analysis indicates that concerted land use targeted GBI conservation (i.e. street tree and residential gardens) policies are the minimum action required to prevent significant future declines in GBI and RES.

Overall, the thesis provides a multi-stage analysis workflow to investigate various GBI and RES management scenarios within the context of planned and unplanned urban development. GBI loss is a common urban trend across the globe, whilst cyclical variation in RES may prove more important for cities with greater seasonal extremes in climate conditions. The ecological modelling, map classification and change analysis methods here work with accessible research data and are therefore theoretically adaptable to a range of urban conditions. Indicators are mapped at scales (100m grid) suitable to investigate GBI retrofits of existing built infrastructure and can accommodate different data assumptions regarding proxy model parameterisation.

Declaration

No portion of the work referred to in this thesis has been submitted in support of an application for another degree or qualification of this or any other university or institute of learning.

Contents

List of figures

List of tables

Acronyms/abbreviations

Reference	*Description*
BLD_{POP}	Population disaggregation method weighted to mapped building extents
CN	Curve Number
GBI	Green-blue infrastructure
GWR	Geographically weighted regression
HAB_{POP}	Population disaggregation method weighted to residential housing locations
LDF	Local development framework
LL00	Topographic features generated from Ordnance Survey land-line (year 2000) data
LST	Land surface temperature
LULC	Land use landcover
MM17	Topographic features generated from Ordnance Survey Mastermap (year 2017) data
NDVI	Normalised difference vegetation index
NLUD	National land use database
OLS	Ordinary least squares
OS	Ordnance survey
RES	Regulating ecosystem services
SCS-CN	Soil conservation service curve number model
ULU	Urban land use

Chapter 1: Introduction

1.1 Background

Urbanisation is a disruptive process. The degradation of natural resources from construction of urban infrastructure interferes in natural ecological cycles, and negatively impacts local environmental conditions. For example, urban heat islands result from a prevalence of thermal energy storing manmade materials, that elevate urban temperatures above neighbouring rural areas, and exacerbate heatwave conditions for urban residents (Heaviside et al. 2016, Paravantis et al. 2017). Sealing of pervious natural surfaces, also increases runoff during extreme precipitation events, increasing the risk of flooding from the inundation of urban drainage systems (Kaspersen et al. 2017, Reynard et al. 2001). Urbanisation can also disrupt soils and vegetation structures that sequester and store atmospheric carbon (Zhang et al. 2015). In this manner urban areas may adversely affect local climate conditions, by contributing directly to global warming. As growth in global urban population is projected to continue in coming years (UN 2018), and climate change may increase risks of extreme weather events in many parts of the world (Madsen et al. 2014, Miller & Hutchins 2017), effective strategies to improve urban resilience are an increasing urban planning concern (Araos et al. 2016, Shi et al. 2016).

Improving urban resilience is a multi-faceted consideration which requires adaptation of both community and institutional practices, in addition to the physical adaptation of new and existing infrastructure (Hamin & Gurran 2009, Lwasa 2010). Physical adaptations can alleviate environmental stressors (e.g. flood water levels, excessive noise levels) using manmade and/or natural infrastructure interventions (Arnbjerg-Nielsen & Fleischer 2009, Carter et al. 2015, Larsen 2015). Manmade adaptations such as the enlargement of existing sewers (Arnbjerg-Nielsen & Fleischer 2009, Waters et al. 2003), or using solar reflecting building materials to reduce heat exposure (Georgescu et al. 2014) are highly beneficial, but can assume a high financial cost (Lennon et al. 2014, Muller 2007). In comparison, green-blue infrastructure, which provides benefits such as urban cooling (Norton et al. 2015), surface runoff reduction (Zhang et al. 2012), capture of atmospheric particulates (Escobedo et al. 2011), excessive noise buffering (Gidlöf-Gunnarsson & Öhrström 2007) and reduced carbon footprints (Nowak & Crane 2002), can provide a lower cost solution to augment or even replace the need for manmade adaptations. In this context green-blue infrastructure may refer to the planned use of natural green (e.g. street trees, parks) and blue (e.g. reservoirs, balancing ponds) resources for their environmental

benefits (da Silva & Wheeler 2017). However, this definition does not apply to green and blue resources that were not designed for this purpose, which nevertheless provide beneficial environmental functions (McDonald 2015). As such, all vegetation and waterbodies in a city act as beneficial urban green-blue infrastructure (GBI; **Figure 1.1**), that if managed effectively can aid urban resilience to hazards resulting from urban environmental stressors.

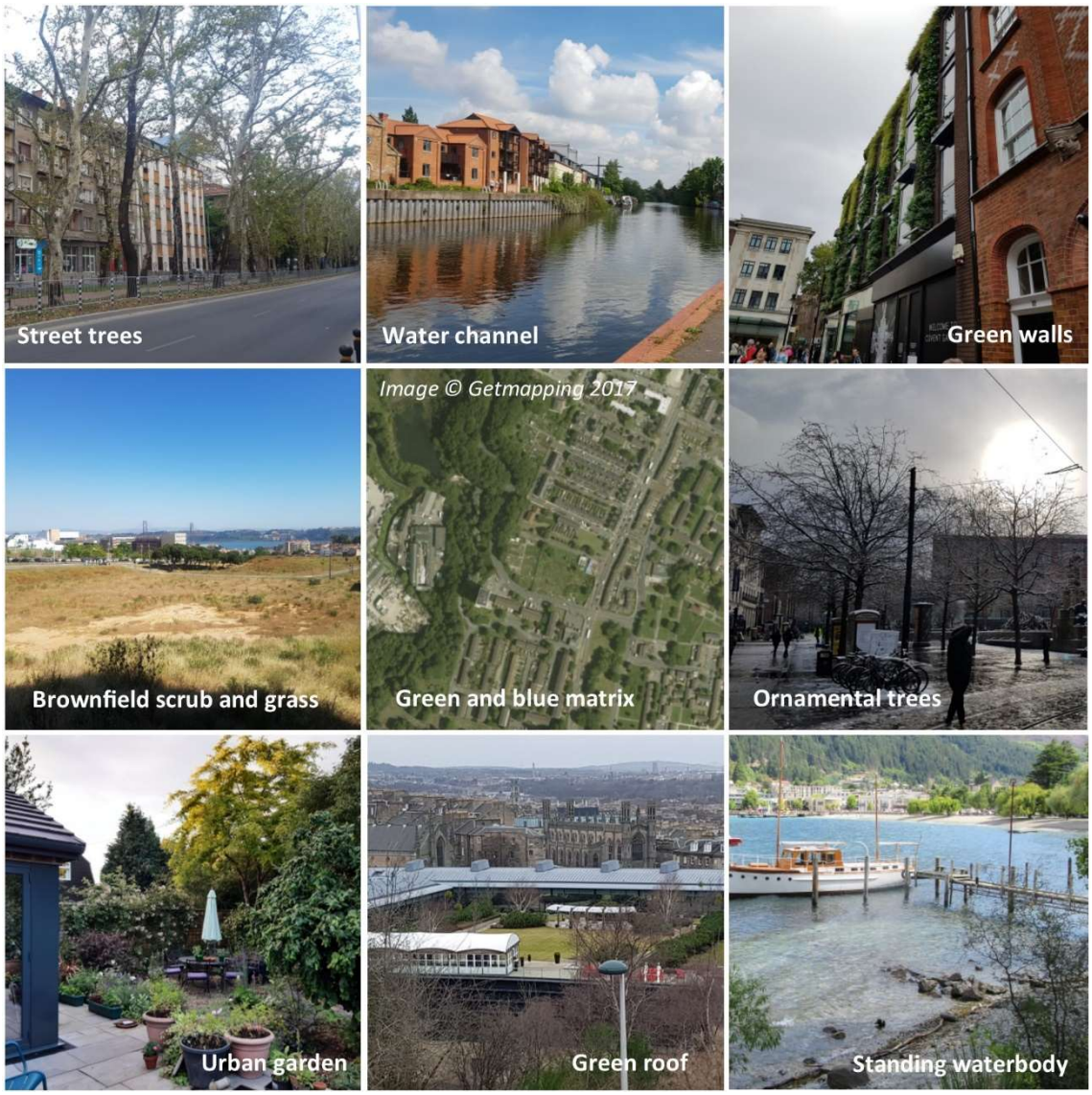

Figure 1.1 – Examples of green-blue infrastructure in urban areas

The management and planning of GBI however, is a complex undertaking. Environmental concerns compete with pressures to develop social and economic capital, and thus replace non-urbanised ecosystems with housing, offices, roads and other types of artificial infrastructure (Bomans et al. 2010). In these circumstances, traditional planning

instruments, such as environmental impact assessments, may be employed to consult stakeholders (e.g. planners, developers, general public) over the environmental impacts of local development (Morgan 2012). Such instruments can help develop actions to preserve GBI and also address environmental concerns in local communities, however their application is not feasible for all development processes within an urban area (Azqueta & Sotelsek 2007). Of serious consequence for GBI management is the lack of planning control over decisions to degrade GBI (e.g. garden paving, brownfield clearing) for land uses outside of direct municipal control (Bibby et al. 2020, Sayce et al. 2012). Protection of GBI may be approached through legislative safeguards or engagement with individuals and organisations to encourage appropriate management practises (Cortinovis & Geneletti 2018). However, this requires a sufficient evidence base on the stock and benefits of GBI resources, to inform strategic spatial GBI investment to build urban resilience throughout a city (Cortinovis & Geneletti 2018, Wilkinson et al. 2013). As such, the conceptualisation of GBI as a resource with inherent societal value is beneficial for this purpose.

Two concepts have gained prominence in recent years. The first relates to Natural Capital, which refers to ecosystems, or ecosystem components that provide goods and services (or benefits) to wider society (Costanza et al. 1997). Ecosystems may be viewed as a managed resource, similar to industrial, human, social and other forms of capital, that require sufficient governance and investment to sustain the capital benefits provided (Guerry et al. 2015). Natural capital accounting frameworks vary in definition and application, but typically imply a number of processes, such as valuing GBI resources, assessing risks posed to GBI vitality, and informing appropriate management systems, to sustain the long-term health of ecosystem benefits (DEFRA 2020, Guerry et al. 2015, Hein et al. 2016). Natural capital values are often described in monetary terms, which can enable consideration of GBI investment within the budgetary constraints of managing organisations (Azqueta & Sotelsek 2007).

Separate to, and also central to the concept of natural capital accounting, is the quantification of ecosystem benefits, or services (Guerry et al. 2015). The term ecosystem services originated as an economic concept to quantify ecosystems and their associated functions, in order to encapsulate all benefits humans receive from ecosystems (Costanza et al. 1997, Fisher et al. 2009). Whereas traditional economic valuations of natural resources focus upon directly marketable goods (e.g. agricultural produce, hydroelectric power, tourism receipts), ecosystem services incorporate additional functions that sustain societal well-being and life upon this earth (Bateman et al. 2013). Ecosystem services are

therefore numerous and are typically categorised as one of four types. Provisioning services refers to the physical goods society receives from ecosystems, such as timber, agricultural yields and water supplies (Kandziora et al. 2013). Supporting services refer to ecosystem functions that can sustain ecosystem vitality and benefits provided, such as soils that encourage diverse plant growth (Dominati et al. 2010). Cultural services refer to benefits humans obtain through interaction with ecosystems, such as cognitive, social, educational and recreational activities supported by parks and other accessible greenspace (Hernández-Morcillo et al. 2013). Regulating services refers to ecosystem functions that regulate ecological and environmental conditions, such as the regulation of global temperatures from forest carbon sequestration and storage (Gauthier et al. 2015). Whilst the scope of individual services may vary between applications, this typology provides a common reference to analyse, communicate and share research into ecosystem benefits within the broader planning and research communities (Gómez-Baggethun & Barton 2013). In the urban context, ecosystem services are typically described as benefits provided by ecosystems, or GBI, located within and immediately surrounding urbanised regions (Luederitz et al. 2015).

Both natural capital and ecosystem services concepts overlap to varying degrees. For example, in the UK natural capital accounting framework (DEFRA 2020) ecosystem services describe only the functions provided by ecosystem structures, which natural capital accounting converts into an appropriate physical or monetary asset value. In contrast, ecosystem services may represent final values of service benefits, and present an alternative framework to evaluate ecosystem benefits (Barbier 2007, Gómez-Baggethun & Barton 2013). Certainly, research into both natural capital and ecosystem services is important to communicate and raise awareness of the environmental value of GBI resources amongst urban planning stakeholders (Gómez-Baggethun & Barton 2013, Haase et al. 2014). Natural capital accounting is therefore focused on generating economic accounts of natural assets, whereas ecosystem service analysis has broader application, with additional emphasis on the methods to quantify the ecological functions and benefits of natural assets (Guerry et al. 2015).

In relation to the use of GBI to build urban resilience, the ecosystem services concept provides a useful framework to map spatially explicit flows of regulating functions that mitigate environmental stressors. A growing body of literature is therefore devoted to assessing spatial and temporal variation in ecosystem service values across urban areas (**Table 1.1**). This process varies from study to study, but is typically conceptualised in terms

of structures, functions and services (**Figure 1.2**). Improving access to high resolution geospatial data, including satellite imagery, topographical maps and species occurrence data, enables synoptic mapping of the extent and condition of GBI across urban areas (de Araujo Barbosa et al. 2015). Functions, that provide a societal benefit, are then estimated considering the environmental and locational context of different biophysical structures (Andrew et al. 2015). Modelling approaches for functions vary widely from approaches for individual services, through to integrated ecosystem service modelling software (e.g. InVEST; Stanford University 2020, ARIES; Villa et al. 2009). For example, the InVEST software suite, which is used widely ecosystem service research (Cabral et al. 2016, Grafius et al. 2016, Sieber & Pons 2015), enables spatially explicit estimation of ecosystem services, and demonstrates the development of openly accessible tools to value natural capital (Stanford University 2020). In terms of services, maps of ecosystem functions can be overlaid with other data indicating demand in the population, in order to assess mismatches between the supply and use of function benefits (Baró et al. 2016, Larondelle & Lauf 2016). This is particularly beneficial for regulating functions (e.g. localised GBI cooling, particulate capture) that moderate harmful environmental stressors at the local scale. For example, areas of high and low regulating functionality may be cross-examined with spatial maps of environmental risk exposure (e.g. flood risk, vulnerable populations) to indicate respective hotspots and coldspots in hazard reduction benefits (Langemeyer et al. 2020, Schröter et al. 2017). Such information can therefore engage multi-disciplinary discussion of appropriate GBI management strategies of where, and how, to conserve and/or improve GBI resources to build urban resilience to environmental stressors (Langemeyer et al. 2020). This information may also serve as spatial evidence of regulating GBI benefits within natural capital accounting and other asset evaluation frameworks (Paulin et al. 2020).

Table 1.1 – Urban ecosystem service mapping case studies

Case study (ordered chronologically)	*Ecosystem services studied*	*Spatial measures of structure*	*Spatial units for functions*	*Spatial units for services*	*Period of change analysis*
Leipzig-Halle, Germany (Burkhard et al. 2012)	See article (9 x Regulating; 11 x Provisioning; 2 x Cultural)	LULC cover polygons	LULC cover polygons	Land use - Landcover	1990 – 2007
Four European cities (Larondelle & Haase 2013)	Temperature regulation; Carbon storage; recreation	LULC cover polygons	LULC polygons	1km buffers from city core to outer city limits	N.A.
Greater Manchester (Radford & James 2013)	Aesthetic; Recreation; Spiritual; Genetic/biodiversity; Air quality/carbon seqREStration; Noise buffering; Climate; Pollination; Water flow regulation	Landcover polygons through image digitisation and field visits	250,000m^2 grid cells	Urban gradient classification (Rural, peri-urban, suburban, urban)	N.A.
Rotterdam, Netherlands (Derkzen et al. 2015)	Air Purification; Carbon Storage; Noise reduction; Run-off retention; Cooling & Recreation	Continuous landcover raster data	1m pixel grid	Urban districts	N.A.
Sheffield, UK (Holt et al. 2015)	Air particulate reduction; Temperature regulation; Stormwater storage; Carbon storage; Cultural; Habitat - flora/fauna	LULC polygons	LULC	500m grid cells, census area & Land use landcover	N.A.
Bordeaux, France (Cabral et al. 2016)	Food provisioning; Flood regulation; Water quality; Erosion regulation; Recreation; Climate regulation; Biodiversity	LULC polgyons	LULC	Urban sub-districts	1990 – 2016

Table 1.1 (Continued) – Urban ecosystem service mapping case studies

Case study (ordered chronologically)	*Ecosystem services studied*	*Spatial measures of structure*	*Amalgamation units for functions*	*Amalgamation units for services*	*Period of change analysis*
Stockholm, Sweden (Kain et al. 2016)	Food supply; Energy supply; Urban cooling; Air quality regulation; Carbon seqREStration; Storm water retention; Physical recreation; Mental recreation	Service providing land use units	2500m^2 grid cells	Various scales: Region, City, Municipality and Neighbourhood	N.A.
New York City (Kremer et al. 2016a)	Stormwater storage; Local climate regulation; Carbon storage; Air Pollution removal; Recreation	Continuous landcover raster data	1m pixel grid	1m pixel grid	N.A.
Barcelona, Spain (Baró et al. 2017)	Food provision; Global climate regulation; Air purification; Erosion control; Outdoor recreation	LULC polygons	Municipal area boundaries	Municipal area boundaries	N.A.
Shanghai, China (Haas & Ban 2018)	See article (7 x Ecological Integrity; 9 x Regulating; 11 x Provisioning; 2 x Cultural)	Image classified landcover objects	Land use – landcover object groups	LULC object groups	2000 – 2009
Bogota, Colombia & Santiago, Chile (Dobbs et al. 2018)	Global climate regulation; Local microclimate regulation; Recreation potential	Continuous NDVI raster data	30m grid pixel	Urban gradient classification & Socio-economic analysis units	1985 – 2014
Barcelona, Spain (Zhang & Ramirez 2019)	17 x Regulating; 6 x Provisioning; 2 x Habitat; 7 x Cultural	LULC polygons	LULC	LULC	N.A.

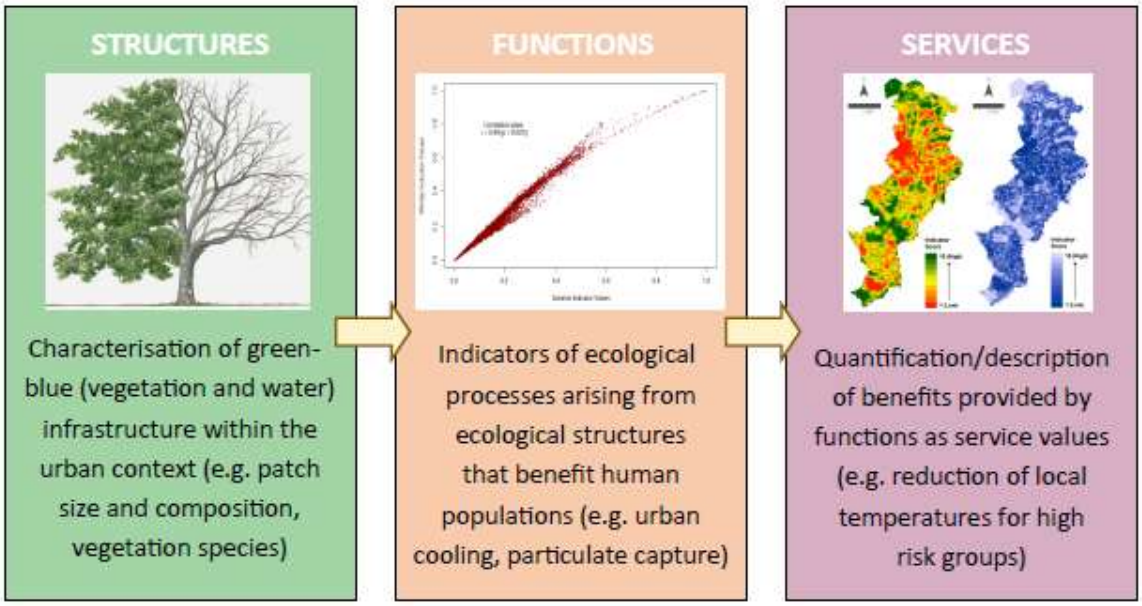

Figure 1.2 – Basic framework of urban ecosystem services research

Location targeted investment in GBI is therefore increasingly evident in cities around the world. Examples of large scale initiatives include the MillionTreesNYC project (2007 – 2015) where tree canopy coverage in New York, USA increased by 20% (Jones & Goodkind 2019), and the Green Corridor development in Lisbon, Portugal, that added 190 hectares of green areas between 2009 and 2017 (Lehner 2018). In the UK, GBI development strategies are evident within many local policy documents, such as the "London Environment Strategy" (GLA 2018) and the city of Manchester's green and blue infrastructure strategy (MCC 2015). The need to improve GBI (natural capital) and ecosystem services, and thus build urban resilience to current and future environmental stressors, is therefore an important goal described in these documents. However, despite increasing recognition of the environmental value of GBI, explicit incorporation of ecosystem service concepts within urban planning strategy appears to be limited (Haase et al. 2014, Woodruff & BenDor 2016). For example, a recent study into urban planning documents in Italy revealed that only 11 out of a total of 136 urban plans explicitly used analysis of ecosystem benefits to guide planning policy (La Rosa 2019). Other studies evidence that while the concept of ecosystem services is at least widely acknowledged, barriers persist for the strategic utilisation of this concept by urban planners (Albert et al. 2014, Rall et al. 2015). This is concerning, as is evident in many cities around the world, the process of GBI degradation is an ongoing process (Chen et al. 2017, Dallimer et al. 2011).

In the face of projected increases in extreme weather in coming years, it is therefore questionable whether urban residents are receiving the maximum potential of regulating ecosystem service benefits.

Certainly, there is potential for further efforts to address this issue through the improved communication of GBI as a nature-based solution to build urban resilience. This discussion of course is not inherently constricted within the confines of natural capital and ecosystem services. However, as evidenced, analytical approaches associated with these concepts describe usable frameworks to quantify and communicate regulating GBI benefits within the climatological, ecological and socio-economic contexts of a given urban area. Urban ecosystem service research, and in particular the mapping of urban ecosystem services, can provide spatially explicit evidence to inform environmental policy from within other planning frameworks (Langemeyer et al. 2020, Paulin et al. 2020). To employ this information more effectively, and help build resilience to environmental hazards in urban areas, requires increasing the usefulness of this information for decision-making purposes.

1.2 Useful ecosystem service information

Usefulness, in terms of decision making, may refer to a number of information requirements. Of primary concern is that indicators of ecosystem service functions and value, should provide information of sufficient scientific quality, and at suitable geographic scales to represent the spatial flow of service benefits (Layke 2009). This is to ensure that decisions regarding GBI investment are informed by sound scientific evidence, so that planning decisions provide intended environmental outcomes (Seppelt et al. 2011). In relation to the concept of GBI as a long-term Natural capital asset, there is also a need for information on the trends, or developments that may alter GBI and associated services in the future (Rodriguez et al. 2006, De Groot et al. 2010). This may guide planning policy to prevent, or encourage, actions causing either degradation or improvement in GBI resources (Cortinovis & Geneletti 2018, Lam & Conway 2018). Trend analysis may also inform modelling of future GBI change, in order to predict future patterns of GBI (e.g. future service coldspots), and thus identify priority areas for long term GBI investment (Lauf et al. 2014).

In addition to quantification processes, there is also need to present findings in an accessible manner to a range of technical and non-technical stakeholders. Accessible

information can therefore support inter-disciplinary development of GBI planning policy, and improve awareness within planning circles on the importance of urban ecosystem services (Sheate et al. 2012). Accessibility is also important in relation to data and methods. Findings generated using transferable methods and concepts of ecosystem services can enable the transfer and sharing of knowledge between different study areas and build knowledge within the research community (Daily et al. 2009). In addition, as environmental planning budgets are often limited, mapping exercises that generate useful results with minimal expenditure are ultimately beneficial (Albert et al. 2014). Mismatches in the content of information, between what is produced and what is actually required by planners, is also a limiting factor in the effective uptake of ecosystem services in planning circles (Albert et al. 2014). These aforementioned information requirements may be addressed further by investigating research gaps within current ecosystem service mapping literature.

1.3 Current research gaps

For regulating ecosystem services, that influence environmental stressors resulting in hazards, challenges remain in the effective representation of spatial flows in GBI functions and utilisation of such functions by urban residents. As shown in **Table 1.1**, services are often amalgamated within various spatial units, such as census tracts, administrative boundaries and land use/landcover (LULC) areas. These units are useful to compare RES benefits to either local demand for services, such as in neighbourhoods containing high risk demographic groups (e.g. elderly people requiring air cooling services), or within areas of local planning concern (Baró et al. 2017, Cabral et al. 2016, Kroll et al. 2012). However, as RES benefits may occur at the micro-scale (e.g. particulate capture by individual trees, or localised air cooling) this spatial scale may under-estimate variation in benefit transfer to local communities (Andrew et al. 2015). For example, an administrative area may consist of a distinct residential zone with minimal GBI cover, adjacent to a large park with considerable GBI cover. Due to morphological constraints, temperature regulation cooling functions of the parkland are limited within the residential area (Coseo & Larsen 2014), and therefore have minimal impact in reducing risk of hot temperature stressors among local residents. However, the significant presence of parkland GBI in this instance results in overestimation of temperature regulation benefits when calculated as a single service value for the administrative area as a whole (**Figure 1.3**; Gómez-Baggethun

& Barton 2013). Alternative spatial units, such as regular grid-based representations may better approximate regulating ecosystem service flows across continuous urban landscapes (Holt et al. 2015, Kremer et al. 2016a). However, studies that implement service demand indicators at this resolution are limited in number, and may rely on data relevant for the local study area (Baró et al. 2016, Larondelle & Lauf 2016).

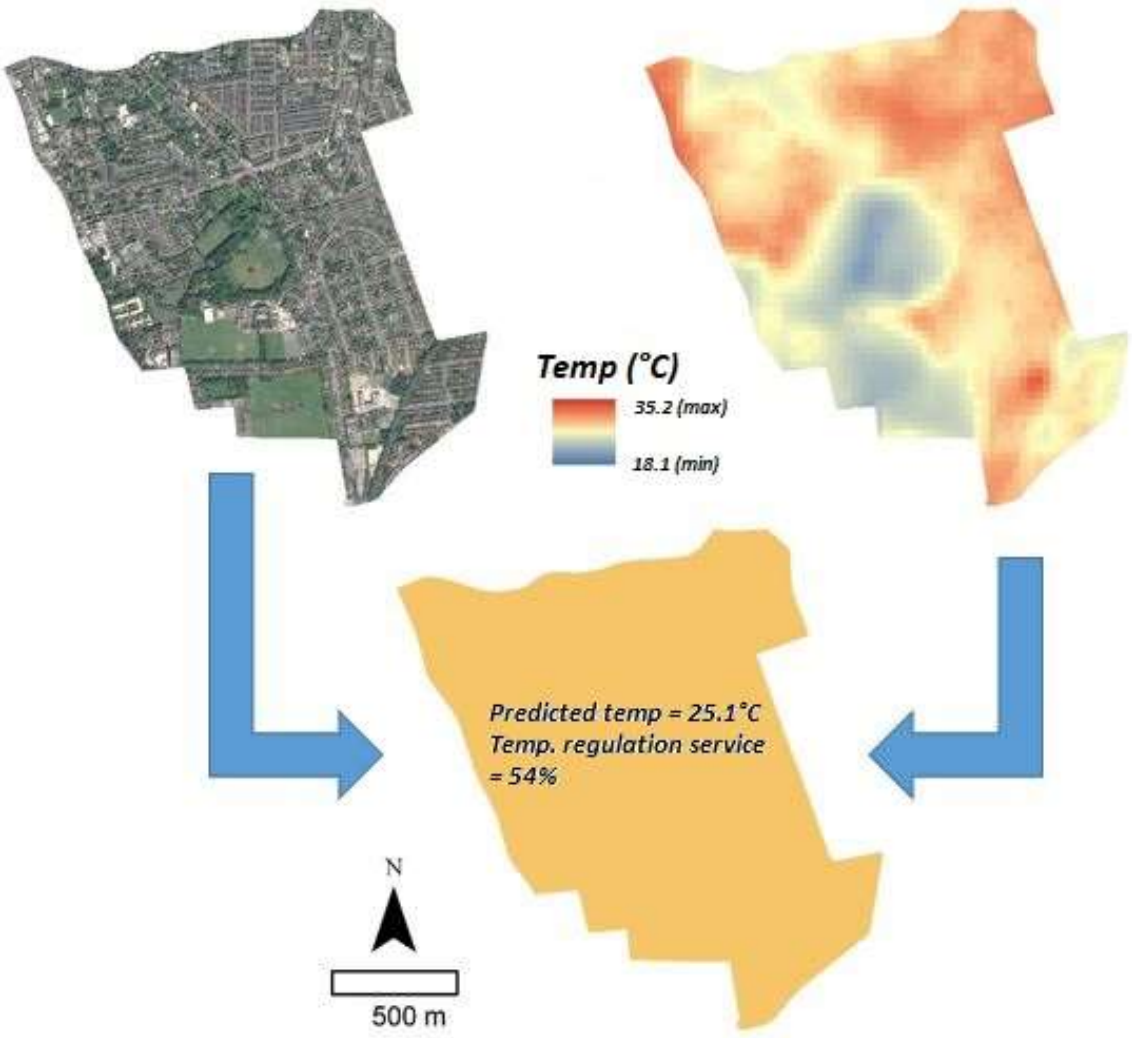

Figure 1.3 – Green-blue infrastructure and associated temperature phenomena aggregated to coarse resolution ecosystem service value

Limitations in current mapping may also result from the various methods used to model ecosystem service indicators. Whilst models validated with primary data that represent local ecological and environmental conditions are preferred, the costs to collect and process such data for certain services is often prohibitive for whole city areas (Schröter et al. 2015). In comparison, proxy methods provide a time and cost-effective alternative

but can result in spurious map outputs due to the direct transfer of findings to inappropriate conditions (Eigenbrod et al. 2010). Studies may counter this issue through approaches tailored to the local urban environment and associated data. However, as quality of input data may vary considerably between study areas, such mapping approaches may have limited application in other urban areas (Haase et al. 2014). Due in part to a current lack of standardisation in methods, RES knowledge transfer between urban areas is limited (Kremer et al. 2016b). RES mapping approaches applicable to different urban environments require understanding of how input data of varying quality may cause ambiguity in the parameterisation of component methods, and thus influence final maps (Schulp et al. 2014).

Addressing the above limitations may improve usefulness of RES maps, however mapped indicator values may be of limited use lacking consideration of change in RES over an annual cycle. For example, seasonal leaf loss associated with deciduous vegetation reduces the ability of green infrastructure foliage to intercept precipitation (Armson et al. 2013a, Asadian & Weiler 2009), capture airborne particulates that are harmful to health (Lin et al. 2016) and transpire moisture to cool surrounding temperatures (Armson et al. 2013b, Rahman et al. 2015). Extreme precipitation for example, may occur during months of the year when vegetation canopy cover is reduced (Fowler & Kilsby 2003, Kassomenos et al. 2012), resulting in enhanced runoff and increased risk of flooding hazards for urban residents. Phenological change will also reduce the magnitude of urban cooling by green infrastructure during cold weather months but may remain as an ecosystem disservice by increasing resident exposure to cold temperature conditions and associated health hazards (Hajat et al. 2007, Lowe 2016). Urban resilience to environmental stressors is therefore dependent upon complex interactions between ecosystem structures and environmental conditions that vary over an annual cycle. Current citywide assessment of ecosystem services (**Table 1.1**) assume GBI functions are temporally static (e.g. full canopy cover year-round to reduce precipitation), and therefore provide limited assessment of GBI as a year-round functional ecosystem service resource. Whether incorporation of seasonal variation in regulation service indicators is a concern for spatial planning of GBI is currently poorly understood.

In contrast to cyclical change, ecosystem service change over inter-year periods has received more attention in the current literature. This is often analysed according to change in land use, as this drives ecosystem service alteration through the re-configuration of landcover components that govern ecosystem functions (Cabral et al. 2016, Haas & Ban

2018). GBI change also occurs within static land use areas over time, impacting ecosystem services (Wellmann et al. 2020). For example, studies of landcover change in residential areas indicate the potential magnitude of GBI degradation that may occur from decisions to pave garden space and extend private dwellings (Pauleit et al. 2005, Perry & Nawaz 2008, Verbeeck et al. 2011). Appropriate planning strategies are therefore required to counteract degradation in ecosystem conditions where necessary, to conserve and improve RES in the future (De Groot et al. 2010, Rodriguez et al. 2006). Quantification of coarse scale LULC change can inform this process (**Table 1.1**). However, this scale of representation may over aggregate important micro-level trends in GBI change (e.g. paving over of garden areas; Perry & Nawaz 2011) as the appropriate GBI metrics remain aggregated within the altered spatial extents of LULC (Andrew et al. 2015). As trends in GBI change due to land use management decisions are poorly understood, RES planning strategies developed on a static information baseline may not be appropriate to address potential future losses in RES benefits (Wellmann et al. 2020).

1.4 Opportunities to address research gaps

As evidenced in **Table 1.1**, the mapping of ecosystem services in urban areas is a relatively new area of research. Improving access to appropriate data resources should enable the further development of current mapping methods to address the aforementioned research gaps. This in turn may improve the usability of spatially explicit regulating ecosystem service information to guide strategic spatial planning of RES to build urban climate resilience. For example, improvements in the spatial representation of regulating ecosystem structures (**Figure 1.2**) may be achieved through use of very high spatial resolution remotely sensed imagery to map urban green-blue infrastructure patches (e.g. trees, grasses water) (de Araujo Barbosa et al. 2015). A large number of existing models can be applied at the patch level to estimate varying levels of ecosystem service functions for different GBI components (Davies et al. 2011, Derkzen et al. 2015). Methods developed using widely accessible research data (e.g. imagery, census records, topographic map data) presents an opportunity to improve the consistency and usability of current ecosystem service map indicators across multiple urban areas (Layke 2009, Daily et al. 2009). For example, application of similar mapping approaches may enable the comparison of factors that influence ecosystem service dynamics (e.g. morphology, GBI species, weather patterns) in different cities. This may then improve knowledge sharing regarding

appropriate strategies to conserve and improve GBI for different urban conditions (Gill et al. 2007, Kremer et al. 2016b). Moreover, as the quality of input data may vary for different mapping exercises, analysis of how this may influence map results is beneficial to convey the overall usefulness of map information to end users (Eigenbrod et al. 2010). Fine scale mapping of ecosystem services can thus provide useful baseline information which can be spatially aggregated to support analysis at different spatial (e.g. administrative, census) scales (Derkzen et al. 2015).

In addition, image data representing different seasons can also be analysed to identify vegetation species, in turn enabling models of cyclical change in ecosystem service functions (Marando et al. 2019, Xiao & McPherson 2016). Seasonality may also apply to demand measures, as disaggregation methods applied to census data enable upscaling of human demand measures to the micro-scales of regulating ecosystem service benefits. For example, this may include assessing resident exposure to localised seasonal environmental hazards, such as pluvial flooding (Cavan & Kaźmierczak 2011), and exposure to extreme temperatures (Dugord et al. 2014), in order to gauge how localised GBI functions can regulate associated environmental stressors. Citywide mapping of cyclical variation in regulating ecosystem services is therefore a novel concept that can assess whether exclusion of seasonal dynamics is an oversight in current mapping ecosystem service analyses.

For inter year study periods the comparison of present-day maps of GBI with historical information (e.g. aerial photographs, satellite imagery, national map data) enable change detection in GBI over time. For example, change detection has been successfully applied to assess the extent of pervious cover change upon local runoff rates in private urban gardens (Perry & Nawaz 2008, Warhurst et al. 2014) and to assess the depletion of carbon sequestration rates according to decline in urban forest cover (Nowak & Greenfield 2012). Automated and semi-automated methods are also applicable with the same geospatial data resources to enable categorisation of land use at various time points (Gill et al. 2008). Assessing how land management may influence future GBI degradation, enables planners to consider socio-economic management pressures influencing regulating ecosystem service change (Pauleit et al. 2005), and also identifies communities at heightened risk from future environmental stressors (Gill et al. 2007).

The ability to address research gaps in regulating ecosystem service mapping approaches, using the aforementioned methods, could support a multi-stage

spatiotemporal analysis of regulating ecosystem services that provides a range of practical benefits. Citywide variation in current regulating ecosystem services is beneficial to identify pockets of year-round ecosystem service deprivation in order to inform localised GBI investment to match resident needs (Majekodunmi et al. 2020). Inter-year trends in GBI change may also provide important evidence of wider environmental concerns, such as biodiversity conservation, or the impacts of urban population and economic growth upon GBI change (Dallimer et al. 2011, Hostetler et al. 2011). Ultimately, there is opportunity to incorporate differing stages of temporal analysis to inform appropriate planning strategies to address resident demands for urban resilience.

In this respect, the concept of land use is again useful. Land use planning is commonly applied in many countries, to ensure that the distribution of human activities is adequate to support economic and environmental policy goals (Barker 2006). In the UK for example, the Town and Country planning order (1987) defines “use” classes, as a framework to manage land use conversion for sustainable economic development. Land use is therefore applied to describe zones of change in strategic spatial planning documents (MCC 2020c) and to guide consultation with stakeholders in relation to planned development (Baker et al. 2010). Interacting GBI with land use will therefore not only relate ecosystem services to different types of human activity, but also information for scenario examination of future GBI investment strategies. Scenario planning of GBI and ecosystem service change, in relation to land use units and approximations, has been successfully investigated in a number of cities around the world (Cortinovis & Geneletti 2018, Gill et al. 2007, Kain et al. 2016). There is potential to build upon this research, and incorporate GBI change analysis to investigate “what if” GBI and ecosystem service management scenarios (e.g. 10% improvement in street trees) within static or changing land use areas (Gill et al. 2007, Kain et al. 2016). Analysis of trends in GBI change per land use and the resulting impact upon regulating ecosystem services is important to identify potential socio-economic pressures influencing GBI change for urban areas in general (Pauleit et al. 2005) and should also highlight applicable measures to conserve future regulating ecosystem services (Gill et al. 2007).

1.5 Regulating ecosystem services

This study will focus upon temperature regulation, stormwater storage and above-ground carbon storage services. As aforementioned, these services are an increasing planning concern in cities around the world, due to their role in mitigating urban environmental stressors that may be exacerbated by climate change (Araos et al. 2016, Shi et al. 2016). Omission of seasonally adjusted RES indicators may therefore represent a concern for current ecosystem service estimates, as extreme climate conditions increase in frequency and severity coming decades (Madsen et al. 2014, Miller & Hutchins 2017). A summary of the regulating ecosystem services examined in this study are provided in **Table 1.2**.

Urban areas are susceptible to enhanced flooding risks due to dense surface sealing, which increases water runoff depths and rates during precipitation events and increases pressures upon local drainage systems (Ahiablame & Shakya 2016). Fluvial (inundation causes water to overflow river banks) or pluvial (inundation of existing drainage systems) flooding thus occur when drainage (e.g. sewers, water channels) capacity is overloaded (Kazmierczak & Kenny 2011). Green infrastructure can alleviate such pressures as water is absorbed by plant holding soils and captured within above-ground biomass material, thus reducing pluvial flooding risks for the surrounding area (Beven 2000). Blue infrastructure capacity for precipitation absorption is dependent upon the capacity for additional water volume provided by water containing structures (Voskamp & Van de Ven 2015). GBI implementation measures such as tree planting and wetland creation, are increasingly employed as sustainable urban drainage system practices in UK urban areas (Ashley et al. 2015). The benefits of GBI flood risk reduction can vary throughout the year as vegetation canopy change may reduce water capture capacity, whilst seasonal wetness levels may determine the absorption capacity of soils and waterbodies (Asadian & Weiler 2009, Hankin et al. 2008, Silveira et al. 2000). Seasonal variation in stormwater storage services have received limited attention in previous ecosystem service studies. This may present a concern, as assumptions of fully functioning GBI may overestimate service benefits during periods when ecological functions are reduced, and precipitation stressors upon local residents are increased.

Urbanisation also modifies natural solar and hydrological cascades, resulting in enhanced urban land surface and ambient air temperatures (e.g. island of heat) when compared to surrounding rural and peri-rural areas (Oke 1978). The so-called urban heat

island phenomenon is observed in cities across the globe, with urban warming considered a significant environmental hazard in hot climate regions, where urban heat islands exacerbate already high local ambient temperatures by several degrees (Grimmond 2007). This artificial enhancement in temperature causes increased prevalence of heat stress related medical conditions and fatalities during heatwave events (Harlan et al. 2006). Patches of GBI, consisting of various configurations of trees, shrubs, grasses and waterbodies help to break up the density of thermal energy storing materials prevalent in urban areas (Cavan et al. 2014, Guo et al. 2015, Weber et al. 2015). The release of latent heat through evaporative cooling of vegetation and waterbodies, aids air and surface cooling, whilst vegetation also provides shading, significantly reducing the amount of solar radiation reaching below canopy surfaces (Hamada & Ohta 2010, Hathway & Sharples 2012). Pockets of shaded cool air that form under vegetation canopies circulate with warmer air resulting in an air-cooling influence for surrounding areas (Dimoudi & Nikolopoulou 2003). Cooling by GBI thus provides a clear benefit to local residents which will become increasingly important as climate change enhances the frequency and intensity of heatwave events in urban areas (Cavan 2011).

However, in comparison to stormwater storage functions, potential urban cooling effects in winter months may provide a disservice to local residents by reducing the benefits of urban heat island warming of cool temperature conditions. Longitudinal studies of relationships between temperature and health outcomes in the UK, indicate worsening death rates as temperatures fall (Hajat et al. 2002, Hajat et al. 2007). Localised temperature cooling thus places additional pressure on household budgets for heating costs, which is a concern for households in urban areas that may suffer from existing high levels of fuel poverty (Robinson et al. 2018). In this context, it is important to consider whether urban cooling benefits in warm weather conditions outweigh negative implications of urban cooling during winter months, and the degree this compares to temporally static indicators in the current literature (**Table 1.1**).

Table 1.2 – Regulating ecosystem services included in this thesis

Ecosystem Service	*Ecological functions of green-blue infrastructure*	*Seasonal dynamics*	*Benefits to local residents*
Temperature Regulation	Air cooling through latent energy transfer of solar radiation from transpiring photosynthesizing plant material, and evaporation in water. Shading by plant canopies to a) reduce radiation absorption in shaded surfaces to reduce above air warming from surface thermal radiation energy transfer; b) form cool air pockets that cool nearby air temperatures through displacement.	Canopy leaf-loss and reduced sunlight in winter months lowers transpiration in plants and reduces ground shading potential. Cooling function of blue infrastructure depends upon temperature disparity between air and water, which varies as water temperatures change according to annual variation in solar warming.	Cooling of ambient temperatures around green-blue infrastructure resources, providing alleviation of thermal discomfort in hot weather conditions. Urban cooling benefits may reverse during cold weather conditions.
Stormwater storage	Interception and temporary storage of precipitation in vegetation material during rainfall events. Absorption of precipitation in soils associated with vegetation and existing waterbodies.	Tree canopy leaf-loss reduces rain-water interception capacity of green-infrastructure material. Pre-event water volume contained in soils and waterbodies may vary according to antecedent weather conditions.	Reduction of water flows flowing into local drainage systems during precipitation events reducing localised flooding risks.
Carbon storage	Sequestration of carbon into biomass during plant growth. Carbon temporarily retained from atmosphere as biomass whilst plant is alive.	Growth patterns vary throughout the year depending upon species, affecting carbon uptake.	Current carbon stocks determine communal contribution to offset climate change.

Urbanisation also replaces carbon storing vegetation and soils with manmade infrastructure. Loss of ecosystems, and increased pollution emissions compound to ensure that urban areas are a major contributor to global warming. As such, there is increasing interest in the reduction of carbon footprints amongst urban planning stakeholders (Sovacool & Brown 2010). Traditional estimates of carbon storage in urban areas are relatively low when compared with rural and natural ecosystems (Davies et al. 2011). However, an increasing body of empirical research demonstrate that urban trees, shrubs,

grasses, turfs, plant litter and underlying soils can provide a significant carbon pool (Davies et al. 2011, Edmondson et al. 2012). Preservation and improvement of GBI resources therefore has implications for building urban resilience to environmental hazards. Stored carbon is prevented from contributing to global warming, which in turn results in climate change and projected increases in extreme weather events (Herzog & Golomb 2004). Carbon storage levels in GBI also vary on an annual cycle. For example, soil respiration of organic carbon can vary according to seasonal change in wetness and temperature levels (Raich & Schlesinger 1992). Trees and other types of vegetation sequester carbon during leaf-growth periods, which is then retained within woody biomass (Nowak & Crane 2002). Loss of vegetation sequestered carbon occurs in winter months when leaf canopies fall to the ground and decompose into either soil organic, or atmospheric carbon (Zak et al. 2008).

Seasonal exchanges in carbon storage between GBI components are thus complex and can result in variation in the total amount of carbon stored over a year. However, it is unclear how this variation directly relates to the mitigation of seasonally varying environmental stressors at the neighbourhood scale. Leaf canopy loss may result in a temporary reduction of above-ground carbon storage services. However, whether this temporary variation increases or reduces seasonal environmental stressors in an urban area is difficult to assess as this ecosystem service function is pooled with carbon storage capacities of natural resources across the globe. As such, for the purpose of mapping ecosystem service values, the carbon storage function of GBI is viewed as a temporally static ecosystem service here. In addition, only above-ground carbon storage is considered here. Soils provide a significant carbon pool in urban areas, which vary according to soil structure, density, depth, supported vegetation structures, levels of disturbance and management practices (Pouyat et al. 2002, Strohbach et al. 2012). However, studies into urban soil storage outside of North America are limited (Edmondson et al. 2014). In comparison to information on above-ground GBI structures, which can be collected from synoptic resources (e.g. imagery, topographic maps), data at the appropriate resolution to estimate variation in soil carbon is less accessible (Edmondson et al. 2014). As such, due to lack of expertise on how to appropriately map spatial variation in soil organic carbon stores, this source of carbon storage was omitted from this study.

Of course, there are other regulating benefits provided by GBI, which are not included here. Notably particulate capture is considered an important function to reduce pollution exposure hazards amongst urban residents. However, the modelling of GBI particulate reduction services is complex, requiring knowledge of both flows of particulates

from anthropogenic sources (Amorim et al. 2013, Kulshrestha et al. 2009), and the biophysical construction of plant species for particulate removal potential (Nowak et al. 2006, Speak et al. 2012). In addition, noise buffering can reduce hazards associated with resident exposure to high levels of acoustic pollution (Fang & Ling 2003). However, the number of studies dedicated to mapping this function across urban areas remain few in number. In contrast to the other regulating ecosystem services (**Table 1.2**), which mitigate extraneous climate stressors, negative particulate and noise stressors may be better addressed by efforts to regulate the human activities that cause them. These services were therefore omitted due to the estimated time required to map seasonal variation for both temperature regulation and stormwater storage services.

As extreme temperature and flooding risks may increase in frequency in the coming years, the focus on regulating ecosystem services here, is beneficial to provide information to build urban resilience through conservation and investment in GBI (Carter et al. 2015). Recent guidance from the UK Department for Environment Food & Rural Affairs indicate that understanding of natural flood management approaches (stormwater storage), cooling effect of vegetation in cities (temperature regulation) and habitat creation (above-ground carbon storage) can support climate resilience and greenhouse gas reduction policy goals (DEFRA 2020, p 30). Methods developed for mapping spatiotemporal dynamics in the three RES here may therefore prove beneficial for enabling current natural capital accounting practises in the UK. A full appreciation of GBI values is not possible here, due to the exclusion of other important ecosystem services (e.g. well-being benefit from resident exposure, social and physical recreation in parks) (Haase et al. 2014). However, it is hoped that by investigating the aforementioned research gaps a framework emerges that can incorporate additional services in future research, to provide a fuller account of GBI benefits within ecosystem service and natural capital terms. Essential to this process therefore is the critical examination of the usefulness of this information for planning purposes in order to identify remaining gaps for future research. Application in a case study area will generate usable local planning information, and may also serve to further raise awareness of GBI benefits in building urban resilience amongst urban planning stakeholders.

1.6 Thesis aims & objectives

The aim of this thesis was to develop approaches to map spatiotemporal dynamics of urban green-blue infrastructure (GBI) and associated regulating ecosystem services (RES), in order to improve the usefulness of ecosystem service information to plan urban environmental resilience. The research aim was investigated through the objectives listed below:

1. Assess how spatial scale and proxy-based methods in current ecosystem service mapping approaches can be improved (Chapter 2).

2. Identify whether incorporation of seasonal dynamics in regulating ecosystem service maps present a concern for planning green-blue infrastructure (Chapter 3).

3. Examine whether the magnitude of change in green-blue infrastructure over time varies for different land uses (Chapter 4).

4. Assess how the methods and findings of previous objectives can inform scenario planning of regulating ecosystem services (Chapter 5).

1.7 Structure of thesis

According to the above aim and objectives the thesis is structured in the following chapters:

- **Chapter 2** describes the development of a regulating ecosystem service mapping approach to address Objective 1. A literature review examines strengths and limitations of models for mapping regulating ecosystem services to address current research gaps. Chosen models are implemented in a case study investigation of the mapping approach. Variation in proxy-based conceptualisation of ecosystem functions investigates how assumptions regarding data impacts relationships between modelled ecosystem service indicators. Review of this process serves as a guide to adapt the approach for other applications.

- **Chapter 3** employs the mapping approach developed in **Chapter 2** to spatially examine seasonal dynamics in temperature regulation and stormwater storage services across the study area. Object-based image analysis is applied to map GBI patches and other landcovers across the study area. Model approaches are updated to examine seasonal interactions between ecological functions and demand for

reduction in seasonal environmental stressors. Results indicate whether seasonal dynamics represent a concern for planning and future research.

- **Chapter 4** develops and implements methods to examine study area GBI change in consistent land use areas (Objective 3). GIS methods are developed to map recent land use to spatially backdate consistent land use area samples. Error adjusted post-classification change detection quantifies high resolution GBI change across the study area. Urban land use change trends indicate future GBI vulnerability between land uses, and across the study area at neighbourhood scales.

- **Chapter 5** draws together the research methods and findings from the previous chapters to demonstrate how they can be implemented to investigate future change in regulating ecosystem services according to different development scenarios. Planned development and conservation data from the local council are integrated with land use GBI change trends. This helps to assess the levels of GBI investment required to offset potential future ecosystem service degradation. This analysis provides useful planning information to raise awareness of land use targeted solutions to conserve and improve green-blue infrastructure for the benefits of urban residents.

- **Chapter 6** provides the concluding discussion regarding the wider implications of the thesis. This includes an overview of the contribution to research resulting from each chapter. Methodological extensions concern limitations in methods used throughout this thesis, and how they may be addressed in future research. Future research directions discusses the avenues of further investigation that emerge from the thesis as a whole.

1.8 Study area

Manchester is a city in north west England, United Kingdom (City centre, Piccadilly Gardens - WGS 84 coordinates: 53°28’51” North 2°14’14” West) with a current population of approximately 547,000 (2018 mid-year estimate; ONS 2019) that serves as the economic centre for the Greater Manchester metropolitan region (population 2.8 million; ONS 2019). Patterns of built and green-blue infrastructure reflect various phases of development in the city’s history (**Figure 1.4**). From the beginning of industrialisation in the late 18th century,

the city grew in phases throughout the 19th (population 70,409 in 1801) and early 20th centuries reaching a maximum population of 766,311 in 1931 (**Figure 1.5**; MCC 2016a). The city's population gradually declined throughout the remainder of the 20th century to approximately 400,000 at the turn of the new millennium (MCC 2016a), reflecting population displacement due to inner-city slum clearance, and emigration due to post-industrial economic decline (Williams 1996). Manchester's industrial legacy is encapsulated by Victorian and Edwardian-era commercial and industrial buildings in and around the city centre (Williams 1996). In addition, a large proportion of the resident population resides in pre-1919 housing stock, ranging from small terraced houses through to large Victorian mansions (Hall et al. 2012, MacKillop 2012).

The city of Manchester presents an interesting case study area to investigate RES methods, as resident exposure to service benefits and environmental stressors is moderated by varying development patterns throughout the city. In Greater Manchester for example, Hall et al. (2012) estimated that areas surrounding pre-1919 residential housing contained an average 11.8% tree cover in comparison to an average 37.8% tree cover for later residential development. Areas of GBI are generally lower within the city centre and inner wards, in comparison to the leafier outer suburbs (Dennis et al. 2018). Variation in GBI cover is also likely to change due to continued economic development and population growth in the city. Indications of how continued development may affect future regulating ecosystem services in the city can be obtained by quantifying trends in GBI change from the turn of the century when recent population growth in the city began.

The city of Manchester's climate is designated as Cfb (C = Warm Temperate; f = Fully Humid; b = Warm Summer) using the Koppen-Geiger classification system (Kottek et al. 2006). Average monthly maximum temperatures range between 7.3°C (January) to 20.6°C (July), whilst average monthly minimums range between 1.6°C (February) and 12.6°C (July) (1981 – 2010 baseline) (Met Office 2013). Average monthly precipitation varies between 51.4mm (February) and 92.5mm (October) (1981 – 2010 baseline) (Met Office 2013). The city experiences rainfall for over one third of the year, with 143 days per year on average recording precipitation > 1mm (Met Office 2013). In a study of frequency of extreme climate events within Greater Manchester (1961 – 2009 baseline) it was revealed that flood events present a significant regional concern, accounting for on average 37-55% of decadal extreme events (Smith & Lawson 2012). Pluvial flooding is a recurring issue in Manchester, which occurred as recently as July 2019, causing damage to infrastructure and private residences throughout the city (BBC 2019a). As extreme precipitation events may increase

in frequency in Greater Manchester from 1 to 4 times a year by the 2050s, the stormwater storage benefits of local green-blue infrastructure will be increasingly vital for reducing associated flood related hazards for local residents (Cavan 2011). Heatwave events, whilst currently less of a concern due to relatively mild climate conditions within Manchester, are projected to increase in frequency in coming decades (Cavan 2011, Smith & Lawson 2012).

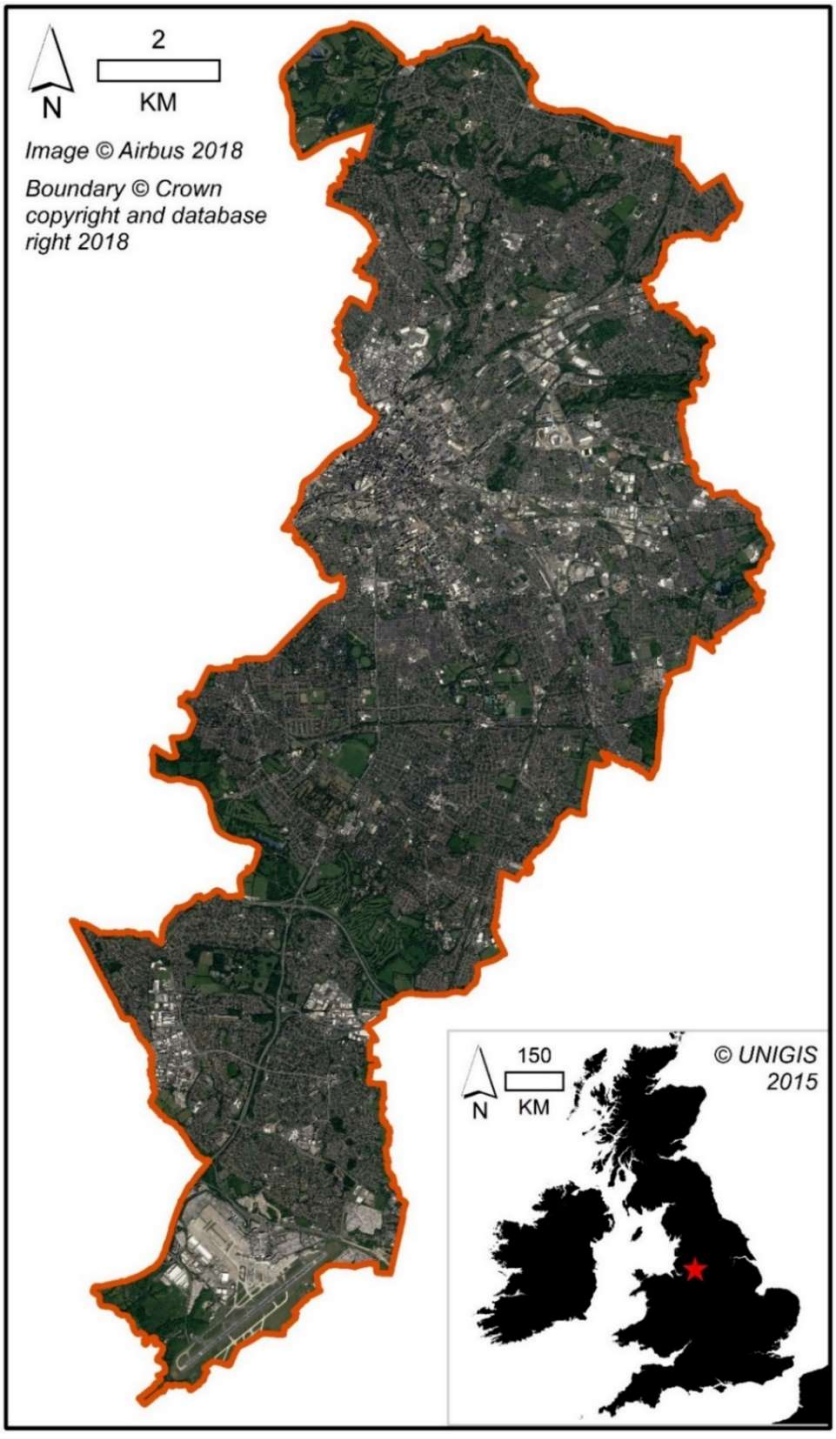

Figure 1.4 – Configuration of landcover in the city of Manchester

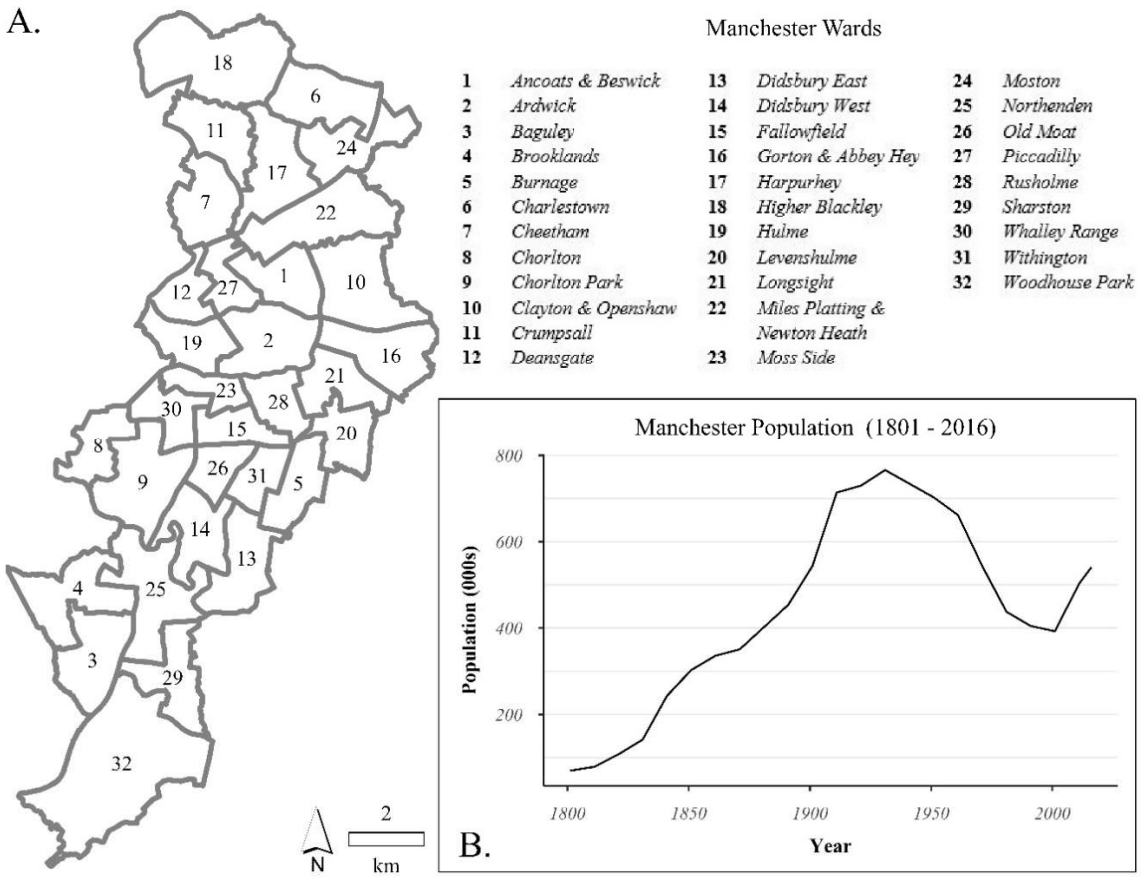

Figure 1.5 – A) Current administrative wards and **B)** Population change (1801 – 2016) for the city of Manchester

This is of course a concern for the local city council. The "Green and Blue Infrastructure Strategy for Manchester (2015 – 25)" describes a number of location based GBI strategies to improve "climate change adaptation and mitigation" in relation to the aforementioned environmental stressors (MCC 2015). Mapping temperature regulation and stormwater storage services across the study area may therefore inform implementation of environmental policies by providing evidence of where green-blue infrastructure investment is most needed in the city. In addition, Manchester city council and other local organisations indicate a commitment to ensure a low-carbon future within the city (MCC 2009, MCCA 2020a), therefore estimates of current and future carbon storage values will be beneficial to inform the local council of the benefits of local GBI resources to achieve this policy aim.

Chapter 2: Mapping regulating ecosystem services

2.1 Introduction

As outlined in **Chapter 1**, expanding access to geospatial datasets and ecosystem service modelling methods provides opportunities to examine research gaps in current regulating ecosystem service (RES) mapping approaches. This will be beneficial to guide strategic spatial planning of GBI resources in order to build urban resilience to environmental stressors. Spatial representation of RES values remains a key concern, as indicator values are required to identify balances between ecosystem service functions, and societal demand for function benefits (Burkhard et al. 2012). Mismatches in supply and demand, at the scale of ecosystem service functions flows therefore indicate where investment in GBI may improve environmental conditions for local residents. For the ecosystem services considered here, the flow of benefits from GBI operate at varying spatial scales and levels of societal demand.

Temperature regulation benefits are typically associated with GBI functions that reduce temperature levels, and in turn reduce health hazards resulting from exposure to extreme temperatures. The magnitude of urban heat islands are negatively correlated with the proportion of GBI in an urban area, therefore GBI resources (e.g. trees, waterbodies) can provide temperature regulation (cooling) benefits to all residents in a city (Peng et al. 2012). This cooling effect also occurs at the local scale, as temperatures around GBI resources are on average lower than areas with limited GBI coverage (Dugord et al. 2014). Residents who live close to a large park for example, should receive greater temperature regulation benefits, than residents who live in highly built-up zones with limited GBI coverage (Kolokotroni & Giridharan 2008). In cold weather conditions the scale of benefits may reverse, as residents in close proximity to GBI may potentially experience a greater degree of negative temperature cooling below ambient levels.

Stormwater storage benefits are associated with the ability of GBI to store precipitation during rainfall events and in turn reduce volume loading upon natural water channels and manmade urban drainage systems. GBI resources may therefore contribute to an overall stormwater storage stock at the river catchment level, reducing flooding associated hazards for residents within fluvial flood risk zones (Voskamp & Van de Ven

2015). In contrast, pluvial flooding occurs when urban drainage systems are completely overwhelmed by surface water (Cavan & Kaźmierczak 2011). Pluvial flood occurrence is complex process, as topography, buildings, road structure, landcover and drainage capacity can impact on surface water flow (Houston et al. 2011). During an extreme rainfall event, pluvial flooding can therefore occur at multiple locations in an urban area (Salvo et al. 2018). As such, GBI can mitigate pluvial flooding risks at the neighbourhood scale, therefore GBI stormwater storage benefits can flow to residents within close proximity of GBI resources (Sjöman & Gill 2014).

GBI also functions to sequester and store atmospheric carbon as plant biomass, therefore providing some mitigation of global warming and associated climate change (Strohbach & Haase 2012). This is a function which provides a benefit to humans both within and outside an urban area. Hence, various GBI patches may be considered as part of a global, or citywide stock of beneficial ecosystem resources (Nowak & Crane 2002). In contrast to temperature regulation and stormwater storage services, the link between above-ground carbon storage and mitigation of hazardous environmental conditions at the neighbourhood scale is less direct. However, there is a growing societal demand for solutions to reduce humanity's carbon footprint, and thus preserve liveable conditions on this planet (Attari et al. 2019). Carbon storage in local GBI resources is therefore important to ensure that neighbourhoods play their role in meeting this wider societal demand (Kennedy & Sgouridis 2011).

Due to localised scale of RES benefits, mismatches between service supply and demand should be mapped according to heterogeneity in GBI that provide varying levels of regulating functions. This is certainly not a novel concept. For example, Burkhard et al. (2012) introduced the ecosystem service matrix, to quantify budgets between ecosystem service supply and demand according to different types of land use. This method has since been upscaled from regional to urban scales to provide a mapping approach for urban ecosystem services (Haas & Ban 2018, Zhang & Ramirez 2019). However, as land use may provide an aggregate measure of GBI, by assuming all land use units contain the same coverage of different GBI resources (Gill et al. 2008, Grafius et al. 2018), there is benefit in refining the resolution of this approach towards the scale of GBI patches (e.g. tree canopies, grass lawns, ponds).

Population density is a useful measure to approximate demand for ecosystem services at this scale, as this indicates the number of people who will benefit within the

affected zone of ecosystem functions (Baró et al. 2016, Larondelle & Lauf 2016). Representing RES values as a regular sized grid may better approximate continuous RES function flows, and thus provide improved estimates of heterogeneity in GBI ecosystem service benefits (Holt et al. 2015, Kremer et al. 2016a). From a planning perspective fine-scale mapping of RES is beneficial to examine GBI investment opportunities at the resolution of GBI interventions suitable to retrofit existing built infrastructure. The mapping of ecosystem service coldspots, or locations where values of multiple ecosystem services are consistently low, is useful in this context to prioritise areas for GBI investment to low levels of RES for local urban residents (Schröter et al. 2017). In addition, improved indicators may provide information to build accounts of GBI values using the natural capital framework, which is important to consider RES and urban resilience strategies within budgetary constraints (Azqueta & Sotelsek 2007).

In order to provide the aforementioned outcomes, an improved mapping approach is required to satisfy a number of demands for 'useful' RES information from both researchers and planning stakeholders. Of primary concern, is that methods are cost effective and accessible, and thus ultimately transferable to different urban areas and conditions. This will support improvements in the wider analysis of RES through improved indicators, and may facilitate knowledge sharing of factors affecting RES (e.g. urban morphology, weather events) between urban areas (Kremer et al. 2016b). Current mapping approaches are often tailored towards specific urban conditions, and therefore have limited application in other urban areas (Haase et al. 2014). For example, the ecosystem service matrix method (Burkhard et al. 2012, Haas & Ban 2018) currently relies on expert assessment, which may be difficult to replicate elsewhere lacking consultation with the appropriate personnel. There is currently little indication of how outputs from this approach may vary according to practical considerations regarding access to methods and appropriate data. Transferable mapping approaches should therefore not only employ affordable methods but should also consider how map information may vary according to applications using input data of varying quality (Schulp et al. 2014).

In addition, the mapping approach should also be adaptable for temporal analysis. Models to estimate RES functions and demand values for temperature regulation and stormwater storage services are required to assess seasonal variation in these services. This is to address the current research gap regarding lack of seasonal variation in RES indicators, and satisfy **Objective 2** of this project. Another key concern is that models use data which can be feasibly updated according to potential landcover change. This is to ensure that

scenario analysis (**Objective 4**) of GBI policies can be implemented efficiently to generate knowledge for the study area and encourage stakeholder consideration of long term GBI conservation and management policies. A review of this process will assess the degree that this approach addresses current research gaps this research gaps into spatial scale and proxy modelling of mapped RES indicators.

2.2 Aims and Objectives

Chapter aim: Assess how spatial scale and proxy-based methods in current ecosystem service mapping approaches can be improved

Chapter objectives:

1. Identify appropriate models to calculate ecosystem service function and demand indicators.

2. Develop and apply model to the city of Manchester, UK.

3. Examine variation in mapping outputs according to variation in quality of potential data inputs.

2.3 Review of ecosystem service models

The identification of research gaps in current RES mapping studies (see **Section 1.3**) determined a general conceptual approach to map spatiotemporal variation in RES. In accordance with ecological modelling approaches, a regular size analysis grid structure is suitable to represent variation in real world RES processes according to continuous spatial variation in GBI across a city (Holt et al. 2015, Kremer et al. 2016a). In this approach each grid cell amalgamates various GBI, RES function and demand metrics to estimate how RES functions satisfy the needs of local residents (Baró et al. 2016). For temporal analysis, model inputs are updateable within the grid structure to provide consistent mapping of spatiotemporal RES change over various study periods. A suitable cell resolution will identify clusters in RES values (e.g. areas of GBI deprivation) at the scale of GBI interventions required to retrofit existing built infrastructure.

A review of methods to evaluate ecosystem service functions and demand models was undertaken to identify pragmatically implementable models to examine service benefit to demand dynamics at high spatial resolution across entire urban areas. In order to address mapping uncertainties, models were assessed in relation to the following criteria:

1. That they are feasible to implement for entire urban areas using regular environmental, GBI and demand metrics aggregated to a chosen analysis area.
2. That model software and associated data are cost-effective and accessible for planning and research.
3. That models are validated with primary data to local ecological and environmental conditions.

In addition, for temperature regulation and stormwater storage services, there was an additional requirement that models enable analysis of seasonal variation in RES functions. **Table 2.1** provides a summary of the models chosen for estimating RES indicators. An overview of the strengths and limitations of models reviewed for each RES, and rationale for each choice, are described in the following sections.

Table 2.1 – Methods and indicators for estimating regulating ecosystem services

RES	*Description of service*	*Summary of chosen method*	*Modelled indicator measure*	*Study area verification**
Temperature regulation	Reduction of localised temperatures during hot weather conditions	Geographically weighted regression models to estimate the influence of local GBI on remotely sensed Land Surface Temperature (LST; °C).	Predicted LST (max LST = 0 service value; min LST = 100% service value)	YES
Above-ground carbon storage	Storage of carbon within above-ground biomass	Transfer of carbon storage values per Land-use Land-cover categories in UK based carbon storage studies to landcover categories within the case study.	Predicted C kg m^2 (max C kg m^2 = 100% service value; min C kg m^2 = 0% service value)	NO
Stormwater storage	Reduction of runoff and local flooding pressures through capture of precipitation by GBI	SCS-CN (USDA 1986) method to estimate runoff reduction potential (CN) of localised GBI resources.	Quantified CN (Max CN = 0% service value; Min CN = 100% service value)	NO

** Model estimates validated to independent measures of environmental conditions within the study area.*

2.3.1 Ecosystem service software packages

A number of open access software packages are currently available to assess and map RES and associated natural capital values. For example, the Land Utilisation and Capability indicator tool assesses the impacts of LULC upon Carbon sequestration (Above-ground carbon storage), and flood mitigation (stormwater storage) ecosystem services (Jackson et al. 2013). This software supports decision making by identifying interventions that will improve synergies in multiple ecosystem services. However, this software currently doesn't include a module to assess temperature regulation services. In

comparison, the ARIES (Artificial Intelligence for Ecosystem Services) software enables mapping of a range service benefit flows from ecosystems to human beneficiaries (Villa et al. 2009). This supports the need to identify mismatches between service supply and demand. However, ARIES software uses artificial intelligence to choose, train and output ecosystem service models according to user specified model inputs (e.g. data, analysis goals, study area extent) (Villa et al. 2009). Due to this complexity, and currently limited application of the model in urban environments, there is limited guidance on how this software may be adapted to assess seasonal change in RES.

In this regards the InVEST, or Integrated Valuation of Ecosystem Services and Tradeoffs tool holds more promise. InVEST presents modules to estimate values for urban cooling (temperature regulation), carbon (above and below ground carbon storage) and urban flood risk mitigation (stormwater storage) services (Stanford University 2020). InVEST quantifies ecosystem service functions, which are then used to estimate benefit values in monetary terms following concepts within natural capital accounting (Tallis et al. 2014). Currently the Urban cooling and Urban flood risk mitigation models are not explicitly designed for seasonal analysis. Urban cooling indicators are estimated using an urban energy exchange model with parameters that are adjustable for seasonally varying climate conditions. However, despite the potential use of this model to investigate seasonal variation in temperature regulation services, the indicators generated by this model are focused specifically upon cooling benefits during hot weather conditions (Zardo et al. 2017). In comparison, other studies have investigated seasonal variation in GBI urban temperature cooling using alternative regression methods (Hamada & Ohta 2010, Zhang et al. 1998). The above software packages provide adaptable methodological frameworks, and service indicators, which can be used in different urban environments. However, due to the relatively novel need to investigate seasonal variation in ecosystem services (**Chapter 3**), methods that have been used successfully for seasonal analysis in urban ecosystem functions in other studies were preferred in this project. Rationale for chosen physical models for each service are therefore described in the following sections.

2.3.2 Temperature regulation

Considerable research has focused upon the benefits of GBI for reducing urban temperatures during hot weather conditions. However, the quantification of citywide function indicators for temperature regulation remains a challenge. Heterogeneity in surface features, building geometry, and vegetation types, creates a complex interplay in thermal energy exchange balances, which when combined with diurnal and seasonally varying meteorological conditions, result in considerable micro-scale variation in urban climate conditions (Arnfield 2003, Oke 1978). Urban climate models, such as three-dimensional computational fluid dynamic models are of sufficient resolution to assess complex interactions between GBI and air temperatures at the micro-scale (Grêt-Regamey et al. 2013, Skelhorn et al. 2014). However, for standard computer systems the required data, processing and verification requirements currently prohibit practical implementation of such advanced techniques for entire urban areas (Acero & Arrizabalaga 2013, Mirzeai 2015).

In contrast, other studies have defined statistical models to assess the relationship of GBI measures to on-site ambient air temperatures (Emmanuel & Kruger 2012, Smith et al. 2011). For example, Kolokotroni & Giridharan (2008) quantified ambient air temperatures at several sites along transects from central London to suburban areas and found a negative relationship between neighbourhood greenspace cover and ambient air temperatures. Automated sensor networks/stations may capture spatiotemporal (diurnal and seasonal) variation in air temperatures (Schwarz et al. 2012), but due to implementation and maintenance costs, are typically restricted to a limited number of sample sites within a city (Weber et al. 2015). As such, citywide assessments using air temperature statistical models often extrapolate findings from sample data across wider LULC categories, to map the spatial variation in temperature regulation (Azevedo et al. 2016, Cheng et al. 2008, Stewart & Oke 2012).

A cost effective alternative to the above approaches is through analysis of satellite sensor (e.g. LANDSAT, MODIS, AVHRR) derived Land Surface Temperature (LST). LST measures the temperature of upper near to ground surface layers and is a governing indicator of thermal energy transfer for above-ground ambient air warming (Oke 1978). Spatial formation of LST and ambient air temperatures have been found to be positively correlated in a number of studies (Azevedo et al. 2016, Cheng et al. 2008, Schwarz et al. 2012), although the strength of this relationship may be modified depending on local

meteorological conditions (Arnfield 2003, Coseo & Larsen 2014). For example, the assortment of vertical structures along regular pathways such as roads for example, form urban canyons that aerodynamically modify the flow and velocity of circulating wind within urban areas (Arnfield 2003). Wind patterns, both dynamically altered within the urban environment, and from incoming weather fronts, alter the spatial formation of ambient air temperatures, causing spatial dislocation in the patterns of ambient air and land surface temperatures (Azevedo et al. 2016). Despite a potentially weak relationship between ambient air temperatures and LST during certain conditions, the prevalence of extreme LST values remains a useful proxy to indicate where extreme urban ambient air temperatures are likely to occur on any given day (Smargiassi et al. 2009). In practical applications, extreme LST values have thus been positively related to increased mortality rates in Paris, France (Laaidi et al. 2012) and Phoenix, USA (Harlan et al. 2006) during heatwave events. However, as urban surface layers warm-up at different rates, consideration is required as to whether the time of image collection represents urban surface warming at its maximum impact for above-ground air temperatures (Schwarz et al. 2012).

In accordance to urban energy balance theory (Arnfield 2003, Oke 1978), urban LST heat island studies find an inverse statistical relationship between GBI cover and LST values (Guo et al., 2015, Weber et al. 2015). A typical approach is to measure local configurations of vegetative/non-vegetative surfaces through classification of high-resolution multi-spectral imagery, and then to statistically model the explanatory relationship of GBI measures to local LST (Chen et al. 2014a, Deilami et al. 2018, Zhou et al. 2011). Images representing seasonal variation in LST are openly accessible, thus enabling seasonal analysis using this approach, with RES indicators verified through estimated model error (Weber et al. 2015). This method however is scale dependent, with minimum spatial analysis unit size typically scaled to resolution of LST imagery, which can range from 30m (Landsat 8, NASA 2020a) through to 1000m (MODIS, NASA 2020b) depending upon sensor.

A summary of how temperature regulation models meet the requisite criteria is provided in **Table 2.2**. An LST statistical model approach was chosen above the others as this satisfied all three criteria.

Table 2.2 – Justification of model approach for temperature regulation services

Definition of service: Cooling of ambient temperatures around green-blue infrastructure, alleviating thermal discomfort in hot weather conditions.

Modelling methods reviewed	*Model/study examples*	*Description*	*Pragmatic implementation across study area*	*Accessible data/software*	*Verified outputs*	*Criteria score*
Ambient air statistical models	Studies: Kolokotroni & Giridharan (2008), Coseo & Larsen (2014), Stewart & Oke (2012)	As above – ambient air temperature measured on-site in relation to variables affecting temperature to parameterise statistical models	No – *infeasible to implement monitoring scheme across study area*	No – *costs for acquiring and maintaining sensors can be extensive*	Yes – *model outputs are verified against sensor measures*	1/3
Urban climate models	Models: ENVI-MET (Skelhorn et al. 2014), Urbclim (De Ridder et al. 2015)	Complex spatial computational models to calculate temperature conditions based on local conditions; accuracy depends on effective model parameterisation for field measured variables affecting temperature	No – *excessive data input and computational requirements for large-scale urban areas*	No – *software is not typically open source*	Yes – *verified by in-situ climate measurements*	1/3
LST statistical models	Studies: Chen et al. (2014a), Guo et al. (2015), Zhou et al. (2011)	Land surface temperature (LST) as proxy measure for ambient air temperatures; predictive statistical relationship for GBI reduction of remotely sensed LST values	Yes – *wide range of studies demonstrate feasibility of this method for study area*	Yes – *LST derived from open source image repositories such as Earth Explorer (USGS 2018) and Earth data (NASA 2020c)*	Yes – *model outputs are verified within the modelling process*	3/3

2.3.3 Above-ground Carbon storage

Biomass estimation, and thus the above-ground carbon storage functions of green infrastructure should consider above and below ground vegetative biophysical structure, including vegetation height above-ground, branch density, and root depth (Cunniff et al. 2015) for all GBI resources. For urban areas that may contain a multitude of vegetation specimens of different species, citywide biomass is often estimated using survey and extrapolation methods. Carbon is quantified for sample plots within LULC areas, and then extrapolated per relevant LULC class to map spatial variation in carbon storage ecosystem service indicators (Rogers et al. 2015). A focus of many studies is the carbon storage potential of trees, due to the comparatively high biomass levels in contrast to other types of GBI (e.g. grass, shrubs). Allometric regression models that are parameterised using independent variables representing tree size and shape (e.g. trunk diameter, crown spread) are used to predict tree biomass and potential biomass growth through sequestration (Basuki et al. 2009, Monteiro et al. 2016). For example, Nowak et al. (2013), collected tree data through in-situ surveys for cities in the USA, used allometric modelling to calculate carbon and sequestration rates for individual trees, and then extrapolated findings according to estimated citywide species distribution, to provide final monetary values for citywide carbon storage ecosystem services. In comparison, Raciti et al. (2014) combined field sampling of tree biomass with canopy coverage and height estimates obtained from analysis of high resolution multi-spectral and LiDAR imagery, to provide spatially explicit maps (1m resolution) of carbon storage in Boston, USA. The high-resolution mapping products provide an effective tool for policy makers to investigate local tree planting schemes, in addition to providing a reference for assessing the effect on carbon storage resulting from future tree canopy removal (Raciti et al. 2014). Spatially explicit biomass estimation methods can improve upon the uncertainties of LULC extrapolation methods (Alonzo et al. 2016, Tigges et al. 2017), and are useful for estimating spatial variance in carbon storage potential of various GBI resources (Holt et al. 2015).

In the context of trees, precision in biomass estimation depends largely on the accuracy of allometric equations for tree species within a local urban context, as locally dependent factors such as soil type, urban morphology, age of urban forest, pollution levels, and competition, impact upon species growth rates (Monteiro et al. 2016). Generating such allometric equations however, requires considerable expertise and investment in field investigation and laboratory analysis, requiring destruction of plant

material to estimate dry biomass weight (Hutyra et al. 2011, McHale et al. 2009). Alternatively, field sampling of tree characteristics (e.g. species, trunk size) may be supported using existing allometric biomass models (Ter-Mikaelian & Korzukhin 1997) and to estimate tree carbon storage potential using inventory models (NCASI 2020, USFS 2018). Where it proves difficult to collect primary data to support the above methods, alternative estimations of above-ground carbon storage are available from existing national and citywide carbon storage inventories (Holt et al. 2015, Whitford et al. 2001). In comparison to tree focused studies, carbon storage values provided for both tree and non-tree GBI types, and enables estimation of the collective function of this RES for all green infrastructure in an urban area. For example, field quantified estimates of carbon storage for multiple GBI types are available for the city of Leicester, UK (Davies et al. 2011), thus offering proxy above-ground carbon storage parameter values, which can be assigned to GBI categories obtained from landcover mapping exercises. As discussed previously, proxy methods should be used with care in order to ensure that transplanted service benefits do not replicate spurious results within final RES mapping outputs (Eigenbrod et al. 2010, Seppelt et al. 2011).

A summary of how carbon storage models meet the requisite criteria is provided in **Table 2.3**. Proxy measure were chosen for the mapping approach due to project constraints required to collect sample data for both allometric and inventory model approaches.

Table 2.3 – Justification of model approach for carbon storage services

Definition of service: Current carbon stocks determine communal contribution to offset climate change.

Modelling methods reviewed	*Model/study examples*	*Description*	*Pragmatic implementation across study area*	*Accessible data and software*	*Verified outputs*	*Criteria score (out of 3)*
Allometric studies of urban forest structure	Studies: Davies et al. (2011), Raciti et al. (2014), Tigges et al. (2017)	Tree growth and biomass models quantified for primary data in study area	No – infeasible to collect site data for sample inputs	Yes – models are open access	No – infeasible to collect and analyse on site tree samples for validation	1/3
Inventory models	I-Tree eco (USFS 2018), COLE: Carbon On-line Estimator (NCASI 2020)	Tree growth and biomass models from look-up inventories used to calculate carbon storage values for mapped forest data	No – infeasible to collect site data for sample inputs	Yes – models are open access	No – infeasible to collect and analyse on site tree samples for validation	1/3
Proxy measures	Used in RES studies: Derkzen et al. (2015), Holt et al. (2015), Kremer et al. (2016a)	Carbon storage values obtained from other studies/inventories assigned directly to GBI measures in study	Yes – easy to assign carbon storage values directly to map classes	Yes – easy to implement with accessible software	No – infeasible to collect and analyse on site tree samples for validation	2/3

2.3.4 Stormwater storage

An ideal assessment of GBI surface runoff reduction would require consideration of GBI benefits amongst all possible factors governing urban flood risks during a heavy rainfall event (Wainwright & Mulligan 2005). Precipitation levels determine modelled surface runoff according to natural/non-natural surface perviousness and roughness. This then determines the depths and rates of water flow over topography for a given return period, and estimates the volume of water forming on overland sinks (e.g. depressions, water channels), or within sewerage systems (Beven 2000). These models may be augmented with locally surveyed phenomena. For example, levels of overland evaporation rates or existing groundwater saturation, can be incorporated as additional model processes, to provide high-resolution assessment of GBI resources for reducing flood risks (Salvadore et al. 2015). However, due to data acquisition and processing costs, this resolution of analysis is currently difficult to achieve for large-scale heterogeneous urban areas (Hammond et al. 2015). Advanced integrated surface and drainage flow models, capable of modelling spatiotemporal variation in 3D hydraulic overland and sewer system flows, are thus generally limited to the micro (or neighbourhood) scale on standard computing systems (Leandro et al. 2014, Massoudieh et al. 2017, Pan et al. 2011).

Large-scale urban runoff models are typically adapted from numerical models for non-urbanized areas such as agricultural basins and forests (Salvadore et al. 2015). Adapted hydrological models incorporate measures of urbanization (e.g. surface perviousness) to combine surface feature maps, topography and other environmental data to map spatial variation in surface runoff for unique catchment areas (Berezowski et al. 2012, Chormanski et al. 2008, Kalcic et al. 2015). Catchment based models are verified against measured channel gauge hydrographs, which enable optimisation of parameters, such as runoff coefficients for unique surface types (Franczyk & Chang 2009, Verbeiren et al. 2013). This method usefully provides some validation of GBI impact upon reducing fluvial/pluvial flood risks and has been implemented for spatiotemporal analysis of GBI change on runoff conditions within a number of urban areas (Cuo et al. 2008, Dixon et al. 2012). However, a limitation of such models in urban areas is that sewerage systems are not considered in water flow calculations (Hammond et al. 2015). Urban runoff flows may be aggregated over important areas of potential pluvial flooding (Boonya-Aroonnet et al. 2007) and may not sufficiently represent flow volumes from urbanised surfaces into local watercourses (De Risi et al. 2015). In addition, as adapted hydrological models are based upon catchment

hydrology, acquiring the data required to model GBI effects for the numerous catchments covering a citywide study area may be excessive.

Alternative approaches, including the US Soil Conservation Society Curve Number (SCS-CN) model, have merit in quantifying flood risk, and have been verified using field studies (USDA 1986). The SCS-CN model equation calculates total excess precipitation surface runoff for a 24-hour precipitation event according to seasonal surface runoff coefficients (curve numbers) for different vegetation types (Sjöman & Gill 2014). Composite curve numbers, obtained from proportional land surface cover within spatial analysis units, provide an indication of each area's contribution to both localised pluvial and larger scale fluvial flooding risks (Sjöman & Gill 2014). The SCS-CN model is suitable for spatiotemporal analysis as rainwater volume input can replicate any extreme 1-day precipitation event (USDA 1986). However, unless calculated runoff is verified against relevant catchment channel stream hydrographs, SCS-CN serves as a proxy model (Mishra et al. 2018) with potential ambiguity in the choice of appropriate Curve Number values, and limitations in the precision of runoff estimates using un-verified Curve numbers (Eli & Lamont 2010, Ogden et al. 2017, Garen & Moore 2005). However, as spatial analysis units for this model are also scale independent, the method provides a flexible and easy to implement approach for generating stormwater storage RES indicators (Mishra et al. 2018), and as such has been used extensively in other urban RES studies (Kremer et al. 2016a, Tratalos et al. 2007, Whitford et al. 2001).

A summary of how stormwater storage models meet the requisite criteria is provided in **Table 2.4**. As demonstrated, two of the approaches satisfied 2 out of 3 criteria. Adapted hydrological catchment models provide a verified approach but require excessive amounts of data to cover the various catchment areas overlapping the boundary of the study area. As such the one-dimensional SCS-CN approach (USDA 1986) was chosen for inclusion within the mapping approach of this research.

Table 2.4 – Justification of model approach for stormwater storage function indicators

Definition of service: Reduction of water flows flowing into local drainage systems during precipitation events reducing localised flooding risks.

Modelling methods reviewed	*Model/study examples*	*Description*	*Pragmatic implementation across study area*	*Accessible data and software*	*Verified outputs*	*Criteria score*
Combined overland-sewer models	Aquacycle (Mitchell et al. 2001); HEDUDM (Pan et al. 2011); Adapted SWMM (Leandro et al. 2014)	As above, but incorporates sewer flows to calculate both overland and underground hydrological flow processes	No – *data and computational software requirements excessive for areas above neighbourhood size*	No – *high resolution models are generally not open source; sewer system data is not openly accessible for UK urban areas*	Yes – *hydrographs for stream gauges are available for local study area to validate surface runoff volumes*	1/3
Adapted Hydrological Catchment Models	DHVM (Cuo et al. 2008); SWAT (Franczyk & Chang 2009); SWMM (Krebs et al. 2014); WetSPA (Verbeiren et al. 2013)	Spatial variance in runoff calculated according to landcover attributes within hydrological analysis units covering a catchment area; does not incorporate sewer flows	No – *study area is covered by multiple catchments which extend out of study area extents. Require considerable effort to acquire data for extraneous areas*	Yes – *dependent upon specific model software is open source; landcover, elevation data and other input data obtainable for study area*	Yes – *hydrographs for stream gauges are available for local study area to validate surface runoff volumes*	2/3
Proxy hydrology models	SCS Curve Number approach (USDA 1986)	Runoff calculated according to surface and sub-surface ground composition for an analysis area; does not incorporate sewer flows	Yes – *flexible approach fitted to analysis units of any scale; requires landcover data only*	Yes – *simple numerical model; implementable with open source software; landcover data obtainable for study area*	No – *verification of surface runoff not conducted for UK urban areas; model is however widely used in RES research*	2/3

2.3.5 Measuring ecosystem service demand

Explicit measures of demand for ecosystem services in current ecosystem service mapping studies vary. For example, Burkhard et al. (2012) describe a scalar ranking scheme (1 = minimal demand; 5 = maximum demand) whereby expert opinion determines the level of demand for individual ecosystem services per LULC. This provides a spatial indication of disparities between service provision and service demand across a study area (Burkhard et al. 2012, Haas & Ban 2018). LULC also supports the use of other quantified metrics, drawn from census and economic data, to estimate demand according to the need to offset the negative impacts of land-use activities upon the local environment (e.g. demand for water, pollution levels; Larondelle & Lauf 2016).

In contrast, other studies define demand measures according to population factors. This may represent simple population levels, where ecosystem services are estimated to the total number of people served (Baró et al. 2017) or specific socio-economic groups at risk from various environmental hazards, such as elderly people to extreme urban temperatures (Dugord et al. 2014, Larondelle & Lauf 2016). A limitation of LULC and the population demand methods is that spatial RES analysis is constrained by analysis units (e.g. LULC, census areas) that may fail to represent the scale at which urban residents consume RES benefits (Andrew et al. 2015). However, population disaggregation methods are available to up-scale population estimates from census units to the required scale of RES analysis (Zandbergen & Ignizio 2010). This approach provides an accessible measure of ecosystem service demand that can be applied in different urban areas and suitable for the mapping approach developed in this project. However, further research is required to accurately disaggregate multiple additional social factors for demand purposes.

2.4 Assessing the mapping approach

As indicated in the above literature review, models that can be parameterised to specific urban conditions using primary data are available. However, the efforts required to collect primary data, and associated processing costs to compute complex environmental are prohibitive for citywide RES mapping exercises, especially where multiple RES are under consideration. Proxy models remain popular within current RES mapping approaches and were thus chosen for the above-ground carbon storage, stormwater storage and demand disaggregation models for the mapping approach in this

project. Implementation of these methods may vary, due to differences in the quality of data available for different mapping exercises. To ensure the mapping approach in this project is adaptable for different urban areas (Seppelt et al. 2011) and attempt to resolve this research gap in current RES mapping approaches, the influence of data upon mapping approach implementation was investigated here. This followed a process described by Eigenbrod et al. (2010) that compared variation in ecosystem service prioritisation (i.e. coldspots) between proxy and primary data-based methods. Model choice upon relationships between different RES, in addition to mapping priority areas for GBI investment, was investigated by comparing mapping outputs from multiple proxy model service (*n = 16*) parameter settings for different demand (*n = 3*) methods. **Figure 2.1** presents the workflow for the assessment of the mapping approach. The methods are described in the following case study.

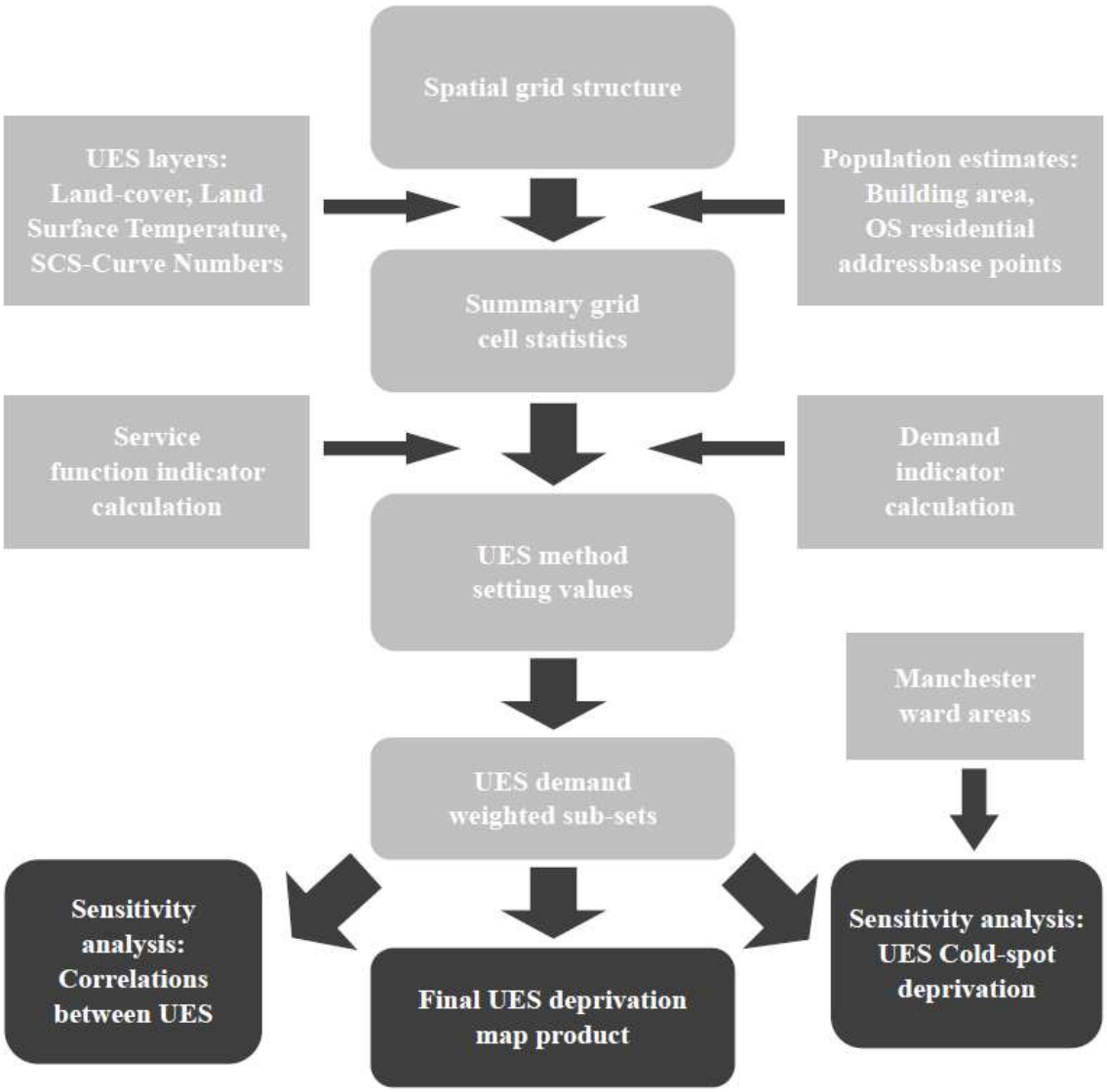

Figure 2.1 – Mapping approach assessment workflow

2.5 Methods

2.5.1 Landcover data

At the time of mapping approach development, an application was underway to gain access to image repositories from the European Space Agency (ESA 2018). As aforementioned (**Section 1.4**), very high-resolution multispectral imagery will enable classification of landcover, which will then serve as inputs into RES models (Dennis et al. 2018, Derkzen et al. 2015). In order to develop and assess the mapping approach, while this application was still underway, an urban landcover map (2m resolution) was created to replicate the spatial and thematic resolution expected from a typical classification exercise. **Table 2.5** presents the main processing steps, data used and methods to create the urban landcover map. Detailed processing steps are provided in **Appendix 2.1**. An example of the final landcover map data is provided in **Figure 2.2**.

Table 2.5 – Processing steps for the generation of the urban landcover map

Processing step	Reference data	Methods	Classes from methods*
1	Mastermap topography layer (May 2017 version; Edina digimap 2017)	Land parcel and surface feature extents represented as polygon areas; attribute data used to categorise initial class area where possible	All classes
2	Tree audit data (City Of Trees 2011)	Represents canopy extents (> 1.5m) of trees and woodland; provides masking feature to re-classify all landcover classes as trees	Tree canopy
3	True-colour aerial imagery (12.5cm resolution; collected June 2009 – 2015; Getmapping 2017)	Classified into a vegetation mask using a threshold with image band data; used to assign non-classified pixels as either non-tree vegetation or non-vegetation appropriate	Non-tree vegetation; Non-vegetation

* Buildings = permanent building structures; Non-vegetation = Artificial and Bare Earth; Water = Water bodies and channels; Tree Canopy = tree canopy extents; Non-tree vegetation – vegetation not considered as trees, such as shrubs and grasses. Non-tree vegetation

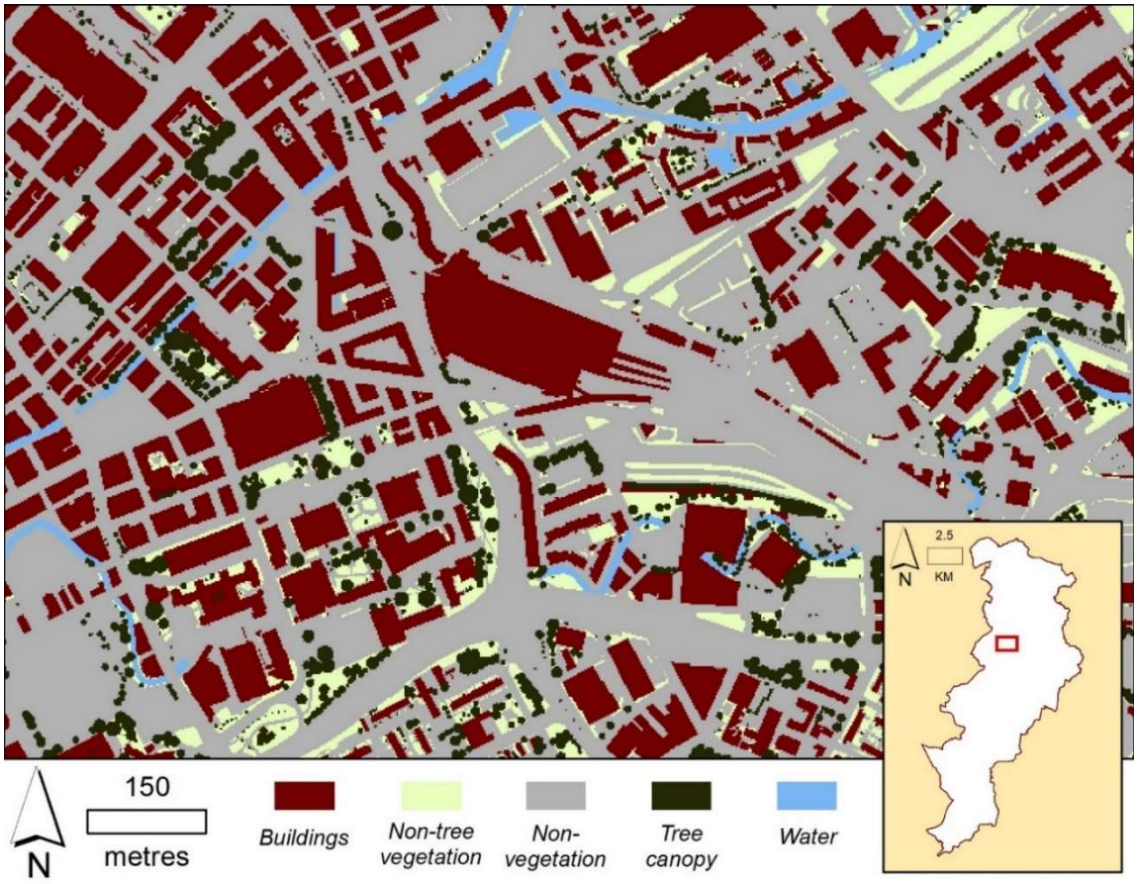

Figure 2.2 – Landcover data for central Manchester

2.5.2 Temperature regulation indicators

A Land Surface Temperature (LST) surface was generated using the mono-window method (Wang et al. 2015) using cloud-free imagery (17 July 2017; 30m resolution) from the Landsat-8 Operational Land Imager sensor (USGS 2017). Image bands were geo-rectified to British National Grid. The exact location of corresponding features (e.g. buildings vertices, road junctions) are difficult to identify between the image and landcover data, due to a large difference spatial resolution. Precise geo-rectification of the LST layer was therefore not attempted. However, the general outline of park and other largescale landscape areas in the image data coincided with the location and outline of corresponding areas in the landcover data, indicating that the two datasets were spatially aligned. Daytime conditions during image collection were warm, with a maximum temperature of 23°C (average 16°C) recorded at the nearby Manchester International Airport weather station (Weather Underground 2017). As spatial patterns of LST in relation to the urban morphology are expected to remain relatively consistent for warmer climate conditions (Oke 1978) the LST surface, generated at 30m resolution, was considered to be representative of more extreme heatwave conditions (**Appendix 2.2**).

Three variables were employed in this process. Percentage GBI per cell represented the percentage of cell area covered by GBI landcover categories (Non-Tree vegetation, Tree vegetation, Water). Mean LST per cell represented the mean of LST pixel values within each cell. Mean NDVI per cell represented the mean of Normalized Difference Vegetation Index (NDVI) pixel values, calculated from the Landsat image bands (**Appendix 2.2**), within each cell. NDVI indicates the level of vegetation activity for the area covered by an image pixel. Areas with high amounts of productive vegetation will have a positive NDVI value (close to 1) in comparison to areas with low vegetation which will be represented by near zero or negative values (Viana et al. 2019). The resolution of analysis cells was initially set at 100m. This represents the finest resolution of disaggregated population estimates within the WorldPop population repository (WorldPop 2020), which provides guidance of a usable resolution to map ecosystem service demand in this approach. This resolution was compared to other grid sizes in order to assess whether this represented a suitable scale to examine LST phenomena across the study area (**Appendix 2.3**).

Strong negative correlation ($r = -0.82$, $p < 0.005$) was recorded between percentage GBI and mean LST per cell. A strong positive relationship ($r = 0.86$, $p < 0.005$) was also recorded between percentage GBI and mean NDVI per cell. General agreement between vegetation metrics and LST values was observed between the urban landcover and Landsat-8 datasets. This indicated the potential application of regression techniques, such as Ordinary Least Squares (OLS), to estimate the causal relationship of percentage GBI upon mean LST per cell across the study area. As aforementioned in **Section 2.3.2**, regression has been used to predict the causal effect of green and blue infrastructure variables upon LST in a number of studies (Chen et al. 2014a, Deilami et al. 2018, Zhou et al. 2011). Global regression models however assume stationarity in the relationship between percentage GBI and LST, by estimating a single coefficient parameter that defines GBI reduction of LST irrespective of cell location. Residuals from global regression models may exhibit spatial autocorrelation, which indicate spatial error structure in the data is not adequately captured within the model (Kong et al. 2014, Li et al. 2010). Any type of autocorrelation in regression models implies potential misspecification and may result in biased estimates of model parameters (Li et al. 2010).

In contrast, local regression techniques, such as geographically weighted regression (GWR), assume non-stationarity in the relationships between independent and dependent variables. GWR is a local regression technique, which uses a distance (bandwidth) defined window kernel to determine averaged regression models for every location in a continuous

field (Comber et al. 2011). In relation to LST, the process of temperature regulation may be locally influenced by interactions between GBI and non-GBI factors (i.e. thermal storage properties of artificial surface types) that are difficult ascertain directly from landcover data. GWR using percentage GBI as the sole independent variable may infer temperature regulation indicators in relation to unknown local independent factors and variation in urban morphology (McMillen 2004). Other studies demonstrate that GWR can reduce autocorrelation in residuals and provide less biased and improved model coefficient estimates (Ivajnšič et al. 2014, Szymanowski & Kryza 2011, Tian et al. 2012, Zhao et al. 2018). OLS and GWR was implemented (ArcMap 10.3; ESRI) using equation 2.1, to statistically predict GBI

LST cooling functions.

$$y = a + bx \qquad [2.1]$$

Where y is the predicted mean LST per cell, x is the percentage GBI coverage per cell. Temperature regulation indicators were calculated from the model providing the least biased fit to analysis cell variables. In this instance cells with lowest predicted LST values provide the largest temperature regulation indicator values (**Table 2.1**).

2.5.3 Above-ground carbon storage indicators

As aforementioned, the cost of collecting primary data to estimate biomass of local GBI resources (e.g. vegetation matter and tree characteristics for allometric models) is prohibitive for whole city areas (Derkzen et al. 2015, Holt et al. 2015). Above-ground carbon storage indicators in the mapping approach were calculated using findings from UK-based empirical carbon storage studies (**Table 2.6**). Descriptions of carbon storage LULC categories were matched to urban landcover classes to identify above-ground carbon storage parameters per landcover class. Above-ground carbon storage was then calculated per square metre (C kg m^2) for the associated landcover area. Due to the potential ambiguity in matching landcover classes to LULC descriptions in empirical studies, four different above-ground carbon storage parameter settings were devised to examine the impact on final RES values (**Table 2.6**). The RES indicator measure is the total carbon stored per cell.

Table 2.6 – Above-ground carbon storage parameter setting values

Setting	Landcover class	Above-ground carbon Storage categorisation	Carbon Storage (kg C m^2)	Justification for carbon Density Method
1[A]	Non-Tree	Herbaceous Vegetation	0.15	Herbaceous vegetation only; Non-tree assumed to represent short grasses
	Tree Canopy	Tree	28.46	Assumed to represent tall trees (> 5m height)
2[A]	Non-Tree	Mean: Herbaceous Vegetation, Shrub	5.19	Assumed to represent a mixture of grasses and low shrubs
	Tree Canopy	Mean: Tree, Tall Shrub	21.33	Assumed to represent a mixture of tall shrubs and trees
3[B]	Non-Tree	Sport and Leisure	0.68	Sports and leisure land use assumed to represent a mixture of vegetation types
	Tree Canopy	Mixed forest	3.28	Mixed forest only
4[B]	Non-Tree	Green Urban Areas	0.09	Green urban areas only (grassy areas)
	Tree Canopy	Broad-leaf Forest	3.80	Broadleaf forest only

[A] Category values obtained from Davies et al. (2011) – study provides a quantified survey and extrapolation analysis of carbon storage according to vegetation categories in Leicester, UK; [B] Category values obtained from Cruickshank et al. (1998) - study provides a national inventory of carbon storage per land-cover land-use classes in Northern Ireland based upon field-based studies.

2.5.4 Stormwater storage indicators

The SCS-CN model works as a one-dimensional numerical model that computes the amount of rainfall converted to surface runoff for a given surface area (represented by

curve number values) during a rainfall event (USDA 1986). Detailed introductions to the model are provided in USDA (1986) and therefore only a general overview of the method is provided here. The SCS-CN model is:

$$Q = \frac{(P - I_a)^2}{(P - I_a) + S} \quad [2.2]$$

Where Q is the total runoff during the event, P is the rainfall amount, I_a is the initial abstraction and S is the maximum potential retention of the surface area after runoff begins. I_a determines all losses, due to structural interception, evaporation and infiltration, before runoff begins. This value can vary but is typically assigned as $I_a = 0.2S$, which has been previously verified in numerous studies of small watersheds (USDA 1986). Substituting this value provides:

$$Q = \frac{(P - 0.2S)^2}{(P + 0.8S)} \quad [2.3]$$

With appropriate values for P and S, calculating Q for a given area is a straightforward process. S is associated to the runoff potential of surface type and is given as the unitless expression (following method described in Whitford et al. 2001 for Urban watersheds):

$$S = \frac{2540}{CN} - 25.4 \quad [2.4]$$

Where CN is the relevant Curve Number for a particular surface type. Following **Equation 2.4** increasing CN values reduce the retention potential of the surface area S, thus increasing the rainwater runoff potential during a rainfall event.

Unless independently verified, SCS-CN serves as a proxy model with curve number parameters (values) assigned directly between SCS-CN surface descriptions, and mapped landcover categories. As is evident for above-ground carbon storage function indicators, ambiguity may thus occur due to this process (see **Section 2.3.3**). Here, four stormwater

storage parameter settings were used to investigate this issue on the resulting mapping outputs (**Table 2.7**). CNs for landcover pixels were assigned by integrating landcover data and underlying soil type (Cranfield University 2018), with stormwater storage indicators calculated from the areal CN average per analysis cell (see **Appendix 2.4** for further details). This landcover approach unfortunately does not consider variation in runoff storage according to varying conditions within landcover classes. For example, some areas of the landcover map may overlap with the location of sustainable urban drainage systems, which represent GBI based systems designed to manage stormwater using natural hydrological processes (Hoang & Fenner 2015). Sustainable urban drainage systems (e.g. detention sinks, rain gardens) will produce greater stormwater storage functions than associated GBI landcover (Dunnett & Clayden 2007, Hoang & Fenner 2015), but are nevertheless excluded from this approach due to limited data on the extent and scale of these systems within the study area.

Table 2.7 – Landcover Curve Number assignment

Study area Landcover	Parameter settings	SCS Landcover	Curve Number per hydrological soil type			
			A	B	C	D
BUILDINGS	1, 2, 3, 4	Paved, roofs, etc.	98	98	98	98
NON-VEGETATION	1, 3	Paved, roofs, etc.[1]	98	98	98	98
	2, 4	Streets and Roads: Paved; open ditches[2]	83	89	92	93
NON-TREE VEGETATION	1, 2	Pasture: good condition[3]	39	61	74	80
	3, 4	Brush: good cover[4]	30	48	65	73
TREE CANOPY	1, 2, 3, 4	Wood: good cover	30	55	70	77
WATER	1, 2, 3, 4	Water	25	25	25	25

1 - *Wholly impervious surfaces i.e. Roofs, Asphalt and concrete roads; 2 – Wholly impervious and pervious non-natural surfaces; 3 - Grassland not protected from grazing such as mown grass typical of lawns, playing fields etc. and rough grassland; 4 - Low-standing vegetation such as bushes, weeds and grass.*

2.5.5 Regulating ecosystem service demand indicators

Methods for population disaggregation vary depending upon available data resources (Stevens et al. 2015, Zandbergen & Ignizio 2010). Two disaggregation methods were used to assess the effect of the choice of method upon final RES map outputs. The first method involves areal upscaling of population estimates within census areas to the areal extents of human habitation represented by building footprint area (termed BLD_{POP} here) (O'Brien & Cheshire 2016). This method is financially cost-effective as building footprint areas from the OS are accessible for research in the UK (Edina Digimap 2017). However, as no distinction is made between building type (e.g. residential, commercial-industrial), population density is extrapolated across non-residential building areas (Jia et al. 2014, O'Brien & Cheshire 2016). In contrast, the HAB_{POP} method uses residential address points from the OS AddressBase Plus product (OS 2018) to weight population towards residential housing (Bhaduri et al. 2007, Zandbergen 2011, Murdock et al. 2015). However, this method is less accessible due to the cost in licensing the associated data. Using both methods, annual population estimates (current estimates available for 2016) for the UK at the Lower Super Output Area (LSOA) level (UKDS 2017) were disaggregated to generate the relative demand indicators (see **Appendix 2.5** for population disaggregation workflows).

2.5.6 Regulating ecosystem service relationships and deprivation

Correlation analysis (R programming language; R Core team 2019) was used to estimate how much measured relationships between individual RES vary when interacting service parameter settings and demand methods (Holt et al. 2015). This indicated how the choice of RES methods may impact the overall RES analysis, for both the mapping approach used in this study, and for models commonly used in the wider RES literature. In addition, the impact of method choice upon RES deprivation mapping was assessed through the comparison of identified multiple RES coldspots at both the neighbourhood (grid cell) and administrative district scale, to simulate an urban planning exercise investigating environmental deprivation at different spatial scales. Coldspots are defined in this study as the lowest 10% of cells using combined rankings of RES indicator scores (see **Table 2.4**) and reverse the hot-spot concept described in other studies of multiple ecosystem services (e.g. Anderson et al. 2009, Schulp et al. 2014). Coldspots were amalgamated at administrative ward level, as this enables comparison of relative RES deprivation levels at the scale of local governance (Baró et al. 2017). The identification of the top 20% RES deprived ward areas

(through percent of demand area that is identified as coldspot) simulated an exercise to identify administrative areas that may benefit the most from GBI investment. The impact of method choice was conducted at both scales using the same procedure. Here, all service parameter settings (n = 16; 1 x temperature regulation; 4 x above-ground carbon storage; 4 x stormwater storage) were interacted within No demand (all cells), BLD_{POP} (where $BLD_{POP} \geq 1$) and HAB_{POP} (where $HAB_{POP} \geq 1$) weighted cells, to compare variation in map outputs.

2.6 Results

Mapped GBI coverage and RES indicator outputs are shown in **Figure 2.3**. To demonstrate the general patterns in above-ground carbon storage and stormwater storage indicators, the figure displays indicator values that are averaged from all parameter settings. Whilst some variation is evident between parameter setting outputs, the overall spatial pattern in indicator values remains relatively consistent for both services (**Appendix 2.6**). In relation to variation in GBI coverage, patterns in the three RES indicators are generally consistent.

Temperature regulation indicator values demonstrate a relatively smooth spatial pattern (**Figure 2.3B**) due to the use of GWR to predict indicator values. This model compared favourably, with R^2 = 0.65 and AIC = 42952, to the ordinary least squares model (y = 33.41 – 0.064x; equation 2.1), with R^2 = 0.45 and AIC = 47871. The Moran's I index (spdep package R programming language; Bivand et al. 2018) identified that spatial autocorrelation was statistically significant for both OLS and GWR residuals. In comparison to OLS residuals (I = 0.59, $p < 0.005$), GWR reduced spatial autocorrelation (I = 0.20, $p < 0.005$), reducing bias in parameter estimates. Temperature regulation indicators follow a non-stationary pattern between GBI and LST, where GBI cover per cell appears to have greater effect in reducing LST, where there is greater coverage of GBI in neighbouring cells. As such, single cells with high GBI coverage, that are within low GBI coverage zones (e.g. city centre, airport), produce lower indicator values than cells with similar GBI coverage in high GBI coverage zones (e.g. parks, urban woodlands). This relationship is reversed for cells with low GBI coverage in either high or low GBI coverage zones, resulting in a comparatively smooth pattern in temperature regulation indicators when compared to other RES.

Patterns in averaged above-ground carbon storage indicators (**Figure 2.3C**) are less contiguous with GBI, as only vegetation landcovers provide functions for this service. This contrasts to temperature regulation (**Figure 2.3B**) and averaged stormwater storage services (**Figure 2.3D**), where water (non-vegetation GBI) provides both temperature cooling and stormwater storage functions respectively. The distribution of above-ground carbon storage indicators demonstrate further dispersion away from large GBI clusters, as many of these areas represent non-urbanised open space that may contain large bodies of water, such as ponds and reservoirs. In contrast, stormwater storage indicators are highly contiguous with GBI coverage patterns. In comparison to temperature regulation, indicators for stormwater storage are dependent solely on landcover values within an individual cell and are therefore are more closely linked to patterns in cell level GBI coverage.

Differences in indicator patterns are more evident for RES demand. BLD_{POP} indicators (**Figure 2.3E**) are spread more evenly across the study area, following the coverage of all building types, irrespective of whether the building houses residents or not. In contrast HAB_{POP} indicators (**Figure 2.3F**) demonstrate a more fragmented pattern and cover a lower percentage of the study area, as demand is weighted specifically towards residential dwellings. HAB_{POP} therefore disregards cells covered exclusively by industrial and commercial type buildings, which often have extremely low GBI coverage, and thus low RES indicator values.

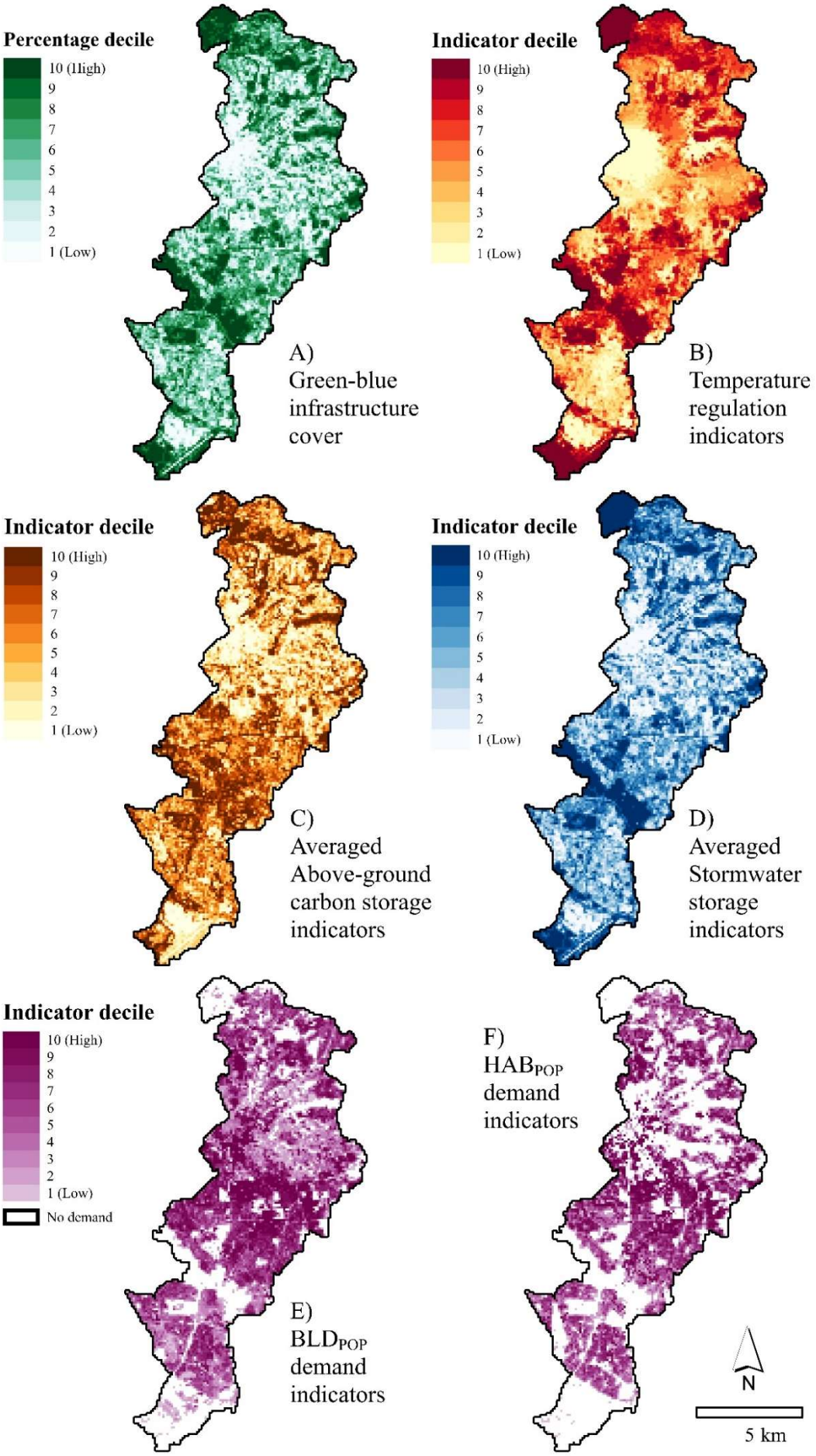

Figure 2.3 - Mapped green-blue infrastructure and indicator outputs

Whilst regression model outputs provide some measure of the quality of temperature regulation function indicators to end users, associated verification measures for above-ground carbon storage, stormwater storage and demand indicators are not available. Variation in map outputs, according to varying proxy model parameterisation is evident, as chosen service parameter settings alter the relationship between individual RES. As demand weighting to both building and residential areas results in a reduction of available demand cells (as % of total study area cells) to 79.2% and 62.9% using BLD_{POP} and HAB_{POP} methods respectively, the relationships between RES are accordingly modified by varying proportions of GBI resources constrained within demand cells (**Figures 2.4 & 2.5**).

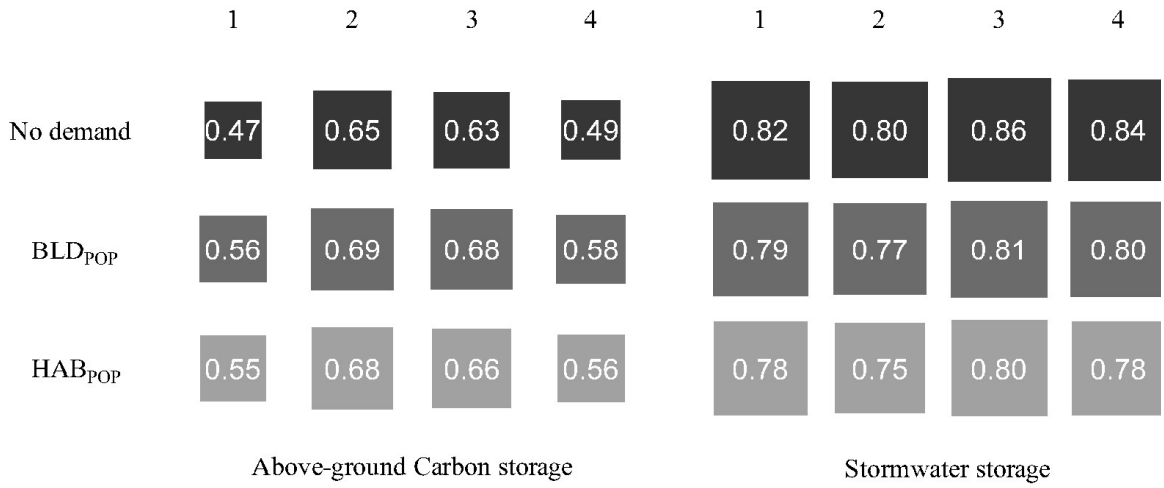

Figure 2.4 – Correlation (r) values ($p < 0.001$) for temperature regulation indicators to above-ground carbon storage and stormwater storage indicators

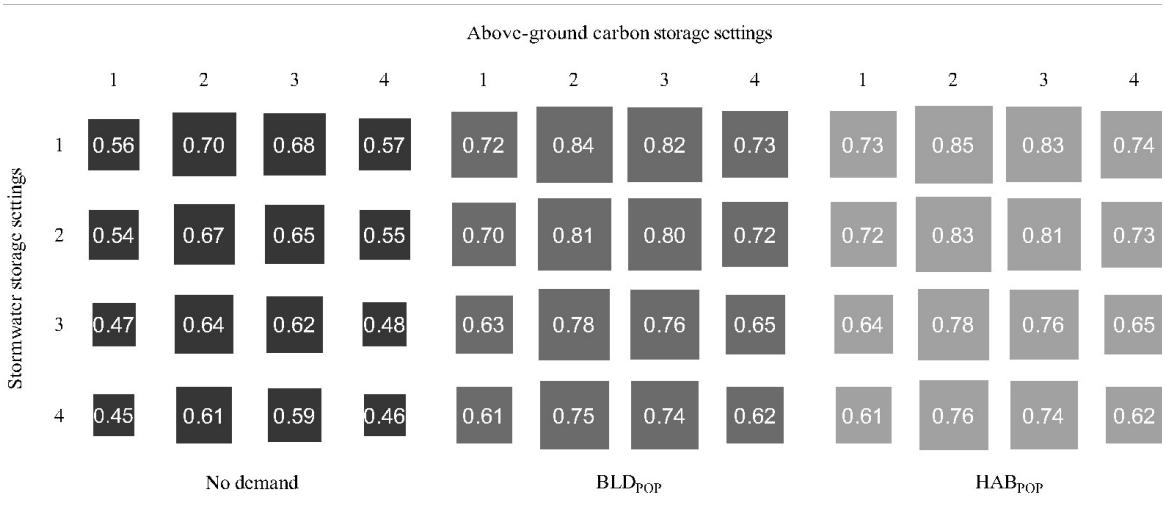

Figure 2.5 – Correlation (r) values ($p < 0.001$) between above-ground carbon storage and stormwater storage indicators

Correlation values (see **Appendix 2.7** for scatterplots) between temperature regulation and above-ground carbon storage services increase from No Demand cells (mean r = 0.56), to the disaggregation methods (mean r = 0.63 and 0.61 for BLD_{POP} and HAB_{POP} respectively). This trend is reversed for correlations between temperature regulation and stormwater storage indicators, with stronger correlation values for no demand cells (mean r = 0.83) in comparison to demand weighted cells (mean r = 0.79 and 0.78 for BLD_{POP} and HAB_{POP} cells respectively). Weighting demand towards building and residential areas in effect removes cells largely covered by water (e.g. cells within reservoirs, water channels) with maximum water coverage per cell varying from 100% for no demand cells, to just 69% and 42.7% for BLD_{POP} and HAB_{POP} cells, respectively. As water is good for stormwater storage and temperature regulation services but has no estimated above-ground carbon storage benefits (**Tables 2.6 and 2.7**), the removal of such cells increases correlation strength between above-ground carbon storage indicators and the other RES (**Table 2.8**). In contrast, correlations between temperature regulation and stormwater storage indicators demonstrate a minor decrease in strength (**Table 2.8**). Variation in indicator correlations are lower between stormwater storage and temperature regulation indicators (**Table 2.8**), as all constituent GBI landcover types contribute positively to overall respective indicator values.

Whilst patterns in relative correlation values between settings remain stable, irrespective of demand method (**Figure 2.4 & 2.5**), ranges in correlation values (**Table 2.8**) appear to vary according to GBI cover levels within demand cells. No demand-weighted cells, with the highest mean GBI cover (46.4%), thus provide the largest range in correlation values. In contrast, BLD_{POP} cells, record both the lowest values for GBI coverage (37.4%), and range in correlation values. These differences, whilst small in value, indicate that choice of proxy model parameter is less consequential in varying relationships between RES with lessening GBI coverage levels. This is due to reduced variation in component GBI resources with varying RES benefits.

Table 2.8 – Summary statistics for correlations between regulating ecosystems services*

Demand cells	Temp. regulation to above-ground carbon storage		Temp. regulation to stormwater storage		Above-ground carbon storage to stormwater storage	
	Mean (r)	*Max.(r) – Min.(r)*	*Mean (r)*	*Max.(r) – Min.(r)*	*Mean (r)*	*Max.(r) – Min.(r)*
No demand	0.56	0.18	0.83	0.06	0.58	0.25
BLD_{POP}	0.63	0.13	0.79	0.04	0.73	0.23
HAB_{POP}	0.61	0.13	0.78	0.05	0.74	0.24

* - Scatterplots of RES indicators for all demand measures are shown in **Appendix 2.7**

For the identification of coldspots, results vary between service parameter settings (**Figure 2.6**). For all cells identified as a coldspot in any service parameter setting, over 78% were consistently identified as a final coldspot when comparing overlapping outputs from different service parameter settings. This percentage differs by 0.8% across all demand weighting methods, indicating relative congruence between service parameter settings irrespective of varying analysis cell area. Maximum difference in coldspot identification between service parameter settings, as a percentage of total coldspot area, is 8.3%, 9.3% and 9.5% for No demand, BLD_{POP} and HAB_{POP} cells respectively. Based upon the parameter values used in this study, the choice of a particular service parameter setting may result in a 10% discrepancy in available coldspot area when compared to outputs using alternative settings. Evidence here suggests that overlapping findings from multiple service parameter settings provides a useful method to establish an overall consensus estimate of RES value.

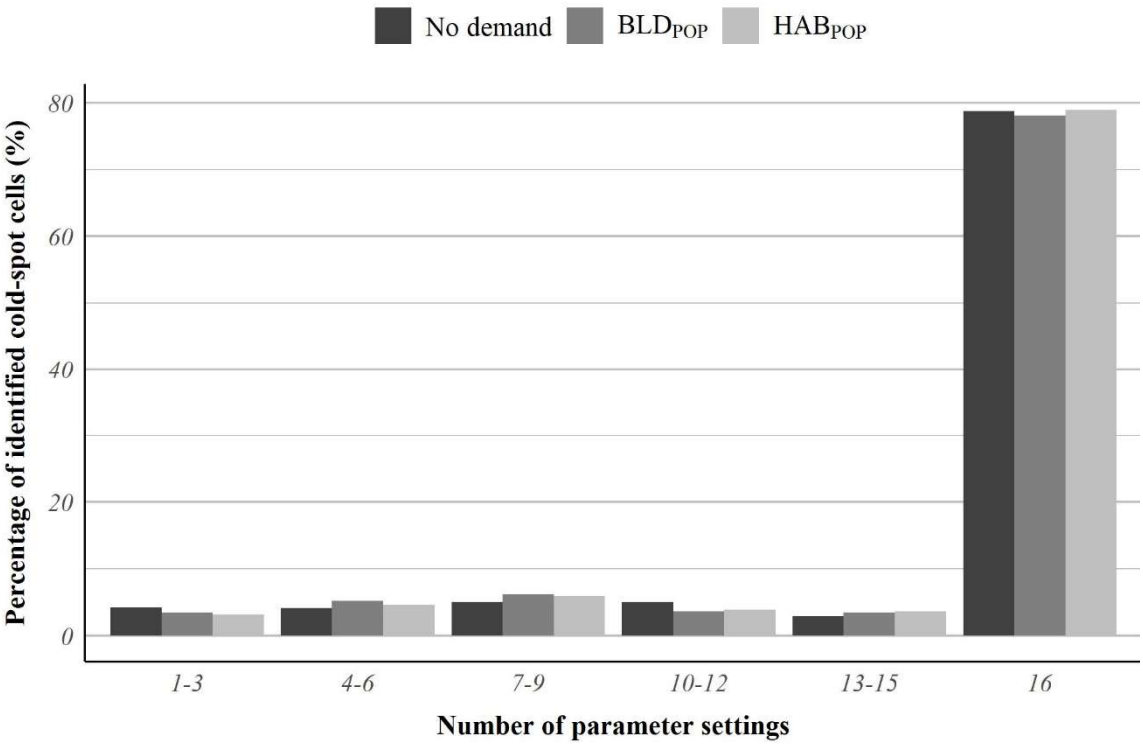

Figure 2.6 – Number of service parameter settings coldspot cells are identified according to demand method

As demonstrated in **Figure 2.7**, the reduction in the number of demand cells necessarily reduces the percentage of the study area, that is identified as a final coldspot, from 8.9%, 7% and 5.6% for No demand, BLD_{POP} and HAB_{POP} cells respectively. Coldspot clusters are iteratively removed due to this process, which in turn alters the prevalence of RES deprivation across the study area. The impact of this process is also evident at coarser spatial scales, as altering demand method results in subtle changes in the identification of deprived ward areas when using final coldspot cells (**Figure 2.8**). Whilst five out of seven wards are consistently identified as the 20% most RES deprived areas, altering the demand measure results in some variation in final map outputs at this resolution.

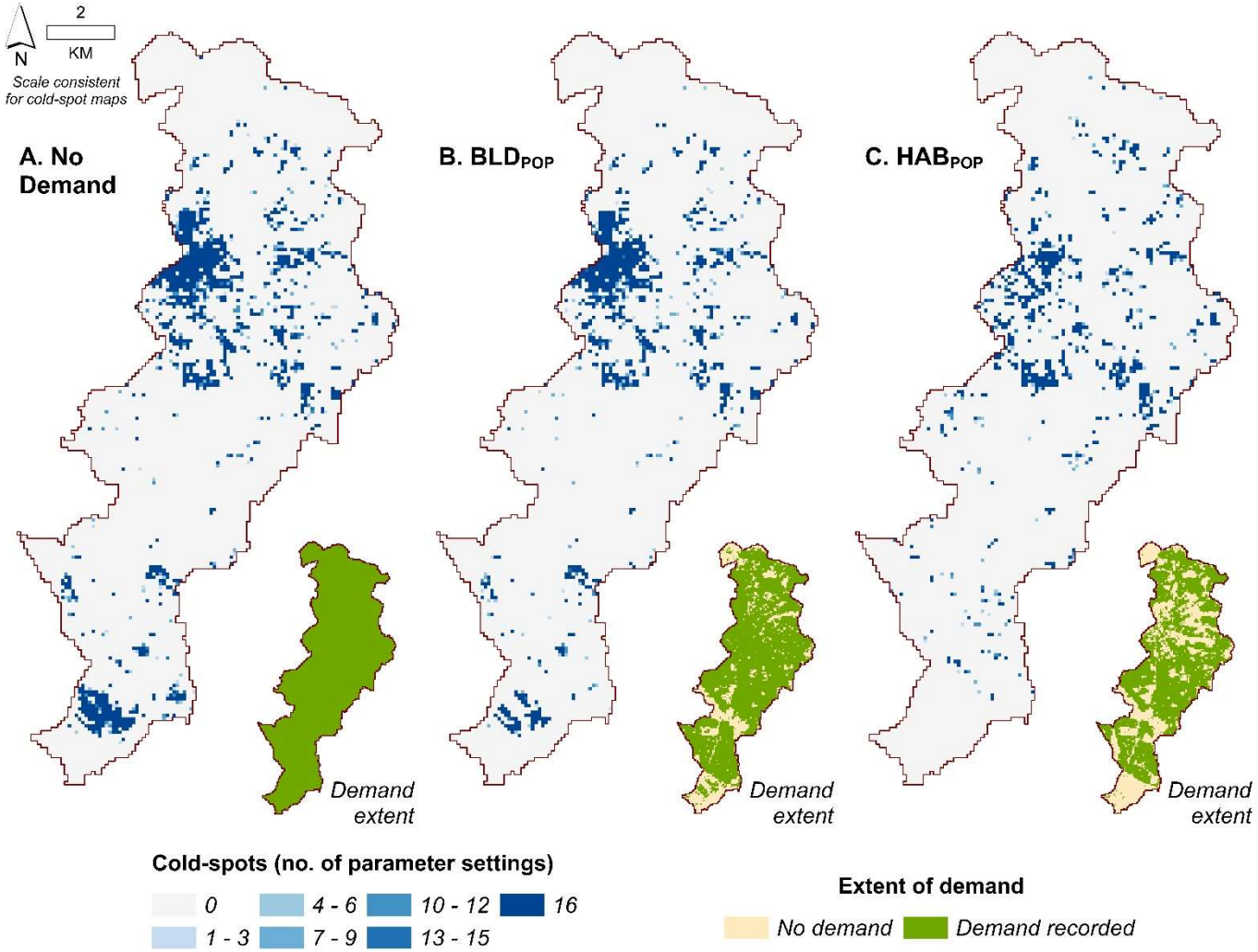

Figure 2.7 – Coldspot identification from overlapping service parameter settings

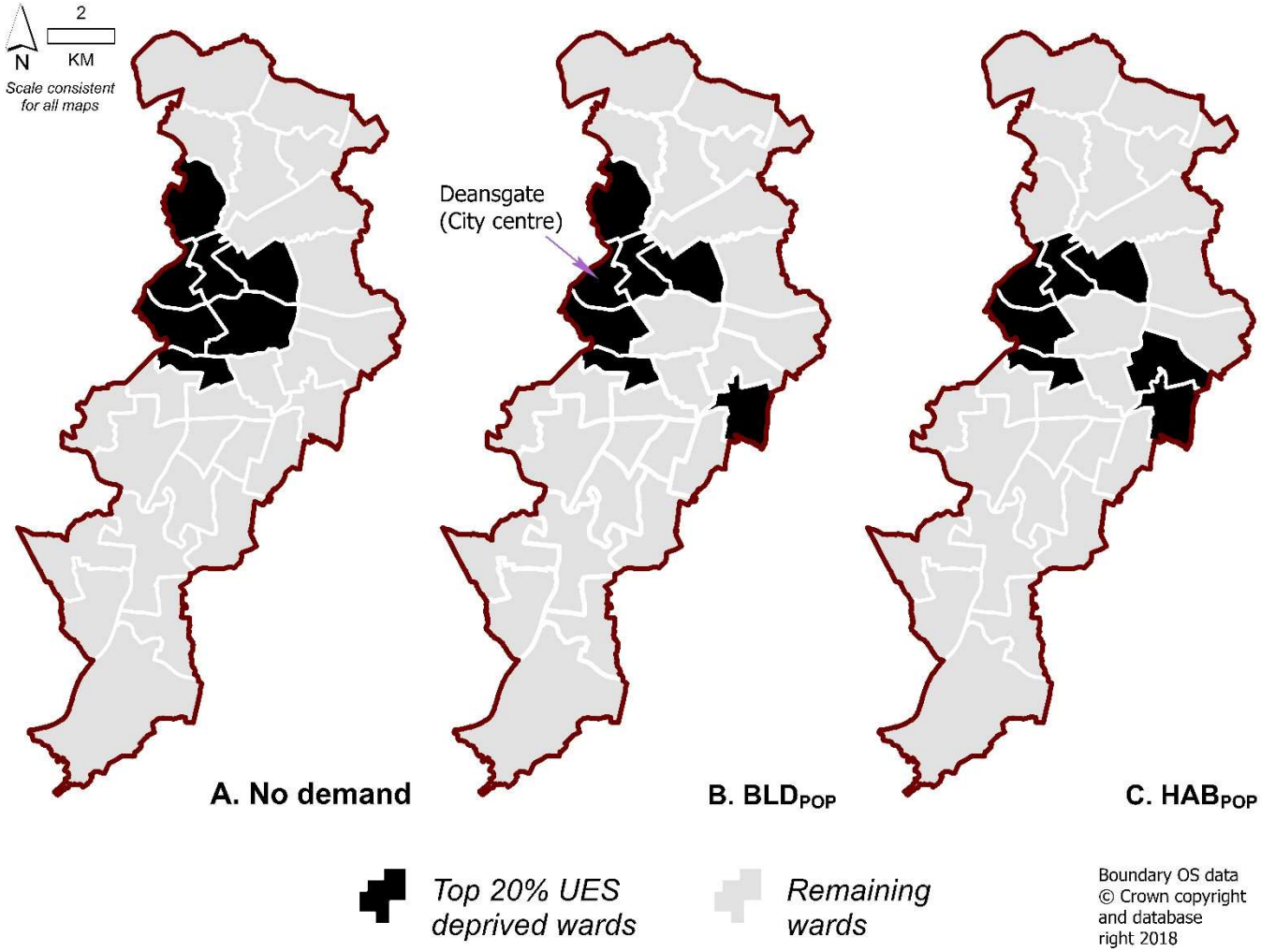

Figure 2.8 - Top 20% RES deprived wards by demand method

The coldspot concept aims to identify the lowest 10% combined regulating RES performing cells per available demand cell area. Overlapping service parameter setting findings to identify final coldspots reduces this percentage further to approximately 8.8% for all demand cells. **Figure 2.9** demonstrates the benefits of the mapping approach at the neighbourhood level. At this resolution, clusters of high RES demand within deprived areas provide a visual analysis tool to identify priority communities for local RES improvement. For example, coldspot areas in **Figure 2.9** mainly fall within residential terraced housing areas that overlap administrative ward districts. The mapping approach provides visual evidence of where intervention strategies such as garden greening could be encouraged (Baker et al. 2018). At this resolution it is possible to envisage the type and scale of GBI investments pragmatically implementable within neighbourhoods.

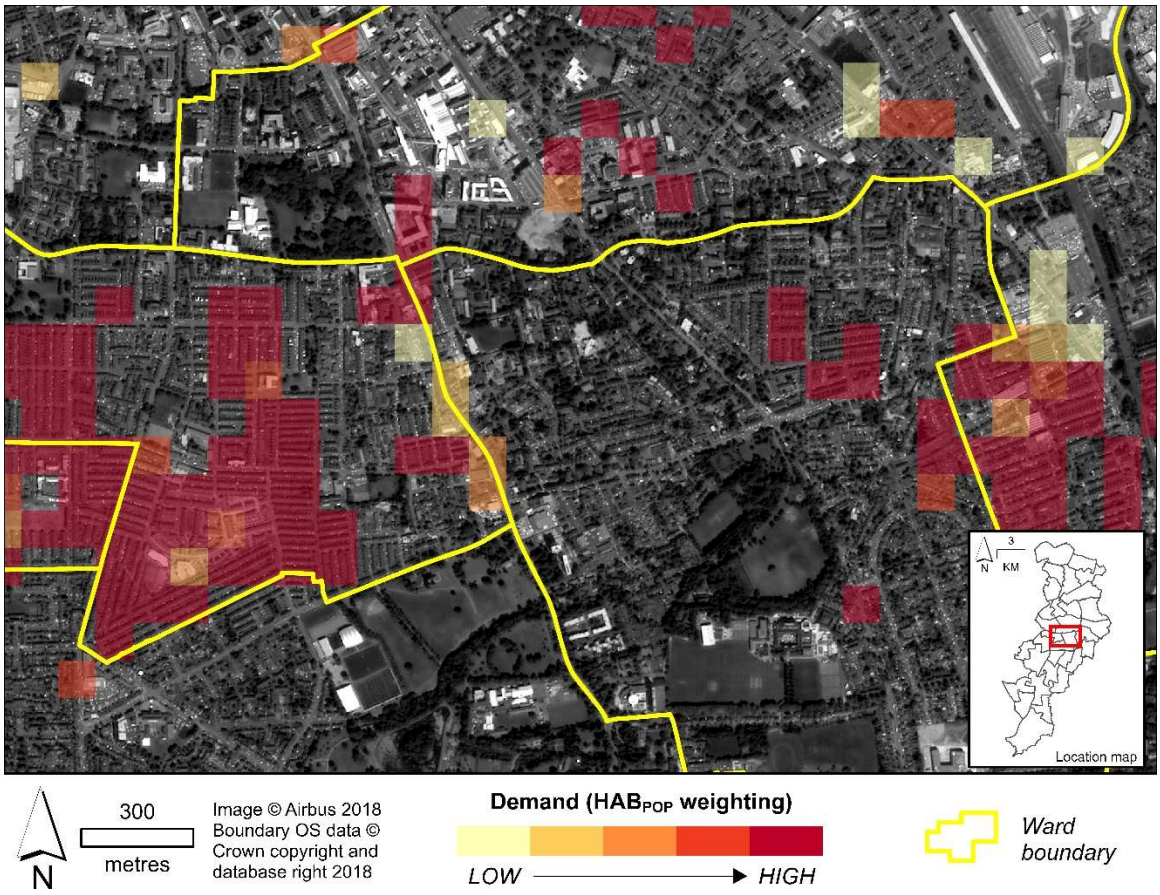

Figure 2.9 - Visualization of RES coldspots (HAB_{POP} demand cells) in relation to urban morphology

2.7 Discussion

This chapter presents a novel mapping approach to identify urban neighbourhoods in need of GBI investment to mitigate environmental stressors. Regulating RES are estimated within the spatial extent of small-scale urban green-blue improvement solutions (e.g. street planting, sustainable urban drainage systems, green walls and roofs) required to effectively retrofit existing urban infrastructure to build environmental resilience (Carter et al. 2015, Voskamp et al. 2015). Whilst this approach currently provides limited information on the specific type of GBI resources required, it usefully indicates RES deprivation at fine spatial scales. This is beneficial to indicate priority locations for improved in-situ monitoring, in order to investigate site specific GBI investment strategies (Massoudieh et al. 2017, Skelhorn. et al. 2014). As GBI and demand inputs are generated using accessible data, the RES indicator to demand concept used here is theoretically adaptable to other urban areas in the UK and further afield. Implementation of this approach in other areas may aid the development of consistent and standardised approaches for mapping RES (Seppelt et al. 2011). For both demand (e.g. mid-year population estimates), and service models (e.g. aerial imagery, national mapping products), the relevant data is typically updated at frequent intervals, therefore RES values may be updated within the spatial analysis grid to assess future change in GBI and RES (Cabral et al. 2016, Haas & Ban 2018). Updated service and demand values should thus enable consistent re-examination of RES dynamics within the changing urban biophysical, socio-economic, and administrative landscape (Dobbs et al. 2018, Schwarz et al. 2011).

As evidenced in the case study, the efficient transfer of proxy findings is often limited due to pragmatic issues in GBI and landcover generation. Where ideal proxy data is not available, then averaging or overlapping indicators from various service parameter settings provides a useful consensus view of combined RES values (Eigenbrod et al. 2010). Whilst exact proxy values can vary distinctly between studies, as is the case for the carbon storage studies used here (**Table 2.6**), the relative performance of GBI associated categories is generally consistent. For example, tree canopy associated categories always store significantly more above-ground carbon than grassy vegetation categories. Therefore, by using simplified indicator metrics to compare multiple RES, congruence between findings from multiple service parameter settings should be present, such as > 78% level for coldspot cells in this study. The identification of RES deprivation coldspots by overlapping findings from multiple parameter settings preferable to a single map output

generated from model averaging. The resulting map output therefore incorporates potential likelihoods for coldspot areas and may prove useful in conveying map usability to end users.

Investigating variation in mapping outputs, according to different implementations of service function and demand models, is useful to indicate how the mapping approach may transfer to other study areas. As resolution in landcover data may vary, and invoke varying levels of ambiguity in model parameterisation, the case study demonstrates how this issue affects relationships between individual RES, and prioritisation mapping of multiple RES. Future investigators are therefore armed with practical information regarding the level of mapping information available from potential data constraints for a given mapping exercise. The findings here may also influence project development, by informing interested parties in the need for investment in data collection or modelling software, to achieve a certain level of information from the subsequent mapping exercise. This is evidenced by demand weighting methods in the case study, as investment in commercial OS Addressbase data (OS 2018) improved the focus of RES deprivation measures to locations where urban residents reside. Other studies have considered the influence of landcover accuracy (Foody 2015) and resolution (Grafius et al. 2016, Holt et al. 2015), in addition to proxy model parameterisation (Zhao & Sander 2018) upon urban ecosystem service maps. The case study here contributes wider research information regarding how variation in function and demand indicators may interact in future ecosystem service mapping exercises.

Correlation analysis in this study provides an indication of how this process is modified by variation in GBI coverage levels for specific RES. This knowledge may aid incorporation of additional proxy derived RES within the approach, as the relationship between various RES can be gauged by relative variation in different GBI components. Correlation analysis was relatively efficient to implement due to the low number of individual RES and demand measures (Holt et al. 2015). However, with increasing RES additional methods may be effective. Quieroz et al. (2015) examined variation in ecosystem service (n = 16) bundles by spatially comparing principal component variation across municipalities representing different social and ecological circumstances. This method, which could be implemented within the mapping approach, could enhance the usefulness of planning information by highlighting additional non-landcover drivers that produce ecosystem service benefits (Quieroz et al. 2015). In addition, variation in combined RES map outputs may be expanded with additional prioritisation analyses (e.g. bundles,

hotspots) using differing combinations of service parameter settings (Holt et al. 2015, Schröter & Remme 2016). This is beneficial to understand how wider ecosystem service mapping approaches may incorporate ambiguities in models to better meet varying needs of urban planning stakeholders.

In relation to RES demand, population disaggregation represents an adaptable methodology to weight the transfer of RES benefits to communities requiring such services. As discussed in **Section 2.3.5**, demand indicators may be further updated to accommodate localised exposure to environmental stressors (i.e. exposure to extreme temperatures, pluvial/fluvial flooding risks), in addition to vulnerability factors within the local population (i.e. age, mobility, economic situation) (Jenerette et al. 2016, Kaźmierczak & Cavan 2011). This is an approach considered in other urban ecosystem service studies (Dugord et al. 2014, Larondelle & Lauf 2016). To match the improved focus on demand may also require re-examination of the scale of ecosystem service function flows, so that RES indicators better approximate the locations where ecosystem services are directly consumed. For example, runoff during a storm event may flow from numerous source points and increase pluvial flooding risks for residents within an afflicted zone (Salvo et al. 2018). The regular analysis grid structure provides a useful basis to investigate verified hydrological models that incorporate cell-based structures and may provide improved estimations of stormwater movement over an urban area (van Dijk et al. 2014). However, as this representation still causes some aggregation of GBI patch information, alternative approaches could be considered to examine the role of interconnected landscape features (Quieroz et al. 2015).

As evidenced in the examination of temperature regulation here, and in other studies, size or clustering of GBI patches in certain locations may determine differing levels of temperature cooling benefits. For example, large parks or urban forests may provide cool islands that confer cooling benefits over a larger neighbouring area than individual trees or small patches (e.g. individual gardens or ponds) (Cheng et al. 2015, Hamada & Ohta 2010). GWR is useful for accounting for non-stationarity in cooling functions of GBI resources according to continuous change in urban morphology. However, this method currently provides limited information on the landscape arrangements (e.g. shading potential of above-ground objects) that may provide strong cooling benefits (Chen et al. 2014b). There is potential within the analysis cell approach to analyse landscape metrics (e.g. connectivity, fragmentation, diversity) in relation to service indicator values for this purpose (Grafius et al. 2018, Syrbe & Walz 2012), and thus provide further usable

information for end users. Indeed, a comparison of indicators produced for irregular landscape units, as used in other urban ecosystem studies, may provide interesting insights into the strengths and limitations of the current analysis cell approach. For example, in a number of field-based carbon storage studies, landscape use and functionality has inferred differing GBI management schemes, and thus differing levels of carbon storage functions from sub-landcover components (Davies et al. 2011, Edmondson et al. 2010). By comparing carbon storage estimates from both cell-based landcover proportions against estimates to differing land use regimes (Grafius et al. 2018) may allow a re-weighting, or averaging, of service indicator estimates from different modelling perspectives.

As evidenced in the investigation of varying model parameterisations upon RES map outputs, continuing limitations remain in the use of proxies to estimate RES values. Overlapping findings from service parameter settings, or simple averaging of proxy findings from multiple studies, can help identify consistent coldspot areas (Derkzen et al. 2015). However, as the final outputs lack validation to study area conditions, an unquantified level of uncertainty may be present in any final RES mapping product (Eigenbrod et al. 2010, Zhao & Sander 2018). As proxy models are often unavoidable for citywide analysis of multiple RES, acceptable levels of uncertain map information should be first considered by end-users before any mapping exercise (Plummer 2009). Whilst proxy models are relatively easy to implement in desktop applications (Kremer et al. 2016b), the findings here should encourage investigators to invest in data collection, in order to validate RES indicators to local environmental conditions (Haase et al. 2014, Seppelt et al. 2011).

Where this type of investment proves excessive for research budgets, improvements in RES modelling may be addressed through specific GBI and landcover categorisations that ensure suitable information transfer from chosen proxies (Andrew et al. 2015, Radford & James 2013). For example, Derkzen et al. (2015) demonstrate how fine-scale categorisation of various GBI types (e.g. trees, short shrubs), according to specific RES benefits measured in other studies (e.g. air purification, noise reduction), may reduce ambiguity in proxy categorisation. In this regard, the landcover data for Manchester may be improved using ancillary information in the classification (e.g. multi-spectral imagery, LiDAR; Baker et al. 2018, Dennis et al. 2018). This may enable stratification of non-tree vegetation into grass and bush categories, and tree canopies according to canopy height, to representing different levels of biomass, or runoff interception. Improved categorisation of landcover according to RES functionality may be beneficial in reducing ambiguity in proxy

category assignment for the stormwater storage (USDA 1986) and above-ground carbon storage models (Davies et al. 2011).

In relation to regression techniques for temperature regulation, use of additional independent variables that explain LST, such as landscape metrics, tree/building shading, and elevation, may also improve the accuracy of verified temperature regulation RES estimates (Chen et al. 2014a, Kong et al. 2014). Certainly, this may also prove useful in reducing bias in parameter estimates due to spatial autocorrelation in model residuals. Indeed, in initial exploration of LST to GBI, regression models built using various independent variables for individual GBI types, indicated that tree canopies may be stronger in reducing LST than non-tree canopy GBI (Wang et al. 2016). Whilst all GBI components are beneficial for LST cooling (Armson et al. 2012), using GBI cell coverage percentages as separate independent variables is problematic, as landcover proportions are dependent upon each other. An improvement of this approach, that may be considered in further research, is to consider the relative LST reduction strength of differing GBI components, in order to form a re-weighted GBI independent variable.

However, use of additional independent variables, (e.g. landscape metrics, tree/building shading, albedo) may improve a snapshot assessment of temperature regulation RES but in turn may prove problematic for future mapping updates. Varying quality of geospatial data may hinder the replication of thematic resolution of existing landcover data (Comber et al. 2004) and prohibit the generation of associated independent variables (e.g. landscape metrics, tree/building shading, albedo) for model prediction. Depending on expected quality of input geospatial data, the use of a single GBI independent variable may represent a reasonable trade-off in future LST prediction applications.

2.8 Conclusion

The overall purpose of this chapter was to satisfy **Objective 1** and assess how spatial scale and proxy-based methods in current ecosystem service mapping approaches can be improved through development of current mapping approaches. With regards to spatial scale, this chapter presents an approach to represent mismatches in RES function to demand dynamics, in order to usefully indicate areas for GBI investment. For example, the map displays of RES coldspots over a synoptic view of urban morphology, present a useful

visual tool to engage interdisciplinary stakeholders on how RES deprivation relates to their local communities. Current indicators may also inform basic estimation of natural capital values of GBI across the study area, or guide precise models and field-based quantification efforts to fully evaluate the potential value GBI investment in relation to societal demand for RES. The mapping approach also provides a potential methodological approach to monitor factors affecting GBI and RES asset values over time, and thus inform appropriate protective planning policies (Guerry et al. 2015).

Overall, the mapping approach represents a trade-off between coarse-scale RES mapping studies where demand from LULC categorisations, or within municipal districts are explicitly considered (Baró et al. 2017, Haas & Ban 2018) to gridded approaches employed in ecological and environmental models (Dobbs et al. 2018, Kremer et al. 2016a). There is potential to compare the current mapping approach against alternative spatial representations of RES processes, such as interconnected landscape features, or differing GBI management regimes (Grafius et al. 2018). As evident, current RES mapping approaches vary widely, and end users' view of RES may depend upon the implementation of certain methods, or certain perspectives in RES evaluation (Haase et al. 2014, Seppelt et al. 2011). Incorporation of alternative methods to estimate RES may prove useful to re-weight RES deprivation measures using different model combinations, and therefore represent different stakeholder views within the mapping process.

Findings from the case study thus inform on the benefits of choosing suitable representations of landcover and demand measures to achieve an accepted resolution in map indicators. Despite this, limitations in input data (e.g. aggregated landcover categories), resulting in ambiguity in model parameterisation may remain unavoidable for certain applications. This chapter therefore contributes valuable research information on how issue may influence final map values, and can be countered within both the mapping approach developed here, and approaches described in other studies. The mapping approach is theoretically transferable to urban areas with similar data resources, and may prove useful to examine concurrences in local scale RES drivers and relationships across the varying urban areas. Overall, the discussion of the model development, guides adaptation of the mapping approach for spatiotemporal analysis in the subsequent chapters. Improvements in landcover categorisation, demand indicators and RES modelling methods will be examined further for seasonal analysis of RES in **Chapter 3**. The potential application of the mapping approach to monitor and assess GBI and RES change will be explored in **Chapters 4 and 5**.

Chapter 3: Seasonal variation in regulating ecosystem services

3.1 Introduction

Seasonal change in biophysical conditions alter the ecological response of green-blue infrastructure (GBI) to changing climate conditions. As such, the level of benefits of some regulating ecosystem service (RES) functions will vary on an annual cycle. For example, GBI may produce a negative effect on urban temperatures throughout the year. Whilst this is beneficial to reduce hot weather stressors, the same effect may also provide a disservice, by increasing resident exposure to cold temperatures during winter months (Hajat et al. 2002, Hajat et al. 2007). In contrast, GBI produces benefits in reducing flood risks throughout the year by temporarily storing precipitation, and thus reducing runoff flows upon drainage systems. Seasonal variation in the condition of both vegetation canopies (e.g. leaf-loss) and supporting soils (e.g. saturation levels) may also alter the ability of green infrastructure to intercept and absorb excess stormwater over an annual cycle (Asadian & Weiler 2009, Silveira et al. 2000). Waterbody volumes may also vary throughout the year altering the storage capacity of blue infrastructure resources (Hankin et. al 2008). Reduced stormwater storage functionality may therefore be apparent when extreme precipitation events occur, and societal need for flood risk reduction is at it's greatest.

Seasonality in GBI functions for both temperature regulation and stormwater storage RES have been examined in a number of field-based (Armson et al. 2013a, Asadian & Weiler 2009, Hamada and Ohta 2010, Hathway & Sharples 2012) and computational modelling studies (Acero & Arrizabalaga 2013, Sjöman & Gill 2014). Methods therefore exist to estimate seasonal variation in RES indicators. However, this opportunity has received limited attention within current ecosystem service literature. This presents a number of concerns in planning urban resilience, as RES estimates typically assume that GBI is fully functional irrespective of the month of the year (de Araujo Barbosa et al. 2015, Cavan et al. 2014). Temporally static service indicators are therefore unable to assess if seasonal reduction in RES clusters in certain areas of a city and whether this represents a concern for community resilience to localised environmental stressors.

Understanding of where, and what type of GBI investment may resolve localised demand for cyclical RES can help to ensure that often constrained municipal resources are suitably allocated (Langemeyer et al. 2020). The RES mapping approach developed in

Chapter 2 presents a framework to examine mismatches between RES functions and demand, and thus indicate potential locations for GBI investment. Updating this approach with seasonal indicators for temperature regulation and stormwater storage RES may present a powerful tool to assess and explore cyclical variation in RES deprivation. This of course will require the adaptation of current model approaches for both RES functions and demand. A case study implementation, and review of the process, will therefore benefit the wider research community by assessing whether inclusion of cyclical variation in RES is required in future research. Methods developed through the case study will also provide guidance on how this analysis may be approached in other study areas.

Mapping seasonal RES indicators will also generate useful information for the local study area. Similar to other cities in the UK, Manchester is subject to periods of hot and cold weather conditions that may cause stress to urban residents (Smith & Lawson 2012). On average, July and August represent the hottest months with average maximum daily temperatures of 20.6°C and 20.3°C respectively (1981 – 2010 baseline) (Met Office 2013). The coldest months are January and February with average minimum daily temperatures of 1.7°C and 1.6°C respectively (Met Office 2013). Heatwave hazards are an occasional concern in the city, with notable heat stress periods recorded for 1995 and 2003 (Smith & Lawson 2012). As such events are likely to increase in frequency in the future (Cavan 2011), adaptation to such stressors is a noted concern within local planning policy (MCC 2015). The city of Manchester currently also suffers from high levels of socio-economic deprivation (Walsh et al. 2010). The ability to adapt to both hot and cold weather extremes (e.g. air conditioning, indoor heating measures) will therefore be constricted for households with tight financial budgets (Robinson et al. 2018). An examination of seasonal variation in temperature regulation may therefore inform local planning stakeholders on how GBI functions affect vulnerable residents over an annual cycle.

Precipitation levels in the city also vary over a year, with average monthly precipitation varying between 51.4mm (February) and 92.5mm (October) (1981 – 2010 baseline) (Met Office 2013). On average, the three wettest months are October (92.5mm), November (81.5mm) and December (80.7mm), which may present a concern for stormwater storage services in the city. A recent field-based survey recorded a minimum of 66 tree species in Manchester, where an approximate 89% of sample specimens were classified as deciduous leaved trees (City Of Trees 2018). Precipitation levels are therefore generally higher over the period of the year, when a large proportion of green infrastructure canopies in the study area are transitioning from leaf-on to leaf-off

conditions (Woodland Trust 2018). Generally wetter conditions may also result in increased soil saturation, and higher water levels in waterbodies. Seasonal variation in the ability of GBI to regulate surface runoff may have an impact upon flooding risks, however the extent to which this varies across the study area is poorly understood. An investigation here may provide an indication to local planners of the locations and types of GBI investment required to improve year-round community resilience to extreme precipitation events.

However, it is important to note here that seasonal dynamics in both temperature regulation and stormwater storage services are complex. The usability of information from this exercise therefore depends upon trade-offs in modelling this complexity, given constraints in the available data, and processing requirements to estimate indicators across the study area. A discussion of how the biophysical response of different GBI components respond to varying climate conditions, is therefore necessary to ascertain what processes are important, and can be quantified within each service model. This will then provide a rationale for the methods employed in the case study, and a foundation to assess the strengths and limitations of the seasonal analysis in RES indicators as a whole.

3.2 Aim and Objectives

Chapter aim: Identify whether incorporation of seasonal dynamics in regulating ecosystem service maps presents a concern for planning green-blue infrastructure.

Chapter objectives:

1. Review the literature to determine seasonal dynamics in regulating ecosystem services that can be evaluated within the mapping approach.
2. Map the distribution of vegetation species, in addition to other urban landcover(s) at high spatial resolution across the study area.
3. Develop and implement methods to map seasonal variation in temperature regulation and stormwater storage ecosystem services across the study area.
4. Assess variation in seasonal ecosystem services and provide current indicators of regulating ecosystem service value across the study area.

3.3 Seasonal dynamics in stormwater storage functions

Urban pluvial (surface water) flooding risks occur during heavy precipitation events, where high levels of rainfall over a certain period (e.g. a few hours) completely overwhelm the storage capacity of local drainage systems, resulting in water concentrating upon above-ground surfaces (Guerreiro et al. 2017). GBI can thus absorb and store rainfall during such events, reducing the rate of rainfall runoff flowing into local drainage systems during peak flows, in turn delaying flooding pressures (Liu et al. 2014). Seasonal changes in GBI conditions thus vary for both green and blue infrastructure, which in turn alters the provision of this service for different periods of the year.

For blue infrastructure, the amount of absorption is determined by the capacity of existing waterbodies (e.g. river or lake banks) to safely accommodate additional volumes from precipitation (Voskamp & Van de Ven 2015). For non-hydraulically connected waterbodies, such as lakes and ponds, stormwater storage requires consideration of the disparity between current water levels, in relation to the storage capacity of associated containing structures (Voskamp & Van de Ven 2015). Conversely, the absorption capacity of water channels (e.g. streams, rivers) may extend over a larger drainage network, where localised precipitation is stored and transported downstream away from the catchment area (Hankin et al. 2008). During periods of lower precipitation, water losses (e.g. outflows of rivers, evaporation) may exceed water gains, in turn lowering water levels and thus improving stormwater storage capacity. In contrast, periods of generally high precipitation can cause a reversal in storage capacity.

In contrast, green infrastructure provides storage benefits through both above-ground interception and soil absorption functions. Interception represents the capture and temporary storage of precipitation in above-ground biophysical structures such as leaves, stems and branches (Berland et al. 2017). Water intercepted by plant material either evaporates during or after a rainfall event or falls to the ground directly from leaves and branches (through-fall), or along plant structures to the adjoining ground supporting stems (stemflow) (Berland et al. 2017). Interception functions are directly related to biophysical plant structure, such as leaf size, gap fraction, and angle of branches between tree specimen (Alves et al. 2018, Xiao & McPherson, 2002). Shedding of plant foliage therefore results in a reduction of canopy interception levels due to the direct loss of plant material available to capture precipitation (Xiao et al. 1998).

Soil absorption is defined as the below ground-surface accumulation of precipitation. As vegetation forms in, and often over permeable soils that absorb and store precipitation during a heavy rainfall event, soil absorption functions are associated with green infrastructure (Whitford et al. 2001). Water throughfall and stemflow from plant material therefore often falls upon an absorbing surface below, which in turn provides additional stormwater storage capacity for the associated green infrastructure resource (Armson et al. 2013a). However, where green infrastructure overhangs impermeable surfaces (e.g. street tree canopies over asphalt), associated soil absorption benefits from throughfall are greatly reduced (Armson et al. 2013a). Soil compaction, and the materials consisting soil layers, determine the ease with which water passes between soil particles (Zölch et al. 2017). Both the rate of soil saturation, and existing water levels within different soils indicates the amount of rainfall that can be absorbed during a precipitation event (Pitt et al. 2005). In addition, vegetation affects the volume of soil water absorbed for plant growth, as the amount of precipitation required for soil saturation may decrease during low to no vegetation growth periods of the year (Silveira et al. 2000).

GBI can be created or modified through sustainable drainage systems to ensure efficient stormwater storage functions. This may include the development of retention basins and swales, green roofs, and devices to improve ground infiltration such as soakaways and trenches (Tourbier & White 2007). However, irrespective of whether GBI is specifically designed for drainage purposes or not, canopy interception and soil absorption rates will be mitigated by climate conditions prior to, and during, an extreme weather event. Temperature and humidity affect the rate of water evaporation from plant material and soils, in turn impacting stormwater storage capacity during extreme events (Schroll et al. 2011). Seasonal variation may occur as warmer and drier weather conditions result in lower pre-event saturation of vegetative structure and associated soils (Ferreira et al. 2015). Characteristics of rain, such as droplet size, temperature, and angle of rainfall also impact interception rates between plant material (Xiao & McPherson 2002), whilst wind conditions can either increase throughfall due to canopy disturbance or increased rates of rainfall evaporation (Asadian & Weiler 2009).

GBI stormwater storage functions will therefore vary between precipitation events. An expectation for temperate climates, is that conditions will in general be wetter during cooler months of the year. In Manchester for example, average precipitation levels are higher during October through to December. GBI stormwater storage capacity may be reduced from the preceding warmer months, as local soils may be wetter, vegetation

canopy cover reduced, and waterbody volumes higher. However, this general assumption should be treated with caution, as intense summer precipitation events have recent caused flooding in the study area (BBC 2019a). Periods of warm weather can dry out soils, which may increase hydrophobicity and reduce GBI stormwater storage as a result (Ferreira et al. 2015).

3.4 Seasonal dynamics in temperature regulation functions

In comparison to non-GBI surfaces (e.g. asphalt, concrete, buildings), GBI is less prone to thermal heating, and has reduced capacity for above-ground air warming (Žuvela-Aloise et al. 2016). For blue infrastructure, this function is provided largely by latent evaporative energy transfer from solar radiative heating of waterbodies (Broadbent et al. 2018, Coutts et al. 2013), resulting in thermal inertia and comparatively lower surface temperatures to non-GBI surfaces during daytime conditions (Webb & Zhang 1997). In addition to evaporation, flowing waterbodies (e.g. rivers and streams) may also transport thermal energy downstream away from an urban area, aiding localised cooling (Hathway & Sharples 2012). Cooling potential varies seasonally as waterbody temperatures vary over the course of a year (Webb & Zhang 1997). For example, Hathway & Sharples (2012) demonstrate that for a small urban river in Sheffield, UK, the cooling potential of surrounding areas is greatest during spring, when the temperature of the river lags behind local ambient air temperatures. However, by late summer/early autumn, temperatures in a river may approach surrounding air conditions, reducing the cooling potential of blue infrastructure resources relative to surrounding non-GBI areas (Hathway & Sharples 2012, Theeuwes et al. 2013). Parity between waterbody and general air temperatures will however dissipate as waterbodies gradually cool during the late autumn and winter months (Hathway & Sharples 2012).

Green infrastructure regulates urban temperatures through a number of primary functions that include evapotranspiration, shading and regulation of wind movements (Kong et al. 2016). Evapotranspiration in vegetation canopy material requires use of shortwave infrared energy to evaporate water required for photosynthesis from leaves (Qiu et al. 2013), resulting in a reduction of above surface ambient air warming through reduced emission of long-wave solar radiation (Shashua-Bar & Hoffman 2000). Stomatal

openings in plant leaves release water vapour; evapotranspiration thus varies according to both leaf area and leaf shape species (Ballinas & Barradas 2016). Climate conditions further affect this process, as changes in ambient air temperature, humidity and wind speed influence the rate of evapotranspiration (Valipour 2014). On a seasonal basis, this function changes due to loss of stomatal water transmission associated with canopy leaf-loss, in addition to potential changes in temperature and humidity levels. For example, evapotranspiration cooling from evergreen trees may dip in association with reduced ambient urban air temperatures in winter (Hamada & Ohta 2010), whereas, antecedent dry conditions for vegetation in summer may reduce plants ability to transpire water, regardless of high temperature and humidity levels (Qiu et al. 2013).

Vegetation shading from above-ground canopies reduces the amount of shortwave energy received by obscured surfaces and affects longwave energy transfer for above-ground air warming (Akbari et al. 2001). This process also enables the development of cool air pockets, which replace surrounding warmer air through displacement, resulting in localised ambient air cooling (Sugawara et al. 2016). In general, vegetative shading improves with an increase in the vertical size of vegetation, and increasing density of foliage, which serves to block out sunlight on nearby surfaces, and decreases due to seasonal loss of light obscuring leaf-canopies (Jaganmohan et al. 2016). In warm weather conditions the relative benefits of GBI shading may improve as solar insolation increases; in this manner shaded areas provide localised cooling by shading artificial materials with increased thermal capacity (Wang et al. 2016). During cool weather conditions, the discrepancy in solar radiation retained between shaded, and non-shaded surfaces is reduced due to the reduced period of radiation exposure (Hamada & Ohta 2010).

Wind-patterns, dynamically altered due to the geometry of above-ground structures, and from incoming weather fronts, can alter the spatial pattern between ambient air and surface temperatures (Arnfield 2003). Tree and shrub green-infrastructure can therefore function as windbreakers. This function is potentially beneficial in reducing resident exposure to cooling winds during winter months (i.e. blocking wind movement around residential buildings), whilst presenting a potential disservice in reducing cool breeze exposure during warm weather conditions (Pataki et al. 2006). Wind regulation therefore relies on physical barriers to air movement, which may decrease due to the loss of green-infrastructure canopies during certain months of the year (Lin et al. 2016). Air temperatures across an urban area therefore vary due to atmospheric movements. As aforementioned, this can result from the formation of cool air pockets around GBI

resources (Kolokotroni & Giridharan 2008). However, relationships in energy transfers between physical surfaces and air pockets can be heavily modified by larger surrounding weather fronts (Coseo & Larsen 2014). Urban surface and air warming, in conjunction with aerodynamic roughness caused by the formation of tall-standing structures can result in the formation of an urban boundary layer (Oke 1978). When energy exchanges between physical surfaces and surrounding air is strong, the boundary layer can act as an insulating atmospheric system, and force larger natural atmospheric fronts over an urbanized zone (Oke 1978). However, when energy interactions are reduced either through reduced solar radiation from cloud cover, or general reductions in the hours of sunshine given parts of the year, this can influence unsettled air temperature conditions (Azevedo et al. 2016). The association between land surface and air temperatures may be weak where wind and air movement is prevalent (Elias & Svensson 2003).

3.5 Modelling seasonal dynamics in ecosystem services

As evidenced in the previous sections, seasonal dynamics between GBI and climate conditions are complex. In order to assess the usability of seasonal indicators, requires consideration of the degree current mapping approaches can be adapted for seasonal analysis. For both RES, canopy loss in deciduous trees may have considerable impacts upon regulating functions. Previous studies demonstrate that the large-scale spatial mapping of tree species is possible through classification of very-high resolution imagery (Immitzer et al. 2012, Raciti et al. 2014). However, implementation of this approach for multiple tree species requires significant time costs to gather appropriate primary data and is unfortunately beyond the scope of this study. A two-class dichotomy between evergreen and deciduous green infrastructure species is however more feasible as classification samples can be identified directly from the imagery itself. Whilst this classification may aggregate variation in ecological functions (e.g. rainwater interception, evapotranspiration) between different vegetation species, it will enable broad city-wide consideration of the implications of seasonal foliage change for both RES here (Sjöman & Gill 2014, Tran et al. 2006). In contrast, calculating both the additional precipitation storage capacity of blue infrastructure waterbodies and thermal volume storage capacity requires topographic modelling of waterbody structures for the entire study area (Liu et al. 2014,

Theeuwes et al. 2013). As the required data (e.g. elevation models for above and sub-water level topographic data) are currently unavailable, then blue infrastructure will be categorised as one class, thus aggregating the RES benefits of differing waterbody structures. This is a limitation for both RES models, but is arguably reasonable given the limited coverage of waterbodies (estimated < 1% study area coverage; **Section 2.5.1**) within the study area.

Due to constraints in available data, the complex dynamics in seasonal RES described previously require approximation into seasonal scenarios. For example, image derived land surface temperature (LST) layers provide a proxy measure of temperature conditions in the study area. A time series of remotely sensed thermal images would therefore enable examination of changes in the magnitude and patterns of LST over a year. Change in LST could then be evaluated against changes in green-infrastructure canopy conditions (i.e canopy senescence), evapotranspiration rates, vegetation growth, in addition to broader environmental conditions (e.g. atmospheric stability, moisture levels) obtained from other datasets, that impact upon GBI cooling functions (Azevedo et al. 2016, Cui & De Foy 2012). Understanding the drivers behind variation in GBI temperature regulation functions could therefore inform planners of appropriate investment in new GBI resources and improve management of existing GBI resources to cope with environmental stressors (Ferreira et al. 2015, Rodriguez et al. 2006). However, as the number of suitable thermal images is limited because of cloud cover, then seasonal analysis here is limited to a pair of thermal images representing warm and cool weather conditions. This will allow the development of novel seasonal temperature regulation indicators, but will provide limited information on temperature regulation functions vary according to different environmental conditions within seasons (Elias & Svensson 2003).

In contrast, for stormwater storage regulation analysis, modelled precipitation data is available to determine various inter-season precipitation scenarios e.g. 95th percentile precipitation volume levels for seasonal extreme stormwater event (Met Office 2020a). However, it is unclear at the present time how such data can be manipulated to determine pre-event soil wetness. Therefore, antecedent soil conditions in the SCS-CN model are assumed to be normal, even though this may provide an over simplification of expected moisture conditions in local soils between seasons (Silveira et al. 2000, Gill et al. 2007). In line with temperature regulation analysis, singular seasonal scenarios will be used to assess variation in stormwater storage services according to cyclical change in both GBI and climate conditions.

3.6 Methods

The following section describes the methods (**Figure 3.1**) required to analyse seasonal variation in RES. **Section 3.6.1** describes the classification of very high spatial resolution multi-spectral imagery to derive landcover, including deciduous and evergreen leaf canopy extents within the study area. Landcover information then functions as the primary input into adapted models for temperature regulation and stormwater storage functions (**Sections 3.6.2 and 3.6.3**). These models then generate indicators for respective seasonal scenarios, in order to assess the degree of seasonal change for each RES respectively. **Section 3.6.4** describes methods to weight RES demand according to population exposure to associated environmental risks, to provide a more focused examination of service to demand dynamics in the study area than evidenced in **Chapter 2**. This section also describes methods to contrast indicators between RES and assess implications of omitting cyclical variation in service indicators from current ecosystem service mapping studies.

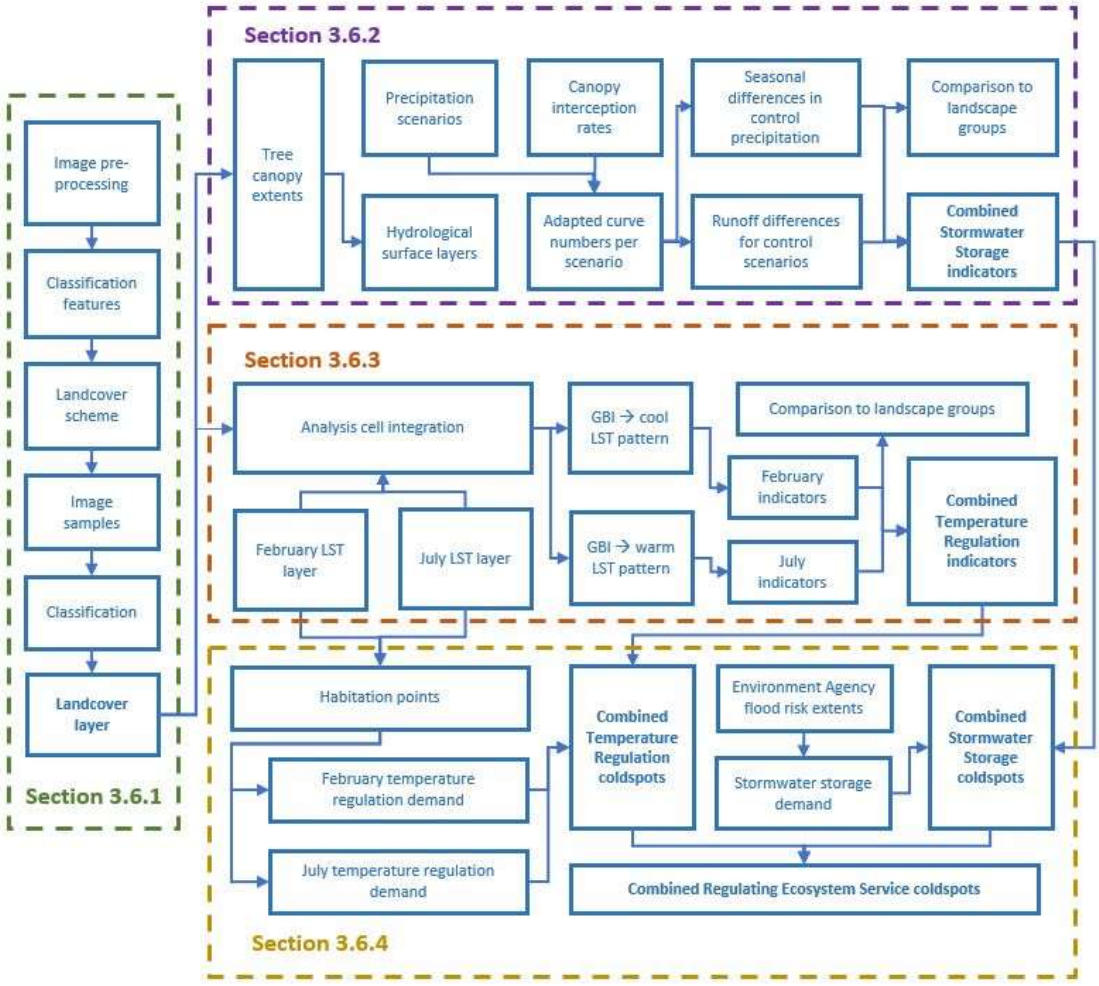

Figure 3.1 – Overview of methods in Chapter 3

3.6.1 Urban landcover mapping

3.6.1.1 Image acquisition and pre-processing

The analysis of multi-temporal remotely sensed imagery enables the consideration of variance in spectral information resulting from cyclical change in canopy conditions, and is useful for the discrimination between deciduous and evergreen vegetation (Hill et al. 2010, Persson et al. 2018). For this exercise, access to a repository of very high spatial resolution (≤ 5m pixel size) multi-spectral imagery, was obtained from the European Space Agency (ESA 2018). A search was undertaken to identify cloud free image tiles that overlapped the study area boundary. Guidance for image selection was based upon Hill et al. (2010), that classified (*n* = 6) tree species in a UK woodland using high resolution imagery recorded at monthly intervals. Here, classification accuracy generally improved with an increasing number of stacked images that ranged from one to five. Images that covered the entire study area, and were constrained within a twelve-month window, in order to minimise effects of land surface changes, were identified for only two dates. These images were from the Spot-7 (1.5m pixel size) and Pleiades-1A (0.5m pixel size) sensors (ESA 2018) for May 26th and October 29th 2017. This is less than the optimum number of images in Hill et al. (2010). However, this study found the use of two images, for 30th May and 27th October was sufficient to produce an overall species classification accuracy of above 75%. Therefore, the images obtained here for similar timepoints were deemed suitable for the classification of deciduous and evergreen vegetation in this exercise.

All images were geo-referenced to British National Grid by the vendor and pre-processed to surface reflectance. As cloud cover was evident in the October Spot-7 imagery, the affected region was replaced by October Pleiades 1A imagery downscaled to Spot-7 resolution using nearest neighbour resampling (Raster package, R programming language; Hijmans 2020). Both Pleiades-1A and Spot-7 sensors share virtually identical spectral characteristics and are processed using the same radiometric correction methods (Airbus 2020). In addition, both images were acquired within a thirty-minute window on the same date, therefore further pre-processing was considered unnecessary to create a composite October image. Technical information on sensor characteristics, and areal coverage of the images is described in **Appendix 3.1**.

3.6.1.2 Classification features

Additional image feature layers were created prior to classification to combine, and further enhance information in the multi-temporal image data (Immitzer et al. 2012, Baker et al. 2018). In addition, ancillary spatial data were processed using the UK Ordnance Survey (OS) Mastermap topography layer (OS 2018) to provide contextual OS landcover data for topological classification purposes (**Figure 3.2**). As the data sets originate from different sources, it was important to check the degree of spatial co-registration, in order to ensure relevant objects (e.g. buildings, roadways) in either data set overlap the same spatial location. Root Mean square spatial alignment error (tested using n = 210 random check points) (Aguilar et al. 2013, Topan & Kutoglu 2009) was less than one (single) pixel. Therefore, geo-rectification was not required for any input data layers. Steps for creating the classification features are described in **Appendix 3.2**.

3.6.1.3 Landcover scheme

A classification scheme was devised to provide suitable landcover information for the following RES analysis. **Table 3.1** provides a description of the classes involved. Both shaded non-vegetation, and shaded vegetation classes were validated during the classification but are subsequently re-assigned to other classes in further classification steps (Baker et al. 2018; see **Section 3.6.1.5**).

Table 3.1 – Image classification scheme

Class ***(t = Temporary class)***	***Class group***	***Description***
Artificial	Non-vegetation	Manmade non-vegetative ground surface e.g. asphalt, concrete, paved materials
Bare Earth		Non-vegetative ground surface consisting of natural materials e.g. soil, sand
Deciduous	Vegetation	Deciduous bole and branch canopy (shrubs/trees) vegetation
Evergreen		Evergreen bole and branch canopy (shrubs/trees) vegetation
Grass		Ground surface herbaceous vegetation
Water	Water	Exposed water i.e. water channels, reservoirs, ponds
Shaded non-vegetation (*t*)	Shadow	Non-vegetation surfaces completely obscured by shadow
Shaded vegetation (*t*)		Vegetation surfaces completely obscured by shadow

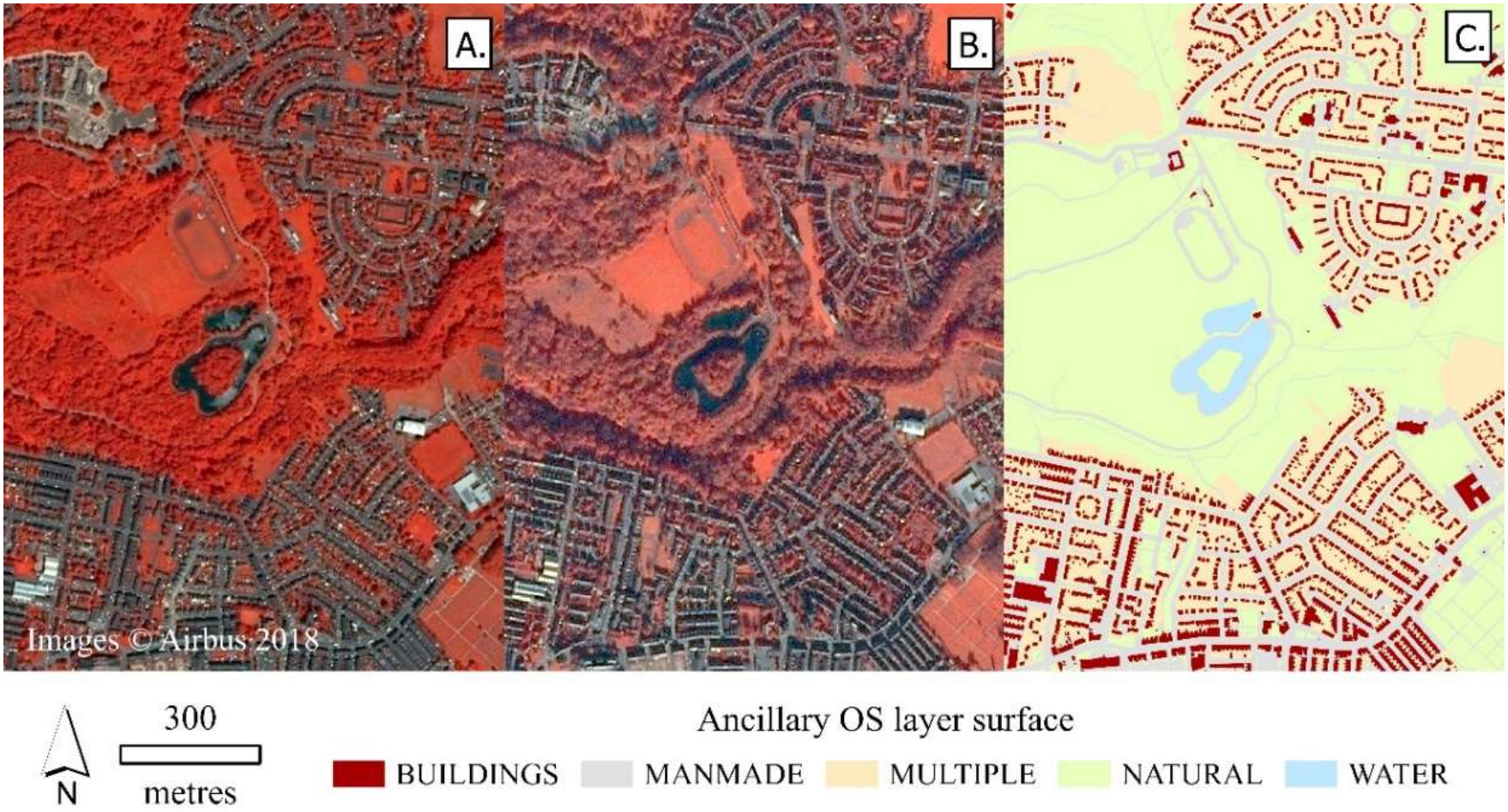

Figure 3.2 - Example of image and ancillary OS classification features: **A.** Spot-7 May 2017 imagery (near infrared false-colour); **B.** Spot-7 October 2017 imagery (near infrared false-colour); **C.** Reclassified ancillary OS classification feature

3.6.1.4 Image samples

Stratified sampling was used to distribute image sample points across the study area (Congalton & Green 2008). Equal area reference zones (*n* = 33) were generated to guide this process, with roughly *n* = 9 points in each zone per class where possible. A total of *n* = 2,376 sample points (*n* determined by multinomial law (Congalton & Green 2008) for both training and validation purposes) were employed in the identification of image class features. Landcover labels were assigned to each sample point, based upon manual identification of corresponding image class for the associated image pixel. For a number of potential sample locations it proved difficult to confirm differences between deciduous and evergreen vegetation using the image data alone. Therefore, Google Earth street-view imagery (various image dates between 2000 and present) was used to assist this process as this provided ground-level view of vegetation types at sample locations. Samples were randomly selected for either training or validation based upon a 70% - 30% training - validation split. Total training samples exceeded *n* = 1000, which has been found to ensure suitable classification accuracy in other studies (Jin & Mountrakis 2013; Jin et al. 2014). A description of the multinomial law method and sample selection scheme for all classes is described in **Appendix 3.3**.

3.6.1.5 Random Forest and topological classification

The Random Forest algorithm (Breiman 2001) is a non-parametric ensemble method widely used for image classification purposes (Immitzer et al. 2012, Millard & Richardson 2015, Rodriguez-Galiano et al. 2012); and was implemented using the 'Random Forest' package in R (Liaw & Wiener 2002). As surface patches can exist at, or close to the size of a single pixel, pixel-based classification was implemented to group image areas into both shadow classes, and main class groups (**Table 3.1**). Water was excluded from the Random Forest process, and classified using ancillary data, due to difficulties in trial runs in achieving sufficient accuracy for this class. Segmentation (all object-based classification was conducted using Trimble eCognition) was implemented for sub-group classification where this improved pixel based results (Aguilar et al. 2013). Deciduous and evergreen extents were the exception, due to difficulties in manually identifying homogenous canopy pixels within overlapping canopy areas.

For all classification nodes, optimum features for both segmentation and classification were selected to enable efficient computational processing (VSURF package,

R programming language, Genuer et al. 2018). Where segmentation was employed, sample points were employed to select the relevant training class objects, with image features calculated from the "within object" mean and standard deviation value. Multi-resolution segmentation parameters were consistent for both segmentation processes, with scale factor = 50, shape = 0.1 and Compactness = 0.1. Random Forest parameters *mtry* (number of random features for each forest tree node) and *ntree* (total number of trees grown in model) were determined for each classification subset through iterative model tuning (Huang & Boutros 2016). See **Appendix 3.4** for Random Forest parameters; **Figure 3.3** for classification workflow.

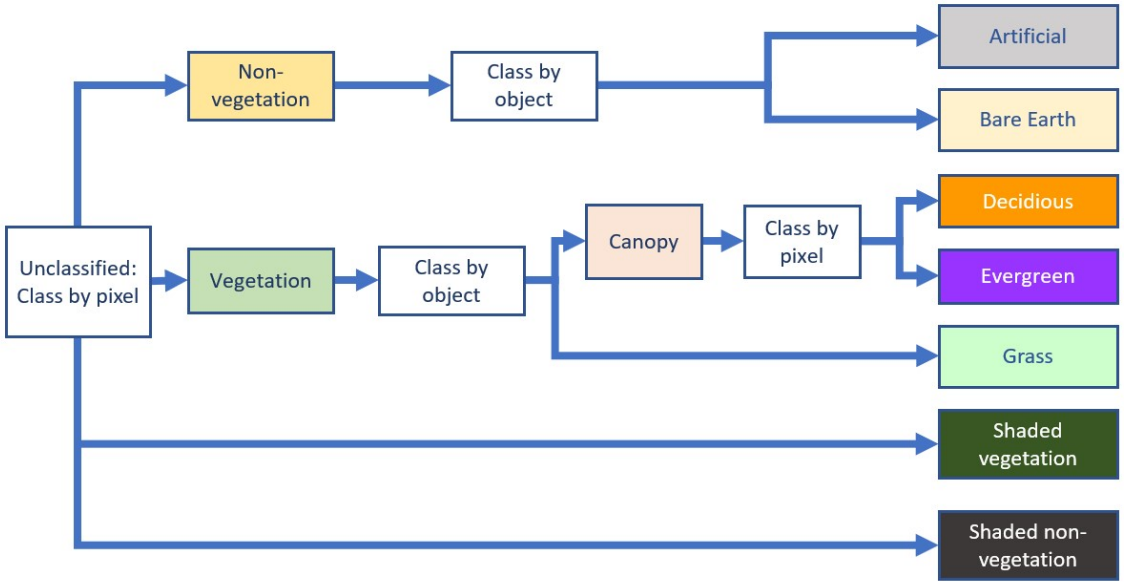

Figure 3.3 - Random Forest classification workflow

Topological processing of classified image object areas refined the classified map. With the exception of Deciduous and Evergreen classes, any pixel that overlapped water areas, as identified in the ancillary OS spatial data, were reclassified to the Water landcover class. Deciduous and Evergreen were however excluded from this process due to potential canopy overhang over water extents. Grass and Bare Earth surfaces within OS landcover manmade and building polygon areas were reassigned to the artificial class. Classification accuracy assessment was conducted using the randomly assigned validation sample points (**Section 3.6.1.4**). An error matrix was populated to calculate both overall and interclass accuracies, in addition to the kappa statistic to ascertain accuracy levels in the map product (Congalton & Green 2008, Viera & Garrett 2005).

The resulting classification layers were then manually examined against the image data. Any areas of misclassification that were identified through this process were then checked and reassigned the appropriate class label. Building extents from the ancillary OS feature layer were used to re-classify overlapping artificial, and shadow class pixels to a new Building class. As the shadow classes represent redundant data, two topological processing routines were used to reassign non-vegetation, and vegetation shadow to classes within the respective class groups (Baker et al. 2018). In the first routine shaded pixels of either class were converted into objects in eCognition, and then reassigned to relevant candidate class if bounded by no other non-shadow class. This process was re-iterated until all appropriate shadow candidates were reassigned (**Appendix 3.5** determines the re-classification rules used in this process). Remaining shaded class pixels were reassigned based on the majority candidate class within a 100m circular buffer around the pixel object centroid. Final checks were made on the classified map, and remaining errors were reclassified where identified to complete the final landcover map, which served as input data into the adapted models described in the following sections.

3.6.2 Seasonal variation in Temperature Regulation indicators

Regular sized polygon grid cells (100m resolution; see **Section 2.5.2**) were generated to cover the administrative extents of the city of Manchester, forming the analysis units for the mapping approach. To quantify seasonal variation in temperature regulation functions required Land Surface Temperature (LST) data to represent both hot and cold temperature conditions. Warm weather (leaf-on) conditions were represented using the LST surface generated (17th July 2017; 30m resolution) to develop the mapping approach (**Section 2.5.2**). For cold weather conditions an additional Landsat-8 image was acquired (USGS 2017a). This image was captured for 7th February 2017 (minimum daily temperature of 2°C, average 6°C), and provides the most suitable cloud-free image data for winter (leaf-off) conditions adjoining the 2017 summer period. Image bands were re-projected to British National Grid. The exact location of corresponding features (e.g. buildings vertices, road junctions) proved difficult to identify between the images and landcover data, due to the large differences in pixel resolution and resulting appearance of image features. Precise geo-rectification of the LST imagery was therefore not attempted. However, the outline of parks and other large features in the image data coincided with the location and outline of the same features in the landcover information, indicating that

the two datasets aligned spatially. A land surface temperature layer was created by applying the mono-window method (see **Section 2.5.2; Appendix 2.2** for workflow) using updated parameter values (**Appendix 3.6**). Mean LST per cell was recorded for both February, and July LST layers respectively (**Figure 3.4**).

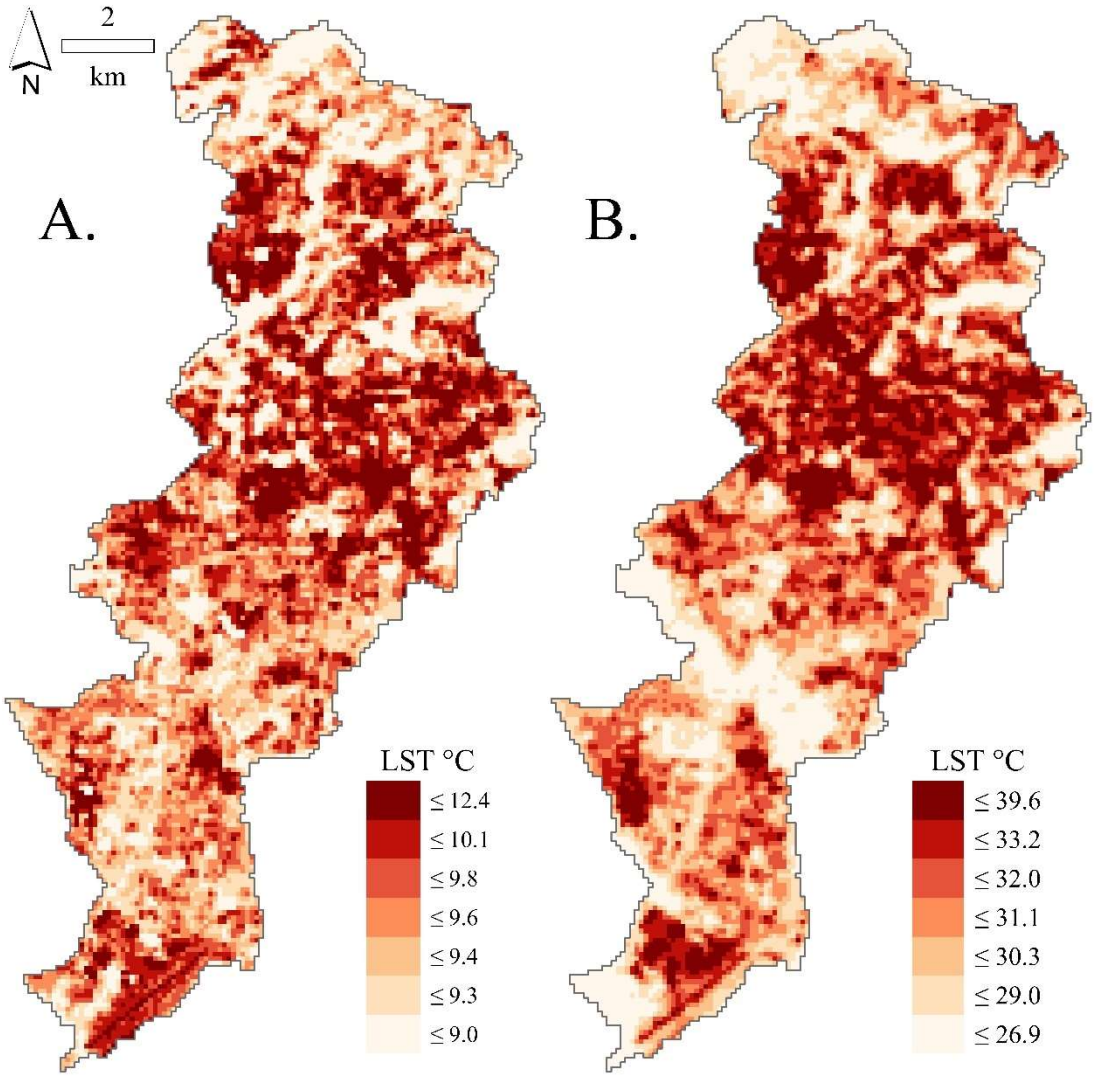

Figure 3.4 – Mean cell Land Surface Temperature (LST) for 7th February (**A**) and 17th July (**B**) 2017

Following the review of temperature regulation methods in **Chapter 2**, an additional analysis was used to investigate whether GBI to LST patterns differ according to categorisations of landscape, or urban morphology. For example, Landscapes associated with high levels of natural infrastructure, such as urban parks and woodland, can result in the formation of cool islands that produce higher temperature cooling effects than opposing built up landscapes (Kolokotroni & Giridharan 2008). To investigate whether

landscape patterns influence relationships in GBI coverage for either February or July LST, all analysis cells were categorised as one of four landscape groups (**Table 3.2**). Ordinary least squares regression (OLS) was then calculated to predict the effect of GBI upon both February and July LST for all cells using **equation 2.1**.

$$y = a + bx \quad \textbf{[2.1]}$$

Table 3.2 – Landscape categorisation of analysis cells

Landscape	Assignment method	Description
Public recreation	Cell coverage by Public recreation land use* > 50%	Managed landscapes for public recreation: Parks, Sports fields and facilities, Urban farming
Non-recreational open space	Cell coverage by Non-recreational open space land use* > 50%	Open-space landscapes not supporting recreation; Agriculture; Waterbodies (e.g. reservoirs, river channels); Woodland
No Demand	Cells not assigned to above Landscapes that with population < 1	Built-up areas not associated with residential housing: Industrial and Commercial zones; community services; transport facilities
Demand	Cells not assigned to any of the above categories (population ≥ 1)	Built-up areas associated with residential housing

* - Land uses obtained from the Urban Land use classification of the study area for the year 2017; class schema and methods described in **Chapter 4, Section 4.5.1**

Where y is the predicted mean LST per cell, x is the percentage GBI coverage per cell. GBI to LST patterns for each landscape category were examined in relation to the OLS regression trendlines. This was beneficial for a number of purposes: a) identify whether high/low service values are associated to certain landscape patterns; c) identify whether general GBI functions improve or degrade according to different categories of landscape usage; c) to evaluate the current regression modelling approaches defined in **Chapter 2**. In contrast to a purely cell-based approach, this analysis should inform local planning

strategies on how general GBI investment may vary in benefits according to landscape patterns across the city.

In addition, the potential effects of leaf-loss upon February LST were investigated by updating x in **equation 2.1** to represent the percent of cell area that is Evergreen, Grass and Water. This measure was used to consider whether the influence of active GBI on LST, produced a stronger effect than combined non-active and active GBI during leaf-off conditions. As discussed in **Section 2.5.2**, potential bias in OLS parameter estimates may be apparent, with evidence of spatial autocorrelation in OLS model residuals. Geographically weighted regression (GWR) was therefore used to assess whether local regression, reduces autocorrelation associated bias in OLS parameter estimates and provided better estimates for temperature regulation indicators (Ivajnšič et al. 2014, Szymanowski & Kryza 2011, Tian et al. 2012, Zhao et al. 2018).

If negative causality of GBI on LST was established for warm weather conditons, positive temperature regulation function indicators were calculated within 0 – 100% range using the method described in **Chapter 2** (**Table 2.1; Section 2.3**). Here, minimum predicted LST produces the highest temperature regulation indicators (i.e. 100%), whereas maximum predicted LST produces the lowest temperature regulation indicators (i.e. 0%). If negative causality of GBI on LST was established for cool weather conditions, negative temperature regulation indicators were calculated by reversing this process (i.e. maximum predicted LST represents the highest temperature regulation indicators = 100%). Indicators for each season were then compared to assess seasonal variation in the temperature regulation indicators.

3.6.3 Seasonal variation in Stormwater Storage indicators

In order to assess the impact of seasonal tree canopy leaf-loss on stormwater storage rates, the SCS-CN model (USDA 1986) was updated according to the methods described by Sjöman & Gill (2014). This study examined seasonal variation in urban residential rainwater surface runoff by adjusting curve numbers for tree areas, according to the impact of changing canopy cover upon canopy interception rates (**Figure 3.5**). This process requires information on both the seasonal interception rates of deciduous and evergreen canopy areas, in addition to the surface runoff potential of understory surfaces. The required adaptation of the SCS-CN model is described in the sections below.

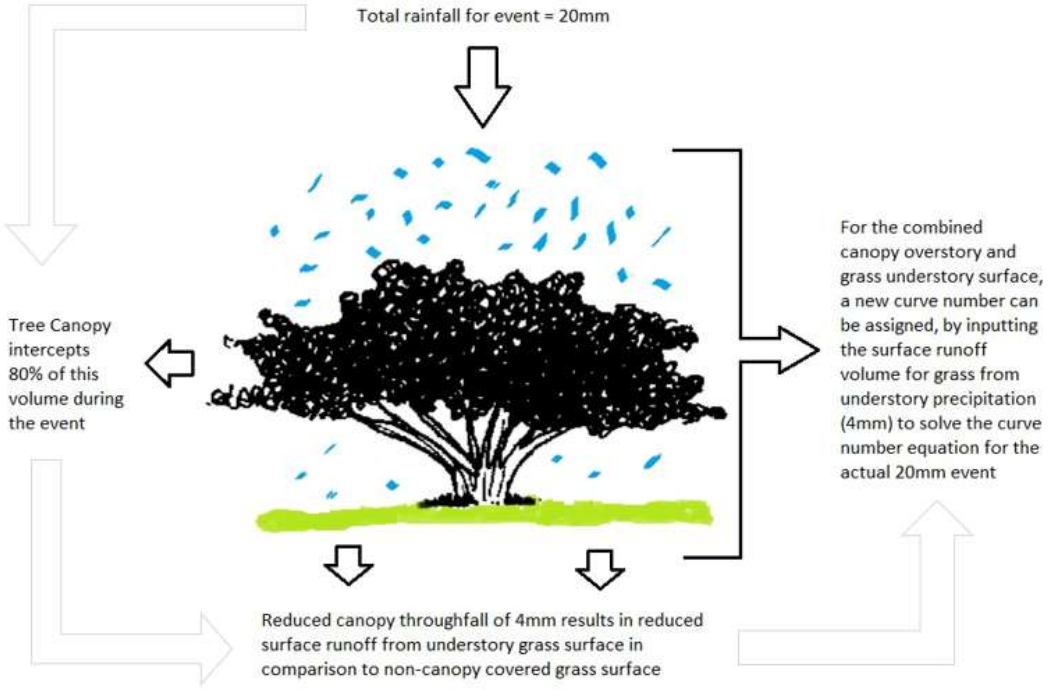

Figure 3.5 – Influence of above-ground canopy interception upon composite curve numbers (USDA 1986)

3.6.3.1 Canopy Interception rates

Field-based investigation of seasonal variation in urban tree canopy interception rates was beyond the scope of this project, therefore interception rates for deciduous and evergreen canopies were identified from peer reviewed literature (Armson et al. 2013a, Asadian & Weiler 2009, Xiao & McPherson 2002, Xiao et al. 2000). A study of interception rates for trees in the UK was identified (Armson et al. 2013a). Unfortunately, this study proved unsuitable as interception rates for "leaf-on" and "leaf-off" conditions were recorded for three deciduous tree specimens across all rainfall days in a year. As interception rates were not reported for individual days, it proved difficult to assess how interception functions vary for heavy precipitation events, or when demand for stormwater storage services may be greatest. In contrast, a study based in Oakland, USA provided information for this purpose (Xiao & McPherson 2011). Here, the total net precipitation flowing under canopies for two deciduous (Gingko [*Ginkgo biloba*] and Sweet Gum [*Liquidambar styraciflua*]) and one evergreen (Lemon [*Citrus limon*]) tree specimen in urban Oakland, USA, was recorded for storm events in a single year period (Xiao & McPherson 2011). Whilst the tree species in this study are not commonly found in UK urban areas, this study provides field-quantification of how seasonal interception rates of urban evergreen,

and deciduous trees differ during intense precipitation events (Asadian & Weiler 2009, Guevara-Escobar et al. 2007).

Differences in mean interception rates between deciduous and evergreen species for both "leaf-on" and "leaf-off" periods (Xiao & McPherson 2011) (see **Appendix 3.7** for a summary of the data) were statistically tested using the non-parametric paired Mann-Whitney U-test (Harris & Jarvis 2014). Significant differences were identified for the leaf-off period ($W = 9, p < 0.01$) only. As no significant difference was recorded for the leaf-on period ($W = 93.5, p > 0.05$) the interception rate of 34.8% (mean of all recorded leaf-on measurements) was assigned to all trees. For "leaf-off" conditions, the ratio between deciduous and evergreen interception rates was used to infer the reduction in interception due to canopy leaf-loss. The mean "leaf-off" interception rate for deciduous trees (25.9%) was thus divided by the mean leaf-off interception rate for evergreen trees (57.8%), resulting in a ratio of 0.44. This determined the proportion of "leaf-on" interception assigned to leafless trees (15.3%) when multiplying the leaf-on interception rate.

3.6.3.2 Tree canopy extents

Tree canopy extents for the study area were extracted from the Greater Manchester Tree Audit data (City Of Trees 2011). This dataset records the extent and height above-ground of both individual tree canopies, and larger tree clusters, across the wider administrative region. This dataset was processed as shown in **Figure 3.6** to classify an interceptive canopy layer from the existing land surface cover map. As the height of the lowest tree specimen was 2.9m in the Xiao & McPherson (2011) study, the height threshold for an interceptive canopy was obtained by rounding up to the nearest whole number (3m above-ground). Any deciduous or evergreen areas intersecting with canopy polygon areas below 3m in height were classified as shrubs for curve number assignment, thus assuming interceptive function remains consistent regardless of potential leaf-loss.

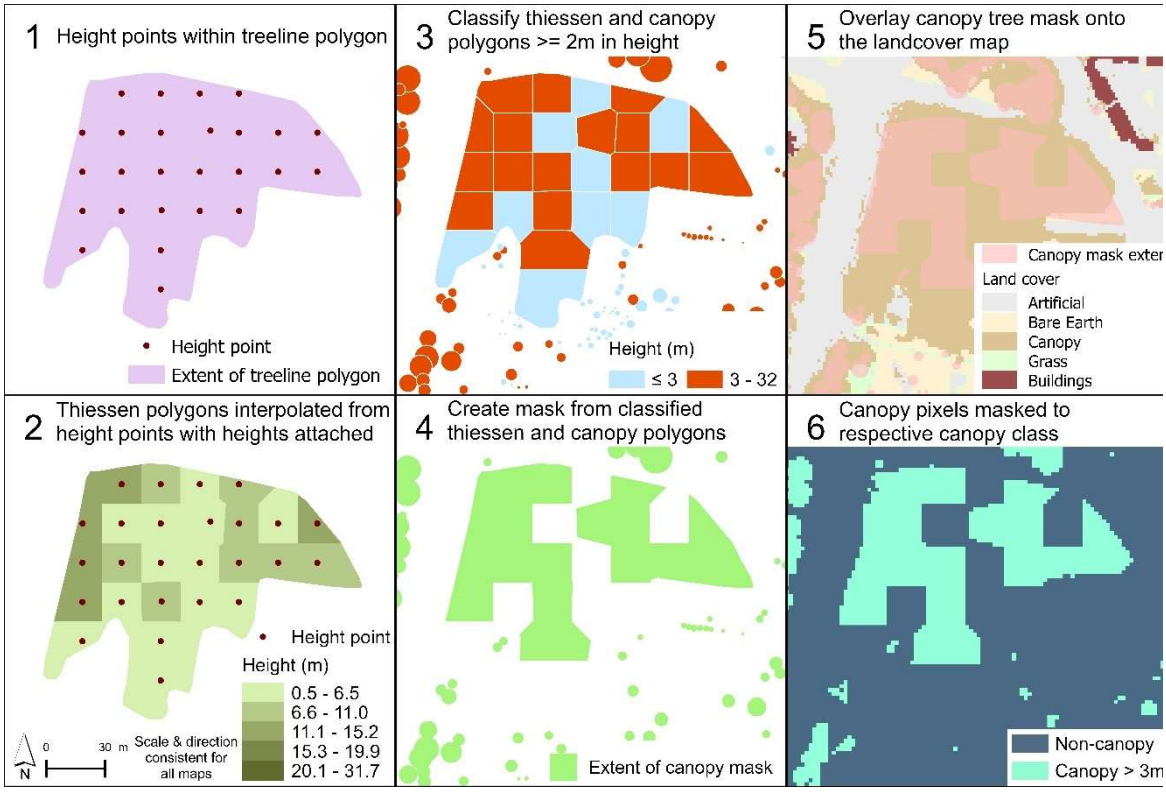

Figure 3.6 – Classification of tree canopies using Tree Audit data (City of Trees 2011)

3.6.3.3 Hydrological surface layers

As tree canopies obscure below ground detail in the imagery, the ancillary OS layer (**Appendix 3.2**) was adapted to assume understory Natural, Manmade (Buildings and Manmade), Multiple, and Water surfaces for the study area. The landcover map (described in **Section 3.6.1**) was then intersected with both the ancillary OS feature layer, and SCS soil map for the study area (see **Section 2.5.4**), to define hydrological surface classes (**Figure 3.7**). Classes excluded from this process were Artificial, Buildings, and Water, as curve numbers (see **Section 2.5.4**) for these classes are the same irrespective of the underlying soil type.

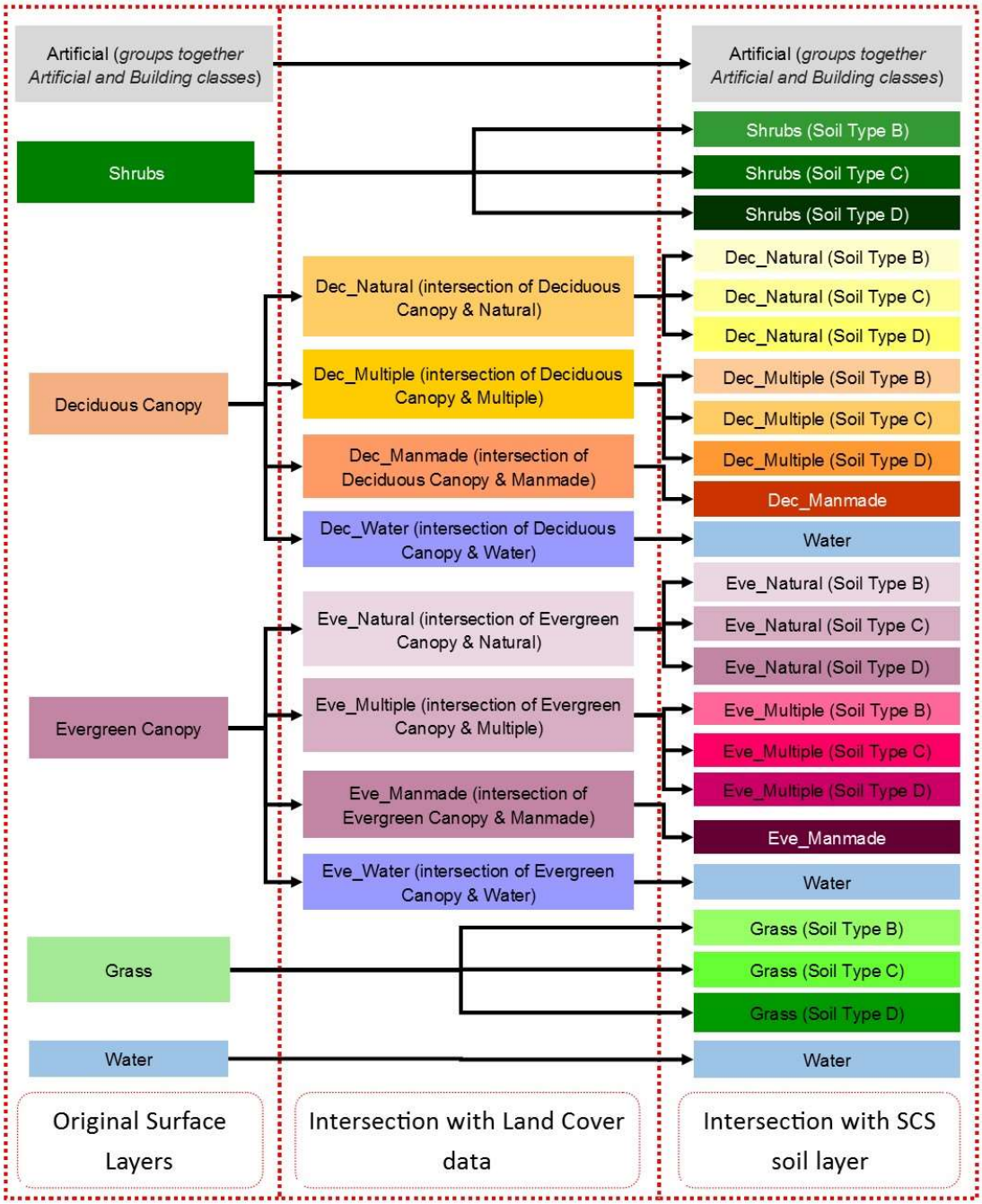

Figure 3.7 – Categorisation of hydrological surface layers

3.6.3.4 Precipitation scenarios

Data required to estimate precipitation level inputs for seasonal scenarios was obtained using the UK climate projections 2009 (Met Office 2020b) Weather Generator tool (Newcastle University 2018). The tool was commissioned by the UK Department for Environment, Food and Rural Affairs (DEFRA) and is designed to support planning and engineering decision-making processes, with statistically sound climate projections based on user guided emission scenarios. The tool uses iterative modelling, to predict daily precipitation levels for both a control baseline period (1961-1990), and for a user defined

projection period based upon carbon emission scenarios. Precipitation outputs are calculated from the baseline period, which are based upon quantified regional precipitation data. The data are generated for a 5km grid cell for the centre of the city of Manchester.

Percentiles were used to identify rainfall thresholds for extreme precipitation events are determined by the event probabilities from the national risk of surface floodwater dataset (EA 2018), which models surface water flood extents for 1 in 30, 1 in 100 and 1 in 1000 probability precipitation events. Precipitation levels were calculated for control and seasonal precipitation inputs. Control inputs considered event probabilities for a whole year to examine variation in cell runoff according to changing leaf conditions only. Seasonal inputs considered event probabilities within “leaf-on” and “leaf-off” time periods to examine the interaction between changing leaf-conditions, and seasonally dependent extreme precipitation.

As vegetation phenology varies year to year, depending upon climate conditions (e.g. temperature, rainfall, and exposure to sunshine etc.) (Jochner & Menzel 2015) national phenology records (circa-2003 – 2016) (Woodland Trust 2018) were examined to estimate monthly blocks representing “leaf-on” and “leaf-off” canopy conditions. For all deciduous species examined in the records, the majority of entries (66.67%) identified April as the month for the beginning of leaf-growth, whilst 92% of records identified November as the month when trees became fully bare of leaves. As such, the “leaf-off” period was determined for the six-month period (November to April) when canopy interception for deciduous trees is assumed diminished or non-existent; the “leaf-on” period thus represents May to October.

3.6.3.5 Adapted SCS-CN method

Curve numbers for Water (including Dec_Water and Eve_Water; see **Figure 3.7**) were updated per precipitation scenario to ensure zero runoff was associated to these areas. In addition, curve numbers were amended for all Dec_ and Eve_ (with exception of Dec_Water and Eve_Water) surfaces to take account of canopy interception function, as follows:

1. Calculate reduced precipitation levels to understory layers:

$$P_r = \left[\frac{100 - Int_{Sp}}{100}\right] \cdot P \qquad \textbf{[3.1]}$$

Where P_r is the reduced understory precipitation (mm); P is the event precipitation; Int_{Sp} is the interception rate for the relevant species canopy condition.

2. For the understory layer, calculate the runoff volume (Q) for the understory layer using P_r as the input P using **Equations 2.3 and 2.4** (**Section 2.5.4**).

3. Calculate curve number values for the Dec_ or Eve_ composite hydrological classes by substituting both the Q value obtained from the step above, and the original event precipitation value for P to solve **Equations 2.3 and 2.4**. This was achieved from a process developed using R statistical programming language (see **Appendix 3.8** for code).

Curve numbers for all other hydrological surface classes remained static for all scenarios (see **Appendix 3.9** for all curve numbers). Hydrological surface layers were amalgamated per analysis cell to calculate weighted composite Curve Numbers for all precipitation scenarios (Whitford et al. 2001). Runoff per cell was calculated for each scenario. The total distribution of cell runoff values was then compared between scenarios, in order to assess how seasonal change in canopy conditions and precipitation events interact to affect seasonal change in stormwater storage services.

3.6.4 Combined ecosystem services

To assess the implications of seasonal analysis for planning purposes required combining seasonal indicator values into overall combined RES metrics. For temperature regulation, an overall year-round indicator was generated by weighting the relative importance of urban cooling between seasonal conditions using the following equation:

$$y = (w1 \cdot x1) + (w2 \cdot x2) \quad \textbf{[3.2]}$$

Where y is the combined temperature regulation indicator value; $w1$ is the weight value for February temperature regulation indicators; $x1$ represents February temperature regulation indicators; $w2$ is the weight value for July temperature regulation indicators; $x2$ represents July temperature regulation indicators. Ranges for predicted February and July LST were divided by the combined sum of ranges to obtain the relative weighting for each set of indicators. Combined temperature regulation indicators were re-scaled to 0-100% range.

Stormwater storage indicators were calculated as the percentage each cell reduces maximum scenario runoff, following the method described in **Chapter 2** (**Table 2.1; Section 2.5.4**). Final seasonal stormwater storage indicators are calculated from the 1 in 30 yearly probability control precipitation inputs. Probabilities for extreme precipitation are not assigned on a seasonal basis for national flood risk assessment, and thus 1 in 30 represents the event probability most likely to affect the study area during a yearly/seasonal cycle. Use of a single precipitation input also ensures seasonal indicators are calculated within a range defined by the same minimum and maximum runoff values. Combined stormwater storage indicators are simply the averaged seasonal value normalized within 0 – 100% range.

As temperature regulation and stormwater storage may alleviate negative environmental conditions at the neighbourhood scale, current RES demand indicators were re-weighted to consider demand in relation to influencing environmental factors. This was achieved for HAB_{POP} demand cells (where $HAB_{POP} > 0$) only, as this measure confines demand specifically to areas of resident habitation. Following previous studies into urban heat stress, demand indicators for temperature regulation RES were weighted by population exposure to seasonal extremes in local temperatures (Dousset et al. 2011,

Dugord et al. 2014, Laaidi et al. 2012, Weber et al. 2015). For the appropriate cells, mean February, and July cell LST were first converted to absolute values. For July demand indicators cells were re-ordered by descending absolute LST values. For February demand indicators, this process was repeated, albeit in order of ascending LST. For unique absolute LST values cells were re-ordered by descending HAB_{POP} value. Ranks were then assigned in this order (highest rank = cell with highest demand) to determine relative resident temperature regulation demand indicators for February and July conditions. Ranks per cell were then averaged and assigned a combined temperature regulation demand group value according to decile membership (e.g. 1 = lowest service demand, 10 = highest service demand).

Stormwater storage demand was weighted by population proximity to modelled urban surface flood risk areas (provided by the Environment Agency; EA 2018) (Jalayer et al. 2014, Kaźmierczak & Cavan 2011). This provided a general indication of where improvements in stormwater storage services may provide the greatest benefits in reducing resident exposure to flood risks. However, a limitation of this method remains the assumption that service function benefits transfer to local residents at the analysis cell scale. Given that surface runoff is transported by overland and underground (i.e. sewer) hydrological flows, stormwater storage services consumed in a particular location may be provided by GBI resources over a considerably larger network (Cuo et al. 2008, Dixon et al. 2012). Whilst the current cell-based demand measure is therefore a simplification of complex urban hydrological processes, the re-weighting of demand to flood risk was considered an improvement over the broader population based method used in **Chapter 2**.

As stormwater storage RES were estimated using a 1 in 30 annual precipitation event, surface stormwater storage demand was estimated using the 1 in 30 probability flooding extents from the Environment Agency data (**Figure 3.8**; EA 2018). Population proximity was calculated by generating spatial buffers in 100m intervals around each zone. The maximum buffer was set at 1000m as this ensured all habitation points resided in at least one interval buffer. Habitation points were then intersected to all buffer intervals and assigned an interval score according to least distance buffer membership (0 = point in flood area; 10 = point in 1000m buffer zone). Interval score values per analysis cell were summed within a matrix (columns = counts for each interval scores; rows = analysis cells). The matrix was re-ordered in descending order on a column by column basis, to rank each cell according to surface stormwater storage demand, for example, the highest ranked cell has

the largest counts for habitation points with interval score of 0. Final demand indicators were assigned a stormwater storage demand group value according to decile membership (e.g. 1 = lowest service demand, 10 = highest service demand).

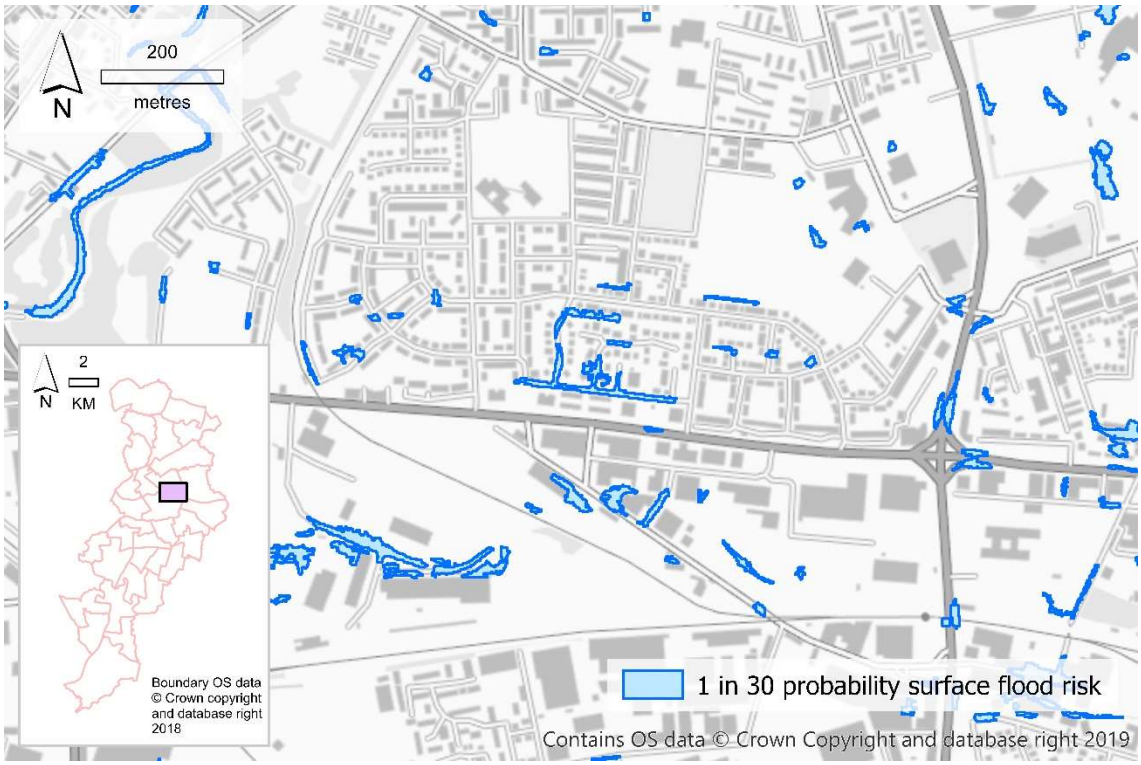

Figure 3.8 – Example 1 in 30 probability surface flood risk extents (EA 2018)

Combined RES function indicators were derived by averaging the rankings between temperature regulation and stormwater storage function indicators, and normalising within 0 – 100% range. This same process was applied to provide overall combined demand indicator values, which were then assigned a combined demand group value according to decile membership (e.g. 1 = lowest service demand, 10 = highest service demand). Relationships and differences in the patterns of final RES function and demand indicators were examined to assess trade-offs RES values. Coldspot analysis was also used to identify patterns in RES deprivation for temperature regulation, stormwater storage and combined ecosystem service values at both the analysis cell and administrative ward level. This information therefore provides usable information to inform further analysis, and potential GBI planning in the study area.

3.7 Results

3.7.1 Landcover classification

The overall accuracy of landcover classification was above 85% (see **Appendix 3.10** for error matrix), which indicates that the landcover information is usable for further analysis (Congalton & Green 2008). In addition, the kappa statistic 0.84 ($p < 0.05$) is significant providing strong indication that the level of interclass agreement is not due to chance (Viera & Garrett 2005). Individual class accuracies vary, however, and require further examination. User accuracy estimates the total percentage of class area that is correctly classified. All classes, with exception of Bare Earth (71.3%) and Evergreen (62.2%), are classified above the 85% threshold, with minimal class confusion to other classes. An estimated 55% of the total misclassified Bare Earth area is assigned to Grass. This may indicate difficulties in separating Bare Earth areas containing some degree of vegetation (i.e. patchy grass) thus resulting in spectral overlap between the respective classes. Evergreen misclassification is spread between Artificial, Deciduous and Shaded classes, indicating a large degree of spectral overlap with these classes.

In contrast, producer accuracy is the estimated percentage of total class areas assigned to other classes (Congalton & Green 2008), with estimates below 85% evident for all vegetation classes. Approximately 20%, 23% and 51% of actual Deciduous, Grass, and Evergreen areas respectively were predicted to belong to other classes in landcover data. This result is poor for Evergreen as a considerable percentage of this class area is hidden within other vegetation classes. Random Forest required more variables to classify deciduous/evergreen (n = 10 variables in comparison to a maximum of n = 5 variables for other routines), which indicates significant noise in variable data between the sample data for the two classes (Goldstein et al. 2011). This result was largely due to limitations in both numbers and quality of samples, and perhaps a lack of ideal variables to differentiate this class. Contiguous areas of evergreen vegetation are less prevalent in the imagery, and therefore it proved difficult to identify clean reference points to obtain a comparative sample distribution for this class.

Post-classification processing (**Section 3.6.1.5**) proved beneficial to correct errors where visually identified. During this process certain errors were easier to identify, such as class encroachment within coarse-scale homogenous areas e.g. deciduous and evergreen encroachment into grass areas such as playing fields, vegetation class encroachment in

waterbodies. In contrast, within heterogeneous canopy areas, identifying misclassification between deciduous and evergreen classes proved more difficult. Errors were also difficult to identify in some cases due to the resolution of the imagery, which prohibits the identification of many small features in the image. An example of the final landcover classification data is shown in **Figure 3.9**.

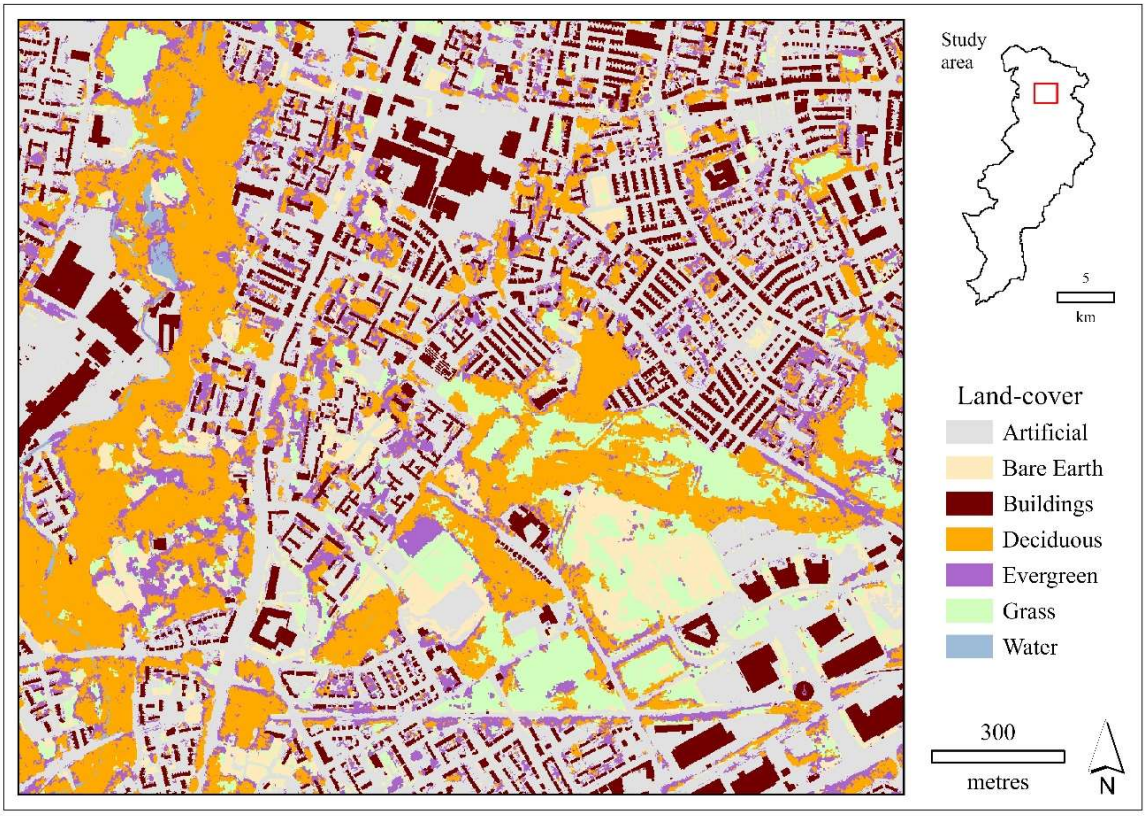

Figure 3.9 – Example of classified Landcover for an area of the city of Manchester

Figure 3.10 shows the proportion of the study area covered by each functional landcover (as determined for surface runoff estimation). Artificial surfaces make-up just over half of the study area with GBI cover estimated at 44.7%. Total functional tree canopy coverage (> 3m) is 14.9%, of which 20.8% is represented by evergreen trees. Shrubs are the largest GBI group representing 18.2%. Due to the resolution of imagery, some small patches of grass are likely to be contained within this class area. The distribution of GBI across the study area is shown in **Figure 3.11**.

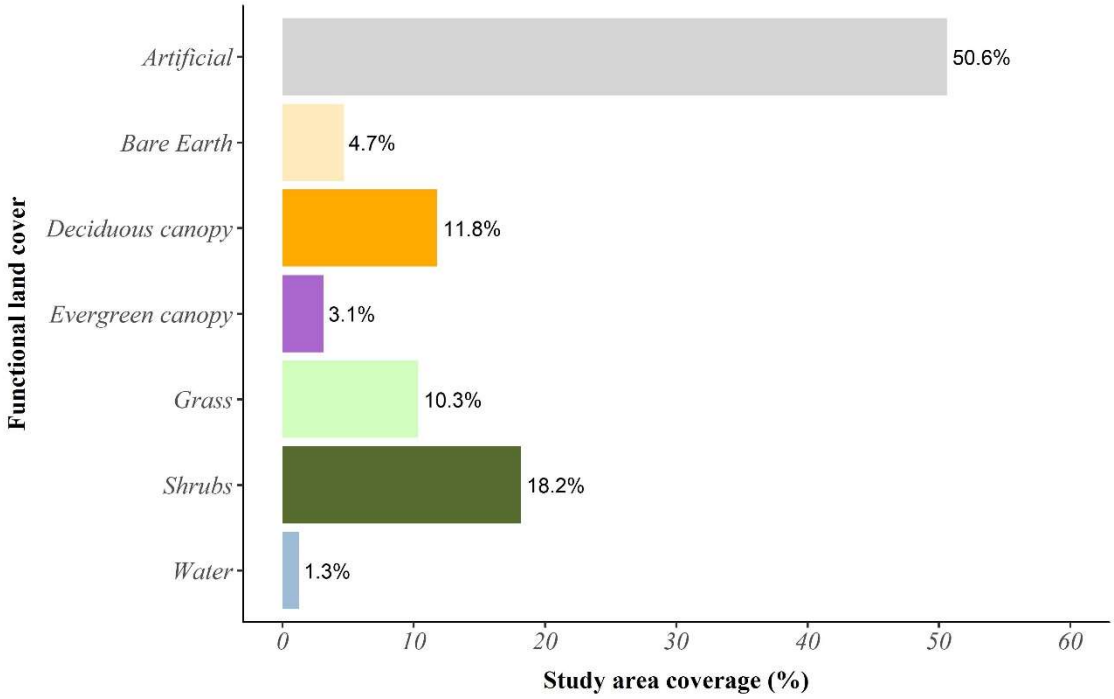

Figure 3.10 - Functional landcover coverage

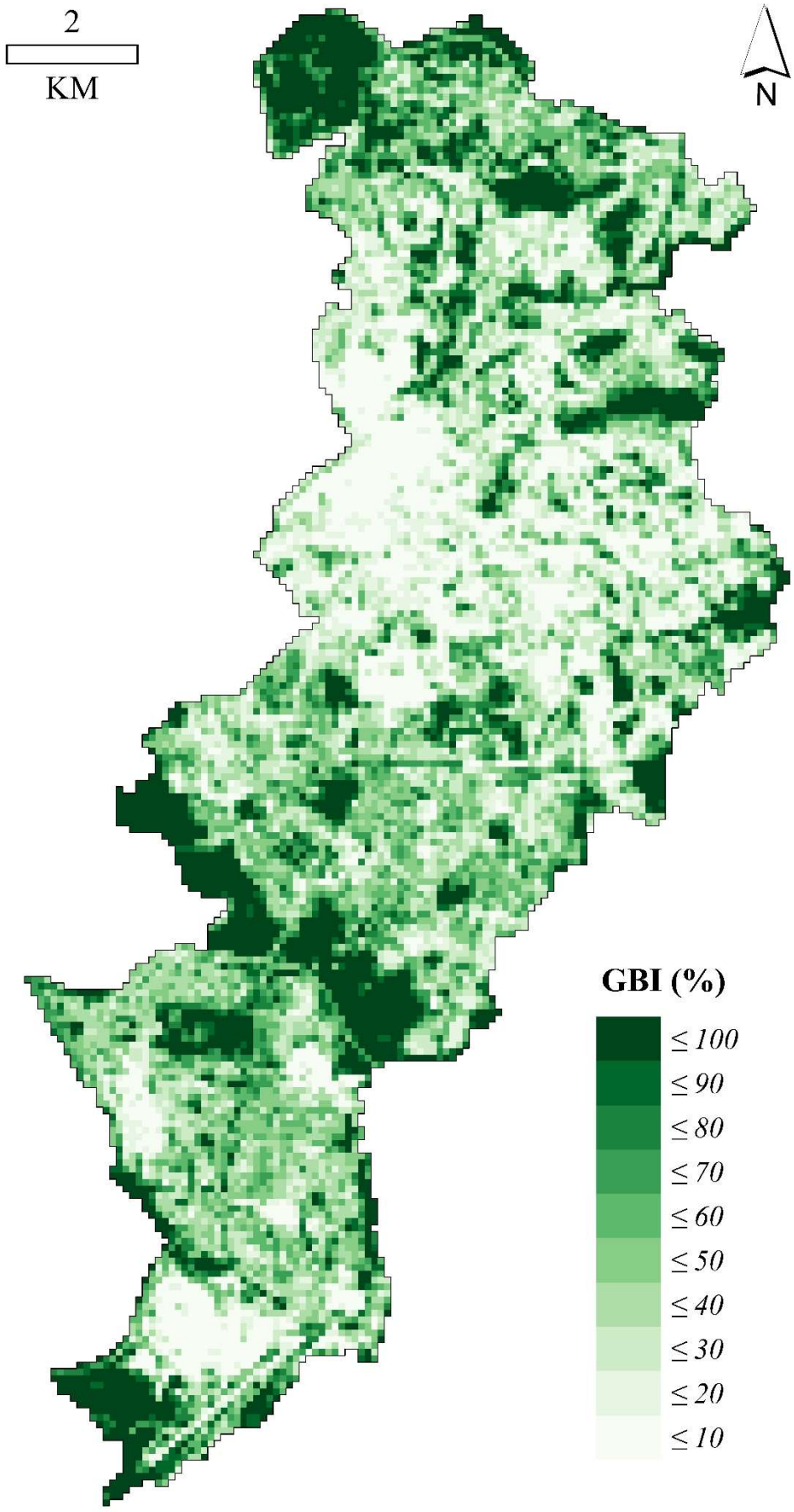

Figure 3.11 - Percentage GBI coverage within the city of Manchester

3.7.2 Seasonal dynamics in temperature regulation functions indicators

Ordinary least squares (OLS) regression indicates that GBI has a negative impact upon July LST values producing a final OLS model: y = 33.777 – 0.079x (where y is the predicted mean July LST value per cell; x the percentage of cell that is GBI). Bias in OLS coefficient estimates may be present due to spatial autocorrelation amongst model residuals. However, cross-validation, implemented to control for spatial error structure, confirmed stability in OLS coefficients irrespective of this issue (**Appendix 3.11**). The model trendline, with confidence and prediction intervals (95% confidence) is shown in **Figure 3.12**. Based on this model definition, an approximate 12.7% increase in cell GBI cover is required to reduce July LST by 1°C.

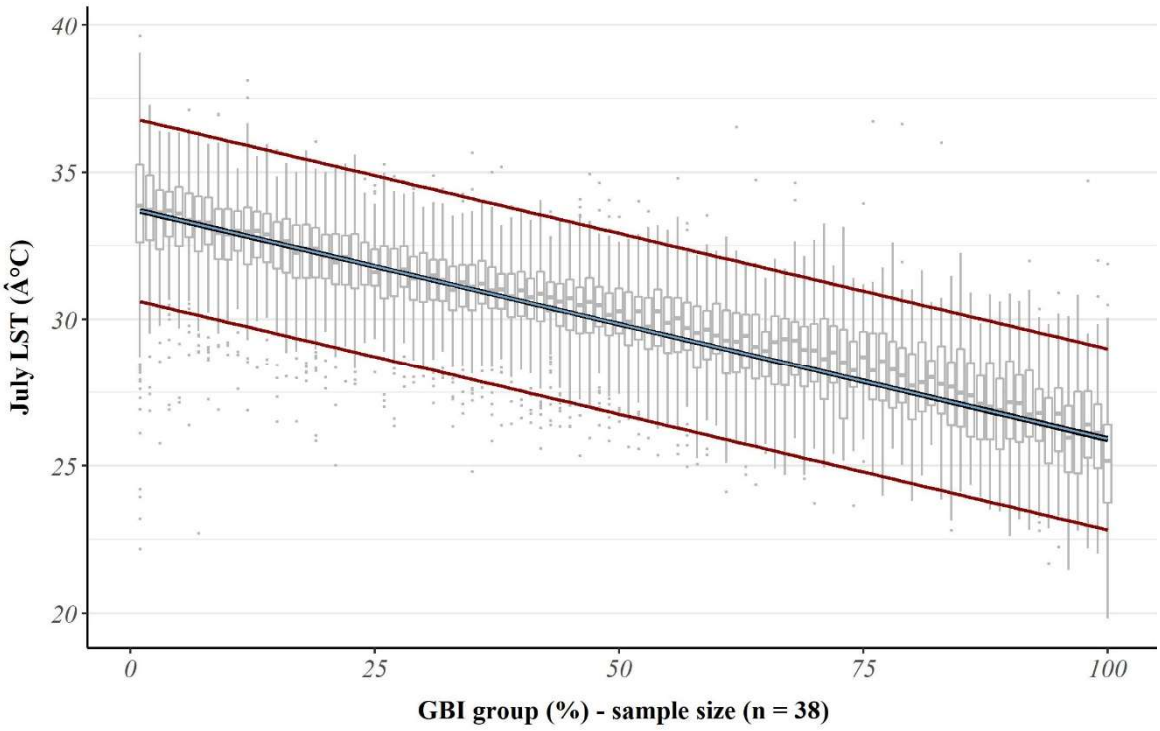

Figure 3.12 – Boxplot for green-blue infrastructure (GBI) percentile bands to July land surface temperature (LST)

Patterns in GBI to July LST are generally consistent for all landscape groups. **Figure 3.13** contrasts the trend between cell GBI and July LST for landscape uses against the trend predicted for the data as a whole. Public Recreation cells (n = 2015; 16.7% of total) are skewed towards higher levels of GBI cell coverage (**Figure 3.13A**). The trend between GBI and July LST is consistent with the trend identified for the data as a whole. However, some cells with < 50% GBI coverage, are positioned below the lower prediction (95% confidence)

interval. These cells are associated with the Sports city development east of the city centre, and contain the city of Manchester football stadium, along with other sporting venues and facilities. Despite low GBI coverage for these cells, the built infrastructure is quite distinct from other built up areas in the city and appears to absorb less solar radiation as a result. Non-recreational open space cells (n = 644; 5.4% of total) are also skewed towards high GBI levels (**Figure 3.13B**). However, cells below the lower prediction (95% confidence) interval are highly clustered at the extreme (> 90%) GBI coverage range. These cells are associated with large waterbodies, such as reservoirs and wetland lakes that are located throughout the study area and produce greater cooling functions than green-infrastructure resources.

GBI coverage is more evenly distributed within No Demand cells (n = 2655; 22.1% of total; **Figure 3.13C**). Trends between GBI and July LST are consistent with the main trend in the data. These cells contain a diverse array of built infrastructure and manmade landcover, with varying capacity to absorb and store solar radiation. Cells above and below the prediction lines are distributed relatively evenly across the GBI range. For demand cells (n = 6723; 55.4% of total), the trend between GBI and LST (**Figure 3.13D**) is more consistent with the main trend in the data than the previous landscape groups, with a minimal number of cells residing outside of the prediction intervals. This indicates that GBI is a relatively stable predictor of LST in cells where residents enjoy the benefits of warm weather temperature cooling.

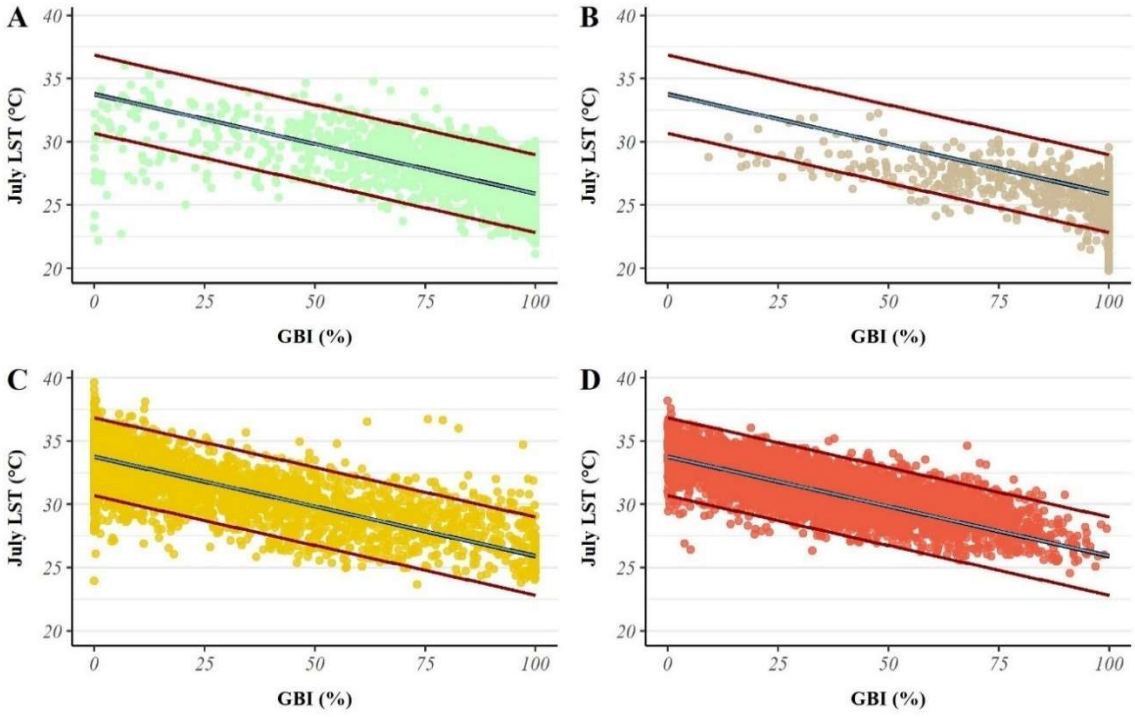

Figure 3.13 – Patterns in green-blue infrastructure (GBI) and July land surface temperature (LST) for Landscape cells

In comparison, a weaker negative relationship is evident between GBI and February LST (**Figure 3.14**). Due to a shortened time window to receive incoming solar radiation during the image date, land surface warming is lessened, which in turn limits the range in absolute LST values. The impact of GBI on cold weather LST thus had limited variation across the study area, with the exception of some outlier cell values (*n = 136* where February LST < 7.53°C). As the results of the OLS models indicate (**Table 3.3**), the removal of non-transpiring vegetation from GBI measure fails to improve prediction of February LST. Deciduous and Evergreen vegetation thus combine with water to negatively impact February LST. The GBI model performs the better out of the two OLS models, predicting a total of 0.8°C LST reduction in February LST when increasing cell GBI coverage from 0 to 100%. Whilst auto-correlation was present in OLS model residuals, cross-validation implemented to control for spatial error structure, confirmed stability in OLS coefficients (**Appendix 3.11**).

Table 3.3 – Ordinary least square results for February LST

Variable	*r **	*OLS Model call ***	*RSE****	R^2
All green-blue infrastructure	-0.387	pLST = 9.876 – 0.008pGB	0.609	0.151
Evergreen, Grass and Water	-0.187	pLST = 9.641 – 0.006pGB	0.641	0.036

* = *r* coefficients significant at ($p < 0.001$); ** = all model coefficients significant ($p < 0.001$); *** = Residual Standard error

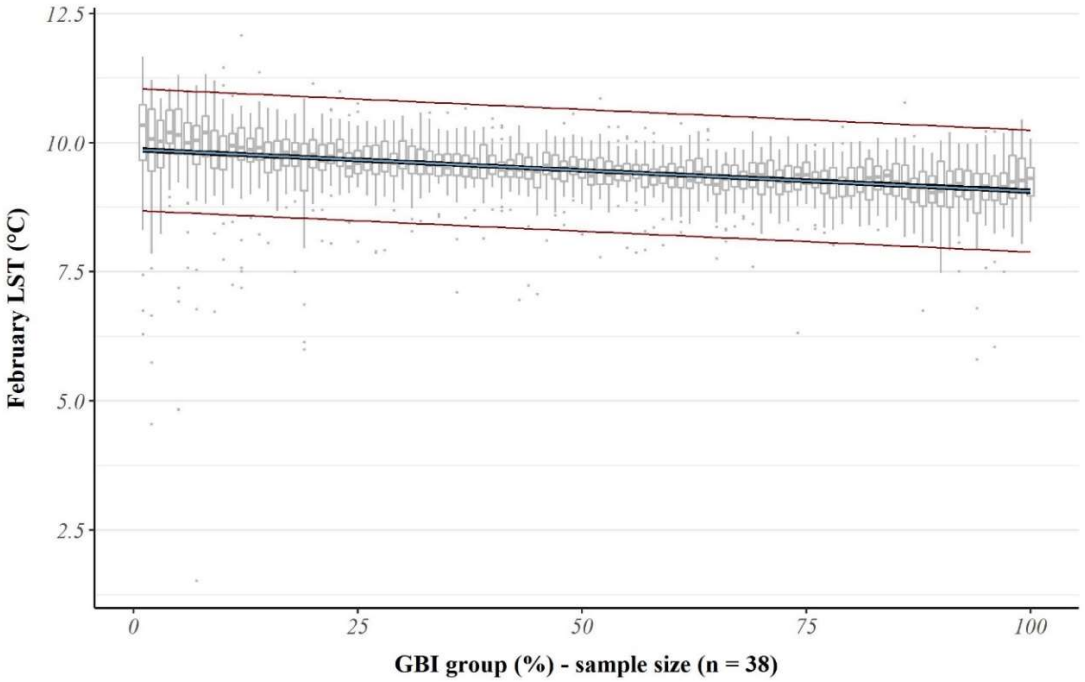

Figure 3.14 – Boxplot for green-blue infrastructure (GBI) percentile bands to February land surface temperature (LST)

Patterns in GBI to February LST for landscape groups (**Figures 3.15**) are generally consistent with patterns exhibited in the landscape groups for GBI to July LST. Notably, Public recreation cells (< 50% GBI) below the lower prediction interval deviate further from the main trend than July LST model values (**Figure 3.15A**). The cooling effect on February LST is therefore greater for a small number of cells, which are again largely associated to the built infrastructure of stadium facilities. For non-recreational open space, cells below the lower prediction interval cluster at the far range of cell GBI coverage, and are again associated with large waterbodies (**Figure 3.15B**). For the no-demand landscape group, patterns in GBI to February LST are generally consistent with the main OLS trend, although variability is evident for cells with minimal (< 5%) GBI coverage (**Figure 3.15C**). This suggests that extremely low LST values, where cool weather temperature stressors may be more prevalent, are associated to a number of areas with predominantly non-GBI landcover. In comparison the demand landscape group, whilst exhibiting some outliers from the main GBI to February LST trend, is highly consistent in relation to the main GBI to February LST trend.

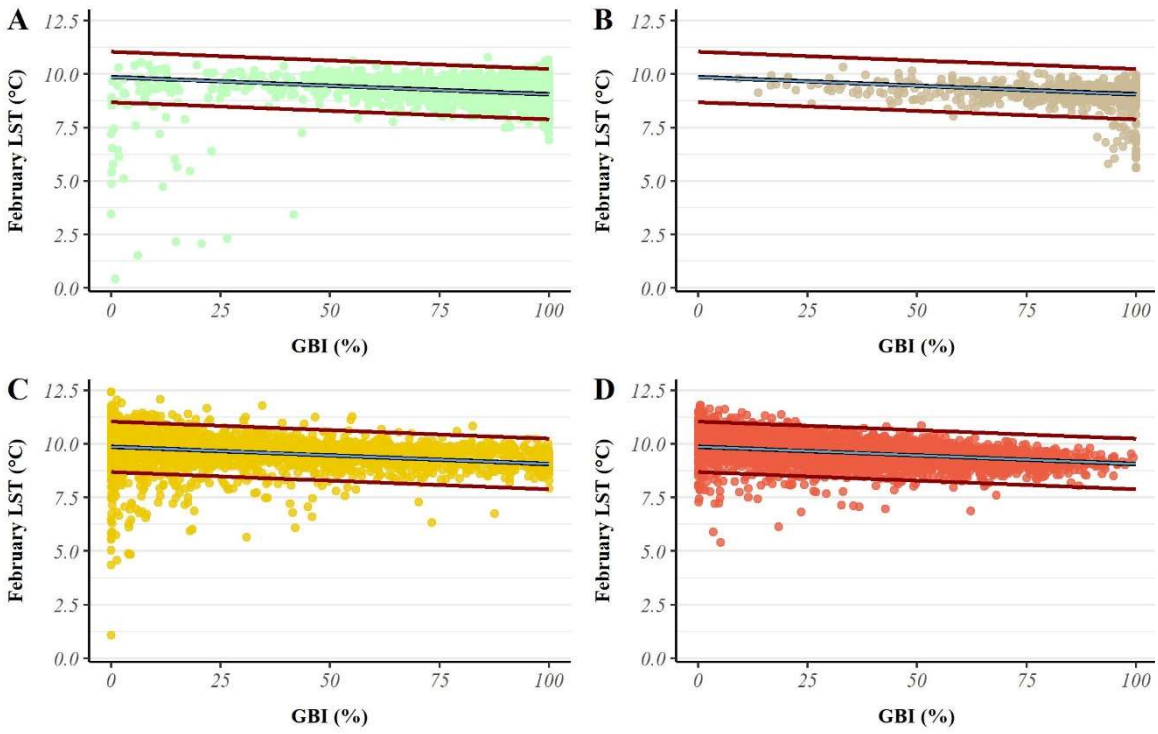

Figure 3.15 – Patterns in green-blue infrastructure (GBI) and February land surface temperature (LST) for Landscape cells

For final temperature regulation indicators, GWR improved prediction of July LST and was used to calculate warm weather temperature regulation indicators. In comparison the OLS model outperformed the GWR for February LST, and was used to calculate cool weather temperature regulation indicators (see **Appendix 3.11** for model comparisons). Modelled LST cooling for July LST, ranges up to 12.2°C, whilst predicted cooling for February LST ranges up to 0.8°C. As such, the magnitude of GBI February cooling disservices, when considering the combined range of total potential year round cooling, is just 6.2% (0.8°C/(0.8°C + 12.2°C)). This range comparison updated **equation 3.2** (see **section 3.6.4**):

$$y = (0.062 \cdot x1) + (0.938 \cdot x2) \quad \textbf{[3.2]}$$

The method thus provides a small adjustment of overall temperature regulation benefits GBI according to limited amount of negative GBI cooling during cool weather seasons. The management of both positive and negative effects of urban cooling will vary therefore this metric also aggregates important dynamics in this relationship. The implications of this planning of GBI and RES are discussed further in **Section 3.8**.

3.7.3 Seasonal dynamics in stormwater storage functions

The effect of increasing input precipitation levels (**Table 3.4**) into the adapted SCS-CN number model resulted in an increased clustering of indicator values towards lower values for all canopy conditions. The model thus replicates the overloading of GBI interception, and infiltration functions, due to increasing precipitation volumes. **Figures 3.16 and 3.17** demonstrate this effect by comparing cell surface runoff between “leaf-on” and “leaf-off” conditions for control period (1961-1990 baseline) input values. The difference in cell surface runoff between “leaf-on” and “leaf-off” conditions grows as precipitation levels increase. Maximum increase in surface runoff is 2.4mm, 4.4mm and 7.1mm for the 1 in 30, 1 in 100 and 1 in 1000 yearly event probability respectively. As precipitation increases, and runoff distribution ranges increase for both leaf-on and leaf-off conditions, stormwater storage functions become more variable across the study area. Differences remain minimal for some cells, as surface runoff is contained to under 1mm for over 75% of cells, irrespective of precipitation input for the SCS-CN model (USDA 1986).

However, these results suggest that loss of deciduous canopies becomes an increasing concern for a small proportion of the study area, as reduced interception functionality compounds with increasingly severe precipitation loads.

Table 3.4 – Precipitation input levels for the SCS-CN model (USDA 1986)

Yearly event probability	***Percentile threshold (%)***	***Precipitation level (mm)***		
		Control period (year)	***Leaf-off (November to April)***	***Leaf-on (May to October)***
1 in 30	96.7	14.5	14.4	14.7
1 in 100	99.0	21.7	20.9	22.5
1 in 1000	99.9	37.5	34.6	39.7
Daily average		*2.7*	*2.8*	*2.6*

Note: November to April (Leaf-off); May to October (Leaf-on)

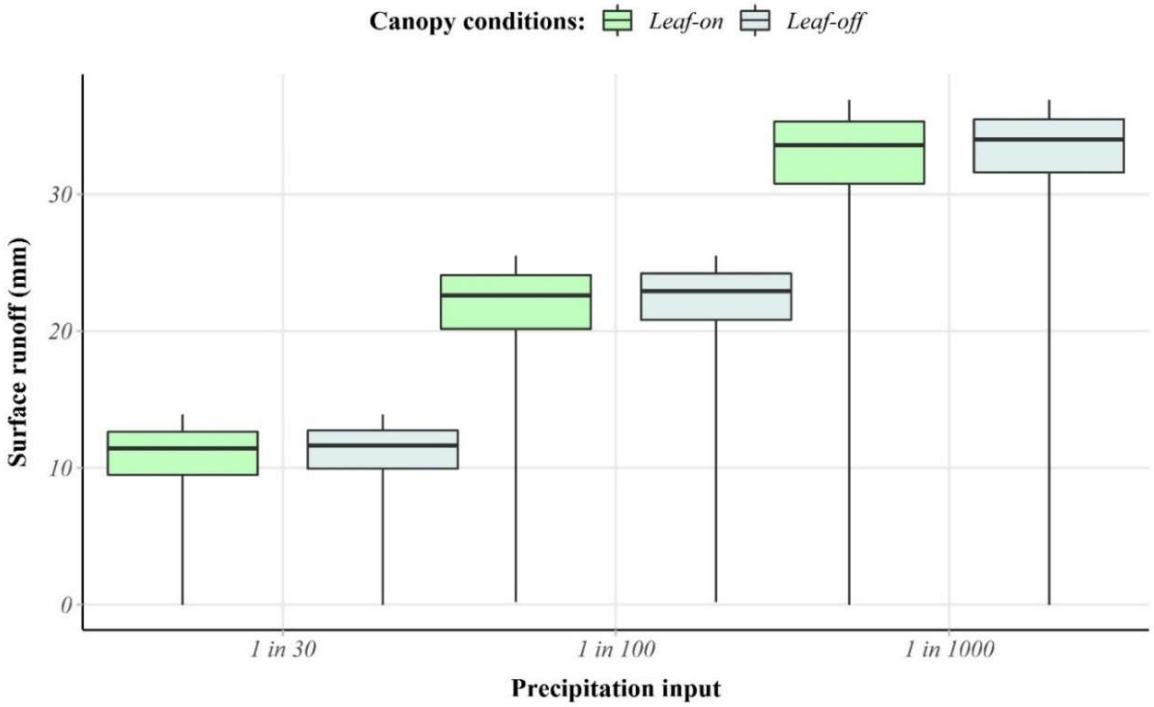

Figure 3.16 – Boxplots of cell surface runoff values for all control precipitation inputs

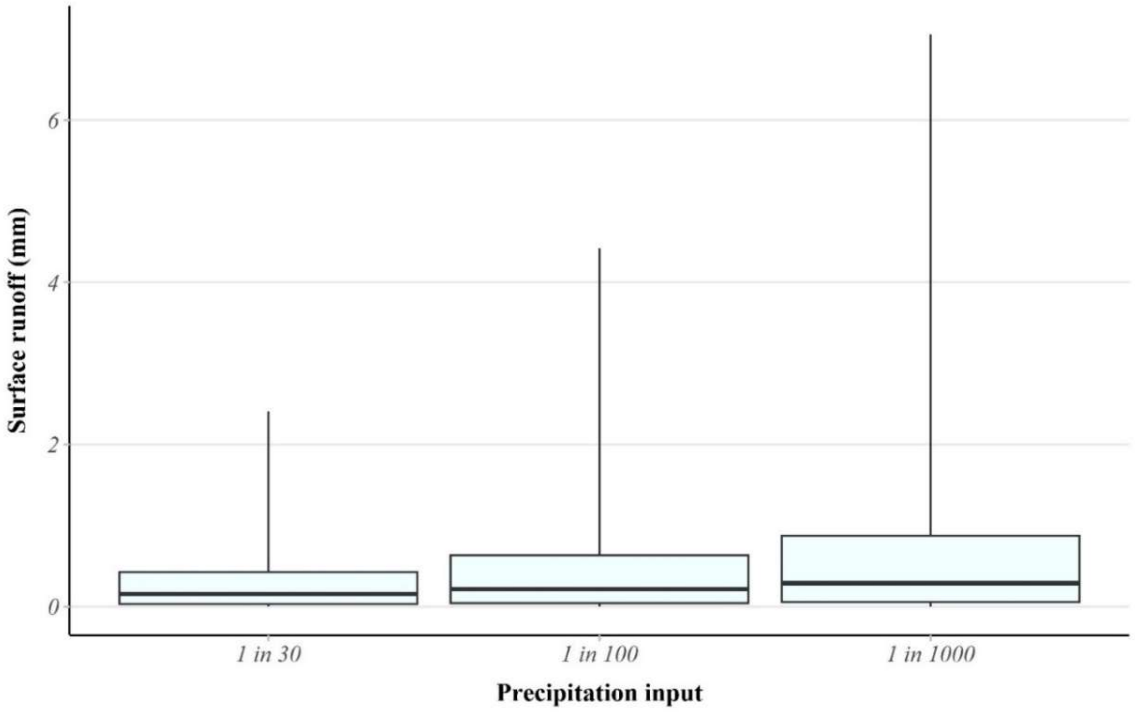

Figure 3.17 - Difference between Leaf-off and Leaf-on conditions in surface runoff for control precipitation inputs

In comparison, differences in surface runoff for seasonally adjusted ("Leaf-on" and "Leaf-off") precipitation events exhibit a different pattern (**Figures 3.18 and 3.19**). As predicted extreme precipitation levels are lower for the "leaf-off" period, the negative impact of leaf-loss for reducing surface runoff is largely reversed. Differences in runoff between seasonal 1 in 30 probability events are minimal due to a minor increase in input precipitation of 0.3mm. For 1 in 100, and 1 in 1000 season events, reduced input precipitation for the leaf-loss period results in reduced surface runoff respectively of over 2 mm, and 4 mm, for the majority of cells. When considering seasonal dynamics in changing canopies and predicted precipitation events, the impact of leaf-loss appears to have minimum impact within the study area. However, as demonstrated for the control precipitation inputs, ranges in distribution values increase with increasing precipitation levels, thus demonstrating that stormwater storage functions become more variable as precipitation events increase in severity.

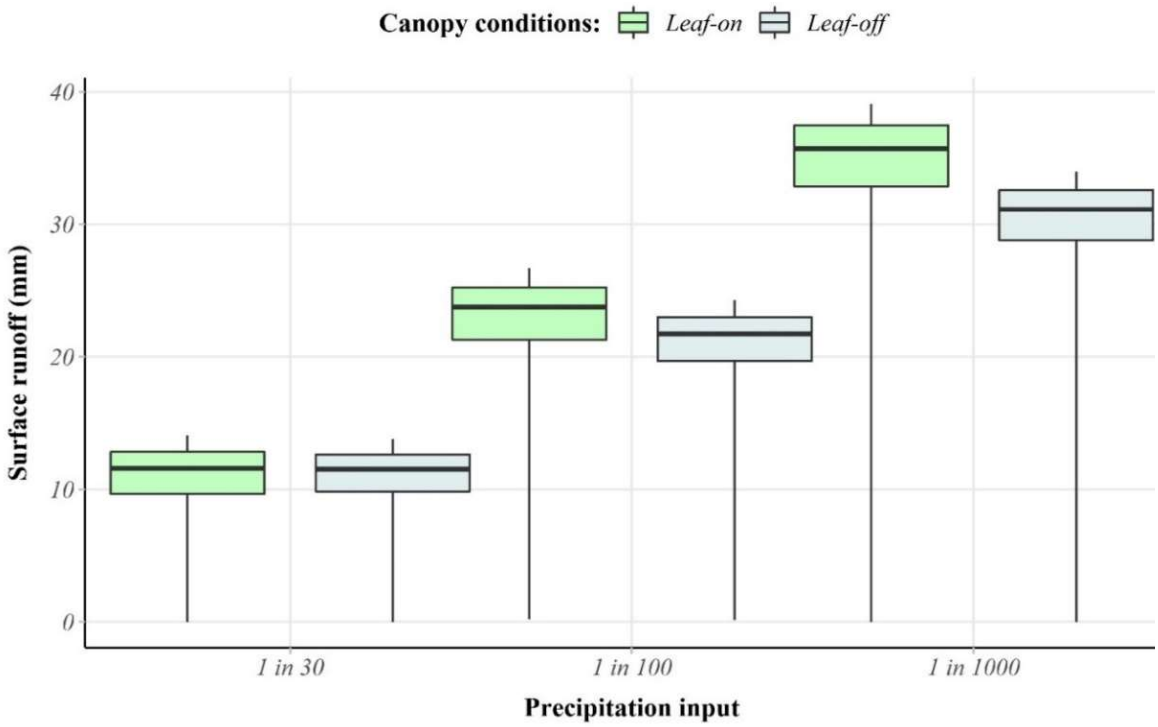

Figure 3.18 – Boxplot of cell surface runoff values for control precipitation inputs

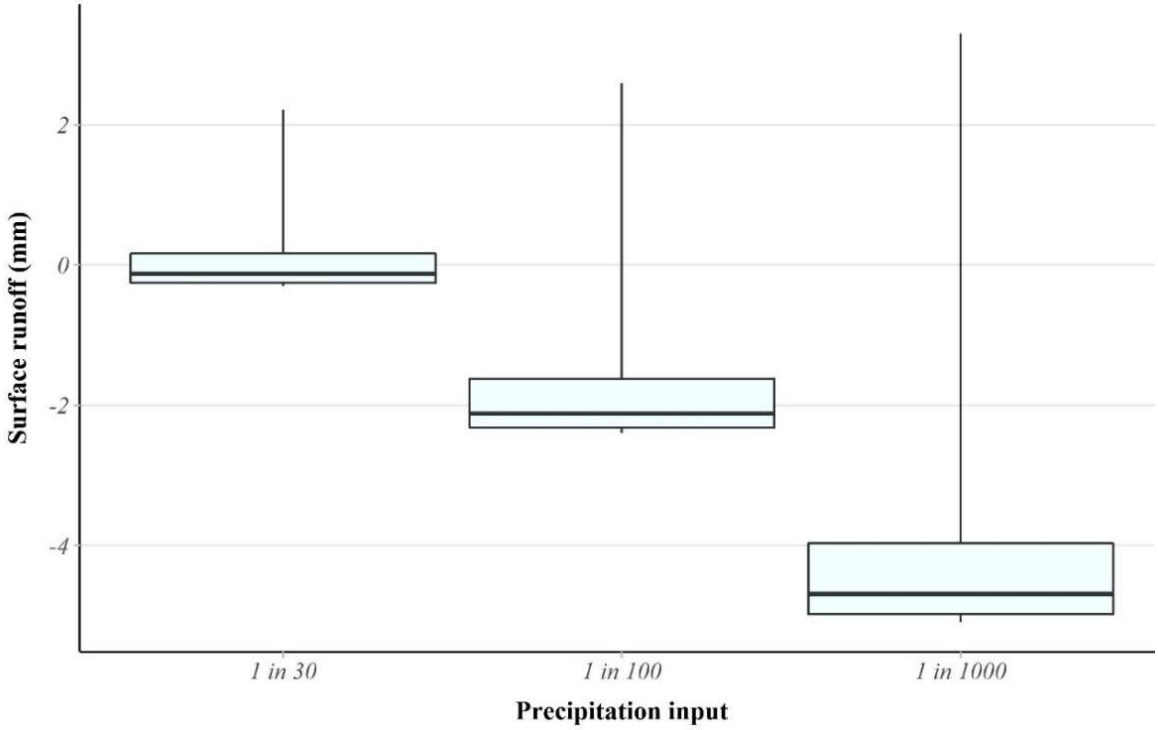

Figure 3.19 - Difference between Leaf-off and Leaf-on conditions in surface runoff for seasonal precipitation inputs

Differences in surface runoff vary considerably between landscape groups. For control precipitation inputs the distribution of surface runoff differences are generally larger for the Public Recreation and Non-recreational Open Space landscape groups (**Figure 3.20**). This is expected given that GBI, and thus deciduous tree canopies, are generally more prevalent in these landscape group cells than the more urbanised No Demand and Demand landscape groups. For example, average deciduous tree cover is 14.8% and 14.4% for Public Recreation and Non-recreational Open Space respectively, which compares favourably to 4.5% and 3.8% respectively for Demand and No Demand landscape group cells. However, in comparison to differences in the interquartile ranges between distributions, differences in overall distribution ranges are less pronounced between landscape groups. This is due to high deciduous tree canopy cover (e.g. > 40%) in a number of No Demand and Demand landscape group cells.

However, irrespective of landscape group, seasonal differences in stormwater storage functions will become increasingly variable as precipitation levels increase. This same pattern is also evident for seasonal precipitation inputs (**Figure 3.21**), as higher precipitation levels for leaf-on conditions, result in increased distribution and range of surface runoff values. Increased runoff levels during leaf-on events are more pronounced for No Demand and Demand landscape groups, due to relatively low GBI coverage in these associated cells. As such stormwater storage services are higher for Public recreation and Non-recreational open space cells. Combined seasonal stormwater storage indicators are based upon surface runoff values for the control 1 in 30 precipitation input. The average runoff for leaf-on and leaf-off conditions for this input are lower for Public recreation and Non-recreational open-space cells with 8.1mm and 8.4mm respectively, when compared to 12.3mm and 11.9mm respectively for No Demand and Demand cells.

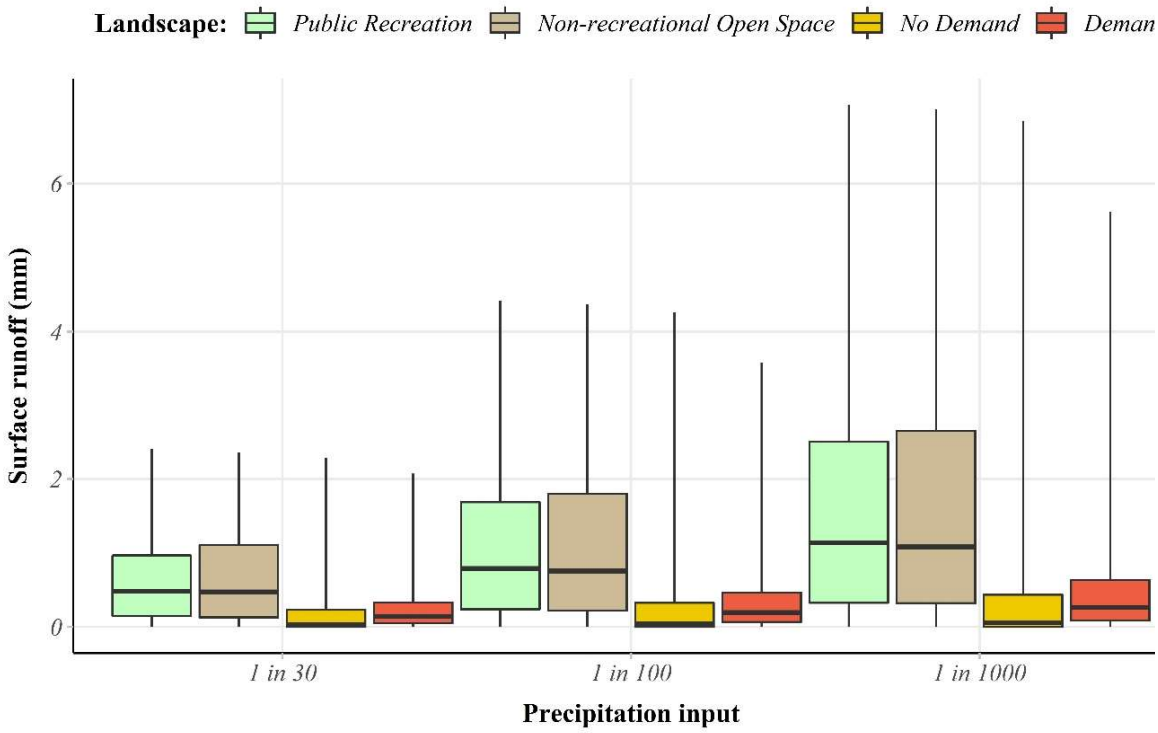

Figure 3.20 – Difference between Leaf-off and Leaf-on conditions per landscape group for control precipitation inputs

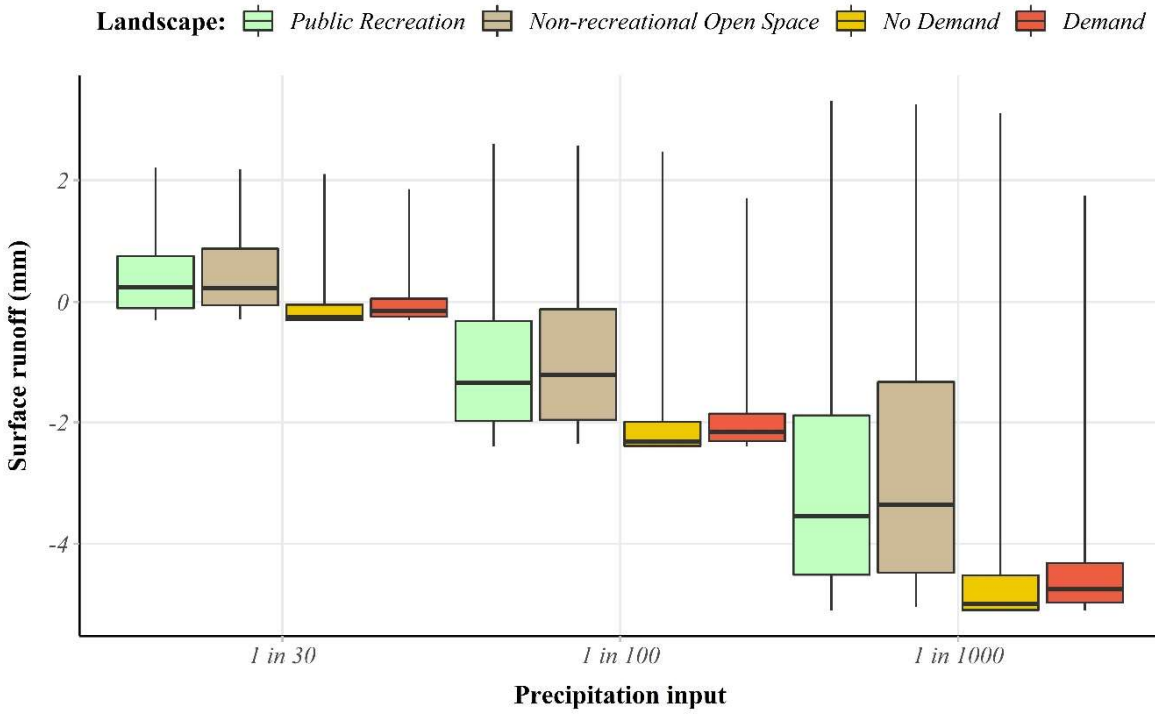

Figure 3.21 – Difference between Leaf-off and Leaf-on conditions per landscape group for seasonal precipitation inputs

Due to design of the SCS-CN model, the impact of varying seasonal interception rates on calculated runoff will vary by associated soil type, with loss of interception worse for less porous soils. This additional factor is of limited concern however, as 92.5% of the study area is covered by SCS-CN soil type D. For cells with stormwater storage demand values, less than 1% are solely associated to a different SCS-CN soil type. In relation to stormwater storage service demand, no distinguishable pattern in surface runoff differences exists between stormwater storage demand groups (see **Figures 3.22 and 3.23**).

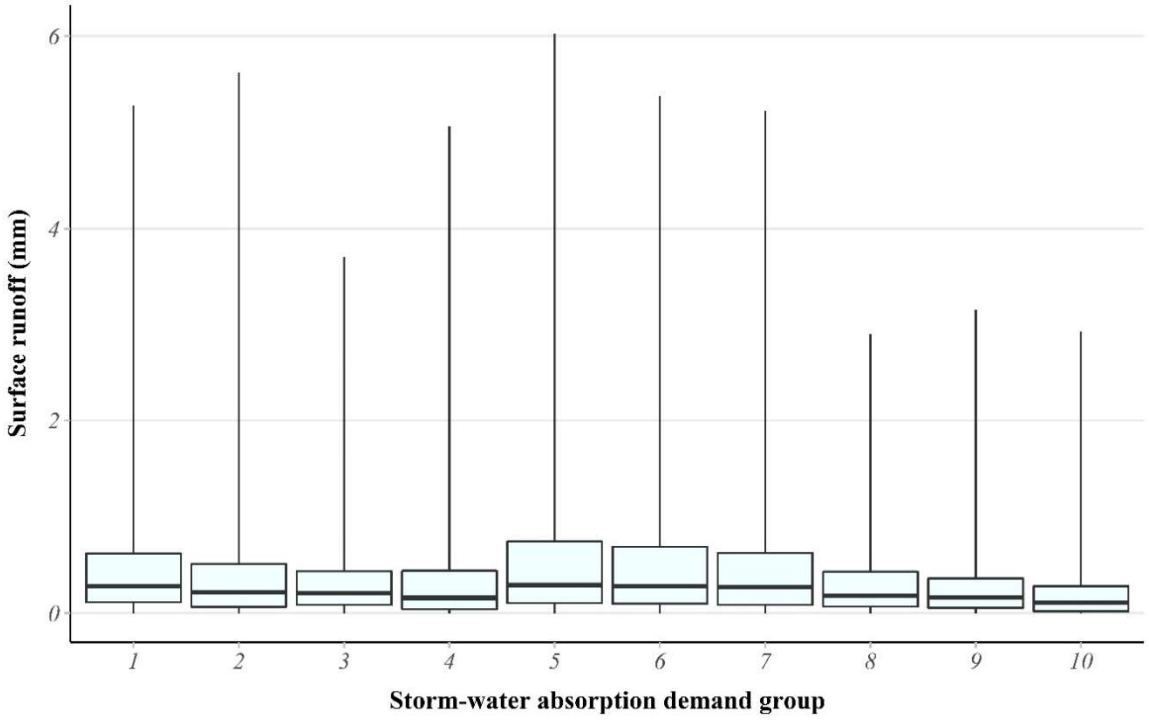

Figure 3.22 – Difference in surface runoff (1 in 30 control precipitation input) per stormwater storage demand group

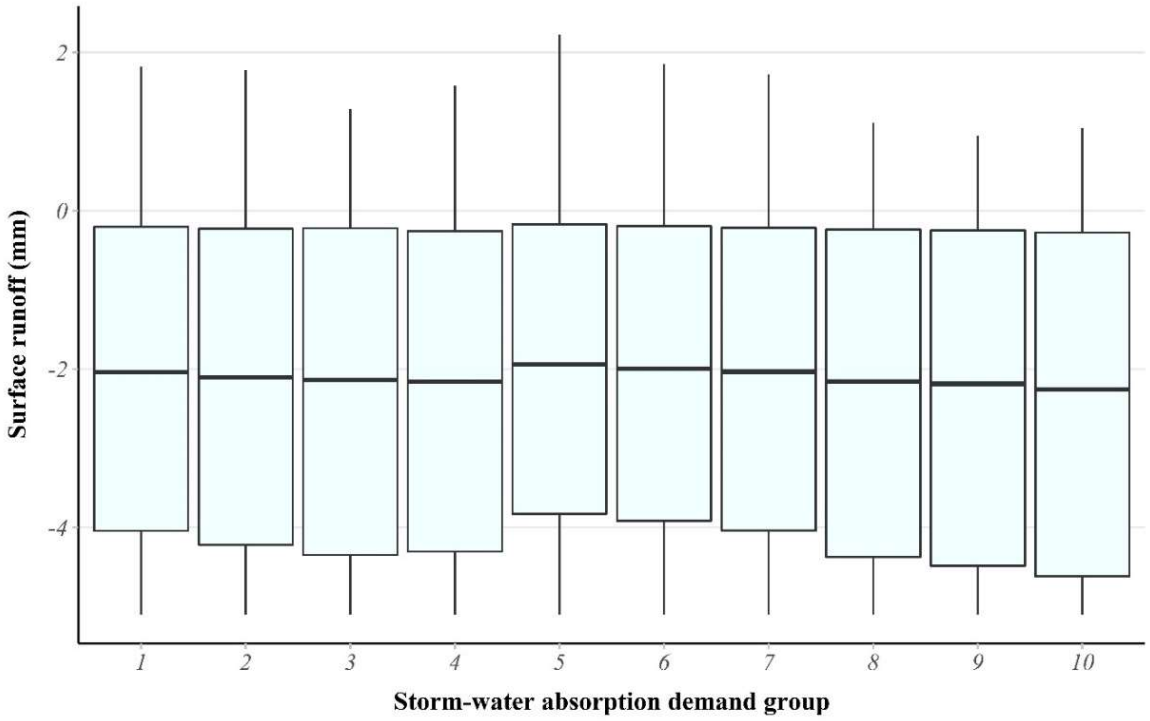

Figure 3.23 – Difference in surface runoff (1 in 30 seasonal precipitation input) per stormwater storage demand group

3.7.4 Comparing ecosystem services

Positive associations exist between both services, as confirmed by correlation analysis ($r = 0.91$; $p < 0.001$). As evident, spatial patterns between RES levels are generally consistent, however, dynamism occurs in this relationship due to variation in localised functions for both RES **(Figure 3.24)**. Stormwater storage functions of GBI, as estimated by the SCS-CN model, are generally consistent with variation in GBI proportions across the study area. In comparison temperature regulation functions are modified at the local level through the interaction of cooling benefits of varying components of both GBI and built infrastructure. As different RES models produce different indicator distributions, comparing RES indicator values directly with one another is difficult without prior consideration of the relative importance of each RES. However, visualisation of differences in raw indicator values between RES **(Figure 3.25)** provides a general guide of where extremities in trade-offs between RES functions occur within the study area.

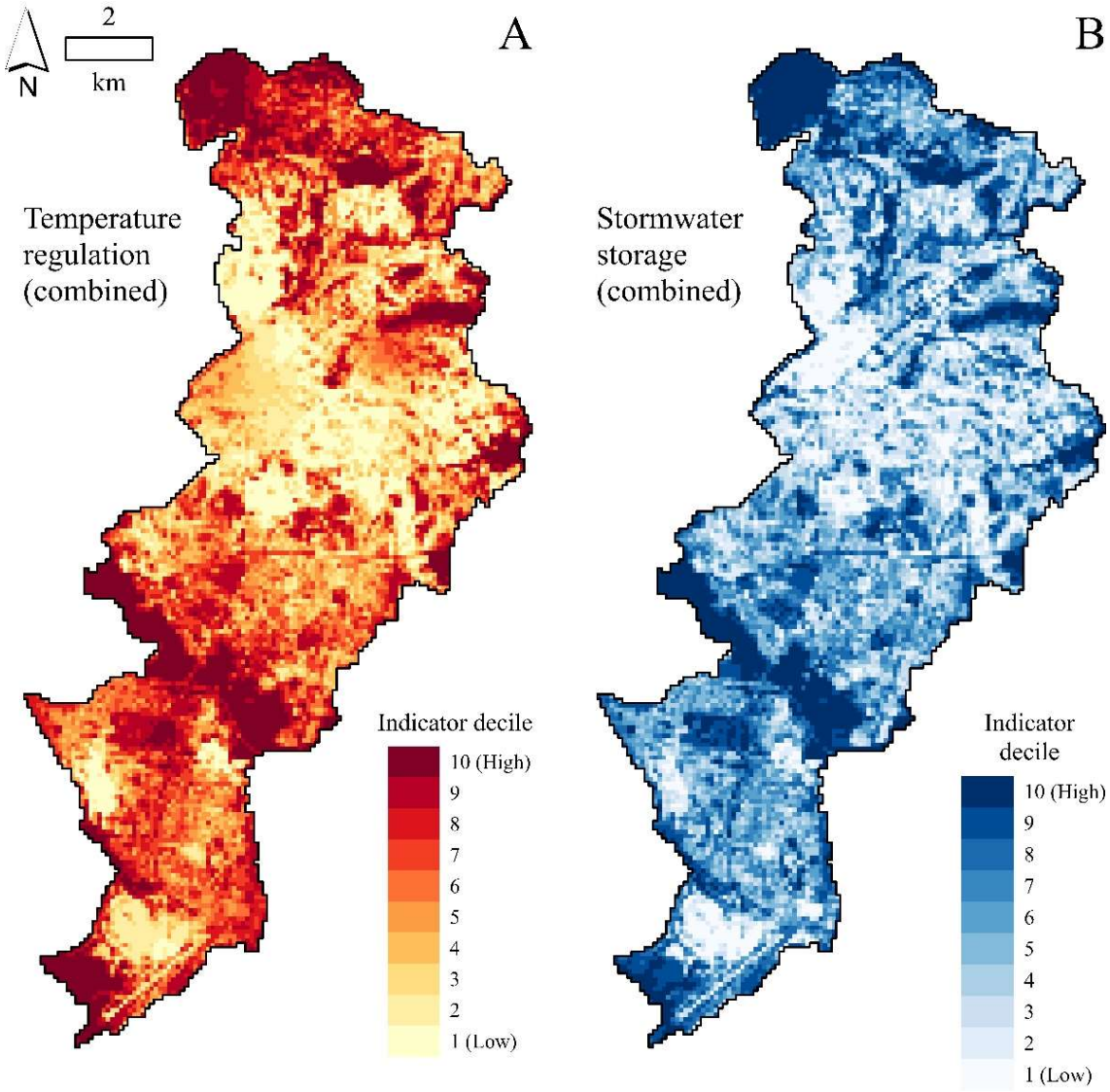

Figure 3.24 –Temperature Regulation (**A**) and Stormwater storage (**B**) function indicator decile values

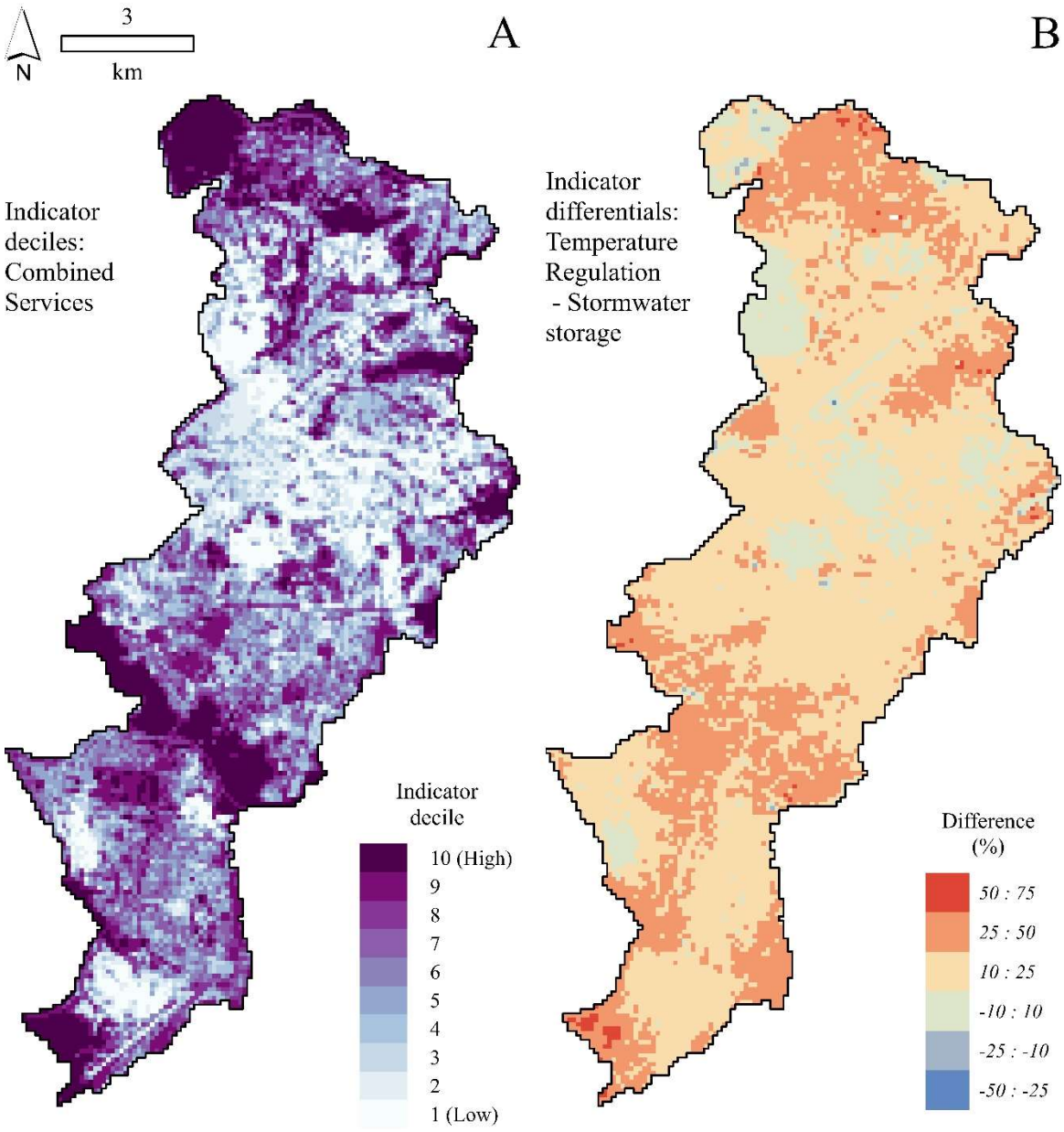

Figure 3.25 – Combined ecosystem service indicator decile values (**A**) and service indicator differentials (**B**)

While there are positive associations between RES function indicators, no distinguishable pattern exists between RES demand indicators (**Figure 3.26),** as strong positive association between RES function indicator deciles contrasts with the seemingly random pattern between demand groups. Spatial extents for environmental heat and flood hazards vary. Local flooding risks are evident according to topographical depressions (EA 2018). In contrast, topography has minimal influence on the degree of local urban warming, which is driven by morphological characteristics of the urban environment (Stewart & Oke 2012).

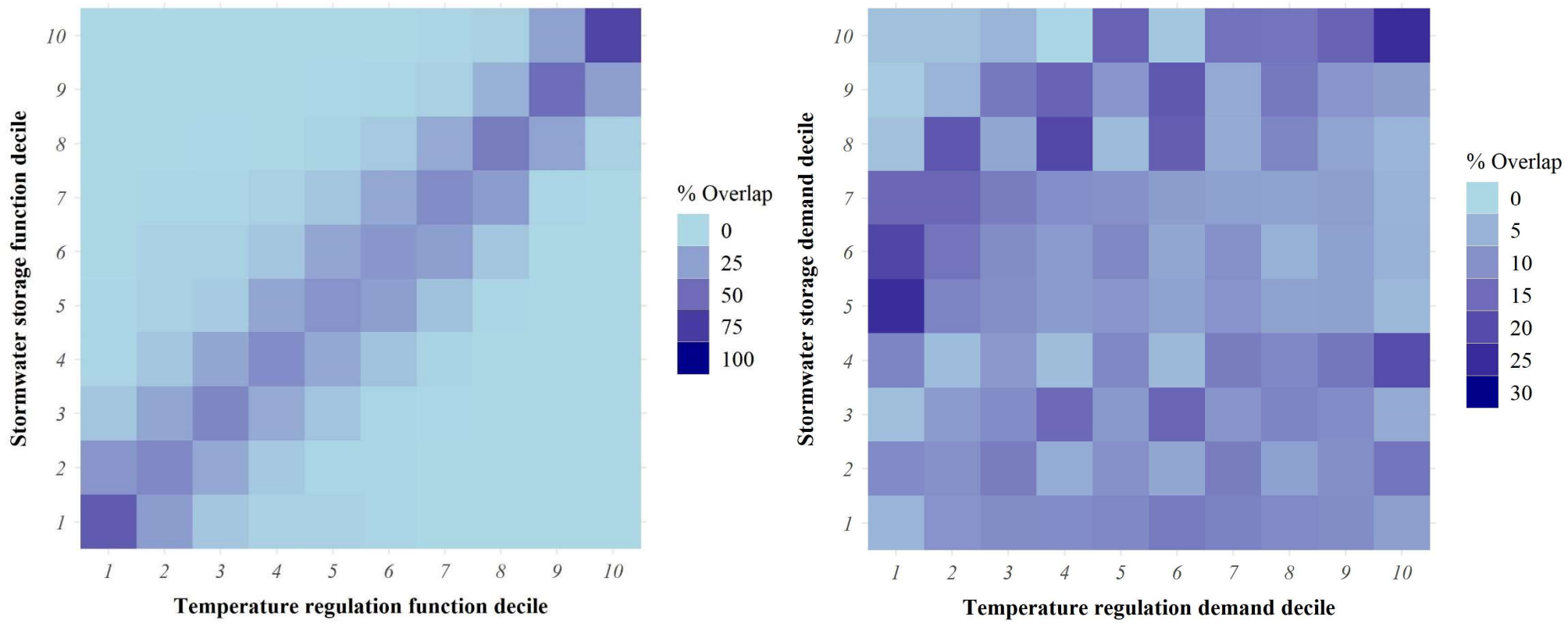

A **B**

Figure 3.26 – Heatmap plots for Stormwater storage and Temperature Regulation function indicator (**A**) and demand deciles (**B**)

RES deprivation, or Coldspot (10% lowest RES per within demand areas; see **Section 2.5.6**) analysis for temperature regulation, stormwater storage, and combined RES demonstrates this dynamism across the study area (**Figure 3.27**). For temperature regulation, coldspots are mainly associated with high demand for LST, whereas the level of demand for stormwater storage coldspots varies considerably. The effect of omitting seasonal metrics on deprivation measures was examined by comparing coldspots calculated using only leaf-on RES function and demand indicators to the aforementioned coldspots from combined seasonal indicators. A total of 95.4%, 97.4% and 95.4% of coldspot cells were identified as such for temperature regulation, stormwater storage and combined services, irrespective of method employed. This indicates that the inclusion of seasonal indicators has a minor effect upon identifying overall RES deprivation, when compared to temporally static indicators used in other ecosystem service studies.

Variation in RES deprivation is also visualised at administrative ward level, as levels of RES deprivation vary according to the RES under consideration (**Figure 3.28**). This is particularly evident for Deansgate ward (city centre) which exhibit relatively high levels of stormwater storage deprivation but exhibits limited deprivation in temperature regulation services. Whilst this area exhibits low GBI levels, the built infrastructure represents the urban core (e.g. high-rise office, retail and residential buildings) and is relatively distinct to other areas of the city. GBI reduction of high temperatures thus benefits from the cooling influence of surrounding buildings (see **Section 3.8.1** for further discussion). In contrast, combined RES deprivation is more evident in wards that generally surround the city centre, and areas represented by comparatively lower rise development.

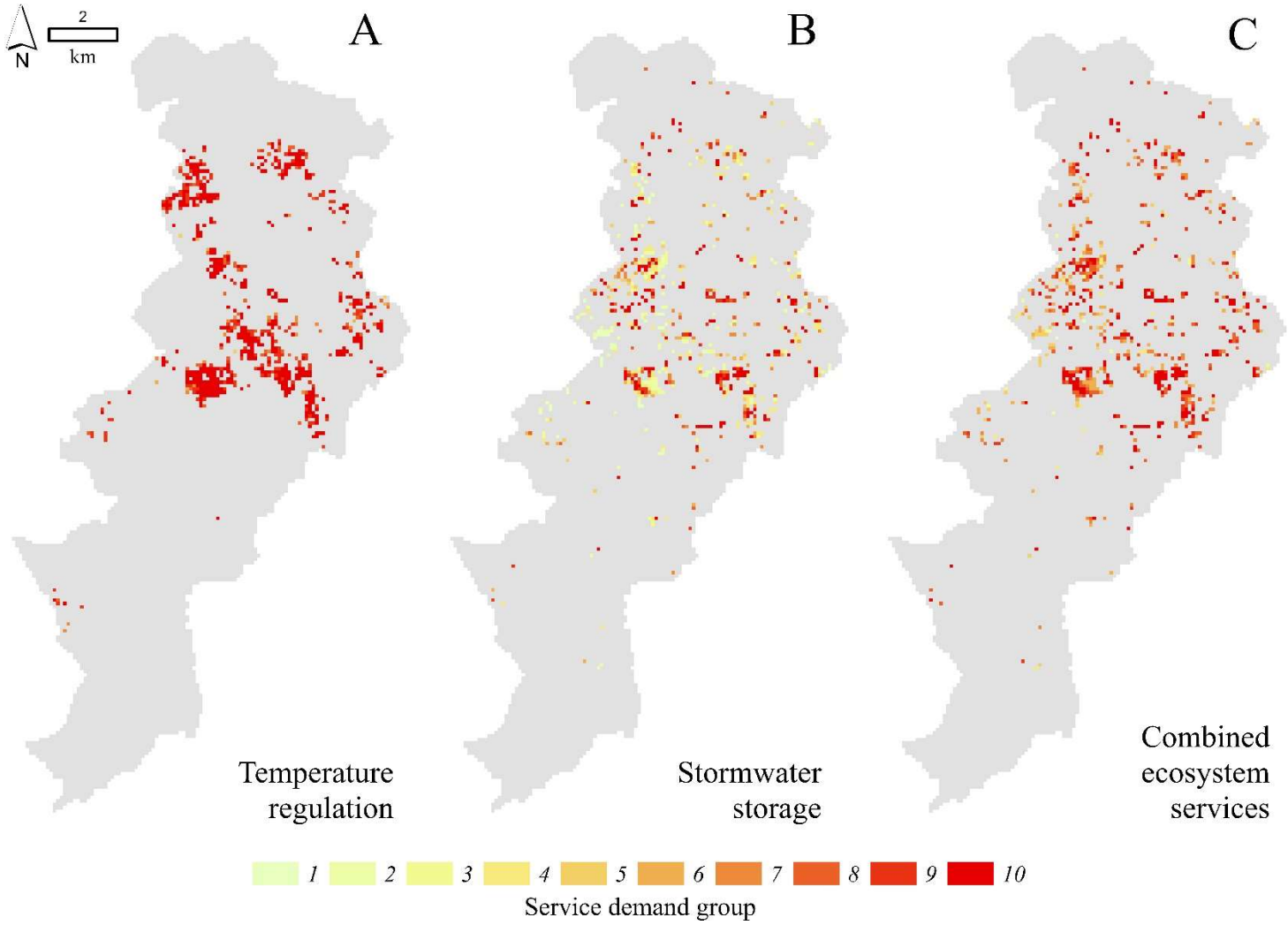

Figure 3.27 – Coldspots for Temperature Regulation (**A**), Stormwater storage (**B**) and Combined Ecosystem services (**C**)

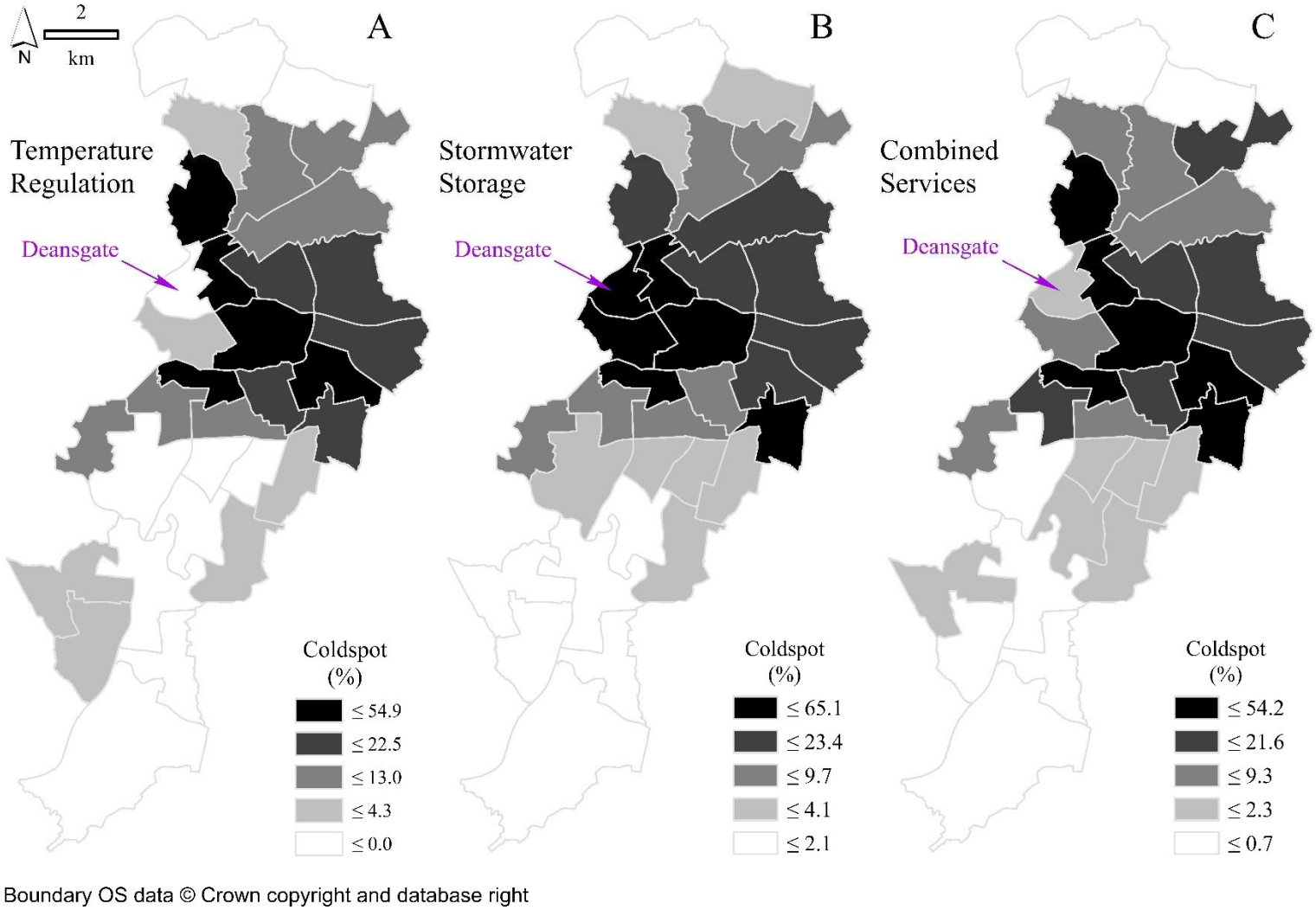

Figure 3.28 - Coldspots (%) per Manchester ward for Temperature Regulation (**A**), Stormwater storage (**B**) & Combined Services (**C**)

3.8 Discussion

3.8.1 Seasonal variation in temperature regulation services

In relation to temperature regulation services, this study found that GBI reduction of land surface temperature (LST) is evident for both warm and cool temperature (i.e. seasonal) conditions. Evidence suggests the magnitude of this ecosystem disservice, a total 0.8°C of potential cool weather LST cooling for example, is likely to have minimal impact (< 1°C) on above-ground air temperatures and associated human discomfort in the study area (Azevedo et al. 2016). Studies of urban heat islands in Asia indicate that the effect of GBI LST reduction lessens as general temperature levels cool (Fan et al. 2008, Hamada & Ohta 2010, Zhang et al. 1998), therefore the relative magnitude of ecosystem disservice may decrease for more extreme cold temperatures. In contrast, spatial patterns in summer GBI LST cooling are expected to remain relatively consistent for hotter weather conditions, although this will vary due to day to day variation in meteorological conditions (e.g. surface wetness, vegetation production) (Azevedo et al. 2016, Li et al. 2018). Studies into seasonal variation in surface urban heat island conditions across multiple cities in USA (Imhoff et al. 2010) and China (Zhou et al. 2016) indicate that daytime surface urban heat island conditions in temperate climate zones are less pronounced for cold weather (winter) temperatures. The balance between beneficial and non-beneficial urban cooling evidenced in this study is consistent with these findings.

The combination of ecosystem service and disservice values is therefore convenient for mapping overall temperature regulation values. However, there are potential limitations in this metric when considering the disparate implications for managing opposing negative or positive GBI functions. In this instance, comparison of seasonal variation in temperature regulation indicators may be more useful for planning purposes, to investigate if interventions are beneficial to manage significant trade-offs in cyclical temperature regulation functions. Relationships between land surface, and above air temperatures, may be more variable in winter months due to generally lower amounts of ground absorbed radiation (Hamada & Ohta 2010, Oke 1978). However, recent evidence suggests that this relationship is not always consistent, as correlations between winter LST and air temperatures can be stronger than the corresponding relationship in summer (Yang et al. 2020).

In-situ monitoring is therefore important given that the current temperature regulation model provides a limited account of other environmental factors such as air movement around urban canyons, or the varying thermal capacities of artificial/natural materials, that might influence temperature stressors under different weather conditions (Coseo & Larsen 2014, Dimoudi & Nikolopoulou 2003, Zheng et al. 2014). The positive effect of different GBI resources on hot weather air temperatures has been investigated at site level in the study area using primary field collected data to parameterise an advanced computational model (Skelhorn et al. 2014). Extension of such in-situ methods over a yearly cycle, could improve understanding of how local GBI impacts cool weather air temperature conditions in the study area (Hamada & Ohta 2010). This is important, given that exposure to cold temperature stressors remains a concern in the city of Manchester, due to high levels of socio-economic deprivation amongst city residents (Walsh et al. 2010). A comparison between the relative effects of GBI cooling in summer and winter would provide validation of the merits of using seasonal indicators for this service, and further indication of the usability of remotely sensed LST for this purpose.

Based on this evidence here, the benefits of GBI cooling of hot weather conditions far exceed negative cooling during cold weather. Increased daylight, and energy absorption by urban surfaces during the summer months results in increased variation of LST values, as warming rates differ between various configurations of landcover (Dugord et al. 2014, Smith et al. 2011). GWR demonstrates that GBI LST cooling varies spatially across the study area, due to varying configurations in GBI components and then cooling influence of adjacent cells (Li et al. 2010, Zheng et al. 2014). As such, advective ambient air-cooling of GBI resources can impact adjacent non-GBI areas by lowering LST (Zheng et al. 2014). The GWR method therefore returns indicator values for some cells with low to none GBI coverage. Investigating dynamism between temperature regulation function and demand indicators for July, has useful implications for planning purposes. For example, where a cell records high levels of both temperature regulation demand (exposure of population to LST) and GBI coverage, then this indicates the associated GBI resources may be relatively poor providers of temperature regulation benefits. Therefore, in contrast to simply improving GBI resources for this area alone (Gill et al. 2007), improvement of surrounding GBI levels, or the use of mixed natural (e.g. forest planting) and non-natural infrastructure (e.g. cool-fitting houses) interventions (Hatvani-Kovacs & Boland 2015, Lanza & Stone 2016, Taylor et al. 2016) may be required to better accommodate service demand for this cell area.

In general, public Recreation and Non-recreational Open Space landscape categories demonstrate higher levels of annual LST cooling than other built-up landscape types (Chen et al. 2014). If considering the need to reduce the urban heat island effect across the city as a whole, then GBI resources in urban parks, woodlands, farms and large waterbodies contribute high level functions for this purpose. The findings here support the concept of investment in green-blue pathways, which can intersect built-up areas and deliver temperature cooling flows along landscape edges to adjoining areas (Kong et al. 2014). In No Demand and Demand landscape areas, GBI also consistently reduces LST (Chen et al. 2014a, Deilami et al. 2018, Zhou et al. 2011). This finding contrasts with assumptions in other RES and natural capital accounting approaches that evaluate temperature cooling benefits from the presence of parks and other large greenspace areas only (Eftec 2018, Majekodunmi et al. 2020). As GBI proved to be a consistent estimator of LST within Demand cells, this suggests that conservation and even improvements in GBI coverage in residential zones should produce a generally positive effect in mitigating localised warm temperature extremes. This is likely to far outweigh any negative cooling effects in cold weather conditions, as extremes in this disservice are associated with high GBI levels (e.g. > 80%) prevalent in non built-up landscapes. In this regard, the council could provide housing insolation grants to counteract negative effects of GBI placement for vulnerable residents, from benefit savings provided by GBI investment for favourable conditions (Dowson et al. 2012). However, given the results in this chapter, this unlikely to be required in Manchester and other cities with similar climate conditions. As direct investment in large scale green-blue investment is an expensive undertaking, active engagement with urban residents and community groups to encourage greening of private and public land, may provide a cost-effective strategy for building urban climate resilience.

3.8.2 Seasonal variation in stormwater storage services

Analysis of seasonal variation in surface runoff indicates that seasonal variation in precipitation conditions are more important for determining seasonal variation in stormwater storage services than changes in canopy condition. Additional precipitation predicted for extreme events during “leaf-on” months appears to overload GBI stormwater storage benefits for the vast majority of cell areas, irrespective of canopy conditions. A small number of cells do record higher levels of runoff for “leaf-off” precipitation inputs as they contain relatively high levels of deciduous tree cover, however, these cells are not

typically associated with high levels of stormwater storage demand. When considering control levels, maximum difference in total modelled cell runoff, according to canopy loss, ranges from just over a total of 200m^3, to over 600m^3 for the most (1 in 30) and least (1 in 1000) probable yearly precipitation events. The degree to which this potential loss of stormwater storage affects local surface flood risk is however difficult to ascertain without further urban hydraulic modelling to assess increased runoff upon local topography and drainage systems (Leandro et al. 2014, Sjöman & Gill 2014).

The indicators derived here may therefore help to identify clusters of stormwater storage deprivation in order to focus application of in-situ, or advanced overland/underground computational models for this purpose (Grêt-Regamey et al. 2013, Leandro et al. 2014). Long-term monitoring of how local vegetation and soil resources change over an annual cycle, and thus react to different levels precipitation, is required to better understand the ecological response of local GBI resources to extreme precipitation events. Whilst the adapted SCS-CN model usefully indicates seasonal variation in stormwater storage, the model is still based on a number of assumptions which could be improved by incorporating local, or even national scale knowledge. This includes the interception capacity of different tree and shrub species found within the study area, in addition to the ability of local soils to absorb storm event precipitation under differing antecedent conditions (Asadian & Weiler 2009, Ferreira et al. 2015). Adaptation of runoff coefficients to local conditions will benefit rainfall runoff modelling both in the study area and elsewhere in the UK, but requires concerted effort to collect the appropriate field data for this purpose (Choi & Ball 2002).

Overall, public recreation and non-recreational open space cells provide higher levels of stormwater storage functions, due to comparatively higher levels of GBI cover than other landscape groups. This again indicates the benefits of developing parkland and green-blue pathways in the city, especially in areas where runoff congregates to increase pluvial flooding risks. Drainage systems may also be adapted to allow runoff to flow towards large scale GBI areas. Sustainable urban drainage systems, such as artificial depressions and soakaways can therefore adapt parks to function as runoff reservoirs during extreme precipitation events (Palazzo 2018). This somewhat negates the need for year-round canopy cover in these areas as storage function is based upon the volume capacity of collections basins. However, evergreen shrub and tree growth in parks may also be encouraged to further reduce stress on these systems over an annual cycle (Guevara-Escobar et al. 2007). Seasonal differences in canopy conditions, and associated stormwater

storage services, appear to become more variable with increasing precipitation levels. Efforts to improve evergreen tree canopy coverage now may therefore provide significant stormwater storage gains in the future, as climate change increases the severity and frequency of extreme precipitation events, and influences unpredictability in flooding risks (Miller & Hutchins 2017). Mapped deprivation for stormwater storage, in conjunction with mapped deprivation for temperature regulation, may therefore serve to identify potential GBI investment locations to satisfy demand for both RES. However, given the current indicatory nature of respective function models, it is advisable that localised site-based research is conducted to identify suitable location specific GBI investment at this scale.

In comparison, No Demand and Demand landscape group cells exhibit lower overall stormwater storage services. Whilst relatively high levels of change in canopy interception functions (> 4 mm additional runoff) are recorded in some demand cells, the results suggest that such areas are more susceptible to seasonal change in precipitation levels, rather than changes in tree canopies. Any improvement in GBI tree, or shrub cover, whether deciduous or evergreen, will improve annual stormwater storage services in low GBI cell areas. Where significant loss of interceptive function occurs, as indicated by cells that record positive difference in runoff ("Leaf-off" runoff – "Leaf-on" runoff) within high demand areas, then evergreen tree planting could be further encouraged. Trade-offs in this strategy may therefore occur, due to the increasing evapotranspiration and shading functions of GBI during cold weather conditions that increase resident exposure to thermal discomfort (Krüger et al. 2013). However, as climate change projections suggest a continuation of global warming into the future (Cavan 2011), then the relative disservices of cold weather temperature cooling may be increasingly outweighed by beneficial service functions during hot weather conditions. Whilst GBI investment in both publicly and privately owned land may provide minor stormwater storage benefits at the parcel scale, a concerted campaign in pluvial flood risk areas may provide flood risk reduction gains at the neighbourhood scale (Perry & Nawaz 2008). Maps of stormwater storage and temperature regulation coldspot clusters therefore indicate where public engagement methods should be located to support urban resilience planning.

3.9 Conclusion

The overall purpose of this chapter was to satisfy **Objective 2** and identify whether incorporation of seasonal dynamics in regulating ecosystem service maps presents a concern for planning green-blue infrastructure. Based on the evidence here, incorporation of seasonal dynamics currently represents a limited concern in mapping RES indicators. Omitting seasonally weighted indicators for both temperature regulation and stormwater storage services results in a near 5% difference in the identification of RES deprivation. This represents a small proportion of the study area and indicates that the use of typical non-seasonally adjusted indicators should still provide usable metrics to explore spatial variation in ecosystem services. However, as seasonal extremes in climate conditions may be more pronounced in other urban areas elsewhere, it may prove beneficial to consider seasonality in future ecosystem service mapping studies. Certainly, cyclical differences in stormwater storage services represent a concern for the city of Manchester, as a number of cells in both demand, and non-demand areas, demonstrate a considerable loss of stormwater storage functions due to canopy change. As climate change is likely to exacerbate extreme precipitation events in urban areas in the future, it is likely that GBI interventions containing certain vegetation types will have increasing importance in building urban resilience (Armson et al. 2013b, Carter et al. 2015). The seasonally adjusted mapping approach thus presents an accessible methodology to identify areas of seasonal RES deprivation where GBI, and other adaptation strategies may be investigated further using models validated to local ecological conditions.

However, as spatiotemporal mapping of RES is rare, the discussion here usefully indicates a number of issues in incorporating seasonal RES map indicators. For temperature regulation the final indicator is weighted according to trade-offs in both positive and negative service functions. This usefully provides a combined measure to compare against seasonally adjusted stormwater storage service indicators, but may aggregate information for the purpose of managing disparate RES benefits and disservices. Further research is therefore required to investigate how the indicators developed here may be incorporated within either wider planning frameworks, or within natural capital accounting methods. In addition, whilst the study here presents transferable methods to investigate seasonal RES change, further research may be beneficial to incorporate seasonal dynamics omitted in this study within future model adaptations (see Methodological extensions in **Chapter 6**). This is the first study to consider the methods and implications of seasonally adjusted RES

indicators at the city scale and therefore generates novel information for the wider research community. Overall, it is hoped that this study raises further awareness of seasonality in RES in order to stimulate further research efforts in this area. Employment and adaptation of the methods here for other ecological and climate conditions will therefore establish further evidence on the relative importance of incorporating seasonal spatiotemporal dynamics within ecosystem services assessments. The adapted indicator methods developed here are thus used to investigate future development scenarios and change in RES in **Chapter 5**.

Chapter 4: Urban land use and green-blue infrastructure change

4.1 Introduction

Continuing urban growth and densification impacts the extent and quality of urban green-blue infrastructure (GBI). Knowledge of whether GBI is vulnerable to various urban development drivers can therefore inform future estimates of environmental conditions, and thus inform appropriate compensatory environmental policies (Henke & Petropoulos 2013). In this context, the concept of anthropogenic land use (as opposed to landcover, or physical material that covers the top surface of the Earth) is useful, as this approximates the various socio-economic pressures that influence GBI management over time (Fisher et al. 2005). Interaction between GBI and land use determine whether GBI change, positive or negative, is associated with particular management practises (Aronson et al. 2017). GBI intervention strategies that are tailored towards specific land managers and stakeholders can therefore address declines in regulating ecosystem services (RES) (Gill et al. 2007). However, as few studies explicitly quantify trends in landcover change within land use, additional research is beneficial to develop methods for this purpose.

Change analysis in a case study approach should generate usable planning information for the study area. Authorities at the city and regional level have issued policy documents that specify a commitment to improve environmental conditions and ecosystem services within the city of Manchester (GMCA 2019, MCC 2015a, MCC 2016b, MCC 2020a). While ensuring current GBI levels is important to achieving policy goals, land use activities that influence GBI change are currently poorly understood in the study area. For example, widespread street tree clearing and garden paving have occurred in a number of UK urban areas in recent years (Kirby 2017, Perry & Nawaz 2008) and may have caused GBI change within the city. In addition, Manchester's population has grown by over 30% since the turn of the century with infrastructure development to facilitate and accommodate this growth (Swinney & Thomas 2015). Quantifying drivers and rates of landcover change can therefore guide future maps of GBI cover, and thus help to identify localised risks posed to environmental conditions (Rodriguez et al. 2006). Land use is useful concept in this regard, as current plans for the city describe targeted GBI research and investment policies towards different land use managers (MCC 2015b, MCC 2016b).

Information on whether GBI is vulnerable within particular land uses is therefore important to ensure that these actions are robust to address different rates of GBI change across the study area (Wellmann et al. 2020).

Despite the aforementioned advantages, analyses of change in urban land use and landcover over time remains a challenge. Of primary concern is that the temporal coverage of geospatial data is consistent (Comber et al. 2004). Whilst a number of pre-designed land use and landcover datasets are available, they are often constrained in either thematic and spatial resolution (Comber 2008) and may not be produced at time stops for the required period of study. Methods to map landcover and land use information may also change between product updates, which results in inconsistencies in class ontologies, and thus limits the effectiveness of change detection analysis (Comber et al. 2004). The literature describes methods to generate bespoke land use and landcover change information (Gill et al. 2008, Dennis et al. 2018, Hermosilla et al. 2013, Rufin et al. 2015) which may be effective in overcoming these aforementioned issues. However, methods vary in both efficiency and accuracy, and implementation of each is dependent upon available resources (Kampouraki et al. 2008). For change analysis here, a review of the current literature is required to identify usable methods. This is ultimately important to ensure that useful change analysis information is generated from the case study, and to identify methodological extensions and avenues for future research.

4.2 Aim and objectives

Chapter aim: Examine whether the magnitude of change in green-blue infrastructure over time varies for different land uses. The temporal period for the analysis of GBI change is a 17-year period from 2000 to 2017. This time window represents a period of significant development in Manchester as the population grew by approximately 30% (400,000 to 540,000; **Section 1.8**) and is consistent with available data resources.

Chapter objectives:

1. To review the literature to identify methods to quantify land use and GBI change.
2. To map change in GBI between 2000 and 2017.
3. To map land use between 2000 and 2017.
4. To quantify GBI change trends within different land uses.

4.3 Mapping change in urban land use

For the temporal analysis of urban land use, a standardised high-resolution geospatial data set was desired. This would limit processing costs and aid the reproducibility and adaptability of the methods to urban areas with the same data coverage. Existing land use data products were thus reviewed according to the following data requirements: a) land use categorised per unique land ownership parcel, or subdivision of land ownership parcel according to land use; b) thematic resolution of land use representing different public sector, commercial sector and residential management areas, and c) consistent thematic and spatial resolution of land use data for the chosen time period. Whilst a range of products were identified, none fully satisfied all of the aforementioned requirements (**Table 4.1**).

An existing dataset limits the examination of GBI change to the temporal resolution evident in the data. Methods to create temporal land use products are beneficial to the wider research community, to enable the examination of land use change for various development periods. Whilst approaches and data sources vary from study to study, all methods follow a common workflow that requires categorisation of features in the original data into spatial representations of contiguous land use classes. As land use areas may comprise complex configurations of topographical features, an approach in many studies is to manually digitise land use types using high-resolution geospatial data as a guide (Gill et al. 2008, Pauleit et al. 2005, Perry & Nawaz 2008). Manual interpretation is relatively accurate, as investigators identify unique land use parcels using expert defined rules (e.g. building configuations, landcover patch composition) (Kampouraki et al. 2007). However, time limitations, which are dependent upon the scale of the study area, and resolution of the spatial thematic information required, can be prohibitive (Kampouraki et al. 2007). In contrast, automatic image classification techniques can speed up this process considerably, as features and indices derived from the spectral data enable rapid classification of image areas to specific land use types (Haas & Ban 2018). For example, the creation of both spatial landcover metrics and object features can enable statistical clustering of landcover configurations into discrete land use class areas (Bauer & Steinnocher 2001). Such techniques are efficient, but may produce information that is limited in thematic resolution and accuracy due to the spatial and spectral limitations of the image data (Diaz-Pacheco & Gutiérrez 2014, Schmit et al. 2006).

In contrast, existing maps can provide the appropriate features (e.g. building typologies, points of interest, land parcel extents) for automatic land use classification. volunteered geographic information, such as OpenStreetMap (Haklay & Weber 2008) and Wikimaps (Kleeb et al. 2012), have been used to map land use in both developing and developed countries (Grippa et al. 2018, Yang et al. 2016). However, the quality of spatial information in such datasets can vary considerably. For example, an investigation into Openstreet map for Manchester revealed significant gaps in useable information across the study area. In contrast, accessible data may be sourced from national and supra-national mapping organisations. For example, Dennis et al. (2018) extracted land use parcels, representing residential and open-space amenities for Greater Manchester, UK, using data from the UK Ordnance Survey (OS) to map human dominated green infrastructure systems.

OS geospatial data layers are openly accessible for academic research, and overlap the study period (Edina 2020), and therefore present an opportunity for temporal mapping of land use. However, as data quality varies considerably over time, limitations in the quality of land use information between study dates will vary. OS land-line data for the year 2000 represents topographic features as point and polyline vector data but in contrast to current (circa 2017) OS data, provides limited information on landcover and land use associated with such features (OS 2004). However, both OS land-line and current OS spatial data products are based upon consistent underlying geographic data models. Changes in sub land use OS features are therefore likely to infer real world structural change in land use (Aspinall & Hill 1997, Schorcht et al. 2016). For example, spatial intersections between overlapping land use polygons have been analysed to assess whether spatial differences represent real land use change or result from inconsistent mapping methods over time (Schorcht et al. 2016). Adaptation of such methods should enable the consistent identification of land use class areas where appropriate attribute information is unavailable in the comparative dataset.

Table 4.1 - Review of current urban land use data for the UK

Product	*Reference*	*Agency*	*Versions*	*Geographic coverage*	*Spatial representation (resolution)*	*Urban specific land use classes*	*Comments*
Urban Morphology Types (UMT)	Gill et al. (2008)	ASCCUE: University of Manchester	2007	Greater Manchester	Various polygon sizes ranging from 0.011- 53 km^2	29 categories urban and peri-urban classes	Good thematic resolution but relatively coarse in spatial resolution, not a multi-temporal product
UK Landcover Map	UK Centre of Ecology and Hydrology (2020)	NERC: Centre for Ecology and Hydrology	1990; 2000; 2007; 2015	UK	25m raster scale	Two classes - Urban and Suburban	Suitable temporal coverage for change analysis, but only two broad urban land use categories
Corine Landcover	Copernicus Land Monitoring Service (2020a)	EU: Copernicus - Land Monitoring System	1990; 2006; 2012; 2018	Europe-wide	0.25km^2 minimum mapping unit area; minimum mapping unit width (100m)	11 classes representing artificial land use land-cover classes commonly found within urban areas	Same as above
Urban Atlas	Copernicus Land Monitoring Service (2020b)	EU: Copernicus - Land Monitoring System	2006; 2012	Europe-wide (urban centres > 50,000 people) - including Manchester	2500m^2 minimum mapping unit area; min-mapping width (10m)	27 in total, depending upon location, representing urban and peri-urban classes	Adaptation of CORINE Land-cover, improved spatial resolution, and thematic categorisation in relation to urban land uses; period between first and last versions not applicable for study period

4.4 Mapping change in green-blue infrastructure

Mapping spatial change in GBI requires finding the difference in extent and quality of city-wide GBI extents between two or more points in time (Coppin et al. 2004). This is achieved through comparison of spatial data, either in the form of existing maps, or using information derived from remote sensing analysis (Coppin et al. 2004, Fuchs et al. 2014, Tomscha et al. 2016). As no map data product, matching the spatial and thematic resolution of the 2017 landcover data (**Section 3.6.1**) was found for the year 2000, only remote sensing methods are considered in this section.

In recent years, remote sensing change detection methods have developed in accordance with increasing proliferation of very high resolution imagery, enabling assessment of GBI change to below sub-metre resolution (Tewkesbury et al. 2015). Commonly cited change detection methods include layer arithmetic and transformations to determine mathematical change indexes, change vector analysis (direction and magnitude of change between image layers), and the direct classification of dynamic and non-dynamic landcovers from multi-temporal image stacks (Hussain et al. 2013, Lu & Moran 2013, Tewkesbury et al. 2015). Whilst these methods have merits, change detection in this investigation is required against an existing GBI baseline measure, therefore only post-classification change detection methods are applicable here (Jensen 2005, Henits et al. 2016).

Standard post-classification change detection is a straightforward method, requiring differencing of classification layers to identify temporal shifts in landcover pixel, or object class values (Peiman 2011, Serra et al. 2003). While this method is suitable for information derived from different sensors, as classifications are conducted independently of each other, classification errors in either input dataset will compound within the final change detection layer (Jensen 2005, Olofsson et al. 2013). For example, Fuller et al. (2003) assessed post-classification change detection accuracy between remotely sensed UK national landcover maps for 1990 and 2000, with recorded accuracies of 85% and 80% respectively. Due to misclassification errors, the study found that whilst change was estimated for 43% of the image area, only 17% of the area had quantifiably changed on the ground. In addition, this method requires stringent geo-rectification between classification layers, to ensure comparison pixels represent the same area of landcover on the ground. For example, Townshend et al. (1992) estimated an error rate in NDVI change detection of up to 50% when recording mis-registration of a single pixel in image pairs, and thus

concluded registration accuracy of 0.2 pixels was required to achieve > 90% change detection accuracy. Inconsistencies between image data such as variation in the nadir image angle, altering the view of vertical standing objects and shadow, in addition to temporal variation in vegetation phenology, may produce differences in classification outputs where in fact no change has occurred (Jensen 2005).

Due to inconsistencies in the quality of image data, which may be unavoidable for given change detection exercises, a range of techniques have been developed to adjust for associated errors (Hester et al. 2010, Hussain et al. 2013, van Oort 2005, Tewkesbury et al. 2015). Adjustment methods thus require prior analysis of drivers in change detection error, which in turn informs semantic rules and object-based methods to re-classify spurious change areas. Examples of this include rules to re-label improbable class conversions (e.g. building to water) (Liu & Zhou 2004), and eroding change areas by a set number of pixels to account for estimated image to image mis-registration error (Serra et al. 2003), through to assessing change detection objects statistics (e.g. shape, size, topological relationships) to identify spurious change areas resulting from archetypes in the post-classification change layer (Chen et al. 2012, Zhou et al. 2008). In addition, Olofsson et al. (2013) describe a method of adjusting estimates of change cover area, using information from verified estimates of change class accuracy.

Change detection of GBI is possible within the study area but will exhibit erroneous change estimates if error is not sufficiently controlled in the change detection process. For example, underestimation of GBI degradation may imply that certain land use management activities cause more environmental damage than actual change in the real world (Fuller et al. 2003) and may therefore support the adoption of over stringent GBI protection measures. In contrast, underestimates of GBI change will omit important environmental developments, and may correspondingly support the adoption of weak and inappropriate GBI protection measures (Falcucci et al. 2007). As evident, accurate GBI change information is ultimately important for both understanding and planning the future provision of RES (Dobbs et al. 2018). Therefore, an error aware GBI change detection method was used in the case study to quantify GBI change within confidence interval estimates (**Sections 4.5.3 and 4.5.4**). Rates of GBI change were then quantified within different land uses (**Sections 4.5.1 and 4.5.2**) to indicate how land use management influences temporal change in GBI across the study area.

4.5 Methods

Methods for this chapter are described in four sections (**Figure 4.1**). **Section 4.5.1** contains detail on the creation of the Urban Land Use (ULU) 2017 layer using OS data. **Section 4.5.2** describes how the ULU class layer and OS land-line derived data are compared topologically to effectively backdate 2017 ULU information to the year 2000. This process in turn identifies consistent no-change ULU class sample areas. **Section 4.5.3** describes the estimation of actual GBI change areas through use of post-classification change detection. **Section 4.5.4** describes how the data layers are combined to analyse GBI change across the study area as a whole, and also within no-change ULU class samples to estimate GBI change trends per ULU class.

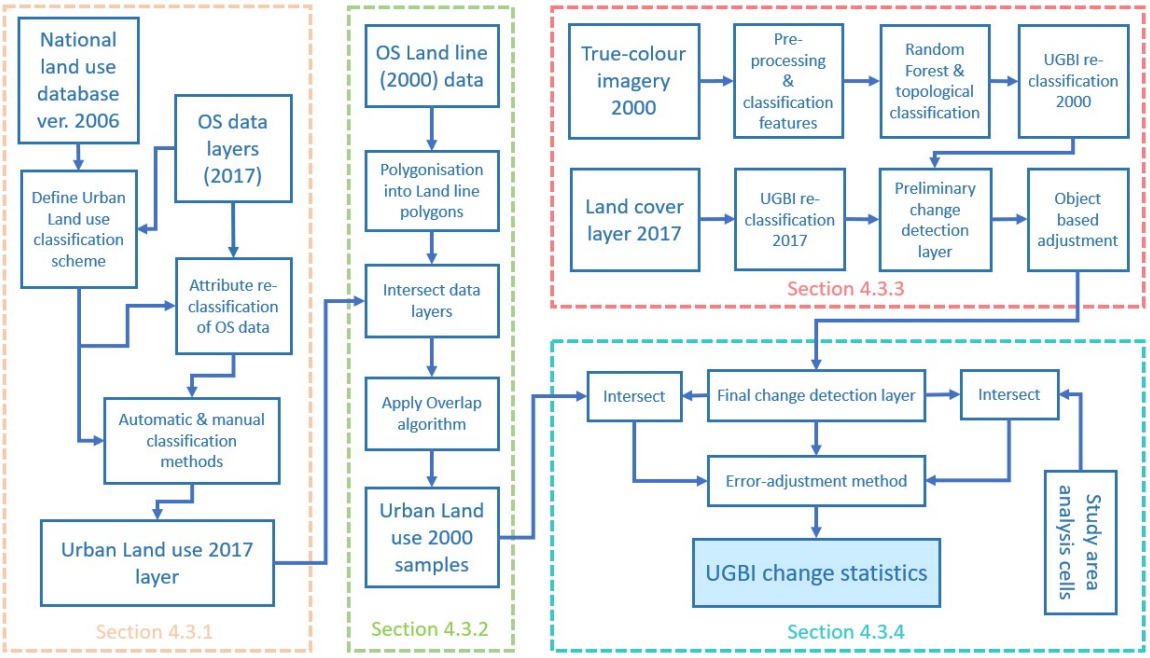

Figure 4.1 – Method sections in Chapter 4

4.5.1 Urban land use 2017 classification

The ULU 2017 classification layer was created using research accessible data from the UK Ordnance Survey (OS). Each data layer contains geospatial vector features (polygons, polylines and points) representing various features of interest. This varies from detailed topographic features (e.g. buildings, unique surface areas, roads), through to the delineation of site areas representing unique land uses (**Table 4.2**). Whilst the combined spatial extent of the input layers cover the entirety of study area, the level of polygon

attribute information (e.g. typology of feature) for unique features varies considerably. Some vector features can be automatically assigned an ULU class label, whereas other features require additional methods. As such, the premise of ULU mapping was to employ automatic re-categorisation of as many ULU areas as possible, and then to apply a combined automatic and manual classification approach for remaining un-assigned features. The definition of ULU classes was ultimately a bottom-up data-driven exercise, based upon pragmatic methods implementable with the input OS data layers (**Table 4.3**). In order to provide general contiguity with wider UK Land use planning information, the 2006 UK (NLUD) National land use database (Harrison 2006) provided the framework for ULU class definition (**Appendix 4.1** details the relationships between ULU and NLUD class relationships).

Table 4.2 – Ordnance Survey (OS) data layers required for urban land use categorisation

Product*	Version	Description
MasterMap Sites Layer	*October 2017*	*Spatial extents of important locations such as airports, schools, hospitals, utility and infrastructure sites*
MasterMap Greenspace Layer	*July 2017*	*Spatial extents of publicly accessible and non-accessible greenspace areas within urban areas*
MasterMap Topography Layer	*May 2017*	*Detailed spatial data representing physical (e.g. surface extents, physical boundaries, buildings, paths) and non-physical (e.g. administrative and electoral boundaries, cartographic text, symbols) features*
Open Map Local (Vector)	*October 2017*	*Open access street-level mapping vector data product containing additional extents of useful urban sites not defined within the above layers*
MasterMap Highways Network	*October 2017*	*Route lines for highways (roads and paths) network for geospatial network analysis*
Building Heights (Alpha)	*October 2017*	*Consisting of a number of different height attributes for each building in the MasterMap Topography Layer.*

* = all Ordnance survey products accessed from the EDINA Digimap digital information service (see https://digimap.edina.ac.uk/; Accessed 09.12.2019); technical information for each layer (see www.ordnancesurvey.co.uk; accessed 18.01.2020)

Table 4.3 - Description of urban land use (ULU) Group and Class categories

ULU Group/ Class	Description
1. Brownfield	**Land without current purpose**
1.1 Brownfield	Brownfield areas, developmental land and construction sites
2. Commercial	**Areas primarily providing commercial and retail services**
2.1 Commercial	Retail and Professional services
3. Community Services	**Government and public community welfare services**
3.1 Safety & well-being	Public safety (e.g. Police, Fire, Social support)
3.2 Cultural facilities	Services supporting cultural recreation
3.3 Health care	Health care services
3.4 Higher education	Non-compulsory adult education services
3.5 Religious facilities	Religious worship in any denomination
3.6 Schools	Compulsory non-adult education services
4. Industrial	**Manufacturing, engineering, construction & energy distribution services**
4.1 Industrial	Manufacturing, warehousing and distribution sites
4.2 Energy Utilities	Generation and distribution of energy supplies
5. Non-recreational Open Space	**Predominantly Open-space not supporting recreation**
5.1 Agriculture	Commercial farming
5.2 Cemeteries	Processing and storage of human remains
5.3 Water	Natural and purpose built water bodies and channels
5.4 Woodland	Continuous tree cover separate to other Land uses
6. Public Recreation	**Outdoor and indoor facilities supporting physical/social recreation**
6.1 Public Open Space	General outdoor amenities and open spaces
6.2 Sports Facilities	Land and facilities designated for sporting activities
6.3 Urban Farming	Non-commercial urban farming
7. Residential	**Primarily residential housing of varying dwellings density**
7.1 Low Density Residential	Majority of dwellings are semi-detached and detached housing
7.2 Medium Density Residential	Majority of dwellings are terraced housing
7.3 High Density Residential	Majority of dwellings that former buildings converted into flats or purpose built multi-dwelling apartment housing
8. Transport	**Infrastructure supporting the transport of people and goods**
8.1 Car Parking	Car parking areas not associated with other land uses
8.2 Limited access roads	Private roads connecting addresses to higher functioning roads
8.3 Linking roads	B-roads connecting significant destinations and feeding A-roads
8.4 Major roads	A roads and dual carriageways
8.5 Minor roads	Roads connecting addresses to higher functioning roads
8.6 Motorways	Motorway roads – as defined in the OS highways dataset
8.7 Railways	Land and infrastructure supporting rail and tram travel
8.8 Roadsides	Access routes between areas for non-vehicular travel
8.9 Transport terminals	Non-rail mass transit travel e.g. bus and tram stations, airports

Figure 4.2 displays the first stage of processing to re-classify and then combine the various OS data layers into ULU class areas. **Figure 4.3** displays a combined method approach required to assign final ULU class labels to remaining un-assigned polygon features (see **Appendix 4.2** processing steps for all methods). This stage involved topological classification methods, where un-assigned features were automatically re-assigned to other classes based upon neighbouring topological relationships. Results from this stage were then manually checked to correct for classification errors as they occurred. In addition, Random forest classification was employed to separate Residential areas into either Low, Medium or High-density residential classes. As potential error may have occurred from the various methods used, final map accuracy was assessed using MasterMap topography layer sample polygons within ULU class areas as reference samples. As thematic accuracy was expected to be extremely high (> 95%), the minimum total number of polygon samples was determined as n = 870 (30 per ULU class * 29 class in total) based upon the minimum required per class sample number to validate overall classification accuracy (Warner et al. 2009). Polygon samples were stratified within areal quintiles to ensure even distribution of polygon area sizes across ULU classes and were then compared to year 2017 multi-spectral imagery (see **Section 3.6.1**) to assign a suitable ULU class label. Accuracy was then assessed using the error matrix method with kappa statistic (Congalton & Green 2008, Viera & Garrett 2005).

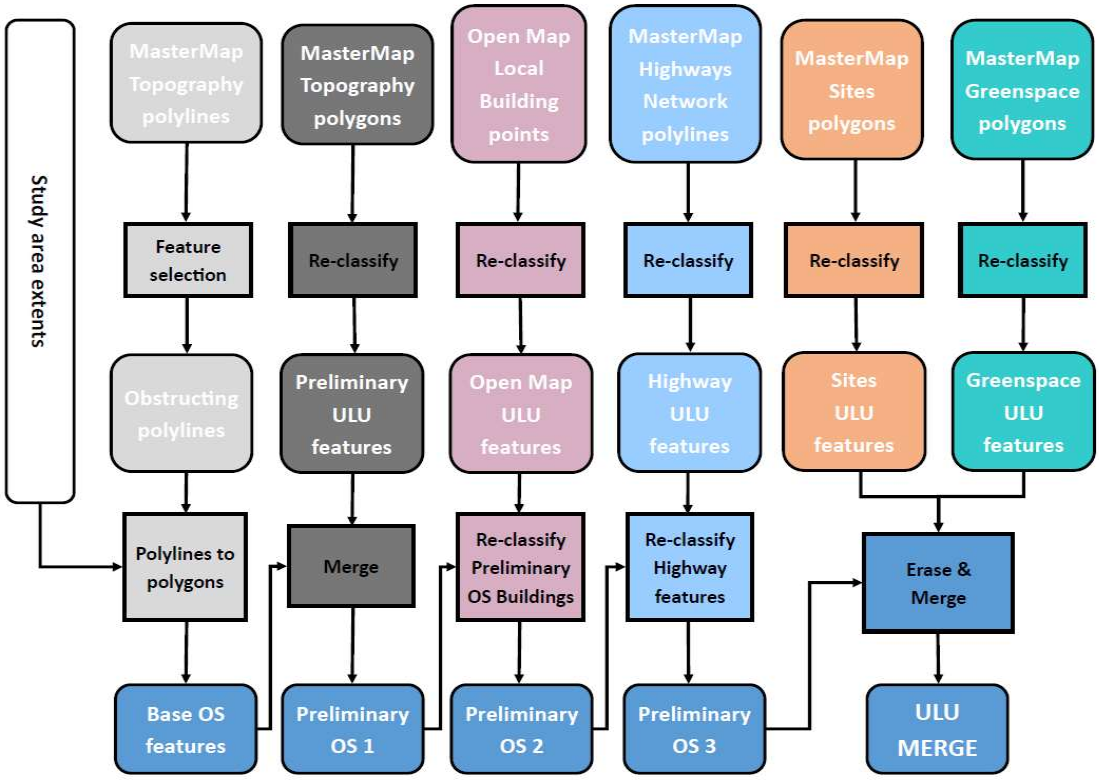

Figure 4.2 - Ordnance Survey layers integration to base urban land use (ULU) class layer

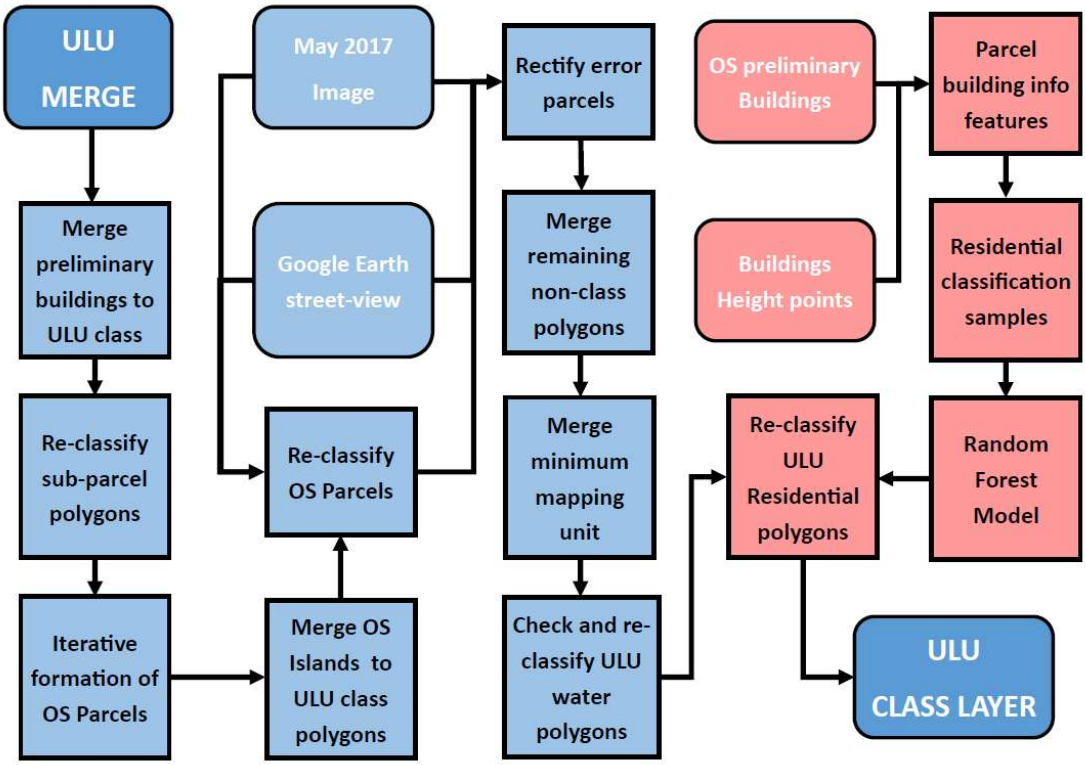

Figure 4.3 - Re-classification of remaining Ordnance survey features into urban land use (ULU) classes

4.5.2 Urban land use

As described in **Section 4.3**, OS land-line data (OS 2004) for the year 2000 provides the reference spatial data to backdate 2017 ULU information using polygon overlap methods. As real-world topographic features remain in position over time (e.g. parcel fence-line, road edge), the representative polyline or polygon line detail should also remain consistent between the OS "land-line" and "MasterMap" products (OS 2020). Polygon-to-polygon comparison between OS data sets enables the identification of sub-ULU features that remain consistent in shape and spatial position over time (Aspinall & Hill 1997).

To develop an appropriate method, overlapping ULU areas from both the 2000 and 2017 OS datasets were first examined to identify potential issues in corresponding feature alignment. land-line polylines representing physical topographic features were thus extracted, and then intersected with the study area extents to generate enclosed land-line polygon areas (LL00). Visual comparison of sub-2017 ULU OS MasterMap features (MM17)

and LL00 polygons revealed both consistencies and inconsistencies in mapping detail between the datasets (**Figure 4.4**).

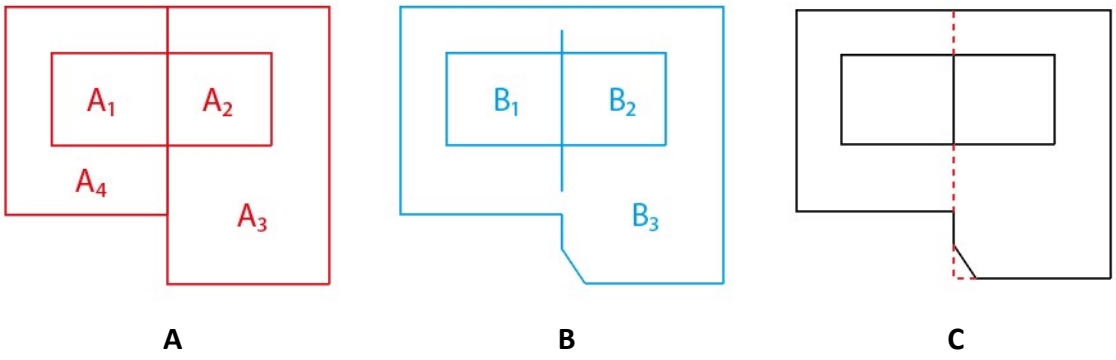

Figure 4.4 – Comparison between Mastermap and land-line features representing a contiguous residential land use area: A MM17 polygons ({A1, A2, A3, A4}) in ULU 2017 layer; B OS land-line 2000 polylines and resulting enclosed LL00 polygons ({B1,B2,B3}); C comparison of both sets of features with inconsistencies in map detail dashed in red.

Comparison of MM17 and LL00 polygons in **Figure 4.4** indicates that each set may represent the same overlapping ULU area (**Figure 4.4C**). However, spatial discrepancies between the features are evident. For example, the central polyline that separates A_1 & A_2 and A_3 and A_4 (**Figure 4.4A**), is not contiguous with polyline length separating B_1 and B_2 (**Figure 4.4B**). This discrepancy may represent either a real-world topographic change, or in this situation, a consistent topographic feature (i.e. boundary fence-line) that is simply not represented in the same detail in both datasets. As such, the combined {A_3, A_4} polygon extents, are approximately contiguous with B_3, and thus represent a consistent group of topographic ULU class feature extents over time. The minor areal discrepancy between {A_3, A_4} and B_3 (**Figure 4.4C**), represents either an inconsistent representation of the same feature between datasets, or an actual real-world change. However, in this case either event does not prevent the identification of the overlapping area in **Figure 4.4C** as a consistent ULU. In this context, an initial polygon overlap method, assessing exact feature position matches, as is the case when comparing polygon sets {A_1, A_2} and {B_1, B_2} was tested, however this returned a disappointing number of consistent ULU polygon areas. As such, an automatic polygon comparison algorithm was developed to allow some degree of variance when assessing varying topological circumstances between corresponding polygon sets (**Figure 4.5**).

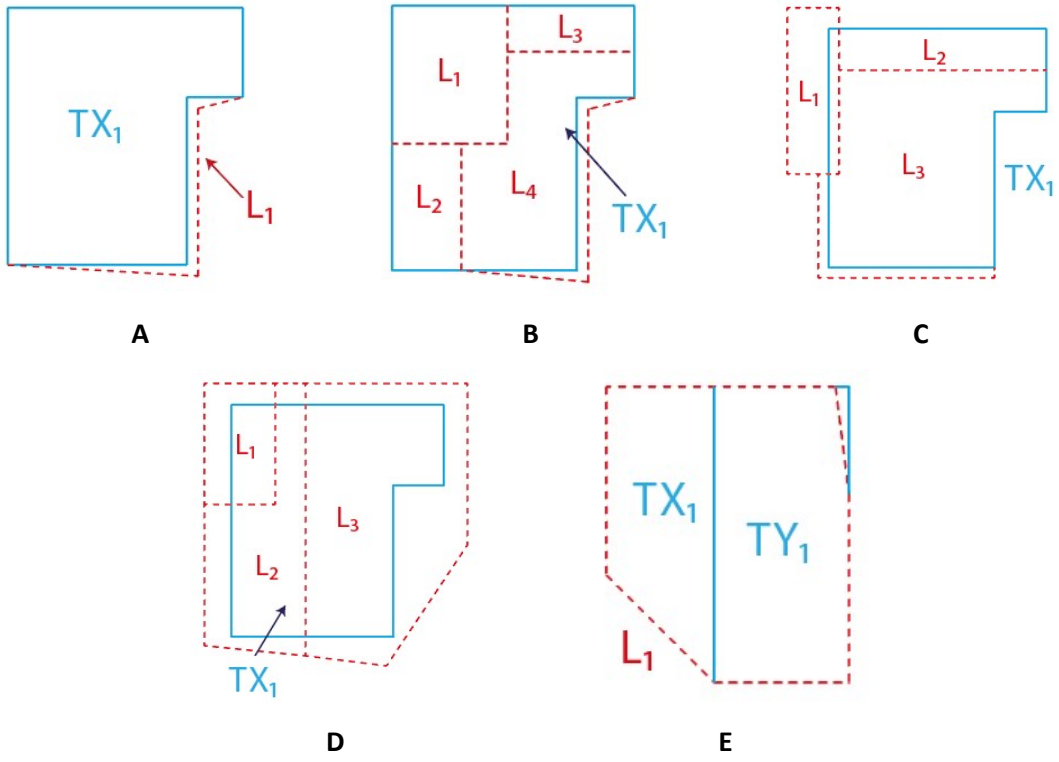

Figure 4.5 – Topological circumstances when comparing overlapping polygon features

The polygon comparison algorithm works as follows. As shown in **Figure 4.5A,** the boundaries of Polygon TX_1 (MM17 polygon of ULU class X_{ULU}) and L_1 (LL00 polygon) mostly coincide, indicating a consistent Land use feature over time. The degree of overlap is calculated as:

$$Overlap = \frac{area(TX_1)}{area(L_1)} \quad \textbf{[4.1]}$$

In this instance, where $Overlap > C.T.$ (where $C.T.$ = user defined conditional parameter defining the proportion of overlap required between comparative polygons) then this is classified as a no-change ULU sample area. **Figure 4.5B** describes a more complex topological arrangement, as TX_1 coincides with combined boundaries of LL00 polygons {L_1, L_2, L_3, L_4}. This could indicate Land use change as year 2000 features of different land use have been combined into a single 2017 ULU area, or that consistent land use features have not been digitised in the 2017 MasterMap layer. Examination of both datasets indicated that the second condition prevails in most circumstances, therefore the degree of overlap between polygons A and {B_1, B_2, B_3, B_4} in this instance is calculated as:

$$Overlap = \frac{area(\{L_1, L_2, L_3, L_4\})}{area(\{TX_1\})} \quad \textbf{[4.2]}$$

Therefore, IF $Overlap > C.T.$ then polygons {*B₁, B₂, B₃, B₄*} are classified as consistent ULU sample areas. In instances where comparison polygons share similar areas but have different shapes, and do not consistently overlap, use of the *Overlap* function as defined in A and B may incorrectly indicate a no-change ULU sample area (**Figure 4.5C**). This is controlled in the process as follows:

i) Subset LL00 polygons that intersect TX_1:

$$LL00 = \{L_1, L_2 \ldots, L_{max}\} \quad \textbf{[4.3]}$$

$$LL\_int = \{LL00 : LL00 \cap TX_1\} \quad \textbf{[4.4]}$$

ii) Select LL00 polygons if ratio of intersected area to LL00 polygon area is > *C.T.*

$$LL\_test = \left\{LL\_int : \left[\frac{area(LL\_int \cap TX_1)}{area(LL\_int)}\right] > C.T.\right\} \quad \textbf{[4.5]}$$

iii) Calculate *Overlap*:

$$Overlap = \frac{area(LL\_test)}{area(TX_1)} \quad \textbf{[4.6]}$$

In this instance, the conditional process removes *L₁* from the *Overlap* comparison, which overlaps *TX₁* slightly due to a slight change in boundary position. The remaining *L₂* and *L₃* polygons are relatively contiguous with the *TX₁* polygon and are thus selected as consistent ULU sample areas. In **Figure 4.5D**, it appears that there has been significant change for the representative polygon area. This may not indicate land use change in itself as neighbouring MM17 features may have been simply re-arranged to define the same land use i.e. reconfiguration of buildings on existing School site. However, establishing different orders of polygon neighbours (i.e. identifying which set of multiple polygons overlaps with another set of multiple polygons) requires significant additional computation using the algorithmic

process. Thus $Overlap$ is simply calculated for either a ONE reference polygon to ONE test polygon, or a ONE reference polygon to MANY test polygons relationship. In this case, reasoning would suggest that no LL00 polygon should be selected as a no-change ULU sample. However, this is dependent on how lenient the conditional overlap threshold ($C.T.$) is set. In **Figure 4.5E**, the roles of MM17 and LL00 polygons are reversed, therefore overlap is calculated by reversing the numerator and denominator references in equation **4.1**. However, L_1 may not be considered a no-change sample area in this instance as:

$$[\, ULU\ of\ TX_1 \neq ULU\ of\ TY_1 \,]\ or\ [\, X \neq Y \,] \qquad \textbf{[4.7]}$$

L_1 is assumed a single Land use feature comprising different 2017 ULU classes, as such it appears that this area in 2000 has now been subdivided for different ULU purposes in 2017 and has thus changed ULU categorisation over the study period. This process was implemented using R (R Core team 2019), with the code provided in **Appendix 4.3**.

As evident the value of $C.T.$ controls this process. Sensitivity analysis was thus conducted to identify an optimal $C.T.$ value that produced a reasonable trade-off between sample error rate and total number of ULU class polygons correctly identified. For this, 300 ULU polygons were randomly selected as validation areas, and were classed as either no-change (*n* = 242), partially changed (*n* = 18) or fully changed (*n* = 40), when comparing changes in features between overlapping 2000 and 2017 imagery. The overlap algorithm was then run for no-change and full-change MM17 polygons, using a sequence of test $C.T.$ values defined as:

$$a_1 = \frac{85}{100};\ a_n = a_{n-1} + \frac{1}{1{,}000{,}000};\ for\ n \leq 100 \qquad \textbf{[4.8]}$$

The correct polygon recall rate was therefore calculated as the percentage of actual no-change polygons identified by the algorithm for each test $C.T.$ value. The process was also run on the full dataset for $C.T.$ values 0.85, 0.90 and 0.999999. This examined how the proportion of identified no-change MM17 polygons varies according to stringency in $C.T.$ value. Three values were tested due to the computational time required to implement this process for full polygon datasets. Comparison between the error and no-change percentage determined a suitable $C.T.$ value for final sample calculation. The final LL00

sample dataset was then validated using an independent sample of ULU class MM17 polygons (*n* = 384). Actual ULU class labels were recorded for sample polygons in order to populate an error matrix with kappa statistic (Congalton & Green 2008, Viera & Garrett 2005), and determine overall accuracy of the chosen Overlap $C.T.$ value.

4.5.3 Mapping green-blue infrastructure change (2000 - 2017)

4.5.3.1 Image pre-processing and feature creation

To map GBI cover for the year 2000, true-colour aerial imagery (25cm resolution; acquired in June 2000) was purchased from Getmapping (2019). In order to generate GBI change objects using post-classification change analysis, this image was downscaled using nearest neighbour resampling (Raster package, R programming language; Hijmans 2020) to the grid resolution (1.5m) of the 2017 classification layer. To improve the accuracy of change detection analysis the image was geo-referenced to within root mean squared error (RMSE) of a single pixel, using OS land-line data from the year 2000 as a reference (Townshend et al. 1992). OS land-line data was used due to a) < 1 pixel RMSE between 2017 OS Mastermap topography layer and year 2017 imagery (see **Section 3.6.1.2**), and b) difficulty in identifying a suitable number of reference points between the year 2017 and year 2000 images. Reference points are typically placed upon image pixels that are identifiable in both images, and represent common vertices of permanent objects, such as building or boundary feature corners. However, this is a time-consuming exercise as vertices that are well defined in one image are often not contiguous with well-defined vertices in the comparison image. In contrast, vertices in the OS land-line data are represented by line intersections at precise coordinates, and therefore provide an easy reference source for image reference points across the entire study area. An initial spatial error of RMSE = 2.89 pixels was estimated between the datasets using *n* = 42 spatially distributed reference points, which is above the recommended minimum number (*n* ≈ 30) of points for geometric rectification and error estimation (Chuvieco 2016).

Initial georeferencing attempts using polynomial transformations at orders 1, 2 and 3 achieved only a marginal improvement in RMSE of 2.75, 2.72 and 2.66 pixels respectively. As visual analysis revealed evidence of variance in distortion across parts of the true-colour image, geo-rectification was implemented using the rubber-sheeting method (Baker & Smith 2019, Shimizu & Fuse 2003). Using a spatial reference grid (*n = 42* cells) as a

stratification layer, reference OS land-line building polygons were randomly selected, and then manually shifted to overlap the boundaries of the respective building feature in the image to create shift polygons. The centroids of original and shift polygons thus provided the reference points to calculate the appropriate rubber sheeting transformation (using ERDAS Imagine). Independent polygons for rubber sheeting translation and validation purposes (Aguilar et al. 2008) (approximately 30% of reference sample number) increased incrementally from 172 and 38, to 504 and 187 polygons respectively, until < 1 pixel RMSE was achieved. Despite this process, some distortion between the image data layers was expected to remain, therefore additional steps were necessary in the post-classification change detection analysis to compensate for this issue.

4.5.3.2 Classification features

Additional image feature layers were created to enhance the limited spectral information in the geo-rectified true-colour imagery and thus improve the accuracy of classification (Baker et al. 2018). In addition, ancillary spatial data was processed using the year 2000 land-line data to provide contextual OS landcover data for topological classification purposes (OS 2004) (see **Appendix 4.4** for further details).

4.5.3.3 Random Forest and object based topological classification

As change detection was required to identify either GBI loss or gain, the year 2000 image was stratified into either GBI or non-GBI, using a mixture of pixel and object-based classification methods. The overall classification process attempted to replicate the methods applied for the 2017 landcover classification as closely as possible (**Section 3.6.1**) in order replicate the quality of this classification layer. The first stage required classification of year 2000 image pixels into one of five preliminary classes representing constituent surfaces of varying spectral signatures. These classes included Vegetation (all vegetated surfaces), Non-Vegetation (bare soil and artificial surfaces), Vegetation shadow (shaded vegetation surfaces), Non-vegetation shadow (shaded non-vegetation surfaces) and Water surfaces. The number of sample points was determined using multinomial law (see **Appendix 3.3**) for the 5 classes in total with confidence level of 95% and precision in overall accuracy of 5%, in order to determine the total number of validation samples (n = 670). This total was doubled to estimate the total number of training samples (n = 1340)

required for an approximate 70% - 30% respective training - testing sample split (see **Appendix 4.5** for sample scheme). Prior information from the 2017 classification determined the stratification of validation samples according to class coverage, which were distributed evenly across the study area using equal area reference grid zones (*n = 33*). Sample positions were manually adjusted to ensure that the point location fell upon a representative landcover pixel in the year 2000 imagery.

All Random Forest classification and tuning was conducted using R programming language. Useful features for classification were selected (VSURF package; Genuer et al. 2018), in order to optimise the computational time required to classify the entire image, model tuning was conducted to optimise the *mtry* and *ntree* parameters (Caret package; Kuhn 2020). It was clear during classification testing that Water surfaces were difficult to separate from other classes using the spectral features alone, therefore this class was processed solely using topological object-based methods. In addition, it also proved difficult to discriminate between Vegetation shadow and Non-vegetation shadow, so these class samples were combined into a single shadow class. Random forest was thus implemented for Vegetation, Non-vegetation and shadow classes only (Random forest package; Liaw & Wiener 2002).

Object-based classification was implemented using the ancillary OS land-line layers to classify water areas within the non-vegetation class, and to reduce instances of mis-classification (see **Appendix 4.6** for object-based classification rulesets). Due to computational issues with the original topological processing of shadow pixels (see **Section 3.6.1.5**) an updated process was developed. The process iterates through individual shadow class areas in the current classification dataset, by de-constructing them into pixel objects, identifying which pixel objects have non-shadow neighbours, and then iterating through the candidate pixel objects, re-classifying where appropriate to the majority neighbouring non-shadow class. If no majority class is discovered then the neighbourhood area is iteratively expanded by 1 x pixel width to incorporate additional pixels until a majority non-shadow class is identified. After this stage the classified data is accuracy assessed using the validation samples to populate an error matrix with kappa statistic (Congalton & Green 2008, Viera & Garrett 2005).

4.5.3.4 Post-change detection

In preparation the year 2017 classification was amalgamated into a GBI (Deciduous, Evergreen, Grass and Water) and Non-GBI (Artificial, Bare Earth and Building) class layer. GBI and non-GBI classes for the years 2000 and 2017 were intersected to form an initial post-classification change detection layer with four change classes: GBI loss, GBI stasis, GBI gain and Non-GBI stasis. Potential errors in this layer were examined in relation to both spatial mis-registration and patterns of misclassification between corresponding classification layers. Object-based adjustment was thus implemented in a number of steps to void spurious change detection class areas (Serra et al. 2003).

First slither polygons of 1-pixel width for all change detection classes were voided from further analysis, as such areas may occur due to mis-registration between the classification data sets. In addition, GBI loss or GBI gain classes within BUILDING polygons were re-classified as Non-GBI stasis. GBI loss and gain class areas that were misclassified due to particular vegetation conditions at time of image capture (e.g. dry canopied vegetation at the time of image collection) were examined and manually re-classified to the appropriate GBI stasis class where identified. Accuracy levels between both the original (CD1) and corrected post-classification layers (CD2) were quantified. Validation class sample numbers, randomly selected within stratifications according to total class area, were determined using multinomial law (n = 618 for 4 classes, and required precision of 5% at 95% confidence interval) (Congalton & Green 2008). Validation point locations were then examined in relation to both the year 2000 and year 2017 imagery to assign an appropriate change class label. Validation points then populated error matrix with kappa statistic (Congalton & Green 2008, Viera & Garrett 2005), which provided an estimate of the overall effectiveness of the change-detection process, and also provided input data for the error-adjustment method.

4.5.4 Analysis of green-blue infrastructure change (2000 – 2017)

GBI change between 2000-2017 was analysed for three spatial scales. The first considers the study area as a whole, to give an overall estimate of GBI change across the study area for this period. The study area is represented by analysis cells that overlap the city of Manchester boundary, which thus represents 95.7% of the actual study area. The second scale considers GBI change at the analysis cell level and thus enables mapping of spatial variation in GBI change across the study area. The final scale considers ULU

classification samples. For each ULU class, change detection class areas are amalgamated from all class samples, thus providing singular GBI change estimates per class.

The error-adjusted method described by Olofsson et al. (2013) was used to estimate net GBI change (within 95% confidence interval bounds) per spatial analysis scale. This method encompasses the knowledge that both change and stasis classes will contain a certain amount of mis-classification, and therefore any hard estimate of actual change area should be adjusted to account for the estimated level of confusion between change detection classes (Olofsson et al. 2013). Information from the error matrix determines the level of class confusion, and samples to calculate upper and lower change area estimates at a confidence interval (e.g. 95%) defined by the investigator (Olofsson et al. 2013) (see **Appendix 4.7** for explanation of this method).

Total error net change with upper (upper GBI gain – lower GBI loss) and lower (lower GBI gain – upper GBI loss) bounds of change was calculated for the analysis areas under consideration. GBI stasis was determined where Upper net GBI change ≥ 0 ≥ Lower net GBI change and was calculated by assuming error levels from the study area error matrix to lower order spatial analysis units (analysis grid cells and total ULU sample area). Net area change estimates were then used to estimate GBI levels in 2000, through use of a class areal weighting method for negative change. For analysis cells net GBI change as percent of cell area enabled visual examination of clusters of GBI change and stasis. GBI change, as a percent of existing GBI was also calculated for the study area, in addition to combined ULU class sample areas. This rate of GBI change enabled estimation of projected study area GBI levels approximately 17 years into the future (i.e. 2034) using both overall rates of change, in addition to rates within ULU class areas. Intersecting ULU class areas with analysis cells also enabled localised mapping of future change, as overall ULU GBI change rates were applied to GBI resources within the intersecting area, and then re-amalgamated at the analysis cell. The resulting map provides a straightforward estimation of potential GBI change in the coming years.

4.6 Results

4.6.1 Urban land use classification for 2017

Cross-validation of the Urban Land use (ULU) 2017 layer yielded an overall accuracy of 96.6% (see **Appendix 4.8** for Urban Land use class confusion matrix). This is above the 85% threshold generally considered acceptable in land use classification exercises (Congalton & Green 2008). User accuracy, or the percentage of actual class area labelled correctly, ranged between 71.1% and 100.0%. Producer accuracy, or percentage of class area not contained within other class areas ranged between 78.8% and 100.0%. With the exception of the Railways class, Residential classes provided the lowest combined accuracy values, as these areas compound additional error from the Random Forest classification process (**Appendix 4.2**). For Railway areas, some unclassified neighbouring OS Mastermap topography parcels have been incorrectly assigned to this class during the parcel merging process, resulting in relatively low classification accuracies for this class. ULU class coverage (**Figure 4.6**), ranged from 0.2% for Cultural facilities through to 22.4% for Low density residential. Residential group areas dominate, exceeding one-third of the study area (**Figure 4.7**). Transport and Recreational Open Space ULU groups are also well represented, covering 23.6% and 18.1% of the study area respectively. An example of the spatial and thematic resolution of the data at both study area and neighbourhood resolution is shown in **Figure 4.8**.

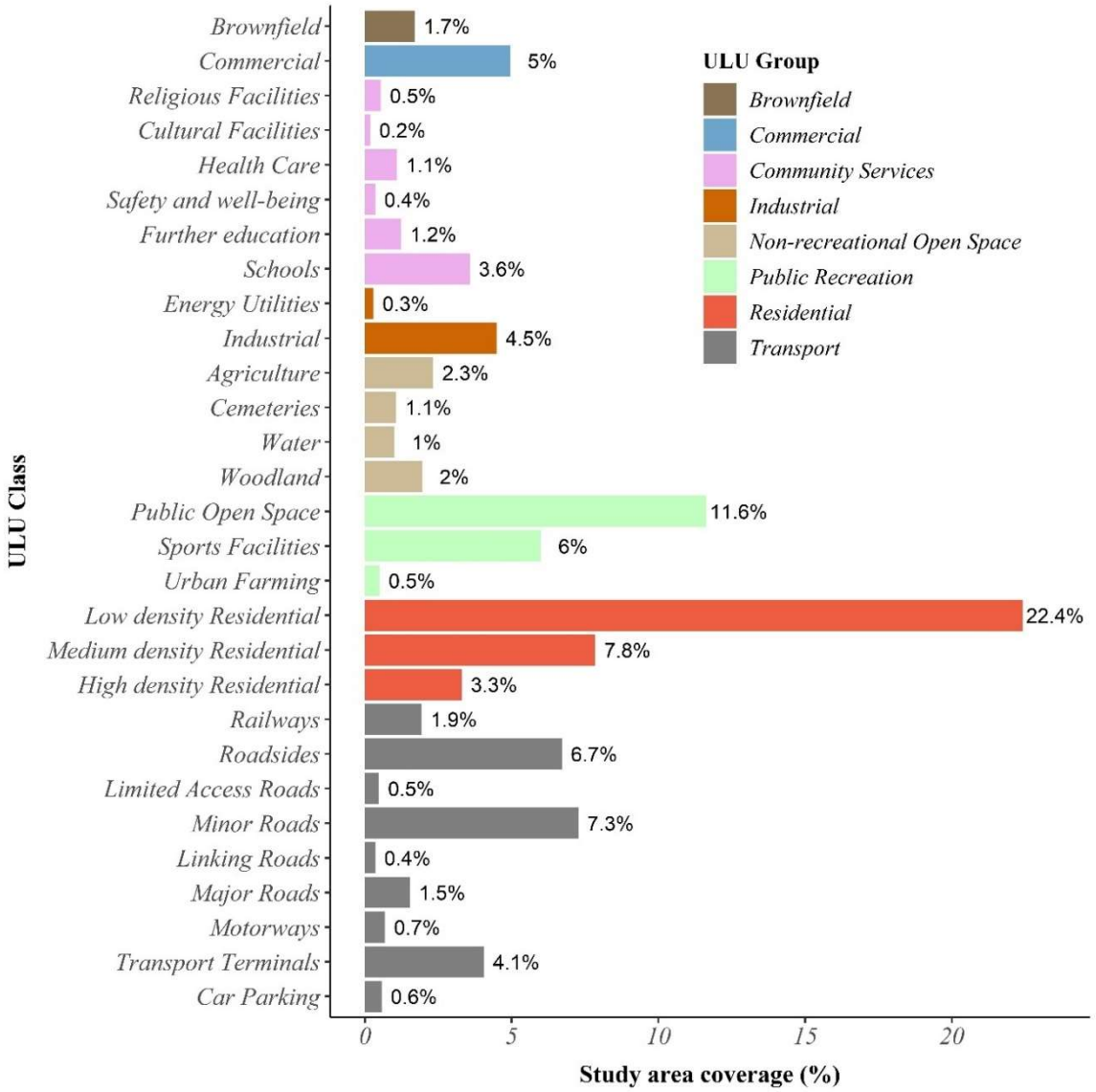

Figure 4.6 – Urban land use class coverage as a percentage of the total study area

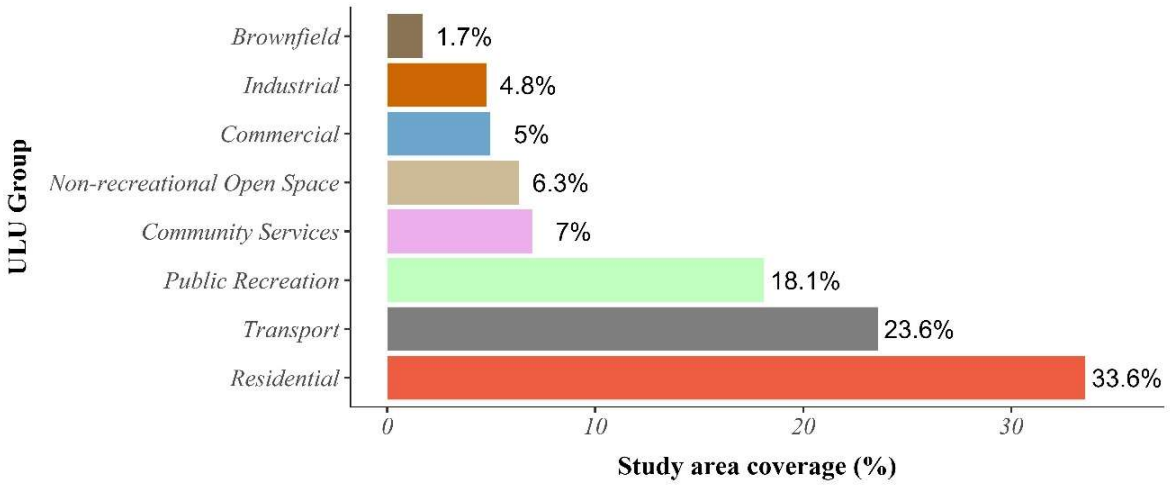

Figure 4.7 – Urban land use group coverage as a percentage of total study area

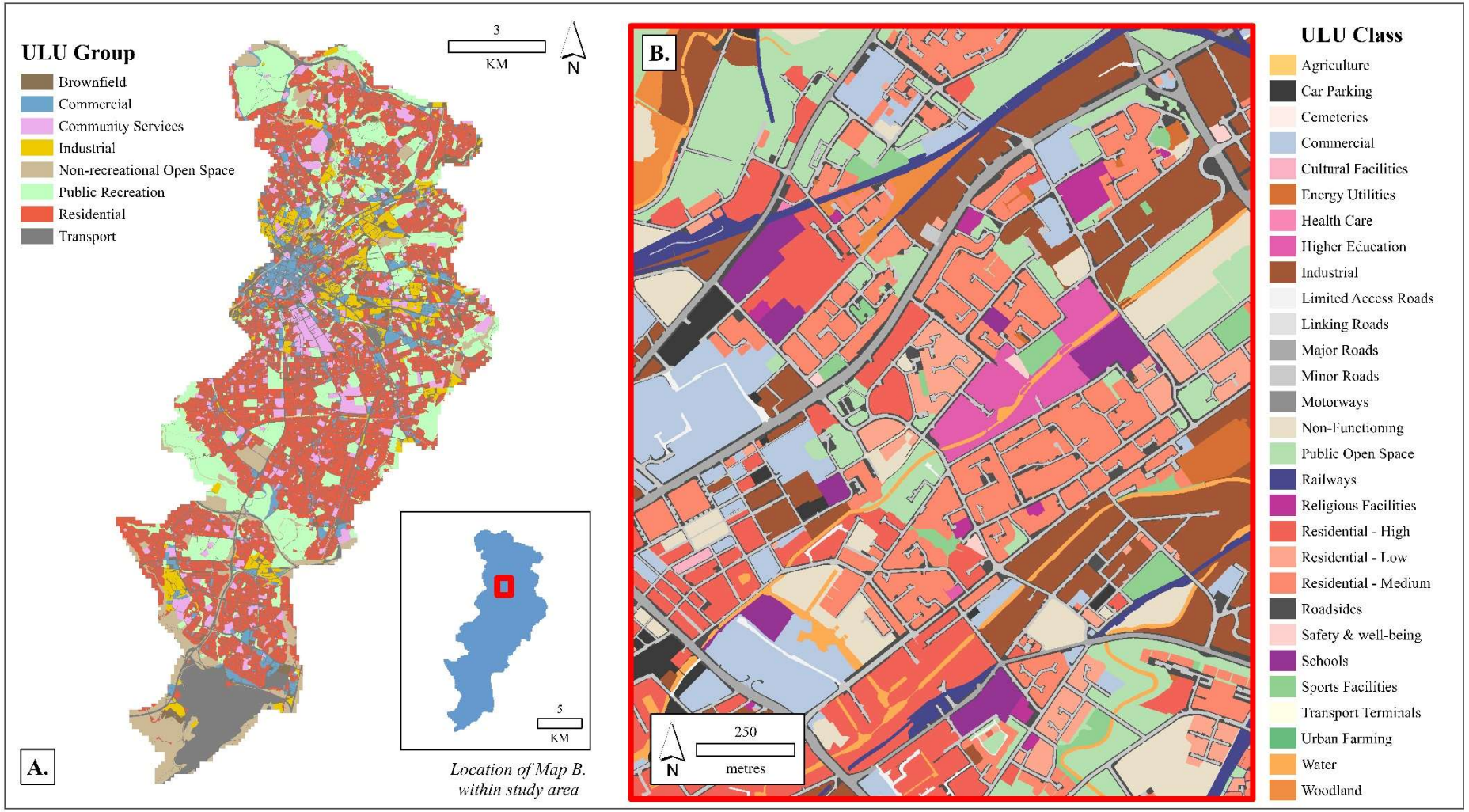

Figure 4.8 –Urban land use 2017 group (**A.**) and class layer (**B.**)

4.6.2 Sampling urban land use of the year 2000

The estimated recall accuracy of the *C.T.* threshold of the *Overlap* algorithm is above 98% for all threshold settings (**Figure 4.9**). A total of 63.5%, 60.2% and 38% of total MM17 candidate sample polygons (*n* = 662,828) were identified as no-change areas for *C.T.* threshold values 0.85, 0.9 and > 0.999 respectively. The first two values return a considerable sample area when considering that the estimated percentage of actual no-change ULU areas is 80.7% (**Table 4.4**).

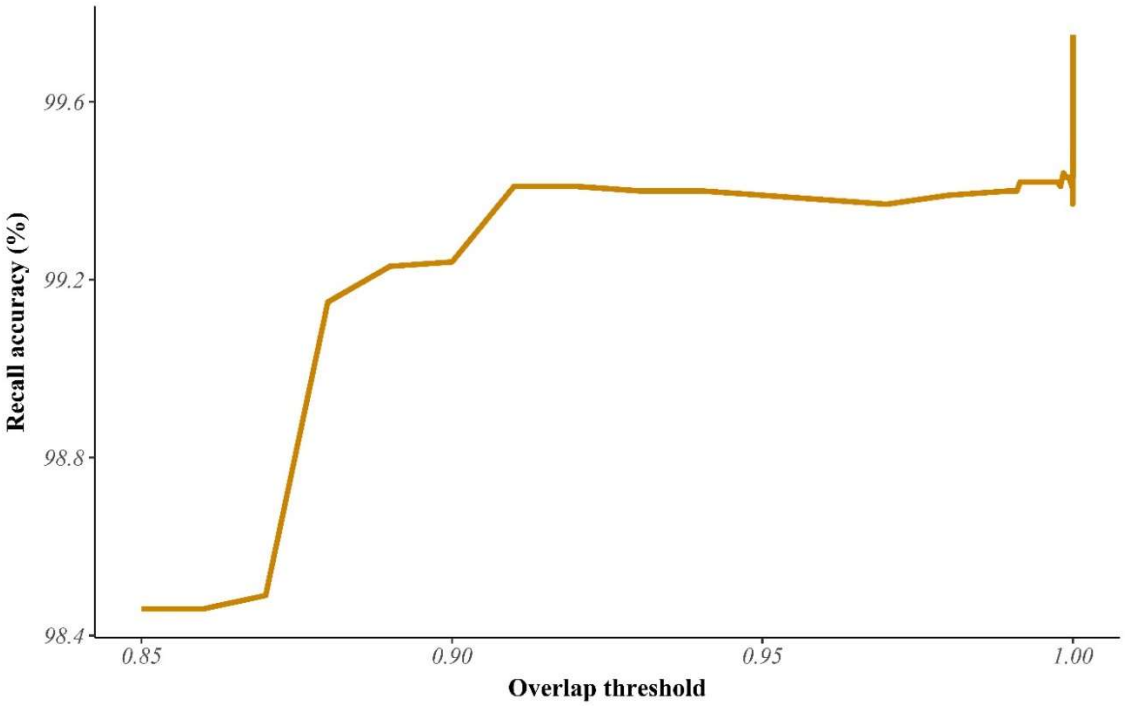

Figure 4.9 – Impact of Overlap threshold upon Overlap algorithm recall accuracy

Table 4.4 - Estimation of ULU change (2000 – 2017)

Change condition	*No. of ULU areas*	*Estimate (%)*	*95% Confidence level estimates**	
			Lower (%)	*Upper (%)*
No change	242	80.7	76.7	85.2
Partial change	18	6.0	2.0	10.5
Full change	40	13.3	9.3	17.8

* = Calculated using Sison-Glaz method with MultinomCI function in DescTools package in R (Signorell et al. 2019)

For selecting final ULU no-change samples, *C.T.* was set at 0.9 as this threshold returns a large sample size with estimated probability sample misclassification at $p < 0.01$. Independent validation of the final sample areas revealed an overall accuracy of 99.5%, with only 2 out of 384 ULU sample areas classed as fully changed. ULU no-change sample area per class varied considerably ranging from 1.4% for Minor roads to 81.5% for Water (**Figure 4.10**). Five ULU classes (Minor Roads, Linking Roads, Limited Access roads, Major Roads and Railways) have no-change sample areas < 10% of the appropriate ULU 2017 class area. Transport group classes in particular had low no-change sample area percentages, due to significant differences in the way road areas are mapped between the 2017 MasterMap and 2000 Land-line data. In MasterMap, roads are subdivided into separate polygon features representing junction boxes and individual road segments, whereas in land-line data, road extents are continuous and may not be clearly defined by a definitive boundary i.e. area defined by road edge polylines extends into non-road areas. The minimum number of GBI change layer pixel sample units within ULU no-change areas is 4,402 (Linking Roads), which is indicated as an appropriate number to estimate change detection class coverage per ULU class (Gill et al. 2008, Pauleit et al. 2005). For example,

Gill et al. (2008) evidence that 400 random sample points for land use classes results in convergence of landcover proportion estimates.

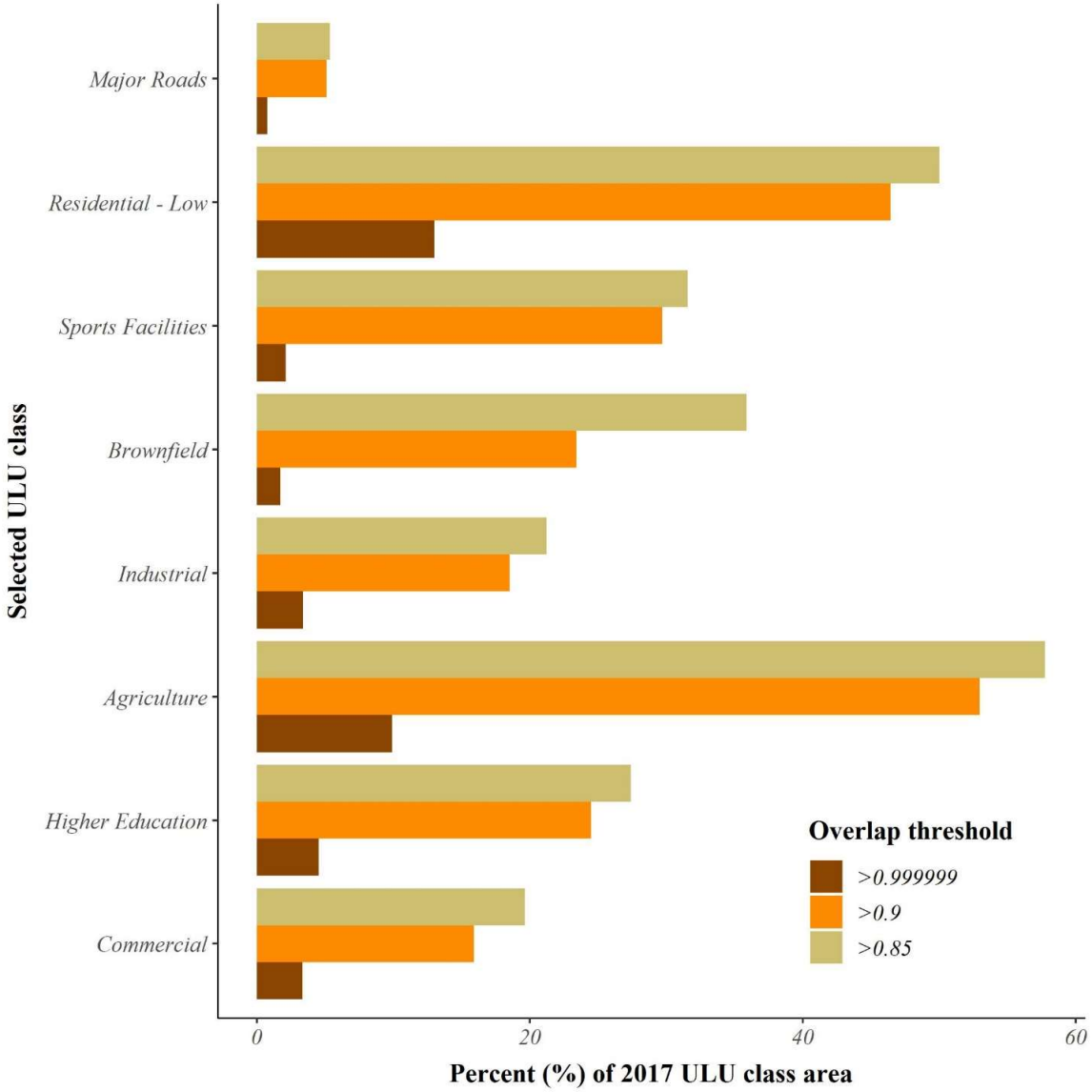

Figure 4.10 – No-change sample area per test *C.T.* value for selected urban land use (ULU) classes

4.6.3 Green-blue infrastructure change layer (2000 – 2017)

Overall accuracy of the year 2000 GBI and Non-GBI classification was 94.2%, which is comparable to the same two-class classification for 2017 (96.8%) (**Tables 4.5 and 4.6**). A rule-of-thumb estimate for basic change detection accuracy, through simple classification differencing, may be obtained by multiplying these two values (Olofsson et al. 2013). This estimate of 91.8%, compares well to the overall accuracy of 92.4% for the CD1 layer. Independent validation (**Table 4.7**) estimates low User's accuracy for the Gain class, thus indicating that Gain areas are considerably over-estimated in the current CD1 layer. Object-based adjustment of CD1, resulting in CD2, accounts for various sources of error and thus results in a marginal improvement in overall accuracy (94.7%) in addition to substantially improving the accuracy of the Gain class (**Table 4.8**). As is evident, CD2 voids 4.6% of CD1 class area, and removes some correctly classified validation points from the CD1 analysis (Serra et al. 2003). However, improvement in the accuracy of the change classes is beneficial for reducing range between high and low confidence interval change estimates using the error-adjusted net-change calculation (Olofsson et al. 2013). An example of the change detection classification data view is provided in **Figure 4.11**. Due to development (2000-2017) GBI in **Figure 4.11A** is converted to non-GBI in **Figure 4.11B**; the reverse is true, as non-GBI in **Figure 4.11C** is converted to GBI in **Figure 4.11D**

Table 4.5 - Error matrix for 2017 GBI classification

	Non-GBI	GBI	User (%)
Non-GBI	248	12	95.4
GBI	9	378	97.7
Producer (%)	96.5	96.9	
Overall accuracy (%)		96.8	
Kappa		0.93	

Table 4.6 - Error matrix for 2000 GBI classification

	Non-GBI	GBI	User (%)
Non-GBI	293	8	97.3
GBI	31	338	91.6
Producer (%)	90.4	97.6	
Overall accuracy (%)		94.2	
Kappa		0.93	

Table 4.7 - Error matrix for CD1 layer

	LOSS	GAIN	GBI Stasis	Non-GBI Stasis	*Users (%)*
LOSS	71	0	6	2	*89.9*
GAIN	1	42	19	5	*62.7*
GBI Stasis	6	0	206	1	*96.7*
Non-GBI Stasis	5	2	0	252	*97.3*
Producers (%)	*85.5*	*95.5*	*89.2*	*96.9*	
Overall accuracy (%)		92.4			
Kappa		0.89			

Table 4.8 - Error matrix for CD2 layer with percentage class change from RCD1 using object-based cleaning

	LOSS	GAIN	GBI Stasis	NVG Stasis	*Users*
LOSS	60	0	4	1	*92.3*
GAIN	0	35	8	2	*77.8*
GBI Stasis	4	3	209	1	*96.3*
Non-GBI stasis	6	2	0	251	*96.9*
Producers	*85.7*	*87.5*	*94.6*	*98.4*	
Areal change (%)	-14.7	-35.2	+2.4	+1.0	
Overall accuracy (%)		94.7			
Kappa		0.92			

Figure 4.11 – Example of Loss and Gain class areas from the RCD2 classification

4.6.4 Green-blue infrastructure change trends (2000 – 2017)

4.6.4.1 Manchester Study area

GBI cover for the study area in 2000 (estimated using error adjustment methods; **Section 4.5.4**) at 50.2% (±2.6%; 95% CI), in comparison to 44.7% in 2017. This change converts to 5.5% net GBI loss (±2.6%; 95% CI) of the total study area, or 10.9% net GBI loss (Low estimate = 6.0%, High estimate = 15.3%; 95% CI) as a percentage of the estimated GBI in 2000. Approximate GBI cover per resident in 2000 was 128.1m^2 compared to 99.8m^2 in 2017 – a reduction of 54.5m^2, or 22.1% of existing GBI per resident. However, despite the overall trend of GBI loss, GBI change varies across the study area. For example, 6.4% (±1.4%; 95% CI) of the study area recorded GBI gain, in comparison to GBI loss for 11.9% (±1.2%; 95% CI).

At the analysis cell level, net gains are recorded for 25.7% of cells in comparison to net losses recorded for 55% of cells. **Figure 4.12** evidences this dynamism in GBI gain and loss: in the gain cells, existing built infrastructure has been removed and replaced with green infrastructure, however car-parking facilities (non-GBI) now replace previous green infrastructure in the cells recording GBI loss. Overall, 42.7% of analysis cells showed relatively minor GBI change (±5%; 95% CI), whilst maximum recorded GBI change was 77.9% and 92.2% for gain and loss cells respectively (**Figure 4.13**). Patterns in analysis cell GBI change exhibit a high degree of spatial autocorrelation as evidenced by the Moran's I test ($I = 0.55$, $p < 0.0001$).

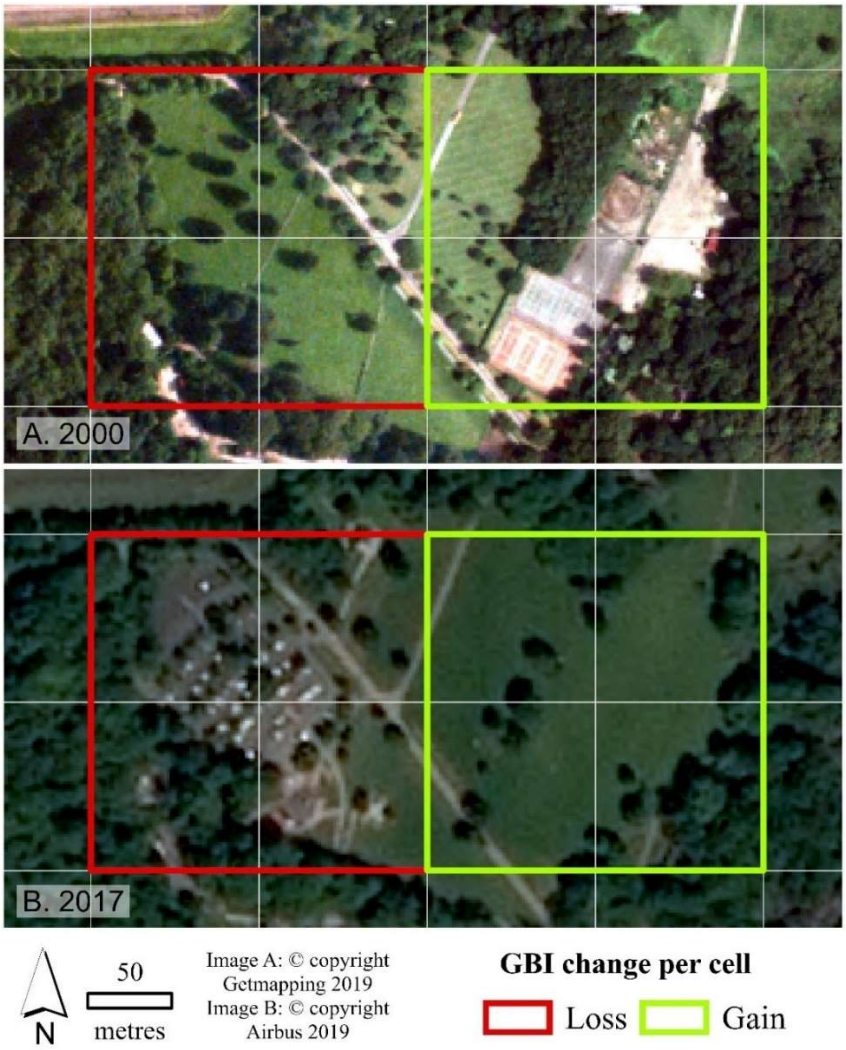

Figure 4.12 – Image comparison for cells recording net green-blue infrastructure Loss and Gain between 2000 (**A**) and 2017 (**B**)

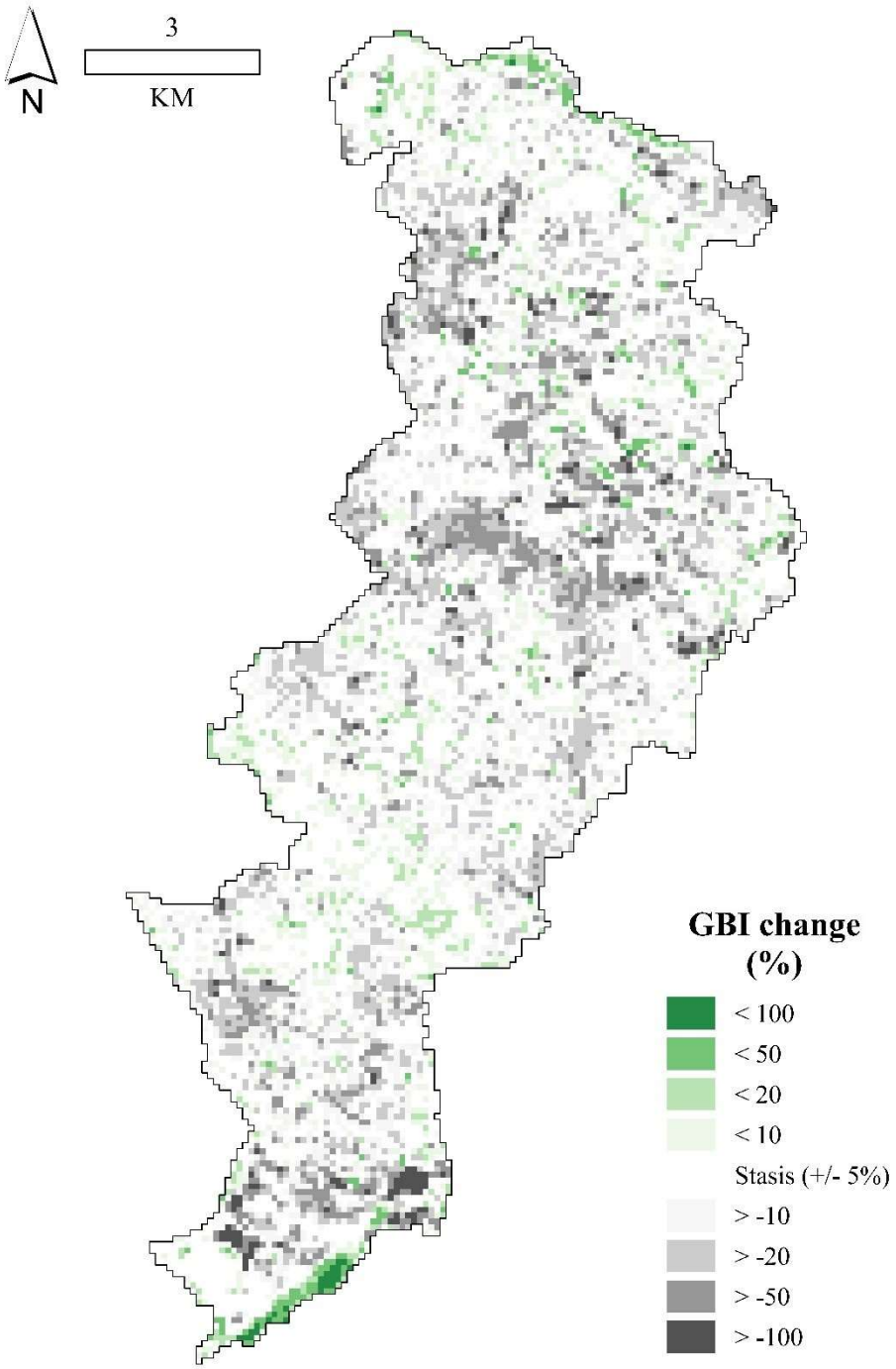

Figure 4.13 – Green-blue infrastructure change (%) per analysis cell area

4.6.4.2 Urban land use

Overall trends for ULU no-change sample areas are largely negative, with 17 out of 29 ULU classes recording statistically significant losses in GBI (**Figure 4.14**). In comparison, just one class records net gain in GBI (Railways), with stasis recorded for all other classes. Rates of GBI change (as percent of estimated year 2000 sample GBI cover) vary considerably between classes (**Figure 4.15**). Large losses in GBI are apparent for Car Parking (74.2%) and Major Roads (41.7%). Declines in GBI resources in Low, Medium and High density residential ULU classes were recorded as 11.9%, 28.3% and 5.7% respectively. This indicates considerable GBI losses between 2000-2017 across residential areas (e.g. gardens), particularly for Medium density Residential areas characterised by terraced housing.

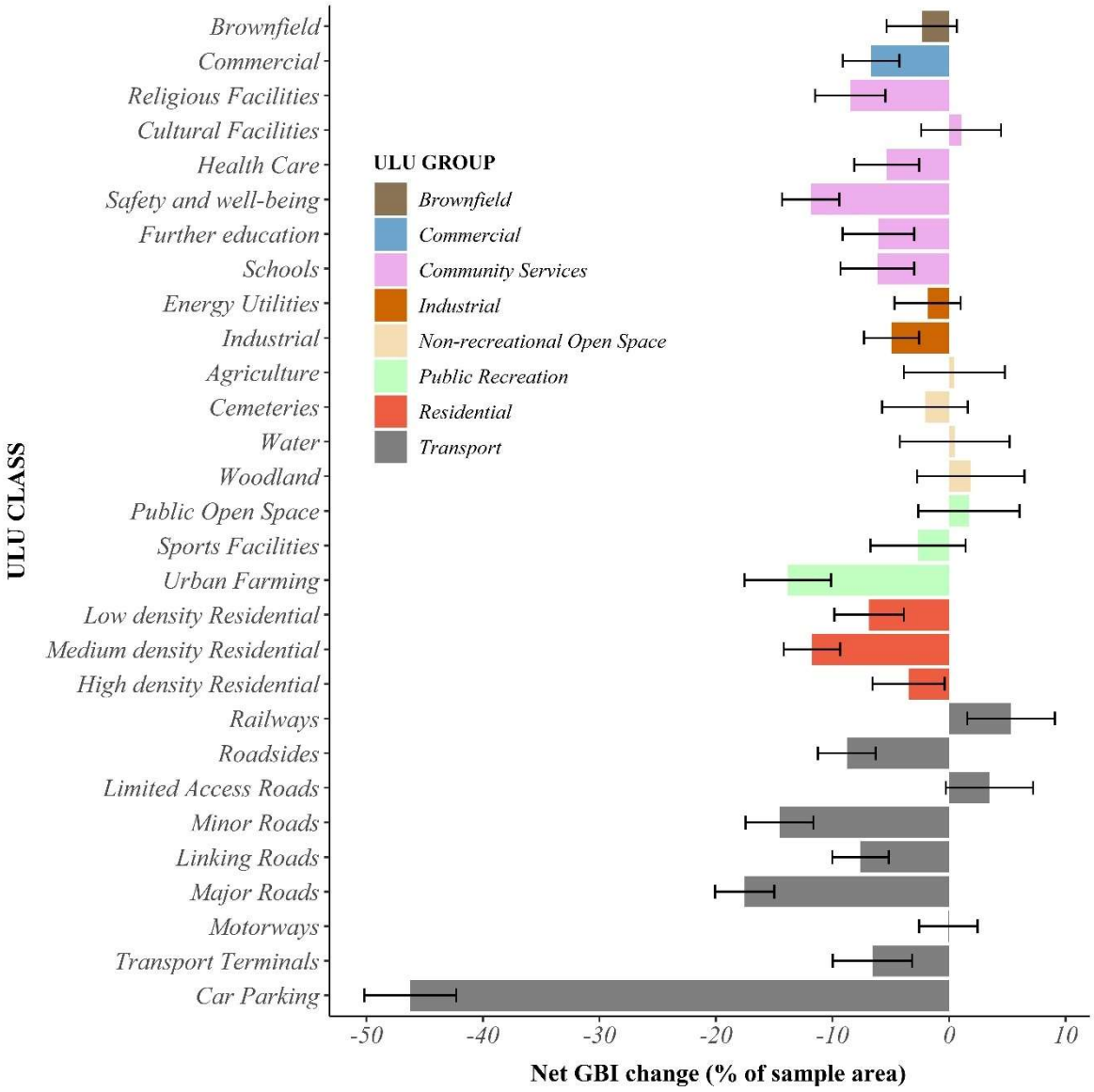

Figure 4.14 – Green-blue infrastructure change area as percentage (± 95% CI) of total urban land use sample area

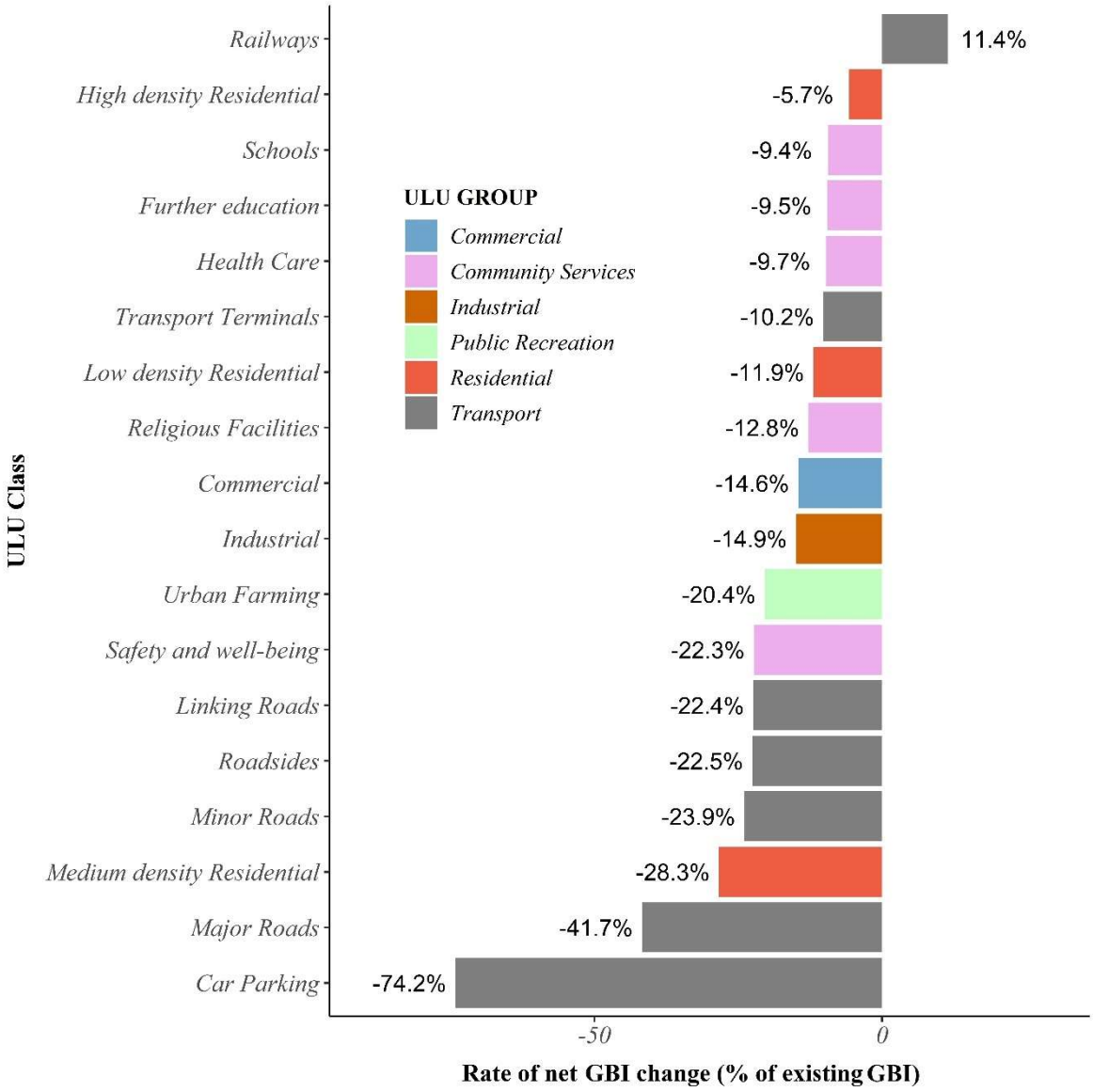

Figure 4.15 - Green-blue infrastructure change as percentage of 2000 green-blue infrastructure per urban land use class

Within overall GBI change trends for ULU classes, dynamism in GBI change areas are evident (**Figure 4.16**) with areas of Loss and Gain recorded for all ULU classes. Overall GBI change trends are determined by the balance between Loss and Gain sample cover (Loss Area Dominance). Whilst the Woodland ULU class exhibits a lower dominance value than Railways, the overall GBI Gain trend is not significant, as the large percentage of GBI stasis inflates the confidence interval change estimates for this class. ULU classes exhibiting overall GBI Loss trends exhibit variation in GBI gain areas (as percent of total sample area) between 1.9% and 10.4%. In comparison, the Railways ULU class (exhibiting GBI change),

shows GBI loss area coverage of 9.8%. ULU classes exhibiting stasis exhibit ranges of 2.5-14.6% and 2.1-11.2% for Gain and Loss area coverage respectively. The degree overall GBI change rates aggregate dynamism between gains and losses in GBI thus varies between ULU classes (**Figure 4.17**).

Comparing overall GBI change rates reveals similar values for a number of classes (**Figure 4.15**), and therefore, in terms of explaining varying rates of GBI change, some redundancy in class categorisation may be apparent. To statistically test whether differences in the distribution of estimated GBI change rates exist, distributions of class GBI change rates were created from exclusive random sample subsets. As ULU no-change sample areas vary considerably in size, thus having variable influence upon overall estimates of class GBI change, equal size pixel groupings representing the ULU minimum mapping unit area ($45m^2$ = 20 pixels) were used as analysis units. The number of groups selected per class (n = 219) was determined from the number of units contained within smallest ULU class sample pixel area (Linking Roads; n = 4402pixels/20 ≈ 219 subsets). GBI change (as percent of existing GBI) was then calculated for each subset.

As the Kruskal-Wallis test ($\chi^2 = 2492$, $p < 0.001$) provided strong evidence of inter-class differences in the distribution of GBI change rates, a pairwise Wilcoxon-Mann-Whitney U-test with Bonferroni correction (Base package, R Statistical Programming language; R Core Team 2019) was used to test for differences between ULU classes. In all, 321 out of a total 406 (79.1%) of class pairings displayed significant differences in estimated GBI change rates, with the majority of non-significant differences (70 out of 85) recorded between classes of different ULU groups and distinct land uses. A notable exception in this regards is the significant pairing between Commercial and Industrial ULU classes, as both ULU classes represent land use for private enterprise (this is discussed further in **Section 4.7**). Significant differences between ULU sub-group class indicated that the current sub-group categorisation scheme provides an approximation of varying GBI change rates within group areas. However, insignificant pairings recorded for Community services (n = 5), Non-Recreational open space (n = 2) and Transport (n = 8) ULU groups, evidence similar development patterns between some sub ULU group classes (see **Appendix 4.9** for results).

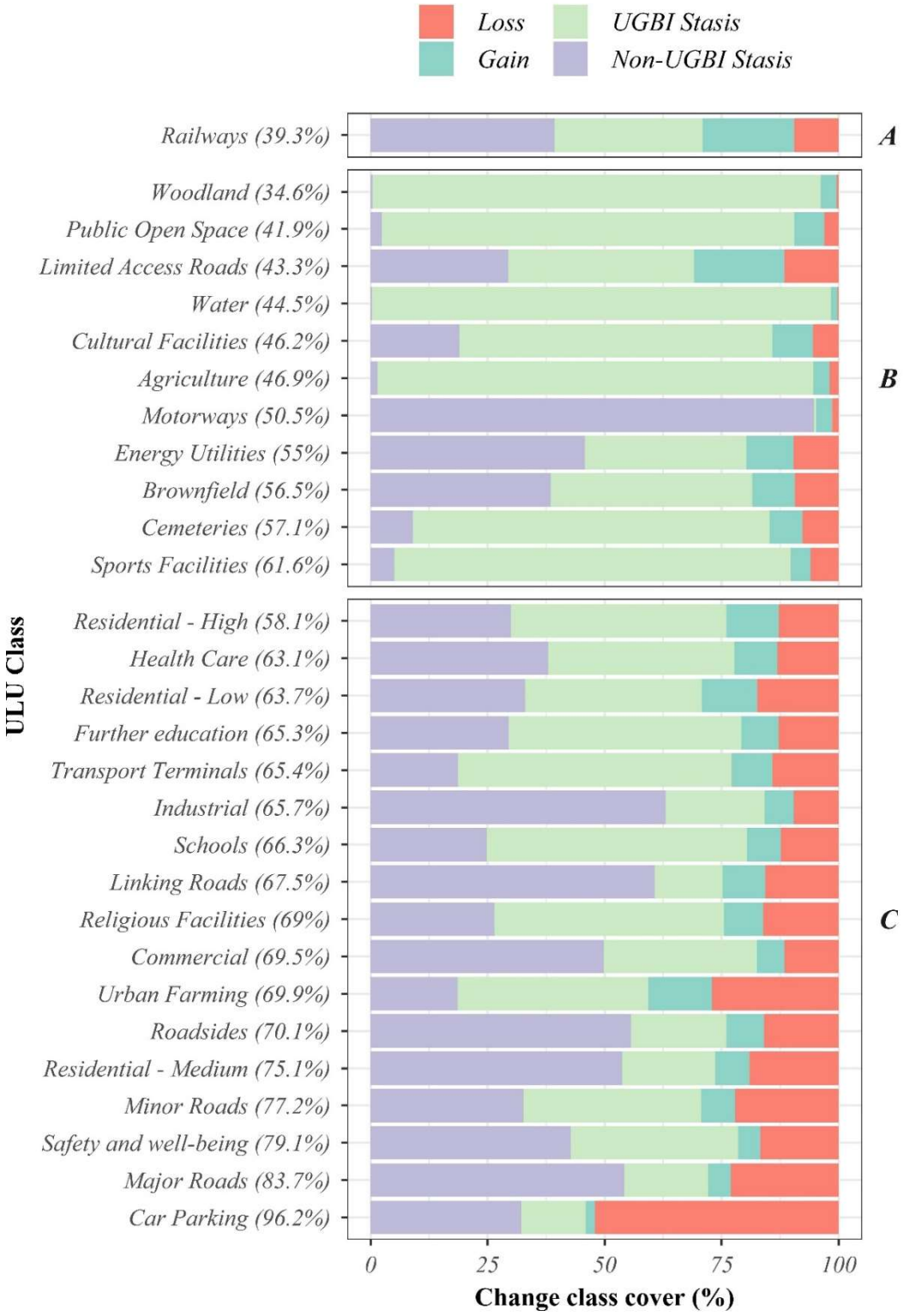

Figure 4.16 – Percentage of green-blue infrastructure (GBI) change class (**A** = Gain, **B** = Stasis, **C** = Loss) area for urban land use (ULU) samples. Bracketed figures represent Loss area dominance [= (Loss area/(Loss area +Gain area)) x 100]

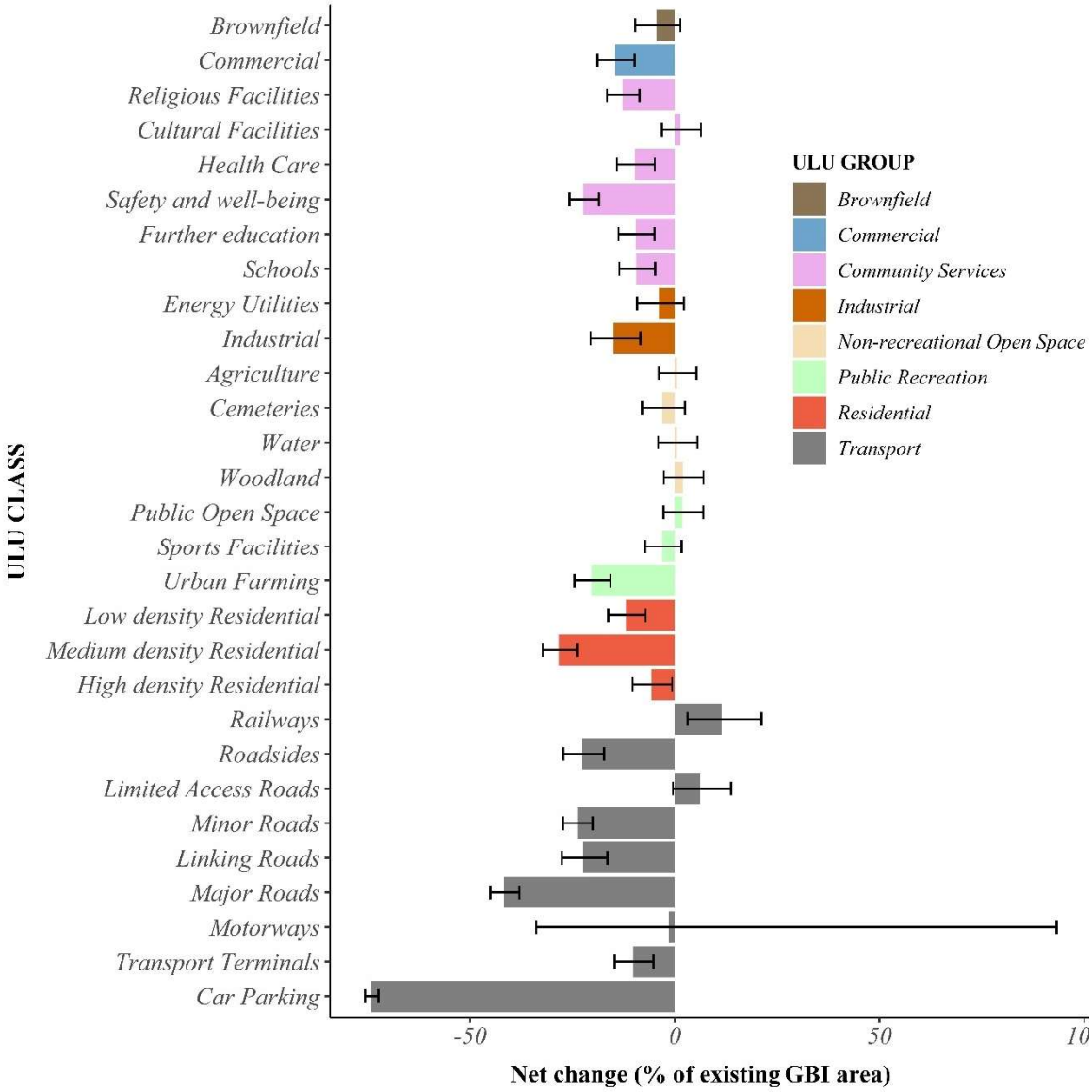

Figure 4.17 – Green-blue infrastructure (GBI) change area (± 95% CI) as percent existing GBI per urban land use (ULU)

4.6.4.3 Future change

When considering total GBI area per ULU class, the greatest loss in GBI is expected to occur within the Roadsides, Medium density Residential and Low density Residential classes (**Figure 4.18**). Whilst rates of GBI change for the Low density Residential class are relatively low (-11.9%), this class contains over 20% of all 2017 GBI. As such, assuming land use areas remain relatively static approximately 17 years into the future, current trends

indicate 45% of total GBI loss will occur within this class. Relatively higher rates of GBI loss for Car parking and the Major roads class, have lower implications for future GBI levels due to respective study area coverage of just 0.6% and 1.5% for these classes. The implications may be examined on a spatial level at both the analysis cell and administrative ward level (**Figure 4.19**). As evidenced, high estimates of potential GBI loss are prevalent within suburban residential areas south of the City Centre, which contain large areas of Low density Residential class areas.

In contrast, when considering the study area as a whole, future GBI cover estimates depend upon the calculation method used. When considering statistically significant GBI change for ULU classes, GBI cover in the 2030s is estimated to decrease by 3.1% (± 1.0%; 95% C.I.). In comparison, using study area baseline change estimates for all GBI resources, future GBI cover is expected to decrease by a total of 4.9% (+1.9%/-2.2%; 95% C.I.). The difference between the two central estimates (1.8%) provides a basic indication of the level of GBI change due to land use conversion. Raw neighbourhood level estimates for GBI decline do not consider GBI change from this process and may therefore currently underestimate the magnitude of GBI decline in the future.

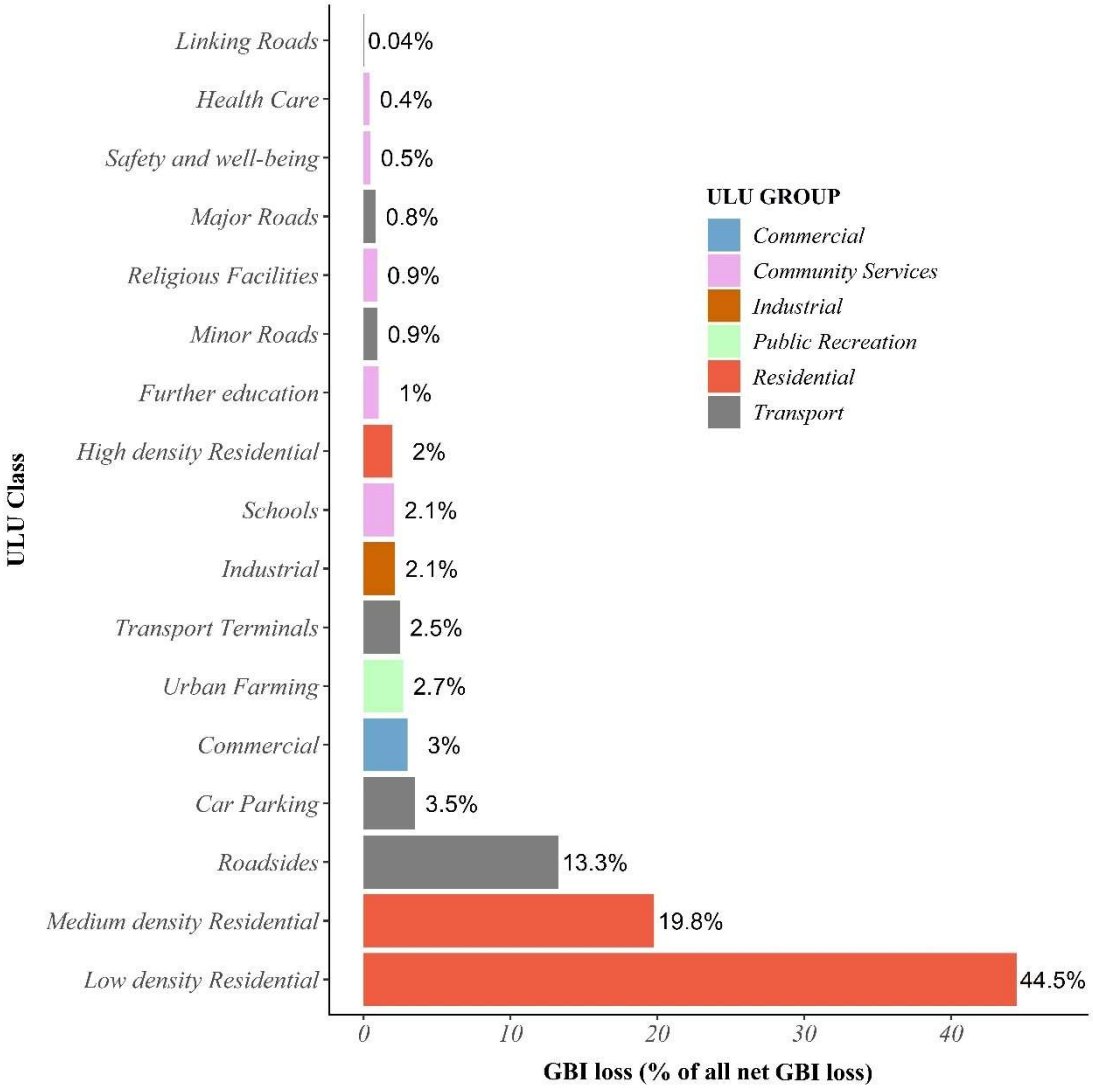

Figure 4.18 – Percentage of all future predicted green-blue infrastructure loss per urban land use class

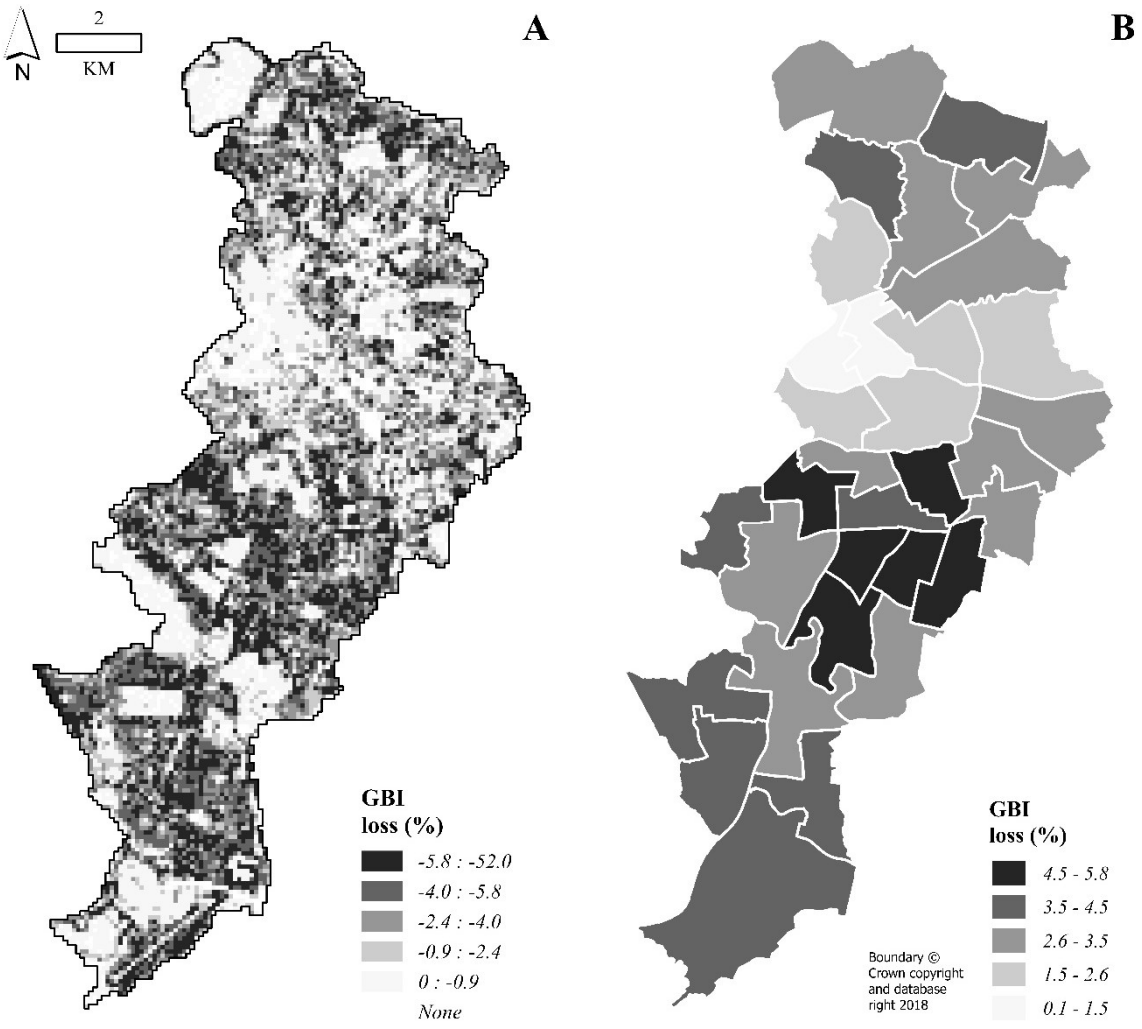

Figure 4.19 – Predicted green-blue infrastructure loss per analysis cell by 2034 (**A**) and predicted GBI loss per administrative ward by 2034 (**B**)

4.7 Discussion

Results indicate a decline in GBI across the study area between the years 2000 and 2017, which may contribute to a trend of longer term degradation in natural resources. A study by Dallimer et al. (2011) measured an approximate 3% decline in greenspace in the city of Manchester's urban core between 1991 and 2006. This study was not representative of the city as a whole but indicates that the GBI degradation recorded here is part of an ongoing process. Additional timesteps between 2000 and 2017 are therefore required to assess whether GBI change reflects various phases of economic growth and decline during this period. Certainly, the indications of GBI decline are contiguous with efforts to regenerate the city. Efforts to re-build the city of Manchester's post-industrial economy began in the 1980s with regeneration of the city centre and has continued apace with substantial re-development since the year 2000 (Swinney & Thomas 2015). Notable developments between 2000 and 2017, such as Manchester Sports-City (Smith 2010), and the New Islington district close to central Manchester (Urban Splash 2020), are representative of overall economic and population growth during this period. GBI degradation will have occurred due to this process of densification in built infrastructure (Haaland & van Den Bosch 2015), through either land use conversion or infill development in consistent ULU areas. The results in this chapter demonstrate that this process varies spatially in intensity according to both location and land use across the city.

For the majority of ULU Transport road classes, GBI change will occur within associated road sidings and central reservations. Losses or gains in vegetation canopy will impact both Roadsides (where vegetation is likely to be planted) and adjoining road areas (where tree canopy may overhang). GBI losses in Transport road classes are not unexpected given that countrywide urban street tree losses have been documented in the UK national press (Kirby 2017). This trend however has not been previously quantified through quantified study. Rates of GBI decline are high for Linking, Minor and Major roads, but do not represent a significant loss of GBI, when considering total GBI coverage within the study area. GBI losses in Roadside areas are, however, concerning given that such resources are accessible to pedestrians and provide additional RES including particulate capture and noise buffering (Salmond et al. 2016). Associated GBI degradation in Minor Roads indicate

that roadside GBI losses are linked to road infrastructure supporting Residential ULU group areas.

GBI decline recorded for Residential ULU group classes coincide with temporal declines in garden green infrastructure/porous surface area identified in other studies (Perry & Nawaz 2008, Warhurst et al. 2014, Verbeeck et al. 2011). For Medium density Residential areas estimated year 2000 GBI levels (27.3%) were already relatively low in comparison to Low (46.3%) and High (37.7%) density Residential classes, and existing low provision of ecosystem services may have degraded significantly further in these ULU class areas (Perry & Nawaz 2008, Whitford et al. 2001). GBI losses in low density housing are less severe but are a serious concern for ecosystem service management given that this class covers over a fifth of the study area. Evidence indicates that population growth may influence conversion of single dwellings into multi-occupancy units, where garden paving occurs to provide car parking space for tenants (Bibby et al. 2018, Perry & Nawaz 2008). In addition, population pressures on households may also influence decisions to extend existing housing units, or subdivide existing garden areas for new housing, in turn pressurising existing GBI in residential areas (Sayce et al. 2012). GBI change rates for high density residential class (e.g. apartment blocks or flats) are significantly lower than other residential classes, as these areas are not subject to the 'tyranny of small decisions' from private garden owners (Dewaelheyns et al. 2016, Goddard et al. 2010). As current predictions of GBI change indicate that approximately two-thirds of all future GBI loss may occur in Residential areas, the conservation of residential GBI should be a key concern for citywide green-blue infrastructure planning strategy.

GBI change for both Transport Terminals and Car Parking classes appear to follow similar patterns found in other ULU classes, whereby GBI is lost by expanding built infrastructure e.g. impervious surfaces for parking, extensions of existing building areas. GBI decline is also prevalent in areas under public (Community Services: Schools, Further Education, Health Care, Safety and well-being) and commercial sector (Commercial and Industrial group) management. As indicated by pairwise significance testing, rates of GBI change are relatively consistent for these groupings. GBI in these areas may thus have been removed and replaced with landcover types that are more economically beneficial for the managing organisation (Mell et al. 2013). Pressures to convert GBI to more economic 'grey-

space' covers may compound, as population growth causes public and economic services to produce 'more with less' land (Kabisch 2015, Whitten 2019). Interestingly, Cultural facilities record no significant change in GBI, which may indicate that pressures for GBI conversion are more evident for public services that are indispensable to the general population.

In contrast, net gains are recorded for Railways (11.4%), whilst overall GBI stasis is recorded for all ULU Non-recreational Open Space group classes, in addition to Public Open Space, and Sports Facilities. Indeed, a surprising finding from this investigation is the amount of dynamism between GBI gain and loss within the study area (see **Figures 4.11 and 4.12**). In addition, there is also evidence that canopies for some trees (e.g. street trees) and tree lines (e.g. edge of woodland or tree clusters) have expanded in coverage over the time period, thus contributing to the total amount of GBI gain recorded. Green infrastructure schemes initiated by the local government (MCC 2016b) and various non-governmental organisations (e.g. City of Trees 2020, Groundwork 2020) have thus contributed to GBI gain measured in this investigation. Overall GBI change trends for ULU classes are thus limited in accounting for this dynamism, and indeed without further evidence it is only possible to speculate on the causal factors above that may influence GBI change within the study area.

Overall, given the local council's commitment to improving environmental conditions in the city, the overall trends in GBI loss should present a concern. Manchester, in common with many cities around the world, is attempting to improve ecosystem services, whilst also pursuing policies of economic growth (MCC 2015a, MCC 2020b). To achieve environmental goals the council has published a number of actions within it's Green and Blue infrastructure action plan (MCC 2015b), that if implemented, will improve local GBI resources and ecosystem services in the study area. Funded projects, such as the £500,000 Clean city programme to deliver community greening initiatives, and the Environment Agency's multi-million pound northwest river basin management plan, will see future environmental improvements (MCC 2015b). The council has also defined actions to embed GBI as part of new public and private infrastructure developments. Measures in the plan include green infrastructure retrofits (e.g. green walls, roof gardens) to existing buildings, sustainable urban drainage systems, and streetscape improvements (MCC

2015b). Given the considerable loss of GBI in many areas of the city, implementation of these actions is essential in order to ameliorate some of the GBI degradation experienced in previous years, and also limit the environmental damage caused by new development.

To develop the aforementioned strategies further, the measures of GBI change, and current RES indicators (**Chapter 3**), could be compared to identify priority locations to enforce GBI conservation measures. The remote sensing and GIS methods employed here could also be re-employed in the future as a process to examine the relative success of GBI investment strategies implemented by the council and other local bodies (e.g. housing associations, non-profit organisations). Further research is also necessary to improve current limitations in temporal change information here. For example, it may be beneficial to stratify abundant land use classes (e.g. Low density residential) using proxies for differing land management practises (e.g. private and non-private home ownership, residential socio-economic status) that may also influence differing rates of GBI change (Dewaelheyns et al. 2016, Goddard et al. 2010). Synoptic land use mapping for different timestops would also be beneficial for quantifying GBI change according to different land use conversions, in order to assess the environmental implications of prospective infrastructure developments in the study area (Borzacchiello et al. 2010, Tayyebi et al. 2010). Improvements to the GBI change detection process is also beneficial to refine confidence intervals in landcover change estimates. For example, negating the need to void classification areas will reduce redundancy in GBI change estimates, whilst access to improved image data may enable change detection amongst additional landcover classes (Liu et al. 2019, Huang et al. 2017). This is especially important for modelling future levels of RES by estimating change for differing functions of GBI components (Kain et al. 2015). Opportunities to improve current methods are therefore discussed in more depth in **Chapter 6**. As tracking the performance of local environmental policies is a concern for the council and given the scale of GBI degradation in parts of Manchester, there is incentive for the council to fund programmes to monitor the rates and implications of GBI change. Whilst investment in new GBI will bring environmental improvement, it is equally important to conserve existing GBI resources and RES to achieve collective social, environmental, biodiversity and carbon neutrality goals in the study area (GMCA 2019, MCC 2015a).

4.8 Conclusion

This chapter developed a novel geospatial workflow to assess GBI change within land use, and thus predict urban locales where GBI decline may occur in the future. The overall balance of GBI change over this period was therefore negative, with GBI decline representing approximately 5.5% of the study area. Severe declines in GBI are recorded for the Car Parking and Major Roads ULU classes, although declines in residential areas are of greatest concern, given the areal coverage (33.6%) of this ULU group across the study area. Since the turn of the century, city residents have likely experienced declining trends in RES benefits as a result. This trend is expected to continue in the future as projected population growth in the city (4% growth 2018 - 2028; ONS 2020) causes GBI decline through residential infill development and land use conversion. An increase in the number of residents, coupled with increases in the severity of environmental stressors is likely to increase RES demand in the future. Understanding the level of GBI investment and conservation required to sustain urban resilience within dynamically changing urban environments will become increasingly important for urban planning stakeholders (Carter et al. 2015, Gill et al. 2007, Kain et al. 2016). The following chapter (**Chapter 5**) therefore builds on the evidence base in this, and the previous chapter, to examine the effectiveness of GBI management scenarios in maintaining future RES benefits in Manchester.

Overall, as population growth and urban development has occurred throughout the country during this period, the trends highlighted here provide indication of the scale of GBI degradation that may have occurred in other UK urban areas (Dallimer et al. 2011). As cities in the UK and across the world face the continuing implications of climate change, GBI resources will become ever more important for regulating the impacts of environmental stressors upon local residents (Carter et al. 2015). Given the evidence of vulnerability of GBI resources for numerous urban centres across the world (Kabisch & Haase 2013, Zhou et al. 2018), the methods described in this chapter should be adapted in other study areas to examine important trends in environmental change. Overall, additional research is beneficial to identify consistent land use factors causing GBI and RES decline across different urban areas, which will then contribute to the existing knowledge

base to support RES protection policies at local and national levels (Cortinovis & Geneletti 2018).

Chapter 5: Scenario analysis

5.1 Introduction

In the previous chapters, methods were developed to examine spatiotemporal dynamics in green-blue infrastructure (GBI) and regulating ecosystem services (RES) in urban areas. This is not only beneficial to guide future efforts to research and map urban ecosystem services but is also useful to highlight environmental concerns that impact both the study area, and other urban centres (Burkhard et al. 2012, Kremer et al. 2016b). Overall trends in GBI loss should therefore present a concern for environmental planning in the city of Manchester, as this indicates future loss of RES is likely, at a time when demand for RES is also likely to grow. Increases in population levels, coupled with projected increases in temperature and precipitation stressors, is likely to increase the need for GBI as a resource to fortify urban climate resilience (Carter et al. 2015). As demand for RES to mitigate negative environmental conditions varies across the study area, it is important to consider the impact of future development upon spatial distribution of GBI, and how this affects the supply of RES (Gill et al. 2007). Whilst local policy documents describe a range of environmental targets and strategies, it is unclear whether such actions are suitably robust to counter projected declines in GBI in coming years (Wellmann et al. 2020).

In response to the need for improved planning information, this chapter will develop the methods and findings in preceding chapters to examine how differing levels of strategic spatial GBI investment may address future declines in RES. GBI change, measured over an inter-year period, will provide a projection of GBI change rates for differing land uses (**Chapter 4**). This information can then be combined with local land use planning information, to provide a future baseline of GBI and seasonally adjusted RES (**Chapter 3**). Working within the constraints of the mapping approach (**Chapter 2**), this future baseline may then enable an examination of how alternative GBI investment scenarios benefit future RES conservation within the study area. Drawing together work from previous chapters should therefore enable an improvement of current land use ecosystem service scenario planning approaches, by incorporating estimates of unplanned landcover change with defined investment strategies. Findings from scenario analysis will then provide an

indication of the scale of GBI investment required to conserve current RES levels, and thus benefit urban resilience in the study area.

5.2 Aims and objectives

Chapter aims: Assess how the methods and findings of previous objectives can inform scenario planning of regulating ecosystem services.

1. Combine information from local planning policies and trends in spatiotemporal GBI change to identify future urban development scenarios in the study area

2. Compare the impact of GBI management scenarios upon the provision of future regulating ecosystem services

3. Discuss implications of findings for environmental management for the city of Manchester

5.3 Introduction to scenario analysis

Knowledge of how urbanisation impacts environmental processes is key to the sustainment and even enhancement of future urban ecosystem services. In this regards, comparison of development scenarios enables assessment of environmental benefits provided by various urban green-blue infrastructure interventions (Carter et al. 2015, Lee & Mayer 2018). For example, Gill et al. (2007) demonstrate this by examining the effects of either a 10% increase or decrease in 'greenspace' upon land surface temperature and rainfall runoff volumes within Greater Manchester urban morphology zones, according to climate conditions in the 2050s and 2080s. Predictive scenarios concern the planning goals of end-users and are therefore constrained by the quality of information for this purpose. As such, scenario development methods in the literature vary and may include use of

spatially explicit land-use development models (Petrov et. al 2009, Stürck et. al 2018), adaptation of qualitative information from policy literature (Deilami & Kamruzzaman 2018, Kain et al. 2016), and/or stakeholder engagement to gather expert views on factors influencing urbanisation and urban environmental change (MacPherson et al. 2013, Reed et al. 2013). As planning stakeholders are typically concerned with improving urban living conditions (Karatas & El-Rayes 2015), the scenario approach described here builds upon previous objectives to identify appropriate GBI management strategies to maintain and even improve RES in Manchester in the coming decades.

Achieving this requires consideration of projected spatiotemporal change in GBI in relation to urban land use (ULU), as this represents the varying land management processes influencing GBI development, that must be considered when defining planning legislation (Aronson et al. 2017, Young & McPherson 2013). As described in **Chapter 4**, spatiotemporal GBI change over time relates to either development within stable land uses (Gill et al. 2007), or development resulting from land use conversion (Pauleit et al. 2005), therefore GBI development scenarios benefit from consideration of both processes (Le Roux et al. 2014). For the Manchester study area, future directions in land use conversion is described in planning documents issued by the city council (MCC 2020b), and as such can inform spatially explicit scenario development. A template for this structure is described in the study by Kain et al. (2016), where local planning policy *documentation* in Stockholm, Sweden is examined to inform and contrast spatially explicit ecosystem service improvement scenarios. Following this approach, the findings from **Chapter 4**, regarding GBI *change* per ULU, allow consideration of how various GBI management schemes within different ULU areas may protect future RES, especially when detrimental GBI change is expected *elsewhere* (Le Roux et al. 2014).

The following sections thus describe the application of this approach within the study area. **Section 5.4** explores local planning policy to incorporate land-use change within the current GBI change model for the study area. **Section 5.5** describes the definition and implementation of various GBI management scenarios, within an updated land-use change model. **Section 5.6** assesses the impact of GBI management strategy upon future combined RES deprivation levels in the study area.

5.4 Land use conversion: Local planning policy

The city of Manchester is one of ten local authorities that comprise the Greater Manchester region. The Greater Manchester combined authority draws all of the local councils together under an executive mayor to develop policies that benefit the city-region as a whole. In 2009, the authority released "The Greater Manchester Strategy" which describes broad economic, educational and environmental strategies to make the region "one of the best places in the world to grow up, get on and grow old" (GMCA 2009). Additional documents, such as the "Greater Manchester Local industrial strategy" (GMCA 2019a) and the "5-Year Environment Plan for Greater Manchester 2019-2024" (GMCA 2019b) develop this existing strategy further, and will support the Greater Manchester spatial framework, which is due for release in 2021. Economic and environmental policies in these GMCA documents are likely influence GBI levels in the city of Manchester in the future, but do not provide information at sufficient resolution to identify the locations and types of land use change.

For the city of Manchester itself, there is no overarching masterplan. However, since 2004, the city, in common with all council districts in England & Wales, has been legally required to produce a series of documents to define a Local Development Framework (LDF) to create strong, safe and prosperous communities using local spatial planning (MCC 2020b). In mid-2012, Manchester City Council (MCC) formally adopted its LDF, with spatial planning initiatives described within the city's openly accessible Core Strategy documents (MCC 2020b). The city council also provides spatially explicit information as to the location of various policies through an accessible online interactive proposal map (MCC 2020c). This aids future land use change assessment, as it is possible to identify the spatial extents of land use development areas in relation to the current urban land use 2017 (ULU) classification. In addition, other sources of land use change, such as private sector development (CityCo 2020) and local urban greening initiatives led by local public bodies, such as the Ignition (GMCA 2020a) and GrowGreen (GMGC 2020) were also investigated. However, as spatially explicit information for such initiatives are currently unavailable, such land use information was not used in this analysis. Current environmental policy documents for the city provide limited spatially explicit information on where

environmental improvement will occur, but were nevertheless useful, in conjunction with the relevant literature sources, for developing GBI management scenarios (MCCA 2020a).

Spatial layers representing the areal extents of future LDF development and conservation plans were extracted from the online interactive proposals map (MCC 2020c). Layers were then identified that represent: a) spatial extents of explicit planning policies to be implemented within the study area; b) policies associated to spatial extents that describe land use development or conservation. LDF layers labelled as *Development*, represent policy extents implementing either land use conversion or re-development that may actively alter the composition of GBI resources within the spatial policy extents. LDF layers labelled as *Conservation* represent areas where GBI is potentially conserved through efforts to preserve the character and functionality of the spatial policy extents. LDF layers chosen through this process are described in **Table 5.1**.

In total the combined extents of identified *Development* and *Conservation* LDF spatial policy areas cover an approximate 25% of the Manchester study area. However, in relation to administrative ward boundaries, representing areas of local governance, coverage of spatial policies vary considerably, with some wards highly impacted by LDF policies and others not at all. Therefore, to compare the impact of various scenario management strategies, in areas of contrasting GBI coverage and LDF planning, two wards were chosen for comparative scenario analysis (**Figure 5.1**). Ardwick was selected as the first ward, as this is a highly urbanised area close to the city centre with low GBI coverage (20.4% of ward area), that contains a number of LDF *Development* areas likely to negatively impact future GBI and RES (**Figure 5.2**). In contrast the second ward Chorlton is mainly comprised of suburban housing with considerable GBI coverage (56.5% of ward area). In contrast to Ardwick, this ward contains no LDF *Development* but is covered by a significant area of LDF *Conservation* (**Figure 5.3**).

Table 5.1 – Description of chosen local development framework layers

LDF Layer	*Land use development represented*	*LDF classification*
Airport Strategic Site (MA1)	Conversion of spatial areas into Commercial and Transport ULU group classes	*Development*
Conservation Areas	Policy area indicating conservation of built environment and GBI	*Conservation*
Economic Development Economic Improvement Area	Conversion to Commercial and Industrial ULU group classes to aid local economy	*Development*
Education and Community Sites	Conversion to Community service ULU group classes to provide public services	*Development*
Green Belt	Designation of green belt to protect existing GBI	*Conservation*
Leisure Use	Conversion to Commercial, Public recreation and other ULU classes to provide leisure services	*Development*
Mixed Use site	Conversion to Commercial, Industrial and Residential ULU classes	*Development*
New Housing	Conversion to Residential ULU group classes	*Development*
New Shops Retail Allocation (CC18)	Conversion to Commercial ULU group class	*Development*

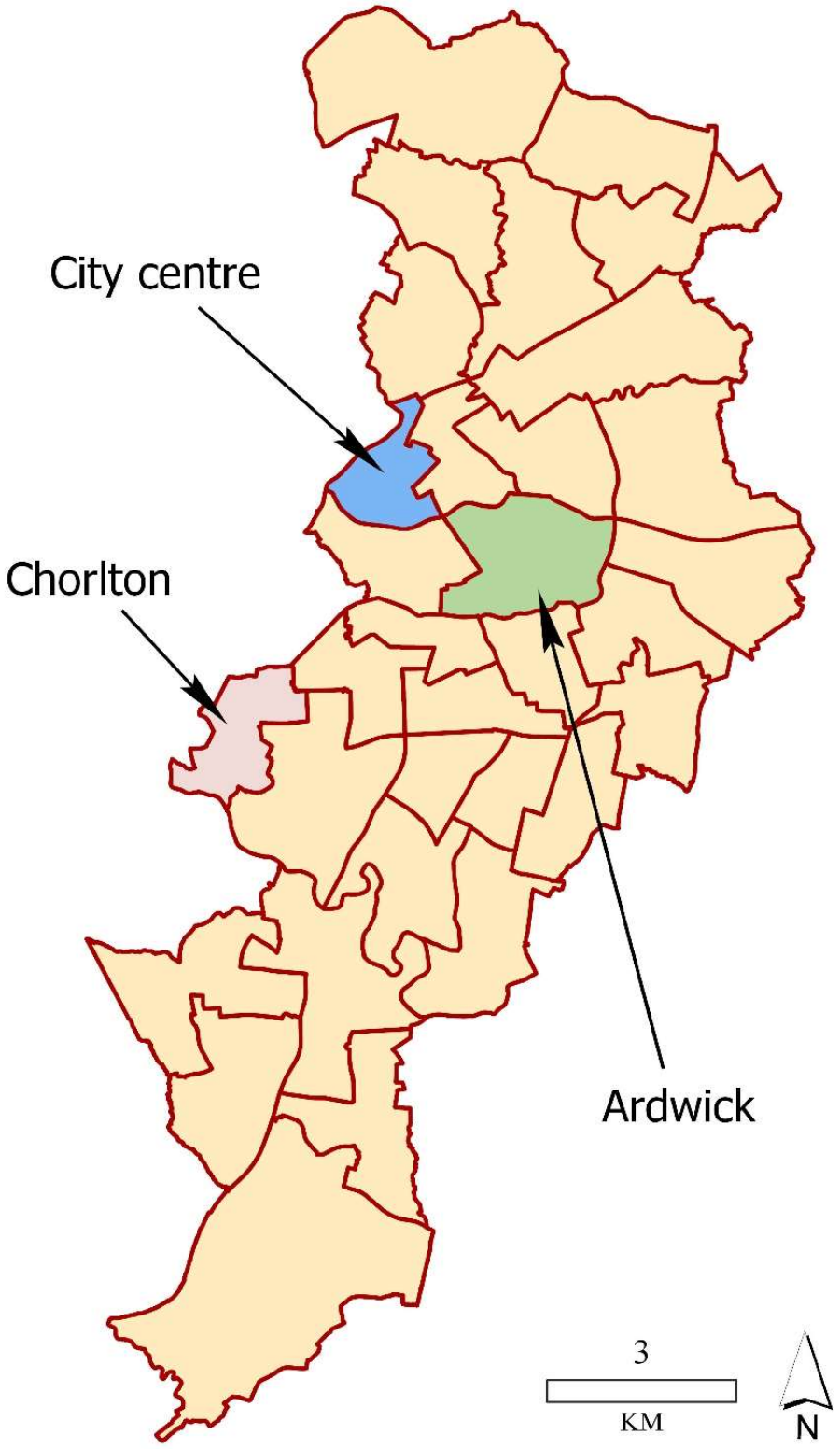

Figure 5.1 – Location of Ardwick and Chorlton wards in relation to Manchester city centre

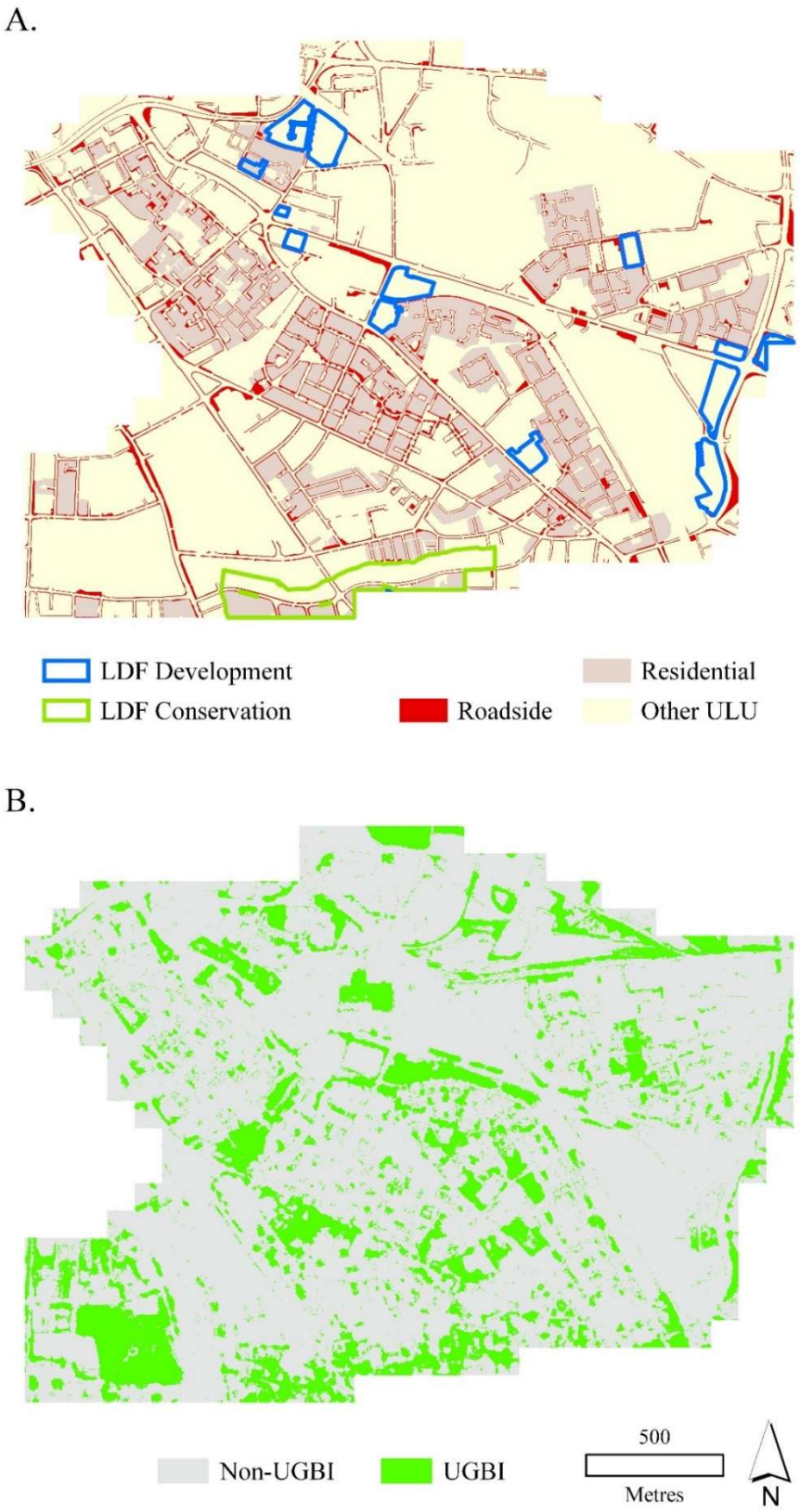

Figure 5.2 – Planning areas (**A.**) and (**B.**) GBI cover within Ardwick

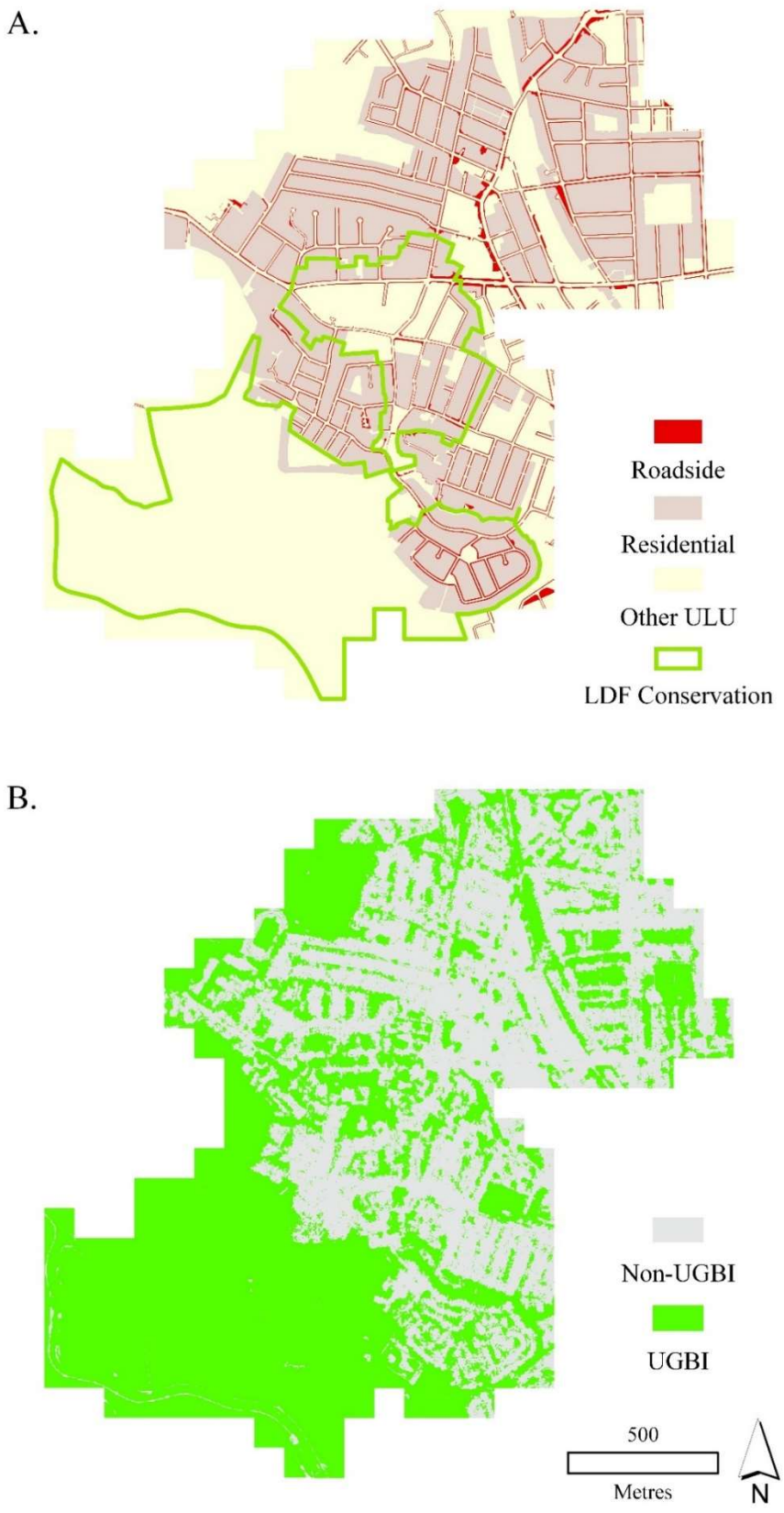

Figure 5.3 – Planning areas (**A.**) and (**B.**) GBI cover within Chorlton

5.5 Scenario implementation

Scenarios were developed according to theoretical management policies to conserve or improve UBGI within ward areas of planning concern. Based upon the assumption that current rates of GBI change per ULU will occur over the same time period as the previous analysis (i.e. approximately 17 years; 2000 – 2017), scenarios consider estimated GBI levels for the 2030s. **Table 5.2** describes the rationale for choosing the areas of planning concern, where management schemes are targeted, and the methods required to integrate them with the existing ULU dataset. In total three GBI management schemes were developed to represent possible management actions the local council may undertake in the future. These are defined as: *No management* - the council takes no active interest in GBI management; *Conservation* – the council applies policies to ensure existing GBI resources are maintained; *Improvement* – the council intervenes and takes direct action to improve the extent of GBI. Scenarios were therefore defined through application of certain GBI management schemes within differing areas of planning concern. Rules to apply GBI management schemes are described in **Table 5.3**, whereas overall GBI management scenarios are defined in **Table 5.4**.

The scenarios therefore assess differing GBI management schemes upon levels of temperature regulation, stormwater storage and above-ground carbon storage RES in the 2030s. GBI management scheme rules in **Table 5.3** were applied within each scenario to estimate spatial change in GBI within ULU planning areas. Updated GBI estimates were then amalgamated to analysis cell level to enable calculation of updated scenario regulating RES indicators. To enable comparison of scenarios between ward areas, function indicators per RES were weighted on the same scale. Temperature regulation function indicators therefore varied between the minimum and maximum outputs for all 2017 study area indicators using geographically weighted regression (see **Section 3.6.2**). Stormwater storage function indicators were calculated from cell curve numbers within the range of seasonal curve numbers for 1 in 30 probability control event (see **Section 3.6.3**). The method for above-ground carbon storage function indicators was updated from the model described in **Chapter 2**, and therefore incorporates additional information regarding biophysical attributes of GBI in the 2017 classification layer (see **Appendix 5.1** for description). Above-ground carbon storage function indicators were calculated within the

range of minimum and maximum potential study area above-ground carbon storage values.

Table 5.2 - Planning area description

Planning area	*Description*
DEVELOPMENT	LDF spatial areas designated as land use change that replace areas of existing ULU class parcels where appropriate. ULU classification for such areas determines the new GBI percentage (2017 ULU estimates) to apply. Where LDF policy indicates multiple land-uses then the average 2017 ULU GBI estimate between these classes applies. The difference in percentage GBI coverage between 2017 and post-development levels determines whether GBI increases or decreases according to the No management method.
CONSERVATION	LDF spatial areas designated for GBI conservation. Intersection between CONSERVATION and ULU class areas determines the spatial extents of CONSERVATION within the scenarios.
ROADSIDES	ULU Roadsides– considered a key area for GBI investment (i.e. Tree planting) under council control. Class is ubiquitous across study area and borders other ULU class areas, which therefore enjoy the adjoining RES benefits provided by GBI investment in Roadsides areas (Salmond et al. 2016).
RESIDENTIAL	All ULU RESIDENTIAL group classes – Residential areas house urban citizens, therefore policies designed to conserve and improve GBI resources are vital to improve regulating RES, and thus reduce resident exposure to urban hazards (Lin et al. 2015a).
NON-PLANNING	ULU areas not covered by one of the categories above.

Table 5.3 – Rules for green-blue infrastructure (GBI) management schemes

Scheme	*Rules*
No management	Assume statistically significant GBI change rates per ULU where applicable GBI change is only applicable in ULU areas containing existing GBI resources Negative change rates are applied for all GBI classes, with removed area replaced by Artificial surfaces Positive change results in GBI replacement of Bare Earth and Artificial surfaces: • For stormwater storage indicators these surfaces are replaced with hydrological Shrubs surfaces assigned by soil type • For above-ground carbon storage indicators these surfaces are replaced by the Tall Shrubs 2-5m class In ULU areas recording no significant change, GBI coverage remains static
Conservation	GBI areas remain static within applied areas
Improvement	Applied using a 10% rate where GBI replaces the percentage of combined non-GBI area, and existing GBI levels remain unchanged. The rate is based upon the study by Gill et al. (2007) that found a 10% 'green or tree cover' improvement provided noticeable benefits to reduce extreme hot weather temperatures and urban surface runoff. Benefits from the same level of greening improvement are therefore examined at the micro-scale using the scenario approach here. GBI replacement rate is applied equally to Artificial and Bare Earth surfaces: • For stormwater storage indicators these surfaces are replaced by hydrological Tree cover > 3m height covering natural surfaces to maximise the potential of any GBI improvement scheme (surfaces assigned by soil type and stratified by proportional Deciduous and Evergreen cover in the 2017 classification) • For above-ground carbon storage indicators these surfaces are replaced by Tall shrubs 2-5m

Table 5.4 - Scenario implementation

Management focus	*Scenario*	**Management scheme within area of planning control***				
		DEVELOPMENT	*CONSERVATION*	*ROADSIDES*	*RESIDENTIAL*	*NON-PLANNING*
Council disregards GBI management in these scenarios	Business as usual	N	N	N	N	N
	Development applied**	D	N	N	N	N
GBI conservation applied in various areas of planning concern in these scenarios	Conservation and development**	D	C	C	C	C
	Conservation applied	D	C	N	N	N
	Conserving Roadsides	D	N	C	N	N
	Conserving Residential	D	N	N	C	N
	High level conservation	D	C	C	C	N
GBI Improvement applied in various areas of planning concern in these scenarios	General Improvement	I	I	I	I	I
	Improvement and development**	D	I	I	I	I
	Improving Conservation	D	I	N	N	N
	Improving Roadsides	D	N	I	N	N
	Improving Residential	D	N	N	I	N
	High level improvement	D	I	I	I	N

* Management scheme key: D = LDF development implemented to alter GBI levels, N = No GBI management, C = GBI Conservation applied, I = GBI improvement applied; ** Scenarios not applied to Chorlton as LDF development areas are not present within this ward

5.6 Future ecosystem services

Differences between scenario and base RES function indicators per ward, enable examination of whether scenario management schemes maintain current RES levels into the 2030s. **Figures 5.4 and 5.5** display the distribution of cell RES function indicator differentials for Ardwick and Chorlton wards respectively. As evident, the application of no active GBI management results in the greatest declines in RES functions for both wards, as rates of GBI decline for the majority of ULU classes result in declining RES for the vast majority of cells in both ward areas. For Ardwick the range of RES function change is exacerbated through GBI change from land use conversion within the *Development applied* scenario. Combined with GBI change within static ULU areas, declines of above 10% are recorded across all RES in some cells, demonstrating the considerable impact ULU re-development may have upon future local RES.

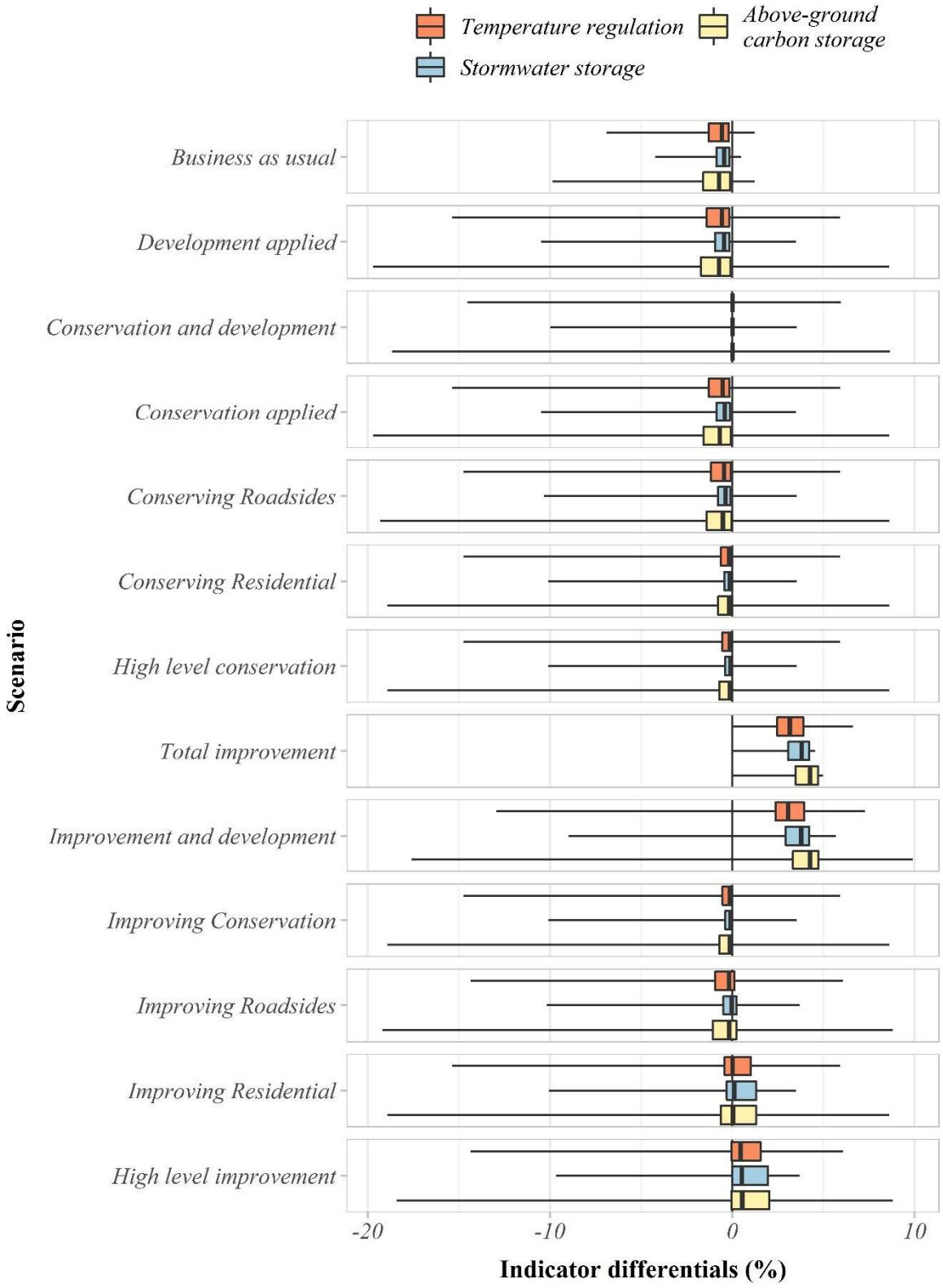

Figure 5.4 - Distribution of regulating ecosystem service (RES) indicator differentials per scenario for Ardwick ward

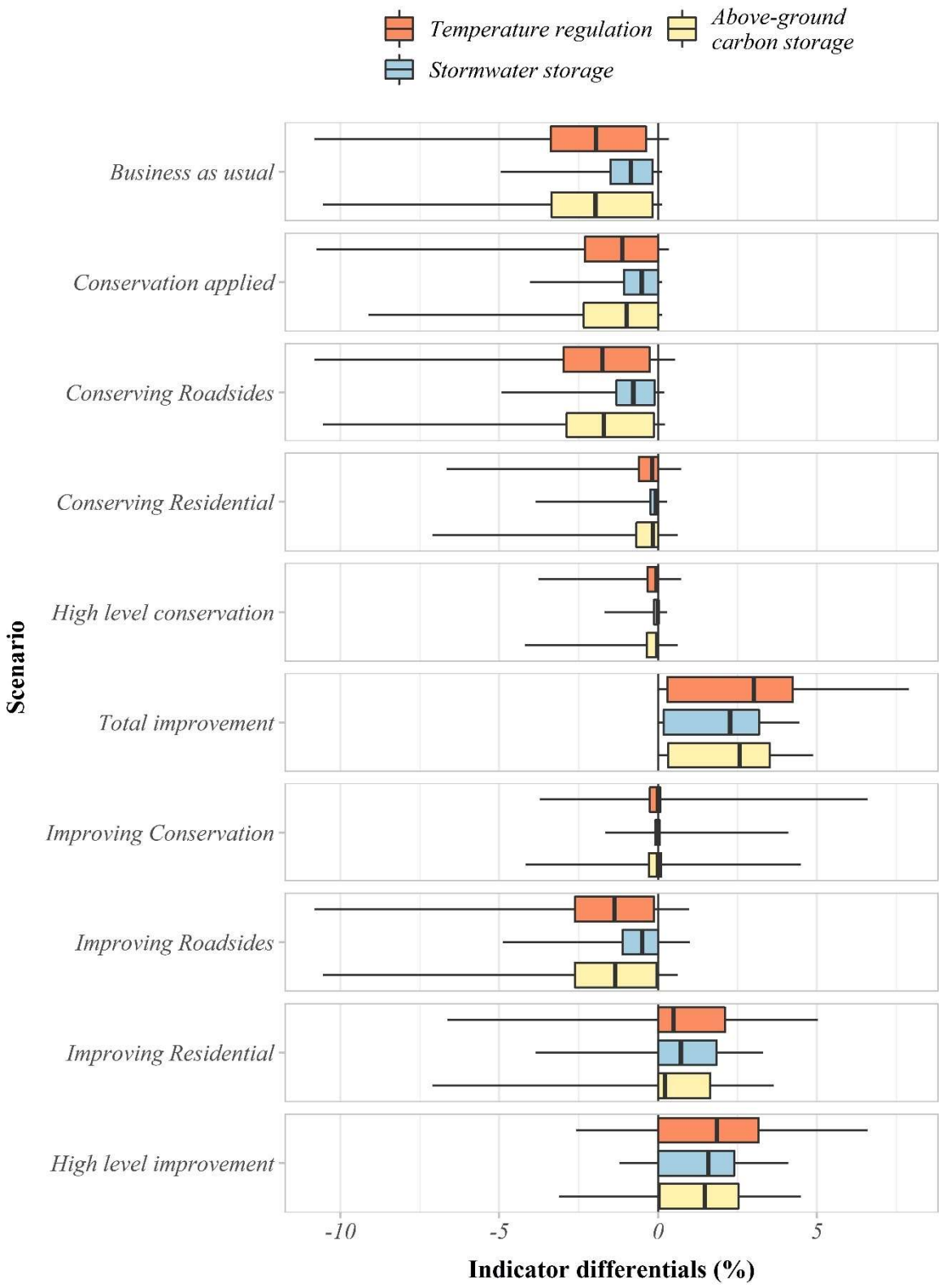

Figure 5.5 - Distribution of regulating ecosystem service (RES) indicator differentials per scenario for Chorlton ward

In contrast, conservation scenarios can limit declines in RES, although the benefits of conservation vary according to where this management scheme is applied. *Conservation applied* and *Conserving Roadsides* scenarios appear to have limited effect in halting declines in RES when compared to conservation in Residential areas. Roadsides follow the Road network and are well distributed across each ward area but cover just 8.6% and 5.9% of each ward, with GBI coverage of 19.2% and 27.3% for Ardwick and Chorlton respectively. Whilst estimated rates of GBI decline in Roadsides are considerable, at approximately 22% of existing GBI resources, conserving GBI levels in this ULU class alone saves just 1.8% and 0.6% of existing GBI for Ardwick and Chorlton respectively. *Conservation applied* has minimal effect in Ardwick, which is covered by just 2.6% in LDF conservation area. In contrast, 36.9% of Chorlton's area is covered by LDF *conservation*, however, approximately 60% of this LDF *conservation* area is covered by ULU classes recording stasis in GBI resources. Whilst conserving GBI resources in the remaining 40% of conservation area is beneficial, it appears to have limited effect in halting declines in GBI for the ward area as a whole. In contrast, conservation in Residential areas provides considerably more benefits for both wards, preserving an improved 3.4% and 3.7% of total GBI resources for Ardwick and Chorlton respectively. Combining conservation in all of the above areas of course compounds these effects to provide the greatest benefit of conservation management schemes.

Improvement scenarios follow a similar pattern in benefitting RES levels. *Total improvement* demonstrates the levels of RES gains from 10% GBI improvement in all ULU areas. The distribution of indicator improvement values varies according to RES, but for majority of cells is constricted between 2.5-5%. In Ardwick, overall improvements are limited by LDF *development* (*Improvement and development* scenario) resulting in declines in RES for some cells. *Improving Conservation* and *Improving Roadsides* improves RES but only with limited effect. In contrast, *Improving Residential* and *High level improvement* results in indicator gains for all three RES in the majority of cells. As demonstrated in **Figures 5.4 and 5.5**, Improvement scenarios (excluding *Total improvement*) result in a mixture of gains and declines in RES.

In relation to maintaining RES within wards, it is useful to assess whether more cells record gains than declines for RES within each scenario. **Figures 5.6 and 5.7** demonstrate that *Improving Residential* and *High level improvement* scenarios maintain general levels

of RES for both wards. Due to the limited initial GBI coverage, the areal extents of scenario GBI improvement area is slightly greater for Ardwick (*Improving Residential* requires 83749m^2, *High level improvement* requires 117537m^2) than Chorlton (*Improving Residential* requires 82046m^2, *High level improvement* requires 100982m^2). The scenarios indicate the magnitude of GBI investment required to offset negative rates in GBI is approximately 8 hectares in each ward in comparison, ensuring improvement for all cells requires over 36 and 13 hectares GBI investment for Ardwick and Chorlton respectively, although these levels may vary according to the exact GBI improvement rate used. For 10% improvement, the greater area required for Ardwick is representative of overall lower GBI coverage of 20.4%, in comparison to 56.5% for Chorlton, demonstrating that efforts to normalise RES levels across the study area will require considerable GBI investment in areas of low RES performance.

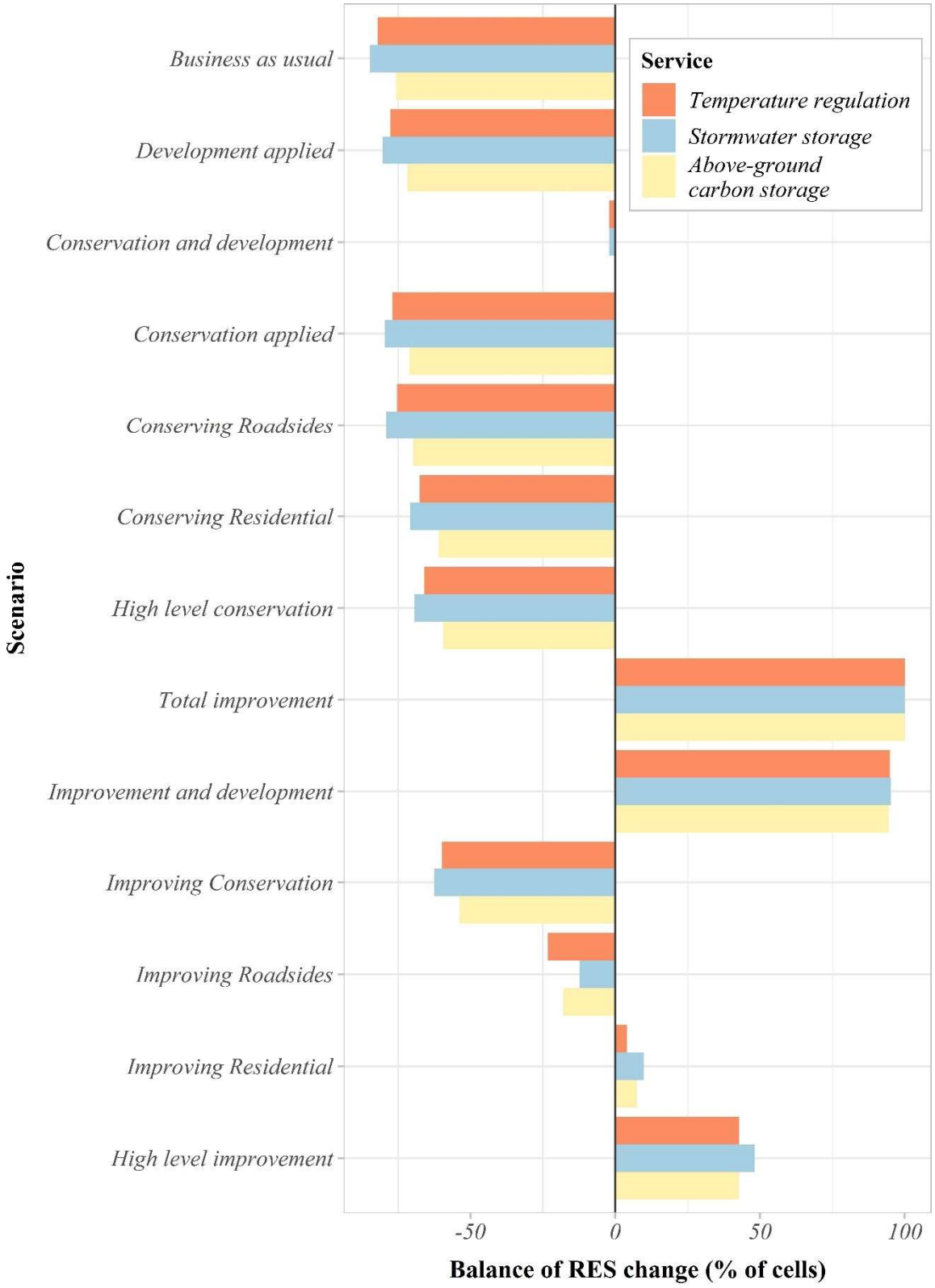

Figure 5.6 - Balance of regulating ecosystem service (RES) change for each scenario in Ardwick

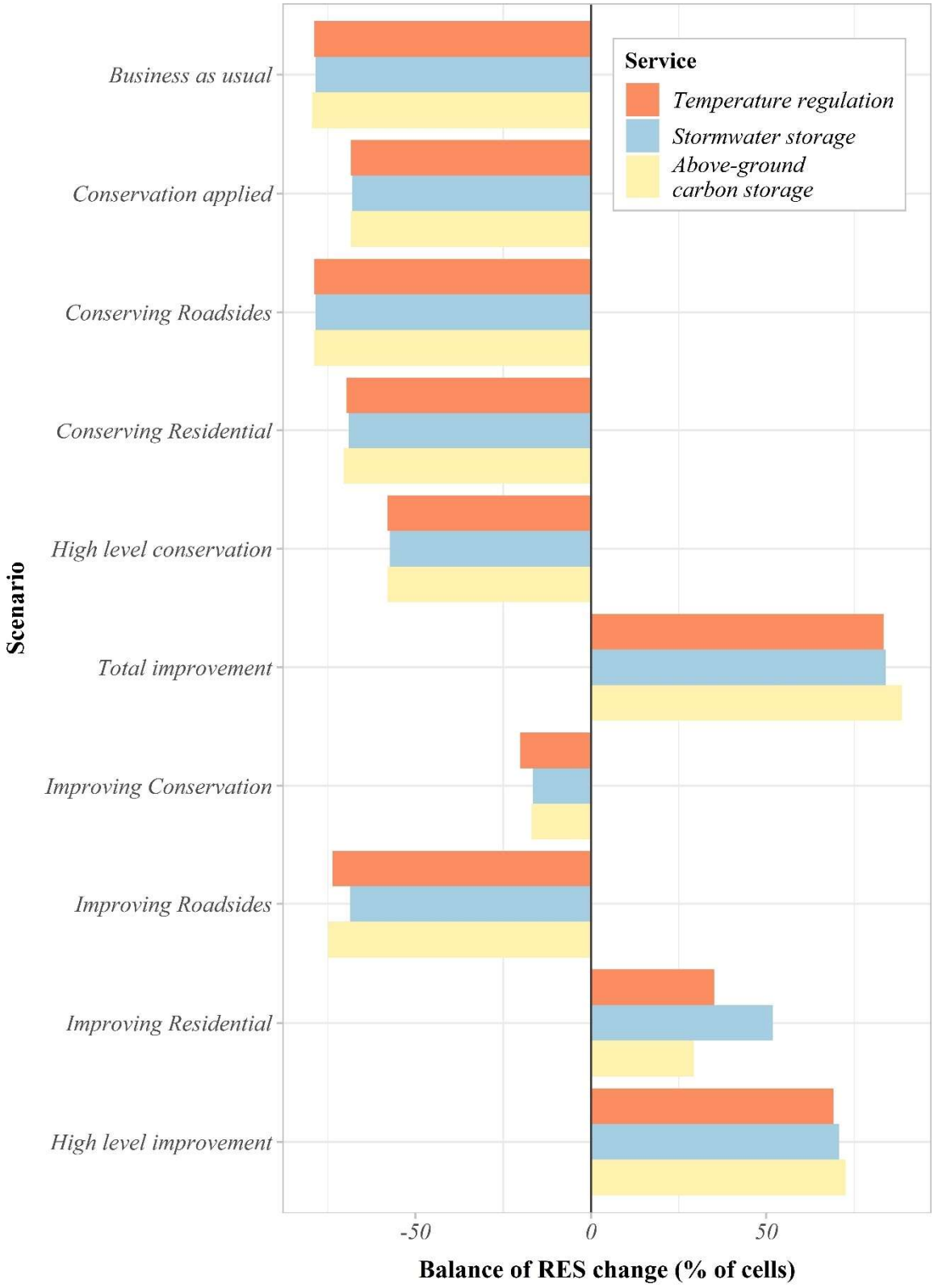

Figure 5.7 - Balance of regulating ecosystem service (RES) change for each scenario in Chorlton

This discrepancy in required GBI investment is further demonstrated when comparing management scenarios to improve existing levels of RES deprivation. RES coldspots, which represent the lowest 10% of existing demand weighted cells using combined rankings of RES function indicators (see **Section 2.5.6**), were calculated for each scenario using updated RES values. Scenario coldspot cells per ward were then compared to the number of coldspots identified using current 2017 RES levels, to assess whether RES deprivation declines or grows in each scenario (see **Figures 5.8 and 5.9**). Trends of declining GBI estimated for both change and conservation scenarios result in the growth of RES deprivation in both ward areas. In Ardwick, where 31.1% of existing demand area is classed as RES deprived, the combined effect of no GBI management combined with LDF development results in an additional 19.6% of demand cells falling into RES deprivation. In comparison, *High level conservation* has minor impacts on limiting this growth, as 12.2% of demand cells in this scenario are re-classified as coldspots. Improvement scenarios in Ardwick mitigate growth in deprivation further, with *Improving Residential* and *High level improvement* respectively recording just 3.7% and 2.2% growth in new coldspots, whilst simultaneously causing a reduction in existing cold-spot area of 3.3% and 9.6%. In comparison, *Total improvement* sees no growth in RES deprivation, but records a remaining 7% of demand cells as coldspots, indicating that measures above 10% total improvement are required to remove RES deprivation within this ward.

Patterns in RES deprivation change are similar, albeit less extreme for Chorlton, which has an overall greater proportion of existing GBI and thus much lower levels of deprivation with just 6.7% of demand cells identified as an existing coldspot. *Conserving Residential* and *High level conservation* scenarios retain RES deprivation approximately at existing levels, with each scenario recording just 1.4% growth in cold-spot area. *Improving Residential* and *High level improvement* virtually halt the growth in new cold-spots whilst simultaneously removing deprivation from 4.3% and 5.2% of demand cells respectively. In comparison, *Total improvement* virtually eradicates RES deprivation in Chorlton with just 0.5% of demand area remaining as a coldspot in this scenario.

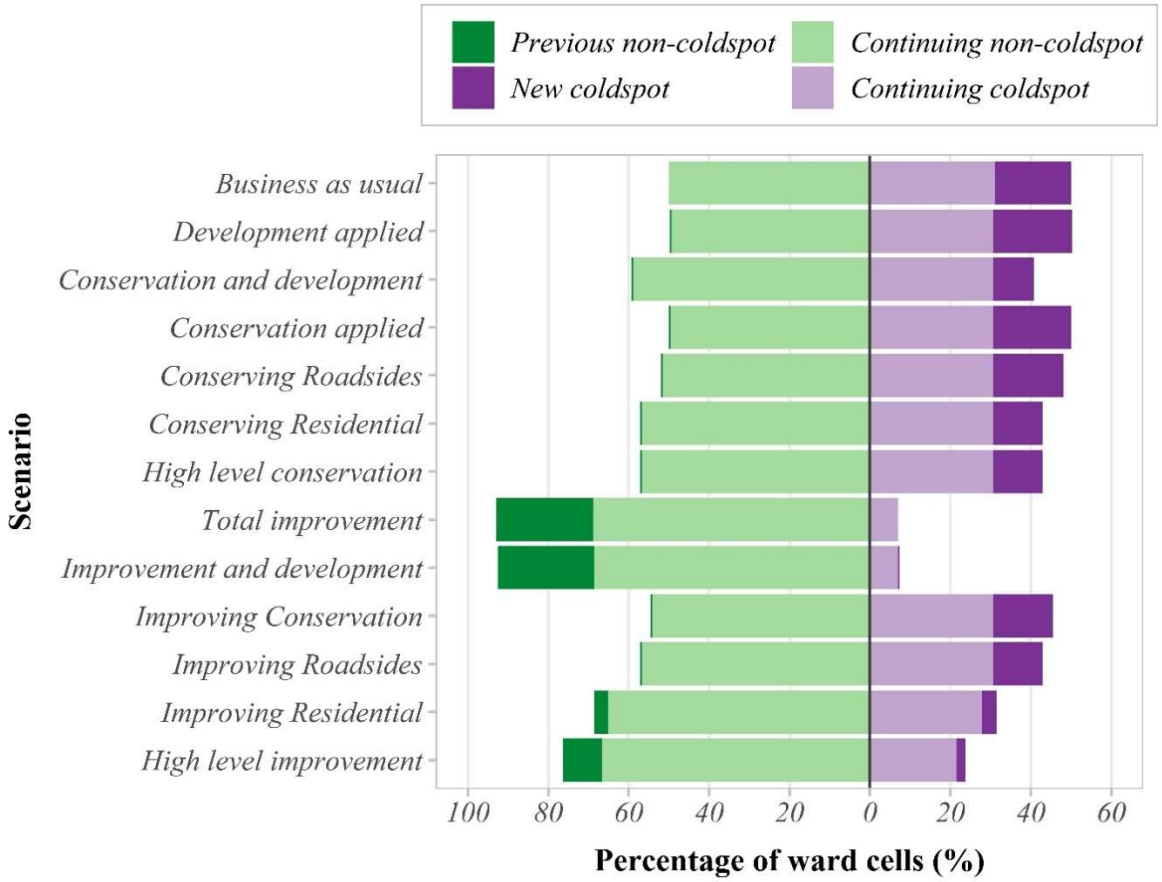

Figure 5.8 - Percentage change in scenario regulating ecosystem service deprived (coldspot) cells in Ardwick

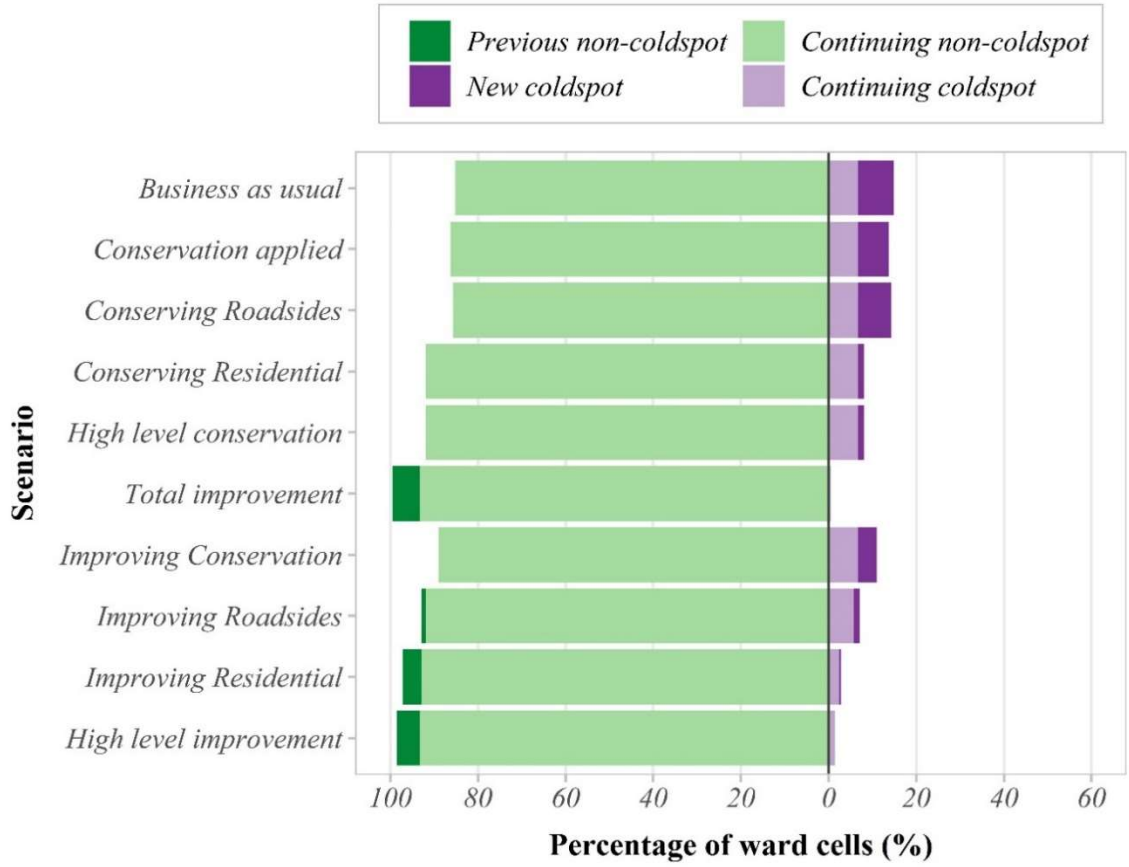

Figure 5.9 - Percentage change in scenario regulating ecosystem service deprived (coldspot) cells in Chorlton

5.7 Implications of scenario analysis

GBI change rates quantified in **Chapter 4** and applied in scenario analysis evidence that the course of no active GBI management (*Business as usual* and *Development applied* scenarios) is an undesirable option for maintaining current levels of RES. Whilst conservation and improvement interventions, enacted together or independently, present actions to halt and even reverse declines in regulating RES (Carter et al. 2015, Le Roux et al. 2014), the associated costs are likely to vary widely. For example, the costs to install and maintain a single tree within existing built infrastructure (e.g. removing artificial surface, preparing a planting pit, labour costs) is considerable, with sources ranging from approximately £5000 (GreenBlue Urban 2018) to £10000 (BBC 2019b). Improving tree cover by 10% within paved over roadsides may therefore cost considerably more than the

same level of improvement on bare ground or other GBI types in residential and conservation areas for example. Whilst ascribing costs to any large-scale greening scheme is problematic lacking the requisite level of planning (i.e. specific zones for tree planting, number of trees required), the scale of improvement area evident in scenario analysis may require substantial financial investment. Further to this, declines in GBI often result in the removal of highly developed and ecologically beneficial GBI resources (e.g. established hedgerows, mature trees), whereas replacement resources may take considerable time to mature and develop the same level of benefits (Le Roux et al. 2014). These reasons alone therefore indicate the importance of local strategies to arrest declines in GBI and to help maintain regulating RES.

In addition, as the frequency and magnitude of extreme weather events may increase in the future due to climate change, GBI improvement is an option to maintain urban resilience in the face of deteriorating environmental conditions. As evidenced in the *Improving Residential* scenario, that maintains positive balances in RES for both wards, theoretically the council needs only devise GBI investment policies for residential areas only. This finding has real-world significance as it supports efforts by Manchester City Council and other local organisations to encourage green-blue infrastructure improvement and conservation within residential domestic gardens (Cavan et al. 2018). Scenario analysis between wards is thus beneficial to tailor policies to address local discrepancies in RES, and thus ensure efficient expenditure of limited resources. For example, *Improving Residential* will provide more benefits for Ardwick (residential GBI cover 21.8%) in reducing local RES deprivation than *Conserving Residential*, which in turn is sufficient to maintain existing levels of RES deprivation in Chorlton (residential GBI cover 39%). Apart from tree protection orders and planning restrictions on certain types of development (i.e. new buildings, size of building extensions), the local council and other governmental bodies in the UK enforce little control over home-owner's decisions to degrade GBI (Baker & Smith 2019, Perry & Nawaz 2008). The findings from this scenario analysis therefore highlight the need for improved legislation to protect GBI in residential land use areas.

As evidenced by seasonal variation in RES functions (**Chapter 3**) GBI improvement policy may consider the planting of evergreen vegetation species, to improve annual coverage of stormwater storage services. In contrast, for temperature regulation services there is limited evidence into the scale of differences in warm-weather cooling benefits

between evergreen and deciduous vegetation. Evidence suggests that evergreen and deciduous vegetation can transpire at similar levels (Peters et al. 2011), although this along with shading functions varies according to biophysical structure (i.e. canopy density, plant stress) between specimens of different species (Armson et al. 2013b, Rahman et al. 2015). In comparison, evidence from this study suggests that potential increases in negative cool weather cooling due to shading and evapotranspiration from additional evergreen trees are of limited concern for overall annual temperature hazard reduction. Particulate reduction ecosystem services may also benefit from evergreen intervention, as foliage change of deciduous vegetation can result in considerable declines in particulate capture during leaf-off conditions (Lin et al. 2016). The ecosystem service maps in **Chapter 3,** and findings from scenario analysis here thus provide spatial indications of where evergreen planting may occur to reduce seasonal variation in stormwater storage hazards, or indeed to provide a general boost to RES in low functioning areas with high demand for associated services.

However, evergreen planting is a general policy recommendation, as studies indicate that GBI interventions should consider whether the introduction of certain plant specimens are appropriate given local ecological and built infrastructure conditions (Monteiro et al. 2017). Plants poorly adapted to the local environment are therefore less able to produce ecosystem services, as for example studies indicate varying impacts of plant stress upon street tree evapotranspiration rates (Rahman et al. 2015) and tree growth cycle benefits for sequestration and lifetime storage of carbon (Nowak et al. 2002). As evidenced in **Chapter 3** any green-infrastructure investment should provide net gains in local regulating RES benefits, irrespective of whether plants have deciduous or evergreen leaves. For a broader range of RES, seasonal variation in service benefits are more related to changing conditions in the surrounding environment over physiological changes in plant conditions. For example, peoples' recreational engagement with GBI typically depends upon the climate conditions rather than canopy coverage (Roberts et al. 2017b), whilst psychological improvement by nearby GBI resources may not decline with canopy de-greening in winter (Sato et al. 2006). Assessment of GBI extents to local population levels allows additional examination of where policy led GBI interventions may best serve to improve a range of vital ecosystem services.

5.8 Conclusion

This chapter demonstrates how the methods developed throughout this thesis, can be utilised for pragmatic planning purposes. Previous studies have assessed ecosystem service change either to projected land use change (Estoque & Murayama 2012, Wu et al. 2019), or GBI improvement within land use (Gill et al. 2007, Kain et al. 2016). This study developed both approaches, by combining both GBI change processes within scenario analysis. This process therefore beneficially evidences the need for robust environmental policies throughout the study area. Current environmental policies in the city of Manchester acknowledge ecosystem services, and indeed describe broad policies to encourage greening and other environmental improvement actions amongst land use managers (e.g. private householders, commercial businesses, public sector organisations) (MCC 2020a). However, it is clear from the scale of potential losses in RES, and resulting GBI investment required to offset this degradation, that firmer legislative protection against GBI destruction may be required to help maintain urban resilience across the study area (Sayce et al. 2012, Perry & Nawaz 2008).

In this regard, the study demonstrated the benefits of strong GBI conservation policies for two wards in the city. The scenario approach should therefore be adapted to examine and contrast GBI investment strategies in other ward areas. The current scenario analysis is of course unable to consider all proposed land use change within the study area. There is therefore emphasis on the further development of publicly accessible spatial databases, with land use change and development from private sector organisations. This source of land use development is largely obscured from council policy documents and will therefore facilitate more realistic scenario analysis across the whole study area. This thesis therefore describes a methodological blueprint for this purpose, which may be adapted and improved upon in future analyses. The following concluding chapter therefore evidences avenues for future research and provides a discussion on the wider implications of the thesis for both ecosystem service research, and broader environmental planning concerns in the UK and further afield.

Chapter 6 – Conclusion

6.1 Implications for research and urban planning

The aim of this thesis was to develop approaches to map spatiotemporal dynamics of urban green-blue infrastructure (GBI) and associated regulating ecosystem services (RES), in order to improve the usefulness of ecosystem service information to plan urban environmental resilience. To achieve this aim a total of four research objectives were devised. Objective 1 concerned how spatial scale and proxy-based methods in current ecosystem service mapping approaches can be improved (**Chapter 2**). Maps of urban ecosystem services are often coarse in spatial resolution and may fail to assess spatial variation in the production and consumption of regulating ecosystem services across an urban area. Current mapping approaches are also often tailored towards specific datasets and may lack transferability due to limited consideration of how proxy models vary for data constraints found in different urban areas. **Chapter 2** therefore examined both issues through the development of a new mapping approach.

Overall, this process resulted in a trade-off between coarse-scale ecosystem service mapping studies where demand within LULC categorisations, or municipal districts are considered (Baró et al. 2017, Haas & Ban 2018) to gridded approaches employed in ecological and environmental models (Dobbs et al. 2018, Kremer et al. 2016a). Grid-based demand measures are evident in studies published prior to, and during completion of this thesis (Baró et al. 2016, Langemeyer et al. 2020, Paulin et al. 2020). The mapping approach developed in **Chapter 2** therefore aligns with methodological attempts to represent regulating ecosystem service dynamics as approximations of continuous ecological and environmental processes. In contrast, coarser scale LULC and administration units are useful representations when ecosystem services are a function of landscapes (e.g. recreational function of parks) or need to be considered in relation to areas of management concern (e.g. commercial sites, ward areas) (Baró et al. 2017, Burkhard et al. 2012). The benefits of gridded ecosystem service information for urban planning purposes, in contrast to traditional representations is therefore an avenue of future research. Certainly, the approach developed here contrasts to assumptions that landcover proportions, or

ecosystem functions, are consistent for all LULC of a certain label (Cabral et al. 2016, Gill et al. 2007). Given heterogeneity in urban GBI coverage evidenced in this thesis, this may provide a simplified view of spatial variation in RES. The mapping approach developed here, therefore incorporates recently developed methods to map urban landcover and associated ecosystem service functions at the scale of GBI components (Derkzen et al. 2015, Kremer et al. 2016). As evidenced in other studies, this is a flexible approach which enables aggregation of fine-scale ecosystem service maps to various levels of planning concern (Derkzen et al. 2015, Grafius et al. 2016).

This mapping scale was therefore beneficial to examine RES in relation to demand for localised urban resilience. However, the use of proxy methods remains a general concern in ecosystem service research (Haase et al. 2014, Seppelt et al. 2011). The review of modelling approaches for RES in this chapter is therefore consistent with other studies, that describe practical limitations in the collection and application of primary data for citywide ecosystem service models (Holt et al. 2015). How proxy model choice impacts mapping outputs is however a relatively novel aspect of this research. As demonstrated, choice of proxy method for ecosystem service functions and demand can produce a significant influence on mapped ecosystem service values. This analysis was not intended as a critique of current mapping approaches, but to identify implications for transferring this approach elsewhere. Urban ecosystem service mapping remains a relatively new field, and this chapter aligns with previous studies that examine methodological issues in ecosystem service maps. This includes the impact of landcover accuracy (Foody 2015), resolution of analysis units (Grafius et al. 2016, Holt et al. 2015), proxy model parameterisation (Zhao & Sander 2018) and relative weighting of indicator values (Kremer et al. 2016). The chapter contributes research knowledge regarding limitations in proxy-based methods to map ecosystem services, and how this may inform application of methods in future studies. It is hoped that by explicitly modelling such limitations, this approach is useful for communicating the usability of RES mapped indicators to end users.

Overall **Chapter 2** developed a spatial approach which provided the basis for analysis in succeeding chapters. Objective 2 (**Chapter 3**) assessed whether incorporation of seasonal dynamics in regulating ecosystem service maps present a concern for planning urban GBI. Current RES mapping studies assume that GBI functions are fully functional,

irrespective of the period of the year (de Araujo Barbosa et al. 2015, Cavan et al. 2014). Temporally static service indicators are therefore unable to assess if seasonal reduction in RES can cluster in certain areas of a city, and whether this represents a concern for community resilience to localised environmental stressors. Whether incorporation of seasonal variation in RES indicators is a concern for spatial planning of GBI is poorly understood within the current body of research.

Seasonal variation in RES functions have been quantified in various field-based studies (Armson et al. 2013a, Cohen et al. 2014, Hamada & Ohta 2010, Lin et al. 2016) albeit for a limited number of sites. **Chapter 3** contributes novel information of seasonal variation in temperature regulation services across an entire urban area. Current findings indicate that this is currently a limited concern for the city of Manchester. Land surface temperature cooling by GBI is much weaker during winter, which is consistent with urban heat island studies in Asia (Fan et al. 2008, Hamada & Ohta 2010, Zhang et al. 1998). The relationship between land surface temperature and air conditions is of course heavily influenced by climatological conditions (e.g. cloud cover, wind patterns) on a given day (Azevedo et al. 2016, Elias & Svensson 2003). The current findings however indicate that in general, negative cooling for cool temperature months is far outweighed by beneficial temperature cooling during warm weather months. This evidence does not present a significant concern for current ecosystem service studies that describe indicators for hot weather conditions only. Areas of high and low temperature regulation functionality are thus broadly consistent in the study area, irrespective of additional weighting of cool weather disservices. Climate change is projected to increase both summer and winter temperatures in the UK (Met Office 2018), therefore the implications in managing a potential disparity in temperature regulation services and disservices may lessen in coming years.

Seasonal variation in stormwater storage functions in the study area is largely governed by seasonal variation in extreme precipitation conditions. Despite the loss of interception capacity in above-ground vegetation, heightened precipitation levels in summer result in increased runoff values for the vast majority of the study area. Similar to seasonally adjusted temperature regulation service indicators, this finding should not present a serious concern for studies that assume constant functionality in GBI stormwater

storage services. However, changes in canopy condition had a significant impact on runoff for some parts of the study area, as a number of cells with high deciduous tree cover recorded higher runoff volumes, irrespective of precipitation levels. Model outputs indicate that variability in runoff increases with the severity of a precipitation event. This is consistent for example, with the study by Gill et al. (2007), that found differences in runoff between landscapes of differing greenspace levels increased when precipitation inputs into the SCS-CN model also increased. Despite the lack of validation of stormwater storage indicators here, this general finding suggests that seasonal differences in GBI functions may become more important for planning urban resilience in the future. Extreme precipitation events are projected to increase in frequency and severity over the next decades (Madsen et al. 2014), and therefore adaptations to reduce local flooding pressures could benefit from investment in evergreen vegetation that provide year-round functionality.

As to the best of the authors' knowledge, no other study has mapped seasonal variation in RES indicators across a city, it is difficult to state definitively whether seasonal indicators should be included in future ecosystem service studies. Whilst omitting seasonal indicators resulted in less than 5% difference in cells recording RES deprivation for Manchester, a difference in seasonal indicators may be more important in cities with greater extremes in seasonal conditions. Models using remotely sensed LST, and the SCS-CN approach are described in a number of urban ecosystem service studies (Dobbs et al. 2018, Holt et al. 2015, Kremer et al. 2016a, Schwarz et al. 2011, Tratalos et al. 2007). The methods developed in this chapter can therefore be adapted to other ecosystem mapping approaches, either directly, or through further research to examine the potential implications of seasonality in RES (see **Section 6.2**).

Chapter 4 (Objective 3) examined whether the magnitude of change in GBI over time varies for different land uses. Change in RES is often assessed according to mapped changes in land use (Burkhard et al. 2012, Cabral et al. 2016, Haas & Ban 2018). This can indicate general changes in GBI and ecosystem services over an inter-year period, however this scale of analysis typically excludes landcover changes within land use. As trends in GBI change according to urban land management decisions are poorly understood, RES planning strategies developed on a static information baseline may not be appropriate to

address future losses in GBI (Wellmann et al. 2020). This chapter therefore developed land use and landcover change mapping methods to examine these trends in Manchester over a 17 year-period.

The overall loss of GBI (approximately 5.5% of study area) recorded here is consistent with Dallimer et al. (2011) who measured an approximate 3% decline in greenspace in Manchester's urban core between 1991 and 2006. GBI declines were recorded for the majority of land uses. Declines in GBI in residential areas is consistent with findings in other studies (Perry & Nawaz 2008, Warhurst et al. 2014, Verbeeck et al. 2011) and are of arguably greatest concern given that these are areas where residents live and thus may consume RES. For example, Perry & Nawaz (2008) recorded an approximate 140% increase in impervious surface cover in a residential area of Leeds, UK, between the years of 1971 and 2004. Similar to this study, the findings in this chapter suggest that residential land management decisions, such as garden front paving, building extensions, and redevelopment of sub-divided garden plots are causing a serious decline in GBI resources across the study area (Sayce et al. 2012). In previous studies, landcover change within land use has been limited to neighbourhoods. However, the mapping methods developed here, enabled consideration of this relationship for multiple land uses across the majority of a large urban area.

GBI change rates estimated for different land uses enabled spatial prediction of varying levels of GBI decline at the scale of analysis cells (see mapping approach in **Chapter 2**). This information alone is relatively novel, and should be useful for local urban planning stakeholders, in indicating where declines in environmental conditions may occur in the future. Certainly, the city of Manchester is not alone amongst cities in the UK, in experiencing both economic and population growth in recent years (Centre for Cities 2021). Resulting development pressures on GBI, as indicated in **Chapter 4**, require widespread adoption of methods to continually monitor GBI change and thus better plan protective urban environmental policies. The landcover and land use change mapping methods here, in conjunction with the spatial mapping approach in **Chapter 2**, evidence a methodological framework to pursue this future research. For example, the high spatial resolution landcover change map identified not only losses in GBI, but also GBI gains which indicate

positive land management processes (e.g. private tree planting, greening of formerly developed land) that could be encouraged within local planning policy.

Overall, objectives 1 – 3 (**Chapters 2 – 4**) were designed to answer a number of research gaps identified in **Chapter 1**. As discussed in the preceding text, each chapter contributes useful information to the wider research community, and should improve the usefulness of ecosystem service maps for planning purposes. The mapping approach and seasonal deprivation indicators should therefore function as a useful visual RES assessment tool, that is widely interpretable amongst planning stakeholders of various disciplines. It is also hoped that the aforementioned spatial predictions of GBI change are useful for raising awareness of this issue for urban resilience in both Manchester, and other cities within the UK. In line with other studies, the mapping approach demonstrates that all GBI is potentially beneficial for RES and urban resilience (Derkzen et al. 2015, Kremer et al. 2016a). The approach is also contiguous with landscape measures in other ecosystem service studies, by demonstrating the importance of non-urbanised landscapes or land uses (e.g. urban woodlands, public recreation areas) as large-scale providers of GBI and RES (Baró et al. 2017, Cabral et al. 2016). Whilst the methods employed throughout this thesis require technical expertise, the resources involved are cost-effective, and should be widely available for both research and planning purposes. Environmental, Remote sensing and Ordnance survey datasets used here ensure that the methods here are theoretically transferable to any other city in the UK. The methods therefore are not only useful as ready-made or an adaptable mapping approach, but may also enable knowledge transfer of RES and urban resilience planning between different urban areas. For example, similar methods and indices applied to measure seasonal dynamics in RES may provide further clarity on whether seasonality represents a concern in estimating ecosystem service indicators.

The overall usefulness of this thesis was the examination of the importance of spatiotemporal dynamics in RES for research and planning purposes. Objective 4 (**Chapter 5**) thus concluded the analysis, by demonstrating how methods and findings developed for the preceding objectives could be utilised as a useful urban resilience planning tool. Certainly, the scenario planning approach adopted is not novel, as the impact of planned landcover change within land use upon ecosystem services has been used in other studies (Gill et al. 2007, Kain et al. 2015). However, in comparison to assessing the effect of GBI

change against a fixed baseline, the approach here incorporates both planned and unplanned development within the scenario model. The seasonally adjusted indicators also present an updated estimate of future RES against traditionally static service indicators. Overall, this analysis demonstrates the considerable challenge planners in Manchester face, in conserving GBI and RES to help build future urban resilience. Tree-planting and investment in parks is occurring in the study area and will be beneficial in improving local environmental conditions (City of Trees 2020, Groundwork 2020), however the evidence suggests that more decisive action may be required to arrest declines in GBI in other areas. Environmental policy documents from Manchester city council direct actions towards different land use managers (MCC 2015b, MCC 2016b). Therefore, the planning approach may prove beneficial in devising GBI protection policies for specific land uses. This may include legislation to restrict development on private gardens or ensuring mature street trees managed by private contractors are retained (Sayce et al. 2012, Coles 2019). In the wider context, it is hoped that this finding raises awareness of the importance of conserving urban GBI resources in the fight to improve urban resilience to a projected exacerbation of environmental stressors in the future. GBI investment will also be required to maximise future RES benefits in urban areas, and therefore the findings here indicate that planners should consider GBI components that provide year-round functionality and are resilient to changing climate conditions (Armson et al. 2013a, Asadian & Weiler 2009).

As the thesis is largely methodological in approach, it is important to consider the implications of assumptions and limitations in the methods developed, and how they may be improved upon in future research. Estimating spatiotemporal dynamics in RES for both annual and inter-year periods is a complex undertaking, and any indicators developed from this process can only ever provide a limited approximation of reality. As discussed in **Chapter 3**, estimating seasonal RES variation for a whole city required disregarding influential ecological and environmental processes, in order to ensure the overall approach remained computationally feasible. For example, RES function indicators could be updated by incorporating additional influential variables to explain land surface temperature, or updating SCS-CN curve numbers to incorporate varying stormwater storage rates of urban soils and above-ground non-tree GBI resources (Chen et al. 2014b, Romero et al. 2007). Certainly, there are alternative modelling tools that vary in complexity and efficiency to

implement, that may nevertheless provide more useful approximations of RES processes as they occur in the real world (Mirzaei 2015, Salvadore et al. 2015). In addition, future research may improve methods in estimating GBI and land use change over time. This may include the development of methods to backdate all land use class areas, in order to assess the implications of land use conversions on GBI change, or mapping change in GBI components of varying ecological functionality (Haas & Ban 2018, Liu et al. 2019). Whilst limitations are evident, the methods developed in this thesis attempted to address novel aspects of ecosystem service research. The methods therefore demonstrate the benefits of expanding access to geospatial data, and the opportunity this provides to further develop methods to map ecosystem service information.

In addition to methodological concerns, the thesis not only attempts to address gaps in current ecosystem service analysis, but also raises further research questions. The mapping approach provides a useful approach to examine spatiotemporal RES dynamics, but requires input from actual end-users to embed the approach as an effective planning tool (Daily et al. 2009, Muller et al. 2010). The analysis cell approach may also differ from current estimates of ecosystem services at the landscape or administrative scale, and may require consideration of the implications of adopting new ecosystem service information within existing planning policy (Woodruff & BenDor 2016). Certainly, further research would be beneficial to develop the map indicators within natural capital accounting frameworks, in order to strengthen links between spatially targeted ecosystem service gains and management budgets (Guerry et al. 2015). This of course will require consideration of how the mapping approach may be adapted to evaluate other regulating and non-regulating ecosystem services. Given that climate change is likely to increase environmental stressors in the future, further improvements in the usefulness of ecosystem service information are vital to effectively plan build urban resilience in the coming years (Carter et al. 2015). As such the concluding sections of this chapter will discuss how limitations and assumptions in current methods, in addition to further research questions, may be addressed in future studies.

6.2 Methodological extensions

Landcover classification of multi-temporal very high spatial resolution imagery achieved acceptable overall accuracy levels (**Chapter 3**), and thus enabled consideration of ecological functions of various amalgamations of component GBI resources. Despite this, some intra-vegetation classes performed relatively poorly in comparison to non-vegetation classes. Physical ground truthing of vegetation species is required to both improve the quality, and number of samples for this purpose. Time constraints did not allow for this here, but this should be certainly employed for similar analysis in the future. For example, Le Louarn et al. (2017) demonstrate that reasonable accuracy of urban tree species classification (6 in total for study) is achievable (OA ≈ 79%) with multi-temporal Pleiades image data (as used in this study), with sufficient species sample size (average of 462 recorded per species class) for classification purposes. As the vegetation species classification may be limited with remote sensing data, field-based sampling is also beneficial to provide inventory estimates of tree species distribution (Brack 2002, Raciti et al. 2014). This enables extrapolation of functions specific to certain species within broad GBI classes to further refine environmental models (Davies et al. 2011, Nowak et al. 2013). As improved estimates of functional GBI extents can result in a considerable refinement in estimates of associated RES (Foody 2015), the error adjustment method (Olofsson et al. 2013; **Chapter 4**) was considered to adjust landcover estimates according to interclass error. However, due to a) pragmatic difficulties in incorporating updated class estimates within adapted SCS-CN approach, and b) limited information on misclassification error within re-assigned shadow areas, this method was not implemented in this chapter. Global sensitivity analysis may prove useful to sample the effect of changing landcover distribution within confidence levels, in order to build a variance based estimate of ecosystem service indicators (Baker et al. 2021). Investigation of landcover accuracy, in conjunction with ambiguity in proxy category transfer, may therefore provide an improved estimate of map usability to end-users.

Estimation of temperature regulation function indicators using geographically weighted regression (GWR) usefully depicts spatial variation in GBI benefits across the urban landscape. However, as evidenced in other studies, the presence of non-built

surfaces (GBI) alone is unable to predict full variation in LST (Chen et al. 2014b, Zhou et al. 2011). In this exercise, GBI proved, to be an effective predictor of both cool and warm weather LST using regression methods. Some cells contain unique configurations of either GBI or built infrastructure, which alter the relationship of GBI to LST away from the main trends evident in the data as a whole. This is an effect that is evident for localised clusters of cells. As was evident in the findings of **Chapter 2** and **Chapter 3**, GWR provided a better fit to local variance in GBI to LST relationships over the global OLS model, reducing autocorrelation in model residuals, and associated bias in model parameter estimates. Notably, patterns in GBI to LST relationships were generally consistent between land use categories, although the pattern of outliers from the main GBI to LST trend varied due to unique GBI and built infrastructure components within cells. An improved predictive process may therefore require a thorough examination of additional independent variables that impact LST values (e.g. built infrastructure materials, GBI patch configuration).

Attempts to incorporate different temperature regulation properties of varying GBI surfaces were made, but eventually abandoned due to difficulties in accommodating dependence between analysis cell surface proportions. By contrast, the reflective properties of varying configurations of built surfaces will influence localised variation in LST (Zheng et al. 2014, Zhou et al. 2011). For example, Zheng et al. (2014) examined spatial variation in LST in Phoenix and found stronger positive associations on LST for dull coloured paving areas, in comparison to buildings roofs constructed of lighter coloured materials. As evidenced in **Chapter 3**, cells with low GBI coverage indicate considerable variation in LST values, indicating the influence of varying thermal storage capacities of non-GBI sources upon this pattern. An alternative approach to regression analysis techniques therefore is to examine LST patterns according to non-GBI, and GBI structure classifications within the spatial analysis grid structure, in order to characterise complex climatological interactions between GBI, and non-GBI components of varying thermal capacities (Cavan et al. 2014, Stewart & Oke 2012). For example, the Local Climate Zone method is an increasingly popular approach, as studies identify statistically significant explanation of LST between different urban site categorisations (e.g. Dense trees, Sparsely built, Open High-rise) (Cai et al. 2018, Geletič et al. 2016). This approach could be approached using urban structure information associated with urban land uses categorised in **Chapter 4** (Dennis et al. 2018).

The influence of GBI configurations upon LST within and between climate zones, thus provides an avenue of further research to examine complexity in seasonal GBI temperature regulation services within heterogenous urban environments (Ferreira & Duarte 2019).

In relation to stormwater storage indicators, some limitations in the seasonal SCS-CN approach are evident due to limited information regarding interception rates between different tree species. The calculated 56% reduction in interception function for leaf-loss between species is based upon single site locations for three tree specimen species that are not prevalent in the city region (City Of Trees 2018). Seasonal interception variance is the same for all areas within the evergreen and deciduous classes, regardless of intra-class species or biophysical considerations (Xiao & McPherson 2002, Livesley et al. 2014). For example, Van Stan et al. (2015) measured a significant 6.3% difference in average interception rates between deciduous urban based American Beech and American Tulip canopies, whereas Asadian & Weiler (2009) measured 11.8% difference in average canopy interception rates between urban coniferous Douglas-fir and western Red Cedar canopies. As such, an alternative approach in future studies may be informed by species distribution estimates, obtained by remote sensing and/or extrapolated from field-based samples within GBI classes (City of Trees 2018). This data may then feed numerical models to estimate interception rates according to diversity in urban vegetation species (Xiao & McPherson 2002), and thus provide alternative estimates of stormwater storage capacity according to diversity in urban tree resources.

In contrast input SCS-CN model parameters, are not validated for UK urban surfaces (Beck et al. 2009). Field based measurement of precipitation runoff enables urban surface curve number validation in relation to varying precipitation and pre-event antecedent conditions (Romero et al. 2007). However, this process requires considerable investment for data collection. An alternative method may require use of spatially distributed hydraulic models, parameterised to reference catchment hydrographs, to validate runoff coefficients for natural surfaces (Kalcic et al. 2015, Palla & Gnecco 2015). This a time-consuming approach requiring consideration of numerous parameter configurations (e.g. soil infiltration, surface roughness) upon model outputs (Choi & Ball 2002). However, given the benefits of the SCS-CN approach for stormwater storage indicators, validation should estimate refined seasonal indicators for local ecological conditions. In contrast, a validated

SCS-CN is still limited in estimating stormwater storage capacities of waterbody structures, however given that water represents < 2% of total study area, this was considered an acceptable trade-off for pragmatic citywide mapping of stormwater storage RES.

Mapping indicators of demand for urban resilience is useful to gauge resident consumption of RES. Methods were therefore derived from studies that spatially quantify levels of resident exposure to local environmental stressors. Population disaggregation usefully weights demand from statistical areal measures (i.e. census areas) to the ecological scale of RES functions. Primarily as the population weighting mechanism assumes each habitation point represents a single household, differences in housing structure (e.g. single household dwellings, nursing homes, halls of residence) should be considered to repurpose weights per habitation point (Jia et al. 2014). As information in the OS Addressbase dataset enables classification of habitation points according to residential address types (OS 2018), census data regarding household size should be further examined to attach population weights accordingly. This approach may be investigated further using census-based socio-demographic measures of vulnerability in the local population as an additional demand weighting mechanism (Wei et al. 2017, Wolff et al. 2015). Certainly this is an avenue of further research, as other studies demonstrate the use of multiple sources of socio-economic and demographic data to estimate daytime and night-time population levels between places of work/play/education and rest/sleep (Bhaduri et al. 2007, HSE 2020). Where urban residents are during extreme weather events is therefore important in determining the level of risk exposure and thus demand for RES (HSE 2020, Laaidi et al. 2012).

Urban land use (ULU) mapping proved largely successful for examining varying rates of GBI change (**Chapter 4**). Despite this, some improvements are recommended in further applications of the ULU mapping process. Firstly, future research may improve the thematic resolution for certain ULU class groups. For example, the Residential class group covers a considerable proportion of the study area and thus may benefit from further stratification into classes approximating various public and private management concerns. In Manchester for example 32% of households in the city are publicly rented from either a housing association or directly from the council (ONS 2013b). This may represent a considerable proportion of land in the study area, where differing communal management

practises over time may influence GBI change at differing rates to residential areas under the direct control of private owners (Dewaelheyns et al. 2016, Goddard et al. 2010). In addition, different pressures may occur between private owner-occupiers who have an active interest in maintaining their own garden space, and private landlords interested in implementing low maintenance land management solutions (Perry & Nawaz 2008). Any methods to advance thematic resolution in Residential group classification will therefore require additional efforts and access to data, that may or may not be freely accessible. However, the additional costs may be worth consideration to assess differing land management processes and thus direct appropriate GBI conservation engagement policies for various residential stakeholders (Azadi et al. 2011, Aronson et al. 2017).

Further stratification may also prove useful in commercial and industrial group classes, to examine whether commercial land uses described in the NLUD 2006 dataset (e.g. Retail, Entertainment facilities, Offices, Manufacturing) significantly explain differing rates of GBI change. Again however, this may require taking on considerable additional costs to acquire and analyse data. Certainly, the current ULU mapping approach requires some manual analysis which maybe improved through automatic classification methods. Random forest was implemented with housing block statistics for Residential ULU classification, and there is scope to augment this approach with additional features derived from remote sensing sources (Bauer & Steinnocher 2001, Haas & Ban 2018). For example, Bauer & Steinnocher (2001) describe a method to classify landcovers at high resolution, thus generating hierarchical object neighbour features to identify land uses of unique land-ownership parcels. The further development of such methods proved beyond the pragmatic scope of this investigation. However, given that this study records statistically significant differences in GBI change rates between ULU classes, further development of ULU classification methods are beneficial to examine increasing complexity in interactions between urban landcover and land use.

For backdating ULU class areas to the year 2000, the automated *Overlap* algorithm was validated to a high level of accuracy and generated an appropriate number of consistent ULU sample polygons (and accompanying pixels) to estimate rates of GBI change per ULU class. This was intended to serve as a preliminary step for the complete re-classification of OS land-line polygons into ULU categories. However, the scale of this

exercise proved beyond the scope of this investigation. Due to incomplete mapped land uses between the study dates it thus proved difficult to estimate the extent that GBI change per ULU is influenced by independent spatial factors e.g. proximity of ULU parcel to hotspot of development, socio-economic characteristics of parcel (Millington et al. 2007). As GBI change is dynamic across the study area this analysis may reveal local statistical models that better explain variation in GBI change rates within ULU classes (Borzacchiello et al. 2010, Tayyebi et al. 2010). Complete ULU class data for the study period would also enable the determination of probabilistic land use change models according to various independent variables (Ballestores & Qiu 2012, Stevens et al. 2007). Combining estimates of GBI change through land use conversion, and GBI change within consistent land use areas thus presents a powerful tool to predict future levels of GBI.

Cross-validation enabled implementation of the error adjustment approach, which usefully incorporates change detection error resulting from misclassification and geometric displacement between data sets to adjust change class area estimation (Olofsson et al. 2013). However, a limitation of this method is that confidence level interval estimates for ULU samples and analysis cells work on the assumption that error is evenly distributed across classes regardless of location and size of analysis area. As spatial clustering in class error rates may occur (Comber et al. 2013), consideration of whether the error adjustment method is adjustable for spatially biased error, should be a concern of future research.

As demonstrated in this investigation, remote sensing change detection analysis remains a challenge. Whilst topological change detection cleaning improved accuracies for individual change detection classes, it is acknowledged that some valid change detection class areas were removed due to this process. In contrast, other studies demonstrate advanced object-based change detection methods, that compare shape and topologies between overlapping multi-temporal objects to assess whether detected change is real or not (Liu et al. 2019, Huang et al. 2017). Whilst such methods are advanced and computationally expensive to implement, associated improvements in change detection accuracy may negate the need to void class areas of the change detection layer. In addition, as the change layer is limited thematically to one class, it is difficult to adequately quantify change in types of GBI (e.g. trees, grass, shrubs) over the study period. Conversion between GBI types providing varying levels of RES benefits is thus a concern in understanding

changes in individual RES. Thematic resolution for the year 2000 was limited largely by the spectral resolution of the aerial imagery. However, continued availability of high-resolution multi-spectral imagery (i.e. Spot-7, Pleiades 1A) for vegetation classification thus presents opportunities to monitor future change of multiple GBI components.

6.3 Future research directions

An important focus of this thesis was to explore the potentials of research accessible tools and data for the analysis of spatiotemporal dynamics in RES. As evidenced in the preceding chapters, usable spatiotemporal information can be derived with limited expenditure (< £500 total spend upon data in this project) for associated resources. The continuing proliferation of open-access data used here (e.g. High-resolution imagery, Ordnance survey data) should therefore encourage further research to improve current GBI and Land use change detection methods for monitoring purposes. This is important to continually re-assess GBI stock and RES levels, and thus embed spatial measures of GBI within natural capital accounting frameworks (Guerry et al. 2015). For example, Eftec (2018) demonstrate the conversion of ecosystem service estimates within Greater Manchester, into monetary values, which is useful to quantify in hard planning terms the wider social and economic benefits of GBI. Re-appraisal of monetary natural capital values could therefore provide further justification to address GBI declines within urban planning policy (Tallis et al. 2008). Such an approach could also support existing efforts to reduce losses in biodiversity through planned development. For example, Natural England in the UK have released “The Biodiversity Metric tool” which provides a systematic accounting approach to trade biodiversity impacts through compensatory natural infrastructure investments (Natural England 2019). Incorporating spatial ecosystem service indicators with this approach in urban areas could therefore encourage municipal led actions to ensure current baselines for environmental conditions are conserved, or improved in the future. The scenario analysis demonstrated in **Chapter 5** therefore provides a workflow to assess various land use based compensatory investment/management measures. Further research is therefore required to develop methods to link spatially explicit RES indicators

with natural capital values, and assess the economic impacts of GBI change at various levels (i.e. ward council, non-profit organisation) of management concern.

Improvements in the usefulness of mapped ecosystem service indicators may therefore be required by end-users to implement a large-scale monitoring approach. Application of the mapping approach in the UK could benefit from the examination of additional open access, or affordable, national coverage datasets to improve estimates of RES indicators. For example, this may include the national population dataset and additional census for further demand weighting purposes (**Chapter 2**). In addition, the UK Environment Agency has also set a target to provide LiDAR data at 1-metre resolution for the full extents England by 2021 (EA 2020). This may prove useful to improve stratification of mapped vegetation types (**Chapter 3**). Online species occurrence databases could also be investigated for the purpose of modelling urban plant species distribution and update the models for RES functions (Hill et al. 2017). Additional investment in both data collection (either digital or field-based methods) and software may therefore be required to ensure RES analysis is validated to local environmental conditions (Haase et al. 2014). This is also consistent with pay-to-use proprietary software for environmental modelling purposes which may provide improved indicator data, such as ambient air or physiological stress temperatures for temperature regulation modelling (Skelhorn et al. 2014, De Ridder 2015), or advanced coupled overland-underground urban drainage models (Salvadore et al. 2015) for stormwater storage assessment. This would be beneficial to incorporate some of the ecological processes omitted in seasonal analysis here (**Chapter 3**); such as wind and other climate conditions that may affect temperature stressors on a given day, or antecedent soil conditions that affect GBI stormwater storage functions during a precipitation event (Azevedo et al. 2016, Romero et al. 2007). This is of particular use for future scenario planning, as model parameters may be altered to account for future environmental conditions, and therefore consider whether additional GBI conservation or improvement is required to offset increased environmental stressors (Cavan & Kazmierczak 2011).

Where appropriate resources are available then validated high resolution models should be investigated for citywide RES mapping purposes. In contrast, where resources are constricted then further research may consider the application of the current indicatory RES mapping approach as part of a multi-stage analysis framework. Pockets of RES

deprivation may be initially identified across the study area using the current mapping approach, and then high-resolution models validated by primary data, may assess the ecosystem service benefits of various GBI interventions at the neighbourhood scale (Acero & Arrizabalaga 2013, Grêt-Regamey et al. 2013, Skelhorn et al. 2014). This level of approach may also serve as validation of the citywide mapping layer, by assessing how differences in RES values agree between mapped data and modelled findings at various points throughout the city (De Ridder 2015, Eigenbrod et al. 2010). This offers a better approach for validating ecosystem service map layers than the method described in **Chapter 2**, but inevitably requires additional expenditure in resources. As a number of openly accessible methods are available for each of the RES here, it may be beneficial to investigate the implications of model averaging (Wilcock et al. 2020). For example, the InVEST (Stamford University 2020) suite provides software solutions to model of each of the RES studied in this thesis. Comparison of indicators obtained in the current mapping approach, against derived values from InVEST and other modelling software may therefore improve the robustness of investigatory RES function indicators (Wilcock et al. 2020).

In this regard, additional investment in data collection and processing software alone may not always provide an easy solution to limitations in current RES analysis. Certain ecological processes are not yet fully accommodated in service models, and thus further research is required, either through developing ecological and physical theory of ecological/environmental processes, or through long-term scientific monitoring and assessment of ecological processes in the field (Seppelt et al. 2011). The former may relate to improvements in spatial statistical modelling of GBI LST or ambient air reduction for temperature regulation indicators (Doick et al. 2014, Stewart & Oke 2012). Method development of remote sensing methods to improve categorisation of GBI species and associated biophysical characteristics for more detailed analysis of RES benefits (e.g. carbon storage, canopy interception) of varying GBI species types (Raciti et al. 2014, Sjöman & Gill 2014) is also beneficial. Longer term field-based enquiry may concern the study of how ecological functions of common UK urban-based tree and shrub species alter on an annual basis to regulate for example temperature (Armson et al. 2013b, Rahman et al. 2015) and precipitation (Armson et al. 2013a). This will enable improved estimates of seasonal variation in regulating RES, in addition to providing validation of existing seasonal

environmental models. In addition, continued study is required into the type of GBI interventions suited to local ecological (e.g. soil types, water availability) and built infrastructure (e.g. space for vegetation rooting/canopies, modification of environmental hazards) conditions to better inform future RES scenario analysis (McBride & Laćan 2018, Speak et al. 2012).

Whilst the aforementioned research will be beneficial for the purposes of ecosystem service mapping research, the degree to which any RES mapping exercise meets local planning objectives certainly requires engagement with end-users (Daily et al. 2009, Muller et al. 2010). Primarily this is important to engage multi-disciplinary discussion of the usefulness mapped RES information developed in this thesis (Gómez-Baggethun et al. 2013). Of particular importance is the implications of incorporating service and disservice values from seasonal analysis and what implications this may have for environmental management (Pataki et al. 2006). In addition, stakeholders may wish to consider the relative importance of individual RES values (Koschke et al. 2012, Kremer et al. 2016a). Combined RES deprivation metrics for example, may therefore consider disparity in resident demand for both services and thus provide an updated view of current need for GBI investment within the study area (Koschke et al. 2012). For example, a recent study in Barcelona, Spain combines ecosystem service mapping and local citizen priorities regarding service needs within a Bayesian belief network model to address local ecosystem service deficits using green roofing interventions (Langemeyer et al. 2020). Stakeholder engagement may also require a re-purposing of the ULU classification to better represent land use managers of local importance, who may be referenced for specific GBI interventions (Li et al. 2005, Mackillop 2012). For Manchester this may include Local Housing Associations that oversee various housing areas, large estates of companies and charitable organisations, through to land controlled by various public sector institutions. However, this again requires access to additional information, such as land deed ownership (Demir & Çoruhlu 2009, Nimbus Maps 2020) to aid identification of land use manager areas.

Engagement with local citizens and members of the planning community may also reveal the importance of other RES within the local area. For example, consideration of how recreational interaction with GBI may benefit the physical and social health of urban residents is a key research and planning concern (Niemelä et al. 2010, Bastian et al. 2012),

and is likely to be highlighted in any stakeholder engagement exercise. In this regards, studies of resident travel accessibility to recreational GBI areas (Comber et al. 2008, Maroko et al. 2009, Stessens et al. 2017) define spatially explicit ecosystem service indicators to improve public well-being. Additional RES considered important by planning stakeholders may include regulating services such as particulate capture (Escobedo & Nowak 2009, Speak et al. 2012) and noise buffering (Radford & James 2013), supporting services such as biodiversity and wildlife habitation (Andersson et al. 2007), through to provisioning services of urban and peri-urban agriculture (Lin et al. 2015b). Even where certain services may not be considered important to local planners, future research should consider methods to incorporate as many RES within the analysis workflow as possible in order to provide a systematic account of the multiple GBI benefits within a given study area. However, it is important to note that incorporation of additional RES will inevitably induce increasing complexity, and perhaps uncertainty, through the incorporation of additional service and demand indicator dynamics (Fu et al. 2011, Layke 2009).

Overall, further research into improved RES mapping methods is vital to support continuing technological developments in fields such as city modelling software, and smart city monitoring systems to enable use of fully integrated urban planning support tools. For example, 3D urban modelling software demonstrate integrated analysis to assess the effect of proposed infrastructural developments upon local planning concerns such as pedestrian and vehicle traffic levels, building sightlines and conservation issues (ESRI 2020, VU.CITY 2020). High resolution ecosystem service analysis software (Grêt-Regamey et al. 2013, Nakata-Osaki et al. 2018) demonstrate the potential to adapt such city models for contextual RES assessment by incorporating 3D representations of trees and other GBI resources. Scenario analysis may then usefully assess whether proposed built-infrastructure (e.g. high-rise apartments, new roads) or GBI investments (e.g. street trees, artificial ponds) heightens or reduces environmental risks for residents within the local environment. Continuing developments in smart-city technology may also support these developments, as improvements in the cost-effectiveness, software and coverage of monitoring networks should improve data collection and ultimately the modelling of various urban ecological/environmental phenomena (Azevedo et al. 2016, Kolokotroni & Giridharan 2008). Further research is therefore required to continually evaluate new

technologies and data for ecosystem service analysis and thus ensure cities are appropriately resilient to the potential risks of climate change in the future (Carter et al. 2015).

Appendices

Appendix 1 – Paper published from thesis

Ecological Indicators 121 (2021) 107058

Contents lists available at ScienceDirect

Ecological Indicators

journal homepage: www.elsevier.com/locate/ecolind

Mapping regulating ecosystem service deprivation in urban areas: A transferable high-spatial resolution uncertainty aware approach

Fraser Baker *, Graham R. Smith, Stuart J. Marsden, Gina Cavan

Ecology & Environment Research Centre, Department of Natural Sciences, John Dalton Building, Manchester Metropolitan University, Chester Street, Manchester M1 5GD, UK

ARTICLE INFO

Keywords:
Regulating ecosystem services
Mapping
Deprivation
Urban
Environmental risk
Uncertainty analysis

ABSTRACT

Maps of regulating urban ecosystem services (UES) aid identification of priority areas for green–blue infrastructure investment to improve urban resilience to environmental hazards. Current mapping approaches however may present coarse spatial resolutions, and often fail to consider how UES flows serve resident demand at the appropriate micro-scale. In addition, prohibitive costs involved in collecting primary data to validate UES model parameters to local conditions may enforce the use of proxy methods, thereby inferring ambiguity in parameterisation and uncertainty in mapping outputs. This study examines both issues through the implementation of a high-spatial resolution approach to map multiple urban regulating ecosystem service (temperature regulation, stormwater absorption, and carbon storage) deprivation in Manchester, UK. Poorly performing UES areas are defined as the lowest 10% combined ecosystem service indicator values ('coldspots') at 100m grid resolution. Coldspots are compared to population demand levels, disaggregated from weighted population estimates, indicating neighbourhoods deprived of UES. Ambiguity in proxy method implementation is examined using combinations of UES parameter settings ($n = 16$) within various demand measures ($n = 3$) to measure changes in relationships between UES, and variation in final map outputs across the study area. Uncertainty is therefore quantified as an interactive process, whereby input parameter ambiguity affects local uncertainty in map outputs, due to varying landcover composition. As explicit sensitivity analysis in current UES mapping studies is limited, the study demonstrates how ambiguity in method parameterisation may impact UES mapping exercises. Complex interactions governing spatial variance in map uncertainty may therefore be addressed through identification of consistent areas of interest (e.g. hotspots, coldspots) by contrasting outputs realised from different parameterisations. As such, the study demonstrates the mapping approach as a transferable city-wide visualisation tool, using accessible data and methods, to investigate regulating UES deprivation at practical scales required to retrofit existing urban infrastructure with green-blue infrastructure investment.

1. Introduction

Regulating ecosystem services of urban green–blue infrastructure (UGBI) benefit urban residents by moderating environmental hazards associated with urbanization (Gómez-Baggethun and Barton, 2013). As climate change is projected to increase the frequency and severity of extreme weather conditions, the localised provision of regulating urban ecosystem services (UES) such as temperature cooling, atmospheric carbon storage, and stormwater absorption, will become increasingly important to safeguard human health and well-being (Kabisch et al., 2016). The spatial mapping of multiple regulating UES is therefore useful to identify neighbourhoods where strategic UGBI interventions may benefit local resident well-being (Kabisch et al., 2016, Pulighe et al., 2016). However, despite increased access to high-spatial resolution geospatial data in recent years, that has enabled improvements in UES mapping methods, the practical influence of resulting information products within urban planning concerns appears limited (Haase et al., 2014, Woodruff and BenDor 2016). Improvements in the effective spatial communication of UES benefits are arguably required to support the conservation and enhancement of UGBI resources.

Abbreviations: UES, Regulating urban ecosystem services; UGBI, Urban green–blue infrastructure; SCS-CN, Soil conservation society curve number method; CN, Curve Number.

* Corresponding author.
E-mail address: f.baker@mmu.ac.uk (F. Baker).

https://doi.org/10.1016/j.ecolind.2020.107058
Received 10 February 2020; Received in revised form 30 August 2020; Accepted 7 October 2020
Available online 3 November 2020

A primary challenge for UES analyses is the appropriate spatial representation to represent real world UES processes. Service indicators amalgamated within census tracts, administrative boundaries or land-use/land-cover areas, are beneficial for comparing a wide range of ecosystem benefits (e.g. economic, social and cultural) to either local demand for such services, such as in neighbourhoods containing high-need demographic groups, or within areas of local planning concern (Baró et al., 2017, Cabral et al., 2016, Kroll et al., 2012). However, as regulating benefits may occur at the micro-scale (e.g. particulate capture by individual trees, or localised air cooling) alternative spatial representations may better represent micro-scale variation in benefit flows to local residents (Andrew et al., 2015). For example, an administrative district may consist of a distinct residential urbanised area with minimal UGBI cover, adjacent to a large park consisting primarily of UGBI. Due to morphological constraints, the temperature regulation benefits provided by the parkland may have limited impact within the residential area (Coseo and Larsen, 2014). However, in this instance the significant presence of parkland UGBI results in overestimation of temperature regulation benefits when calculating a single service value for the area as a whole (Gómez-Baggethun and Barton, 2013). In contrast, UES represented within grid structures provide more appropriate measures of spatial variation in continuous environmental processes across heterogeneous urban environments (Holt et al., 2015; Kremer et al., 2016a; Langemeyer et al., 2020). Studies demonstrate the benefits of service demand indicators at fine scale resolution to map overall UES values (Baró et al., 2016; Larondelle and Lauf, 2016), but remain limited in number, and may rely on data relevant to a specific study area. To improve applicability of UES mapping approaches, further investigation of grid based service to demand indicators adaptable for different urban areas are required.

In addition, current mapping outputs may implicate an unquantified level of uncertainty, through the combination of various methods and assumptions required to assess multiple UES values. Whilst models validated with primary data that represent local ecological and environmental conditions are preferred, the costs to collect and process such data for particular UES may prove prohibitive for whole city areas (Schröter et al., 2015). In comparison, proxy methods provide a time and cost-effective alternative but may result in spurious map outputs due to the direct transfer of findings to inappropriate ecological representations (Eigenbrod et al., 2010). Studies may counter this issue through approaches tailored to the local urban environment and associated data. However, as quality of input data may vary considerably between study areas, such mapping approaches may have limited application in other urban areas (Haase et al., 2014). Due in part to a current lack of standardisation in methods, UES knowledge transfer between urban areas is limited (Kremer et al., 2016b). UES mapping approaches applicable to different urban environments thus require understanding of how input data of varying quality may cause ambiguity in the parameterisation of component methods, and thus influence final map products (Schulp et al., 2014). Whilst consideration of mapping uncertainty is often discussed in UES studies, it is rarely investigated in quantified terms (Andrew et al., 2015; Zhao and Sander, 2018).

In order to advance current methods for mapping UES, this study aims to address the aforementioned issues by transforming current UES mapping methods into a transferable high-spatial resolution uncertainty aware regulating ecosystem service mapping approach. A case study implementation for Manchester, UK, demonstrates the benefits of the methods applied. Results from this exercise provide recommendations for application of the approach in other urban areas, in addition to generating knowledge for wider urban ecosystem service research.

2. Methods

2.1. Study area

Manchester is a post-industrial city located in the North-west region of England, UK (Fig. 1) covering an approximate area of 115 km^2 (UKDS, 2017), with an estimated 2016 population of 541,000 (4716 people/km^2) (MCC, 2018). Currently, UGBI covers approximately 49% of the total city area, with significant UGBI contained within parklands and other natural resource areas (Dennis et al., 2018). In addition, UGBI varies according to residential housing characteristics, with pre-1919 (46.2% of housing stock; typically terraced housing), and post-1919 residential areas estimated to contain on average 11.8% and 37.8% tree cover respectively (Hall et al., 2012). Due to heterogeneity in local UGBI resources, residents in the city experience varying regulating UES (Gill et al., 2007); therefore, the city provides a useful case study area to develop a UES mapping approach.

2.2. Overview of mapping approach

Environmental hazards affecting study area residents include pluvial and fluvial flooding and heat stress from extreme temperatures, in addition to larger scale environmental risks posed by global warming (Carter et al., 2015). Therefore, regulating services chosen for the mapping approach include temperature regulation, carbon storage, and stormwater absorption, due to benefits in regulating urban environmental risks for current and future climate conditions (Carter et al., 2015). Models for UES indicators that are feasible for micro-scale

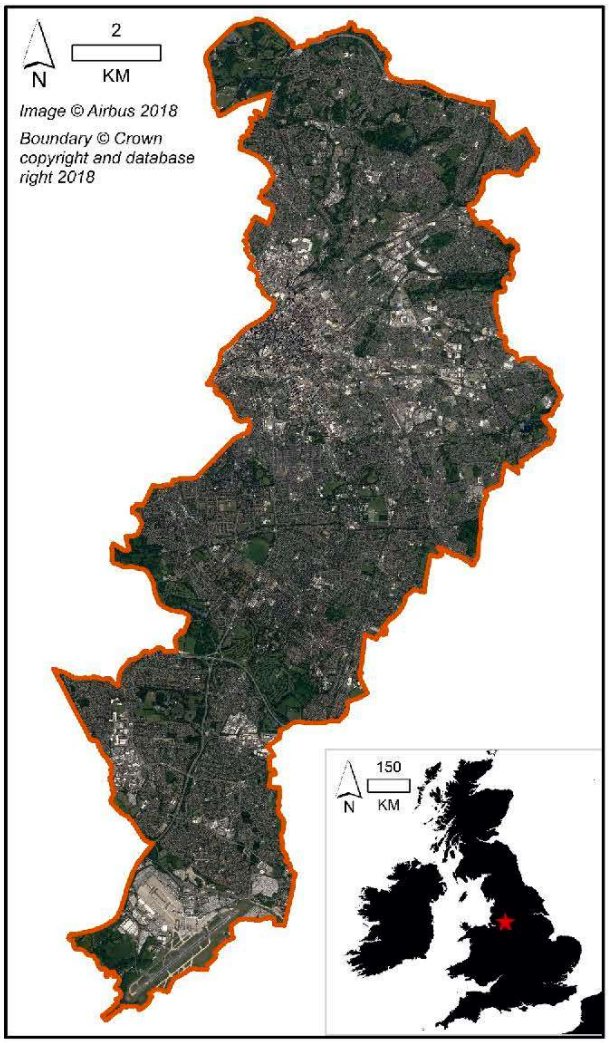

Fig. 1. Location of Manchester within UK.

citywide analysis were chosen following a review of UES mapping literature (Table 1). The approach uses a regular grid cell structure (100 m resolution) to provide a measure of UES indicators in relation to UGBI change across the continuous urban environment (Holt et al., 2015). Within this approach, disaggregated census population estimates represent levels of resident demand for local UES (Baró et al., 2017).

Due to the excessive costs of acquiring independent reference data, parameters for carbon storage and stormwater absorption models (Table 1), in addition to demand disaggregation methods, are not validated to study area conditions, and therefore infer a degree of uncertainty. Following a pragmatic interpretation of the mapping approach, sensitivity analysis was used to investigate how ambiguity in proxy method assumptions may impact map outputs. The influence of proxy method choice upon relationships between unique UES, and combined UES indicators, in addition to identifying regulating UES deprivation ('Coldspots') was therefore investigated using ($n = 16$) service model parameter settings within various ($n = 3$) demand measures (Eigenbrod et al., 2010). Combined UES deprivation (*Coldspot*) areas identified through overlap of deprivation areas for each parameter setting, aim to reduce potential mapping uncertainty and thus demonstrate the overall benefits of the approach. Fig. 2 presents the case study workflow, with methods described in the following sections.

2.3. Urban landcover

An urban landcover map representing five classes (buildings, non-vegetation (artificial and bare Earth surfaces), tree Canopy, non-tree vegetation and water) was generated to provide geo-referenced ecological map data to estimate UES values (see Table 2 and Fig. 3). The data was scaled at 2 m pixel resolution (now widely available) to generate land-cover products available in similar UES mapping studies (see Derkzen et al., 2015; Kremer et al., 2016a).

Table 1
Methods and indicators chosen for UES.

UES	Description of service	Chosen method*	Modelled indicator measure	Study area validation**
Temperature regulation	Reduction of localised temperatures during hot weather conditions	Geographically weighted regression models to estimate the influence of local UGBI on remotely sensed Land Surface Temperature (LST; °c).	Predicted LST (max LST = 0 service value; min LST = 100% service value)	YES
Carbon storage	Storage of carbon within vegetation biomass	Transfer of carbon storage values per Land-use Land-cover categories in UK based carbon storage studies to Land-cover categories within the case study.	Predicted C kg m^2 (max C kg m^2 = 100% service value; min C kg m^2 = 0% service value)	NO
Stormwater absorption	Reduction of runoff and local flooding pressures through capture of precipitation by UGBI	SCS-CN (USDA, 1986) method to estimate runoff reduction potential (CN) of localised UGBI resources.	Quantified CN (Max CN = 0% service value; Min CN = 100% service value)	NO

* Further description of methods provided within the following sections; ** Model estimates validated to environmental conditions within the study area.

2.4. Temperature regulation

Land surface temperature (LST) represents the temperature of ground surface layers and is a governing indicator of thermal energy transfer for above ground ambient air warming (Oke, 1988), with excessive LST empirically associated with negative health outcomes (Harlan et al., 2014; Laaidi et al., 2011). In comparison to measured ambient air temperatures, which may require significant expense in implementing citywide in-situ monitoring networks (Muller et al., 2013), remotely sensed LST data is available for entire urban areas, enabling statistical modelling of temperature regulation indicators. A LST surface was generated using the mono-window method (Wang et al., 2015) using cloud-free imagery (17 July 2017; 30 m resolution) from the Landsat-8 Operational Land Imager sensor (USGS, 2017). Daytime conditions were warm, with a maximum temperature of 23 °C (average 16 °C) recorded at the nearby Manchester International Airport weather station (Weather Underground, 2017). As spatial patterns of LST in relation to the urban morphology are expected to remain relatively consistent for warmer climate conditions (Oke, 1988) the LST surface generated was considered a reasonable representation of excessive heatwave conditions. Geographically weighted regression was implemented (ESRI ArcMap 10.3) using ordinary least squares regression (Eq. (1)) to statistically infer the causal relationship of UGBI (proportion of UGBI per cell = pUGBI) upon LST as it varies according to localised variation in urban morphology. Predicted mean LST per cell (pLST) provided the measure for estimating temperature regulating indicators.

$$pLST_{CELL} = a + b \cdot pUGBI_{CELL} \quad (1)$$

2.5. Carbon storage

Due to the prohibitive cost of collecting primary data to estimate biomass of local UGBI resources (e.g. vegetation matter and tree characteristics for allometric models) (Derkzen et al., 2015; Holt et al., 2015) above-ground carbon storage was calculated based upon findings in UK-based empirical carbon storage studies (Table 3). Descriptions of carbon storage landcover/land-use categories were matched to case study landcover classes to calculate above ground carbon storage per square metre (C kg m^{-1}) for the associated landcover area. Due to realistic difficulties in interpreting some landcover classes to landcover/land-use descriptions in empirical study, four different parameter settings were devised to examine parameter ambiguity on final UES values (Table 3). The UES indicator measure is the total carbon stored per cell.

2.6. Stormwater absorption

Combined overland-underground catchment scale models enable estimation of stormwater absorption rates of UGBI types through validation of modelled catchment outputs to measured channel outflows (Salvadore et al., 2015). Such methods are computationally expensive for urban districts overlapped by numerous catchment areas, requiring significant data and expertise for effective model parameterisation. In comparison, the Soil Conservation Society curve number (SCS-CN) method (USDA, 1986) is a pragmatic alternative widely used in other UES mapping studies (Gill et al., 2007; Kremer et al., 2016a; Tratalos et al., 2007). SCS-CN works as a one-dimensional numerical model that computes the amount of rainfall converted to surface runoff for a given surface area (represented by curve number values) during a rainfall event (USDA, 1986). However, unless independently validated, SCS-CN is a proxy model with curve number values assigned directly between SCS-CN and mapped landcover categories. In the same manner as carbon storage, parameter ambiguity may occur through the interpretation process (see Section 2.7) for some landcover classes, therefore four stormwater absorption parameter settings were used to investigate this issue (Table 4). Curve numbers (CN) for landcover pixels were assigned by integrating landcover data and underlying soil type (Cranfield

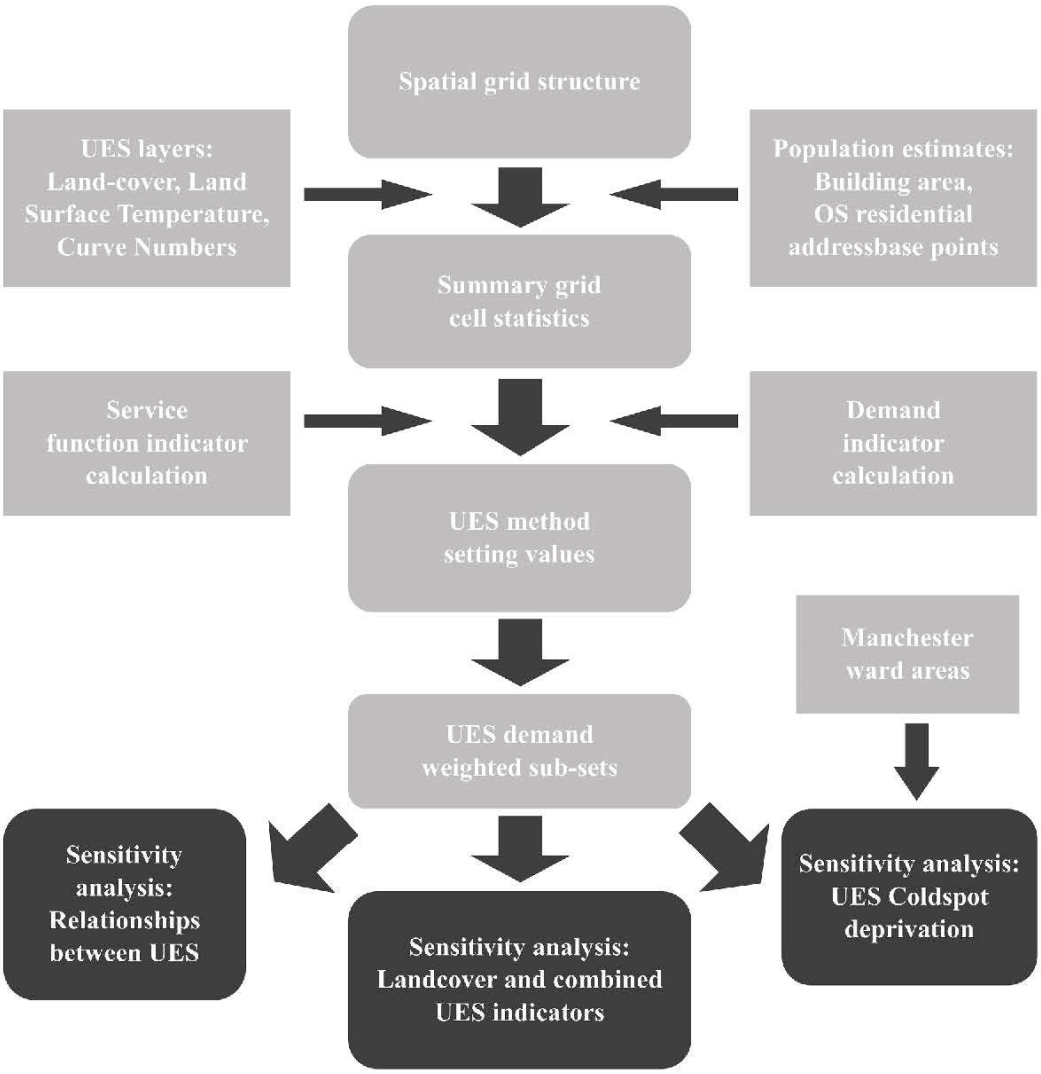

Fig. 2. Case study workflow.

University, 2018), with stormwater absorption indicators calculated from the areal CN average per analysis cell.

2.7. Regulating ecosystem service demand

Methods for population disaggregation vary depending upon available resources (Stevens et al., 2015; Zandbergen and Ignizio, 2010) therefore two disaggregation methods were used to assess choice of method upon final UES map outputs. The first method involves areal upscaling of population estimates within census areas to the areal extents of human habitation represented by building footprint area (termed BLD_{POP} here) (O'Brien and Cheshire, 2016). This method is cost-effective as building footprint areas are accessible for research in the UK (Edina digimap, 2017). However, as no distinction is made between building type (e.g. residential, commercial-industrial), population density is extrapolated across non-residential building areas (Jia et al., 2014; O'Brien and Cheshire, 2016). In contrast, the RES_{POP} method uses residential address points from the UK ordnance survey AddressBase Plus product (OS, 2018) to weight population towards residential housing (Bhaduri et al., 2007; Zandbergen, 2011). However, this method is less accessible due to licensing costs of the associated data. Using both methods, annual population estimates (current estimates available for 2016) for the UK at the Lower Super Output Area (LSOA) level (UKDS, 2017) were disaggregated to generate the respective demand indicators (see Appendix A for population disaggregation workflows).

2.8. Sensitivity analysis – UES relationships and deprivation

Three methods were used to examine the effect of parameter ambiguity upon UES map outputs. First, correlation analysis estimated how chosen service parameters and demand methods interact to alter relationships between individual UES (Holt et al., 2015). UES indicators were calculated for all parameter settings ($n = 16$; 1 Temperature regulation $\times$ 4 Carbon storage $\times$ 4 Stormwater absorption settings) within No demand (all cells), BLD_{POP} (where $BLD_{POP} \geq 1$) and RES_{POP} (where $RES_{POP} \geq 1$) demand cells. This analysis considered how the mapping approach may perform under differing data assumptions, and the impact of parameter ambiguity upon UES indicators for models commonly employed in other UES mapping studies.

Second, a manual parameter comparison approach investigated the degree parameter ambiguity influences spatial variation in combined

Table 2
Data, methods and class descriptions used to generate the urban landcover map.

Process	Reference data	Methods	Classes from methods*
1	Mastermap topography layer (May 2017 version; Edina Digimap, 2017)	Land parcel and surface feature extents represented as polygon areas; attribute data used to categorise initial class area where possible	All classes
2	Tree audit data (CityOfTrees, 2011)	Represents canopy extents (>1.5 m) of trees and woodland; provides masking feature to re-classify all landcover classes as trees	Tree canopy
3	True-colour aerial imagery (12.5 cm resolution; collected June 2009–2015; Getmapping, 2017)	Classified into a vegetation mask using a threshold with image band data; used to assign non-classified pixels as either non-tree vegetation or non-vegetation appropriate	Non-tree vegetation; Non-vegetation

* Buildings permanent building structures; Non-vegetation Artificial and Bare Earth; Water Water bodies and channels; Tree Canopy tree canopy extents; Non-tree vegetation – vegetation not considered as trees, such as shrubs and grasses.

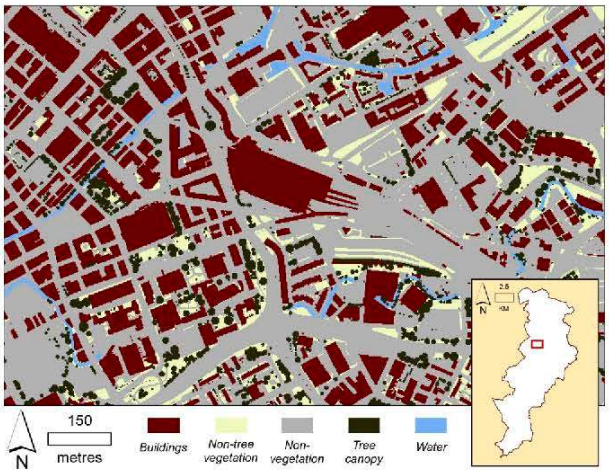

Fig. 3. Example of mapped urban land cover for central Manchester.

UES indicators, defined as percentiles of summed ranks for individual UES (see Table 1). Assuming a uniform probability distribution function (PDF) for each uncertain parameter, nine unique parameter values were calculated from equal intervals within permitted input parameter range (see Table 5). Parameter values were thus altered one by one, in pairs, triples and all parameters together considering all possible parameter interactions for each combination. Mid parameter range values represented the default position for non-altered parameters where applicable. Combined UES indicators per cell were calculated for all parameter interactions, with the range in combined cell UES indicator values defining the level of variation, or uncertainty per parameter combination. This 'brute-force' method was undertaken over a simulation based global sensitivity approach for example, as combined UES indicators require individual service indicators for all cells calculated from a uniform set of parameter inputs (Lilburne and Tarantola, 2009). This analysis enabled consideration of a) spatial variation in uncertainty across all cells in the study area, b) whether uncertainty increases due to different orders of uncertain parameters, and c) considered the influence of relative magnitudes in parameter uncertainty upon potential mapping outputs.

Finally, a method to counter potential uncertainty in outputs was assessed by comparing identified 'coldspot' areas at both the neighbourhood (grid cell) and administrative district resolution, to simulate an urban planning exercise to map environmental deprivation at various spatial scales. Coldspots are defined in this study as the lowest 10% of cells using combined UES indicators, and therefore reverse the hotspot concept described in other ecosystem service studies (Anderson et al., 2009; Schulp et al., 2014). Coldspots are then amalgamated to identify the 20% most UES deprived administrative ward areas (Holt et al., 2015) according to the ratio of Coldspot to demand area. Wards were used in this instance, as socio-economic statistics produced at the administrative

Table 3
Carbon storage values for four parameter settings.

Setting	Land-cover class	Carbon storage categorisation	Carbon storage (kg C m $^{-2}$)	Justification for carbon density method
1[a]	Non-Tree	Herbaceous Vegetation	0.15	Herbaceous vegetation only; Non-tree assumed to represent short grasses
	Tree Canopy	Tree	28.46	Assumed to represent tall trees (>5m height)
2[a]	Non-Tree	Mean: Herbaceous Vegetation, Shrub	5.19	Assumed to represent a mixture of grasses and low shrubs
	Tree Canopy	Mean: Tree, Tall Shrub	21.33	Assumed to represent a mixture of tall shrubs and trees
3[b]	Non-Tree	Sport and Leisure	0.68	Sports and leisure land use assumed to represent a mixture of vegetation types
	Tree Canopy	Mixed forest	3.28	Mixed forest only
4[b]	Non-Tree	Green Urban Areas	0.09	Green urban areas only (grassy areas)
	Tree Canopy	Broad-leaf Forest	3.80	Broadleaf forest only

[a] Category values obtained from Davies et al. (2011) – study provides a quantified survey and extrapolation analysis of carbon storage according to vegetation categories in Leicester, UK.
[b] Category values obtained from Cruickshank et al. (1998) – study provides a national inventory of carbon storage per land-cover land-use classes in Northern Ireland based upon field-based studies.

Table 4
Curve Number values according to soil groups and chosen Soil Conservation Society (SCS) landcovers per parameter setting.

Study area Landcover	Parameter settings	SCS Landcover	Curve Number (CN) per Hydrological Soil Type		
			B	C	D
BUILDINGS	1, 2, 3, 4	Paved, roofs, etc.	98	98	98
NON-VEGETATION	1, 3	Paved, roofs, etc.[1]	98	98	98
	2, 4	Streets and Roads: Paved; open ditches[2]	89	92	93
NON-TREE VEGETATION	1, 2	Pasture: good condition[3]	61	74	80
	3, 4	Brush: good cover[4]	48	65	73
TREE CANOPY	1, 2, 3, 4	Wood: good cover	55	70	77
WATER	1, 2, 3, 4	Water	25	25	25

1 – Wholly impervious surfaces i.e. Roofs, Asphalt and concrete roads; 2 – Wholly impervious and pervious non-natural surfaces; 3 – Grassland not protected from grazing such as mown grass typical of lawns, playing fields etc. and rough grassland; 4 – Low-standing vegetation such as bushes, weeds and grass.

Table 5
Probability distribution function values for ambiguous parameters.

Uncertain carbon storage parameter (kg C m^2)	Key*	PDF parameter range values (Minimum | Maximum | Default)		
Non-tree vegetation	**A**	0.09 | 5.19 | 2.64		
Tree canopy	**B**	3.28 | 28.46 | 15.87		
Uncertain stormwater absorption parameter (CN)		Soil type		
		B	*C*	*D*
Non-vegetation	**C**	89 | 98 | 93.5	92 | 98 | 95	93 | 98 | 95.5
Non-tree vegetation	**D**	48 | 61 | 54.5	65 | 74 | 69.5	73 | 80 | 76.5

* – Identifier for input parameter within parameter combinations; varied parameters notated within brackets e.g. {A, B} represents combined interaction between parameters A and B.

level therefore enable comparison of relative deprivation levels at the scope of local governance (Baró et al., 2017). As per correlation analysis, this was conducted for all parameter settings across all demand cell weightings.

3. Results

Geographically weighted regression resulted in a model with $R^2 = 0.65$ and $AIC = 42{,}952$, comparing favourably to the ordinary least squares model ($R^2 = 0.45$ and $AIC = 47{,}871$). Modelled temperature regulation indicators therefore remain strongly associated with pUGBI ($r = 0.88$, $p < 0.001$), and are therefore positively associated with other UES. Uncertainty in proxy UES model parameterisation therefore alters these relationships in varying magnitudes according to the relative demand weighting method (Figs. 4 and 5). Mapped indicators for all UES parameter settings and demand methods are provided in Appendix B.

Correlation values between temperature regulation and carbon storage indicators increases from no demand cells (mean $r = 0.56$), to the disaggregation methods (mean $r = 0.63$ and 0.61 for BLD_{POP} and RES_{POP} respectively). This trend is however reversed for correlations between temperature regulation and stormwater absorption indicators, with stronger correlation values for no demand cells (mean $r = 0.83$) in comparison to demand weighted cells (mean $r = 0.79$ and 0.78 for BLD_{POP} and RES_{POP} cells respectively). Weighting demand towards building and residential areas in effect removes cells largely covered by water (e.g. cells within reservoirs, water channels) with maximum water coverage per cell varying from 100% for no demand cells, to just 69% and 42.7% for BLD_{POP} and RES_{POP} cells respectively. As water is beneficial for stormwater absorption and temperature regulation services but has no estimated carbon storage benefits (see Table 5), the removal of such cells alters relationships between individual UES.

Whilst patterns in relative correlation values between settings remain stable, irrespective of demand method (Figs. 4 and 5), ranges in correlation values (Table 6) vary between demand method cells with different landcover proportions. For example, no demand cells provide the largest range in correlation values and the highest mean UGBI cover (46.4%), contrasting with BLD_{POP} cells, with lowest UGBI coverage (37.4%), and range in correlation values. Correlation differences are small but indicate that variation in relationships between individual UES is constrained somewhat by spatial variation in cell landcover proportions.

For combined UES indicators, uncertainty (range in combined UES indicators per cell) generally increases according to the number of interactions between uncertain parameters (Fig. 6) which influence uncertainty individually by varying magnitudes. As evident, median and maximum combined UES indicator range values for single parameter combinations ({A}, {B}, {C}, {D}) are considerably lower than interacting variations between all parameters ({A, B, C, D}). However, this is not a consistent pattern when travelling from lower to higher order combinations. For example within No Demand cells, parameter variation in tree canopy carbon storage ({B}) values result in more uncertain outputs than parameter combinations {A, C}, {A, D} and {C, D}. The relative importance of single uncertain parameters therefore varies (1st = {B}, 2nd = {A}, 3rd = {D}, 4th = {C}), with carbon storage parameters B and then A interacting to produce greater uncertainty for 2nd and 3rd order parameter combinations. This relationship is associated with the ratio of PDF parameter values against the total range (between no service to maximum service values) of permissible parameter values for each service. For example, permissible parameter ranges are 28.46 for carbon storage (minimum = 0 C kg m^2, maximum = 28.46 C kg m^2) and 73 for stormwater absorption (minimum CN = 98, maximum CN = 25). Dividing PDF ranges by the permissible range for the appropriate service, provides the ratio, or magnitude of uncertain parameter value range ({B} = 0.88, {A} = 0.18, {D} = 0.13 (average for soil types), {C} = 0.09 (average for soil types)) which concurs with the relative order of individual parameter influence. Variation in uncertainty between parameter combinations is relatively consistent between demand measures, as median combined ranges exhibit minor differences, whilst increased variation in maximum combined UES indicator ranges has minimal impact upon the order of uncertainty between parameter combinations.

Variation in parameter driven uncertainty between individual cells (Fig. 6) is thus influenced by variation in cell landcover proportions. Fig. 7 displays landcover proportions, averaged for all cells by unique combined UES indicator range values for each parameter combination

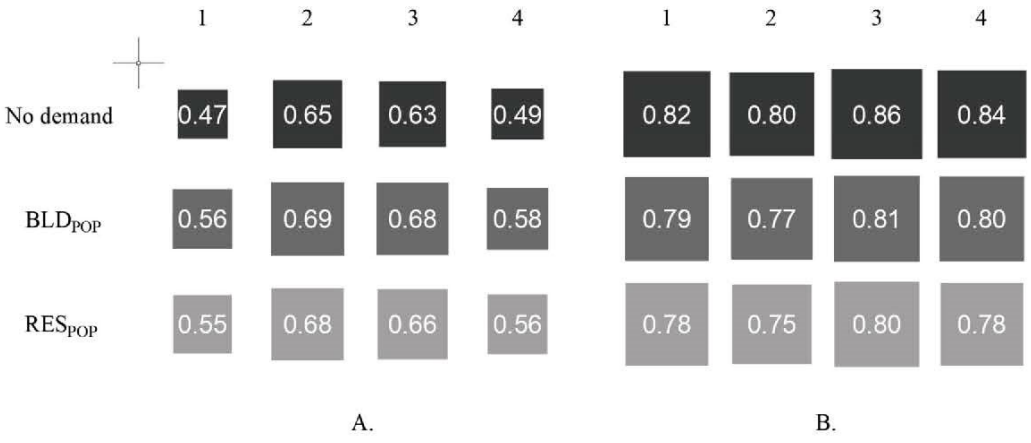

Fig. 4. Correlation (r) values between temperature regulation indicators to carbon storage (A) and stormwater absorption (B) indicators for all parameter settings and all demand weighting methods. All r values significant ($p < 0.001$).

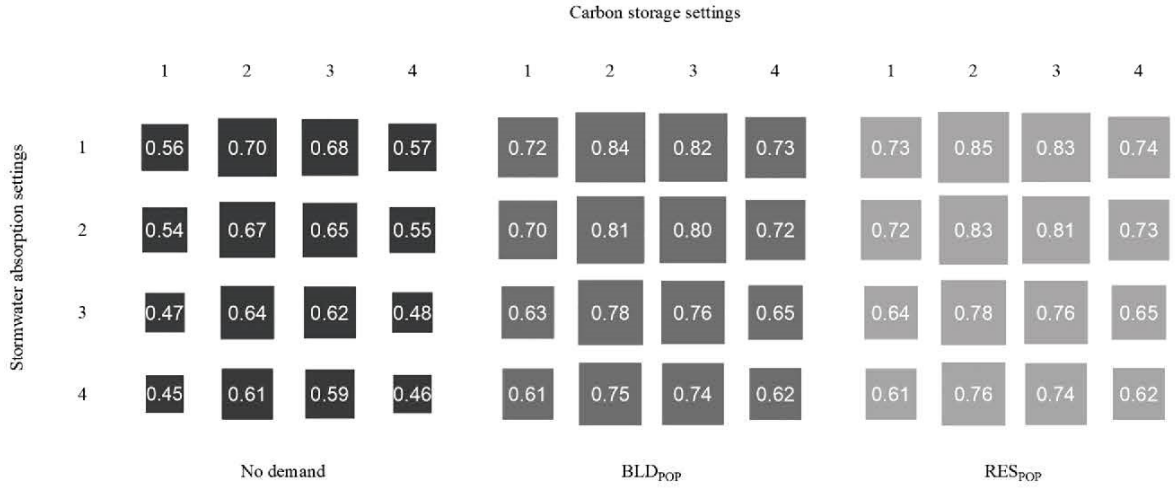

Fig. 5. Correlation values (r) between Carbon storage and Stormwater absorption indicators between all parameter settings for for all demand methods. All r values significant ($p < 0.001$).

Table 6
Summary statistics for correlations between UES.

Demand cells	Temp. regulation to Carbon storage		Temp. regulation to Stormwater absorption		Carbon storage to Stormwater absorption	
	Mean (r)	*Max .(r)–Min. (r)*	*Mean (r)*	*Max. (r)–Min. (r)*	*Mean (r)*	*Max. (r)–Min. (r)*
No demand	0.56	0.18	0.83	0.06	0.58	0.25
BLD_{POP}	0.63	0.13	0.79	0.04	0.73	0.23
RES_{POP}	0.61	0.13	0.78	0.05	0.74	0.24

(ordered by least [1] to most [15] uncertainty in combined UES values) for No demand cells. A general pattern emerges across all parameter combinations, whereby a single landcover proportion becomes increasingly dominant for cells with relatively higher levels of uncertainty. Tree canopy dominates parameter combination {D}, non-vegetation dominates parameter cobmination {C} and {C, D}, whilst for all subsequent combinations non-tree vegetation increasingly dominates. Interestingly, the patterns for single parameter combinations {D} and {B} are not associated directly to the respective non-tree vegetation and tree canopy parameters. This may be explained by the dependency of combined UES indicators between cells, as variation in UES parameter values produce a dependency upon the relative ranking index of other cells. Whilst individual cell landcover proportions vary for unique combined UES values, overall patterns indicate that this is not a random spatial process. The figure therefore evidences where high levels of uncertainty in combined UES indicators may occur within the study area.

Parameter ambiguity therefore impacts the identification of coldspots (Fig. 8). For all cells identified as a coldspot in any parameter setting, over 78% were consistently identified as a final coldspot through overlaying outputs across all parameter settings. This percentage differs by 0.8% across all demand weighting methods, indicating relative congruence in coldspot identification between UES parameter settings irrespective of varying analysis cell area. Maximum difference in coldspot identification between parameter settings, as a percentage of total coldspot area, is 8.3%, 9.3% and 9.5% for No demand, BLD_{POP} and RES_{POP} cells respectively. Based upon the proxy values used in this study, choice of a particular parameter setting results in a near 10% discrepancy in available coldspot area when compared to maps generated using alternative parameters.

As demonstrated in Fig. 9, the reduction in the number of demand cells necessarily reduces the total study area percentage identified as a final coldspot from 8.9%, 7% and 5.6% for No demand, BLD_{POP} and RES_{POP} cells respectively. Coldspot clusters are iteratively removed due to this process, which in turn alters the mapped extent of deprivation across the study area. The impact of this process is also evident at coarser spatial scales, as altering demand method also results in subtle changes in the identification of UES deprived ward areas (Fig. 10). Whilst five out of seven wards are consistently identified as the 20% most UES deprived areas, altering demand measure causes some variation in final map outputs at this spatial scale.

Overall, Fig. 11 demonstrates the resolution of final map products of UES deprivation within the context of both the built environment and administrative ward landscape. It is therefore possible to envisage the type and scale of UGBI investments pragmatically implementable within local neighbourhoods. For example, coldspot areas mainly fall within residential terraced housing areas that overlap administrative ward districts in some areas, in turn providing visual evidence of where ward councils could act collectively to direct local garden greening strategies (Baker et al., 2018).

4. Discussion

This study presents a novel mapping approach to indicate priority locations to reduce resident exposure to climate related hazards. The approach is therefore transferable to other urban areas using accessible geospatial data and methods, with accompanying sensitivity analysis to indicate the impact upon map outputs due to pragmatic considerations required of investigators in different urban areas. Given that UES analysis methods are often opaque (e.g. expert based, black box software) or rely on data specific for an urban area (Haas and Ban, 2017; Langemeyer et al., 2020) efforts to improve provide basic and adaptable framework to consider UES knowledge transfer between urban areas (Haase et al., 2014; Luederitz et al., 2015). In particular this approach provides additional support to an environmental/ecological scale representation of UES indicators, especially where services flow continuously across heterogeneous urban landscapes (Baró et al., 2016; Langemeyer et al., 2020).

Spatial resolution in regulating UES in this study are thus important to indicate UES benefits within the spatial extent of small-scale urban greening solutions (e.g. street tree planting, sustainable urban drainage systems, green walls and roofs) required to effectively retrofit existing urban infrastructure (Carter et al., 2015; Voskamp and Van de Ven,

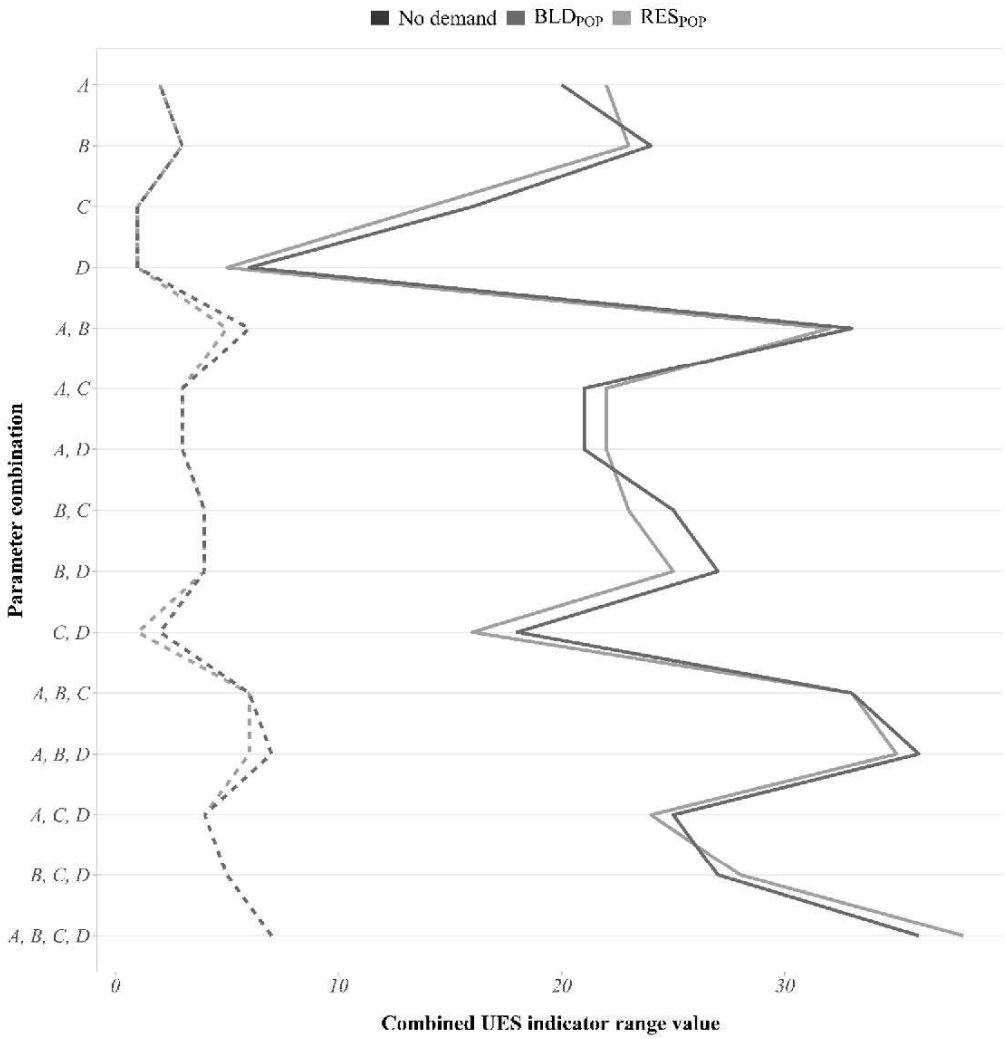

Fig. 6. Median (dashed) and Maximum (solid) range in combined UES indicators for all parameter combinations for all demand methods.

2015). Whilst the approach provides limited information on the type of beneficial UGBI resources for each location, it currently indicates UES deprivation at scales where improved in-situ monitoring exercises may be feasibly implemented to investigate appropriate local UGBI investment strategies (e.g. Massoudieh et al., 2017; Skelhorn et al., 2014). For both demand (e.g. mid-year population estimates) and service estimation (e.g. aerial imagery, national mapping products) the relevant geospatial data is typically updated at frequent intervals, as such there is potential to adapt the mapping approach to monitor UES change (Haas and Ban, 2017; Cabral et al., 2016). Service and demand values updated within the fixed analysis grid structure may therefore enable consistent re-examination of UES dynamics according to continual change in the urban biophysical, socio-economic, and administrative landscape (Dobbs et al., 2018; Schwarz et al., 2011).

In addition to aiding transferability of this approach, novel incorporation of sensitivity analysis provides beneficial insights for further UES research. For example, UES deprivation maps in this approach are highly sensitive to associated demand weightings, that may result in skewed views of UES service to demand dynamics if not considered, such as UES deprivation mapped to no population areas such as airport runways, large car parks etc. The findings serve to raise further awareness as to the benefits of including demand measures in further UES mapping research, particularly where UES flows exhibit high levels of spatial dependency at the micro-scale (Baró et al., 2016; Larondelle and Lauf, 2016). The various quality of UES deprivation maps in turn provide a general indication as to whether data for a particular demand method, using this or a similar approach, is worth the investment in resources to meet a desired level of accuracy.

In addition, as proxy models remain a popular choice in UES mapping approaches, sensitivity analysis indicates that increasing relative magnitudes in proxy parameter uncertainty may reflect uncertainty in mapping outputs when applied linearly to landcover area estimates. This is evidently a spatially dependent process that becomes increasingly complex as additional sources of landcover associated uncertainty are compounded within aggregated UES indicators. Variation in map uncertainty across the study area therefore varies widely and may apply to other approaches that use similar methods in proxy to landcover extrapolation (Zhao and Sander, 2018). Due to interdependencies in landcover proportions per cell, associated uncertainty is difficult to model using standard statistical techniques. Therefore, overlapping findings, obtained from different interactions in uncertain inputs, can provide an easy to implement consensus view of combined UES indicators (Eigenbrod et al., 2010; Schröter and Remme, 2016).

Despite benefits to sensitivity analysis, some limitations in proxy based UES methods remain, as the lack of independent validation to primary data limits understanding of remaining uncertainty within

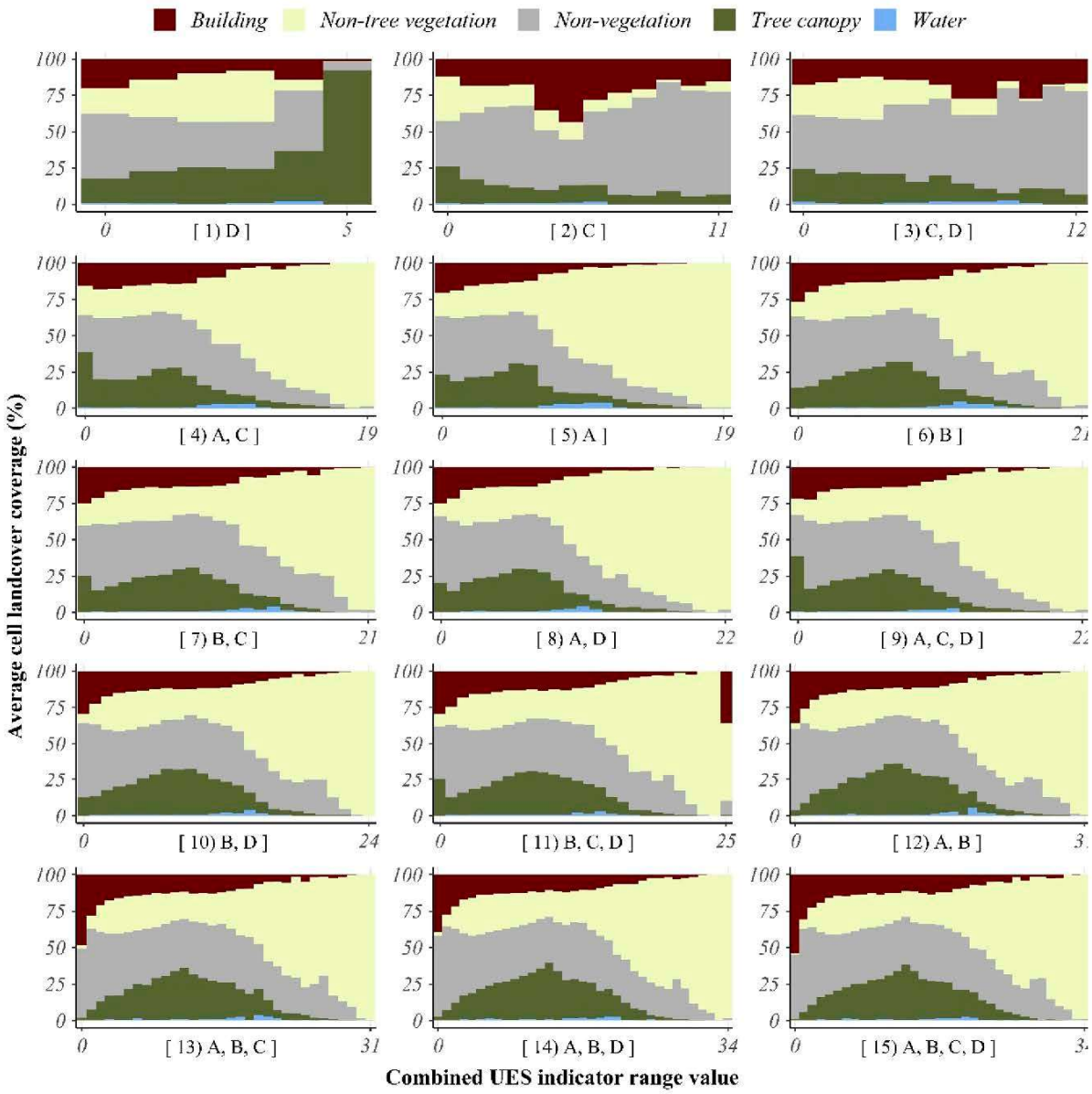

Fig. 7. Average landcover proportions (%) for combined UES indicator range values per parameter combination; designated in order of importance (1 least importance) within '[ ]' brackets.

current mapping outputs (Eigenbrod et al., 2010; Zhao and Sander, 2018). Efforts to address this issue may therefore begin with improvements in the thematic resolution of landcover data from use of ancillary information in the classification process (e.g. multi-spectral imagery, LiDAR; Baker et al., 2018; Dennis et al., 2018). For example, stratification of non-tree vegetation into grass and bush categories, and tree canopies according to canopy height, can support extrapolation of independent field based carbon storage estimates of local vegetation types for these categories (Davies et al., 2011; Raciti et al., 2014). Improved landcover data could also be incorporated with topographical elevation and underground drainage data to support both advanced hydraulic modelling of UGBI flooding reduction within urbanised catchments (Sjöman and Gill, 2014), in addition to high resolution climate models to assess UGBI impacts upon localised temperatures under various heat-wave scenarios (Skelhorn et al., 2014).

Models validated to local environmental conditions have been employed successfully to examine UGBI benefits at various scales of analysis. However, the associated resource investments (e.g. software, primary data) required are typically prohibitive for entire urban areas when multiple UES are concerned (Kremer et al., 2016b). Where use of proxy methods is unavoidable, uncertainty may be further addressed through UGBI and landcover categorisations designed for appropriate UES indicator transfer from suitably chosen proxies (Andrew et al., 2015; Derkzen et al., 2015). In relation to regression techniques for temperature regulation, improved landcover categorisation and use of additional variables such as landscape metrics, tree/building shading, and elevation for example, may also improve the accuracy of validated temperature regulation UES estimates (Chen et al., 2014; Kong et al., 2014). Demand indicators may be further updated to accommodate localised exposure to environmental hazards (i.e. exposure to extreme temperatures, pluvial/fluvial flooding risks) in addition to vulnerability factors within the local population (i.e. age, mobility, economic

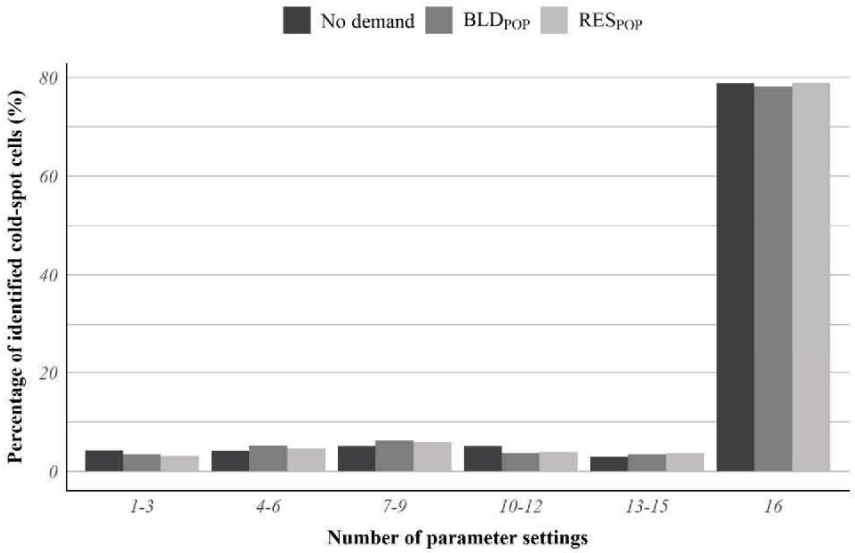

Fig. 8. Number of parameter settings that coldspot cells are identified by demand method.

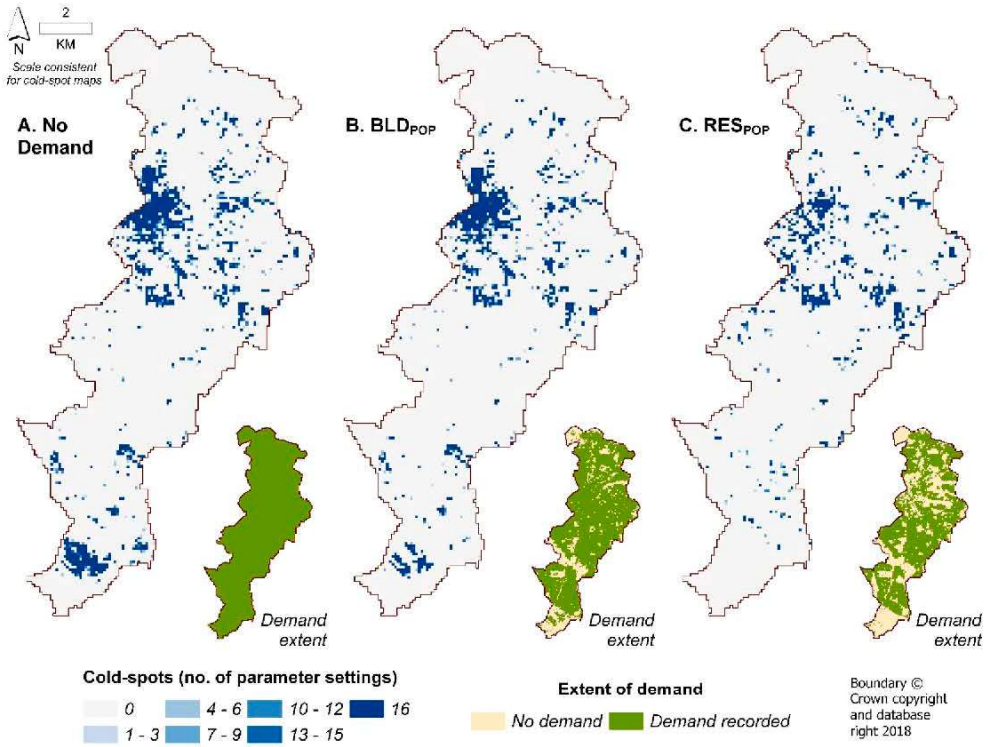

Fig. 9. Overlap of parameter setting coldspots by demand method.

situation) (Jenerette et al., 2016; Kaźmierczak and Cavan, 2011). In addition, as service benefits may flow outside single cell areas (i.e. runoff from neighbouring areas could flow into, and thus increase flooding risks for cell residents) the regular analysis grid structure should prove useful to investigate service to demand dynamics at various scales of benefit transfer (Baró et al., 2016).

Future research may therefore consider validation of uncertainty in popular UES proxy methods using samples of primary data, and/or models validated by primary data at sample locations (Eigenbrod et al., 2010). In addition, extensions to sensitivity should be considered in future studies for other sources of uncertainty such as landcover misclassification errors (Convertino et al., 2014), importance weighting of individual UES according to stakeholder needs (Kremer et al., 2016a), in addition to parameterisation assumptions for additional UES models incorporated within the mapping approach. Whilst parameter comparison enabled consideration of spatially dependent interactions between all ambiguous parameter combinations, this method will become less computationally feasible when considering additional sources of

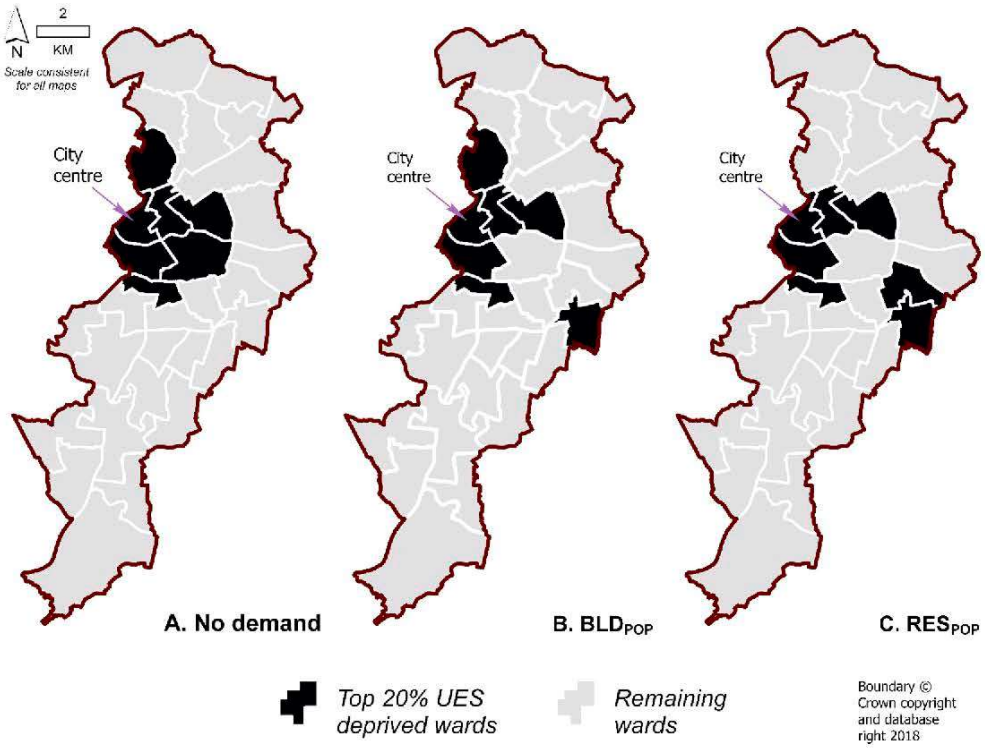

Fig. 10. Top 20% UES deprived wards by demand method.

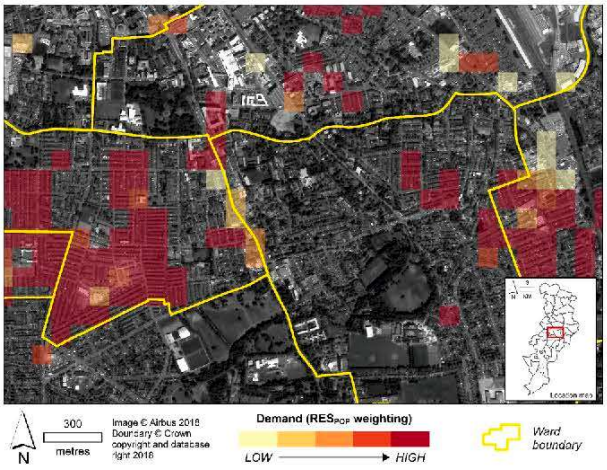

Fig. 11. Visualization of UES coldspots (RES$_{POP}$ demand cells) in relation to urban morphology.

uncertainty. Variance based global sensitivity analysis have been successfully applied to examine complex interactions between multiple sources of uncertainty in spatial models (Convertino et al., 2014; Lilburne and Tarantola, 2009) and may therefore provide a pragmatic solution in this respect. Further examination of this, and other sensitivity/uncertainty analyses is therefore required to improve standardisation of uncertainty estimation for various UES indicator metrics and prioritisation measures (Hou et al., 2013; Schröter and Remme, 2016), and is ultimately required to improve communication of the overall usability of UES maps to end users. The case study here therefore explicitly considered realistic pragmatic difficulties in current citywide UES mapping exercises with the intention to guide further research efforts towards this goal.

5. Conclusion

The mapping approach presented in this study, provides a transferable methodology to investigate how current regulating UES fulfils service demand amongst the local urban population. This approach ultimately provides a trade-off between coarse-scale UES mapping studies where demand from Landuse/Landcover categorisations, or within municipal districts are explicitly considered (Baró et al., 2017; Haas and Ban, 2017) to gridded approaches employed at the ecological/environmental scale (Dobbs et al., 2018; Kremer et al., 2016a). As financial resources for UGBI improvement may be constrained, UES deprivation analysis in the mapping approach usefully indicates areas of greatest concern for potential UGBI investment.

Sensitivity analysis in this study proved vital to demonstrate the wide-ranging issues in proxy model implementation for UES mapping studies in general. Explicit examination of uncertainty in proxy methods is useful not only to guide application of the mapping approach for different urban areas, but usefully conveys the overall usability of the mapping outputs for further planning purposes (Haase et al., 2014; Luederitz et al., 2015). Such efforts are thus beneficial to assess and re-appraise issues in current UES mapping methods, to aid the development of consistent and standardised approaches for mapping UES (Seppelt et al., 2011).

In the wider context, the development of UES mapping approaches is useful for highlighting the applicability of UES mapping data for urban planning purposes. It is hoped that this raises awareness and encourages investment in improved environmental modelling software, smart-city monitoring networks (e.g. local temperatures, pollution levels) and mapping data (e.g. high spatial-resolution imagery, three-dimensional data) to better facilitate validated UES analysis, and thus improve provision of regulating UES in urban areas (Schröter et al., 2015; Zhao and Sander, 2018). This improvement will greatly assist efforts to improve

our towns and cities resilience to environmental hazards now and in uncertain future climate conditions.

CRediT authorship contribution statement

Fraser Baker: Conceptualization, Methodology, Software, Formal analysis, Writing - original draft, Writing - review & editing. **Graham R. Smith:** Writing - review & editing, Supervision, Methodology. **Stuart J. Marsden:** Writing - review & editing, Supervision, Methodology. **Gina Cavan:** Conceptualization, Supervision, Project administration, Funding acquisition, Methodology, Writing - review & editing.

Declaration of Competing Interest

The authors declare that they have no known competing financial interests or personal relationships that could have appeared to influence the work reported in this paper.

Acknowledgements

This research was funded by Manchester Metropolitan University and UNIGIS UK. We kindly thank the Ordnance Survey for licensing the AddressBase product for our research. We also kindly thank the independents reviewers for the time and effort for the invaluable comments regarding the manuscript.

Appendix A

Population disaggregation workflows

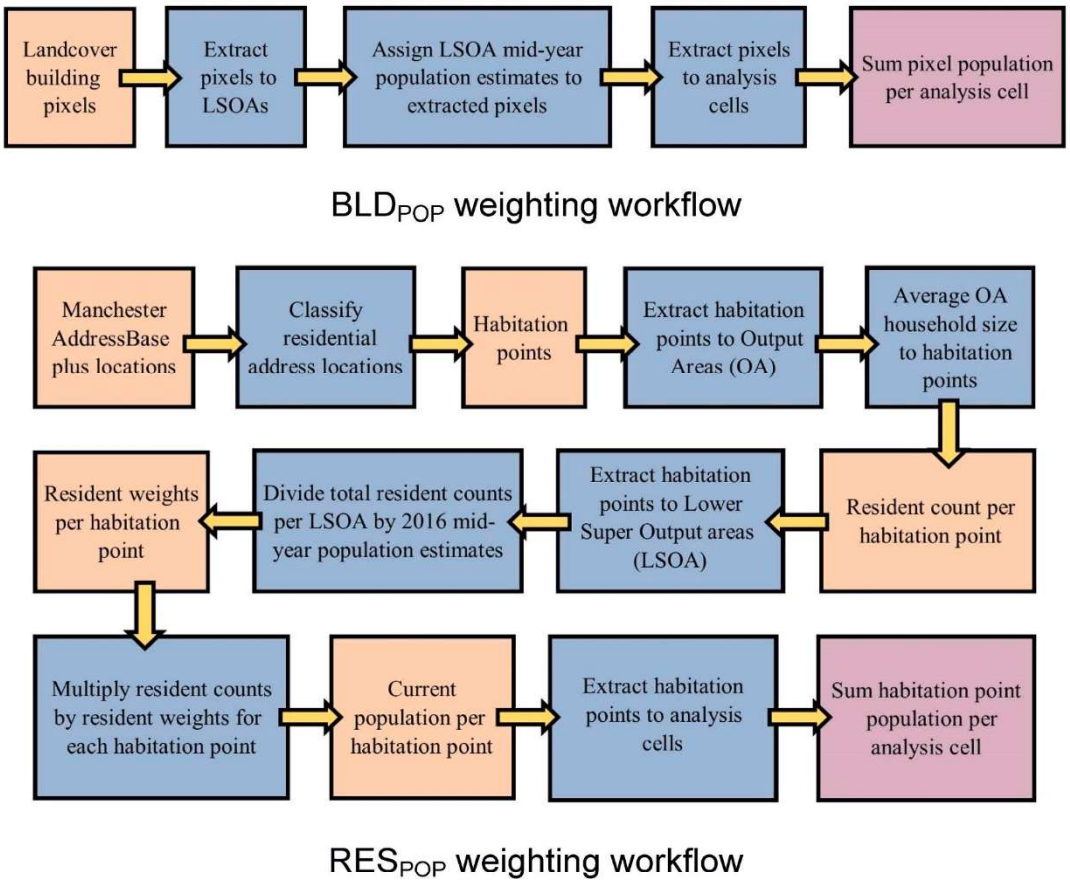

Notes:

Output areas and Lower Super Output areas represent statistical spatial measurement areas in the 2011 UK census (Retrieved from UK Data Service, https://www.ukdataservice.ac.uk/, accessed 2017). Output areas represent resident population groupings averaging 309 people. Lower Super Output areas contain multiple Output areas with average of 1500 people. 2016 LSOA mid-year population estimates from the UK Office of National Statistics (ONS) are for Lower super output areas (Retrieved from ONS, https://www.ons.gov.uk/peoplepopulationandcommunity/populationandmigration/populationestimates/bulletins/annualmidyearpopulationestimates/latest, Accessed 2018). Household size estimates at Output Area level are drawn from the UK 2011 census (Retrieved from ONS: Nomisweb, https://www.nomisweb.co.uk/, accessed 2017).

Appendix B

NOTE:

The following figures show the distribution of indicator values for all UES parameter settings and demand methods.

Indicator values are thus classified into equal number indicator deciles.

No demand cells are where demand weighted population < 1.

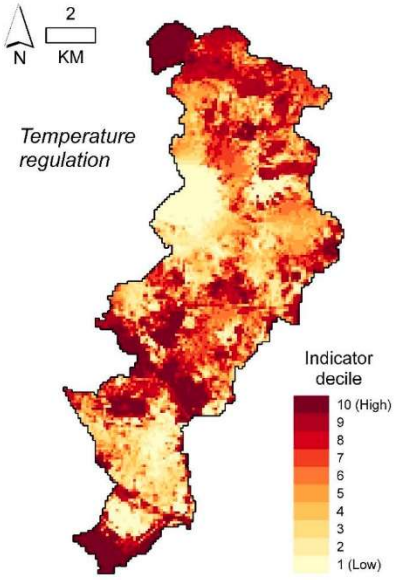

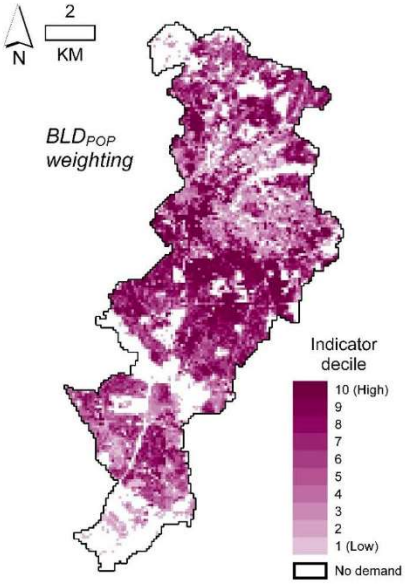

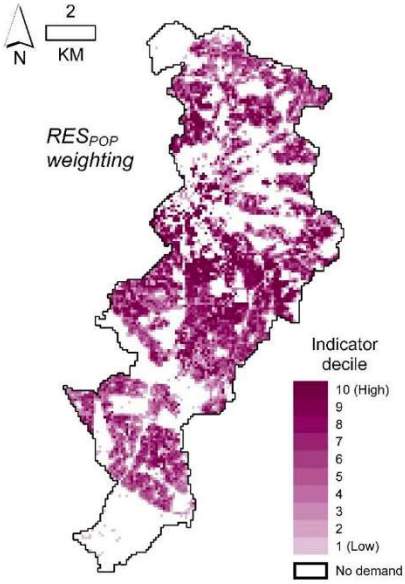

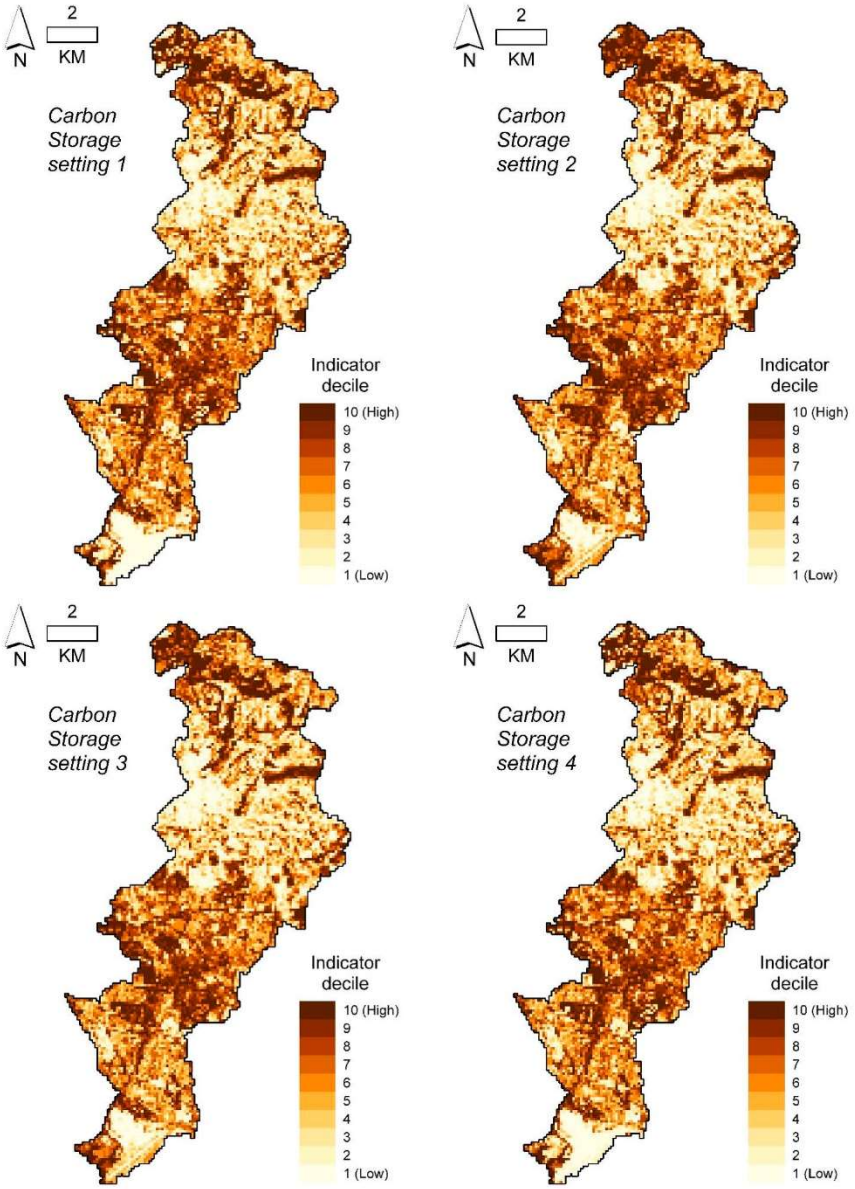
N
2
KM
Carbon Storage setting 1
Indicator decile
10 (High)
9
8
7
6
5
4
3
2
1 (Low)
N
2
KM
Carbon Storage setting 2
Indicator decile
10 (High)
9
8
7
6
5
4
3
2
1 (Low)
N
2
KM
Carbon Storage setting 3
Indicator decile
10 (High)
9
8
7
6
5
4
3
2
1 (Low)
N
2
KM
Carbon Storage setting 4
Indicator decile
10 (High)
9
8
7
6
5
4
3
2
1 (Low)

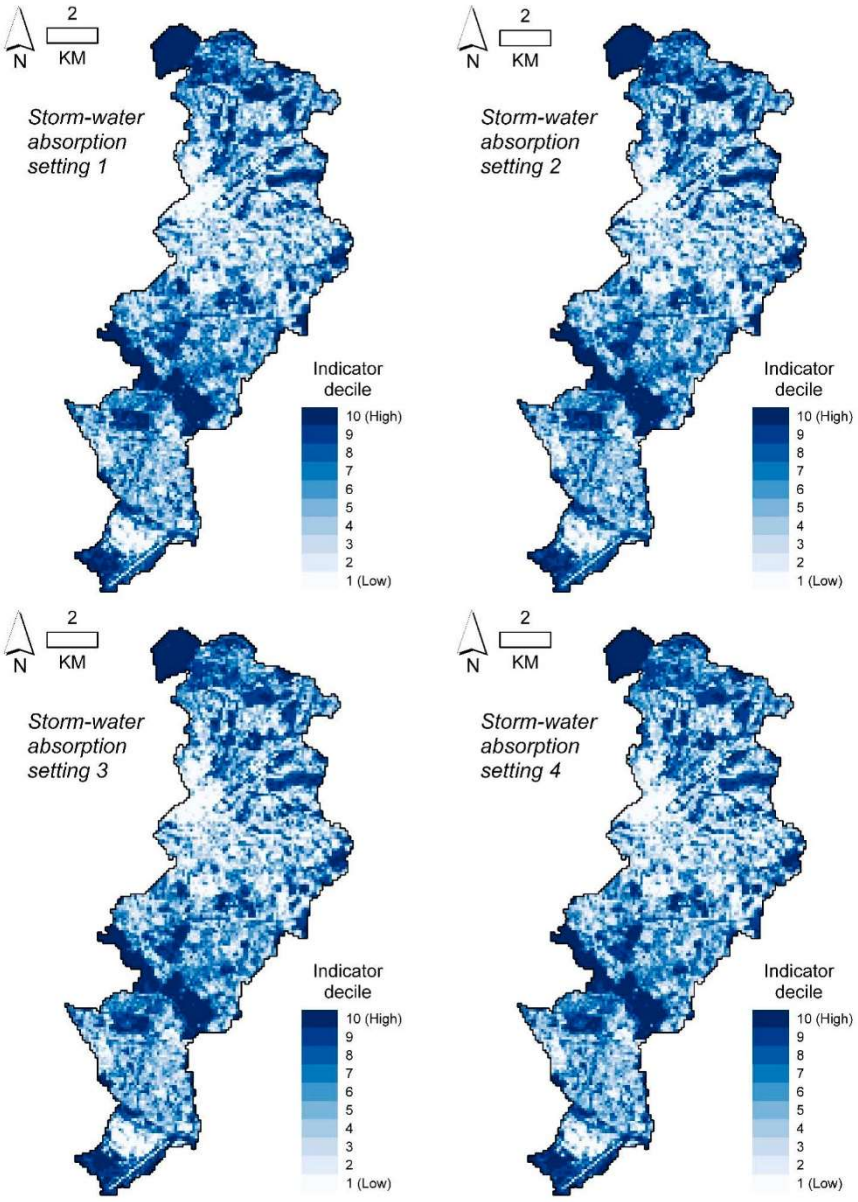

References

Anderson, B.J., Armsworth, P.R., Eigenbrod, F., Thomas, C.D., Gillings, S., Heinemeyer, A., Roy, D.B., Gaston, K.J., 2009. Spatial covariance between biodiversity and other ecosystem service priorities. J. Appl. Ecol. 46 (4), 888–896.

Andrew, M.E., Wulder, M.A., Nelson, T.A., Coops, N.C., 2015. Spatial data, analysis approaches, and information needs for spatial ecosystem service assessments: a review. GIScience Remote Sens. 52 (3), 344–373.

Baker, F., Smith, C., Cavan, G., 2018. A combined approach to classifying land surface cover of urban domestic gardens using citizen science data and high resolution image analysis. Remote Sensing 10 (4), 537.

Baró, F., Palomo, I., Zulian, G., Vizcaino, P., Haase, D., Gómez-Baggethun, E., 2016. Mapping ecosystem service capacity, flow and demand for landscape and urban planning: a case study in the Barcelona metropolitan region. Land Use Policy 57, 405–417.

Baró, F., Gómez-Baggethun, E., Haase, D., 2017. Ecosystem service bundles along the urban-rural gradient: Insights for landscape planning and management. Ecosyst. Serv. 24, 147–159.

Bhaduri, B., Bright, E., Coleman, P., Urban, M.L., 2007. LandScan USA: a high-resolution geospatial and temporal modeling approach for population distribution and dynamics. GeoJournal 69 (1–2), 103–117.

Cabral, P., Feger, C., Levrel, H., Chambolle, M., Basque, D., 2016. Assessing the impact of land-cover changes on ecosystem services: a first step toward integrative planning in Bordeaux, France. Ecosyst. Serv. 22, 318–327.

Carter, J.G., Cavan, G., Connelly, A., Guy, S., Handley, J., Kazmierczak, A., 2015. Climate change and the city: building capacity for urban adaptation. Prog. Plann. 95, 1–66.

Chen, A., Yao, X.A., Sun, R., Chen, L., 2014. Effect of urban green patterns on surface urban cool islands and its seasonal variations. Urban For. Urban Green. 13 (4), 646–654.

CityOfTrees, 2011. Greater Manchester Tree Audit, Manchester, UK. Personal communication.

Convertino, M., Muñoz-Carpena, R., Chu-Agor, M.L., Kiker, G.A., Linkov, I., 2014. Untangling drivers of species distributions: Global sensitivity and uncertainty analyses of MaxEnt. Environ. Modell. Software 51, 296–309.

Coseo, P., Larsen, L., 2014. How factors of land use/land cover, building configuration, and adjacent heat sources and sinks explain Urban Heat Islands in Chicago. Landscape Urban Plann. 125, 117–129.
Cranfield University, 2018. LandIS: Land Information System. Available online: http://www.landis.org.uk/, September, 2018.
Cruickshank, M.M., Tomlinson, R.W., Devine, P.M., Milne, R., 1998. Carbon in the vegetation and soils of Northern Ireland. In: Biology and Environment: Proceedings of the Royal Irish Academy. Royal Irish Academy, pp. 9–21.
Davies, Z.G., Edmondson, J.L., Heinemeyer, A., Leake, J.R., Gaston, K.J., 2011. Mapping an urban ecosystem service: quantifying above-ground carbon storage at a city-wide scale. J. Appl. Ecol. 48 (5), 1125–1134.
Dennis, M., Barlow, D., Cavan, G., Cook, P., Gilchrist, A., Handley, J., James, P., Thompson, J., Tzoulas, K., Wheater, C.P., Lindley, S., 2018. Mapping urban green infrastructure: a novel landscape-based approach to incorporating land use and land cover in the mapping of human-dominated systems. Land 7 (1), 17.
Derkzen, M.L., van Teeffelen, A.J., Verburg, P.H., 2015. Quantifying urban ecosystem services based on high-resolution data of urban green space: an assessment for Rotterdam, the Netherlands. J. Appl. Ecol. 52 (4), 1020–1032.
Dobbs, C., Hernández-Moreno, Á., Reyes-Paecke, S., Miranda, M.D., 2018. Exploring temporal dynamics of urban ecosystem services in Latin America: the case of Bogota (Colombia) and Santiago (Chile). Ecol. Ind. 85, 1068–1080.
Edina Digimap, 2017. Ordnance Survey. Available online: https://digimap.edina.ac.uk/os, (accessed May, 2017).
Eigenbrod, F., Armsworth, P.R., Anderson, B.J., Heinemeyer, A., Gillings, S., Roy, D.B., Thomas, C.D., Gaston, K.J., 2010. The impact of proxy-based methods on mapping the distribution of ecosystem services. J. Appl. Ecol. 47 (2), 377–385.
Getmapping, Aerial Data, 2017. High Resolution Imagery. Available online: http://www.getmapping.com/products-and-services/aerial-imagery-data/aerial-data-high-resolution-imagery (accessed on 29 March 2018).
Gill, S.E., Handley, J.F., Ennos, A.R., Pauleit, S., 2007. Adapting cities for climate change: the role of the green infrastructure. Built Environ. 33 (1), 115–133.
Gómez-Baggethun, E., Barton, D.N., 2013. Classifying and valuing ecosystem services for urban planning. Ecol. Econ. 86, 235–245.
Haas, J., Ban, Y., 2017. Mapping and monitoring urban ecosystem services using multitemporal high-resolution satellite data. IEEE J. Sel. Top. Appl. Earth Obs. Remote Sens. 10 (2), 669–680.
Haase, D., Larondelle, N., Andersson, E., Artmann, M., Borgström, S., Breuste, J., Gomez-Baggethun, E., Gren, Å., Hamstead, Z., Hansen, R., Kabisch, N., 2014. A quantitative review of urban ecosystem service assessments: concepts, models, and implementation. Ambio 43 (4), 413–433.
Hall, J.M., Handley, J.F., Ennos, A.R., 2012. The potential of tree planting to climate-proof high density residential areas in Manchester, UK. Landscape Urban Plann. 104 (3–4), 410–417.
Harlan, S., Chowell, G., Yang, S., Petitti, D., Morales Butler, E., Ruddell, B., Ruddell, D., 2014. Heat-related deaths in hot cities: estimates of human tolerance to high temperature thresholds. Int. J. Environ. Res. Public Health 11 (3), 3304–3326.
Holt, A.R., Mears, M., Maltby, L., Warren, P., 2015. Understanding spatial patterns in the production of multiple urban ecosystem services. Ecosyst. Serv. 16, 33–46.
Hou, Y., Burkhard, B., Müller, F., 2013. Uncertainties in landscape analysis and ecosystem service assessment. J. Environ. Manage. 127, S117–S131.
Jenerette, G.D., Harlan, S.L., Buyantuev, A., Stefanov, W.L., Declet-Barreto, J., Ruddell, B.L., Myint, S.W., Kaplan, S., Li, X., 2016. Micro-scale urban surface temperatures are related to land-cover features and residential heat related health impacts in Phoenix, AZ USA. Landscape Ecol. 31 (4), 745–760.
Jia, P., Qiu, Y., Gaughan, A.E., 2014. A fine-scale spatial population distribution on the high-resolution gridded population surface and application in Alachua County, Florida. Appl. Geogr. 50, 99–107.
Kabisch, N., Frantzeskaki, N., Pauleit, S., Naumann, S., Davis, M., Artmann, M., Haase, D., Knapp, S., Korn, H., Stadler, J., Zaunberger, K., 2016. Nature-based solutions to climate change mitigation and adaptation in urban areas: perspectives on indicators, knowledge gaps, barriers, and opportunities for action. Ecol. Soc. 21 (2).
Kaźmierczak, A., Cavan, G., 2011. Surface water flooding risk to urban communities: analysis of vulnerability, hazard and exposure. Landscape Urban Plann. 103 (2), 185–197.
Kong, F., Yin, H., James, P., Hutyra, L.R., He, H.S., 2014. Effects of spatial pattern of greenspace on urban cooling in a large metropolitan area of eastern China. Landscape Urban Plann. 128, 35–47.
Kremer, P., Hamstead, Z.A., McPhearson, T., 2016a. The value of urban ecosystem services in New York City: a spatially explicit multicriteria analysis of landscape scale valuation scenarios. Environ. Sci. Policy 62, 57–68.
Kremer, P., Hamstead, Z., Haase, D., McPhearson, T., Frantzeskaki, N., Andersson, E., Kabisch, N., Larondelle, N., Rall, E.L., Voigt, A., Baró, F., 2016b. Key insights for the future of urban ecosystem services research. Ecol. Soc. 21 (2), 29.
Kroll, F., Müller, F., Haase, D., Fohrer, N., 2012. Rural–urban gradient analysis of ecosystem services supply and demand dynamics. Land Use Policy 29 (3), 521–535.
Laaidi, K., Zeghnoun, A., Dousset, B., Bretin, P., Vandentorren, S., Giraudet, E., Beaudeau, P., 2011. The impact of heat islands on mortality in Paris during the August 2003 heat wave. Environ. Health Perspect. 120 (2), 254–259.
Langemeyer, J., Wedgwood, D., McPhearson, T., Baró, F., Madsen, A.L., Barton, D.N., 2020. Creating urban green infrastructure where it is needed–a spatial ecosystem service-based decision analysis of green roofs in Barcelona. Sci. Total Environ. 707, 135487.
Larondelle, N., Lauf, S., 2016. Balancing demand and supply of multiple urban ecosystem services on different spatial scales. Ecosyst. Serv. 22, 18–31.
Lilburne, L., Tarantola, S., 2009. Sensitivity analysis of spatial models. Int. J. Geogr. Inf. Sci. 23 (2), 151–168.
Luederitz, C., Brink, E., Gralla, F., Hermelingmeier, V., Meyer, M., Niven, L., Abson, D.J., 2015. A review of urban ecosystem services: six key challenges for future research. Ecosyst. Serv. 14, 98–112.
Massoudieh, A., Maghrebi, M., Kamrani, B., Nietch, C., Tryby, M., Aflaki, S., Panguluri, S., 2017. A flexible modeling framework for hydraulic and water quality performance assessment of stormwater green infrastructure. Environ. Modell. Software 92, 57–73.
MCC [Manchester City Council], 2018. Population: Manchester's population, ethnicity and migration. Retrieved from: https://secure.manchester.gov.uk/info/200088/statistics_and_intelligence/438/population, July, 2018.
Muller, C.L., Chapman, L., Grimmond, C.S.B., Young, D.T., Cai, X., 2013. Sensors and the city: a review of urban meteorological networks. Int. J. Climatol. 33 (7), 1585–1600.
O'Brien, O., Cheshire, J., 2016. Interactive mapping for large, open demographic data sets using familiar geographical features. J. Maps 12 (4), 676–683.
Oke, T.R., 1988. Boundary Layer Climates. Routledge.
OS [Ordnance Survey], 2018. Addressbase Products. Available online: https://www.ordnancesurvey.co.uk/business-and-government/products/addressbase-products.html, May 2018.
Pulighe, G., Fava, F., Lupia, F., 2016. Insights and opportunities from mapping ecosystem services of urban green spaces and potentials in planning. Ecosyst. Serv. 22, 1–10.
Raciti, S.M., Hutyra, L.R., Newell, J.D., 2014. Mapping carbon storage in urban trees with multi-source remote sensing data: Relationships between biomass, land use, and demographics in Boston neighborhoods. Sci. Total Environ. 500, 72–83.
Salvadore, E., Bronders, J., Batelaan, O., 2015. Hydrological modelling of urbanized catchments: a review and future directions. J. Hydrol. 529, 62–81.
Schröter, M., Remme, R.P., Sumarga, E., Barton, D.N., Hein, L., 2015. Lessons learned for spatial modelling of ecosystem services in support of ecosystem accounting. Ecosyst. Serv. 13, 64–69.
Schröter, M., Remme, R.P., 2016. Spatial prioritisation for conserving ecosystem services: comparing hotspots with heuristic optimisation. Landscape Ecol. 31 (2), 431–450.
Schulp, C.J., Burkhard, B., Maes, J., Van Vliet, J., Verburg, P.H., 2014. Uncertainties in ecosystem service maps: a comparison on the European scale. PLoS One 9 (10), e109643.
Schwarz, N., Bauer, A., Haase, D., 2011. Assessing climate impacts of planning policies—an estimation for the urban region of Leipzig (Germany). Environ. Impact Assess. Rev. 31 (2), 97–111.
Seppelt, R., Dormann, C.F., Eppink, F.V., Lautenbach, S., Schmidt, S., 2011. A quantitative review of ecosystem service studies: approaches, shortcomings and the road ahead. J. Appl. Ecol. 48 (3), 630–636.
Sjöman, J.D., Gill, S.E., 2014. Residential runoff–the role of spatial density and surface cover, with a case study in the Höjeå river catchment, southern Sweden. Urban For. Urban Green. 13 (2), 304–314.
Skelhorn, C., Lindley, S., Levermore, G., 2014. The impact of vegetation types on air and surface temperatures in a temperate city: a fine scale assessment in Manchester, UK. Landscape Urban Plann. 121, 129–140.
Stevens, F.R., Gaughan, A.E., Linard, C., Tatem, A.J., 2015. Disaggregating census data for population mapping using random forests with remotely-sensed and ancillary data. PLoS One 10 (2), e0107042.
Tratalos, J., Fuller, R.A., Warren, P.H., Davies, R.G., Gaston, K.J., 2007. Urban form, biodiversity potential and ecosystem services. Landscape Urban Plan. 83 (4), 308–317.
UKDS [UK Data Service], 2017. Census Boundary Data. Retrieved from https://www.ukdataservice.ac.uk/, April, 2017.
USDA [United States Department of Agriculture, Soil Conservation Society], 1986. Urban hydrology for small watersheds. Techn. Release 55, 2–6.
USGS [United States Geological Survey], 2017. Earth Explorer Service. Available online: https://earthexplorer.usgs.gov/, September 2017.
Voskamp, I.M., Van de Ven, F.H., 2015. Planning support system for climate adaptation: composing effective sets of blue-green measures to reduce urban vulnerability to extreme weather events. Build. Environ. 83, 159–167.
Wang, F., Qin, Z., Song, C., Tu, L., Karnieli, A., Zhao, S., 2015. An improved mono-window algorithm for land surface temperature retrieval from Landsat 8 thermal infrared sensor data. Remote Sens. 7 (4), 4268–4289.
Weather Underground, 2017. Manchester Airport, GB. Available online: https://www.wunderground.com/weather/EGCC, September 2017.
Woodruff, S.C., BenDor, T.K., 2016. Ecosystem services in urban planning: comparative paradigms and guidelines for high quality plans. Landscape Urban Plann. 152, 90–100.
Zandbergen, P.A., 2011. Dasymetric mapping using high resolution address point datasets. Trans. GIS 15, 5–27.
Zandbergen, P.A., Ignizio, D.A., 2010. Comparison of dasymetric mapping techniques for small-area population estimates. Cartogr. Geogr. Inf. Sci. 37 (3), 199–214.
Zhao, C., Sander, H.A., 2018. Assessing the sensitivity of urban ecosystem service maps to input spatial data resolution and method choice. Landscape Urban Plann. 175, 11–22.

Appendix 2.1 – Steps to create a landcover layer

Main processes described in **Table 2.5, Section 2.5.1**.

Appendix 2.1.1 – Classify Ordnance Survey Mastermap Topography layer

The UK Ordnance Survey Mastermap Topography layer (Edina Digimap 2017) is a digital geospatial product covering entire UK which represents topographical features in the physical world. Linear features such as fences, verges, building footprints and water edges for example, are represented as lines with attribute information. Areas enclosed by linear features are defined as polygons and represent topographic areas such as enclosed land parcels, uniform surfaces such as paths, roads and buildings, and waterbodies for example. Polygon attribute information enables re-classification of such areas into broad landcover classes, replicating the thematic resolution of high-resolution landcover mapping exercises in other studies (Dennis et al. 2018, Derkzen et al. 2015, Zhou et al. 2011). Landcover classes were re-classified following the step by step process below (**Table A2.1**):

Table A2.1 – Process to classify landcover

Step	Landcover class	Class Description	Assignment Rules*	Rationale for Processing
1	*BUILDINGS*	Permanent building structures	Feature attributes *Buildings, Buildings; Rail/Buildings; Roads, Tracks and Paths/Buildings* in the THEME field	Features that identified as Building class
2	*NON-VEGETATION*	Non-vegetative hard surfaces	Features with *Manmade* attribute in MAKE field	Features identified with wholly artificial surface coverage
3	*WATER*	Water surfaces	Features with *Inland water, Inland water; Natural Environment/Inland Water; structure*	Features containing waterbodies
4	*TREE CANOPY*	Tree Canopy areas	Features with *Natural* in MAKE filed **and** with description *"Trees"* found anywhere in any DescTERM categories	Natural features containing Tree vegetation; assumed to contain full canopy coverage – even though such areas may contain various mixtures for Tree

				canopy and non-Tree canopy areas
5	*NON-TREE VEGETATION*	Vegetation not considered as Trees, such as low standing shrubs and grasses	Features with *Natural* in MAKE field	Remaining Natural features assumed to contain non-Tree areas such as open Grassland, areas of Cultivation, Shrubbery
6	*MANMADE*	(See above)	Features with *Unclassified/Unknown* values in the MAKE field	Feature description may imply multiple surface coverage within such polygons, however, general observation of the polygons in relation to IMG revealed that such polygons are largely covered by non-vegetative surfaces and therefore they were re-assigned to the Manmade class
7	*UNKNOWN (Preliminary non-PLS class)*	Temporary PLS class to be processed in subsequent steps	All remaining features	Features containing multiple surface types. Largely attributed to private garden areas where multiple vegetative and non-vegetative surface types exist. Retained for further processing with Image processed vegetation mask (see below).

* = Features re-classified in a step are not re-classified in any following step

To replicate the formatting of remote sensing image data that would be used for thesis objectives II. and III. the above polygons were transformed into a 2m resolution raster classification layer.

Appendix 2.1.2 – Tree canopy mask

Tree Audit layer geospatial data for the study area (City of Trees 2011), which represents individual tree canopies and woodland areas in the city of Manchester as polygon shapes, was merged into a single polygon feature area to create a tree canopy cover mask. This mask was then transformed into a raster layer to match the resolution and grid position of the preliminary classification layer described above. The tree mask layer then re-classified classification pixels as TREE CANOPY where the overlap occurred between the two layers.

Appendix 2.1.3 – Vegetation extent mask

True-colour aerial imagery (12.5cm resolution) covering the study area (acquired in June 2009 & June 2015) (Getmapping 2017) was processed to create a vegetation mask. For this process, the Green Red Vegetation Index (GRVI), which provides a measure of pixel greenness (representing vegetation) using optical bands (Motohka et al. 2010), was created using the following equation:

$$GRVI_{Pixel} = \frac{(GreenBand_{Pixel} - RedBand_{Pixel})}{(GreenBand_{Pixel} + RedBand_{Pixel})} \quad [A2.1]$$

Where $GRVI_{Pixel}$ is the GRVI value per pixel, $GreenBand_{Pixel}$ is the green band value per pixel, $RedBand_{Pixel}$ is the red band value per pixel. Exploration of the image data identified a GRVI threshold of > 0.2 to classify image pixels as vegetation. Vegetation pixels were then subsequently polygonised to create a non-tree vegetation Mask at the same resolution and grid position of the layers above. The non-tree vegetation mask layer then re-classified *UNKNOWN* class pixels in the classification layer as *NON-TREE VEGETATION* where the two layers overlapped. Remaining UNKNOWN classification pixels were assigned as NON-VEGETATION.

Appendix 2.1.4 – Landcover process diagram

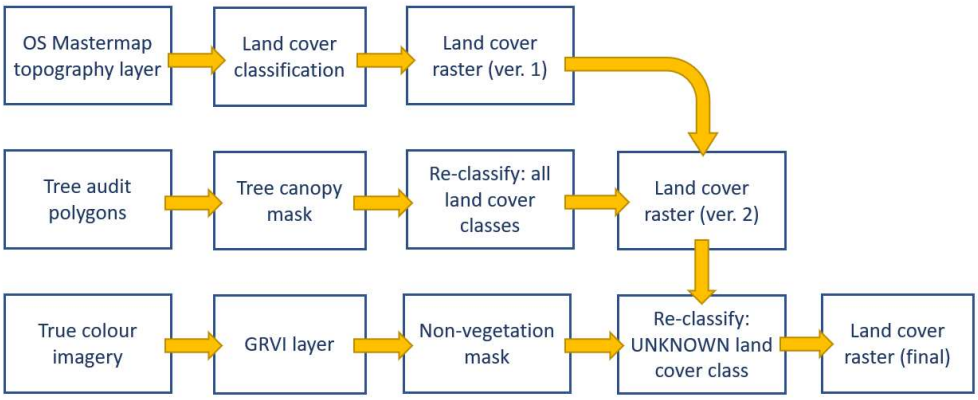

Appendix 2.2 – Process to create land surface temperature layer

Land Surface Temperature (LST) images were generated according to the mono-window method described by Wang et al. (2015). This method works specifically with Landsat-8 image band data and accounts for light contamination in the 2nd thermal infrared channel (TIR2) (USGS 2017b) by requiring data from one thermal infrared channel (TIR1) only.

Appendix 2.2.1 – LST layer key steps

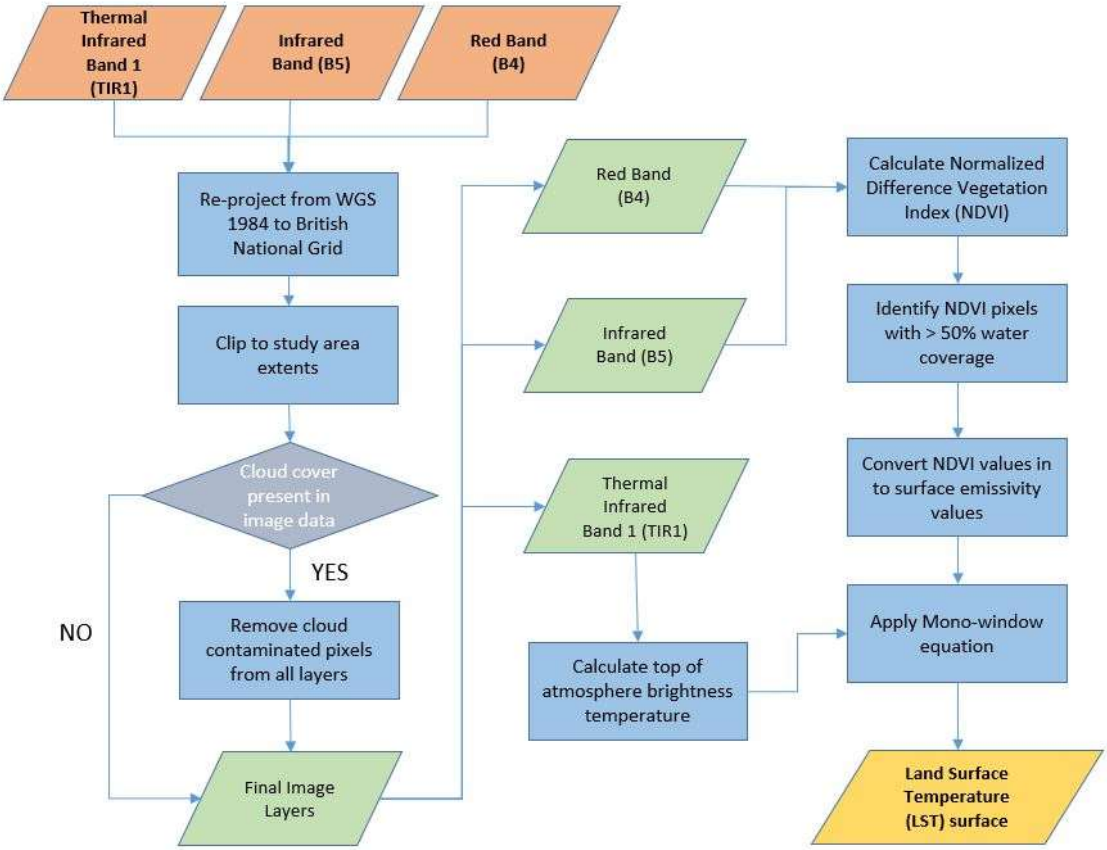

Appendix 2.2.2 – Land surface layer creation

Image selection and pre-processing

The USGS Earth Explorer Landsat-8 archive was explored for a cloud-free image representing hot weather conditions for the city of Manchester. The image chosen for 17th July 2017 represented the most appropriate image available for the given criteria. The image was collected at approximately 11:10 am and is thus close to mid-day maximum surface warming. Image bands 4 (Red), 5 (Near-infrared) and 10 (Thermal infrared 1) were extracted and re-projected from WGS-1984 to British National Grid projection. The bands were then clipped to study area extents using a 400m buffer around the city of Manchester boundary.

NDVI and surface emissivity

The Normalized difference vegetation index (NDVI) was created using the equation below:

$$NDVI = \frac{(Band\ 5 - Band4)}{(Band\ 5 + Band\ 4)} \quad \text{[A2.2]}$$

Surface emissivity, represents a measure of thermal energy emittance of a given surface layer and was approximated from the NDVI layer (Sobrino et al. 2008, Wang et al. 2015). In this method, pixels covered by water are assigned emissivity of 0.991. These pixels were identified by overlapping a water mask created from landcover class polygons (see **Appendix 2.1.1**). Remaining pixels with NDVI > 0.5 are assigned emissivity of 0.973; pixels with NDVI < 0.2 are assumed as artificial surfaces and assigned emissivity of 0.962; any pixel with NDVI between 0.2 and 0.5 is assigned a scaled emissivity value between 0.962 and 0.973.

Conversion of Band 10 to top of atmosphere brightness

In contrast to Bands 4 & 5, which are atmospherically corrected, Band 10 is provided at Level-1 processing and thus requires re-calculation to top of atmosphere brightness values. First step requires calculation to top of atmosphere radiance as follows:

$$L_\lambda = M_L Q_{cal} + A_L \quad \text{[A2.3]}$$

Where L_λ = Top of atmosphere radiance (Watts/(m2*srad*µm)); M_L = Band-specific multiplicative rescaling factor from the metadata (= 3.342 x 10^{-4}); A_L= Band-specific additive rescaling factor from the metadata (= 0.1); Q_{cal} = Quantized and calibrated standard product pixel values (Level-1 Band 10 digital image numbers). Top of atmosphere brightness is calculated as follows:

$$T = \frac{K_2}{\ln\left(\frac{K_1}{L_\lambda} + 1\right)} \quad \text{[A2.4]}$$

Where T = Top of atmosphere brightness temperature (K); L_λ = Top of atmosphere radiance (Watts/(m2*srad*µm)); K_1 = Band-specific thermal conversion constant from the metadata (= 774.8853); K_2 = Band-specific thermal conversion constant from the metadata (= 1321.0789).

Calculation of Land Surface Temperature Values

Land surface temperature (T_s) in kelvins (k) is calculated using the equation below (**Table A2.2** for parameters):

$$T_s = [a_{10}(1 - C_{10} - D_{10}) + (b_{10}(1 - C_{10} - D_{10}) + C_{10} + D_{10})T_{10} - D_{10}T_a]/C_{10} \quad \text{[A2.5]}$$

Table A2.2 – Parameters for equation A2.5

Parameter	*Description*	*Method/value*
T_a	Mean atmospheric temperature value (k)	Assumed values from testing phase (Wang et al. 2015) = 15.34°C + 273.12
T_{10}	At sensor Brightness temperature of Landsat-8 Band 10	See equation 4 above
a_{10}	Constant to approximate derivative of Planck's function; derived from expected LST temperature range in degrees Celsius	Chosen from look up table for expected temperature values ranging from 0 – 50°C; = -62.7182
b_{10}	Another constant based on expected LST temperature range in degrees Celsius	0.4339
C_{10}	Internal parameter for equation	$C_{10} = \tau_{10\varepsilon 10;}$ where ε_{10} is surface emmissivity
D_{10}	Internal parameter for equation	$D_{10} = (1 - \tau_{10})[1 + (1 - \varepsilon_{10})\,\tau_{10}]$
τ_{10}	Atmospheric transmittance	Calculated using online Atmospheric Correction Parameter Calculator (Barsi et al. 2017) for Landsat missions 5 – 8. Following parameters are required: Near surface air temperature = 20°C; Humidity = 56%; Surface Pressure = 1024 (all values obtained from Manchester Airport at 11.20AM; Weather Underground 2017)*

* = Weather Underground provides openly accessible information for airport stations around the world. In contrast the nearest UK Met office weather station is at Woodford, Stockport, UK, which represents a rural setting some 15km from Manchester city centre (Met Office 2020a). Manchester airport was chosen as it is both within the urban fabric of the city and is expected to provide a better representation of Urban heat island conditions across the city in general (Oke 1978).

Note: To convert from kelvins to Celsius, the constant 273.12 was subtracted from the resulting LST (k) layer. A caveat to the above approach is the assumption that near surface air temperature and humidity values remain constant across the study area. Variation in LST values was thus assessed by altering near surface temperatures ± 2°C and humidity ± 5% in various configurations. Maximum differentials in LST ranged from -1.15°C to +0.78°C. This indicates the range calculated LST values are likely to deviate from actual LST on the ground.

Appendix 2.3 – Investigating analysis cell size

The resolution of lattice grid cell structure determines the scale at which spatial heterogeneity in RES is measured across the study area. As discussed in **Section 2.5.2**, the LST modelling approach is largely constrained to the pixel resolution of the LST surface layer. Depending upon the analysis scale of interest, this resolution may be altered through downscaling, either through pixel resampling or amalgamation of pixel values within an analysis unit area. This process in turn may introduce zoning effects into analysis, whereby variance in the data is increasingly averaged over coarser spatial scales (Openshaw 1984), thus altering the statistical relationship between GBI and LST measures (Weng et al. 2004).

The analysis cell resolution was originally set at 100m as evidence suggests that this represents a useful scale to assess spatial variation in LST (Weng et al. 2004, Zhou et al. 2014) and thus consider the benefits of cell based GBI to reduce urban warming risks for the associated population. To assess the suitability of this resolution sensitivity analysis was conducted by comparing the strength of statistical associations between GBI and LST for additional cell resolutions detailed in **Table A2.3** below:

Table A2.3 – Grid cell resolutions included in sensitivity analysis

Grid cell resolution	Rationale for implementing scale	Number of cells required for study area extents	Number of remaining cells (% of total) for analysis*
50m	Scale near to LST pixel resolution (30m x 30m) providing high resolution analysis of spatial heterogeneity in LST	47326	45251 (95.6%)
100m	Original chosen cell resolution as described above	12088	11055 (91.5%)
200m	Enables comparison to the 100m scale	3148	2648 (84.1%)
500m	Cell size resolution used in a recent UK RES study (see Holt et al. 2015) and thus considered the coarsest scale for the mapping approach	556	372 (66.9%)

* = Cell extents overlap the administrative boundary for Manchester; cells that overlapped the boundary were removed from further sensitivity analysis.

The regular sized grid cell structures were created for the above resolutions. For all cells at each resolution, the percentage GBI and mean LST was calculated. To void incomplete values, grid cells that extended in coverage beyond the extent of the landcover data were removed from further analysis. As demonstrated, the percent of cells removed increases at coarser scales as the area of overlap increases, thus decreasing the suitability of the grid cell representation to approximate the

extents of complex boundary areas. Correlation analysis was conducted to assess the strength of relationship between percentage GBI and mean LST per cell for each resolution – see **Table A2.4** below:

Table A2.4 – Results of correlation analyses (GBI and LST) for each grid cell resolution

Grid Cell resolution (m)	*Correlation coefficient (r)**
50	-0.761
100	-0.822
200	-0.870
500	-0.914

** significant at p < 0.005*

The results of this analysis demonstrate the zoning effect according to modified areal unit problem (Openshaw 1984). Thus, as grid cell resolution coarsens noise in the relationship between GBI and LST becomes increasingly aggregated, and correlation strength improves as a result. However, as evident in **Figure A2.1**, at coarsening grid resolution spatial variation in LST is increasingly aggregated. 50m resolution presents the most suitable representation in this regards, whereas at 500m it is evident that grid cells may contain clusters of both relatively warm and cool LST areas. However, at finer scales it is evident that incomplete cell coverage at cell boundary edges will contribute additional noise in the relationship between GBI and LST.

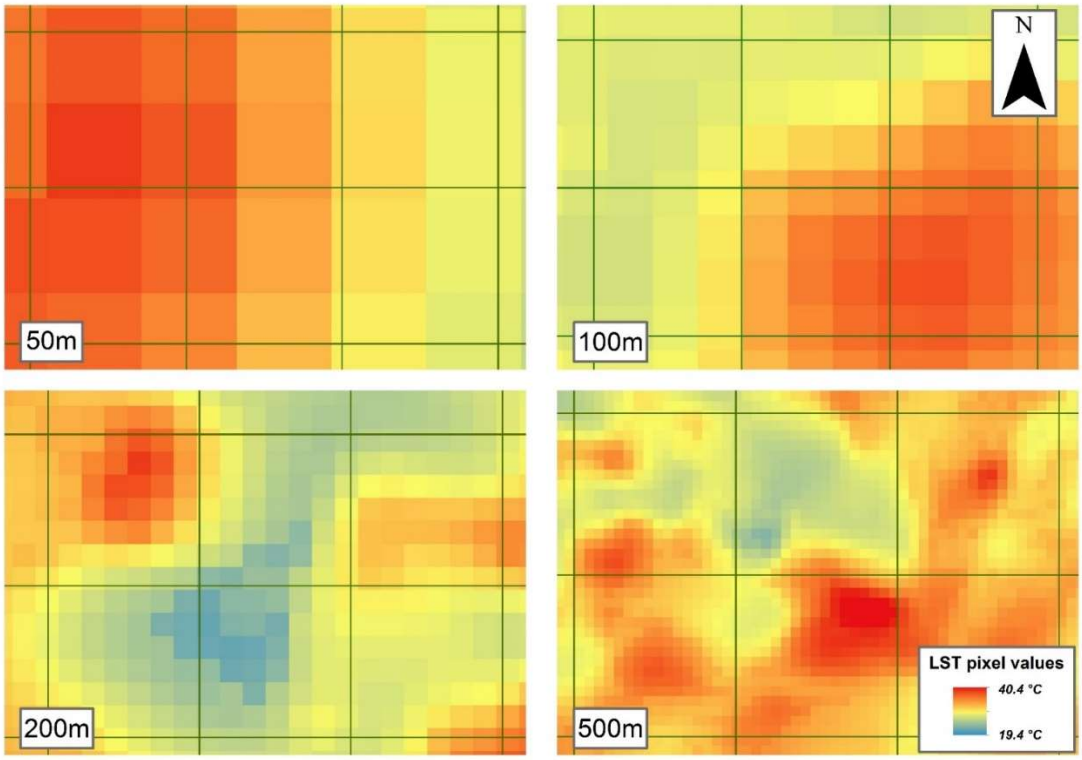

Figure A2.1 – Spatial patterns of LST in relation to grid cell resolution

For further mapping purposes the 100m grid cell resolution was retained. Based on the above analysis this resolution appears to represent a reasonable compromise in amalgamation of spatial variation in LST values, and strength in statistical relationship between pUGBI and mLST. However, it is important to note that use of additional variables may improve associations between GBI and LST further, making the use of < 100m resolution grid cell resolution more appropriate in this regards. In future applications of the mapping approach the availability of additional data may thus allow a re-consideration of analysis scale presented in this thesis.

Appendix 2.4 – Soil type data for curve number method

Appendix 2.4.1 – Classification of SCS-CN soil types

The SCS-CN model (USDA 1986) considers water absorption capacity of varying soil types, which then modifies the Curve Number values for above-ground landcover material. Implementation in study areas outside the United States requires conversion of local soil types into SCS-CN soil categories. Maps of soil types and conditions in the UK are provided in reports by the LandIS: Land Information System (Cranfield University 2018). Soil maps were georeferenced to the study area using common ordnance survey grid intersections. Soil area extents were digitised and relevant Hydrology of Soil type (HOST) class attached. SCS-CN soil classes were assigned to HOST categories based on guidance from SEPA (2011) – see **Table A2.5** below:

Table A2.5 – SCS-CN soil classification

Standard Percentage Runoff (HOST*)	SCS-CN Soil Class	HOST Soil classes
< 10%	A	1, 2, 13
10-20%	B	3, 4, 5, 7, 11
20-40%	C	6, 8, 9, 16, 17, 18, 20, 28
> 40%	D	10, 12, 14, 15, 19, 21, 22, 23, 24, 25, 26, 27, 29

* HOST (Hydrology of Soil Type) is a scheme to classify UK soil types within 29 classes according to the soils ability to transmit water.

Appendix 2.4.2 – Extent of HOST and SCS-CN soil classes (% of study area)

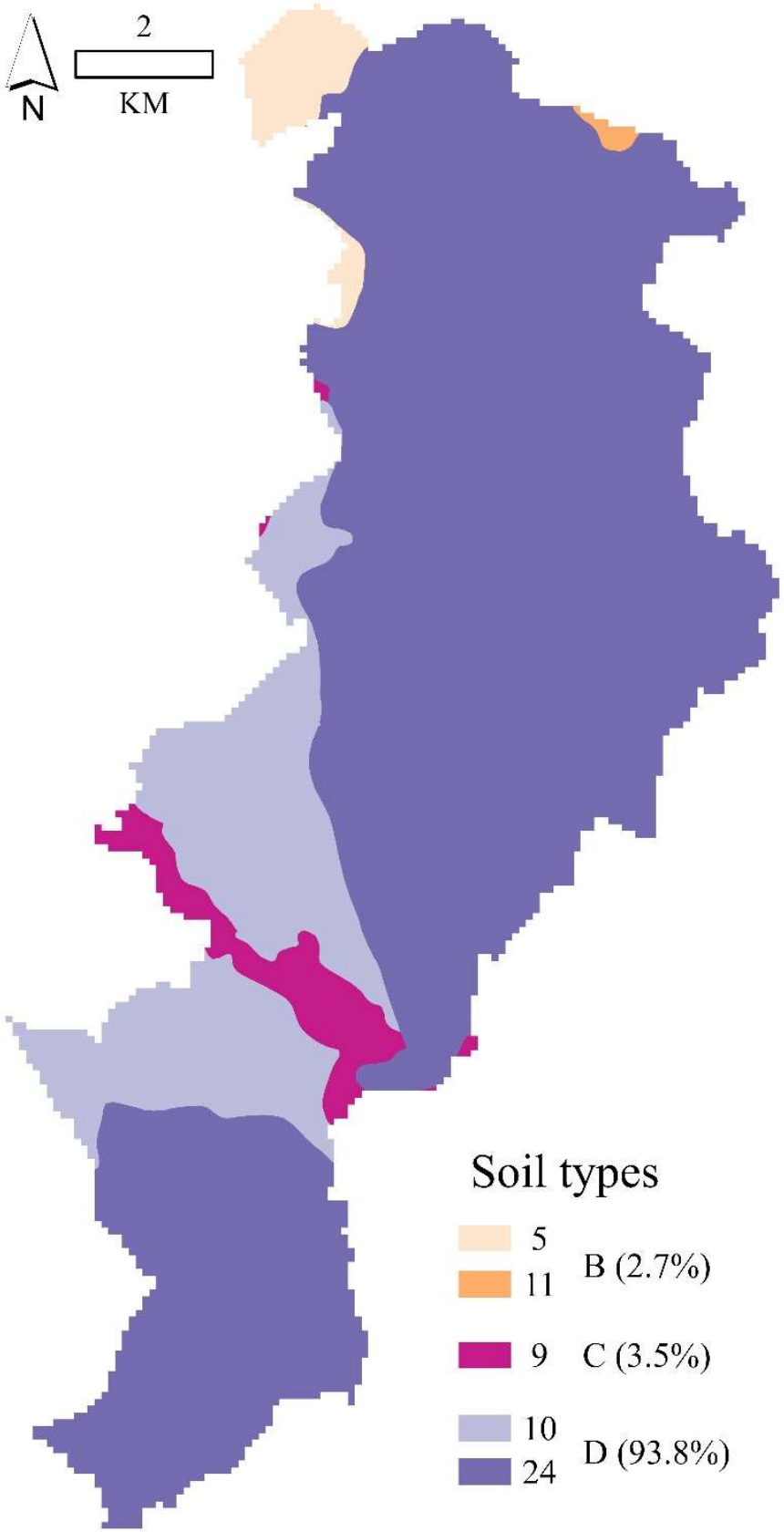

Appendix 2.5 – Population disaggregation workflows

Appendix 2.5.1 – Workflow for BLD_{POP} method

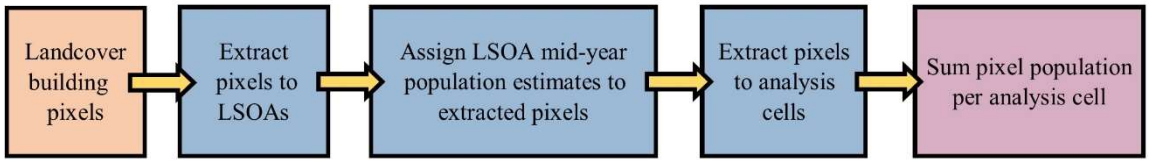

Appendix 2.5.2 – Workflow for HAB_{POP} method

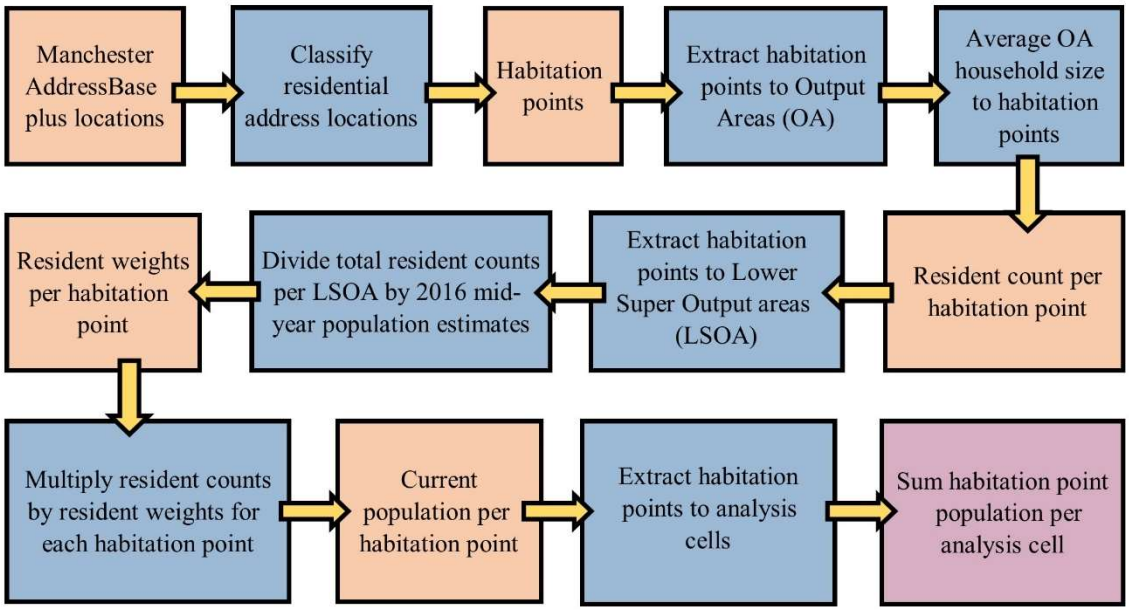

Notes:

Average Household Size per Output Area (OA) calculated from UK Census 2011 table QS406EW: Household Size (ONS 2013a). This table provides counts of all individual households per OA, with breakdown of (n = 8) household size categories (1 → 8+). Average household size per OA calculated accordingly.

Addressbase plus (July 2018 update; OS 2018) data for Manchester was provided by the Ordnance survey on a research license. Addressbase records were classified as residential (habitation) addresses with any CLASS code beginning with the letter R (= *Residential address class*; OS 2018)

Appendix 2.5.3 – Visual display of HAB_{POP} method

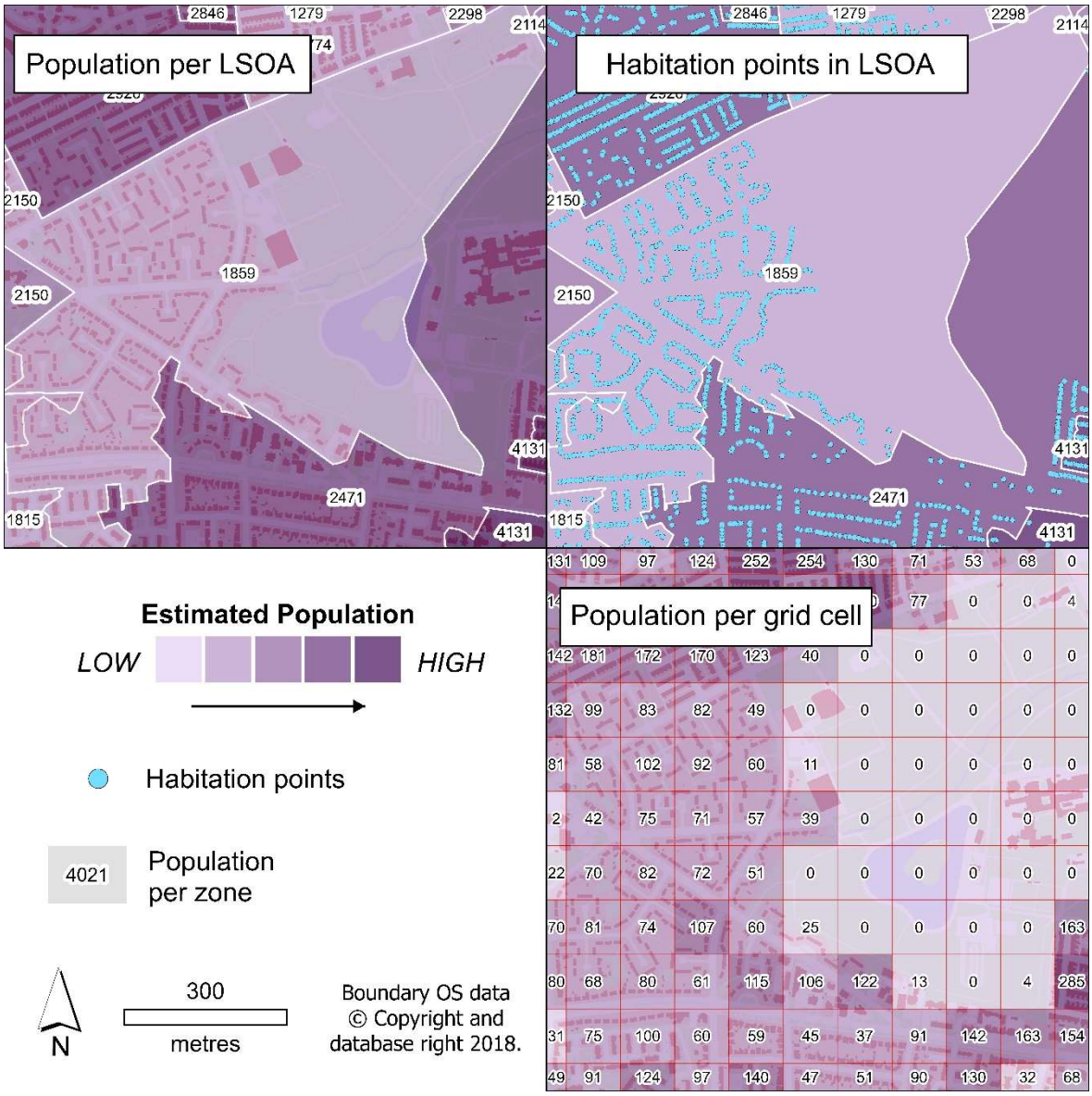

Appendix 2.6 – Mapped RES function and demand indicators

Appendix 2.6.1 – Above-ground carbon storage indicators

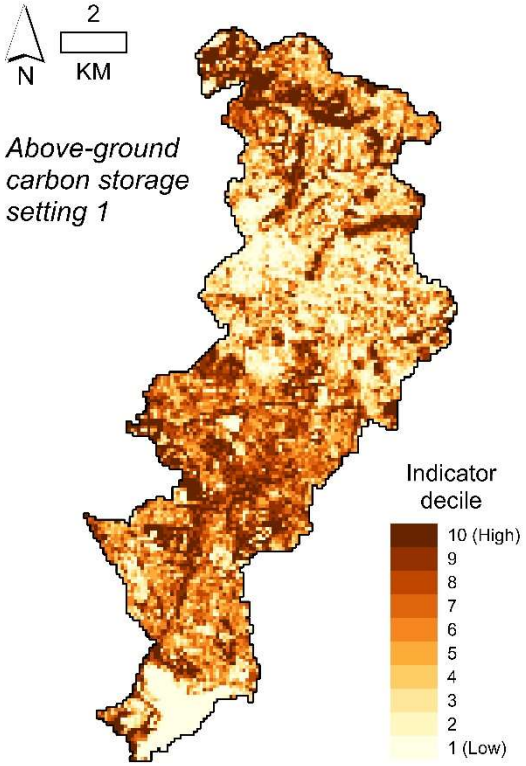

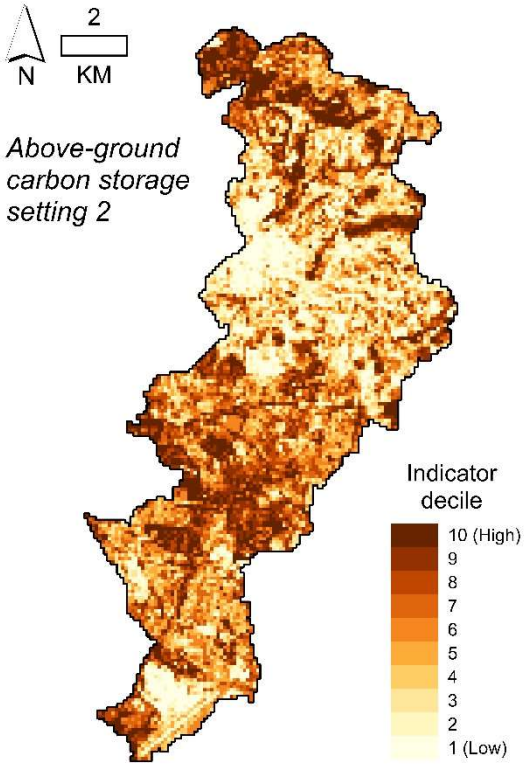

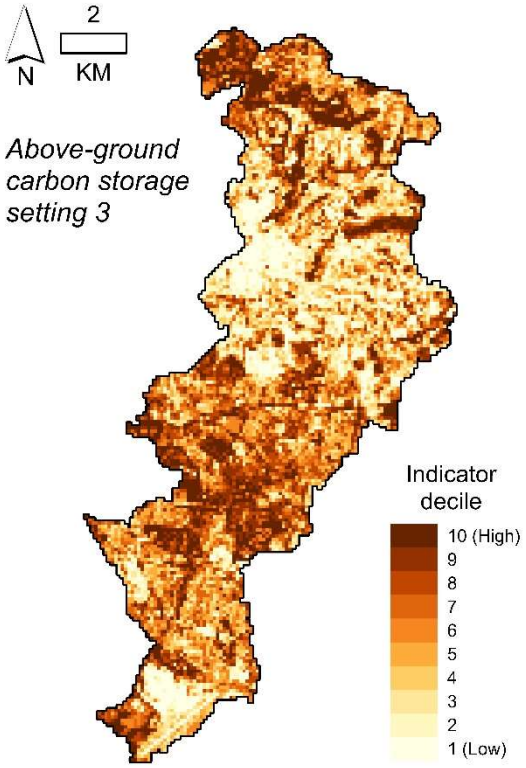

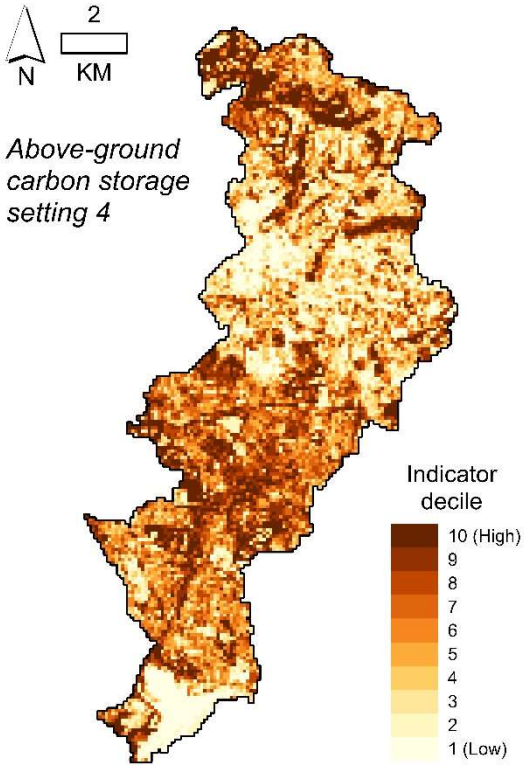

Appendix 2.6.2 – Stormwater storage indicators

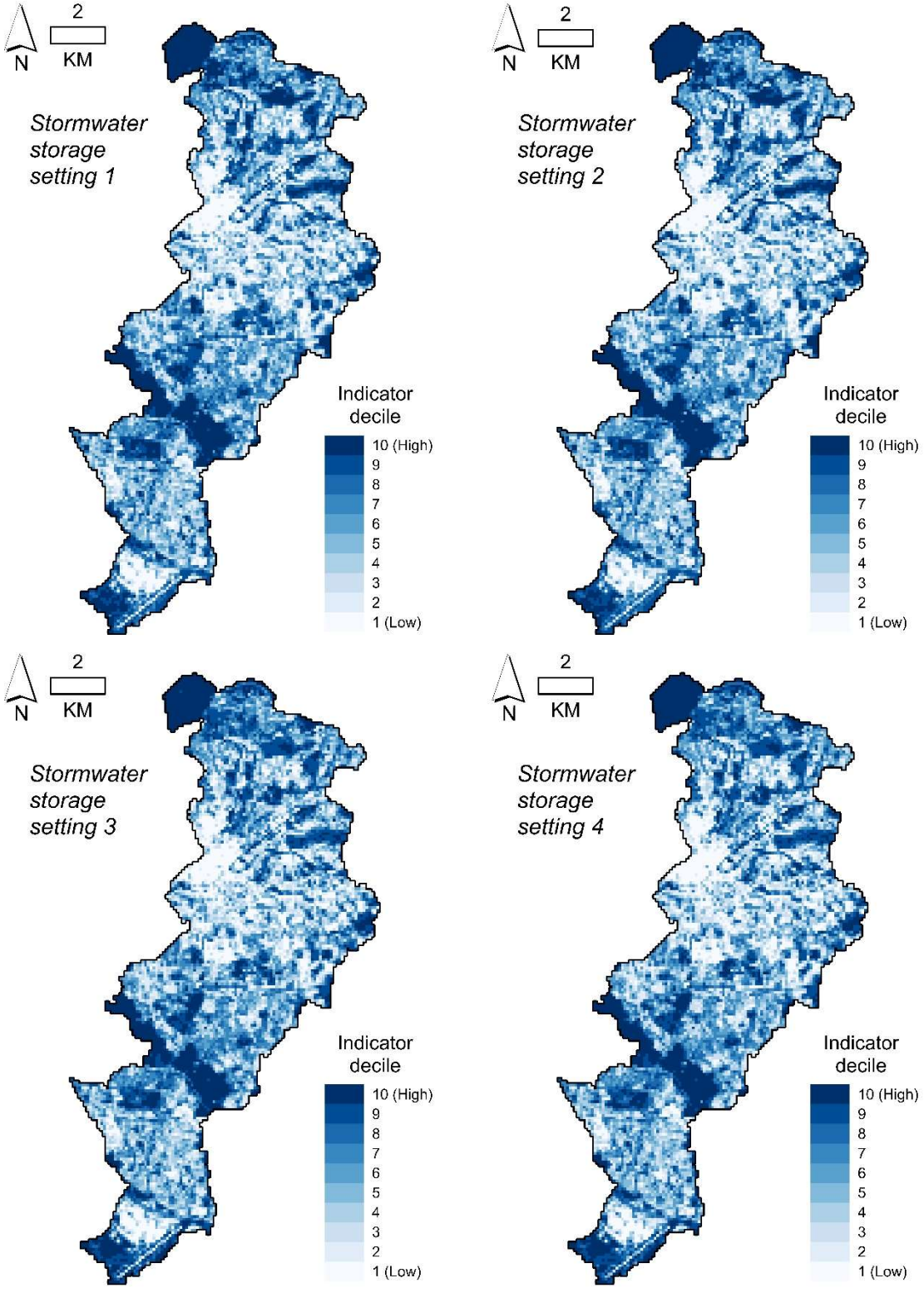

Appendix 2.7 – Scatterplots between RES indicators

The following appendices present scatterplots between Temperature regulation (TR), Stormwater storage (S) and Above-ground carbon storage (C) indicators for each group of demand cells. Parameter setting is indicated next to the indicator letter key where appropriate (i.e. C3 represents Above-ground carbon storage indicators for parameter setting 3). From initial investigation, a general linear relationship was identified in each of the scatterplots. As such, Pearson's correlation coefficient was used to test the strength of association between indicator values. **Table A2.6** provides a summary of correlation statistics (see **Table 2.8**; **Section 2.6**). Scatterplot patterns vary for each demand measure.

No demand cells are both the most numerous and therefore contain the greatest degree of variation in landcover proportions. As a result, outliers are more visible in scatterplots for this demand measure. This results in generally lower strength correlation values for Temperature regulation → Above-ground carbon storage, and Above-ground carbon storage → Stormwater storage. Outliers are also present for Temperature regulation → Stormwater storage, however the linear pattern remains consistent for the overwhelming majority of cells. As such correlation values are stronger than other RES indicator pairings. Scatterplot patterns are visually similar for both BLD_{POP} of HAB_{POP}. This is also reflected in the correlation values which vary by small margins between each demand measure.

Table A2.6 – Summary statistics for correlations between RES

Demand cells	Temp. regulation to Above-ground carbon storage		Temp. regulation to Stormwater storage		Above-ground Carbon storage to Stormwater storage	
	Mean (r)	*Max.(r) – Min.(r)*	*Mean (r)*	*Max.(r) – Min.(r)*	*Mean (r)*	*Max.(r) – Min.(r)*
No demand	0.56	0.18	0.83	0.06	0.58	0.25
BLD_{POP}	0.63	0.13	0.79	0.04	0.73	0.23
HAB_{POP}	0.61	0.13	0.78	0.05	0.74	0.24

Appendix 2.7.1 – Scatterplots for No demand cells

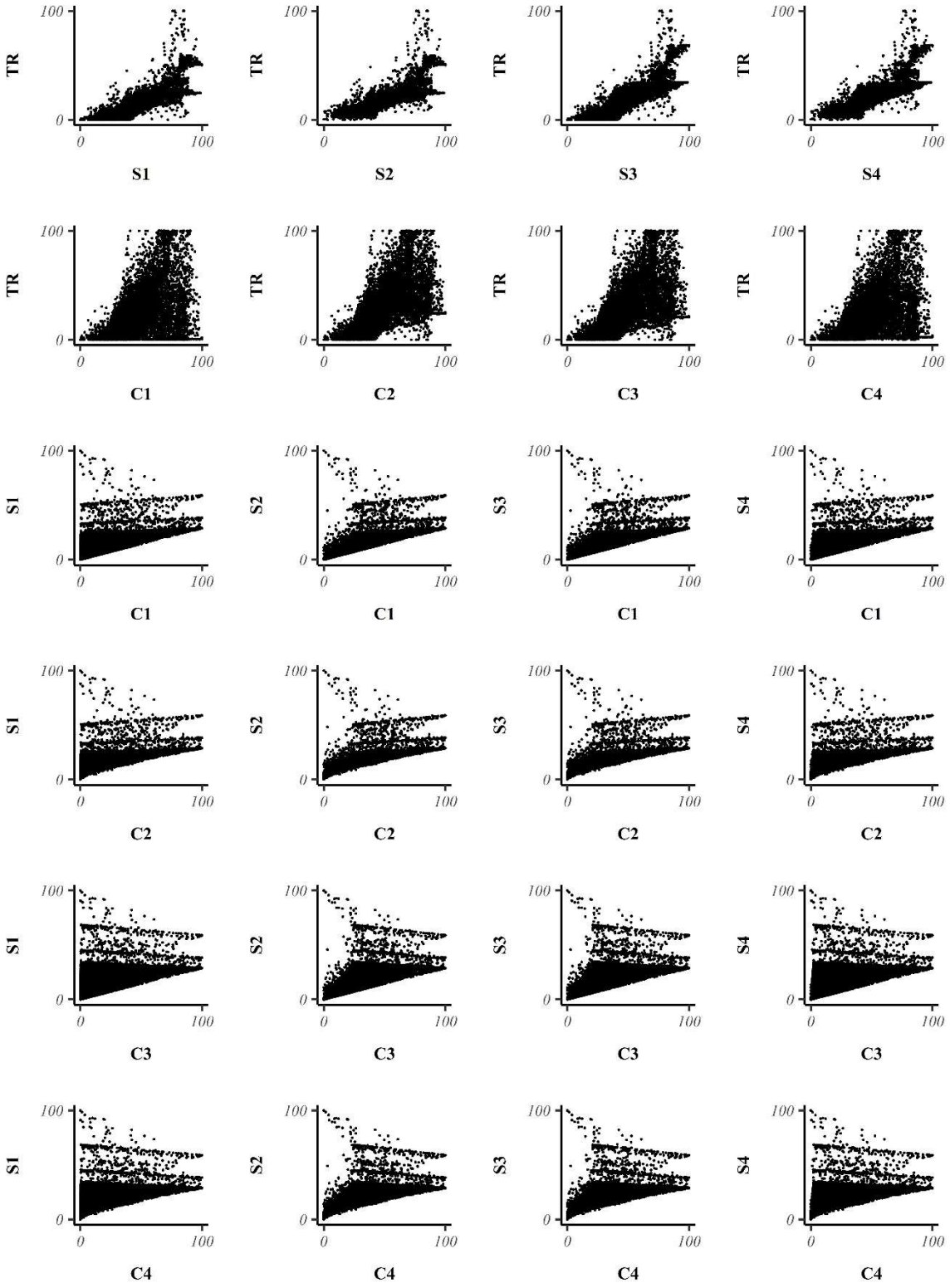

Appendix 2.7.2 – Scatterplots for BLD_{POP} demand cells

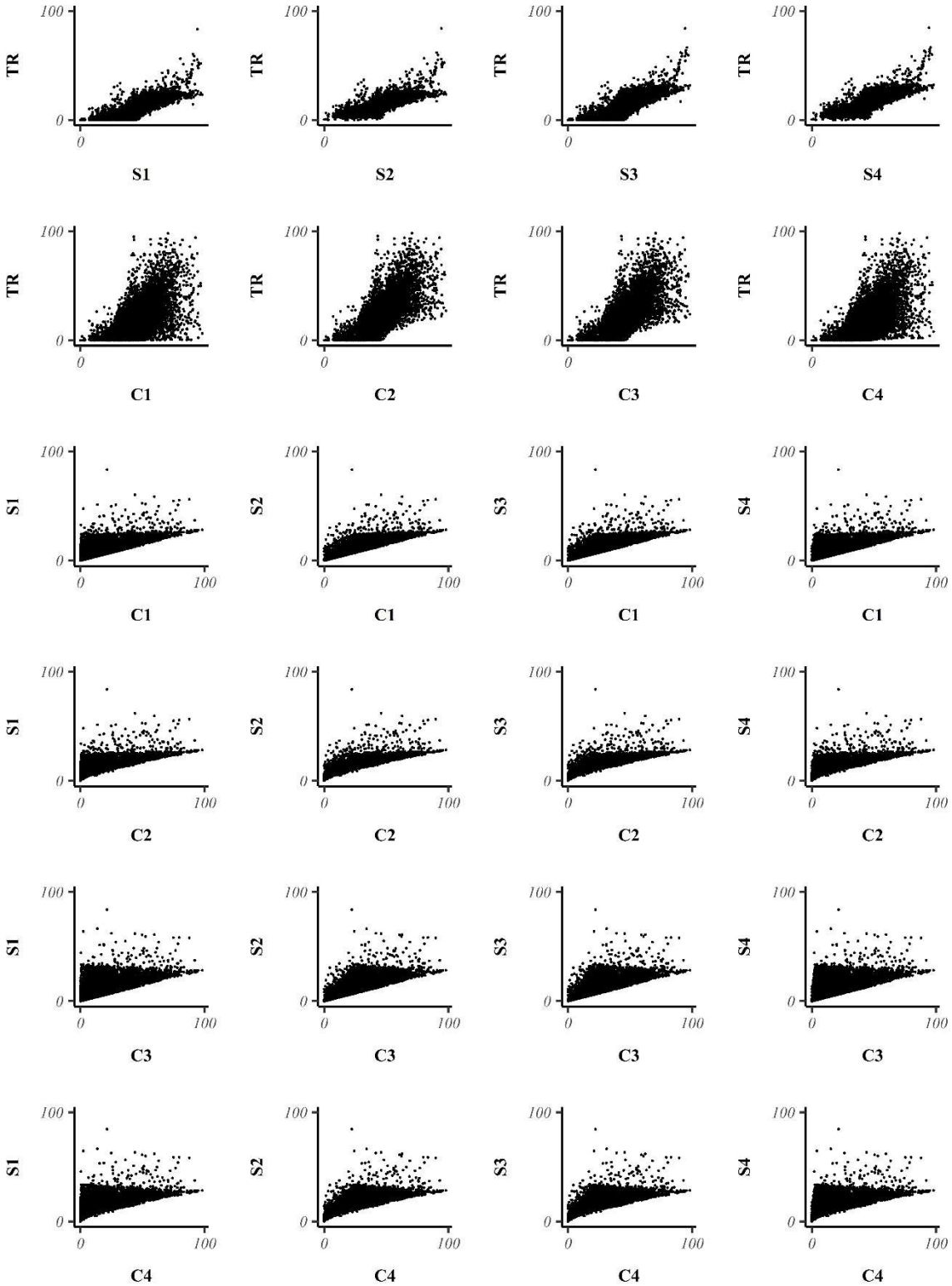

Appendix 2.7.3 – Scatterplots for HAB_{POP} demand cells

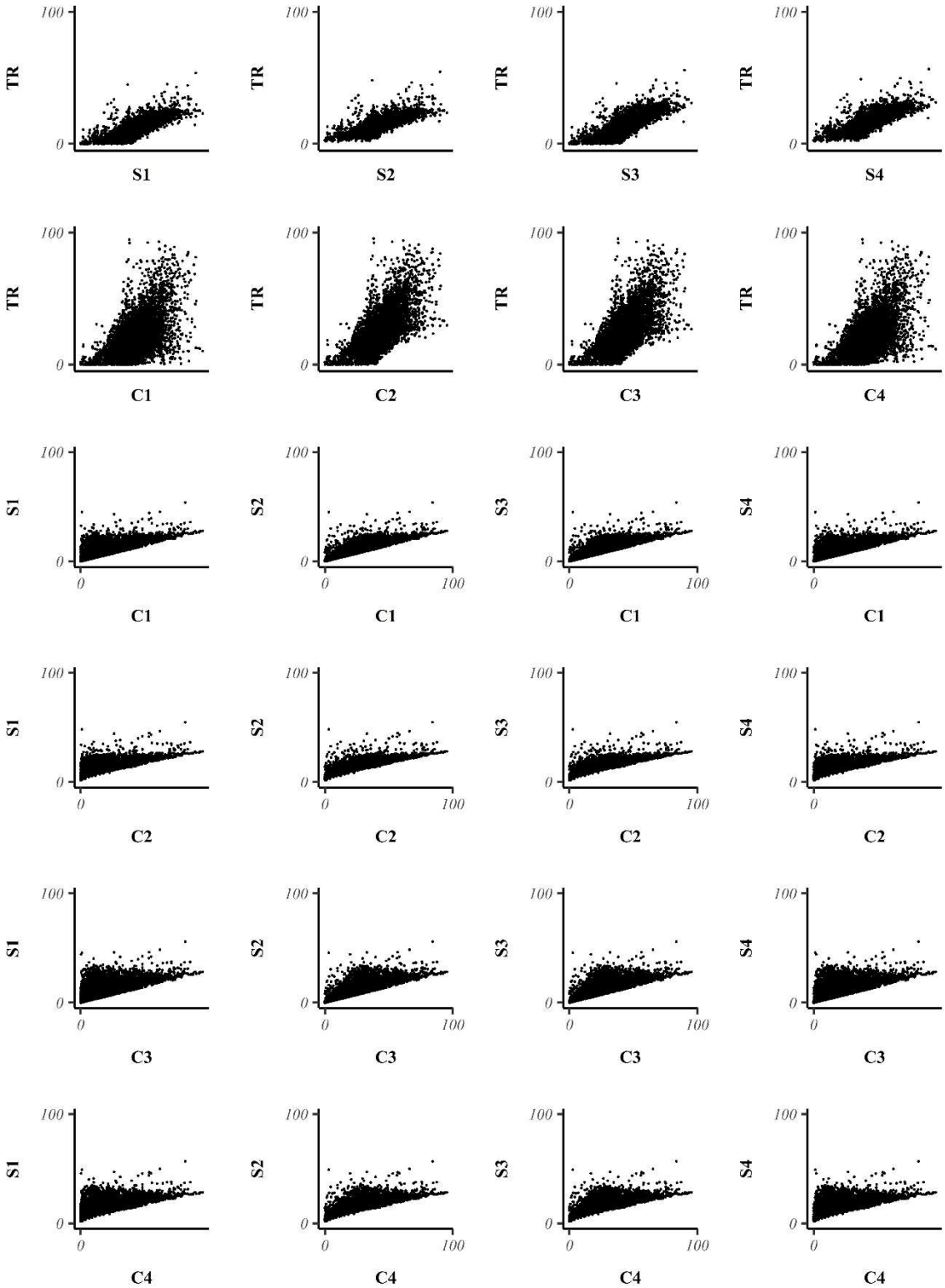

Appendix 3.1 – Multi-temporal image data for Landcover classification

Appendix 3.1.1 – Sensor characteristics for study image data

Sensor	*Spectral band*	*Bandwidth*	*Spatial Resolution*
Spot-7[1]	Panchromatic	0.45-0.745µm	1.5m
	Blue	0.45-0.52µm	6m
	Green	0.53-0.59µm	
	Red	0.625-0.695µm	
	Near Infrared (NIR)	0.76-0.89µm	
Pleiades-1A[2]	Panchromatic	0.47-0.83µm	0.5m
	Blue	0.43-0.55µm	2m
	Green	0.5-0.62µm	
	Red	0.59-0.71µm	
	Near Infrared (NIR)	0.74-0.94µm	

[1] ASTRIUM (October, 2012). Pleiades Imagery User Guide. Retrieved from https://www.intelligence-airbusds.com/en/8289-imagery-services (accessed 05/01/19)

[2] ASTRIUM (July, 2013). SPOT 6 & SPOT 7 Imagery User Guide. Retrieved from https://www.intelligence-airbusds.com/en/8289-imagery-services (accessed 05/01/19)

Appendix 3.1.2 – Extents of October SPOT-7 and Pleiades-1A image masks in relation to May SPOT-7 image

Note: percentage figures for coverage of May SPOT-7 by each October mask is given in the image.

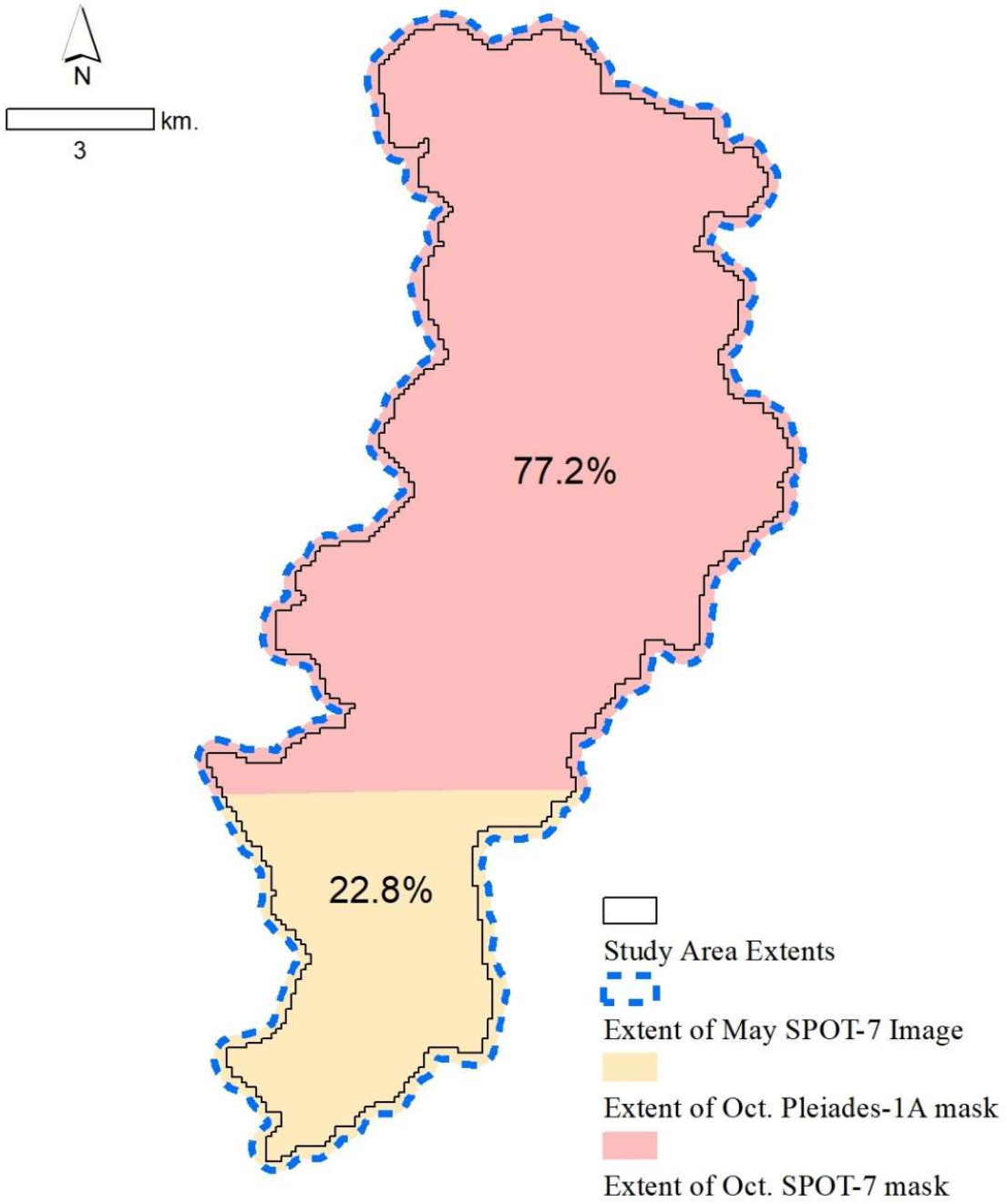

Appendix 3.2 – Image and OS ancillary layer classification features

Appendix 3.2.1 – Image classification feature layers

Image features	*Description*	*Calculation method*
Red $Green$ $Blue$ NIR (Near Infrared)	Original image layers	No processing required
$NDVI$	Normalized difference vegetation index –measure of pixel biomass photosynthetic production (Chuvieco 2016)	$NDVI = \frac{NIR - Red}{NIR + Red}$
$NDWI$	Normalized difference water index – measure of water content in water bodies (Chuvieco 2016)	$NDWI = \frac{Green - NIR}{Green + NIR}$
$Mean_{RGB}$	Measure of brightness of visible radiation layers – useful for determining *dark* pixels (Baker et al. 2018)	$Mean_{RGB} = \frac{Red + Green + Blue}{3}$
Sd_{RGB}	Measure of pixel saturation or greyness (Baker et al. 2018)	$Sd_{RGB} = \sqrt{\frac{\sum_{i=1}^{n}(x_i - Mean_{RGB})^2}{n-1}}$ Where n = 3 for Red, Green and Blue layers; x is pixel value for Red, Green or Blue layer
Red_{CHR} $Green_{CHR}$ $Blue_{CHR}$	Chromatic values for Red, Green and Blue layers; reduces variance in pixel illumination in image and useful for other vegetation indices (Meyer & Neto 2008)	$Lyr_{CHROMATIC} = \frac{Lyr}{Red + Green + Blue}$ Where Lyr represents the relevant layer for chromatic value calculation
$GRVI$	Green Red Vegetation index – measure of pixel greenness (Motohka et al. 2010)	$GRVI = \frac{Green_{CHR} - Red_{CHR}}{Green_{CHR} + Red_{CHR}}$
EXG	Excess green vegetation index – measure of pixel	$EXG = 2Green_{CHR} - Red_{CHR} - Blue_{CHR}$

	greenness (Meyer & Neto 2008)	
$EXGEXR$	Excess green minus excess red index - alternative greenness index to the above (Huang & Zhang 2013)	$EXGEXR = EXG - (1.4Red_{CHR} - Green_{CHR})$
$PCA1$ $PCA2$ $PCA3$ $PCA4$	4 x principal component layers calculated from the Red, Green, Blue and NIR layers	Calculated using principal component function in ArcMap (version 10.5)
$NDVI_{RAT}$	Ratio *NDVI* feature between May and October images to create single index for seasonal *NDVI* variation	$NDVI_{RAT} = \frac{ocNDVI}{NDVI}$
$NDWI_{RAT}$	Additional ratio feature created to improve Deciduous and Evergreen classification	$NDWI_{RAT} = \frac{NDVI_{RAT}}{NDWI}$

Note: Image features were calculated for both May and October images; for May image features the layer name acronym remains the same as in the table above, for October image features the prefix oc is added to the relevant acronym. For example, $Mean_{RGB}$ *is referenced as* $ocMean_{RGB}$ *when calculated for October image data only.*

Appendix 3.2.2 –OS Mastermap Topography layer classification features

Surface Class (in order of processing)	*Description*	*Classification ruleset (terms in italic represent OSMT attribute field)*
WATER	Exposed water i.e. water channels, reservoirs, ponds	*descriptiveGroup* **IS** Inland Water, Natural Environment **OR** Inland Water, Structure **OR** Inland Water
BUILDINGS	Vertical standing built structures	*Theme* **IS** Buildings **OR** Buildings, Roads Tracks and Paths **OR** Buildings, Rail
NATURAL	Natural non-water surface such as Bare Earth, Grass and other vegetative surfaces	*Make* **IS** Natural **OR** *descriptiveGroup* **IS** Landform OR Landform, Road Or Track **OR** Landform, Rail **OR** Landform, Historic Interest **OR** Landform, Inland Water
MANMADE	Non-natural surfaces such e.g. Asphalt, Concrete	*Make* **IS** Manmade
MULTIPLE	Mixed NATURAL and MANMADE surface	All remaining records

Appendix 3.3 – Sampling scheme for Random Forest classification

Appendix 3.3.1 – Sample size calculation and selection

The minimum number of samples (n) required for overall accuracy assessment was determined through use of the Multinomial Law equation (Congalton & Green 2008):

$$n = \frac{B}{4b^2} \quad \textbf{[A3.1]}$$

Where n is the overall number of samples; B is determined from the required confidence level (e.g., 95%) and is the chi-square critical value for 1 d.f and $\chi^2_{(1-\alpha/k)}$ (where k is the number of classes, α is 1 minus the required confidence level e.g., 95% = 1 − 0.95); b is the desired level of precision (e.g., 5% = 0.05). Minimum number of samples were calculated for (k = 8) classes in total, confidence level of 95% and accuracy of 5%. See equation below:

$$n = B/(4 \cdot b^2) = \frac{7.23}{4 \cdot 0.05^2} = 723 \quad \textbf{[A3.1]}$$

The minimum number of training samples was calculated by doubling the number of samples required for validation (2 x 723 = 1446), to approximate a 70% (training) to 30% (validation) sample split. To ensure samples were distributed spatially across the study area, a reference grid of 33 zones was created to cover the image extents. The general aim was to place 9 points for each class within each zone, so that total collected samples (*n* = 2,376) exceed the minimum total for required sample points (*n* = 2,169). Image samples were identified from the study images, with additional cross-referencing of Google Earth imagery and street view (various image dates between 2000 and present) to examine leaf-on and leaf-off canopy conditions, to help identify samples for the deciduous and evergreen image classes. For all classes, with the exception of Evergreen, the minimum number of samples (*n* = 271) was acquired. Despite evergreen canopies being prevalent in the Google Earth imagery, these areas were often closely intermixed with deciduous vegetation, thus limiting the amount of spectrally pure sample areas available for this class. For some classes, the minimum number of samples was not identified in each zone, therefore where possible additional samples were collected from neighbouring zones to make up the shortfall. Samples were randomly selected for either training or validation. Class proportion of total sample size determined the proportion of required number of validation samples per class.

Appendix 3.3.2 – Sample size per landcover class

Class	*Total no. of samples*	*Proportion of total samples (%)*	*No of training samples*	*No. of validation samples*
Artificial	297	13.8	197	100
Bare Earth	299	13.9	198	101
Deciduous	285	13.2	189	96
Evergreen	109	5.1	72	37
Grass	296	13.7	196	100
Water	277	12.8	184	93
Shaded non-vegetation	296	13.7	197	99
Shaded vegetation	297	13.8	197	100
Total	2,156	100	1,430	726

Appendix 3.4 – Selected parameters for Random Forest classification

Classification subset	Input Classes	Output Classes	Method	Segmentation & Classification layers	RF settings	
					mtry	*ntree*
Initial	Unclassified	Non-vegetation class, Vegetation class, Shaded vegetation and Shaded non-vegetation	Pixel	*Blue, Red, PCA1, $Green_{CHR}$, EXGEXR*	3	50
Artificial	Non-vegetation	Artificial & Bare Earth	Object	*$Blue_{CHR}$, NDWI, PCA3, Red_{CHR}, NDVI, PCA4, Sd_{RGB}, ocNDV, SDEV_$Blue_{CHR}$, $ocBlue_{CHR}$*	3	1000
Canopy	Vegetation	Grass and Canopy (combines Deciduous and Evergreen)	Object	*$Green_{CHR}$, Sd_{RGB}, $Blue_{CHR}$, Red, EXGEXR, PCA3, $Mean_{RGB}$, NDWI, NDVI, PCA1, PCA4, ocPCA2, SDEV_$Blue_{CHR}$, Blue*	5	1000
Canopy Species	Canopy	Deciduous and Evergreen	Pixel	*NDVI, PCA1, PCA2, PCA4, NDVI, ocRed, $ocRed_{CHR}$, ocEXGEXR, $NDVI_{RAT}$, $NDWI_{RAT}$*	10	1500

Appendix 3.5 – Ruleset for topological shadow re-classification

Candidate class	Rules for Shaded non-Vegetation
Artificial	Relative Border to Artificial > 0 **AND** Relative Border to Bare Earth = 0 **AND** Relative Border to Water = 0
Bare Earth	Relative Border to Bare Earth > 0 **AND** Relative Border to Artificial = 0 **AND** Relative Border to Water = 0
Water	Relative Border to Water > 0 **AND** Relative Border to Artificial = 0 **AND** Relative Border to Bare Earth = 0
Candidate class	**Rules for Shaded Vegetation**
Deciduous	Relative Border to Deciduous > 0 **AND** Relative Border to Evergreen = 0 **AND** Relative Border to Grass = 0 **AND** Relative Border to Water = 0
Evergreen	Relative Border to Evergreen > 0 **AND** Relative Border to Deciduous = 0 **AND** Relative Border to Grass = 0 **AND** Relative Border to Water = 0
Grass	Relative Border to Grass > 0 **AND** Relative Border to Evergreen = 0 **AND** Relative Border to Deciduous = 0 **AND** Relative Border to Water = 0
Water	Relative Border to Water > 0 **AND** Relative Border to Evergreen = 0 **AND** Relative Border to Deciduous = 0 **AND** Relative Border to Grass = 0

Note: Relative Border is a feature calculated in eCognition which calculates shared borders with neighbouring classes as a ratio of the reference object shape perimeter

Appendix 3.6 – Mono-window parameters for February land surface temperature

Parameter	*Description*	*Method/value altered from July LST creation*
T_a	Mean atmospheric temperature value (k)	Assumed values from testing phase (Wang et al. 2015) = -5.87°C + 273.12
a_{10}	Constant to approximate derivative of Planck's function; derived from expected LST temperature range in degrees Celsius	Chosen from look up table for expected temperature values ranging from −20 °C → 30 °C; = -55.4276
b_{10}	Another constant based on expected LST temperature range in degrees Celsius	0.4086
τ_{10}	Atmospheric transmittance	Calculated using online Atmospheric Correction Parameter Calculator (Barsi et al. 2017) for Landsat missions 5 – 8. Following parameters are required: Near surface air temperature = 8°C; Humidity = 81%; Surface Pressure = 1012 (all values obtained from Manchester Airport at 11.20AM; Weather Underground 2017)*; Final value = 0.81

Note: Cloud cover was evident in Landsat imagery data. Therefore, this was removed using a manually digitised masking feature to re-classify cloud contaminated pixels where appropriate. Less than 1% of total pixel area was removed from the final February LST layer through this process.

Appendix 3.7 – Table of tree interception data (Xiao & Mcpherson 2011)

Leafing period	*Date*	*Rainfall (mm)*	*Interception rate (%) for deciduous trees*		*Interception rate (%) for Lemon (evergreen) tree*
			Gingko	*Sweet Gum*	
	05.10.05	17.5	23.9	15	96.8
	13.11.05	24.2	n/a	11.8	n/a
	26.02.06	7.9	100	14.1	96.3
"Leaf-off"	05.03.06	74.0	28.3	11	28.8
	09.03.06	6.7	25.9	17.4	49.1
	12.03.06	24.7	30	18.4	28.1
	15.03.06	86.3	26.6	14.4	47.5
Mean (SE in brackets) period interception (%) (all species values)			25.91 (6.4)		57.77 (12.8)
	24.03.06	15.5	33.3	25.2	21
	27.03.06	18.5	33.3	3.5	31.6
	31.03.06	15.5	28.4	19.4	18.6
	03.04.06	45.0	25.6	18	4.7
"Leaf-on"	07.04.06	20.4	25.8	23	25.8
	11.04.06	33.9	48.2	25.2	19.9
	15.04.06	32.1	37.7	30	49.6
	19.05.06	8.6	72	64.3	55.5
	21.05.06	15.4	72	73	55.5
Mean (SE in brackets) period interception (%) (all species values)			36.55 (4.28)		31.36 (6.06)

Appendix 3.8 – R code to calculate canopy adjusted curve numbers

The code below (R statistical programming language) provides an example of how to calculate curve numbers by accounting for above-ground canopy interception rates. The same process can be used to calculate curve numbers for water surfaces with zero runoff for various precipitation inputs.

```
#############################################################################
#
# ~~~~~~>> Input parameters
#
# Data-frame containing curve Numbers for Ancillary OS layers used in study
#
aCN.df <- data.frame(Soil.group = c("B","C","D"),
                     Impermeable = c(98,98,98),
                     Multiple = c(79.5,86.0,89.0),
                     Natural = c(61,74,80),
                     stringsAsFactors = F)
#
# Scenario precipitation (e.g. 14.5mm)
#
prc <- 14.5
#
# Interception rate (%) for canopy above surface (e.g. 34.82%)
#
intc <- 34.82
#
# ~~~~~~~~~~~~~~~~~~~~~~~~~~~~~~~~~~~~~~~~~~~~~~~~~~~~~~~~~~~~~~~~~~~~~~~
# ~~~~~~>> Find solution
#
# 1. Calculate runoff for ancillary OS surfaces according to adjusted
# understory levels
#
intc <- intc/100
undp <- (1-intc) * prc # Understory precipitation
svals <- (2540/as.matrix(aCN.df[,2:4]))-25.4
# S values for curve numbers - select correct columns
und.runoff <- ((undp - (0.2*svals))^2)/(undp + (0.8*svals))
# runoff calculate from s-values
#
# 2. Get runoff values for all curve numbers for overall Scenario precipitation
#
# Function returns CN producing minimal difference to expected runoff: CN.INTERVAL
# determines how close the runoff solution is to absolute zero; EXP.RUNOFF is runoff
# calculated for the below canopy ancillary OS layer surface; P is the scenario
# precipitation value
#
all_CN <- function(CN.INTERVAL = 0.001,EXP.RUNOFF = 0,P = 15) {
 #
 test.CN <- seq(5,98,CN.INTERVAL) #
 S <- (2540/test.CN)-25.4
 Q.df <- data.frame(CN = test.CN,Q=((P - (0.2*S))^2)/(P + (0.8*S)))
 #
```

```
  Q.df$DIFF <- abs(Q.df$Q - EXP.RUNOFF)
  choo <- Q.df$DIFF == min(Q.df$DIFF)
  return(Q.df[choo,])
  #
}
# WARNING: No error messages with this - if EXP.RUNOFF is too high then function
# will output incorrect results
#
# Output is data.frame with selected Curve Number, calculated runoff and absolute
# difference between calculated runoff and expected runoff
#
# Default settings - calculates Curve Number value for Water surface runoff for a
# 15mm precipitation event - P is adjustable and EXP.RUNOFF is static to calculate
# Water Curve Numbers for other precipitation input values
#
# 3. Example - calculate curve numbers for below canopy ancillary OS surface runoff
# values
#
und.CN <- und.runoff # copy below canopy surface runoff matrix to new variable
#
# Run loop below to calculate Curve Number values for all below canopy runoff volumes
for(i in 1:ncol(und.runoff)){
  for(j in 1:nrow(und.runoff)){
    #
    und.CN[i,j] <- all_CN(EXP.RUNOFF = und.runoff[i,j],P = prc)[1,1]
  }
}
# Outputs data.frame with updated CN values
updated.CN.df <- data.frame(Soil.group = c("B","C","D"),
                            as.data.frame.matrix(und.CN),
                            Water = rep(all_CN(P = prc )[1,1],3))
#
print(updated.CN.df)
```

Appendix 3.9 – Input curve numbers for adapted SCS-CN method

Appendix 3.9.1 – Fixed curve numbers that remain consistent irrespective of precipitation scenario

Landcover (*Ancillary OS layer in italics*)	SCS-CN class (USDA 1986)	SCS soil type		
		B	C	D
Bare Earth	Streets and roads: Dirt (including right-of-way)	82	87	89
Grass & *Natural*	Open space (lawns, parks etc): Good condition (grass cover > 75%)	61	74	80
Impervious & *Manmade*	Paved parking lots, roofs, driveways etc.	98	98	98
Shrubs	Woods: Poor	66	77	83
Multiple	Average between *Natural* and *Manmade*; represents mixture of both	79.5	86	91

Note: Includes curve numbers for below canopy ancillary OS layer surfaces. Hydrological surface classes were designed to represent distinct landcover types which can be assigned to specific SCS-CN categories

Appendix 3.9.2 – Curve numbers for DEC_, EVE_ and Water surfaces: all seasonal precipitation scenarios

Hydrological surface layers	SCS-CN soil type	Control precipitation / Leaf-on conditions			Control precipitation / Leaf-off conditions			Seasonal precipitation / Leaf-on conditions			Seasonal precipitation / Leaf-off conditions		
		1:30	*1:100*	*1:1000*	*1:30*	*1:100*	*1:1000*	*1:30*	*1:100*	*1:1000*	*1:30*	*1:100*	*1:1000*
DEC_NATURAL	B	44.78	42.15	37.85	53.86	52.49	49.97	44.70	41.90	37.35	53.88	52.63	50.4
	C	55.56	52.08	46.09	66.07	64.24	60.67	55.46	51.73	45.38	66.10	64.43	61.29
	D	61.00	57.00	50.02	71.91	69.80	65.67	60.88	56.59	49.19	71.94	70.03	66.39
DEC_MULTIPLE	B	60.54	56.58	49.69	71.42	69.34	65.25	60.42	56.18	48.87	71.45	69.56	65.96
	C	66.8	62.16	54.04	66.07	64.24	60.67	66.66	61.69	53.08	77.93	75.73	71.53
	D	69.84	64.84	56.09	80.94	78.35	73.23	69.69	64.33	55.06	80.98	78.63	74.11
DEC_MANMADE	B, C, D	79.67	73.31	62.37	90.32	87.13	80.86	79.48	72.66	61.10	90.37	87.47	81.95
EVE_NATURAL	B	44.78	42.15	37.85	44.78	42.15	37.85	44.70	41.90	37.35	44.82	42.42	38.55
	C	55.56	52.08	46.09	55.56	52.08	46.09	55.46	51.73	45.38	55.62	52.44	47.07
	D	61.00	57.00	50.02	61.00	57.00	50.02	60.88	56.59	49.19	61.06	57.41	51.16
EVE_MULTIPLE	B	60.54	56.58	49.69	60.54	56.58	49.69	60.42	56.18	48.87	60.6	56.99	50.82
	C	66.80	62.16	54.04	66.80	62.16	54.04	66.66	61.69	53.08	66.87	62.64	55.36
	D	69.84	64.84	56.09	69.84	64.84	56.09	69.69	64.33	55.06	69.92	65.35	57.51
EVE_MANMADE	B, C, D	79.67	73.31	62.37	79.67	73.31	62.37	79.48	72.66	61.10	79.77	73.96	64.13
WATER	B, C, D	25.94	18.97	11.93	25.94	18.97	11.93	25.68	18.42	11.34	26.08	19.55	12.80

Appendix 3.10 – Classification error matrix

		Reference								
		Artificial	*Bare Earth*	*Deciduous*	*Evergreen*	*Grass*	*Shaded Artificial*	*Shaded Vegetation*	*Water*	***User's accuracy (%)***
Classification	*Artificial*	**90**	0	0	1	9	0	0	0	*90*
	Bare Earth	6	**72**	2	3	16	0	0	2	*71.3*
	Deciduous	0	0	**83**	9	1	1	2	0	*86.5*
	Evergreen	3	0	6	**23**	0	2	3	0	*62.2*
	Grass	0	3	4	4	**89**	0	0	0	*89.0*
	Shaded Artificial	0	0	0	0	0	**95**	4	0	*96.0*
	Shaded Vegetation	2	0	3	5	0	3	**86**	1	*86.0*
	Water	0	0	5	2	0	0	0	**86**	*92.5*
	Producer's accuracy (%)	*89.1*	*96*	*80.6*	*48.9*	*77.4*	*94.1*	*90.5*	*96.6*	

Overall accuracy: 86.0%; Kappa: 0.84 (*p < 0.05*)

Appendix 3.11 – Comparison between regression models

The OLS model to predict mean July cell LST results in y = 33.77 – 0.079x, with RSE = 1.573, adjusted R^2 = 0.72 and AIC = 48889. Moran's I test (spdep package R programming language; Bivand et al. 2018) was implemented to assess spatial autocorrelation in model residuals, percentage of cell that is GBI, and July LST values (**Table A3.1**).

Table A3.1 – Moran's I values for the July LST OLS model

Variable	*I (statistic)*	*p-value*
OLS Residuals	0.56	< 0.01
GBI	0.68	< 0.01
julMEAN	0.86	< 0.01

Where *I* > 0 is statistically significant this indicates positive spatial autocorrelation in data under examination (Brunsdon & Comber 2015). Positive autocorrelation in OLS regression residuals is unsurprising given autocorrelation in both the dependent and independent variables. Cross-validation was used to assess the stability of the regression model when providing control spatial autocorrelation (Roberts et al. 2017a). Here, 20 mutually exclusive subsets of randomly sampled analysis cells were generated (each set represents 5% of total number of cells available), with identical regression models re-built for all subsets. As cells in each subset are scattered across the study area and are thus disconnected (i.e. not first order neighbours). Variation in subset model coefficients (**Table A3.2**) indicates the level of stability in estimated model parameters (Hawkins et al. 2007, Roberts et al. 2017a).

Table A3.2 – Cross-validated OLS model statistics

	Intercept	*Coefficient*	R^2	*RSE**	*MAE***
Mean	33.77	-0.079	0.714	1.572	1.204
Standard Deviation	0.118	0.002	0.02	0.05	0.034
Minimum	33.56	-0.083	0.675	1.487	1.153
Maximum	34.07	-0.075	0.755	1.653	1.264

* = Residual Standard error; ** = Mean Absolute Error

Geographically Weighted Regression (GWR) improved prediction of July LST. Optimal kernel bandwidth for GWR determined as 593.5 m (using the GWR function in ArcMap, ESRI). The model resulted in *RSE* = 1.201, R^2 = 0.84 and AIC = 41967 which provides an improvement in model outputs from OLS. As with the July OLS model, Moran's I test with Monte-Carlo simulation (999 permutations) strongly indicates spatial autocorrelation for February LST (*I = 0.704, P < 0.01*) and OLS residuals (*I = 0.683, p < 0.01*) respectively. Using the same cross-validation method as the July OLS LST model, demonstrates that model coefficients and outputs vary little when accounting for spatial autocorrelation (**Table A3.3**). Unlike the July GWR LST model, GWR fails to provide significant gains in the explanation of February LST. The OLS model to predict February LST results in y = 9.88 – 0.008x, with RSE = 0.609, adjusted R^2 = 0.151 and AIC = 23653. The GWR model at optimal kernel bandwidth 593.5m (ArcMap 10.3; ESRI) resulted in RSE = 0.666, R^2 = 0.510, and AIC = 26559.

Table A3.3 – Cross-validated OLS model statistics

	Intercept	*Coefficient*	R^2	*RSE**	*MAE**
Mean	9.869	-0.008	0.151	0.598	0.387
Standard Deviation	0.044	0.001	0.044	0.062	0.018
Minimum	9.798	-0.009	0.087	0.497	0.358
Maximum	9.956	-0.007	0.246	0.756	0.424

* = Residual Standard error; ** = Mean Absolute Error

Appendix 4.1 – Relationships between National Land Use database (NLUD 2006) and Urban Land use 2017 classification

NLUD 2006 (v4.4)		ULU 2017	
ORDER	*GROUP*	*CLASS*	*GROUP*
AGRICULTURE & FISHERIES	Agriculture	5.1 Agriculture	Non-recreational Open Space
	Fisheries		
FORESTRY	Managed forest	5.4 Woodland	
	Un-managed forest		
MINERALS	Mineral workings & quarries	**Not identifiable**	**Not identifiable**
RECREATION & LEISURE	Outdoor amenity & open spaces	6.1 Public open space	Public recreation
	Amusement & show places	**Not identifiable**	**Not identifiable**
	Libraries, museums & galleries	3.2 Cultural facilities	Community Services
	Sports Facilities & grounds	6.2 Sports facilities	Public recreation
	Holiday parks & camps	7.1 Low density residental	Residential
	Allotments & city farms	6.3 Urban Farming	Public recreation
TRANSPORT	Transport tracks & ways	8.6 Motorways	Transport
		8.4 Major Roads	
		8.3 Linking Roads	
		8.5 Minor Roads	
		8.2 Limited Access Roads	
		8.8 Roadsides	
		8.7 Railways	
	Transport terminals & interchanges	8.9 Transport Terminals	
	Car parks	8.1 Car Parking	
	Other Vehicle storage		
	Goods & freight handling	4.1 Industrial	Industrial
	Waterways	5.3 Water	Non-recreational Open Space

Continued over page…

NLUD 2006 (v4.4)		ULU 2017	
ORDER	*GROUP*	*CLASS*	*GROUP*
UTILITIES & INFRASTRUCTURE	Energy production & distribution	4.2 Energy Utilities	Industrial
	Water storage & treatment	5.3 Water	Non-recreational Open Space
	Refuse disposal	4.1 Industrial	Industrial
	Cemeteries & crematoria	5.2 Cemeteries	Non-recreational Open Space
	Post & telecommunications	2.1 Commercial	Commercial
RESIDENTIAL	Dwellings	7.1 Low density Residential	Residential
	Dwellings	7.2 Medium density Residential	
	Dwellings	7.3 High density Residential	
	Hotels, boarding & guest houses		
	Residential institutions		
COMMUNITY SERVICES	Medical & health care services	3.3 Health Care	Community Services
	Places of worship	3.5 Religious Facilities	
	Education	3.6 Schools	
	Education	3.4 Higher Education	
	Community services	3.1 Safety and Well-being	
RETAIL	Shops	2.1 Commercial	Commercial
	Shops		
	Financial & professional services		
	Restaurants & cafes		
	Public houses, bars & nightclubs		
INDUSTRY & BUSINESS	Manufacturing	4.1 Industrial	Industrial
	Offices	2.1 Commercial	Commercial
	Storage	4.1 Industrial	Industrial
	Wholesale distribution		
VACANT & DERELICT	Vacant	1.1 Brownfields	Brownfield
	Derelict		
DEFENCE	Defence	Safety & Well-being	Community Services
UNUSED LAND	Unused land	1.1 Brownfields	Brownfield

Appendix 4.2 – Creating 2017 Urban Land use layer

Appendix 4.2.1 - Process to create Urban land use layer

<table>
<tr><th>Step</th><th>Description</th></tr>
<tr><td>1</td><td>Select and extract OSMT: Polylines features with PhysicalPresenceValue = “obstructing” to create Obstructing polylines data. Obstructing polylines represent above-ground features such as fences, walls, hedges etc. that prevent pedestrian access to enclosed areas. Obstructing polylines thus represent features that define distinct land parcel areas within the OS Topography dataset.</td></tr>
<tr><td>2</td><td>Intersect Obstructing polylines with SA boundary to create set of polygon areas (BASE OS) with unique ID reference and all with MERGE label pOSMT.</td></tr>
<tr><td>3</td><td>Re-classify OSMT: Polygons with MERGE labels where the following attribute conditions are met:
<table>
<tr><th>MERGE label*</th><th>THEME contains</th><th>THEME excludes</th><th>DESCRIPTION contains</th></tr>
<tr><td>pBUILDINGS</td><td>Buildings</td><td>Rail OR Roads Tracks and Paths OR Water</td><td>n.a.</td></tr>
<tr><td>pPATH</td><td>Roads Tracks And Paths</td><td>Rail OR Water</td><td>Path</td></tr>
<tr><td>pROAD</td><td>Roads Tracks And Paths</td><td>Rail OR Water</td><td>Road Or Track</td></tr>
<tr><td>pWATER</td><td>Water</td><td>Rail OR Roads Tracks and Paths</td><td>n.a.</td></tr>
<tr><td>Railways</td><td>Rail</td><td>n.a.</td><td>n.a.</td></tr>
<tr><td>Roadsides</td><td>Roads Tracks And Paths</td><td>Rail OR Water</td><td>Roadside</td></tr>
</table>
* Labels beginning with a lower case p represent preliminary class polygons to be categorised to final ULU classes in subsequent steps. Other labels represent final ULU classes. Extract re-class label polygons only from the OSMT: Polygons data to create PRLM ULU.</td></tr>
<tr><td>4</td><td>Erase BASE OS polygons using the extents of PRLM ULU, and then merge to form PRLM OS dataset.</td></tr>
<tr><td>5</td><td>Re-classify Openmap (OPMP: Important Building points) points with MERGE labels where the following conditions are met:
<table>
<tr><th>MERGE label</th><th>CLASSIFICATION contains</th></tr>
<tr><td>Community services</td><td>Fire station OR Police station</td></tr>
<tr><td>Cultural facilities</td><td>Art Gallery OR Library OR Museum OR Tourist Information</td></tr>
<tr><td>Health Care</td><td>Hospice OR Hospital OR Medical Care Accommodation</td></tr>
<tr><td>Higher Education</td><td>Further education OR Higher or University education</td></tr>
<tr><td>Religious facilities</td><td>Place of worship</td></tr>
</table></td></tr>
</table>

	Schools	Non state Primary education OR Non state secondary education OR Primary education OR Secondary education OR Special needs education
	Sports Facilities	Sports and Leisure Centre
	Transport Terminals	Airport OR Bus station OR Coach station

6	Re-classify PRLM OS buildings containing re-classified OPMP building points with appropriate MERGE label.

7 Re-classify Highways – All: FGDB Network (NTWK) Polylines where the following conditions are met:

MERGE label	*routeHierarchy attributes*
Motorways	Motorway
Major Roads	A Road Primary, A Road
Linking Roads	B Road, B Road Primary
Minor Roads	Minor Road, Local Road, Local Access Road
Limited Access Roads	Restricted Local Access Road, Restricted Secondary Access Road, Secondary Access Road

8	Re-classify PRLM OS pROADs polygons with MERGE label from contained NTWK polyline.

9 Re-classify MasterMap Sites Layer (SITES) polygons where the following conditions are met:

MERGE label	*Site Layer attribute: Function*
Energy Utilities	Gas Distribution or Storage OR Electricity Distribution
Health Care	Hospice OR Hospital OR Medical Care Accommodation
Higher Education	Further Education OR Further Education, Higher or University Education OR Higher or University Education
Railways	Railway Station
Schools	Further Education, Non State Primary Education OR Further Education, Non State Secondary Education OR Further Education, Secondary Education OR Non State Primary Education OR Non State Primary Education, Non State Secondary Education OR Primary Education OR Primary Education, Secondary Education OR Secondary Education OR Special Needs Education OR Non State Secondary Education
Transport Terminals	Airport or Bus station or Coach station

10

Re-classify and retain MasterMap Greenspace (GRNS) layer polygons where the following conditions are met:

MERGE label	*Greenspace Layer: Primary Function (priFunc)*
Brownfield	Non-functioning
Cemeteries	Cemetery
Public Open Space	Public Park Or Garden
Religious Facilities	Religious Grounds
Residential	Camping Or Caravan Park OR Private Gardens
Sports Facilities	Bowling Green OR Golf Course OR Play Space OR Playing Field OR Tennis Court OR Other Sports Facility OR Formal Recreation
Urban Farming	Allotments Or Community Growing Spaces

11

Erase GRNS polygons using SITES polygons and then erase PRLM OS using GRNS & SITES layer in turn. Merge GRNS, SITES and PRLM OS polygons to form ULU MERGE dataset.

12

Re-classify ULU MERGE pBUILDINGS and pOSMT labels where polygons are surrounded by polygons with single ULU (excludes Roadsides) class label. Re-classify pPATH polygons that border pBUILDING and either any pOSMT, ULU Group Road or Roadsides polygons as pBUILDINGS.

13

Re-classify pOSMT polygons to PRLM OS classes; enables iterative grouping of non-ULU class polygons into self-contained parcels based upon observations of topological relationships in the OS data. Re-classify as follows:

Topological rule	PRLM OS *	Class hierarchy
Polygon shares common boundary with pBUILDING polygon AND ULU Group Road polygon	OS_Access_Build	1
Polygon shares common boundary with pBUILDING polygon AND NOT ULU Group Road polygon	OS_Build	2
Polygon shares common boundary with ULU Group Road polygon and NOT pBUILDING polygon	OS_Access	3
Polygon shares no common boundary with ULU Group Road polygon OR pBUILDING polygon	OS_Island	4

* Topological class definition: OS_Access_Build: polygon links pBUILDING that supports a particular land-use to an access road, enabling land-use to function self-sufficiently; OS_Build: polygon is attached, and thus supports a building area supporting a particular land-use; OS_Access: polygon acts as link between access road to larger land-use parcel, but is not directly associated with a building area; OS_Island: polygon does not satisfy any of the above conditions

14 Topological class polygons into single parcel areas following the processes described below:

Process	Method
1	Re-assign unique IDs of OS_Build and OS_Access_Build polygons according to neighbouring pBUILDING polygon with largest area
2	Find pBUILDING objects with IDs different to IDs of neighbouring topological class polygons
3	Use neighbouring IDs to link areas together; assign new ID to all polygons with any of the neighbouring IDs; iterate this process until no further polygon IDs can be reassigned; re-assign topological class labels to OS_Access_Build if any polygons with new ID is this class, else re-assign class labels as OS_Build
4	Assign IDs of OS_Build polygons to OS_Access polygons based upon majority shared border, and reclassify combined area as OS_Access_Build
5	Merge remaining OS_Build polygons to OS_Access_Build polygons based upon majority shared border
6	Re-classify remaining OS_Build polygons neighbouring Roadsides AND OS_Access_Build polygons as OS_Land_Parcels
7	Re-classify remaining OS_Build polygons as OS_Islands

15 Merge OS_Islands with neighbouring class polygons (excluding pWATER, pPATH and Brownfield) based upon majority shared border; re-classify remaining OS as OS PARCELS if this condition is not satisfied; dissolve all polygons according to updated classification.

16 Manually inspect OS PARCELS polygons in conjunction with May 2017 and Google Earth street-view imagery to assign appropriate ULU class labels; if OS PARCELS do not represent homogenous ULU class parcel area then re-classify as *error* parcels.

17 Rectify *error* parcels by using polygons to select original contained OS Mastermap polygon areas; group error parcels into homogenous land parcel areas and assign appropriate class label

18 Merge remaining non-ULU class polygons (excluding pWATER) to neighbouring ULU polygons according to majority border relationship.

19 Identify polygons below the minimum mapping unit of $45m^2$ and merge with neighbouring class areas according to majority shared neighbouring border. The minimum mapping unit area ($45m^2$) was determined by a general observation that polygons of this size would

	contain 20 complete classification pixels, and thus maintain the expected change detection accuracy of 85% when considering whole pixel numbers (85% of 20 is thus 17).
20	Manually select pWATER areas that are neither water channels, canals, rivers or reservoirs (shared water utilities) and merge to neighbouring class polygons based upon majority shared boundary.
21	Create parcel based building info features for Residential polygons using Building heights polygons by extract building polygons with area ≥ 30m^2 (representing actual dwelling areas) contained inside residential polygon areas (see **Appendix 4.1.2**).
22	Classify ULU Residential polygons as follows:

Process	*Method*
1	Select classification samples for Low, Medium and High residential classes (using ancillary imagery and Mastermap polygons as a guide) and split into training and validation samples
2	Use the Random Forest algorithm to re-classify residential polygons ensuring overall classification accuracy ≥ 85% (see **Appendix 4.1.3** for further details)
3	Manually re-classify (using ancillary imagery and Mastermap polygons as a guide) any residential polygons that do not contain Building Heights data

23	Create final ULU CLASS layer by ensuring topological errors are corrected, with updated ID values, polygon area and length data attached.

Appendix 4.2.2 - Dwelling and Block level features for classification of ULU Residential polygons

Feature	*Method*
MIN_HT	Minimum dwelling building height
MAX_HT	Maximum dwelling building height
AVE_HT	Average dwelling building height
RAN_HT	Difference between MIN_HT and MAX_HT
MIN_AR	Minimum dwelling building area
MAX_AR	Maximum dwelling building area
AVE_AR	Average dwelling building area
RAN_AR	Difference between MIN_AR and MAX_AR
MIN_VL	Minimum dwelling building volume
MAX_VL	Maximum dwelling building volume
AVE_VL	Average dwelling building volume
RAN_VL	Difference between MIN_VL and MAX_VL
LOG_RATIO_AREA	Log of [LU17 polygon area / Total residential dwelling area]
LOG_RATIO_VOLUME	Log of [LU17 polygon area / Total residential dwelling volume]
B_AVE_NB	Average number of dwellings per block
B_AVE_AR	Average area of block
B_MIN_AR	Minimum residential block area
B_MAX_AR	Maximum residential block area
B_RAN_AR	Difference between B_MIN_AR and B_MAX_AR
B_AVE_HT	Average residential block height
B_MIN_HT	Minimum residential block height
B_MAX_HT	Maximum residential block height
B_RAN_HT	Difference between B_MIN_HT and B_MAX_HT
B_AVE_VL	Average residential block volume
B_MIN_VL	Minimum residential block volume
B_MAX_VL	Maximum residential block volume
B_RAN_VL	Difference between B_MIN_VL and B_MAX_VL

Appendix 4.2.3 - Implementation of Random Forest classification

Step	*Description*
1	An initial 300 residential polygons were chosen using random selection (within quantiles for polygon areas) with class labels manually assigned. Due to the limited number of Residential – High (*n* = 26) samples obtained through this process, additional samples (*n* = 54; total of 80) were obtained for this class. Sample numbers for Residential – Suburban (*n* = 134) and Residential – Urban (*n* = 140) remained relatively even. To ensure a reasonable number of polygons for training the data was randomly split (within quantiles for polygon areas) ensuring a 75/25% split for training and validation polygons respectively.
2	The final Random Forest model was tuned with features (B_AVE_AR, AVE_VL, B_AVE_NB, AVE_AR, MAX_VL & MAX_AR) selected using the VSURF() algorithm in addition to parameters: mtry = 1 and ntree = 1000. Overall accuracy on validation samples = 85.1% (Kappa = 0.767).
3	Residential polygons lacking appropriate classification feature data (186 out of 5867) were manually re-classified.

Appendix 4.3 – Overlap algorithm (R statistical programming language)

The following code can be copied as R script. No libraries are required for the algorithm to function.

```
# ~~~~~~~~~~~~~~~~~~~~~~~~~~~~~~~~~~~~~~~~~~~~~~~~~~~~~~~~~~~~~~~~~~~~~~~~~~~~
# Overlap algorithm - function code with instructions
#
# Author: Fraser Baker; Date: 7th February 2020
# ~~~~~~~~~~~~~~~~~~~~~~~~~~~~~~~~~~~~~~~~~~~~~~~~~~~~~~~~~~~~~~~~~~~~~~~~~~~~
# Pre-processing - requires input data as follows:
#
# -> REFERENCE POLYGONS: THESE ARE POLYGONS WITH LAND-USE CLASS
# LABELS; MUST CONTAIN UNIQUE POLYGON ID REFERENCE (REF.ID),
# POLYGON AREA (AREA.REF) AND LAND-USE CLASS LABEL (CLASS)
#
# -> TEST POLYGONS: THESE ARE POLYGONS WITHOUT LAND-USE CLASS
# LABELS; MUST CONTAIN UNIQUE POLYGON ID REFERENCE (TES.ID)
# AND POLYGON AREA (AREA.TES)
#
# Intersect REFFERENCE and TEST POLYGONS to create new dataset
# with the required fields below:
#
#   REF.ID = ID OF INTERSECTED REFERENCE POLYGON
#   TES.ID = ID OF INTERSECTED TEST POLYGON
#   AREA.INT = AREA OF POLYGON INTERSECTION
#   AREA.REF = ORIGINAL AREA OF INTERSECTED REFERENCE POLYGON
#   AREA.TES = ORIGINAL AREA OF INTERSECTED TEST POLYGON
#   RATIO.TES = AREA.INT / AREA.TES
#   RATIO.REF =  AREA.INT / AREA.REF
#   CLASS = LAND-USE CLASS ASSIGNED TO REFERENCE POLYGON
#
# data.frame (DF) required from this dataset only
# ~~~~~~~~~~~~~~~~~~~~~~~~~~~~~~~~~~~~~~~~~~~~~~~~~~~~~~~~~~~~~~~~~~~~~~~~~~~~
# overlap() function defined below - requires following inputs from user:
#
# DF = data.frame of REFERENCE to TEST polygon intersection
# ID = unique ID of REFERENCE polygon under investigation
# c.t = conditional threshold to assess polygon overlap
#
# all other variables in function call should be assigned NULL
#
overlap <- function(DF,ID,c.t,rel.REF.2.TES = NULL,TES.sub.of.RES = NULL,
                    a = NULL,a.TES.ov.REF = NULL,a.REF.ov.TES = NULL){
 #
 a <- DF[DF$REF.ID%in%ID,] #subset main dataframe according to ID of
 # REFERENCE polygon under investigation
 #
 if(length(a$TES.ID)>1){
  # If a has multiple records then REFERENCE polygon is subdivided by
  # multiple TEST polygons
  #
  a.REF.ov.TES <- a[a$RATIO.REF>c.t,] # subset all records where RATIO.TES > c.t
  #
  if(length(a.TES.ov.REF$TES.ID) > 0){ # assess if any records for TEST polygons remain
  rel.REF.2.TES <- ifelse((sum(a.TES.ov.REF$AREA.TES)/unique(a.TES.ov.REF$AREA.REF))>c.t,1,0)
  # If TRUE TEST polygons form part of group that sub-divides and overlaps a REFERENCE
  # polygon within threshold tolerance; CON = 1 in this case
  #
```

```
   TES.sub.of.REF <- unique(a.REF.ov.TES$TES.ID)  # store ID's of TEST polygons intersected
   # with the REFERENCE polygon
   }
  } else {
   # If a has single record then this this suggests REFERENCE may be matched to a single
   # TEST polygon or forms a group of REFERENCE polygons that sub-divides a single TEST
   # polygon
   a.TES.ov.REF <- DF[DF$TES.ID%in%a$TES.ID,] # subset all records from main dataframe by
   # TEST.ID in a
   #
   a.TES.ov.REF <- a.TES.ov.REF[a.REF.ov.TES$RATIO.REF > c.t,] # subset all records where
   # RATIO.REF > c.t.
   #
   if(length(a.TES.ov.REF$REF.ID) > 0){ #
    if((sum(a.TES.ov.REF$AREA.REF)/unique(a.TES.ov.REF$AREA.REF)) > c.t){
    # If TRUE REFERENCE polygons form part of group that sub-divides and
     # overlaps a TEST polygon within threshold tolerance
     if(length(unique(a.TES.ov.REF$CLASS))==1){ # multiple land-use classes are not acceptable
      #
      rel.REF.2.TES <- ifelse(length(a.TES.ov.REF$REF.ID)>1,2,1)
      # If TRUE TEST polygon is part of group that sub-divides
      # and overlaps REFERENCE polygon within threshold tolerance: CON = 2;
      # ELSE REFERENCE polygon overlaps single TEST polygon only: CON = 1
     }
     #
     TES.sub.of.REF <- unique(a.TES.ov.REF$TES.ID) # store relevant ID values for TEST polygons
     #
    }
   }
  }
  #
  return(list(REF.ID=ID,CLASS=unique(a$CLASS),RL.CON=rel.REF.2.TES,
  TES.ID=TES.sub.of.REF))
  # function returns list for input REFERENCE polygon with: REF.ID;
  # CLASS (Class of REFERENCE polygon);RL.CON (relative condition of overlap);
  # TES.ID (IDs of TEST polygons intersected to REFERENCE polygons)
 }
 #
 # Note: for large datasets that parrallel processing may be required to loop through all
 # unique REFERENCE polygon IDs
```

Appendix 4.4 – Image and OS land-line ancillary features for classification

Appendix 4.4.1 – Image classification feature layers

Image features	*Description*	*Calculation method*
Red $Green$ $Blue$	Default image layers	No further processing required
$Mean_{RGB}$	Measure of brightness of visible radiation layers – useful for determining *dark* pixels (Baker et al. 2018)	$Mean_{RGB} = \frac{Red + Green + Blue}{3}$
Sd_{RGB}	Measure of pixel saturation or greyness (Baker et al. 2018)	$Sd_{RGB} = \sqrt{\frac{\sum_{i=1}^{n}(x_i - Mean_{RGB})^2}{n-1}}$ Where n = 3 for Red, Green & Blue layers; x is pixel value for Red, Green or Blue layer
Red_{CHR} $Green_{CHR}$ $Blue_{CHR}$	Chromatic values for Red, Green & Blue layers; reduces variance in pixel illumination in image & useful for other vegetation indices (Meyer & Neto 2008)	$Lyr_{CHROMATIC} = \frac{Lyr}{Red + Green + Blue}$ Where Lyr represents the relevant layer for chromatic value calculation
$GRVI$	Green Red Vegetation index – measure of pixel greenness (Motokha et al. 2010)	$GRVI = \frac{Green - Red}{Green + Red}$
EXG	Excess green vegetation index – measure of pixel greenness (Meyer & Neto 2008)	$EXG = 2Green_{CHR} - Red_{CHR} - Blue_{CHR}$
EXR	Excess green vegetation index – measure of pixel redness (Meyer & Neto 2008)	$EXG = 1.4Red_{CHR} - Green_{CHR}$
$EXGEXR$	Excess green minus excess red index - alternative greenness index to the above (Huang & Zhang 2013)	$EXGEXR = EXG - EXR$

Appendix 4.4.2 – Ancillary OS land-line classification feature layers

Ancillary feature	Description	Method
BUILDINGS	Extents of building features within Land-line data	Land-line polygons containing Land-line points representing building features*
ROADS	Extents of road features within Land-line data	Polygon created using a 2.5 metre buffer around Land-line polylines representing road centre lines
WATER	Extents of water features & channels within Land-line data	Land-line polygons identified with maximum shared border to Land-line polyline features representing water*

* = Some manual processing required to correct mis-identified features where appropriate

Appendix 4.5 – Sampling scheme for Random forest and object-based classification

Class	Total no. of samples	Proportion of total samples (%)	No. of training samples	No. of validation samples
Non-Vegetation	693	36.47	462	231
Shadow (Shaded Non-Vegetation)	210	11.05	140	70
Shadow (Shaded Vegetation)	240	12.63	160	80
Vegetation	702	36.95	468	234
Water	55	2.89	0	55
Total	1900	100	1230	670

Appendix 4.6 – Ruleset for object-based classification

Candidate class	***Rules for Shadow classes***
Non-Vegetation	Relative border to Non-vegetation = 1
Vegetation	Relative border to Vegetation = 1
Merge all objects and intersect with WATER and BUILDING layer polygons	
Candidate class	***Rules for Shadow class***
Non-Vegetation	Minimum overlap with BUILDINGS > 0
Water	Minimum overlap with WATER > 0
Non-Vegetation	Relative border to Non-vegetation = 1
Non-Vegetation	Relative border to Water AND Non-vegetation = 1
Vegetation	Relative border to Water AND Vegetation = 1
Merge all objects and intersect with WATER layer polygons	
Candidate class	***Rules for Non-vegetation class***
Water	Minimum overlap with WATER > 0
Merge all objects	
Candidate class	***Rules for Vegetation class***
Non-Vegetation	Minimum overlap with ROAD ≥ 0.8
Non-Vegetation	Minimum overlap with BUILDING ≥ 0.8
Re-classify non-shadow classes to either GBI or NON-GBI; Segment shadow class into pixel objects	

Appendix 4.7 – Implementation of error-adjustment method to estimate net change GBI change

Theory and development of the error adjustment method is provided by Olofsson et al. (2013). The following practical example demonstrates how this method was implemented in this investigation. The first stage of the method requires an independent accuracy assessment using an error matrix. Final class area estimates are also required to calculate proportional class coverage for the area under investigation. This information is provided in the below **Table A4.1** for the change detection classes used in this investigation.

Table A4.1 – Example error matrix for error adjustment method

	Loss	Gain	GBI Stasis	Non-GBI stasis	Total	Class Area (m^2)	Proportion of total area
Loss	115	0	8	2	125	767993	0.13
Gain	0	97	22	6	125	432567	0.08
GBI Stasis	5	3	241	1	250	2007921	0.35
Non-GBI stasis	6	2	0	242	250	2505441	0.44
				Totals		5713922	1

The second stage thus requires this information to calculate error-adjusted class proportions of total area per class:

$$p_{.j} = \sum_i W_i \frac{n_{ij}}{n_i} \qquad [A4.1]$$

Where $p_{.j}$ is the error adjusted proportion per column wise class *j* ; W_i is the proportion of total area for row wise class *i* ; n_{ij} is error matrix count for row wise class *i* & column wise class *j* ; n_i is total row cells count for row wise class *i*. Using this equation an adjusted error matrix is calculated (see below). For each cell the proportion of total area is calculated according to appropriate error count, with column sums per class providing the total error adjusted area proportion per class (**Table A4.2**).

Table A4.2 – Error adjusted proportion of total class area for change classes

	Loss	Gain	GBI Stasis	Non-GBI stasis
Loss	0.124	0.000	0.009	0.002
Gain	0.000	0.059	0.013	0.004
GBI Stasis	0.006	0.005	0.338	0.002
Non-GBI stasis	0.010	0.003	0.000	0.425
Error-adjusted proportion of total area	0.14	0.07	0.36	0.43
Error-adjusted area (m^2)	801607.0	382778.3	2059179.6	2470357.1

As shown above the central error-adjusted area is thus calculated by multiplying error adjusted proportions to total area. To calculate confidence interval estimates first find the Standard error of the error-adjusted proportion using the following equation:

$$S(p_{.j}) = \sqrt{\sum_{i=1}^{q} W_i^2 \frac{\frac{n_{ij}}{n_i}\left(1-\frac{n_{ij}}{n_i}\right)}{n_i - 1}} \quad [A4.2]$$

Where q is the total number of classes. For example, the standard error of the error adjusted proportion for the lost class is calculated as follows:

$$S(Loss) = \left(0.13^2 \frac{\frac{115}{125}\left(1-\frac{115}{125}\right)}{125\ -\ 1} + 0.08^2 \frac{\frac{0}{125}\left(1-\frac{0}{125}\right)}{125\ -\ 1} + 0.35^2 \frac{\frac{5}{250}\left(1-\frac{5}{250}\right)}{250\ -\ 1} + 0.44^2 \frac{\frac{6}{250}\left(1-\frac{6}{250}\right)}{250\ -\ 1} \right)^{\frac{1}{2}} = 0.0075 \quad [A4.3]$$

Confidence interval estimates of error adjusted area are calculated by converting the standard error proportion into an areal figure & multiplying this figure by the z-score for the required confidence level (e.g. 95% here) – see below:

$$Area\big(S(Loss)\big) = z \cdot Area_{tot} \cdot\ S(Loss) = 1.96 \cdot 5713922 \cdot 0.0075 = \pm 83991.7m^2 \quad [A4.4]$$

Error adjusted area estimates are thus required for Loss & Gain classes only. The total change area is calculated using the high & low class estimates for both classes. Central, upper & lower net change are calculated as follows:

$$\hat{A}(Net) = \hat{A}(Gain) - \hat{A}(Loss) = 382778.3 - 801607.0 = -418828.7m^2 \quad [A4.5]$$

$$\hat{A}(UpperNet) = \left[\hat{A}(Gain) + Area\left(S(Gain)\right)\right] - \left[\hat{A}(Loss) - Area\left(S(Loss)\right)\right] = [382778.3 + 58402.7] - [801607.0 - 83991.7] = -276434m^2 \quad [A4.6]$$

$$\hat{A}(LowerNet) = \hat{A}(Net) + \left[\hat{A}(Net) - \hat{A}(UpperNet)\right] = -418828.7 + [-418828.7 - (-276434)] = -561223.1m^2 \quad [A4.7]$$

This process is repeated for all areas of analysis (i) Study area; ii) Analysis cells; iii) ULU class samples). Error matrix values remain consistent in all cases, whilst change class & total area values vary between analysis areas. Upper & Lower net change values thus confine the boundaries of potential GBI change. If Lower net change ≤ 0 ≤ Upper net change for analysis area then no-change (stasis) condition is recorded.

Appendix 4.8 – Cross-validation of urban land use layer

ULU group	ULU class	User accuracy (%)	Producer accuracy (%)	Class confusion (row-wise) counts
Brownfield	Brownfield	100	97.1	
Commercial	Commercial	93.9	93.9	Public Open Space x 1 | Residential – Low x 1
Community Services	Religious Facilities	100	100	
	Cultural Facilities	100	100	
	Health Care	100	97.1	
	Safety and well-being	100	97.1	
	Further education	100	100	
	Schools	100	100	
Industrial	Energy utilities	90.9	100	Railways x 2 | Woodland x 1
	Industrial	93.9	96.9	Residential – Low x 2
Non-Recreational Open Space	Agriculture	93.9	100	Health Care x 1 | Residential – Low x 1
	Cemeteries	100	100	
	Water	100	100	
	Woodland	90.9	100	Major Roads x 1 | Public Open Space x 1 | Residential – Low x 1
Recreational Open Space	Public Open Space	93.9	93.9	Residential – Low x 1 | Roadside x 1
	Sports Facilities	100	97.1	
	Urban Farming	97.0	100	Sports Facilities x 1
Residential	Residential – Low	84.4	71.1	Residential – Medium x 5
	Residential – Medium	100	80.5	
	Residential – High	78.8	100	Residential – Low x 4 | Residential – Medium x 3
Transport	Railways	87.9	93.5	Commercial x 2 | Brownfield x 1 | Residential – Low x 1
	Roadsides	97.0	97.0	Minor Roads x 1
	Limited Access Roads	100	100	
	Minor Roads	100	97.1	
	Linking Roads	100	100	
	Major Roads	100	97.1	
	Motorways	100	100	
	Transport Terminals	100	100	
	Car Parking	97.0	100	Industrial x 1

Overall accuracy = 96.6%; Kappa = 0.96

Appendix 4.9 – Insignificant differences between urban land use classes

ULU class 1	ULU class 2	p-values	ULU group
Agriculture	Water	1	NON-PUBLIC OPEN SPACE
Agriculture	Woodland	0.1	NON-PUBLIC OPEN SPACE
Further education	Health Care	1	COMMUNITY SERVICES
Further education	Religious Facilities	1	COMMUNITY SERVICES
Further education	Schools	1	COMMUNITY SERVICES
Health Care	Religious Facilities	1	COMMUNITY SERVICES
Health Care	Schools	1	COMMUNITY SERVICES
Limited Access Roads	Railways	1	TRANSPORT
Linking Roads	Minor Roads	1	TRANSPORT
Linking Roads	Motorways	1	TRANSPORT
Linking Roads	Roadsides	1	TRANSPORT
Major Roads	Motorways	1	TRANSPORT
Minor Roads	Motorways	0.8	TRANSPORT
Minor Roads	Roadsides	1	TRANSPORT
Motorways	Roadsides	1	TRANSPORT

Note: Insignificant differences detected using Pairwise Wilcoxon-Mann-Whitney U-test (R Core Team 2019).

Appendix 5.1 – Above-ground carbon storage values

To map above-ground carbon storage function indicators in the study area, above-ground carbon storage values per GBI class were extracted from the Davies et al. (2011) study (see **Section 2.5.3**). To improve upon the uncertainties regarding parameterisation in the previous analysis, four above-ground carbon storage categories were classified by intersecting 2017 landcover data with the tree audit data (City Of Trees 2011). Following the method described in **Section 3.6.3** individual tree and treeline Thiessen polygons were classified into three height bracket classes: Shrubs = < 2m, Tall Shrubs = 2 – 5m & Trees = > 5m. Height classes were intersected with deciduous and evergreen class areas, to classify above-ground carbon storage classes (see **Table A5.1**). Deciduous and Evergreen classes not overlapping tree audit data extents was re-classified to the Shrubs above-ground carbon storage class. All Grass class areas were assigned as Herbaceous Vegetation. Above-ground carbon storage classes were amalgamated per analysis cell to calculate m^{-2} per class, with total above-ground carbon storage per cell calculated according to c kg m^{-2} extracted from the Leicester study (see **Table A5.1** for above-ground carbon storage values).

Table A5.1 – Above-ground carbon storage classes and values from Davies et al. (2011)

Class	***Class description***	***Land Ownership***	***Carbon Density (kg C m^2)***	***Averaged carbon storage value per class (kg C m^2)***
Herbaceous Vegetation	Near-to-ground Vegetation (i.e. Grass, Non-woody plants)	Mixed	0.14	0.145
		Public	0.15	
Shrub	Woody bushes and trees with mean height typically <2 m	Mixed	13.79	10.225
		Public	6.66	
Tall Shrub	Woody bushes and trees with mean height generally 2-5m	Mixed	12.35	14.19
		Public	16.03	
Tree	Trees > 5m tall	Mixed	28.06	28.46
		Public	28.86	

Above-ground carbon storage function indicators per analysis cell were calculated as the percentage of maximum possible above-ground carbon storage i.e. cell with 100% Tree class cover.

Bibliography

Acero, J. A., Arrizabalaga, J., Kupski, S., & Katzschner, L. (2013). Urban heat island in a coastal urban area in northern Spain. *Theoretical and applied climatology*, *113*(1-2), 137-154.

Aguilar, M. A., Agüera, F., Aguilar, F. J., & Carvajal, F. (2008). Geometric accuracy assessment of the orthorectification process from very high resolution satellite imagery for Common Agricultural Policy purposes. *International journal of remote sensing*, *29*(24), 7181-7197.

Aguilar, M. A., Saldaña, M. M., & Aguilar, F. J. (2013). GeoEye-1 and WorldView-2 pan-sharpened imagery for object-based classification in urban environments. *International Journal of Remote Sensing*, *34*(7), 2583-2606.

Aguirre-Gutiérrez, J., Seijmonsbergen, A. C., & Duivenvoorden, J. F. (2012). Optimizing landcover classification accuracy for change detection, a combined pixel-based and object-based approach in a mountainous area in Mexico. *Applied Geography*, *34*, 29-37.

Ahiablame, L., & Shakya, R. (2016). Modeling flood reduction effects of low impact development at a watershed scale. *Journal of environmental management*, *171*, 81-91.

Airbus (2020). Pléiades User Guide & SPOT 6/7 User Guide. Retrieved from: https://www.intelligence-airbusds.com/docs/9326-resource-centre#section-3672 (Accessed 09/04/2020)

Akbari, H., Pomerantz, M., & Taha, H. (2001). Cool surfaces and shade trees to reduce energy use and improve air quality in urban areas. *Solar energy*, *70*(3), 295-310.

Albert, C., Hauck, J., Buhr, N., & Von Haaren, C. (2014). What ecosystem services information do users want? Investigating interests and requirements among landscape and regional planners in Germany. *Landscape Ecology*, *29*(8), 1301-1313.

Alonzo, M., McFadden, J. P., Nowak, D. J., & Roberts, D. A. (2016). Mapping urban forest structure and function using hyperspectral imagery and lidar data. *Urban forestry & urban greening*, *17*, 135-147.

Alves, P. L., Formiga, K. T. M., & Traldi, M. A. B. (2018). Rainfall interception capacity of tree species used in urban afforestation. *Urban Ecosystems*, *21*(4), 697-706.

Amorim, J. H., Rodrigues, V., Tavares, R., Valente, J., & Borrego, C. (2013). CFD modelling of the aerodynamic effect of trees on urban air pollution dispersion. *Science of the Total Environment*, *461*, 541-551.

Andrew, M. E., Wulder, M. A., Nelson, T. A., & Coops, N. C. (2015). Spatial data, analysis approaches, and information needs for spatial ecosystem service assessments: a review. *GIScience & Remote Sensing*, *52*(3), 344-373.

Anderson, B. J., Armsworth, P. R., Eigenbrod, F., Thomas, C. D., Gillings, S., Heinemeyer, A. & Gaston, K. J. (2009). Spatial covariance between biodiversity and other ecosystem service priorities. *Journal of Applied Ecology*, *46*(4), 888-896.

Andersson, E., Barthel, S., Ahrné, K., (2007). Measuring social-ecological dynamics behind the generation of ecosystem services. Ecological Applications 17, 1267–1278.

Aronson, M. F., Lepczyk, C. A., Evans, K. L., Goddard, M. A., Lerman, S. B., MacIvor, J. S., Nilon, C. H. & Vargo, T. (2017). Biodiversity in the city: key challenges for urban green space management. *Frontiers in Ecology and the Environment*, *15*(4), 189-196.

Araos, M., Berrang-Ford, L., Ford, J. D., Austin, S. E., Biesbroek, R., & Lesnikowski, A. (2016). Climate change adaptation planning in large cities: a systematic global assessment. *Environmental Science & Policy*, *66*, 375-382.

de Araujo Barbosa, C. C., Atkinson, P. M., & Dearing, J. A. (2015). Remote sensing of ecosystem services: a systematic review. *Ecological Indicators*, *52*, 430-443.

Armson, D., Stringer, P., & Ennos, A. R. (2012). The effect of tree shade and grass on surface and globe temperatures in an urban area. *Urban Forestry & Urban Greening*, *11*(3), 245-255.

Armson, D., Stringer, P., & Ennos, A. R. (2013a). The effect of street trees and amenity grass on urban surface water runoff in Manchester, UK. *Urban Forestry & Urban Greening*, *12*(3), 282-286.

Armson, D., Rahman, M. A., & Ennos, A. R. (2013b). A comparison of the shading effectiveness of five different street tree species in Manchester, UK. *Arboriculture & Urban Forestry*, *39*(4), 157-164.

Arnbjerg-Nielsen, K., & Fleischer, H. S. (2009). Feasible adaptation strategies for increased risk of flooding in cities due to climate change. *Water Science and Technology*, *60*(2), 273-281.

Arnfield, A.J. (2003). Two decades of urban climate research: a review of turbulence, exchanges of energy and water, and the urban heat island. *International journal of climatology*, *23* (1), 1-26.

Aronson, M. F., Lepczyk, C. A., Evans, K. L., Goddard, M. A., Lerman, S. B., MacIvor, J. S., Nilon, C. H. & Vargo, T. (2017). Biodiversity in the city: key challenges for urban green space management. *Frontiers in Ecology and the Environment*, *15*(4), 189-196.

Asadian, Y., & Weiler, M. (2009). A new approach in measuring rainfall interception by urban trees in coastal British Columbia. *Water Quality Research Journal*, *44*(1), 16-25.

Ashley, R. M., Walker, A. L., D'Arcy, B., Wilson, S., Illman, S., Shaffer, P., & Chatfield, C. (2015). UK sustainable drainage systems: past, present and future. In *Proceedings of ICE-Civil Engineering* (Vol. 168, No. 3, pp. 125-130). Thomas Telford.

Aspinall, R. J., & Hill, M. (1997, August). Landcover change: a method for assessing the reliability of landcover changes measured from remotely-sensed data. In *IGARSS'97. 1997 IEEE International Geoscience and Remote Sensing Symposium Proceedings. Remote Sensing-A Scientific Vision for Sustainable Development* (Vol. 1, pp. 269-271). IEEE.

Attari, S. Z., Krantz, D. H., & Weber, E. U. (2019). Climate change communicators' carbon footprints affect their audience's policy support. *Climatic Change*, *154*(3-4), 529-545.

Azadi, H., Ho, P., Hafni, E., Zarafshani, K., & Witlox, F. (2011). Multi-stakeholder involvement and urban green space performance. *Journal of Environmental Planning and Management*, *54*(6), 785-811.

Azqueta, D., & Sotelsek, D. (2007). Valuing nature: From environmental impacts to natural capital. *Ecological economics*, *63*(1), 22-30.

Azevedo, J.A., Chapman, L. and Muller, C.L. (2016). Quantifying the daytime and night-time urban heat island in Birmingham, UK: A comparison of satellite derived land surface temperature and high resolution air temperature observations. *Remote Sensing*, *8* (2), 153.

Baker, F., & Smith, C. (2019). A GIS and object based image analysis approach to mapping the greenspace composition of domestic gardens in Leicester, UK. *Landscape and urban planning*, *183*, 133-146.

Baker, F., Smith, C., & Cavan, G. (2018). A combined approach to classifying land surface cover of urban domestic gardens using citizen science data and high resolution image analysis. *Remote Sensing*, *10*(4), 537.

Baker, M., Hincks, S., & Sherriff, G. (2010). Getting involved in plan making: participation and stakeholder involvement in local and regional spatial strategies in England. *Environment and Planning C: Government and Policy*, *28*(4), 574-594.

Ballestores Jr, F., & Qiu, Z. (2012). An integrated parcel-based land use change model using cellular automata and decision tree. *Proceedings of the International Academy of Ecology and Environmental Sciences*, *2*(2), 53.

Ballinas, M., & Barradas, V. L. (2016). The urban tree as a tool to mitigate the urban heat island in Mexico city: a simple phenomenological model. *Journal of environmental quality*, *45*(1), 157-166.

Barbier, E. B. (2007). Valuing ecosystem services as productive inputs. *Economic policy*, *22*(49), 178-229.

Baró, F., Palomo, I., Zulian, G., Vizcaino, P., Haase, D., & Gómez-Baggethun, E. (2016). Mapping ecosystem service capacity, flow and demand for landscape and urban planning: A case study in the Barcelona metropolitan region. *Land use policy*, *57*, 405-417.

Baró, F., Gómez-Baggethun, E., & Haase, D. (2017). Ecosystem service bundles along the urban-rural gradient: Insights for landscape planning and management. *Ecosystem Services*, *24*, 147-159.

Barsi, J. (2017). Atmospheric Correction Parameter Calculator. Retrieved from: https://atmcorr.gsfc.nasa.gov/ (Accessed 26/03/2020)

Bastian, O., Haase, D., & Grunewald, K. (2012). Ecosystem properties, potentials and services–The EPPS conceptual framework and an urban application example. *Ecological indicators*, *21*, 7-16.

Basuki, T. M., Van Laake, P. E., Skidmore, A. K., & Hussin, Y. A. (2009). Allometric equations for estimating the above-ground biomass in tropical lowland Dipterocarp forests. *Forest Ecology and Management*, *257*(8), 1684-1694.

Bateman, I.J., Harwood, A.R., Mace, G.M., Watson, R.T., Abson, D.J., Andrews, B., Binner, A., Crowe, A., Day, B.H., Dugdale, S. and Fezzi, C. (2013). Bringing ecosystem services into economic decision-making: land use in the United Kingdom. *science*, *341*(6141), 45-50.

Bauer, T., & Steinnocher, K. (2001). Per-parcel land use classification in urban areas applying a rule-based technique. *GeoBIT/GIS*, *6*, 24-27.

Beck, H. E., de Jeu, R. A., Schellekens, J., van Dijk, A. I., & Bruijnzeel, L. A. (2009). Improving curve number based storm runoff estimates using soil moisture proxies. *IEEE Journal of Selected Topics in Applied Earth Observations and Remote Sensing*, *2* (4), 250-259.

Berezowski, T., Chormański, J., Batelaan, O., Canters, F., & Van de Voorde, T. (2012). Impact of remotely sensed landcover proportions on urban runoff prediction. *International Journal of Applied Earth Observation and Geoinformation*, *16*, 54-65.

Berland, A., Shiflett, S. A., Shuster, W. D., Garmestani, A. S., Goddard, H. C., Herrmann, D. L., & Hopton, M. E. (2017). The role of trees in urban stormwater management. *Landscape and Urban Planning*, *162*, 167-177.

Beven, K.J. (2000). *Rainfall-runoff modelling: the primer*. John Wiley & Sons.

Bhaduri, B., Bright, E., Coleman, P., & Urban, M. L. (2007). LandScan USA: a high-resolution geospatial and temporal modeling approach for population distribution and dynamics. *GeoJournal*, *69*(1-2), 103-117.

Bibby, P., Henneberry, J., & Halleux, J. M. (2018). Under the radar? 'Soft'residential densification in England, 2001–2011. *Environment and Planning B: Urban Analytics and City Science*, 2399808318772842.

Bibby, P., Henneberry, J., & Halleux, J. M. (2020). Under the radar?'Soft'residential densification in England, 2001–2011. *Environment and Planning B: Urban Analytics and City Science*, *47*(1), 102-118.

Bivand, Roger S. and Wong, David W. S. (2018) Comparing implementations of global and local indicators of spatial association. Test, 27(3), 716-748

Bomans, K., Steenberghen, T., Dewaelheyns, V., Leinfelder, H., & Gulinck, H. (2010). Underrated transformations in the open space—The case of an urbanized and multifunctional area. *Landscape and urban planning*, *94*(3-4), 196-205.

Boonya-Aroonnet, S., Maksimovic, C., Prodanovic, D., & Djordjevic, S. (2007). Urban pluvial flooding: development of GIS based pathway model for surface flooding and interface with surcharged sewer model. *NOVATECH 2007*.

Borzacchiello, M. T., Nijkamp, P., & Koomen, E. (2010). Accessibility and urban development: a grid-based comparative statistical analysis of Dutch cities. *Environment and Planning B: Planning and Design*, *37*(1), 148-169.

Brack, C. L. (2002). Pollution mitigation and carbon sequestration by an urban forest. *Environmental pollution*, *116*, S195-S200.

Breiman, L. (2001). Random forests. *Machine learning*, *45*(1), 5-32.

BBC [British Broadcasting Service] (29th July 2019a). Heavy rain causes travel disruption in North West. Online news article retrieved from: https://www.bbc.co.uk/news/uk-england-manchester-49149281 (Accessed 03/05/2020)

BBC [British Broadcasting Service] (27th June 2019b). *Blackpool street trees cost £10k each, council admits*. Retrieved from https://www.bbc.co.uk/news/uk-england-lancashire-48790943 (Accessed 16/03/2020)

Broadbent, A. M., Coutts, A. M., Tapper, N. J., & Demuzere, M. (2018). The cooling effect of irrigation on urban microclimate during heatwave conditions. *Urban climate*, *23*, 309-329.

Burkhard, B., Kroll, F., Nedkov, S., & Müller, F. (2012). Mapping ecosystem service supply, demand and budgets. *Ecological indicators*, *21*, 17-29.

Cabral, P., Feger, C., Levrel, H., Chambolle, M., & Basque, D. (2016). Assessing the impact of landcover changes on ecosystem services: A first step toward integrative planning in Bordeaux, France. *Ecosystem Services*, *22*, 318-327.

Cai, M., Ren, C., Xu, Y., Lau, K. K. L., & Wang, R. (2018). Investigating the relationship between local climate zone and land surface temperature using an improved WUDAPT methodology–A case study of Yangtze River Delta, China. *Urban Climate*, *24*, 485-502.

Carter, J. G., Cavan, G., Connelly, A., Guy, S., Handley, J., & Kazmierczak, A. (2015). Climate change and the city: Building capacity for urban adaptation. *Progress in planning*, *95*, 1-66.

Cavan, G. (2011). Climate change projections for Greater Manchester. *EcoCities project, University of Manchester, Manchester, UK*.

Cavan, G., & Kazmierczak, A. (2011). Urban greening to adapt urban areas to climate change: The Oxford Road Corridor Case Study. *EcoCities project, The University of Manchester, Manchester, UK*.

Cavan G., Lindley S., Jalayer F., Yeshitela K., Pauleit S., Renner, F. & Kibassa, D. (2014). Urban morphological determinants of temperature regulating ecosystem services in two African cities. *Ecological indicators*, *42*, 43-57.

Cavan, G., Smith, C., Tzoulas, K., Baker, F., & Barlow, D. (2018). My Back Yard: An Action Plan. Retrieved from mybackyard.org.uk/docs/mby-actionplan.pdf (Accessed 16/03/2020)

Centre for Cities (2021). City Monitor. Retrieved from: https://www.centreforcities.org/city-monitor/ (Accessed 06/02/2021)

Chen, X., Chen, J., Shi, Y., & Yamaguchi, Y. (2012). An automated approach for updating landcover maps based on integrated change detection and classification methods. *ISPRS Journal of Photogrammetry and Remote Sensing*, *71*, 86-95.

Chen, A., Yao, X.A., Sun, R. and Chen, L. (2014a). Effect of urban green patterns on surface urban cool islands and its seasonal variations. *Urban forestry & urban greening*, *13* (4), 646-654.

Chen, A., Yao, L., Sun, R., & Chen, L. (2014b). How many metrics are required to identify the effects of the landscape pattern on land surface temperature?. *Ecological indicators*, *45*, 424-433.

Chen, B., Nie, Z., Chen, Z., & Xu, B. (2017). Quantitative estimation of 21st-century urban greenspace changes in Chinese populous cities. *Science of the Total Environment*, *609*, 956-965.

Cheng, K.S., Su, Y.F., Kuo, F.T., Hung, W.C. and Chiang, J.L. (2008). Assessing the effect of landcover changes on air temperature using remote sensing images—A pilot study in northern Taiwan. *Landscape and Urban Planning*, *85* (2), 85-96.

Cheng, X., Wei, B., Chen, G., Li, J., & Song, C. (2015). Influence of park size and its surrounding urban landscape patterns on the park cooling effect. *Journal of Urban Planning and Development*, *141*(3), A4014002.

Choi, K. S., & Ball, J. E. (2002). Parameter estimation for urban runoff modelling. *Urban water*, *4*(1), 31-41.

Chormanski, J., Van de Voorde, T., De Roeck, T., Batelaan, O., & Canters, F. (2008). Improving distributed runoff prediction in urbanized catchments with remote sensing based estimates of impervious surface cover. *Sensors*, *8*(2), 910-932.

Chuvieco, E. (2016). *Fundamentals of satellite remote sensing: An environmental approach*. CRC press.

City Of Trees (2011) Greater Manchester Tree Audit [computer file]. (Manchester, UK). Retrieved through personal communication, 2011.

City Of Trees (2018) Greater Manchester i-tree sample data [computer file]. (Manchester, UK). Retrieved through personal communication, 2018.

City of Trees (2020). About City of Trees. Retrieved from https://www.cityoftrees.org.uk/about-city-trees (Accessed 02/02/2020)

CityCo (2020). *Property Developments Map: Tracking city growth.* Retrieved from https://cityco.com/manchester-development-map/ (Accessed 16/03/2020)

Cohen, P., Potchter, O., & Schnell, I. (2014). The impact of an urban park on air pollution and noise levels in the Mediterranean city of Tel-Aviv, Israel. *Environmental Pollution*, *195*, 73-83.

Coles, J. (2019). What Sheffield felling investigation means for the future. Woodland Trust website. Retrieved from: https://www.woodlandtrust.org.uk/blog/2019/08/sheffield-felling-investigation/ (Accessed 06/02/2021)

Comber, A., Fisher, P., & Wadsworth, R. (2004). Assessment of a semantic statistical approach to detecting landcover change using inconsistent data sets. *Photogrammetric Engineering & Remote Sensing*, *70*(8), 931-938.

Comber, A., Brunsdon, C., & Green, E. (2008). Using a GIS-based network analysis to determine urban greenspace accessibility for different ethnic and religious groups. *Landscape and urban planning*, *86*(1), 103-114.

Comber, A. J., Brunsdon, C., & Radburn, R. (2011). A spatial analysis of variations in health access: linking geography, socio-economic status and access perceptions. *International journal of health geographics*, *10*(1), 44.

Comber, A., See, L., Fritz, S., Van der Velde, M., Perger, C., & Foody, G. (2013). Using control data to determine the reliability of volunteered geographic information about landcover. *International Journal of Applied Earth Observation and Geoinformation*, *23*, 37-48.

Congalton, R. G., & Green, K. (2008). *Assessing the accuracy of remotely sensed data: principles and practices*. CRC press.

Copernicus Land Monitoring Service (2020a). CORINE Landcover. Retrieved from https://land.copernicus.eu/pan-european/corine-landcover (Accessed 22/06/2020)

Copernicus Land Monitoring Service (2020b). Urban Atlas. Retrieved from https://land.copernicus.eu/local/urban-atlas (Accessed 22/06/2020)

Coppin, P., Jonckheere, I., Nackaerts, K., Muys, B., & Lambin, E. (2004). Review ArticleDigital change detection methods in ecosystem monitoring: a review. *International journal of remote sensing*, *25*(9), 1565-1596.

Cortinovis, C., & Geneletti, D. (2018). Ecosystem services in urban plans: What is there, and what is still needed for better decisions. *Land use policy*, *70*, 298-312.

Coseo, P., & Larsen, L. (2014). How factors of land use/landcover, building configuration, and adjacent heat sources and sinks explain Urban Heat Islands in Chicago. *Landscape and Urban Planning*, *125*, 117-129.

Costanza, R., d'Arge, R., De Groot, R., Farber, S., Grasso, M., Hannon, B., Limburg, K., Naeem, S., O'neill, R.V., Paruelo, J. & Raskin, R. G. (1997). The value of the world's ecosystem services and natural capital. *nature*, *387*(6630), 253-260.

Coutts, A. M., Tapper, N. J., Beringer, J., Loughnan, M., & Demuzere, M. (2013). Watering our cities: The capacity for Water Sensitive Urban Design to support urban cooling and improve human thermal comfort in the Australian context. *Progress in Physical Geography*, *37*(1), 2-28.

Cranfield University (2018). LandIS – Land Information System [Data download]. Retrieved from http://www.landis.org.uk/ (Accessed 26/03/2018)

Cruickshank, M. M., Tomlinson, R. W., Devine, P. M., & Milne, R. (1998, August). Carbon in the vegetation and soils of Northern Ireland. In *Biology and Environment: Proceedings of the Royal Irish Academy* (pp. 9-21). Royal Irish Academy.

Cui, Y. Y., & De Foy, B. (2012). Seasonal variations of the urban heat island at the surface and the near-surface and reductions due to urban vegetation in Mexico City. *Journal of Applied Meteorology and Climatology*, *51*(5), 855-868.

Cunniff, J., Purdy, S. J., Barraclough, T. J., Castle, M., Maddison, A. L., Jones, L. E., & Karp, A. (2015). High yielding biomass genotypes of willow (Salix spp.) show differences in below ground biomass allocation. *biomass and bioenergy*, *80*, 114-127.

Cuo, L., Lettenmaier, D. P., Mattheussen, B. V., Storck, P., & Wiley, M. (2008). Hydrologic prediction for urban watersheds with the Distributed Hydrology–Soil–Vegetation Model. *Hydrological Processes*, *22*(21), 4205-4213.

Daily, G. C., Polasky, S., Goldstein, J., Kareiva, P. M., Mooney, H. A., Pejchar, L., & Shallenberger, R. (2009). Ecosystem services in decision making: time to deliver. *Frontiers in Ecology and the Environment*, *7*(1), 21-28.

Dallimer, M., Tang, Z., Bibby, P. R., Brindley, P., Gaston, K. J., & Davies, Z. G. (2011). Temporal changes in greenspace in a highly urbanized region. *Biology Letters*, *7*(5), 763-766.

Davies, Z. G., Edmondson, J. L., Heinemeyer, A., Leake, J. R., & Gaston, K. J. (2011). Mapping an urban ecosystem service: quantifying above-ground carbon storage at a city-wide scale. *Journal of applied ecology*, *48*(5), 1125-1134.

De Groot, R. S., Alkemade, R., Braat, L., Hein, L., & Willemen, L. (2010). Challenges in integrating the concept of ecosystem services and values in landscape planning, management and decision making. *Ecological complexity*, *7*(3), 260-272.

De Groot, R., Brander, L., Van Der Ploeg, S., Costanza, R., Bernard, F., Braat, L. & Hussain, S. (2012). Global estimates of the value of ecosystems and their services in monetary units. *Ecosystem services*, *1*(1), 50-61.

De Ridder, K., Lauwaet, D. and Maiheu, B., (2015). UrbClim–A fast urban boundary layer climate model. *Urban Climate*, *12*, pp.21-48.

De Risi, R., Jalayer, F., & De Paola, F. (2015). Meso-scale hazard zoning of potentially flood prone areas. *Journal of Hydrology*, *527*, 316-325.

Deilami, K., Kamruzzaman, M., & Liu, Y. (2018). Urban heat island effect: A systematic review of spatio-temporal factors, data, methods, and mitigation measures. *International journal of applied earth observation and geoinformation*, *67*, 30-42.

Demir, Osman, and Yakup Emre Çoruhlu (2009). "Determining the property ownership on cadastral works in Turkey." *Land use policy* 26(1), 112-120.

Dennis, M., Barlow, D., Cavan, G., Cook, P. A., Gilchrist, A., Handley, J. & Lindley, S. (2018). Mapping urban green infrastructure: A novel landscape-based approach to incorporating land use and landcover in the mapping of human-dominated systems. *Land*, *7*(1), 17.

DEFRA [Department of Environment Food & Rural Affairs] (2020). Enabling a Natural Capital Approach: Guidance. Retrieved from https://assets.publishing.service.gov.uk/government/uploads/system/uploads/attachment_data/file/869801/natural-capital-enca-guidance_2_March.pdf (Accessed 27/10/2020)

Derkzen, M. L., van Teeffelen, A. J., & Verburg, P. H. (2015). Quantifying urban ecosystem services based on high-resolution data of urban green space: an assessment for Rotterdam, the Netherlands. *Journal of Applied Ecology*, *52*(4), 1020-1032.

Dewaelheyns, V., Kerselaers, E., & Rogge, E. (2016). A toolbox for garden governance. *Land Use Policy*, *51*, 191-205.

Di Salvo, C., Pennica, F., Ciotoli, G., & Cavinato, G. P. (2018). A GIS-based procedure for preliminary mapping of pluvial flood risk at metropolitan scale. *Environmental modelling & software*, *107*, 64-84.

Diaz-Pacheco, J., & Gutiérrez, J. (2014). Exploring the limitations of CORINE Landcover for monitoring urban land-use dynamics in metropolitan areas. *Journal of Land Use Science*, *9*(3), 243-259.

van Dijk, E., van der Meulen, J., Kluck, J., & Straatman, J.H.M. (2014). Comparing modelling techniques for analysing urban pluvial flooding. *Water science and technology*, *69*(2), 305-311.

Dimoudi, A., & Nikolopoulou, M. (2003). Vegetation in the urban environment: microclimatic analysis and benefits. *Energy and buildings*, *35*(1), 69-76.

Dixon, B., & Earls, J. (2012). Effects of urbanization on streamflow using SWAT with real and simulated meteorological data. *Applied Geography*, *35*(1-2), 174-190.

Dobbs, C., Hernández-Moreno, Á., Reyes-Paecke, S., & Miranda, M. D. (2018). Exploring temporal dynamics of urban ecosystem services in Latin America: The case of Bogota (Colombia) and Santiago (Chile). *Ecological indicators*, *85*, 1068-1080.

Doick, K. J., Peace, A., & Hutchings, T. R. (2014). The role of one large greenspace in mitigating London's nocturnal urban heat island. *Science of the Total Environment*, *493*, 662-671.

Dominati, E., Patterson, M., & Mackay, A. (2010). A framework for classifying and quantifying the natural capital and ecosystem services of soils. *Ecological economics*, *69*(9), 1858-1868.

Dousset, B., Gourmelon, F., Laaidi, K., Zeghnoun, A., Giraudet, E., Bretin, P. & Vandentorren, S. (2011). Satellite monitoring of summer heat waves in the Paris metropolitan area. *International Journal of Climatology*, *31*(2), 313-323.

Dowson, M., Poole, A., Harrison, D., & Susman, G. (2012). Domestic UK retrofit challenge: Barriers, incentives and current performance leading into the Green Deal. *Energy Policy*, *50*, 294-305.

Dugord, P. A., Lauf, S., Schuster, C., & Kleinschmit, B. (2014). Land use patterns, temperature distribution, and potential heat stress risk–the case study Berlin, Germany. *Computers, Environment and Urban Systems*, *48*, 86-98.

Duque, L., Relvas, H., Silveira, C., Ferreira, J., Monteiro, A., Gama, C., & Miranda, A. I. (2016). Evaluating strategies to reduce urban air pollution. *Atmospheric Environment*, *127*, 196-204.

Dunnett, N., & Clayden, A. (2007). Rain gardens. *Managing water sustainably in the garden and designed landscape*. Timber press.

EFTEC [Economics for the Environment Consultancy] (2018). Natural Capital Account for Greater Manchester. Retrieved from https://naturegreatermanchester.co.uk/wp-content/uploads/2018/06/NCA-for-GM-Final-Report-270618.pdf (Accessed 28/10/2020)

Edina Digimap (2017). Ordnance Survey Mastermap Topography Layer [data download]. Retrieved from https://digimap.edina.ac.uk/ (Accessed 17/06/2017)

Edina (2020). Digimap Service: Ordnance Survey. Retrieved from https://digimap.edina.ac.uk/os (Accessed 01/05/2020)

Edmondson, J. L., Davies, Z. G., McCormack, S. A., Gaston, K. J., & Leake, J. R. (2014). Land-cover effects on soil organic carbon stocks in a European city. *Science of the total Environment*, *472*, 444-453.

Eigenbrod, F., Armsworth, P. R., Anderson, B. J., Heinemeyer, A., Gillings, S., Roy, D. B., & Gaston, K. J. (2010). The impact of proxy-based methods on mapping the distribution of ecosystem Services. *Journal of Applied Ecology*, *47*(2), 377-385.

Eli, R. N., & Lamont, S. J. (2010). Curve numbers and urban runoff modeling—Application limitations. In *Low Impact Development 2010: Redefining Water in the City* (pp. 405-418).

Eliasson, I., & Svensson, M. K. (2003). Spatial air temperature variations and urban land use-a statistical approach. *Meteorological Applications*, *10*(2), 135-149.

Elmqvist, T., Setälä, H., Handel, S. N., Van Der Ploeg, S., Aronson, J., Blignaut, J. N., Gomez-Baggethun, E., Nowak, D.J., Kronenberg, J. & De Groot, R. (2015). Benefits of restoring ecosystem services in urban areas. *Current opinion in environmental sustainability*, *14*, 101-108.

Emmanuel, R. and Krüger, E. (2012). Urban heat island and its impact on climate change resilience in a shrinking city: The case of Glasgow, UK. *Building and Environment*, *53*, 137-149.

EA [Environment Agency] (2018). What is the Risk of Flooding from Surface Water map? [Data download] Retrieved from https://assets.publishing.service.gov.uk/government/uploads/system/uploads/attachment_data/file/842485/What-is-the-Risk-of-Flooding-from-Surface-Water-Map.pdf (Accessed 09/04/2018)

ESA [European Space Agency] (2018). Open Access at the European Space Agency. Retrieved from http://open.esa.int/ (Accessed 12/03/2018)

Eftec [Economics for the Environment Consultancy] (2018). Natural Capital Account for Greater Manchester. Retrieved from: https://naturegreatermanchester.co.uk/wp-content/uploads/2018/06/NCA-for-GM-Final-Report-270618.pdf (Accessed 07/02/2021)

Escobedo, F. J., & Nowak, D. J. (2009). Spatial heterogeneity and air pollution removal by an urban forest. *Landscape and urban planning*, *90*(3-4), 102-110.

Escobedo, F. J., Kroeger, T., & Wagner, J. E. (2011). Urban forests and pollution mitigation: Analyzing ecosystem services and disservices. *Environmental pollution*, *159*(8-9), 2078-2087.

ESRI (2020). Esri CityEngine. Retrieved from https://www.esri.com/en-us/arcgis/products/esri-cityengine/overview (Accessed 16//03/2020)

Estoque, R. C., & Murayama, Y. (2012). Examining the potential impact of land use/cover changes on the ecosystem services of Baguio city, the Philippines: a scenario-based analysis. *Applied Geography*, *35*(1-2), 316-326.

Falcucci, A., Maiorano, L., & Boitani, L. (2007). Changes in land-use/land-cover patterns in Italy and their implications for biodiversity conservation. *Landscape ecology*, *22*(4), 617-631.

Fan, Y., & Van den Dool, H. (2008). A global monthly land surface air temperature analysis for 1948–present. *Journal of Geophysical Research: Atmospheres*, *113*(D1).

Fang, C. F., & Ling, D. L. (2003). Investigation of the noise reduction provided by tree belts. *Landscape and urban planning*, *63*(4), 187-195.

Ferreira, L. S., & Duarte, D. H. S. (2019). Exploring the relationship between urban form, land surface temperature and vegetation indices in a subtropical megacity. *Urban Climate*, *27*, 105-123.

Ferreira, C. S. S., Walsh, R. P. D., Steenhuis, T. S., Shakesby, R. A., Nunes, J. P. N., Coelho, C. O. A., & Ferreira, A. J. D. (2015). Spatiotemporal variability of hydrologic soil properties and the implications for overland flow and land management in a peri-urban Mediterranean catchment. *Journal of Hydrology*, *525*, 249-263.

Fiedler, P. E. K., & Zannin, P. H. T. (2015). Evaluation of noise pollution in urban traffic hubs—Noise maps and measurements. *Environmental Impact Assessment Review*, *51*, 1-9.

Fisher, P. F., Comber, A. J., & Wadsworth, R. (2005). Land use and landcover: contradiction or complement. *Re-presenting GIS*, 85-98.

Fisher, B., Turner, R. K., & Morling, P. (2009). Defining and classifying ecosystem services for decision making. *Ecological economics*, *68*(3), 643-653.

Foody, G. M. (2015). Valuing map validation: The need for rigorous landcover map accuracy assessment in economic valuations of ecosystem services. *Ecological Economics*, *111*, 23-28.

Fouillet, A., Rey, G., Laurent, F., Pavillon, G., Bellec, S., Guihenneuc-Jouyaux, C., & Hémon, D. (2006). Excess mortality related to the August 2003 heat wave in France. *International archives of occupational and environmental health*, *80*(1), 16-24.

Fowler, H. J., & Kilsby, C. G. (2003). A regional frequency analysis of United Kingdom extreme rainfall from 1961 to 2000. *International Journal of Climatology: A Journal of the Royal Meteorological Society*, *23*(11), 1313-1334.

Franczyk, J., & Chang, H. (2009). The effects of climate change and urbanization on the runoff of the Rock Creek basin in the Portland metropolitan area, Oregon, USA. *Hydrological Processes*, *23*(6), 805-815.

Fu, B. J., Su, C. H., Wei, Y. P., Willett, I. R., Lü, Y. H., & Liu, G. H. (2011). Double counting in ecosystem services valuation: causes and countermeasures. *Ecological research*, *26*(1), 1-14.

Fuller, R. M., Smith, G. M., & Devereux, B. J. (2003). The characterisation and measurement of landcover change through remote sensing: problems in operational applications?. *International Journal of Applied Earth Observation and Geoinformation*, *4*(3), 243-253.

Fuchs, R., Herold, M., Verburg, P. H., Clevers, J. G., & Eberle, J. (2015). Gross changes in reconstructions of historic landcover/use for Europe between 1900 and 2010. *Global change biology*, *21*(1), 299-313.

Garen, D. C., & Moore, D. S. (2005). Curve number hydrology in water quality modeling: Uses, abuses, and future directions 1. *JAWRA Journal of the American Water Resources Association*, *41*(2), 377-388.

Gauthier, S., Bernier, P., Kuuluvainen, T., Shvidenko, A. Z., & Schepaschenko, D. G. (2015). Boreal forest health and global change. *Science*, *349*(6250), 819-822.

Geletič, J., Lehnert, M., & Dobrovolný, P. (2016). Land surface temperature differences within local climate zones, based on two central European cities. *Remote Sensing*, *8*(10), 788.

Genuer, R., Poggi, J. M., & Tuleau-Malot, C. (2018). VSURF: an R package for variable selection using random forests.

Georgescu, M., Morefield, P. E., Bierwagen, B. G., & Weaver, C. P. (2014). Urban adaptation can roll back warming of emerging megapolitan regions. *Proceedings of the National Academy of Sciences*, *111*(8), 2909-2914.

Getmapping, Aerial Data (2017) High Resolution Imagery [Data download]. Retrieved from http://www.getmapping.com/products-and-services/aerial-imagery-data/aerial-data-high-resolution imagery (Accessed 29/03/2017)

Getmapping (2019) Aerial Data—High Resolution Imagery [Data download]. Retrieved from: http://www.getmapping.com/products-and-services/aerial-imagery-data/aerial-data-high-resolution-imagery (Accessed 29/05/2019).

Gidlöf-Gunnarsson, A., & Öhrström, E. (2007). Noise and well-being in urban residential environments: The potential role of perceived availability to nearby green areas. *Landscape and urban planning*, *83*(2-3), 115-126.

Gill, S. E., Handley, J. F., Ennos, A. R., & Pauleit, S. (2007). Adapting cities for climate change: the role of the green infrastructure. *Built environment*, *33*(1), 115-133.

Gill, S. E., Handley, J. F., Ennos, A. R., Pauleit, S., Theuray, N., & Lindley, S. J. (2008). Characterising the urban environment of UK cities and towns: A template for landscape planning. *Landscape and urban planning*, *87*(3), 210-222.

Goddard, M. A., Dougill, A. J., & Benton, T. G. (2010). Scaling up from gardens: biodiversity conservation in urban environments. *Trends in ecology & evolution*, *25*(2), 90-98.

Goldstein, B. A., Polley, E. C., & Briggs, F. B. (2011). Random forests for genetic association studies. *Statistical applications in genetics and molecular biology*, *10*(1).

Gómez-Baggethun, E., De Groot, R., Lomas, P. L., & Montes, C. (2010). The history of ecosystem services in economic theory and practice: from early notions to markets and payment schemes. *Ecological economics*, *69*(6), 1209-1218.

Gómez-Baggethun, E., & Barton, D. N. (2013). Classifying and valuing ecosystem services for urban planning. *Ecological economics*, *86*, 235-245.

Grafius, D. R., Corstanje, R., Warren, P. H., Evans, K. L., Hancock, S., & Harris, J. A. (2016). The impact of land use/landcover scale on modelling urban ecosystem services. *Landscape Ecology*, *31*(7), 1509-1522.

Grafius, D. R., Corstanje, R., & Harris, J. A. (2018). Linking ecosystem services, urban form and green space configuration using multivariate landscape metric analysis. *Landscape ecology*, *33*(4), 557-573.

Grêt-Regamey, A., Celio, E., Klein, T. M., & Hayek, U. W. (2013). Understanding ecosystem services trade-offs with interactive procedural modeling for sustainable urban planning. *Landscape and Urban Planning*, *109*(1), 107-116.

GLA [Greater London Authority] (2018). London Environment Strategy. Retrieved from: https://www.london.gov.uk/sites/default/files/london_environment_strategy_0.pdf (Accessed 29/10/2020)

GMCA [Greater Manchester Combined Authority] (2019). 5-Year Environment Plan for Greater Manchester: 2019 – 2024. Retrieved from https://www.greatermanchester-ca.gov.uk/media/1986/5-year-plan-branded_3.pdf (Accessed 02/01/2021)

GMCA [Greater Manchester Combined Authority] (2020a). *Ignition project aims to develop innovative solutions for Greater Manchester's natural environment*. Retrieved from https://www.greatermanchester-ca.gov.uk/what-we-do/environment/ignition/ (Accessed 16/03/2020)

GMCA [Greater Manchester Combined Authority] (2020b). *MappingGM*. Retrieved from https://mappinggm.org.uk/ (Accessed 16/03/2020)

GMGC [Greater Manchester Green City] (2020). *GrowGreen: Greater Manchester is getting greener!* Retrieved from http://gmgreencity.com/article/growgreen-greater-manchester-getting-greener (Accessed 16/03/2020)

GreenBlue Urban (2018). Street Tree Cost Benefit Analysis. Retrieved from https://www.treeconomics.co.uk/wp-content/uploads/2018/08/GBU_Street-Tree-Cost-Benefit-Analysis-2018.pdf (Accessed 16/03/2020)

Griffiths, P., Hostert, P., Gruebner, O., & van der Linden, S. (2010). Mapping megacity growth with multi-sensor data. *Remote Sensing of Environment*, *114*(2), 426-439.

Grimmond, S. (2007). Urbanization and global environmental change: local effects of urban warming. *The Geographical Journal*, *173*(1), 83-88.

Grippa, T., Georganos, S., Zarougui, S., Bognounou, P., Diboulo, E., Forget, Y., Lennert, M., Vanhuysse, S., Mboga, N. & Wolff, E. (2018). Mapping urban land use at street block level using openstreetmap, remote sensing data, and spatial metrics. *ISPRS International Journal of Geo-Information*, *7*(7), 246.

Groundwork (2020). Ignition: Nature Based Solutions for Greater Manchester. Retrieved from: https://www.groundwork.org.uk/projects/ignition-nature-based-solutions-for-greater-manchester/?hub=97 (Accessed 14/05/20)

Guerreiro, S. B., Glenis, V., Dawson, R. J., & Kilsby, C. (2017). Pluvial flooding in European cities—A continental approach to urban flood modelling. *Water*, *9*(4), 296.

Guerry, A.D., Polasky, S., Lubchenco, J., Chaplin-Kramer, R., Daily, G.C., Griffin, R., Ruckelshaus, M., Bateman, I.J., Duraiappah, A., Elmqvist, T. and Feldman, M.W. (2015). Natural capital and ecosystem services informing decisions: From promise to practice. *Proceedings of the National Academy of Sciences*, *112*(24), 7348-7355.

Guevara-Escobar, A., González-Sosa, E., Véliz-Chávez, C., Ventura-Ramos, E., & Ramos-Salinas, M. (2007). Rainfall interception and distribution patterns of gross precipitation around an isolated Ficus benjamina tree in an urban area. *Journal of Hydrology*, *333*(2-4), 532-541.

Guo, G., Wu, Z., Xiao, R., Chen, Y., Liu, X. and Zhang, X., (2015). Impacts of urban biophysical composition on land surface temperature in urban heat island clusters. *Landscape and Urban Planning*, *135*, pp.1-10.

Haaland, C., & van Den Bosch, C. K. (2015). Challenges and strategies for urban green-space planning in cities undergoing densification: A review. *Urban forestry & urban greening*, *14*(4), 760-771.

Haas, J., & Ban, Y. (2018). Urban landcover and ecosystem service changes based on Sentinel-2A MSI and Landsat TM Data. *IEEE Journal of Selected Topics in Applied Earth Observations and Remote Sensing*, *11*(2), 485-497.

Haase, D., Larondelle, N., Andersson, E., Artmann, M., Borgström, S., Breuste, J., & Kabisch, N. (2014). A quantitative review of urban ecosystem service assessments: concepts, models, and implementation. *Ambio*, *43*(4), 413-433.

Hajat, S., Kovats, R. S., Atkinson, R. W., & Haines, A. (2002). Impact of hot temperatures on death in London: a time series approach. *Journal of Epidemiology & Community Health*, *56*(5), 367-372.

Hajat, S., Kovats, R. S., & Lachowycz, K. (2007). Heat-related and cold-related deaths in England and Wales: who is at risk?. *Occupational and environmental medicine*, *64*(2), 93-100.

Haklay, M., & Weber, P. (2008). Openstreetmap: User-generated street maps. *IEEE Pervasive Computing*, *7*(4), 12-18.

Hall, J. M., Handley, J. F., & Ennos, A. R. (2012). The potential of tree planting to climate-proof high density residential areas in Manchester, UK. *Landscape and Urban Planning*, *104*(3-4), 410-417.

Hamada, S., & Ohta, T. (2010). Seasonal variations in the cooling effect of urban green areas on surrounding urban areas. *Urban forestry & urban greening*, *9*(1), 15-24.

Hamin, E. M., & Gurran, N. (2009). Urban form and climate change: Balancing adaptation and mitigation in the US and Australia. *Habitat international*, *33*(3), 238-245.

Hammond, M. J., Chen, A. S., Djordjević, S., Butler, D., & Mark, O. (2015). Urban flood impact assessment: A state-of-the-art review. *Urban Water Journal*, *12*(1), 14-29.

Hankin, B., Waller, S., Astle, G., & Kellagher, R. (2008). Mapping space for water: screening for urban flash flooding. *Journal of Flood Risk Management*, *1*(1), 13-22.

Harlan, S. L., Brazel, A. J., Prashad, L., Stefanov, W. L., & Larsen, L. (2006). Neighborhood microclimates and vulnerability to heat stress. *Social science & medicine*, *63*(11), 2847-2863.

Harris, R., & Jarvis, C. (2014). *Statistics for geography and environmental science*. Routledge.

Harrison, A. R. (2006). National land use database: land use and landcover classification. *Office of the Deputy Prime Minister, Ed*.

Hathway, E. A., & Sharples, S. (2012). The interaction of rivers and urban form in mitigating the Urban Heat Island effect: A UK case study. *Building and Environment*, *58*, 14-22.

Hatvani-Kovacs, G., & Boland, J. (2015). Retrofitting precincts for heatwave resilience: Challenges and barriers in Australian context. *Challenges*, *6*(1), 3-25.

Hawkins, B. A., Diniz-Filho, J. A. F., Mauricio Bini, L., De Marco, P., & Blackburn, T. M. (2007). Red herrings revisited: spatial autocorrelation and parameter estimation in geographical ecology. *Ecography*, *30*(3), 375-384.

Hein, L., Bagstad, K., Edens, B., Obst, C., de Jong, R., & Lesschen, J. P. (2016). Defining ecosystem assets for natural capital accounting. *PloS one*, *11*(11), e0164460.

Henke, J. M., & Petropoulos, G. P. (2013). A GIS-based exploration of the relationships between human health, social deprivation and ecosystem services: the case of Wales, UK. *Applied Geography*, *45*, 77-88.

Hernández-Morcillo, M., Plieninger, T., & Bieling, C. (2013). An empirical review of cultural ecosystem service indicators. *Ecological indicators*, *29*, 434-444.

HSE [Health and Safety Executive] (2020). National Population Dataset. Retrieved from https://www.hsl.gov.uk/what-we-do/data-analytics/national-population-database (Accessed 09/04/2020)

Heaviside, C., Vardoulakis, S., & Cai, X. M. (2016). Attribution of mortality to the urban heat island during heatwaves in the West Midlands, UK. *Environmental health*, *15*(1), S27.

Henits, L., Jürgens, C., & Mucsi, L. (2016). Seasonal multitemporal landcover classification and change detection analysis of Bochum, Germany, using multitemporal Landsat TM data. *International Journal of Remote Sensing*, *37*(15), 3439-3454.

Hermosilla, T., Ruiz, L. A., Recio, J. A., & Cambra-López, M. (2012). Assessing contextual descriptive features for plot-based classification of urban areas. *Landscape and Urban Planning*, *106*(1), 124-137.

Hernández-Morcillo, M., Plieninger, T., & Bieling, C. (2013). An empirical review of cultural ecosystem service indicators. *Ecological indicators*, *29*, 434-444.

Herzog, H., & Golomb, D. (2004). Carbon capture and storage from fossil fuel use. *Encyclopedia of energy*, *1*(6562), 277-287.

Hester, D. B., Nelson, S. A. C., Cakir, H. I., Khorram, S., & Cheshire, H. (2010). High-resolution landcover change detection based on fuzzy uncertainty analysis and change reasoning. *International Journal of Remote Sensing*, *31*(2), 455-475.

Hijmans, R. J. (2020). raster: Geographic Data Analysis and Modeling. R package version 3.3-13. https://CRAN.R-project.org/package=raster

Hill, R. A., Wilson, A. K., George, M., & Hinsley, S. A. (2010). Mapping tree species in temperate deciduous woodland using time-series multi-spectral data. *Applied Vegetation Science*, *13*(1), 86-99.

Hoang, L., & Fenner, R. A. (2016). System interactions of stormwater management using sustainable urban drainage systems and green infrastructure. *Urban Water Journal*, *13*(7), 739-758.

Holt, A. R., Mears, M., Maltby, L., & Warren, P. (2015). Understanding spatial patterns in the production of multiple urban ecosystem services. *Ecosystem services*, *16*, 33-46.

Hostetler, M., Allen, W., & Meurk, C. (2011). Conserving urban biodiversity? Creating green infrastructure is only the first step. *Landscape and Urban Planning*, *100*(4), 369-371.

Houston, D, Werritty, A., Bassett, D., Geddes, A., Hoolachan, A., & McMillan, M. (2011). Pluvial(rain-related) flooding in urban areas: the invisible hazard. York: Joseph Rowntree Foundation;. Retrieved from https://eprints.gla.ac.uk/162145/7/162145.pdf (Accessed 11/11/2020)

HSE [Health and Safety Executive] (2020). The National Population Database. Retrieved from: https://www.hsl.gov.uk/what-we-do/data-analytics/national-population-database (Accessed 07/02/2020)

Huang, B. F., & Boutros, P. C. (2016). The parameter sensitivity of random forests. *BMC bioinformatics*, *17*(1), 331.

Huang, H., Chen, Y., Clinton, N., Wang, J., Wang, X., Liu, C., Gong, P., Yang, J., Bai, Y., Zheng, Y., & Zhu, Z. (2017). Mapping major landcover dynamics in Beijing using all Landsat images in Google Earth Engine. *Remote Sensing of Environment*, *202*, 166-176.

Huang, X., & Zhang, L. (2013). An SVM ensemble approach combining spectral, structural, and semantic features for the classification of high-resolution remotely sensed imagery. *IEEE transactions on geoscience and remote sensing*, *51*(1), 257-272.

Hussain, M., Chen, D., Cheng, A., Wei, H., & Stanley, D. (2013). Change detection from remotely sensed images: From pixel-based to object-based approaches. *ISPRS Journal of photogrammetry and remote sensing*, *80*, 91-106.

Hutyra, L. R., Yoon, B., & Alberti, M. (2011). Terrestrial carbon stocks across a gradient of urbanization: a study of the Seattle, WA region. *Global Change Biology*, *17*(2), 783-797.

Imhoff, M. L., Zhang, P., Wolfe, R. E., & Bounoua, L. (2010). Remote sensing of the urban heat island effect across biomes in the continental USA. *Remote sensing of environment*, *114*(3), 504-513.

Immitzer, M., Atzberger, C., & Koukal, T. (2012). Tree species classification with random forest using very high spatial resolution 8-band WorldView-2 satellite data. *Remote Sensing*, *4*(9), 2661-2693.

Ivajnšič, D., Kaligarič, M., & Žiberna, I. (2014). Geographically weighted regression of the urban heat island of a small city. *Applied Geography*, *53*, 341-353.

Jackson, B., Pagella, T., Sinclair, F., Orellana, B., Henshaw, A., Reynolds, B., Mcintyre, N., Wheater, H. and Eycott, A. (2013). Polyscape: A GIS mapping framework providing efficient and spatially explicit landscape-scale valuation of multiple ecosystem services. *Landscape and Urban Planning*, *112*, 74-88.

Jaganmohan, M., Knapp, S., Buchmann, C. M., & Schwarz, N. (2016). The bigger, the better? The influence of urban green space design on cooling effects for residential areas. *Journal of environmental quality*, *45*(1), 134-145.

Jalayer, F., De Risi, R., De Paola, F., Giugni, M., Manfredi, G., Gasparini, P. & Cavan, G. (2014). Probabilistic GIS-based method for delineation of urban flooding risk hotspots. *Natural hazards*, *73*(2), 975-1001.

Jenerette, G. D., Harlan, S. L., Buyantuev, A., Stefanov, W. L., Declet-Barreto, J., Ruddell, B. L. & Li, X. (2016). Micro-scale urban surface temperatures are related to landcover features and residential heat related health impacts in Phoenix, AZ USA. *Landscape Ecology*, *31*(4), 745-760.

Jensen, J. R. (2005). Digital image processing: a remote sensing perspective. *Upper Saddle River, NJ: sPrentice Hall*.

Jia, P., Qiu, Y., & Gaughan, A. E. (2014). A fine-scale spatial population distribution on the high-resolution gridded population surface and application in Alachua County, Florida. *Applied Geography*, *50*, 99-107.

Jin, H., & Mountrakis, G. (2013). Integration of urban growth modelling products with image-based urban change analysis. *International journal of remote sensing*, *34*(15), 5468-5486.

Jin, H., Stehman, S. V., & Mountrakis, G. (2014). Assessing the impact of training sample selection on accuracy of an urban classification: a case study in Denver, Colorado. *International journal of remote sensing*, *35*(6), 2067-2081.

Jochner, S., & Menzel, A. (2015). Urban phenological studies–past, present, future. *Environmental pollution*, *203*, 250-261.

Jones, B. A., & Goodkind, A. L. (2019). Urban afforestation and infant health: Evidence from MillionTreesNYC. *Journal of Environmental Economics and Management*, *95*, 26-44.

Kabisch, N. (2015). Ecosystem service implementation and governance challenges in urban green space planning—The case of Berlin, Germany. *Land use policy*, *42*, 557-567.

Kabisch, N., & Haase, D. (2013). Green spaces of European cities revisited for 1990–2006. *Landscape and urban planning*, *110*, 113-122.

Kabisch, N., Frantzeskaki, N., Pauleit, S., Naumann, S., Davis, M., Artmann, M., & Zaunberger, K. (2016). Nature-based solutions to climate change mitigation and adaptation in urban areas: perspectives on indicators, knowledge gaps, barriers, and opportunities for action. *Ecology and Society*, *21*(2).

Kain, J. H., Larondelle, N., Haase, D., & Kaczorowska, A. (2016). Exploring local consequences of two land-use alternatives for the supply of urban ecosystem services in Stockholm year 2050. *Ecological indicators*, *70*, 615-629.

Kalcic, M. M., Chaubey, I., & Frankenberger, J. (2015). Defining Soil and Water Assessment Tool (SWAT) hydrologic response units (HRUs) by field boundaries. *International Journal of Agricultural and Biological Engineering*, *8*(3), 69-80.

Kampouraki, M., Wood, G. A., & Brewer, T. R. (2008). Opportunities and limitations of object based image analysis for detecting urban impervious and vegetated surfaces using

true-colour aerial photography. In *Object-Based Image Analysis* (pp. 555-569). Springer, Berlin, Heidelberg.

Kandziora, M., Burkhard, B., & Müller, F. (2013). Mapping provisioning ecosystem services at the local scale using data of varying spatial and temporal resolution. *Ecosystem Services*, *4*, 47-59.

Karatas, A., & El-Rayes, K. (2015). Evaluating the performance of sustainable development in urban neighborhoods based on the feedback of multiple stakeholders. *Sustainable Cities and Society*, *14*, 374-382.

Kaspersen, P. S., Ravn, N. H., Arnbjerg-Nielsen, K., Madsen, H., & Drews, M. (2017). Comparison of the impacts of urban development and climate change on exposing European cities to pluvial flooding. *Hydrology and Earth System Sciences*, *21*(8), 4131-4147.

Kassomenos, P., Vardoulakis, S., Chaloulakou, A., Grivas, G., Borge, R., & Lumbreras, J. (2012). Levels, sources and seasonality of coarse particles (PM10–PM2. 5) in three European capitals–Implications for particulate pollution control. *Atmospheric environment*, *54*, 337-347.

Kaźmierczak, A., & Cavan, G. (2011). Surface water flooding risk to urban communities: Analysis of vulnerability, hazard and exposure. *Landscape and Urban Planning*, *103*(2), 185-197.

Kaźmierczak, A., & Kenny, C. (2011). Risk of flooding to infrastructure in Greater Manchester. *Manchester: The University of Manchester*.

Kennedy, S., & Sgouridis, S. (2011). Rigorous classification and carbon accounting principles for low and Zero Carbon Cities. *Energy Policy*, *39*(9), 5259-5268.

Kirby, D. (31st March, 2017). Revealed: The trees on our streets are being felled at a rate of 58 a day. *I-News*. Retrieved from https://inews.co.uk/news/environment/revealed-suburban-trees-felled-rate-58-day-527251 (Accessed 02/02/2020).

Kleeb, R., Gloor, P. A., Nemoto, K., & Henninger, M. (2012). Wikimaps: dynamic maps of knowledge. *International Journal of Organisational Design and Engineering 3*, *2*(2), 204-224.

Kolokotroni, M. and Giridharan, R. (2008). Urban heat island intensity in London: An investigation of the impact of physical characteristics on changes in outdoor air temperature during summer. *Solar energy*, *82* (11), 986-998.

Kong, F., Yin, H., James, P., Hutyra, L. R., & He, H. S. (2014). Effects of spatial pattern of greenspace on urban cooling in a large metropolitan area of eastern China. *Landscape and Urban Planning*, *128*, 35-47.

Kong, F., Sun, C., Liu, F., Yin, H., Jiang, F., Pu, Y. & Dronova, I. (2016). Energy saving potential of fragmented green spaces due to their temperature regulating ecosystem services in the summer. *Applied energy*, *183*, 1428-1440.

Koschke, L., Fürst, C., Frank, S., & Makeschin, F. (2012). A multi-criteria approach for an integrated landcover-based assessment of ecosystem services provision to support landscape planning. *Ecological indicators*, *21*, 54-66.

Kottek, M., Grieser, J., Beck, C., Rudolf, B., & Rubel, F. (2006). World map of the Köppen-Geiger climate classification updated. *Meteorologische Zeitschrift*, *15*(3), 259-263.

Krebs, G., Kokkonen, T., Valtanen, M., Setälä, H., & Koivusalo, H. (2014). Spatial resolution considerations for urban hydrological modelling. *Journal of hydrology*, *512*, 482-497.

Kremer, P., Hamstead, Z. A., & McPhearson, T. (2016a). The value of urban ecosystem services in New York City: A spatially explicit multicriteria analysis of landscape scale valuation scenarios. *Environmental Science & Policy*, *62*, 57-68.

Kremer, P., Hamstead, Z., Haase, D., McPhearson, T., Frantzeskaki, N., Andersson, E., Kabisch, N., Larondelle, N., Rall, E.L., Voigt, A. and Baró, F. (2016b). Key insights for the future of urban ecosystem services research. *Ecology and Society* 21 (2), 29.

Kroll, F., Müller, F., Haase, D., & Fohrer, N. (2012). Rural–urban gradient analysis of ecosystem services supply and demand dynamics. *Land use policy*, *29*(3), 521-535.

Krüger, E., Drach, P., Emmanuel, R., & Corbella, O. (2013). Assessment of daytime outdoor comfort levels in and outside the urban area of Glasgow, UK. *International journal of biometeorology*, *57*(4), 521-533.

Kuhn, M. (2020). The caret package. *R Foundation for Statistical Computing, Vienna, Austria. URL https://cran. r-project. org/package= caret*.

La Rosa, D. (2019). Why is the inclusion of the ecosystem services concept in urban planning so limited? A knowledge implementation and impact analysis of the Italian urban plans. *Socio-Ecological Practice Research*, 1-9.

Laaidi, K., Zeghnoun, A., Dousset, B., Bretin, P., Vandentorren, S., Giraudet, E. and Beaudeau, P. (2012). The impact of heat islands on mortality in Paris during the August 2003 heat wave. *Environmental health perspectives*, *120* (2), 254.

Langemeyer, J., Baró, F., Roebeling, P., & Gómez-Baggethun, E. (2015). Contrasting values of cultural ecosystem services in urban areas: The case of park Montjuïc in Barcelona. *Ecosystem Services*, *12*, 178-186.

Langemeyer, J., Wedgwood, D., McPhearson, T., Baró, F., Madsen, A. L., & Barton, D. N. (2020). Creating urban green infrastructure where it is needed–A spatial ecosystem service-based decision analysis of green roofs in Barcelona. *Science of the Total Environment*, *707*, 135487.

Lanza, K., & Stone Jr, B. (2016). Climate adaptation in cities: What trees are suitable for urban heat management?. *Landscape and Urban Planning*, *153*, 74-82.

Larondelle, N., & Haase, D. (2013). Urban ecosystem services assessment along a rural–urban gradient: A cross-analysis of European cities. *Ecological Indicators*, *29*, 179-190.

Larondelle, N., & Lauf, S. (2016). Balancing demand and supply of multiple urban ecosystem services on different spatial scales. *Ecosystem Services*, *22*, 18-31.

Larsen, L. (2015). Urban climate and adaptation strategies. *Frontiers in Ecology and the Environment*, *13*(9), 486-492.

Layke, C. (2009). Measuring nature's benefits: a preliminary roadmap for improving ecosystem service indicators. *World Resources Institute: Washington*.

Le Louarn, M., Clergeau, P., Briche, E., & Deschamps-Cottin, M. (2017). "Kill Two Birds with One Stone": Urban Tree Species Classification Using Bi-Temporal Pléiades Images to Study Nesting Preferences of an Invasive Bird. *Remote Sensing*, *9*(9), 916.

Le Roux, D. S., Ikin, K., Lindenmayer, D. B., Manning, A. D., & Gibbons, P. (2014). The future of large old trees in urban landscapes. *PloS one*, *9*(6), e99403.

Leandro, J., Chen, A. S., & Schumann, A. (2014). A 2D parallel diffusive wave model for floodplain inundation with variable time step (P-DWave). *Journal of Hydrology*, *517*, 250-259.

Leandro, J., Schumann, A. and Pfister, A., (2016). A step towards considering the spatial heterogeneity of urban key features in urban hydrology flood modelling. *Journal of hydrology*, *535*, pp.356-365.

Lee, H., & Mayer, H. (2018). Maximum extent of human heat stress reduction on building areas due to urban greening. *Urban Forestry & Urban Greening*, *32*, 154-167.

Lehner, M. (2018). Lisbon Green Corridor. Online website article (nextcity.nl – platform for nature inclusive and biodiverse cities) retrieved from: https://nextcity.nl/ (29/10/2020)

Lennon, M., Scott, M., & O'Neill, E. (2014). Urban design and adapting to flood risk: the role of green infrastructure. *Journal of Urban Design*, *19*(5), 745-758.

Li, F., Wang, R., Liu, X., & Zhang, X. (2005). Urban forest in China: Development patterns, influencing factors and research prospects. *The International Journal of Sustainable Development & World Ecology*, *12*(2), 197-204.

Li, S., Zhao, Z., Miaomiao, X., & Wang, Y. (2010). Investigating spatial non-stationary and scale-dependent relationships between urban surface temperature and environmental factors using geographically weighted regression. *Environmental Modelling & Software*, *25*(12), 1789-1800.

Li, H., Zhou, Y., Li, X., Meng, L., Wang, X., Wu, S., & Sodoudi, S. (2018). A new method to quantify surface urban heat island intensity. *Science of the total environment*, *624*, 262-272.

Liaw, A., & Wiener, M. (2002). Classification and regression by randomForest. *R news*, *2*(3), 18-22.

Lin, B., Meyers, J., & Barnett, G. (2015a). Understanding the potential loss and inequities of green space distribution with urban densification. *Urban forestry & urban greening*, *14*(4), 952-958.

Lin, B. B., Philpott, S. M., & Jha, S. (2015b). The future of urban agriculture and biodiversity-ecosystem services: Challenges and next steps. *Basic and applied ecology*, *16*(3), 189-201.

Lin, M. Y., Hagler, G., Baldauf, R., Isakov, V., Lin, H. Y., & Khlystov, A. (2016). The effects of vegetation barriers on near-road ultrafine particle number and carbon monoxide concentrations. *Science of the Total Environment*, *553*, 372-379.

Liu, W., Chen, W., & Peng, C. (2014). Assessing the effectiveness of green infrastructures on urban flooding reduction: A community scale study. *Ecological Modelling*, *291*, 6-14.

Liu, H., & Zhou, Q. (2004). Accuracy analysis of remote sensing change detection by rule-based rationality evaluation with post-classification comparison. *International Journal of Remote Sensing*, *25*(5), 1037-1050.

Liu, S., Marinelli, D., Bruzzone, L., & Bovolo, F. (2019). A review of change detection in multitemporal hyperspectral images: Current techniques, applications, and challenges. *IEEE Geoscience and Remote Sensing Magazine*, *7*(2), 140-158.

Livesley, S. J., Baudinette, B., & Glover, D. (2014). Rainfall interception and stem flow by eucalypt street trees–The impacts of canopy density and bark type. *Urban Forestry & Urban Greening*, *13*(1), 192-197.

Lowe, S. A. (2016). An energy and mortality impact assessment of the urban heat island in the US. *Environmental Impact Assessment Review*, *56*, 139-144.

Lu, D., Li, G., & Moran, E. (2014). Current situation and needs of change detection techniques. *International Journal of Image and Data Fusion*, *5*(1), 13-38.

Luederitz, C., Brink, E., Gralla, F., Hermelingmeier, V., Meyer, M., Niven, L., & Abson, D. J. (2015). A review of urban ecosystem services: six key challenges for future research. *Ecosystem Services*, *14*, 98-112.

Lwasa, S. (2010). Adapting urban areas in Africa to climate change: the case of Kampala. *Current Opinion in Environmental Sustainability*, *2*(3), 166-171.

MacKillop, F. (2012). Climatic city: Two centuries of urban planning and climate science in Manchester (UK) and its region. *Cities*, *29*(4), 244-251.

MacPherson, A. J., Principe, P. P., & Mehaffey, M. (2013). Using Malmquist Indices to evaluate environmental impacts of alternative land development scenarios. *Ecological indicators*, *34*, 296-303.

Madsen, H., Lawrence, D., Lang, M., Martinkova, M., & Kjeldsen, T. R. (2014). Review of trend analysis and climate change projections of extreme precipitation and floods in Europe. *Journal of Hydrology*, *519*, 3634-3650.

Majekodunmi, M., Emmanuel, R., & Jafry, T. (2020). A spatial exploration of deprivation and green infrastructure ecosystem services within Glasgow city. *Urban Forestry & Urban Greening*, *52*, 126698.

MCC [Manchester City Council] (2009) Manchester. A Certain Future*. Manchester City Council*. Retrieved from: http://www.manchesterclimate.com/sites/default/files/MACF%202010-20.pdf (Accessed 30/05/2017)

MCC [Manchester City Council] (2015a). *Manchester's Great Outdoors: a Green and Blue Infrastructure Strategy for Manchester – 2015-25.* Manchester City Council. Retrieved from http://www.manchester.gov.uk/downloads/download/6314/manchester_green_and_blue_strategy (Accessed 05/04/2018)

MCC [Manchester City Council] (2015b). Manchester's Great Outdoors: a Green and Blue Infrastructure Strategy for Manchester: Stakeholder Implementation Plan. Retrieved from https://secure.manchester.gov.uk/download/downloads/id/23418/green_and_blue_action_plan.pdf (Accessed 05/04/2018)

MCC [Manchester City Council] (2016a). A20 1086-2016 Manchester population. Retrieved from: http://www.manchester.gov.uk/download/downloads/id/25393/a20_1086-2016_manchester_population.pdf (Accessed 05/04/2018)

MCC [Manchester City Council] (January, 2016b). Manchester Tree Action Plan. Retrieved from https://www.manchester.gov.uk/downloads/download/6838/manchester_green_and_blue_strategy (Accessed 02/02/2020)

MCC [Manchester City Council] (2020a). Manchester Climate Change Framework 2020-25. Retrieved from http://www.manchesterclimate.com/sites/default/files/Manchester%20Climate%20Change%20Framework%202020-25.pdf (Accessed 16/06/2020)

MCC [Manchester City Council] (2020b). *About the Local Development Framework (LDF)*. Retrieved from https://secure.manchester.gov.uk/info/200074/planning/1562/about_the_local_development_framework_ldf (Accessed 16/03/2020)

MCC [Manchester City Council] (2020c). *Core Strategy: Interactive Proposals Map*. Retrieved from https://secure.manchester.gov.uk/info/200074/planning/3301/core_strategy/2 (Accessed 16/03/2020)

Marando, F., Salvatori, E., Sebastiani, A., Fusaro, L., & Manes, F. (2019). Regulating ecosystem services and green infrastructure: assessment of urban heat island effect mitigation in the municipality of Rome, Italy. *Ecological modelling*, *392*, 92-102.

Maroko A.R., Maantay J.A., Sohler N.L., Grady K.L. & Arno P.S. (2009) The complexities of measuring access to parks and physical activity sites in New York City: a quantitative and qualitative approach. *International Journal of Health Geographics*, *8*(1) 34.

Martín-López, B., Gómez-Baggethun, E., García-Llorente, M., & Montes, C. (2014). Trade-offs across value-domains in ecosystem services assessment. *Ecological indicators*, *37*, 220-228.

Massoudieh, A., Maghrebi, M., Kamrani, B., Nietch, C., Tryby, M., Aflaki, S., & Panguluri, S. (2017). A flexible modeling framework for hydraulic and water quality performance assessment of stormwater green infrastructure. *Environmental Modelling & Software*, *92*, 57-73.

McBride, J. R., & Laćan, I. (2018). The impact of climate-change induced temperature increases on the suitability of street tree species in California (USA) cities. *Urban Forestry & Urban Greening*, *34*, 348-356.

McDonald, R. I. (2015). *Conservation for cities: how to plan & build natural infrastructure*. Island Press.

McHale, M. R., Burke, I. C., Lefsky, M. A., Peper, P. J., & McPherson, E. G. (2009). Urban forest biomass estimates: is it important to use allometric relationships developed specifically for urban trees?. *Urban Ecosystems*, *12*(1), 95-113.

McMillen, D. P. (2004). Geographically Weighted Regression: The Analysis of Spatially Varying Relationships. *American Journal of Agricultural Economics*, *86*(2), 554-556.

Mell, I. C., Henneberry, J., Hehl-Lange, S., & Keskin, B. (2013). Promoting urban greening: Valuing the development of green infrastructure investments in the urban core of Manchester, UK. *Urban forestry & urban greening*, *12*(3), 296-306.

Met Office (2013). Manchester Airport 1981 – 2010 averages. Retrieved from: https://web.archive.org/web/20130116131858/http://www.metoffice.gov.uk/climate/uk/averages/19812010/sites/manchester_airport.html last (Accessed 21/05/2018)

Met Office (2019). UK Climate Projections: Headline Findings September 2019 version 2. Retrieved from: https://www.metoffice.gov.uk/binaries/content/assets/metofficegovuk/pdf/research/ukcp/ukcp-headline-findings-v2.pdf (Accessed 06/02/2021)

Met Office (2020a). Weather stations. Retrieved from https://www.metoffice.gov.uk/weather/learn-about/how-forecasts-are-made/observations/weather-stations (Accessed 26/03/2020)

Met Office (2020b). UK Climate Projections (UKCP). Retrieved from https://www.metoffice.gov.uk/research/approach/collaboration/ukcp/index (Accessed 07/04/2020)

Meyer, G. E., & Neto, J. C. (2008). Verification of color vegetation indices for automated crop imaging applications. *Computers and electronics in agriculture*, *63*(2), 282-293.

Millard, K., & Richardson, M. (2015). On the importance of training data sample selection in random forest image classification: A case study in peatland ecosystem mapping. *Remote sensing*, *7*(7), 8489-8515.

Miller, J. D., & Hutchins, M. (2017). The impacts of urbanisation and climate change on urban flooding and urban water quality: A review of the evidence concerning the United Kingdom. *Journal of Hydrology: Regional Studies*, *12*, 345-362.

Millington, J. D., Perry, G. L., & Romero-Calcerrada, R. (2007). Regression techniques for examining land use/cover change: a case study of a Mediterranean landscape. *Ecosystems*, *10*(4), 562-578.

Mirzaei, P.A. (2015). Recent challenges in modeling of urban heat island. *Sustainable cities and society*, *19*, 200-206.

Mishra, S. K., Singh, V. P., & Singh, P. K. (2018). Revisiting the soil conservation service curve number method. In *Hydrologic modeling* (pp. 667-693). Springer, Singapore.

Mitchell, V. G., Mein, R. G., & McMahon, T. A. (2001). Modelling the urban water cycle. *Environmental modelling & software*, *16*(7), 615-629.

Monteiro, M. V., Doick, K. J., & Handley, P. (2016). Allometric relationships for urban trees in Great Britain. *Urban Forestry & Urban Greening*, *19*, 223-236.

Monteiro, M. V., Levanič, T., & Doick, K. J. (2017). Growth rates of common urban trees in five cities in Great Britain: A dendrochronological evaluation with an emphasis on the impact of climate. *Urban forestry & urban greening*, *22*, 11-23.

Morgan, R. K. (2012). Environmental impact assessment: the state of the art. *Impact assessment and project appraisal*, *30*(1), 5-14.

Motohka, T., Nasahara, K. N., Oguma, H., & Tsuchida, S. (2010). Applicability of green-red vegetation index for remote sensing of vegetation phenology. *Remote Sensing*, *2*(10), 2369-2387.

Muller, M. (2007). Adapting to climate change: water management for urban resilience. *Environment and urbanization*, *19*(1), 99-113.

Muller, N., Werner, P., & Kelcey, J. G. (Eds.). (2010). *Urban biodiversity and design*. John Wiley & Sons.

Murdock, A.P., Harfoot, A.J.P., Martin, D., Cockings, S. and Hill, C. (2015). OpenPopGrid: an open gridded population dataset for England and Wales. GeoData, University of Southampton. Retrieved from http://openpopgrid.geodata.soton.ac.uk/OpenPopGrid_ProductDocumentation.pdf (Accessed 09/05/2020)

Nakata-Osaki, C. M., Souza, L. C. L., & Rodrigues, D. S. (2018). THIS–Tool for Heat Island Simulation: A GIS extension model to calculate urban heat island intensity based on urban geometry. *Computers, Environment and Urban Systems*, *67*, 157-168.

Namdeo, A., & Bell, M. C. (2005). Characteristics and health implications of fine and coarse particulates at roadside, urban background and rural sites in UK. *Environment International*, *31*(4), 565-573.

NASA [National Aeronautics and Space Administration] (2020a). Landsat 8. Retrieved from https://landsat.gsfc.nasa.gov/landsat-8/ (Accessed 23/03/2020)

NASA (2020b). Modis: Specifications. Retrieved from https://modis.gsfc.nasa.gov/about/specifications.php (Accessed 23/03/2020)

NASA (2020c). Earthdata. Retrieved from https://earthdata.nasa.gov/ (Accessed 23/03/2020)

NCASI [National Council for Air and Stream Improvement Foundation] (2020). COLE (Carbon On-Line Estimator). Retrieved from https://www.ncasi.org/technical-studies/forestry/biomass-climate-change/cole-carbon-on-line-estimator/ (Accessed 23/03/2020)

Natural England (2019). The Biodiversity Metric 2.0 (JP029). Article on Natural England website. Retrieved from: http://publications.naturalengland.org.uk/publication/5850908674228224 (Accessed 06/02/2021)

Newcastle University (2018). UKCP09 Weather Generator. Retrieved from https://www.ncl.ac.uk/ceser/research/software/weather-generator/ (Accessed 09/04/2018)

Niemelä, J., Saarela, S. R., Söderman, T., Kopperoinen, L., Yli-Pelkonen, V., Väre, S., & Kotze, D. J. (2010). Using the ecosystem services approach for better planning and conservation of urban green spaces: a Finland case study. *Biodiversity and Conservation*, *19*(11), 3225-3243.

Nimbus Maps (2020). *Nimbus Maps for Property Professionals.* Retrieved from https://www.nimbusmaps.co.uk/ (Accessed 16/03/2020)

Norton, B. A., Coutts, A. M., Livesley, S. J., Harris, R. J., Hunter, A. M., & Williams, N. S. (2015). Planning for cooler cities: A framework to prioritise green infrastructure to mitigate high temperatures in urban landscapes. *Landscape and urban planning*, *134*, 127-138.

Nowak, D. J., & Crane, D. E. (2002). Carbon storage and sequestration by urban trees in the USA. *Environmental pollution*, *116*(3), 381-389.

Nowak, D. J., Stevens, J. C., Sisinni, S. M., & Luley, C. J. (2002). Effects of urban tree management and species selection on atmospheric carbon dioxide. *Journal of Arboriculture. 28 (3): 113-122.*, *28*(3).

Nowak, D. J., Crane, D. E., & Stevens, J. C. (2006). Air pollution removal by urban trees and shrubs in the United States. *Urban forestry & urban greening*, *4*(3-4), 115-123.

Nowak, D. J., & Greenfield, E. J. (2012). Tree and impervious cover change in US cities. *Urban Forestry & Urban Greening*, *11*(1), 21-30.

Nowak, D. J., Greenfield, E. J., Hoehn, R. E., & Lapoint, E. (2013). Carbon storage and sequestration by trees in urban and community areas of the United States. *Environmental pollution*, *178*, 229-236.

O'Brien, O., & Cheshire, J. (2016). Interactive mapping for large, open demographic data sets using familiar geographical features. *Journal of Maps*, *12*(4), 676-683.

Ogden, F. L., Hawkins, R. P., Walter, M. T., & Goodrich, D. C. (2017). Comment on "Beyond the SCS-CN method: A theoretical framework for spatially lumped rainfall-runoff response" by MS Bartlett et al. *Water Resources Research*, *53*(7), 6345-6350.

Oke, T. R. (1978). Boundary layer climates, 372. *Methuen, New York*.

ONS [Office for National Statistics] (2013a). QS406EW: Household Size [Data download]. Retrieved from https://www.nomisweb.co.uk/census/2011/qs406ew (Accessed 26/03/2018)

ONS [Office for National Statistics] (2013b). KS402EW: Tenure. Retrieved from: https://www.nomisweb.co.uk/census/2011/ks402ew (Accessed 15/05/2020)

ONS [Office for National Statistics] (2019). Estimates of the population for the UK, England and Wales, Scotland and Northern Ireland. Retrieved from: https://www.ons.gov.uk/peoplepopulationandcommunity/populationandmigration/populationestimates/datasets/populationestimatesforukenglandandwalesscotlandandnorthernireland (Accessed 01/05/2020)

ONS [Office for National Statistics] (2020). Subnational population projections for England: 2018-based. Online tool retrieved from: https://www.ons.gov.uk/peoplepopulationandcommunity/populationandmigration/populationprojections/bulletins/subnationalpopulationprojectionsforengland/2018based (Accessed 16/05/2020)

Olofsson, P., Foody, G. M., Stehman, S. V., & Woodcock, C. E. (2013). Making better use of accuracy data in land change studies: Estimating accuracy and area and quantifying uncertainty using stratified estimation. *Remote Sensing of Environment*, *129*, 122-131.

Openshaw, S. (1984). Ecological fallacies and the analysis of areal census data. *Environment and planning A*, *16*(1), 17-31.

van Oort, P. A. J. (2005). Improving landcover change estimates by accounting for classification errors. *International Journal of Remote Sensing*, *26*(14), 3009-3024.

OS [Ordnance Survey] (2004). *Land-line user guide*. Retrieved from https://digimap.edina.ac.uk/webhelp/os/osdigimaphelp.htm#data_information/os_products/land-line.htm, (Accessed 18/01/2020)

OS [Ordnance Survey] (2018). Addressbase plus: July 2018 version [Data download]. Obtained on research license from Ordnance Survey (July 2018). Online information: https://www.ordnancesurvey.co.uk/business-government/products/addressbase (Accessed 26/03/2020)

OS [Ordnance Survey] (2020). *OS MasterMap Topography Layer*. Retrieved from https://www.ordnancesurvey.co.uk/business-government/products/mastermap-topography, (Accessed 18/01/2020)

Palazzo, E. (2019). From water sensitive to floodable: Defining adaptive urban design for water resilient cities. *Journal of Urban Design*, *24*(1), 137-157.

Palla, A., & Gnecco, I. (2015). Hydrologic modeling of Low Impact Development systems at the urban catchment scale. *Journal of hydrology*, *528*, 361-368.

Pan, A., Hou, A., Tian, F., Ni, G., & Hu, H. (2011). Hydrologically enhanced distributed urban drainage model and its application in Beijing city. *Journal of Hydrologic Engineering*, *17*(6), 667-678.

Paravantis, J., Santamouris, M., Cartalis, C., Efthymiou, C., & Kontoulis, N. (2017). Mortality associated with high ambient temperatures, heatwaves, and the urban heat island in Athens, Greece. *Sustainability*, *9*(4), 606.

Pauleit, S., Ennos, R., & Golding, Y. (2005). Modeling the environmental impacts of urban land use and landcover change—a study in Merseyside, UK. *Landscape and urban planning*, *71*(2-4), 295-310.

Paulin, M. J., Remme, R. P., de Nijs, T., Rutgers, M., Koopman, K. R., de Knegt, B., van der Hoek, D.C.J. & Breure, A. M. (2020). Application of the Natural Capital Model to assess changes in ecosystem services from changes in green infrastructure in Amsterdam. *Ecosystem Services*, *43*, 101114.

Peiman, R. (2011). Pre-classification and post-classification change-detection techniques to monitor landcover and land-use change using multi-temporal Landsat imagery: a case study on Pisa Province in Italy. *International journal of remote sensing*, *32*(15), 4365-4381.

Peng, S., Piao, S., Ciais, P., Friedlingstein, P., Ottle, C., Bréon, F.M., Nan, H., Zhou, L. and Myneni, R.B. (2012). Surface urban heat island across 419 global big cities. *Environmental science & technology*, *46*(2), 696-703.

Perry, T., & Nawaz, R. (2008). An investigation into the extent and impacts of hard surfacing of domestic gardens in an area of Leeds, United Kingdom. *Landscape and Urban Planning*, *86*(1), 1-13.

Persson, M., Lindberg, E., & Reese, H. (2018). Tree species classification with multi-temporal Sentinel-2 data. *Remote Sensing*, *10*(11), 1794.

Peters, E. B., Hiller, R. V., & McFadden, J. P. (2011). Seasonal contributions of vegetation types to suburban evapotranspiration. *Journal of Geophysical Research: Biogeosciences*, *116*(G1).

Petrov, L. O., Lavalle, C., & Kasanko, M. (2009). Urban land use scenarios for a tourist region in Europe: Applying the MOLAND model to Algarve, Portugal. *Landscape and Urban Planning*, *92*(1), 10-23.

Pitt, R. E., Chen, S., Clark, S., & Lantrip, J. (2005). Soil structure effects associated with urbanization and the benefits of soil amendments. In *Impacts of Global Climate Change* (pp. 1-12).

Plummer, M. L. (2009). Assessing benefit transfer for the valuation of ecosystem services. *Frontiers in Ecology and the Environment*, *7*(1), 38-45.

Pouyat, Richard, Peter Groffman, Ian Yesilonis, and Luis Hernandez. "Soil carbon pools and fluxes in urban ecosystems." *Environmental pollution* 116 (2002): S107-S118.

Pulighe, G., Fava, F., & Lupia, F. (2016). Insights and opportunities from mapping ecosystem services of urban green spaces and potentials in planning. *Ecosystem services*, *22*, 1-10.

Qiu, G. Y., LI, H. Y., Zhang, Q. T., Wan, C. H. E. N., Liang, X. J., & Li, X. Z. (2013). Effects of evapotranspiration on mitigation of urban temperature by vegetation and urban agriculture. *Journal of Integrative Agriculture*, *12*(8), 1307-1315.

R Core Team (2019). R: A language and environment for statistical computing. R Foundati on for Statistical Computing, Vienna, Austria.

Raciti, S. M., Hutyra, L. R., & Newell, J. D. (2014). Mapping carbon storage in urban trees with multi-source remote sensing data: Relationships between biomass, land use, and demographics in Boston neighborhoods. *Science of the Total Environment*, *500*, 72-83.

Radford, K. G., & James, P. (2013). Changes in the value of ecosystem services along a rural–urban gradient: A case study of Greater Manchester, UK. *Landscape and urban planning*, *109*(1), 117-127.

Rahman, M. A., Armson, D., & Ennos, A. R. (2015). A comparison of the growth and cooling effectiveness of five commonly planted urban tree species. *Urban Ecosystems*, *18*(2), 371-389.

Rall, E. L., Kabisch, N., & Hansen, R. (2015). A comparative exploration of uptake and potential application of ecosystem services in urban planning. *Ecosystem Services*, *16*, 230-242.

Reed, M. S., Kenter, J., Bonn, A., Broad, K., Burt, T. P., Fazey, I. R., & Stringer, L. C. (2013). Participatory scenario development for environmental management: A methodological framework illustrated with experience from the UK uplands. *Journal of environmental management*, *128*, 345-362.

Reynard, N. S., Prudhomme, C., & Crooks, S. M. (2001). The flood characteristics of large UK rivers: potential effects of changing climate and land use. *Climatic change*, *48*(2-3), 343-359.

Roberts, D. R., Bahn, V., Ciuti, S., Boyce, M. S., Elith, J., Guillera-Arroita, G. & Warton, D. I. (2017a). Cross-validation strategies for data with temporal, spatial, hierarchical, or phylogenetic structure. *Ecography*, *40*(8), 913-929.

Roberts, H., Sadler, J., & Chapman, L. (2017b). Using Twitter to investigate seasonal variation in physical activity in urban green space. *Geo: Geography and Environment*, *4*(2), e00041.

Robinson, C., Bouzarovski, S., & Lindley, S. (2018). 'Getting the measure of fuel poverty': The geography of fuel poverty indicators in England. *Energy Research & Social Science*, *36*, 79-93.

Rodríguez, J.P., Beard Jr, T.D., Bennett, E.M., Cumming, G.S., Cork, S.J., Agard, J., Dobson, A.P. and Peterson, G.D. (2006). Trade-offs across space, time, and ecosystem services. *Ecology and society*, *11*(1).

Rodriguez-Galiano, V. F., Ghimire, B., Rogan, J., Chica-Olmo, M., & Rigol-Sanchez, J. P. (2012). An assessment of the effectiveness of a random forest classifier for landcover classification. *ISPRS Journal of Photogrammetry and Remote Sensing*, *67*, 93-104.

Rogers, K., Sacre, K., Goodenough, J., & Doick, K. (2015). Valuing London's urban forest: results of the London i-Tree eco project.

Romero, P., Castro, G., Gómez, J. A., & Fereres, E. (2007). Curve number values for olive orchards under different soil management. *Soil Science Society of America Journal*, *71*(6), 1758-1769.

Rufin, P., Müller, H., Pflugmacher, D., & Hostert, P. (2015). Land use intensity trajectories on Amazonian pastures derived from Landsat time series. *International Journal of Applied Earth Observation and Geoinformation*, *41*, 1-10.

Russo, A., Escobedo, F. J., Timilsina, N., Schmitt, A. O., Varela, S., & Zerbe, S. (2014). Assessing urban tree carbon storage and sequestration in Bolzano, Italy. *International Journal of Biodiversity Science, Ecosystem Services & Management*, *10*(1), 54-70.

Salmond, J. A., Tadaki, M., Vardoulakis, S., Arbuthnott, K., Coutts, A., Demuzere, M., Dirks, K.N., Heaviside, C., Lim, S., Macintyre, H., McInnes, R. N. & Wheeler, B.W. (2016). Health and climate related ecosystem services provided by street trees in the urban environment. *Environmental Health*, *15*(1), 95-111.

Salvadore, E., Bronders, J., & Batelaan, O. (2015). Hydrological modelling of urbanized catchments: A review and future directions. *Journal of hydrology*, *529*, 62-81.

Sato, T., Yano, T., & Morihara, T. (2006). Seasonal effects of a tree belt on community response to road traffic noise: A social survey in Tomakomai, Japan. *Journal of Temporal Design in Architecture and the Environment*, *6*(1), 49-56.

Sayce, S., Walford, N., & Garside, P. (2012). Residential development on gardens in England: Their role in providing sustainable housing supply. *Land Use Policy*, *29*(4), 771-780.

Schmit, C., Rounsevell, M. D., & La Jeunesse, I. (2006). The limitations of spatial land use data in environmental analysis. *Environmental Science & Policy*, *9*(2), 174-188.

Schorcht, M., Krüger, T., & Meinel, G. (2016). Measuring land take: usability of national topographic databases as input for land use change analysis: a case study from Germany. *ISPRS International Journal of Geo-Information*, *5*(8), 134.

Schroll, E., Lambrinos, J., Righetti, T., & Sandrock, D. (2011). The role of vegetation in regulating stormwater runoff from green roofs in a winter rainfall climate. *Ecological engineering*, *37*(4), 595-600.

Schröter, M., & Remme, R. P. (2016). Spatial prioritisation 566 for conserving ecosystem services: comparing hotspots with heuristic optimisation. *Landscape ecology*, *31*(2), 431-450.

Schröter, M., Kraemer, R., Ceauşu, S., & Rusch, G. M. (2017). Incorporating threat in hotspots and coldspots of biodiversity and ecosystem services. *Ambio*, *46*(7), 756-768.

Schröter, M., Remme, R. P., Sumarga, E., Barton, D. N., & Hein, L. (2015). Lessons learned for spatial modelling of ecosystem services in support of ecosystem accounting. *Ecosystem Services*, *13*, 64-69.

Schulp, C. J., Burkhard, B., Maes, J., Van Vliet, J., & Verburg, P. H. (2014). Uncertainties in ecosystem service maps: a comparison on the European scale. *PloS one*, *9*(10), e109643.

Schwarz, N., Bauer, A., & Haase, D. (2011). Assessing climate impacts of planning policies—an estimation for the urban region of Leipzig (Germany). *Environmental impact assessment review*, *31*(2), 97-111.

Schwarz, N., Schlink, U., Franck, U. and Großmann, K. (2012). Relationship of land surface and air temperatures and its implications for quantifying urban heat island indicators—An application for the city of Leipzig (Germany). *Ecological Indicators*, *18*, 693-704.

SEPA [Scottish Environment Protection Agency]. (2011). Allan Water Natural Flood Management Techniques and Scoping Study. Retrieved from http://www.cress.stir.ac.uk/allanwater/documents/R001.Allan_Water_NFM.pdf (Accessed 21/04/2018)

Seppelt, R., Dormann, C. F., Eppink, F. V., Lautenbach, S., & Schmidt, S. (2011). A quantitative review of ecosystem service studies: approaches, shortcomings and the road ahead. *Journal of applied Ecology*, *48*(3), 630-636.

Seppelt, R., Fath, B., Burkhard, B., Fisher, J. L., Grêt-Regamey, A., Lautenbach, S., Hotes, S., Spangenberg, J., Verburg, P.H. & Van Oudenhoven, A. P. (2012). Form follows function? Proposing a blueprint for ecosystem service assessments based on reviews and case studies. *Ecological Indicators*, *21*, 145-154.

Serra, P., Pons, X., & Sauri, D. (2003). Post-classification change detection with data from different sensors: some accuracy considerations. *International Journal of Remote Sensing*, *24*(16), 3311-3340.

Sharma, A., Conry, P., Fernando, H. J. S., Hamlet, A. F., Hellmann, J. J., & Chen, F. (2016). Green and cool roofs to mitigate urban heat island effects in the Chicago metropolitan area: Evaluation with a regional climate model. *Environmental Research Letters*, *11*(6), 064004.

Shashua-Bar, L., & Hoffman, M. E. (2000). Vegetation as a climatic component in the design of an urban street: An empirical model for predicting the cooling effect of urban green areas with trees. *Energy and buildings*, *31*(3), 221-235.

Shi, L., Chu, E., Anguelovski, I., Aylett, A., Debats, J., Goh, K., & Roberts, J. T. (2016). Roadmap towards justice in urban climate adaptation research. *Nature Climate Change*, *6*(2), 131-137.

Shimizu, E., & Fuse, T. (2003, May). Rubber-sheeting of historical maps in GIS and its application to landscape visualization of old-time cities: focusing on Tokyo of the past. In *Proceedings of the 8th international conference on computers in urban planning and urban management* (Vol. 11, No. 1, pp. 3-8).

Sieber, J., & Pons, M. (2015). Assessment of urban ecosystem services using ecosystem services reviews and GIS-based tools. *Procedia Engineering*, *115*, 53-60.

Signorell, A., Aho, K., Alfons, A., Anderegg, N., Aragon, T., & Arppe, A. (2016). DescTools: Tools for descriptive statistics. *R package version 0.99*, *18*.

da Silva, J. M. C., & Wheeler, E. (2017). Ecosystems as infrastructure. *Perspectives in ecology and conservation*, *15*(1), 32-35.

Silveira, L., Charbonnier, F., & Genta, J. L. (2000). The antecedent soil moisture condition of the curve number procedure. *Hydrological Sciences Journal*, *45*(1), 3-12.

Sjöman, J. D., & Gill, S. E. (2014). Residential runoff–The role of spatial density and surface cover, with a case study in the Höjeå river catchment, southern Sweden. *Urban forestry & urban greening*, *13*(2), 304-314.

Skelhorn, C., Lindley, S., & Levermore, G. (2014). The impact of vegetation types on air and surface temperatures in a temperate city: A fine scale assessment in Manchester, UK. *Landscape and Urban Planning*, *121*, 129-140.

Smargiassi, A., Goldberg, M.S., Plante, C., Fournier, M., Baudouin, Y. and Kosatsky, T. (2009). Variation of daily warm season mortality as a function of micro-urban heat islands. *Journal of Epidemiology & Community Health*, *63* (8), 659-664.

Smith, A. (2010). The development of "sports-city" zones and their potential value as tourism resources for urban areas. *European Planning Studies*, *18*(3), 385-410.

Smith, C., & Lawson, N. (2012). Identifying extreme event climate thresholds for greater Manchester, UK: examining the past to prepare for the future. *Meteorological Applications*, *19*(1), 26-35.

Smith, C.L., Webb, A., Levermore, G.J., Lindley, S.J. and Beswick, K. (2011). Fine-scale spatial temperature patterns across a UK conurbation. *Climatic Change*, *109* (3), 269-286.

Sobrino, J. A., Jiménez-Muñoz, J. C., Sòria, G., Romaguera, M., Guanter, L., Moreno, J. & Martínez, P. (2008). Land surface emissivity retrieval from different VNIR and TIR sensors. *IEEE Transactions on Geoscience and Remote Sensing*, *46*(2), 316-327.

Sovacool, B. K., & Brown, M. A. (2010). Twelve metropolitan carbon footprints: A preliminary comparative global assessment. *Energy policy*, *38*(9), 4856-4869.

Speak, A. F., Rothwell, J. J., Lindley, S. J., & Smith, C. L. (2012). Urban particulate pollution reduction by four species of green roof vegetation in a UK city. *Atmospheric Environment*, *61*, 283-293.

Stanford University (2020). Natural Capital Project: InVEST. Retrieved from https://naturalcapitalproject.stanford.edu/software/invest (Accessed 29/10/2020)

Stessens, P., Khan, A. Z., Huysmans, M., & Canters, F. (2017). Analysing urban green space accessibility and quality: A GIS-based model as spatial decision support for urban ecosystem services in Brussels. *Ecosystem services*, *28*, 328-340.

Steul, K., Schade, M., & Heudorf, U. (2018). Mortality during heatwaves 2003–2015 in Frankfurt-Main–the 2003 heatwave and its implications. *International journal of hygiene and environmental health*, *221*(1), 81-86.

Stevens, D., Dragicevic, S., & Rothley, K. (2007). iCity: A GIS–CA modelling tool for urban planning and decision making. *Environmental Modelling & Software*, *22*(6), 761-773.

Stevens, F. R., Gaughan, A. E., Linard, C., & Tatem, A. J. (2015). Disaggregating census data for population mapping using random forests with remotely-sensed and ancillary data. *PloS one*, *10*(2), e0107042.

Stewart, I.D. and Oke, T.R. (2012). Local climate zones for urban temperature studies. *Bulletin of the American Meteorological Society*, *93* (12), pp.1879-1900.

Strohbach, M. W., Arnold, E., & Haase, D. (2012). The carbon footprint of urban green space—A life cycle approach. *Landscape and Urban Planning*, *104*(2), 220-229.

Stürck, J., Levers, C., van der Zanden, E. H., Schulp, C. J. E., Verkerk, P. J., Kuemmerle, T., & Schrammeijer, E. (2018). Simulating and delineating future land change trajectories across Europe. *Regional Environmental Change*, *18* (3), 733-749.

Sugawara, H., Shimizu, S., Takahashi, H., Hagiwara, S., Narita, K. I., Mikami, T., & Hirano, T. (2016). Thermal influence of a large green space on a hot urban environment. *Journal of environmental quality*, *45*(1), 125-133.

Swinney P. & Thomas E. (2015). A century of change in Manchester. Retrieved from https://www.centreforcities.org/reader/a-century-of-cities/3-are-cities-bound-by-these-pathways/1-a-century-of-change-in-manchester/ (Accessed 02/05/2020)

Syrbe, R. U., & Walz, U. (2012). Spatial indicators for the assessment of ecosystem services: providing, benefiting and connecting areas and landscape metrics. *Ecological indicators*, *21*, 80-88.

Szymanowski, M., & Kryza, M. (2011). Application of geographically weighted regression for modelling the spatial structure of urban heat island in the city of Wroclaw (SW Poland). *Procedia Environmental Sciences*, *3*, 87-92.

Tallis, H., Kareiva, P., Marvier, M., & Chang, A. (2008). An ecosystem services framework to support both practical conservation and economic development. *Proceedings of the National Academy of Sciences*, *105*(28), 9457-9464.

Tallis, H. T., Ricketts, T., Guerry, A. D., Wood, S. A., Sharp, R., Nelson, E., & Vogl, A. L. (2014). Integrated valuation of environmental services and tradeoffs (InVEST) 3.1. 0 user's guide.

Taylor, J., Davies, M., Mavrogianni, A., Shrubsole, C., Hamilton, I., Das, P., & Biddulph, P. (2016). Mapping indoor overheating and air pollution risk modification across Great Britain: A modelling study. *Building and Environment*, *99*, 1-12.

Tayyebi, A., Delavar, M. R., Yazdanpanah, M. J., Pijanowski, B. C., Saeedi, S., & Tayyebi, A. H. (2010). A spatial logistic regression model for simulating land use patterns: a case study of the Shiraz Metropolitan area of Iran. In *Advances in earth observation of global change* (pp. 27-42). Springer, Dordrecht.

Ter-Mikaelian, M. T., & Korzukhin, M. D. (1997). Biomass equations for sixty-five North American tree species. *Forest Ecology and Management*, *97*(1), 1-24.

Tewkesbury, A. P., Comber, A. J., Tate, N. J., Lamb, A., & Fisher, P. F. (2015). A critical synthesis of remotely sensed optical image change detection techniques. *Remote Sensing of Environment*, *160*, 1-14.

Theeuwes, N. E., Solcerová, A., & Steeneveld, G. J. (2013). Modeling the influence of open water surfaces on the summertime temperature and thermal comfort in the city. *Journal of Geophysical Research: Atmospheres*, *118*(16), 8881-8896.

Tian, F., Qiu, G. Y., Yang, Y. H., Xiong, Y. J., & Wang, P. (2012). Studies on the relationships between land surface temperature and environmental factors in an inland river catchment based on geographically weighted regression and MODIS data. *IEEE Journal of selected topics in applied earth observations and remote sensing*, *5*(3), 687-698.

Tigges, J., Churkina, G., & Lakes, T. (2017). Modeling above-ground carbon storage: a remote sensing approach to derive individual tree species information in urban settings. *Urban ecosystems*, *20*(1), 97-111.

Tomscha, S. A., Sutherland, I. J., Renard, D., Gergel, S. E., Rhemtulla, J. M., Bennett, E. M., Daniels, L.D., Eddy, I.M. & Clark, E. E. (2016). A guide to historical data sets for reconstructing ecosystem service change over time. *BioScience*, *66*(9), 747-762.

Topan, H., & Kutoglu, H. S. (2009). Georeferencing accuracy assessment of high-resolution satellite images using figure condition method. *IEEE Transactions on Geoscience and Remote Sensing*, *47*(4), 1256-1261.

Torno, H. C., Marsalek, J., & Desbordes, M. (Eds.). (2013). *Urban runoff pollution* (Vol. 10). Springer Science & Business Media.

Torres-Vera, M. A., Prol-Ledesma, R. M., & García-López, D. (2009). Three decades of land use variations in Mexico City. *International Journal of Remote SensingInternational Journal of Remote Sensing*, *30*(1), 117-138.

Tourbier, J., & White, I. (2007). Sustainable measures for flood attenuation: sustainable drainage and conveyance systems SUDACS. *Advances in Urban Flood Management. London: Taylor & Francis*, 13-28.

Townshend, J. R., Justice, C. O., Gurney, C., & McManus, J. (1992). The impact of misregistration on change detection. *IEEE Transactions on Geoscience and remote sensing*, *30*(5), 1054-1060.

Tran, H., Uchihama, D., Ochi, S., & Yasuoka, Y. (2006). Assessment with satellite data of the urban heat island effects in Asian mega cities. *International journal of applied Earth observation and Geoinformation*, *8*(1), 34-48.

Tratalos, J., Fuller, R. A., Warren, P. H., Davies, R. G., & Gaston, K. J. (2007). Urban form, biodiversity potential and ecosystem services. *Landscape and urban planning*, *83*(4), 308-317.

Tzoulas, K., Korpela, K., Venn, S., Yli-Pelkonen, V., Kaźmierczak, A., Niemela, J., & James, P. (2007). Promoting ecosystem and human health in urban areas using Green Infrastructure: A literature review. *Landscape and urban planning*, *81*(3), 167-178.

UK Centre of Ecology and Hydrology (2020). Landcover Map 2015. Retrieved from https://www.ceh.ac.uk/services/landcover-map-2015 (Accessed 22/06/2020)

UKDS [United Kingdom Data Service] (2017). English Census Merged Wards, 2011 [data download]. Retrieved from https://borders.ukdataservice.ac.uk/bds.html (Accessed 17/06/2017)

UN [United Nations] (2018). 68% of the world population projected to live in urban areas by 2050, says UN. Retrieved from: https://www.un.org/development/desa/en/news/population/2018-revision-of-world-urbanization-prospects.html (Accessed 29.10.2020)

USDA [United States Department of Agriculture, Soil Conservation Society] (1986). Urban hydrology for small watersheds. *Technical release*, *55*, 2-6.

USFS [United States Forestry Service] (2018). i-Tree: Tools for Assessing and Managing Forests & Community Trees. Retrieved from https://www.itreetools.org/eco/ (Accessed 26/05/2019)

USGS [United States Geological Survey] (2017a). Earth explorer service: L8 image data [data download]. Retrieved from https://earthexplorer.usgs.gov/ (Accessed 24/10/2017)

USGS [United States Geological Survey] (2017b). Using the USGS Landsat 8 Product. Retrieved from https://landsat.usgs.gov/using-usgs-landsat-8-product (Accessed 24/10/2017)

Urban Splash (2020). New Islington, Manchester. Retrieved from https://www.urbansplash.co.uk/regeneration/projects/new-islington (Accessed 15/05/2020)

Valipour, M. (2014). Application of new mass transfer formulae for computation of evapotranspiration. *Journal of Applied Water Engineering and Research*, *2*(1), 33-46.

Van Stan, J. T., Levia Jr, D. F., & Jenkins, R. B. (2015). Forest canopy interception loss across temporal scales: Implications for urban greening initiatives. *The Professional Geographer*, *67*(1), 41-51.

Verbeeck, K., Van Orshoven, J., & Hermy, M. (2011). Measuring extent, location and change of imperviousness in urban domestic gardens in collective housing projects. *Landscape and urban planning*, *100*(1-2), 57-66.

Verbeiren, B., Van de Voorde, T., Canters, F., Binard, M., Cornet, Y., & Batelaan, O. (2013). Assessing urbanisation effects on rainfall-runoff using a remote sensing supported modelling strategy. *International Journal of Applied Earth Observation and Geoinformation*, *21*, 92-102.

Viera, A. J., & Garrett, J. M. (2005). Understanding interobserver agreement: the kappa statistic. *Fam med*, *37*(5), 360-363.

Villa, F., Ceroni, M., Bagstad, K., Johnson, G., & Krivov, S. (2009, September). ARIES (Artificial Intelligence for Ecosystem Services): a new tool for ecosystem services assessment, planning, and valuation. In *Proceedings of the 11th Annual BIOECON Conference on Economic Instruments to Enhance the Conservation and Sustainable Use of Biodiversity, Venice, Italy* (pp. 21-22).

Villa, F., Bagstad, K. J., Voigt, B., Johnson, G. W., Portela, R., Honzák, M., & Batker, D. (2014). A methodology for adaptable and robust ecosystem services assessment. *PloS one*, *9*(3).

van Vliet, J., Bregt, A. K., Brown, D. G., van Delden, H., Heckbert, S., & Verburg, P. H. (2016). A review of current calibration and validation practices in land-change modeling. *Environmental Modelling & Software*, *82*, 174-182.

Voskamp, I. M., & Van de Ven, F. H. (2015). Planning support system 588 for climate adaptation: Composing effective sets of blue-green measures to reduce urban vulnerability to extreme weather events. *Building and Environment*, *83*, 159-167.

VU.CITY (2020). VU.CITY: The Smart City Platform. Retrieved from https://vu.city/ (16/03/2020)

Wainwright, J., & Mulligan, M. (Eds.). (2005). *Environmental modelling: finding simplicity in complexity*. John Wiley & Sons.

Walsh, D., Bendel, N., Jones, R., & Hanlon, P. (2010). It's not 'just deprivation': why do equally deprived UK cities experience different health outcomes?. *Public health*, *124*(9), 487-495.

Wang, F., Qin, Z., Song, C., Tu, L., Karnieli, A., & Zhao, S. (2015). An improved mono-window algorithm for land surface temperature retrieval from Landsat 8 thermal infrared sensor data. *Remote sensing*, *7*(4), 4268-4289.

Wang, Z. H., Zhao, X., Yang, J., & Song, J. (2016). Cooling and energy saving potentials of shade trees and urban lawns in a desert city. *Applied Energy*, *161*, 437-444.

Warhurst, J. R., Parks, K. E., McCulloch, L., & Hudson, M. D. (2014). Front gardens to car parks: changes in garden permeability and effects on flood regulation. *Science of the Total Environment*, *485*, 329-339.

Warner, T. A., Foody, G. M., & Nellis, M. D. (2009). *The SAGE handbook of remote sensing*. Sage Publications.

Waters, D., Watt, W. E., Marsalek, J., & Anderson, B. C. (2003). Adaptation of a storm drainage system to accommodate increased rainfall resulting from climate change. *Journal of Environmental Planning and Management*, *46*(5), 755-770.

Weather Underground (2017). Meteorological data for Manchester Airport station. Retrieved from https://www.wunderground.com/ (Accessed 24/10/17)

Webb, B. W., & Zhang, Y. (1997). Spatial and seasonal variability in the components of the river heat budget. *Hydrological processes*, *11*(1), 79-101.

Weber, S., Sadoff, N., Zell, E. and de Sherbinin, A. (2015). Policy-relevant indicators for mapping the vulnerability of urban populations to extreme heat events: A case study of Philadelphia. *Applied Geography*, *63*, 231-243.

Wei, C., Taubenböck, H., & Blaschke, T. (2017). Measuring urban agglomeration using a city-scale dasymetric population map: A study in the Pearl River Delta, China. *Habitat International*, *59*, 32-43.

Wellmann, T., Schug, F., Haase, D., Pflugmacher, D., & van der Linden, S. (2020). Green growth? On the relation between population density, land use and vegetation cover fractions in a city using a 30-years Landsat time series. *Landscape and Urban Planning*, *202*, 103857.

Weng, Q., Lu, D., & Schubring, J. (2004). Estimation of land surface temperature–vegetation abundance relationship for urban heat island studies. *Remote sensing of Environment*, *89*(4), 467-483.

Whitford, V., Ennos, A. R., & Handley, J. F. (2001). "City form and natural process"—indicators for the ecological performance of urban areas and their application to Merseyside, UK. *Landscape and urban planning*, *57*(2), 91-103.

Whitten, M. (2019). Blame it on austerity? Examining the impetus behind London's changing green space governance. *People Place Policy*, *12*, 204-224.

Wilkinson, C., Saarne, T., Peterson, G. D., & Colding, J. (2013). Strategic spatial planning and the ecosystem services concept–an historical exploration. *Ecology and Society*, *18*(1).

Willcock, S., Hooftman, D. A., Blanchard, R., Dawson, T. P., Hickler, T., Lindeskog, M., Martinez-Lopez, J., Reyers, B., Watts, S.M., Eigenbrod, F. & Bullock, J. M. (2020). Ensembles of ecosystem service models can improve accuracy and indicate uncertainty. *Science of the Total Environment*, *747*, 141006.

Williams, G. (1996). Manchester. *Cities*, *13*(3), 203-212.

Wolff, S., Schulp, C. J. E., & Verburg, P. H. (2015). Mapping ecosystem services demand: A review of current research and future perspectives. *Ecological Indicators*, *55*, 159-171.

Woodland Trust (2018). Natures Calendar: Seasonal Reports [Data download]. Retrieved from https://naturescalendar.woodlandtrust.org.uk/analysis/seasonal-reports/ (Accessed 09/11/2018)

Woodruff, S. C., & BenDor, T. K. (2016). Ecosystem services in urban planning: Comparative paradigms and guidelines for high quality plans. *Landscape and Urban Planning*, *152*, 90-100.

Wu, Y., Tao, Y., Yang, G., Ou, W., Pueppke, S., Sun, X., Chen, G. and Tao, Q. (2019). Impact of land use change on multiple ecosystem services in the rapidly urbanizing Kunshan City of China: Past trajectories and future projections. *Land Use Policy*, *85*, 419-427.

Xiao, Q., McPherson, E. G., Simpson, J. R., & Ustin, S. L. (1998). Rainfall interception by Sacramento's urban forest. *Journal of Arboriculture*, *24*, 235-244.

Xiao, Q., & McPherson, E. G. (2002). Rainfall interception by Santa Monica's municipal urban forest. *Urban ecosystems*, *6*(4), 291-302.

Xiao, Q., & McPherson, E. G. (2011). Rainfall interception of three trees in Oakland, California. *Urban Ecosystems*, *14*(4), 755-769.

Xiao, Q., & McPherson, E. G. (2016). Surface water storage capacity of twenty tree species in Davis, California. *Journal of environmental quality*, *45*(1), 188-198.

Xiao, Q., McPherson, E. G., Ustin, S. L., & Grismer, M. E. (2000). A new approach to modeling tree rainfall interception. *Journal of Geophysical Research: Atmospheres*, *105*(D23), 29173-29188.

Yang, A., Fan, H., Jing, N., Sun, Y., & Zipf, A. (2016). Temporal analysis on contribution inequality in OpenStreetMap: A comparative study for four countries. *ISPRS International Journal of Geo-Information*, *5*(1), 5.

Yang, C., Yan, F., & Zhang, S. (2020). Comparison of land surface and air temperatures for quantifying summer and winter urban heat island in a snow climate city. *Journal of Environmental Management*, *265*, 110563.

Young, R. F., & McPherson, E. G. (2013). Governing metropolitan green infrastructure in the United States. *Landscape and Urban Planning*, *109*(1), 67-75.

Zak, D. R., Holmes, W. E., Burton, A. J., Pregitzer, K. S., & Talhelm, A. F. (2008). Simulated atmospheric NO3− deposition increases soil organic matter by slowing decomposition. *Ecological applications*, *18*(8), 2016-2027.

Zandbergen, P. A. (2011). Dasymetric mapping using high resolution address point datasets. *Transactions in GIS*, *15*, 5-27.

Zandbergen, P. A., & Ignizio, D. A. (2010). Comparison of dasymetric mapping techniques for small-area population estimates. *Cartography and Geographic Information Science*, *37*(3), 199-214.

Zardo, L., Geneletti, D., Pérez-Soba, M., & Van Eupen, M. (2017). Estimating the cooling capacity of green infrastructures to support urban planning. *Ecosystem services*, *26*, 225-235.

Zhang, X., Aono, Y., & Monji, N. (1998). Spatial variability of urban surface heat fluxes estimated from Landsat TM data under summer and winter conditions. *Journal of Agricultural Meteorology*, *54*(1), 1-11.

Zhang, M., Huang, X., Chuai, X., Yang, H., Lai, L., & Tan, J. (2015). Impact of land use type conversion on carbon storage in terrestrial ecosystems of China: A spatial-temporal perspective. *Scientific reports*, *5*, 10233.

Zhang, S., & Ramírez, F. M. (2019). Assessing and mapping ecosystem services to support urban green infrastructure: The case of Barcelona, Spain. *Cities*, *92*, 59-70.

Zhang, B., Xie, G., Zhang, C., & Zhang, J. (2012). The economic benefits of rainwater-runoff reduction by urban green spaces: a case study in Beijing, China. *Journal of environmental management*, *100*, 65-71.

Zhao, C., & Sander, H. A. (2018). Assessing the sensitivity of urban ecosystem service maps to input spatial data resolution and method choice. *Landscape and urban planning*, *175*, 11-22.

Zhao, H., Ren, Z., & Tan, J. (2018). The spatial patterns of land surface temperature and its impact factors: spatial non-stationarity and scale effects based on a geographically-weighted regression model. *Sustainability*, *10*(7), 2242.

Zheng, B., Myint, S. W., & Fan, C. (2014). Spatial configuration of anthropogenic landcover impacts on urban warming. *Landscape and Urban Planning*, *130*, 104-111.

Zhou, W., Huang, G. and Cadenasso, M.L. (2011). Does spatial configuration matter? Understanding the effects of landcover pattern on land surface temperature in urban landscapes. *Landscape and Urban Planning*, *102* (1), 54-63.

Zhou, W., Troy, A., & Grove, M. (2008). Object-based landcover classification and change analysis in the Baltimore metropolitan area using multitemporal high resolution remote sensing data. *Sensors*, *8*(3), 1613-1636

Zhou, W., Wang, J., Qian, Y., Pickett, S. T., Li, W., & Han, L. (2018). The rapid but "invisible" changes in urban greenspace: A comparative study of nine Chinese cities. *Science of the Total Environment*, *627*, 1572-1584.

Zhou, D., Zhang, L., Hao, L., Sun, G., Liu, Y., & Zhu, C. (2016). Spatiotemporal trends of urban heat island effect along the urban development intensity gradient in China. *Science of the Total Environment*, *544*, 617-626.

Zhou, D., Zhao, S., Liu, S., Zhang, L., & Zhu, C. (2014). Surface urban heat island in China's 32 major cities: Spatial patterns and drivers. *Remote Sensing of Environment*, *152*, 51-61.

Zölch, T., Henze, L., Keilholz, P., & Pauleit, S. (2017). Regulating urban surface runoff through nature-based solutions–An assessment at the micro-scale. *Environmental research*, *157*, 135-144.

Žuvela-Aloise, M., Koch, R., Buchholz, S., & Früh, B. (2016). Modelling the potential of green and blue infrastructure to reduce urban heat load in the city of Vienna. *Climatic Change*, *135*(3-4), 425-438.